PNC TJ1214 91-003

地層処分性能評価用解析システムの統合化研究(Ⅱ)

－ 文献集 －

(動力炉・核燃料開発事業団　委託研究文献集)

1991 年 5 月

動力炉核燃料開発事業団
4.6.29
技術管理室

三菱原子力工業株式会社

この資料は，動燃事業団の開発業務を進めるため，特に限られた関係者だけに開示するものです。ついては，複製，転載，引用等を行わないよう，また第三者への開示又は内容漏洩がないよう管理して下さい。また今回の開示目的以外のことには使用しないよう特に注意して下さい。

本資料についての問合せは下記に願います。

〒107　東京都港区赤坂１－９－13

動力炉・核燃料開発事業団

技術協力部　技術管理室

PNC TJ1214 91-003
1991 年 5 月

地層処分性能評価用解析システムの統合化研究(Ⅱ)

池田康博* ・石原義尚*
中原 豊* ・杉崎敬良*
土井英雄**・浜本 浩*
向井 悟**・蜂谷尚之**

要 旨

本研究は，地層処分システムの性能評価システムを体系的に開発していくために，以下に示す研究を実施した。

(1) Site-genericな観点から地層処分システムを包括的に性能評価するための統合モデルの全プロセス構成を体系付け，開発アプローチ法を総括した。

(2) 統合モデル体系を構成するためのプロセスモデル候補及びその検証／確証のステータスをレビューした。

(3) 統合モデル体系を成立させるために必要なプロセス連成関係を同定し，その課題，実行方法を総括した。

(4) 統合モデル体系を構成するためのプロセスモデル候補のモデル信頼性を評価する（確証）方法を確立させるため，INTRAVALフェーズ２の確証ケースの応用を検討した。

(5) 統合 モデル体系を構成するためのプロセスモデル候補のコード信頼性を評価する（検証）方法を確立させるため，FEMWATERを使って検証を実施した。

本報告書は，三菱原子力工業株式会社が動力炉・核燃料開発事業団の委託により実施した研究の成果である。

契約番号：020D0151

事業団担当部課室および担当者：環境開発部地層処分開発室（梅木博之）

* ：系統設計部系統計画チーム

** ：大宮研究所評価・解析チーム

PNC TJ1214 91-003
MAY, 1991

Integration Study (Ⅱ) for Performance Assessment System of Geological Disposal

Yasuhiro Ikeda* ・Yoshinao Ishihara *
Yutaka Nakahara * ・Takayoshi Sugisaki*
Hideo Doi ** ・Hiroshi Hamamoto*
Satoru Mukai** ・Naoyuki Hachiya **

Abstract

In the study, we have performed the following tasks in order to develop a systematic, comprehensive approach and a reliable, integrated computational system for performance assessment of a geologic disposal system.

(1) Develop system integration model concept including an integrated computational approach and a complete set of processes to performance assessment site-generically.

(2) Review candidate models based system integration model, including the status of verification and validation activities.

(3) Identify coupled processes based system integration model and review methodology for models of coupled processes.

(4) Apply test cases in INTRAVAL Phase 2 to develop methodology and techniques to validate candidate conceptual models.

(5) Verify FEMWATER to develop methodology and techniques to assure the numerical accuracy of computer codes.

Work performed by Mitsubishi Atomic Power Industries, Inc. under contract with Power Reactor and Nuclear Fuel Development Corporation.
PNC Liaison:Waste Technology Development Division, Geological Isolation Section, Hiroyuki Umeki.

* : System Engineering Department, System Planning Team.
**: Omiya Technical Institute, Analytical Evaluation Team.

文 献 も く じ

1. Three Dimensional In-Situ Migration Experiment in the Boom Clay Formation at the Mol Site in Belgium,INTRAVAL Phase 2,(1991) ・・・・・・1
2. Proposal for the Waste Isolation Pilot Plant Test Case on Flow and Transport in Heterogeneous Fractured Media INTRAVAL Phase Ⅱ, (1990) ・・・・・・・・・・・・・・・・・・・・・・・・・・・・・・・・15
3. P.Grindrod et al.,Flow THrough Fractured Rock:What does the WIPP site Culebra data reveal?,INTRAVAL Phase 2,(1991) ・・・・・・・・・・・41
4. K.A.Cliffe et al.,Preliminary Results for the WIPP2 Test Case, INTRAVAL Phase 2,(1991) ・・・・・・・・・・・・・・・・・・・・・・・55
5. INTRAVAL Phase Ⅱ Test Case:Las Cruces Trench Site,INTRAVAL Phase 2, (1990) ・・・・・・・・・・・・・・・・・・・・・・・・・・・・・・・67
6. K.Schelkes et al.,INTRAVAL Phase Ⅱ Test Case:Saline Groundwater Movement in an Erosional Channel Crossing a Salt Dome,BGR,(1990) ・・・・85
7. A.Hautojarvi et al.,Comments on tracer tests and data interpretation, VTT,INTRAVAL Phase 2,(1991) ・・・・・・・・・・・・・・・・・・・・・113
8. C.F.Tsang and S.Neuman,Studies of Tracer Experiments in a Fracture Zone at the Finnsjon Research Area-INTRAVAL Test Case 5,INTRAVAL Phase 1,(1991) ・・・・・・・・・・・・・・・・・・・・・・・・・・・・・139

I N T R A V A L

(phase 2)

(Test case description and data)

Three Dimensional In-Situ Migration Experiment in the Boom Clay Formation at the MOL Site in Belgium.

(a joint SCK/CEN - NIRAS/ONDRAF - PNC experiment for model validation.)

February 12,1991

1

1. INTRODUCTION

Since 1974 a Belgian research and development programme is carried out by SCK/CEN on the geological disposal of radio- active waste. Its main objectives are to develop the concept and the techniques, to demonstrate the feasibility and to assess the safety and performance of the geological disposal of conditioned radioactive waste in a deep argillaceous formation.

The parameters required in safety assessment studies are determined in the laboratory on clay samples taken from the underground. Different types of migration experiments are performed on the samples. Reshaped and reconsolidated clay plugs are used for Flow Through type diffusion experiments (1,2). Clay cores drilled parallel with and perpendicular to the stratification of the formation are used for percolation experiments (3). The values of the migration parameters obtained from the small scale laboratory experiments are used for long term safety assessment calculations (PAGIS and PACOMA studies).

Despite the precautions taken during sample collection and the preparation of the diffusion experiments, parameters determined in the laboratory are subject to uncertainty. To improve the confidence in the laboratory data and to validate the safety assessment model, a large scale in-situ experiment has been set up.

In 1982 SCK/CEN has build an underground research laboratory (URL) in the Boom clay formation underlying the Belgian nuclear research facilities at Mol at a depth of 220 meters. Figure 1 shows the underground facility as build up to date. In 1985 a piezometernest has been installed in the clay formation through access hole No. 1 in the concrete plug at the right end of the URL (see CP1 on figure 1).

The aim of this piezometernest was to get a good estimation of the in-situ hydraulic parameters of the clay formation and to start a large scale in-situ migration test. The purpose of the large scale migration test is to validate the safety assessment model and the migration parameters used for the long time predictive calculations.

The described experiment is a joint effort between SCK/CEN, NIRAS/ONDRAF and the Power Reactor and Nuclear Fuel Development Corporation (PNC) of Japan.

2. DESCRIPTION OF THE EXPERIMENT

Figure 2 gives a conceptual view of the piezometernest installed in the URL. The all stainless steel system contains 9 piezometers, interspaced by 0.9 m long tubes, and numbered from 1 to 9. Each piezometer consists of two concentric tubes, the outer one being made of sintered stainless steel. Figure 3 gives an outline of a filter (piezometer) of the piezometernest.

The distance between the filters from center to center is 1 meter. A stand pipe with an internal diameter of 2 mm is connected to the space separating the concentric tubes. The stand pipe makes the connection between the filter and the URL. The internal volume of the stand pipe is 3.14 ml per meter pipe. The volume of the space separating the concentric tubes is 75.4 ml, and the pore volume of the filter is 13.0 ml. The hole system is assembled in the gallery before it is mounted in the bore hole.

A horizontal hole with a diameter of 50 mm and a depth of 10 m in the clay is drilled in the clay formation by rotary drilling. The cuttings are removed by compressed air. Immediately after drilling, the completely assembled piezometernest is pushed in the drilled hole. An inert gas is flushed through the filters to prevent oxidation of the clay. After about 2 days the small gap separating the tubing and the wall of the hole in the clay is completely sealed by convergence creep of the clay, and the gas flow stops. The clay formation acts as a packer and isolates each of the 9 piezometers from each other. The total internal volume of the stand pipes for the different filters are given in the table I.

Table I: Total internal volume of the stand pipes for the different filters.

Filter number	Total volume stand pipe (ml)
1	37.68
2	34.54
3	31.40
4	29.83
5	26.69
6	23.56
7	23.55
8	20.41
9	17.27

3. PRESSURE DISTRIBUTION

The presence of the vertical experimental shaft at the end of the URL (see figure 1) at atmospheric pressure and lined with concrete bricks creates a hydraulic pressure gradient in the neighborhood of the piezometernest. The interstitial water pressure build-up in the piezometers is measured by Bourdon manometers coupled with snap-tite connections to the stand pipes. The steady state pressure distribution as a function of the depth in the clay is given in table II.

Figure 4 shows the pressure distribution in the piezometers as a function of the depth in the clay formation. The numbering of the filters is also indicated together with an indication of the injection filter.

Table II: Steady state pore water pressure distrbution around piezometernest CP1 as a function of the depth in the clay formation.

Filter Nr	Depth in clay (m)	Pore water pressure (MPa)
9	2	0.36
8	3	0.69
7	4	0.92
6	5	1.12
5	6	1.29
4	7	1.43
3	8	1.55
2	9	1.68
1	10	1.78

4. INJECTION OF THE HTO TRACER

About 2.5 years after the installation of the piezometernest the clay formation is supposed to be settled. The injection of the HTO tracer could be done. A stainless steel vessel containing 925 MBq of HTO is connected between filters CP1/2 and CP1/5 from 20/01/88 to 10/03/88. The pressure difference of 0.39 MPa between the two filters drives the HTO tracer into filter CP1/5 with a flowrate of 5.61 ml/d. The volume of the stand pipe from filter CP1/5 amounts to 26.69 ml. The total amount of liquid injected in filter CP1/5 is 280.5 ml or 2.4 times the dead volume of the piezometer. Then the vessel is disconnected an the stand pipes are closed. Now all the filters are closed and there is no water flow in the filters. The system is left alone and the HTO migration is 3-dimensional.

Utmost care is taken not to contaminate the other filters with HTO during loading and injection in CP1/5.

5. SAMPLING STRATEGY AND CONCENTRATION MEASUREMENTS

For the measurement of the HTO concentration in the interstitial liquid in the clay, liquid samples are collected from the filters CP1/4 and CP1/6 adjacent to the injection filter CP1/5 at a distance of 1 meter.

To avoid disturbance of the HTO concentration distribution in the clay formation due to sampling of the interstitial liquid, the sampling frequency and the total amount of sampled liquid is kept as low as possible.

From previous model calculations for the design of the experiment the first sampling should be done about 3 months after start of the injection and continued at a two months interval. The collected liquid sample volume has to be at least equal to the dead volume of the sampled piezometer. The first eight samples from each filter are taken in one fraction to collect sufficient activity for the measurement. For the sampling, weighed sample containers are connected to piezometers CP1/4 and CP1/6 by means of snap-tite connections. After a sampling duration of a few days the containers are disconnected and the amount of water collected is weighed. The HTO content in the sample is measured by liquid scintillation counting.

The interstitial Boom clay water has a high content of organic material causing severe quenching for low energy beta particles of tritium (Emax = 18 KeV). For the first samples with very low activities, quenching was avoided by distillation of the liquid before the addition of the liquid scintilator. Sample 8 and higher were corrected for quenching by measuring with and without the addition of an internal standard.

To obtain the concentration (Cj) of HTO in the interstitial liquid in the vicinity of the filter from the concentration measured in the collected sample (Cs) corrections has to be made for the stagnant liquid in the dead volume of the piezometer. If we assume that the concentration in the stand pipe is equal to the previous concentration in the vicinity of the filter (Ci) and the concentration in the concentric space near the filter and in the pore space of the filter does not differ to much from the concentration in the formation at that position, then the concentration at the filter position may be calculated as:

$$Cj = (Vs*Cs - Vsp*Ci)/(Vs - Vsp)$$

Vs is the total volume and Cs the concentration of the sample, Vsp is the internal volume of the stand pipe and Ci the previous concentration.

Table III: Results of the fractionated sampling of sample CP1/4-9.

Fraction Nr	Total sampled liquid (ml)	Total sampled activity (Bq)
1	21.26	7.11
2	40.40	15.93
3	57.86	28.28
4	73.50	40.08
5	128.41	89.49
6	142.81	102.97
7	160.43	118.84
8	177.29	134.91

To test the hypothesis, sample number 9 is been collected in 8 fractions. Table III gives the results of the fractionated sampling of sample CP1/4-9. Figure 5 gives a plot of the percolated activity as a function of the quantity of the sampled liquid. The line on the figure shows the calculation of the correction formula and proofs the validity of the correction hypothesis.

From sample number 9 on sampling is done in two fractions. A first fraction with a volume of at least two times the volume of the stand pipe of the filter. A second fraction with a volume of at least 100 ml. The concentration of the second fraction is equal to the concentration in the vicinity of the filter and no more correction is needed.

6. MEASURED CONCENTRATION DISTRIBUTION

The results of the concentration measurements in the filters CP1/4 and CP1/6 are given in table IV. The concentration of the sampling number 4 is below detection limit. The elapsed time is the time since injection of the HTO tracer. The last column in the table gives the concentration in the vicinity of the filter in Bq/l.

Table IV: Data on HTO concentrations in filters number CP1/4 and CP1/6.

Sample number	Start sampling (d/m/y)	Sample time (day)	Sample volume (ml)	Sample activ. (Bq)	Elapsed time (day)	Concentration (Bq/l)
CP1/4-4	27/11/88	10.10	184.8	<	311	0.0
CP1/4-5	22/03/89	7.08	128.2	0.372	426	3.8
CP1/4-6	16/05/89	9.30	167.8	3.239	481	22.7
CP1/4-7	18/07/89	9.80	178.0	16.18	544	104.6
CP1/4-8	27/09/89	8.90	161.8	49.83	615	354.0
CP1/4-9	04/12/89	10.02	177.3	-	683	953.9
CP1/4-10	02/04/90	9.00	160.8	-	802	3044.9
CP1/4-11	22/08/90	4.65	83.8	-	944	8148.2
CP1/6-4	27/11/88	10.10	125.4	<	311	0.0
CP1/6-5	22/03/89	7.08	87.8	0.205	426	3.5
CP1/6-6	16/05/89	9.30	112.0	1.579	481	17.9
CP1/6-7	18/07/89	9.80	120.0	9.60	544	100.5
CP1/6-8	27/09/89	8.90	109.7	30.43	615	343.5
CP1/6-9	04/12/89	10.02	125.0	-	683	1063.6
CP1/6-10	02/04/90	9.00	111.6	-	802	3046.1
CP1/6-11	22/08/90	4.65	57.9	-	944	10734.9

The activity in the first three samples of filter CP1/4 are below detection limit. For filter CP1/6 HTO concentrations of 150, 33, 3.7 and 0.0 Bq/l have been measured for sampling after respectively 87, 145, 216 and 311 days. These unexpected results are supposed to be due to a slight contamination during the loading of the HTO tracer.

Figure 6 displays the measured concentration in the filters CP1/4 and CP1/6 as a function of the time since injection of the tracer. A simulation of the experiment with the MICOF program using the parameter values of chapter 7 is also given.

7. PROPOSED PARAMETER VALUES FOR MODEL CALCULATIONS

The proposed best values of the parameters for the calculation of the migration in the Boom clay formation based on the experiments on samples in the surface laboratory are:

- hydraulic conductivity	K	= 3.2E-12	m/s
- hydraulic gradient	dh/dx	= -18.9	m/m
- diffusion access. porosity	n	= 0.35	-
- dispersion length	a	= 0.002	m
- retardation factor	R	= 1	-
- half live HTO	T	= 12.28	year
- Darcy velocity (x direction)	Vd	= 6.0E-11	m/s
- dispersion constant (x)	Dx	= 4.1E-10	m2/s
- dispersion constant (y)	Dy	= 4.1E-10	m2/s
- dispersion constant (z)	Dz	= 2.0E-10	m2/s

The diffusion parameters have been determined in Flow Through type diffusion experiments on reconsolidated clay plugs (2). The apparent dispersion constant and the dispersion length have been measured by percolation experiments on clay cores drilled parallel and perpendicular to the stratification of the Boom clay formation (3).

The hydraulic conductivity of the formation has been determined in-situ in the piezometernest CP1 previous to the injection of the tracer.

The value proposed for the diffusion accessible porosity is 0.35 at an estimated in-situ consolidation pressure of 2.4 MPa.

8. REFERENCES

(1) M. Put and P. Henrion, Radiochimica Acta, 44/45, 343-347 (1988)

(2) P. Henrion, M. Put and M. Van Gompel, The influence of compaction on the diffusion of non-sorbed species in Boom clay. Presented at "MIGRATION 89", Monterey,USA

(3) M. Put, et al., Estimation of the migration parameters for the Boom clay formation by percolation experiments on undisturbed clay cores. MRS 1990 Fall Meeting, Boston

9. CONTACT PERSON

Martin PUT
SCK/CEN
Boeretang 200
B-2400 MOL
Belgium

TEL (014)33.22.30
TFX (014)31.50.21

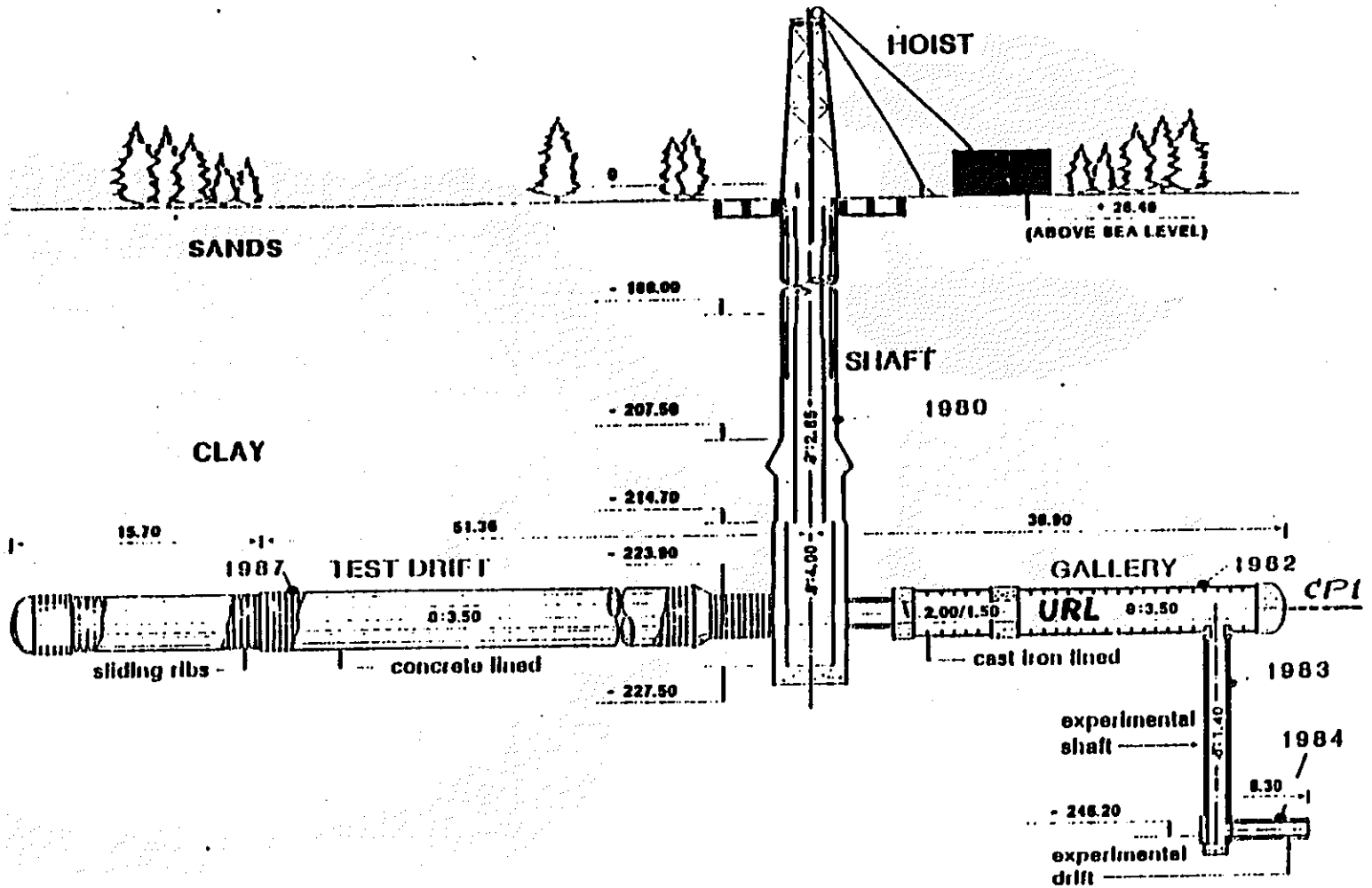


Figure 1: Scheme of the as built underground facility at SCK/CEN MOL Belgium.

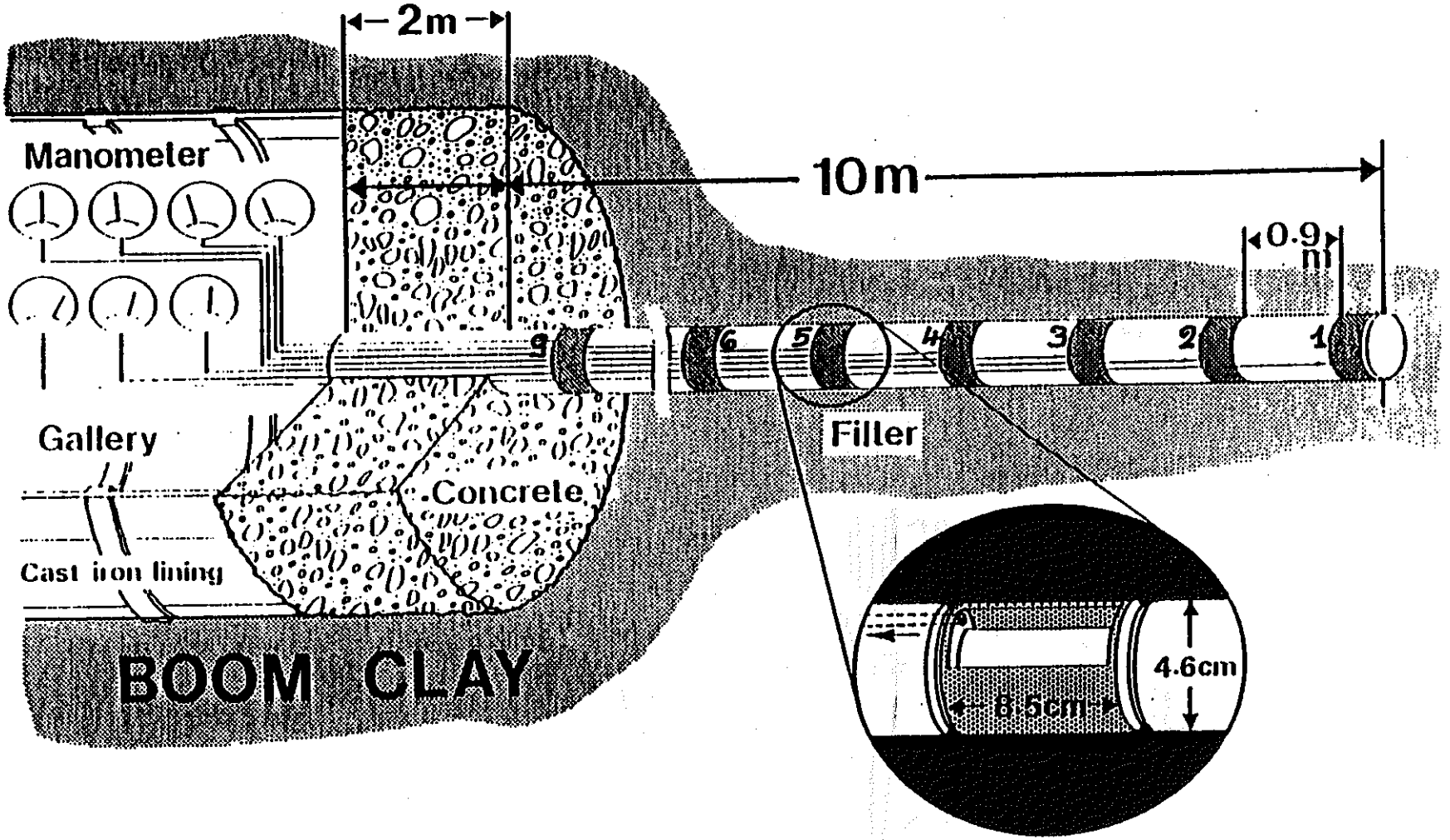


Figure 2: Conceptual view of piezometernest.

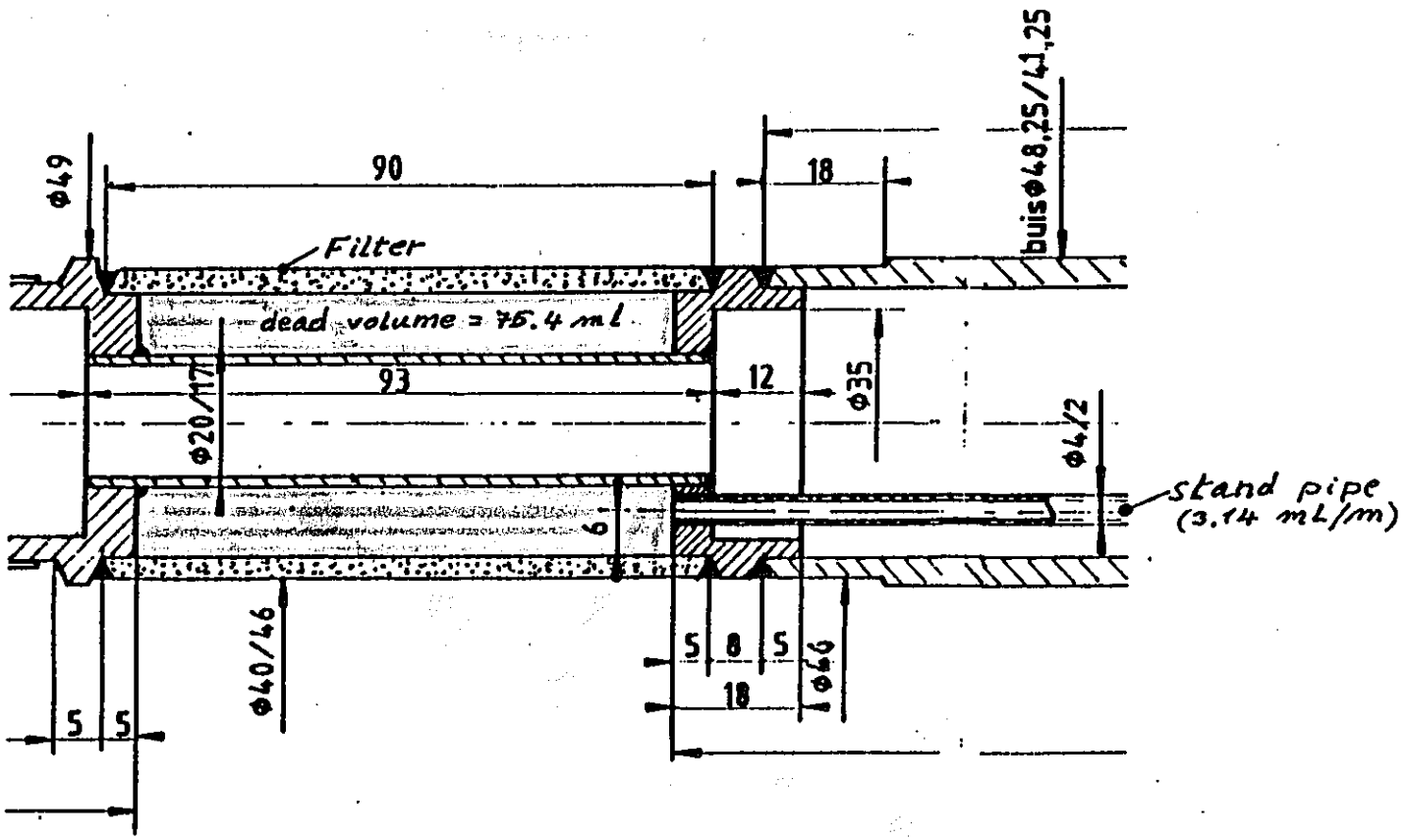


Figure 3 : Outline of a filter from piezometernest CP1.

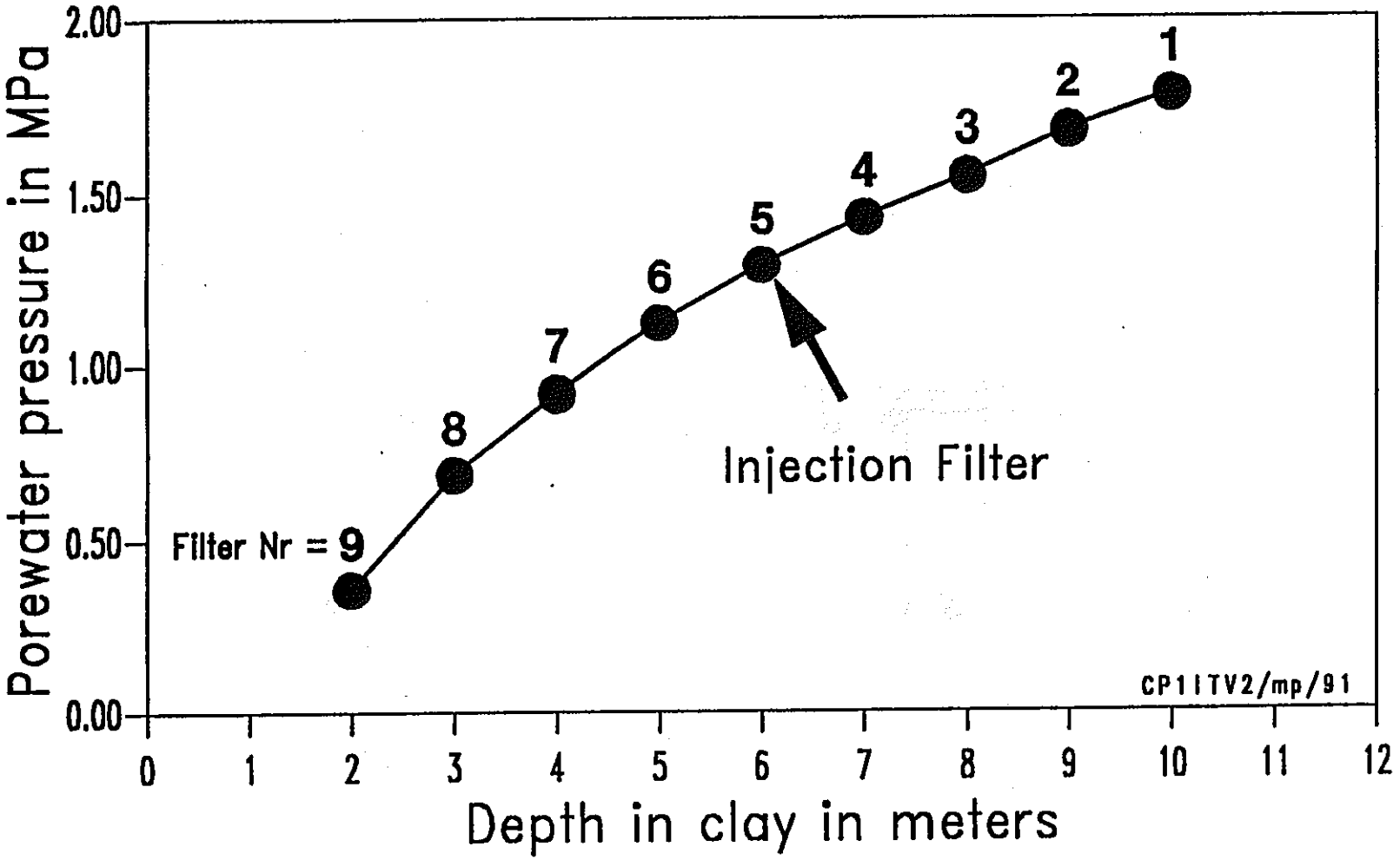


Figure 4: Pressure profile in CP1.

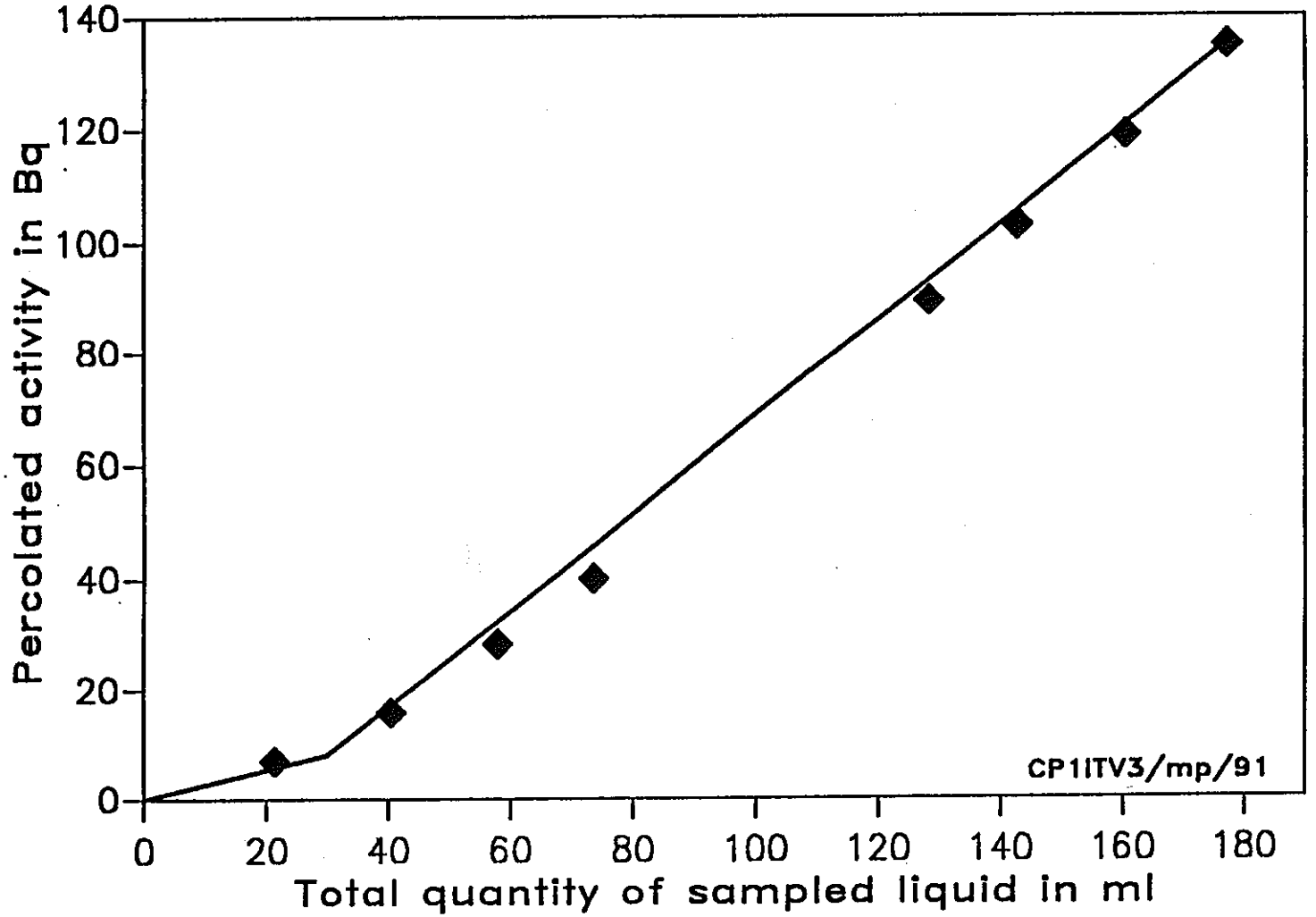


Figure 5 : Percolated HTO activity (Bq) as a function of the quantity of the sampled liquid for sample CP1/4-9.

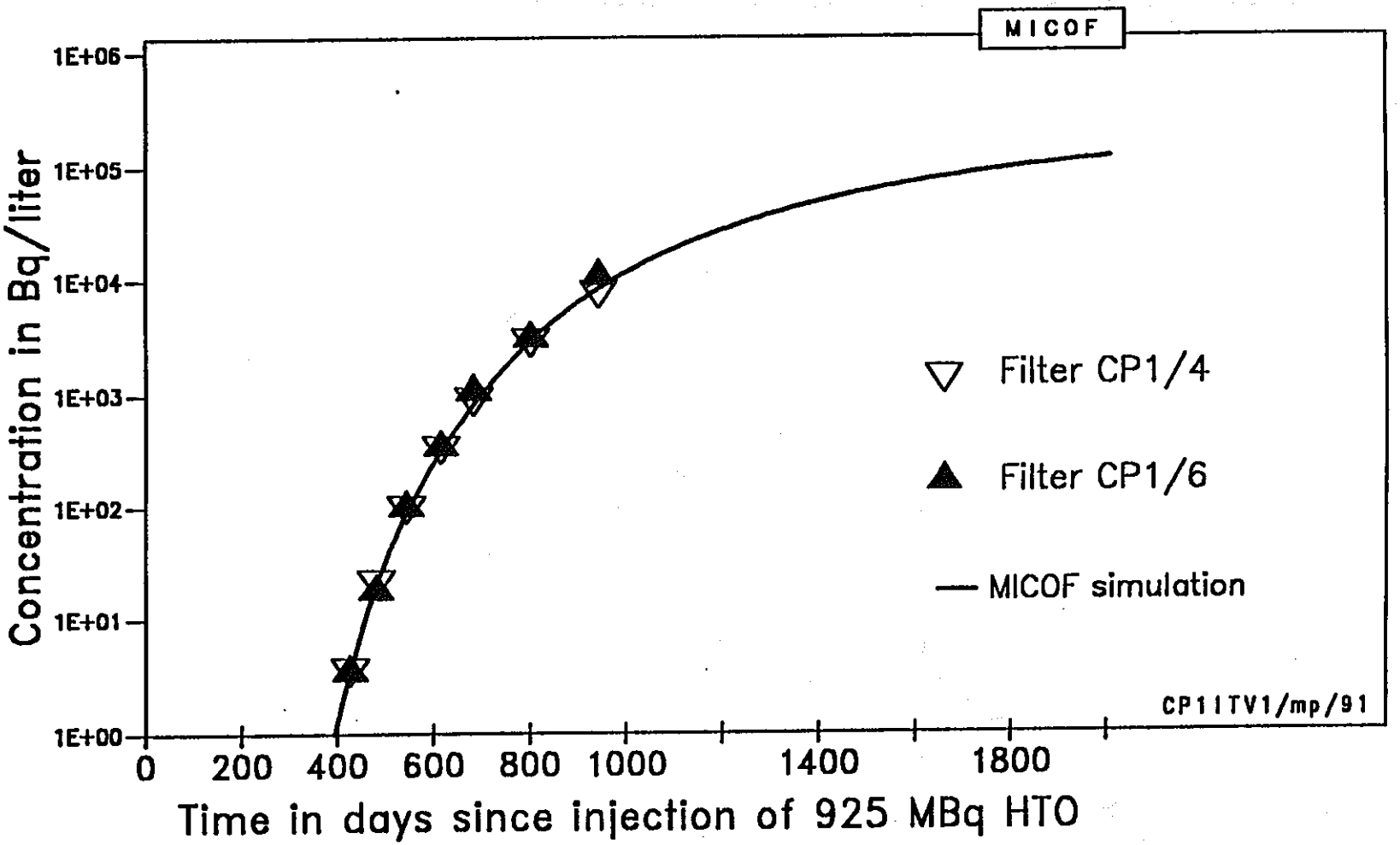


Figure 6 : Concentration in the liquid for the filters CP1/4 and CP1/6.

PROPOSAL FOR THE WASTE ISOLATION PILOT PLANT TEST CASE ON FLOW AND TRANSPORT IN HETEROGENEOUS FRACTURED MEDIA INTRAVAL PHASE II

I. INTRODUCTION

A. Pilot Group

The Pilot Group is the United States Department of Energy, Waste Isolation Pilot Plant (WIPP) Project Office, in Carlsbad, New Mexico, USA, 88221. The pilot group leader is Jerry Carr, Hydrologist, Waste Isolation Pilot Plant, Carlsbad, New Mexico, USA, 88221. The alternate pilot group leader is Vernon Daub, Manager, Waste Isolation Pilot Plant, Carlsbad, New Mexico, USA, 88221.

The technical contact is Elaine D. Gorham, Supervisor, Fluid Flow and Transport Division 6344, Sandia National Laboratories, Albuquerque, New Mexico, USA, 87185.

As the first underground repository in the USA for disposal of radioactive wastes, the Waste Isolation Pilot Plant (WIPP) is subject to rigorous scientific scrutiny. Validation of WIPP computer models used to resolve technical issues important to performance assessment is of great interest to Sandia National Laboratories and the US Department of Energy. Both Sandia and the Department of Energy are committed to such validation. INTRAVAL provides an opportunity to discuss validation methods, participate in various validation activities, and obtain validation of some WIPP models. The Department of Energy expects its commitment to validation and the INTRAVAL to continue throughout Phase II of INTRAVAL. This commitment includes participation in test cases addressing technical issues that may be of importance to WIPP performance assessment. The Department of Energy's commitment to this test case includes data and modeling support from Sandia National Laboratories, timely submission of data to other project teams, and possible new experiments if needed to resolve test case issues. The Department of Energy and Sandia National Laboratories are committed to a high level of interaction between test case modelers and the Sandia experimental team.

B. Experimental Location and Brief Description

The WIPP, located near Carlsbad in southeastern New Mexico, USA (Figure 1), is an underground research and development facility intended to demonstrate safe disposal of radioactive wastes in bedded salt. The WIPP is planned to be a permanent repository for low-level and transuranic wastes generated by the United States' defense programs. The WIPP is currently scheduled to open in 1991.

The WIPP is located in the Delaware Basin (Figure 2), of which the northern part is filled with 8,000 meters of sedimentary Phanerozoic rocks containing

evaporites. The nearest major aquifer is in the Capitan reef, ten miles from the WIPP. Water bearing zones within the rocks that underlie, host and overlie the WIPP repository have low permeabilities and storativities, are generally confined, and contain waters with high salinities and long residence times.

The Pecos river runs from north to south. The ground surface at the WIPP is about 150 m above the river bed and about 130 m above the flood plain. Surface runoff is to the west from areas north, south and west of the site. The WIPP repository lies 655 m below ground surface within bedded evaporites, primarily halite, of the Permian Salado Formation. (Figure 3) Groundwaters from Nash Draw, a feature caused by dissolution in the Salado Formation, drain toward the Pecos river. Overlying the Salado Formation is the Rustler Formation. The Culebra Dolomite Member of the Rustler Formation is the most transmissive water-bearing unit found at the WIPP site. It is an 8 m thick vuggy dolomite layer. Waters in the main waterbearing units over the immediate WIPP site flow to the southwest in the Magenta and to the south in the Culebra.

Sandia National Laboratories supports the Department of Energy with scientific research on issues related to performance assessment and compliance with US Environmental Protection Agency standards. Many technical issues are important to the WIPP's performance. Geologic, hydrologic, geochemical and isotope data have been obtained to resolve several issues concerning the hydrology of the Culebra dolomite. A central issue involves the travel time within the Culebra from a location above the repository to the WIPP site boundary. All or some of these issues could provide the basis for this test case.

Extensive geologic investigations have taken place at the WIPP, beginning in 1975. These include detailed investigation of numerous surface features for the purpose of delineating subsurface features or irregularities that could affect flow in and around the Culebra. A transient electromagnetic survey is planned for 1991-2 in order to better delineate a hypothesized fractured region (high transmissivity zone) in the southeast corner of the site.

Sixty wells have been completed to the Culebra dolomite at 41 locations to provide information on the hydraulic properties of the Culebra (Figure 4). Transmissivity and hydraulic-head data have been used to construct and calibrate a groundwater-flow model for the Culebra. In general, the transmissivity of the Culebra increases from east to west across the WIPP site, with a total range of six orders of magnitude in the vicinity of the site. The variation in transmissivity is related to fracturing. Where present, fracturing causes the Culebra to behave as a double-porosity medium with respect to both hydraulic responses and solute transport.

Well-test data from three wells in the southeastern part of the site (DOE-1, H-3, and H-11; Figure 4) indicate the presence of a zone of relatively high transmissivity within an area of otherwise low transmissivity. Calibration of the groundwater-flow model has indicated that this high-transmissivity zone is a linear "channel" feature extending from approximately the middle

of the site to an area of generally higher transmissivity south of the site (Figure 5). (The word "channel" is not intended to carry any depositional or geological connotation. It is used only to indicate that the north-south dimension of the feature is considerably greater than its east-west dimension.) All flow paths within the Culebra above the waste-storage panels appear to lead toward the high-transmissivity channel and then off site down the channel.

Two pumping tests, each of two months' duration, and two convergent-flow tracer tests have been performed in the vicinity of the channel. One pumping test and one tracer test were performed near the center of the WIPP site near what is believed to be the northwestern edge of the channel. The other pumping test and tracer test were performed in the channel near the southern WIPP site boundary. The transient water-level responses at observations wells within 6 km of the pumping wells during the long-term pumping tests provided data (Figure 6) that were used in calibration of the regional groundwater-flow model. Because the goal of this model was to define regional flow patterns, however, the model was not optimized for delineation of, and calibration within, the high-transmissivity channel. Subsequent modeling of solute transport along flow paths identified by the regional model has shown that the characteristics of the channel, specifically its exact location, width, and transmissivity, exert a controlling influence on groundwater travel time from a location above the repository to the site boundary (Figure 7).

Geochemical and isotope studies have been conducted in order to obtain additional insight into the hydrologic behavior of the Culebra. Figures 7 through 14 summarize some of those results. In general these data have been used to demonstrate that the age of the Culebra waters is of the order of 10,000 years, and that the waters originated during a known pluvial period. In addition, it has been hypothesized that the flow direction during the period of recharge to the Culebra was from the northwest, as shown in Figure 13, and not from the north as is the current flow direction.

C. Original Purpose of the Performed Experiments

The hydraulic tests were originally performed to provide transmissivity data to be used in developing a regional groundwater-flow model. The transient water-level responses to the large-scale pumping tests were subsequently used directly in model calibration. The convergent-flow tracer tests were intended to provide information on some of the double-porosity properties of the Culebra controlling solute transport, specifically matrix-block size and fracture porosity.

The regional groundwater-flow model was intended to provide the basis for performance-assessment calculations involving flow through the Culebra. The regional flow model would be used to define flow lines for one-dimensional transport calculations.

D. Objectives of the Test Case in INTRAVAL Phase II

The data base available for this test case is very large. In order not to present an overwhelming problem to the Project Teams a number of different objectives can be identified which use only a portion of the data base or resolve only portions of larger issues. Therefore the test case may have any number of objectives. One possible objective could be to determine if the hydrologic data support the derived transmissivity distribution and/or the model boundary conditions. Related to this objective could be an evaluation of the uniqueness of the derived transmissivity distribution. A third related objective could be to determine the uncertainty in the transmissivity distribution.

Another important objective could to determine the resolution in transmissivity needed for long time (10,000 years) predictions of radionuclide travel time. Related to this objective could be an evaluation of the uncertainty in predictions of radionuclide travel time. Other objectives could be to determine if the paleoflow directions inferred from the geochemical/isotopic data could be reproduced using the current transmissivity distribution and boundary conditions altered to simulate increased rainfall; to determine if halite gypsum dissolution will take place in the next 10,000 years in the Culebra, resulting in an alteration in the transmissivity distribution; to determine if the hydrologic evidence is sufficient to rule out a significant effect on transport of karst features.

A staged approach to this test case is anticipated. An example would be to begin with the first objective mentioned. The first step might be to use the large-scale pumping test data to refine the model calibration in the area of the high-transmissivity channel. This problem could be approached by defining a subdomain within the regional model as a local-scale model centered on the high-transmissivity channel. The calibrated regional model would provide the boundary conditions for the local-scale model. A new model grid could then be defined for the local-scale model that will allow more sensitive calibration to the large-scale pumping tests.

The second objective mentioned would require determination of the sensitivity of this calibration to the characteristics of the high-transmissivity channel. Are the existing data adequate to define or bound the characteristics of the high-transmissivity channel, or can a number of different conceptualizations of the channel, with different transport properties, allow equally good calibration to the data? As part of this sensitivity evaluation, the calibrated model(s) could be used to simulate the transport of a conservative (non-sorbing) solute from a point source above the repository to the channel, and through the channel to the site boundary. Variations in the treatment of lateral dispersion within the channel are of particular interest.

If the existing data allow alternative calibrations with significantly different travel times, the next step is to identify the data that would be required to reduce the number of alternatives. These data may represent single-well hydraulic tests performed at specific new locations to help

constrain the transmissivity distribution, additional tracer tests, and/or an additional large-scale pumping test performed at a specific location with additional observation wells at other specific locations. Before an additional large-scale pumping test would be performed, the test would be simulated using all alternative calibrated models. Performance of the test should then serve to validate one of the models.

This test case is expected to have a three-year duration. During the first year, project teams would review the existing data and make recommendations for additional data-collection and/or testing activities. During the second and perhaps third year, additional data would be collected and transmitted to the project teams. Final analyses and reporting would be performed during the third year.

E. Validation Aspects

This test case deals with the validation of groundwater flow and transport models of a heterogeneous system. Given that testing can rarely be performed on the same spatial and temporal scales over which behavior is to be predicted, how can we gain confidence that the testing we can perform has given us all the information we need about a system? With respect to validation of a groundwater-flow model, our working hypothesis is that the necessary hydraulic characterization can be achieved by conducting large-scale tests with overlapping spheres of influence that together cover the entire region of interest. Each individual test should involve an area containing as much heterogeneity as possible. In addition to validation of our working hypothesis, other questions that might be answered include: How can the locations for the large-scale tests be optimized? What information (e.g., combination of tests) can rule out the possibility of significant features being missed?

With respect to validation of a transport model, our initial approach is to assume that the same properties and processes governing solute transport on a 20- to 40-m scale under high-induced-gradient conditions will also apply on a scale of several kilometers under natural-gradient conditions. Possible complicating factors include: natural variations in transmissivity, fracture spacing, and/or fracture orientation within the high-transmissivity channel; uncertainty in the position and width of the high-transmissivity channel; uncertainty in the amount of mixing occurring between natural groundwater and the contaminant plume; and uncertain and possibly nonconstant longitudinal and transverse dispersivities.

When the 10,000-yr period of regulatory concern is taken into account, uncertainty is added with respect to the boundary conditions for both the groundwater-flow and transport models. Thus, validation of these models must address potential changes in boundary conditions.

F. Data Available

- o UTM coordinates and surveyed elevations for all wells
- o core logs and/or geophysical logs from all well locations
- o geochemical and isotope data (major ion concentrations, density, etc.) from all well locations
- o raw and interpreted hydraulic-test data from all well locations
- o raw and interpreted tracer-test data
- o core porosity and permeability data from tracer-test and other locations
- o water-level data (hydrographs) from time of well construction to present for all wells
- o estimated steady-state hydraulic heads at all well locations
- o calibrated steady-state regional groundwater-flow model
- o calibrated transient regional groundwater-flow model

G. Partial List of Reference Documents Available

Avis, J.A., and Saulnier, G.J., Jr. 1990. Analysis of the Fluid-Pressure Responses of the Rustler Formation at H-16 to the Construction of the Air-Intake Shaft at the Waste Isolation Pilot Plant (WIPP) Site. Contractor Report SAND89-7067 (Albuquerque, NM: Sandia National Laboratories).

Barr, G.E.; Miller, W.B.; and Gonzalez, D.D. 1983. Interim Report on the Modeling of the Regional Hydraulics of the Rustler Formation. Sandia Report SAND83-0391 (Albuquerque, NM: Sandia National Laboratories).

Bartel, L.C. 1989. Results from Electromagnetic Surface Surveys to Characterize the Culebra Aquifer at the WIPP Site. Sandia Report SAND87-1246 (Albuquerque, NM: Sandia National Laboratories).

Beauheim, R.L. 1986. Hydraulic-Test Interpretations for Well DOE-2 at the Waste Isolation Pilot Plant (WIPP) Site. Sandia Report SAND86-1364 (Albuquerque, NM: Sandia National Laboratories).

Beauheim, R.L. 1987a. Interpretations of Single-Well Hydraulic Tests Conducted At and Near the Waste Isolation Pilot Plant (WIPP) Site, 1983-1987. Sandia Report SAND87-0039 (Albuquerque, NM: Sandia National Laboratories).

Beauheim, R.L. 1987b. Analysis of Pumping Tests of the Culebra Dolomite Conducted at the H-3 Hydropad at the Waste Isolation Pilot Plant (WIPP) Site. Sandia Report SAND86-2311 (Albuquerque, NM: Sandia National Laboratories).

Beauheim, R.L. 1987c. Interpretation of the WIPP-13 Multipad Pumping Test of the Culebra Dolomite at the Waste Isolation Pilot Plant (WIPP) Site. Sandia Report SAND87-2456 (Albuquerque, NM: Sandia National Laboratories).

Beauheim, R.L. 1989. Interpretation of H-11b4 Hydraulic Tests and the H-11 Multipad Pumping Test of the Culebra Dolomite at the Waste Isolation Pilot Plant (WIPP) Site. Sandia Report SAND89-0536 (Albuquerque, NM: Sandia National Laboratories). Cauffman, T.L.; LaVenue, A.M; and McCord, J.P. 1990. Ground-Water Flow Modeling of the Culebra Dolomite: Volume II - Data Base. Contractor Report SAND89-7068/2 (Albuquerque, NM: Sandia National Laboratories).

Cooper, J.B., and Glanzman, V.M. 1971. Geohydrology of Project Gnome Site, Eddy County, New Mexico. USGS Professional Paper 712-A (Washington, D.C.), 24 pp.

Crawley, M.E. 1988. Hydrostatic Pressure and Fluid Density Distribution of the Culebra Dolomite Member of the Rustler Formation Near the Waste Isolation Pilot Plant, Southeastern N.M. DOE/WIPP 88-030 (Carlsbad, NM: US DOE).

Davies, P.B. 1989. Variable-Density Ground-Water Flow and Paleohydrology in the Region Surrounding the Waste Isolation Pilot Plant (WIPP), Southeastern New Mexico. USGS Open-File Rpt 88-490 (Albuquerque, NM).

Dennehy, K.F. 1982. Results of Hydrologic Tests and Water-Chemistry Analyses, Wells H-6A, H-6B, and H-6C, at the Proposed Waste Isolation Pilot Plant Site, Southeastern New Mexico. USGS Water-Resources Investigations 82-8 (Albuquerque, NM), 68 pp.

Dennehy, K.F., and Mercer, J.W. 1982. Results of Hydrologic Tests and Water-Chemistry Analyses, Wells H-5A, H-5B, and H-5C, at the Proposed Waste Isolation Pilot Plant Site, Southeastern New Mexico. USGS Water-Resources Investigations 82-19 (Albuquerque, NM), 83 pp.

Drellack, S.L., Jr., and J.G. Wells. 1982a. Geologic and Well-Construction Data for the H-7 Borehole Complex Near the Proposed Waste Isolation Pilot Plant Site, Southeastern New Mexico. USGS Water-Resources Investigations 82-38 (Albuquerque, NM).

Drellack, S.L., Jr., and J.G. Wells. 1982b. Geologic and Well-Construction Data for the H-9 Borehole Complex Near the Proposed Waste Isolation Pilot Plant Site, Southeastern New Mexico. USGS Water-Resources Investigations 82-4111 (Albuquerque, NM).

Gonzales, M.M. 1989. Compilation and Comparison of Test-Hole Location Surveys in the Vicinity of the Waste Isolation Pilot Plant Site. Sandia Report SAND88-1065 (Albuquerque, NM: Sandia National Laboratories).

Haug, A.; Kelley, V.A.; LaVenue, A.M.; and Pickens, J.F. 1987. Modeling of Ground-Water Flow in the Culebra Dolomite at the Waste Isolation Pilot Plant (WIPP) Site: Interim Report. Contractor Report SAND86-7167 (Albuquerque, NM: Sandia National Laboratories).

Holt, R.M., and Powers, D.W. 1988. Facies Variability and Post-Depositional Alteration Within the Rustler Formation in the Vicinity of the Waste Isolation Pilot Plant, Southeastern New Mexico. DOE/WIPP-88-004 (Carlsbad, NM: US DOE).

Hydro Geo Chem, Inc. 1985. WIPP Hydrology Program, Waste Isolation Pilot Plant, SENM, Hydrologic Data Report #1. Contractor Report SAND85-7206 (Albuquerque, NM: Sandia National Laboratories).

Hydro Geo Chem, Inc. 1986. Two-Well Recirculation Tracer Tests at the H-2 Hydropad, Waste Isolation Pilot Plant (WIPP), Southeastern New Mexico. Contractor Report SAND86-7092 (Albuquerque, NM: Sandia National Laboratories).

INTERA Technologies, Inc. 1986. WIPP Hydrology Program, Waste Isolation Pilot Plant, Southeastern New Mexico, Hydrologic Data Report #3. Contractor Report SAND86-7109 (Albuquerque, NM: Sandia National Laboratories).

INTERA Technologies, Inc., and Hydro Geo Chem, Inc. 1985. WIPP Hydrology Program, Waste Isolation Pilot Plant, Southeastern New Mexico, Hydrologic Data Report =2. Contractor Report SAND85-7263 (Albuquerque, NM: Sandia National Laboratories).

Jones, C.L. 1973. Salt Deposits of Los Medanos Area, Eddy and Lea Counties, New Mexico, with sections on Ground Water Hydrology by M.E. Cooley and Surficial Geology by G.O. Bachman. USGS Open-File Rpt USGS-4339-7, 67 pp.

Kelley, V.A., and Pickens, J.F. 1986. Interpretation of the Convergent-Flow Tracer Tests Conducted in the Culebra Dolomite at the H-3 and H-4 Hydropads at the Waste Isolation Pilot Plant (WIPP) Site. Contractor Report SAND86-7161 (Albuquerque, NM: Sandia National Laboratories).

Kelley, V.A., and Saulnier, G.J., Jr. 1990. Core Analyses for Selected Samples from the Culebra Dolomite at the Waste Isolation Pilot Plant Site. Contractor Report SAND90-7011 (Albuquerque, NM: Sandia National Laboratories).

Lambert, S.J. 1987. Feasibility Study: Applicability of Geochronologic Methods Involving Radiocarbon and Other Nuclides to the Groundwater Hydrology of the Rustler Formation, Southeastern New Mexico. Sandia Report SAND86-1054 (Albuquerque, NM: Sandia National Laboratories).

Lambert, S.J., and Carter, J.A. 1987. Uranium-Isotope Systematics in Groundwaters of the Rustler Formation, Northern Delaware Basin, Southeastern New Mexico, I: Principles and Preliminary Results. Sandia Report SAND87-0388 (Albuquerque, NM: Sandia National Laboratories).

Lambert, S.J., and Harvey, D.M. 1987. Stable-Isotope Geochemistry of Groundwaters in the Delaware Basin of Southeastern New Mexico. Sandia Report SAND87-0138 (Albuquerque, NM: Sandia National Laboratories).

Lambert, S.J., and Robinson, K.L. 1984. Field Geochemical Studies of Groundwaters in Nash Draw, Southeastern New Mexico. Sandia Report SAND83-1122 (Albuquerque, NM: Sandia National Laboratories).

LaVenue, A.M.; Cauffman, T.L.; and Pickens, J.F. 1990. Ground-Water Flow Modeling of the Culebra Dolomite: Volume I - Model Calibration. Contractor Report SAND89-7068/1 (Albuquerque, NM: Sandia National Laboratories).

LaVenue, A.M.; Haug, A.; and Kelley, V.A. 1988. Numerical Simulation of Ground-Water Flow in the Culebra Dolomite at the Waste Isolation Pilot Plant (WIPP) Site: Second Interim Report. Contractor Report SAND88-7002 (Albuquerque, NM: Sandia National Laboratories).

Lowenstein, T.K. 1987. Post Burial Alteration of the Permian Rustler Formation Evaporites, WIPP Site, New Mexico: Textural, Stratigraphic and Chemical Evidence, EEG-36 (Santa Fe, NM: New Mexico Environmental Evaluation Group), 54 pp.

Lyon, M.L. 1989. Annual Water Quality Data Report for the Waste Isolation Pilot Plant, April 1989. DOE/WIPP 89-001 (Carlsbad, NM: US DOE).

Mercer, J.W. 1983. Geohydrology of the Proposed Waste Isolation Pilot Plant Site, Los Medanos Area, Southeastern New Mexico. USGS Water-Resources Investigations Rpt 83-4016 (Albuquerque, NM), 113 pp.

Mercer, J.W.; Beauheim, R.L.; Snyder, R.P.; and Fairer, G.M. 1987. Basic Data Report for Drilling and Hydrologic Testing of Drillhole DOE-2 at the Waste Isolation Pilot Plant (WIPP) Site. Sandia Report SAND86-0611 (Albuquerque, NM: Sandia National Laboratories).

Mercer, J.W.; Davis, P.; Dennehy, K.F.; and Goetz, C.L. 1981. Results of Hydrologic Tests and Water-Chemistry Analyses, Wells H-4A, H-4B, and H-4C at the Proposed Waste Isolation Pilot Plant Site, Southeastern New Mexico. USGS Water-Resources Investigations 81-36 (Albuquerque, NM), 92 pp.

Mercer, J.W., and Orr, B.R. 1979. Interim Data Report on the Geohydrology of the Proposed Waste Isolation Pilot Plant Site, Southeast New Mexico. USGS Water-Resources Investigations Rpt 79-98 (Albuquerque, NM), 178 pp.

Mercer, J.W., and Snyder, R.P. 1990a. Basic Data Report for Drillholes at the H-11 Complex (Waste Isolation Pilot Plant - WIPP). Sandia Report SAND89-0200 (Albuquerque, NM: Sandia National Laboratories).

Mercer, J.W., and Snyder, R.P. 1990b. Basic Data Report for Drillhole H-12 (Waste Isolation Pilot Plant - WIPP). Sandia Report SAND89-0201 (Albuquerque, NM: Sandia National Laboratories).

Mercer, J.W., and Snyder, R.P. 1990c. Basic Data Report for Drillholes H-14 and H-15 (Waste Isolation Pilot Plant - WIPP). Sandia Report SAND89-0202 (Albuquerque, NM: Sandia National Laboratories).

Mercer, J.W., and Snyder, R.P. 1990d. Basic Data Report for Drillhole H-16 Complex (Waste Isolation Pilot Plant - WIPP). Sandia Report SAND89-0203 (Albuquerque, NM: Sandia National Laboratories).

Mercer, J.W., and Snyder, R.P. 1990e. Basic Data Report for Drillholes H-17 and H-18 (Waste Isolation Pilot Plant - WIPP). Sandia Report SAND89-0204 (Albuquerque, NM: Sandia National Laboratories).

Randall, W.S.; Crawley, M.E.; and Lyon, M.L. 1988. Annual Water Quality Data Report for the Waste Isolation Pilot Plant, May 1988. DOE/WIPP-88-006 (Carlsbad, NM: US DOE).

Reeves, M.; Freeze, G.A.; Kelley, V.A.; Pickens, J.F.; and Upton, D.T. 1990. Regional Double-Porosity Solute Transport in the Culebra Dolomite under Brine-Reservoir-Breach Release Conditions: an Analysis of Parameter Sensitivity and Importance. Contractor Report SAND89-7069 (Albuquerque, NM: Sandia National Laboratories).

Reeves, M.; Kelley, V.A.; and Pickens, J.F. 1987. Regional Double-Porosity Solute Transport in the Culebra Dolomite: an Analysis of Parameter Sensitivity and Importance at the Waste Isolation Pilot Plant (WIPP) Site. Contractor Report SAND87-7105 (Albuquerque, NM: Sandia National Laboratories).

Richey, S.F. 1986. Hydrologic-Test Data from Wells at Hydrologic-Test Pads H-7, H-8, H-9, and H-10 Near the Proposed Waste Isolation Pilot Plant Site, Southeastern New Mexico. USGS Open-File Rpt 86-413 (Albuquerque, NM), 126 pp.

Richey, S.F. 1987a. Preliminary Hydrologic Data for Wells Tested in Nash Draw, Near the Proposed Waste Isolation Pilot Plant Site, Southeastern New Mexico. USGS Open-File Rpt 87-37 (Albuquerque, NM), 131 pp.

Richey, S.F. 1987b. Water-Level Data from Wells in the Vicinity of the Waste Isolation Pilot Plant, Southeastern New Mexico. USGS Open-File Rpt 87-120 (Albuquerque, NM), 107 pp.

Robinson, T.W., and Lang, W.B. 1938. Geology and Ground-Water Conditions of the Pecos River Valley in the Vicinity of Laguna Grande de la Sal, New Mexico, in 12th and 13th Biennial Reports: New Mexico State Engineer, pp. 77- 100.

Saulnier, G.J., Jr. 1987. Analysis of Pumping Tests of the Culebra Dolomite Conducted at the H-11 Hydropad at the Waste Isolation Pilot Plant (WIPP) Site. Contractor Report SAND87-7124 (Albuquerque, NM: Sandia National Laboratories).

Saulnier, G.J., Jr.; Freeze, G.A.; and Stensrud, W.A. 1987. WIPP Hydrology Program, Waste Isolation Pilot Plant, Southeastern New Mexico, Hydrologic Data Report #4. Contractor Report SAND86-7166 (Albuquerque, NM: Sandia National Laboratories).

Siegel, M.D.; Leckie, J.O.; Park, S.W.; Phillips, S.L.; and Sewards, T. 1990. Studies of Radionuclide Sorption by Clays in the Culebra Dolomite at the Waste Isolation Pilot Plant Site, Southeastern New Mexico. Sandia Report SAND89-2387 (Albuquerque, NM: Sandia National Laboratories).

Snyder, R.P. 1985. Dissolution of Halite and Gypsum, and Hydration of Anhydrite to Gypsum, Rustler Formation, in the Vicinity of the Waste Isolation Pilot Plant, Southeastern New Mexico. USGS Open-File Rpt 85-229 (Washington, DC: US GPO), 11 pp.

Stensrud, W.A.; Bame, M.A.; Lantz, K.D.; LaVenue, A.M.; Palmer, J.B.; and Saulnier, G.J., Jr. 1987. WIPP Hydrology Program, Waste Isolation Pilot Plant, Southeastern New Mexico, Hydrologic Data Report #5. Contractor Report SAND87-7125 (Albuquerque, NM: Sandia National Laboratories).

Stensrud, W.A.; Bame, M.A.; Lantz, K.D.; Cauffman, T.L.; Palmer, J.B.; and Saulnier, G.J., Jr. 1988a. WIPP Hydrology Program, Waste Isolation Pilot Plant, Southeastern New Mexico, Hydrologic Data Report #6. Contractor Report SAND87-7166 (Albuquerque, NM: Sandia National Laboratories).

Stensrud, W.A.; Bame, M.A.; Lantz, K.D.; Palmer, J.B.; and Saulnier, G.J., Jr. 1988b. WIPP Hydrology Program, Waste Isolation Pilot Plant, Southeastern New Mexico, Hydrologic Data Report #7. Contractor Report SAND88-7014 (Albuquerque, NM: Sandia National Laboratories).

Stensrud, W.A.; Bame, M.A.; Lantz, K.D.; Palmer, J.B.; and Saulnier, G.J., Jr. 1990. WIPP Hydrology Program, Waste Isolation Pilot Plant, Southeastern New Mexico, Hydrologic Data Report #8. Contractor Report SAND89-7056 (Albuquerque, NM: Sandia National Laboratories).

Stevens, K., and Beyeler, W. 1985. Determination of Diffusivities in the Rustler Formation from Exploratory-Shaft Construction at the Waste Isolation Pilot Plant in Southeastern New Mexico. USGS Water-Resources Investigations Rpt 85-4020 (Albuquerque, NM).

Uhland, D.W., and Randall, W.S. 1986. Annual Water Quality Data Report for the Waste Isolation Pilot Plant, September 1986. DOE/WIPP-86-006 (Carlsbad, NM: US DOE).

Uhland, D.W.; Randall, W.S.; and Carrasco, R.C. 1987. Annual Water Quality Data Report for the Waste Isolation Pilot Plant, March 1987. DOE/WIPP-87-006 (Carlsbad, NM: US DOE).

U.S. Geological Survey. 1962. Hydrologic and Geologic Studies for Project Gnome--Final Report. U.S. AEC Plowshare Program Rpt PNE-130F.

Wells, J.G. and S.L. Drellack, Jr. 1982. Geologic and Well-Construction Data for the H-8 Borehole Complex Near the Proposed Waste Isolation Pilot Plant Site, Southeastern New Mexico. USGS Water-Resources Investigations 82-4118 (Albuquerque, NM).

Wells, J.G. and S.L. Drellack, Jr. 1983. Geologic and Well-Construction Data for the H-10 Borehole Complex Near the Proposed Waste Isolation Pilot Plant Site, Southeastern New Mexico. USGS Water-Resources Investigations Rpt 83-4124 (Albuquerque, NM).

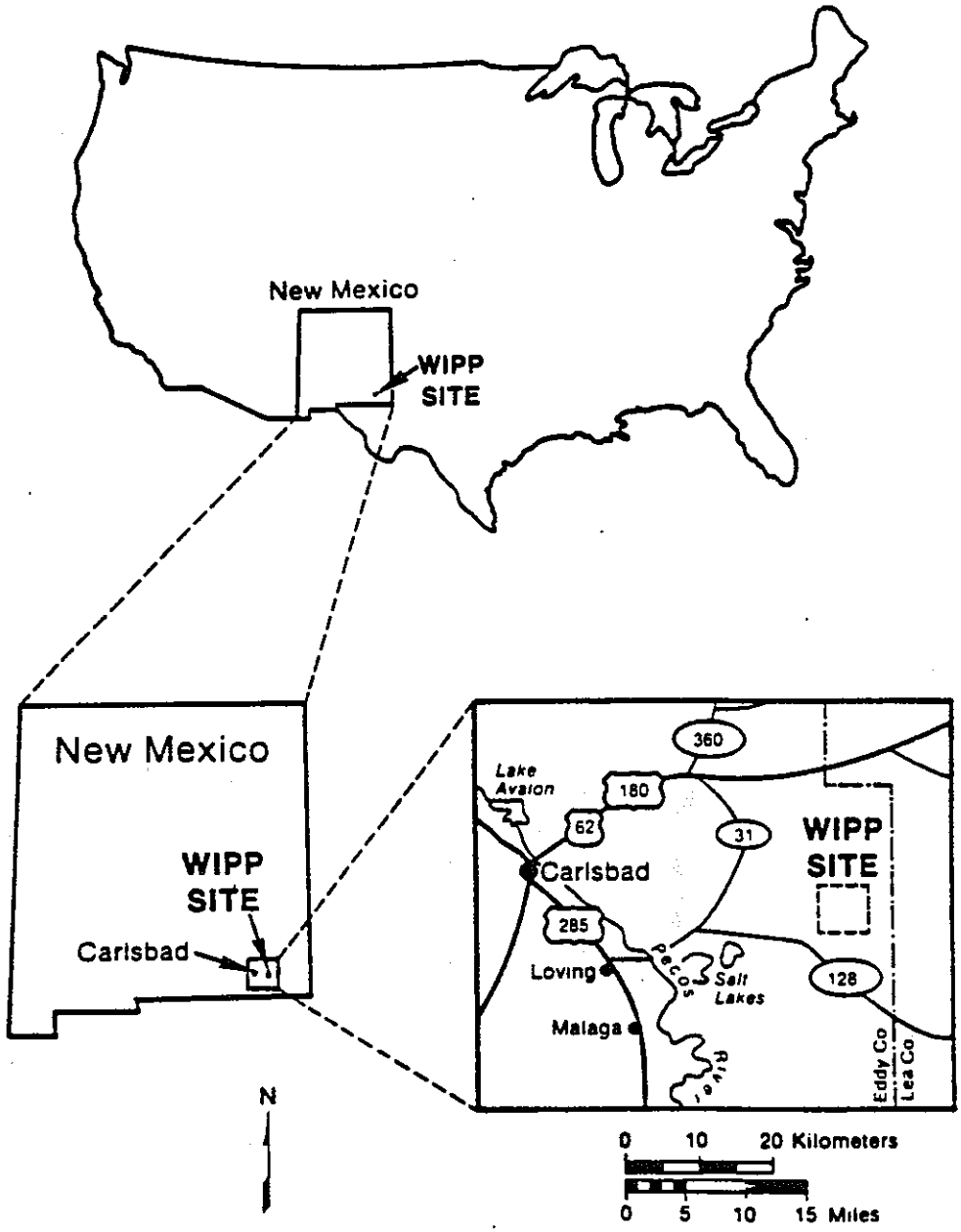


Figure 1. Location of the WIPP Site.

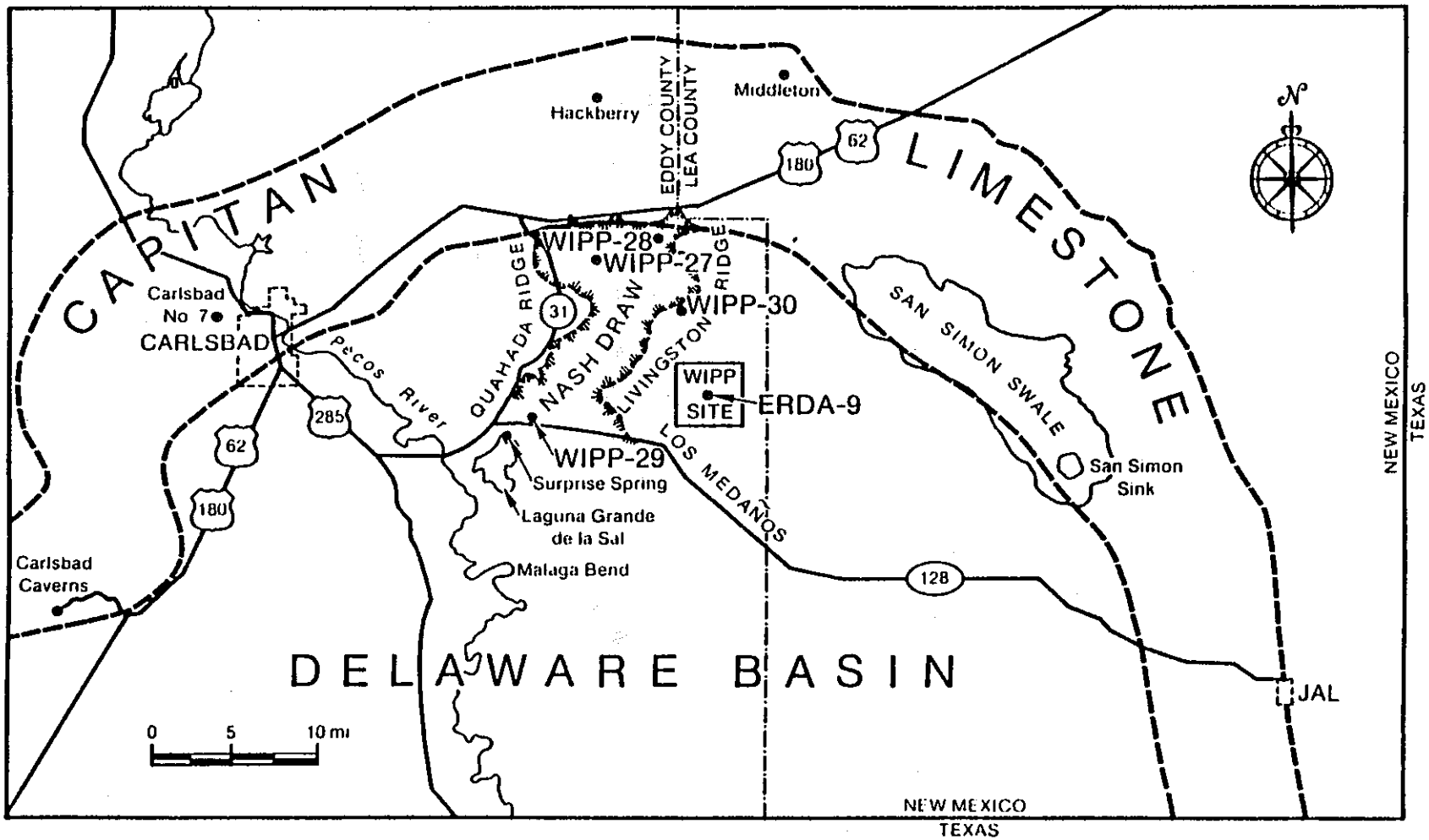


Figure 2. Local Geological Features near the WIPP Site.

SYSTEM	SERIES	GROUP	FORMATION	MEMBER
RECENT	RECENT		SURFICIAL DEPOSITS	
QUATERN-ARY	PLEISTO-CENE		MESCALERO CALICHE	
			GATUNA	
TRIASSIC		DOCKUM	UNDIVIDED	
PERMIAN	OCHOAN		DEWEY LAKE RED BEDS	
			RUSTLER	Forty-niner
				Magenta Dolomite
				Tamarisk
				Culebra Dolomite
				unnamed
			SALADO	
			CASTILE	
	GUADALUPIAN	DELAWARE MOUNTAIN	BELL CANYON	
			CHERRY CANYON	
			BRUSHY CANYON	

Figure 3. WIPP-Area Stratigraphic Column.

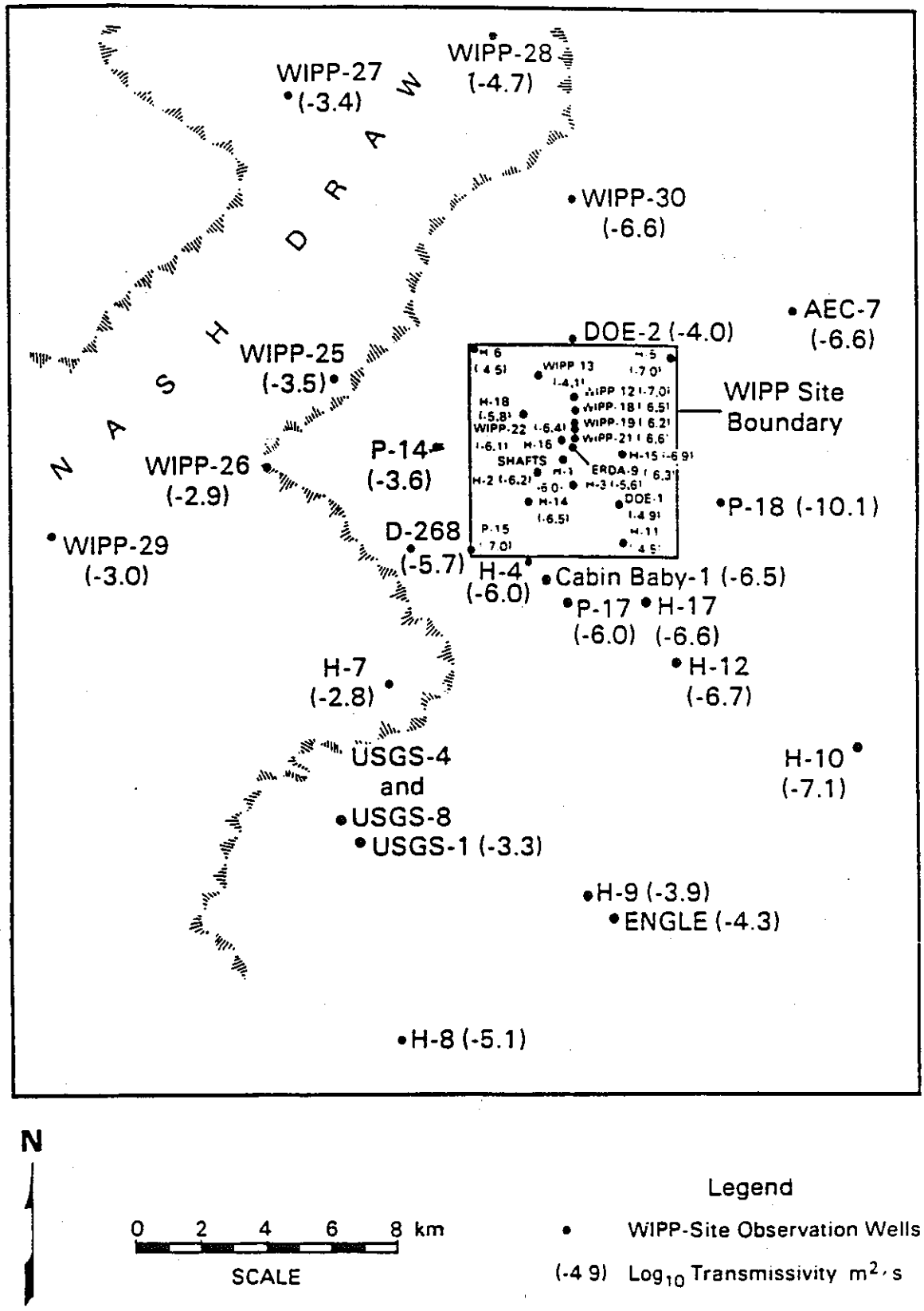


Figure 4. Culebra Wells and Measured Transmissivity Near the WIPP Site.

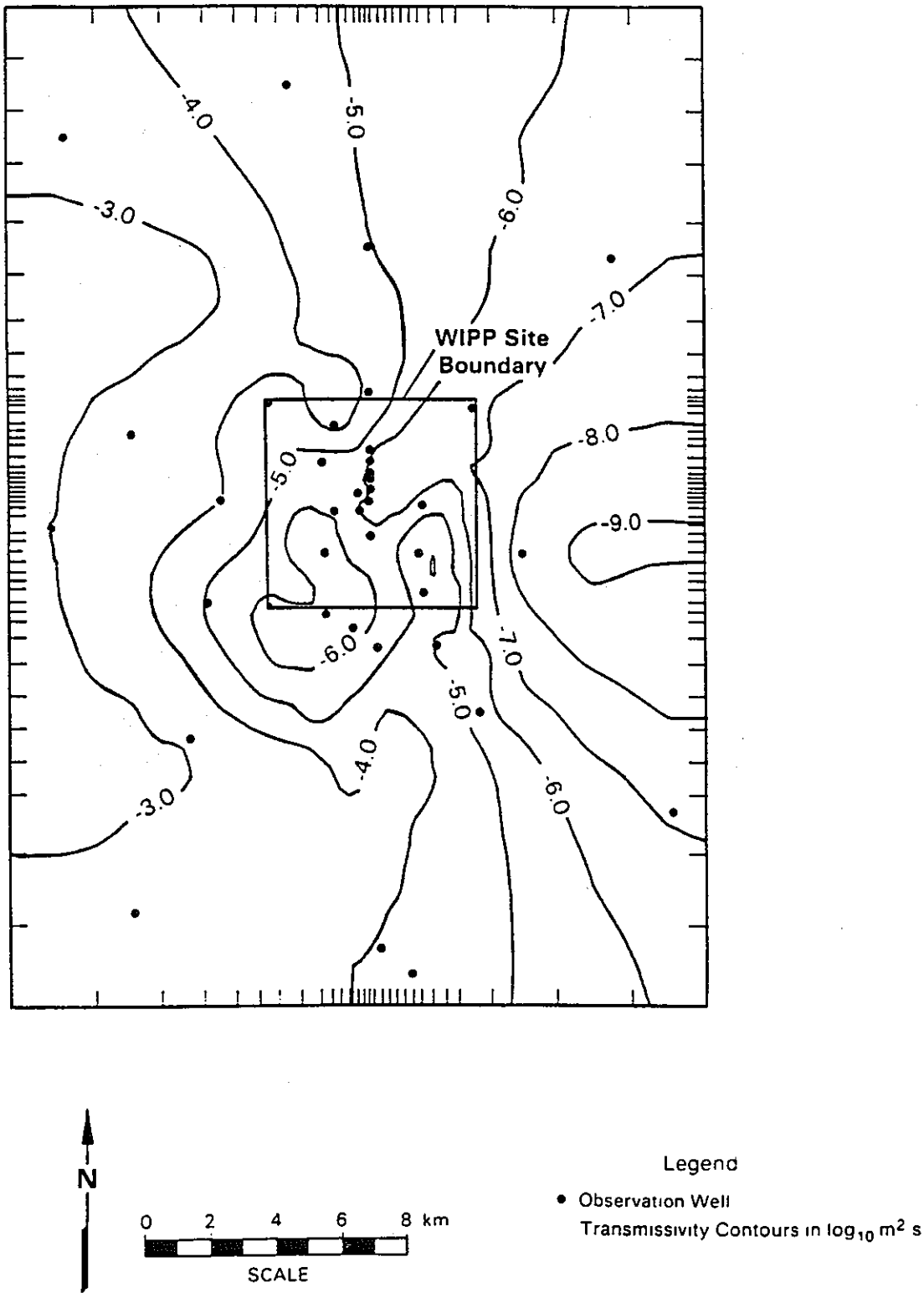


Figure 5. Transient Calibrated Transmissivity Field

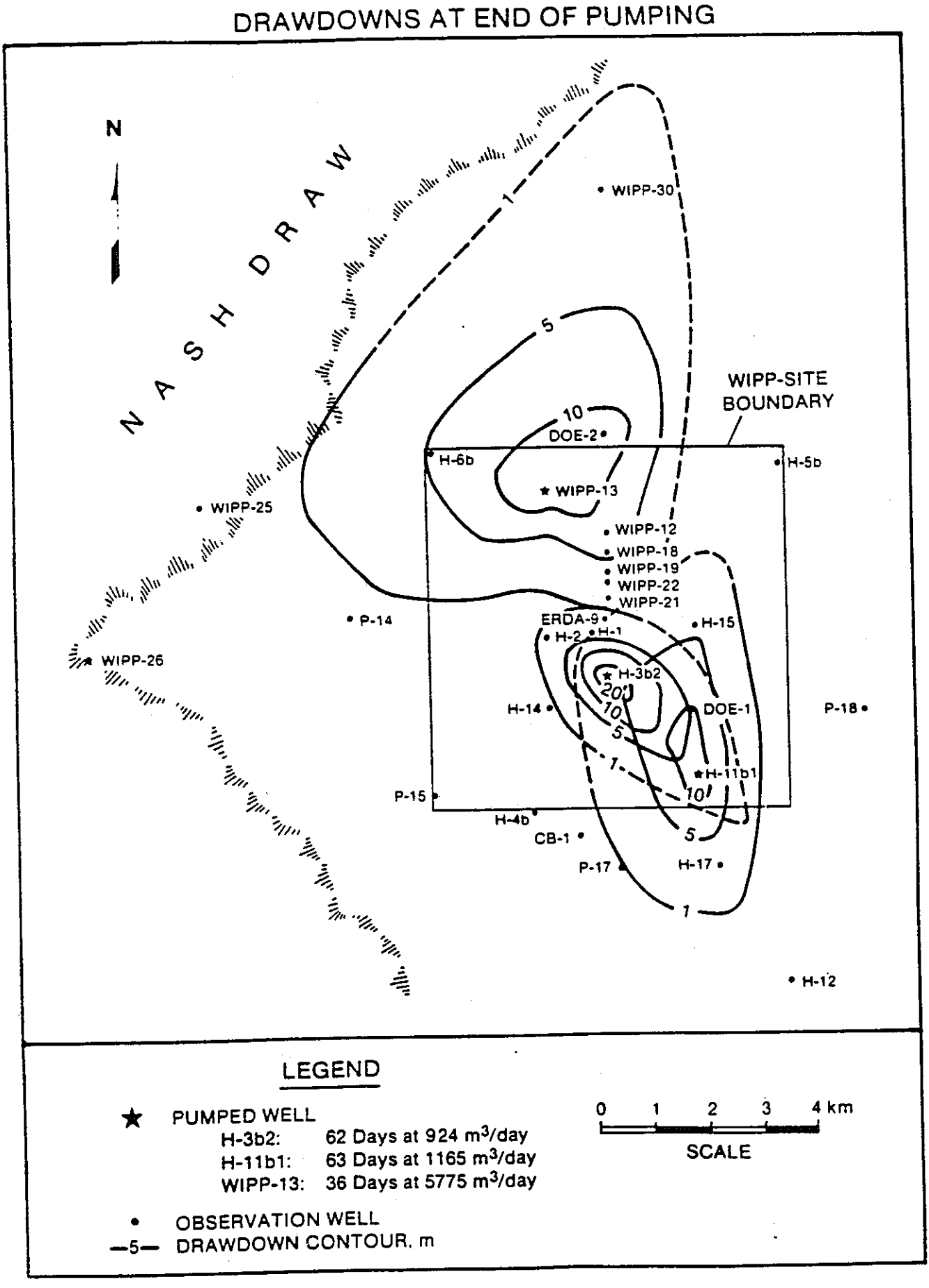


Figure 6. Drawdown Observed at the End of Long Term Pumping Tests.

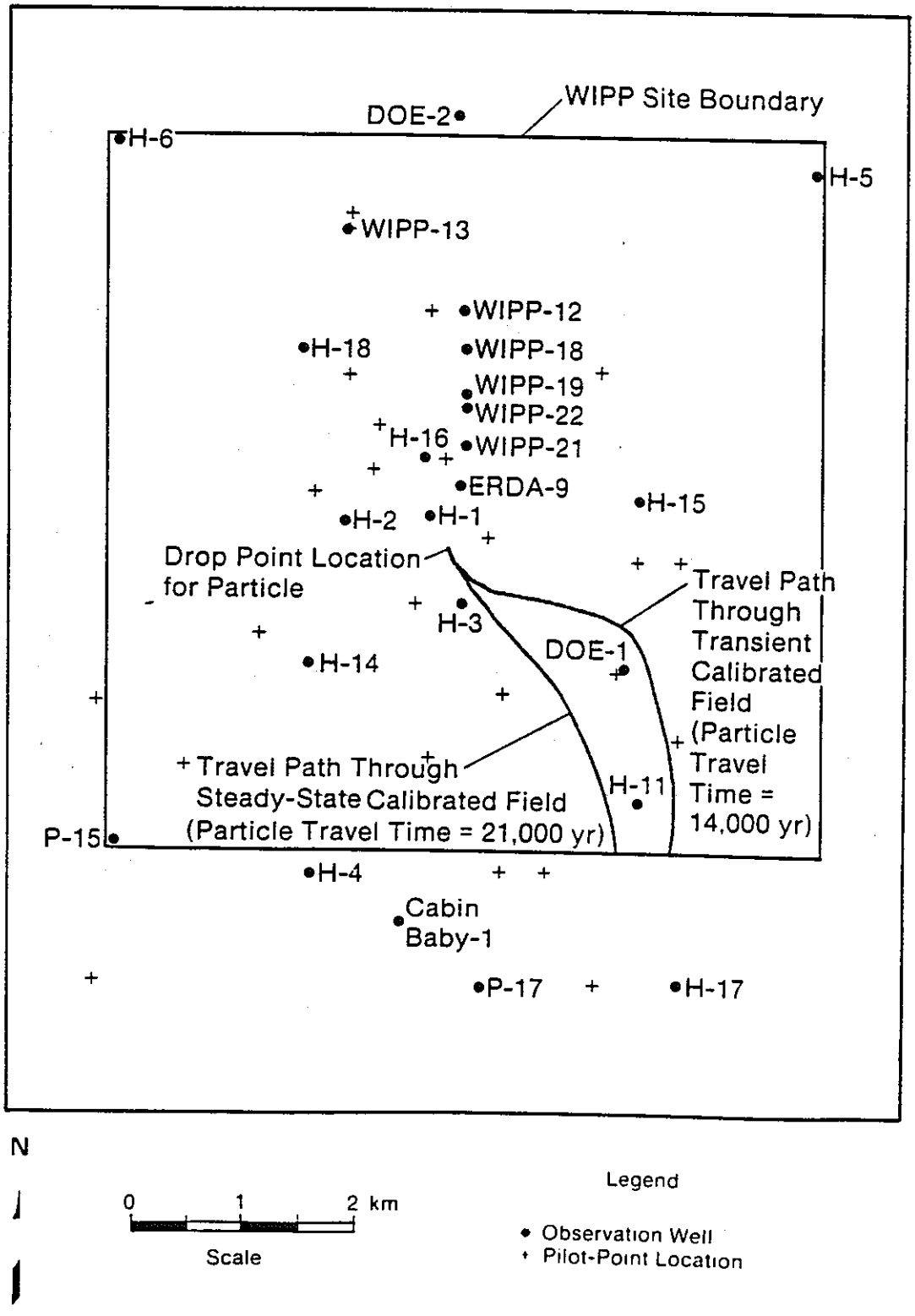


Figure 7. Changes in Flow Paths and Travel Times Between Steady State Calibrated and Transient Calibrated Transmissivity Fields.

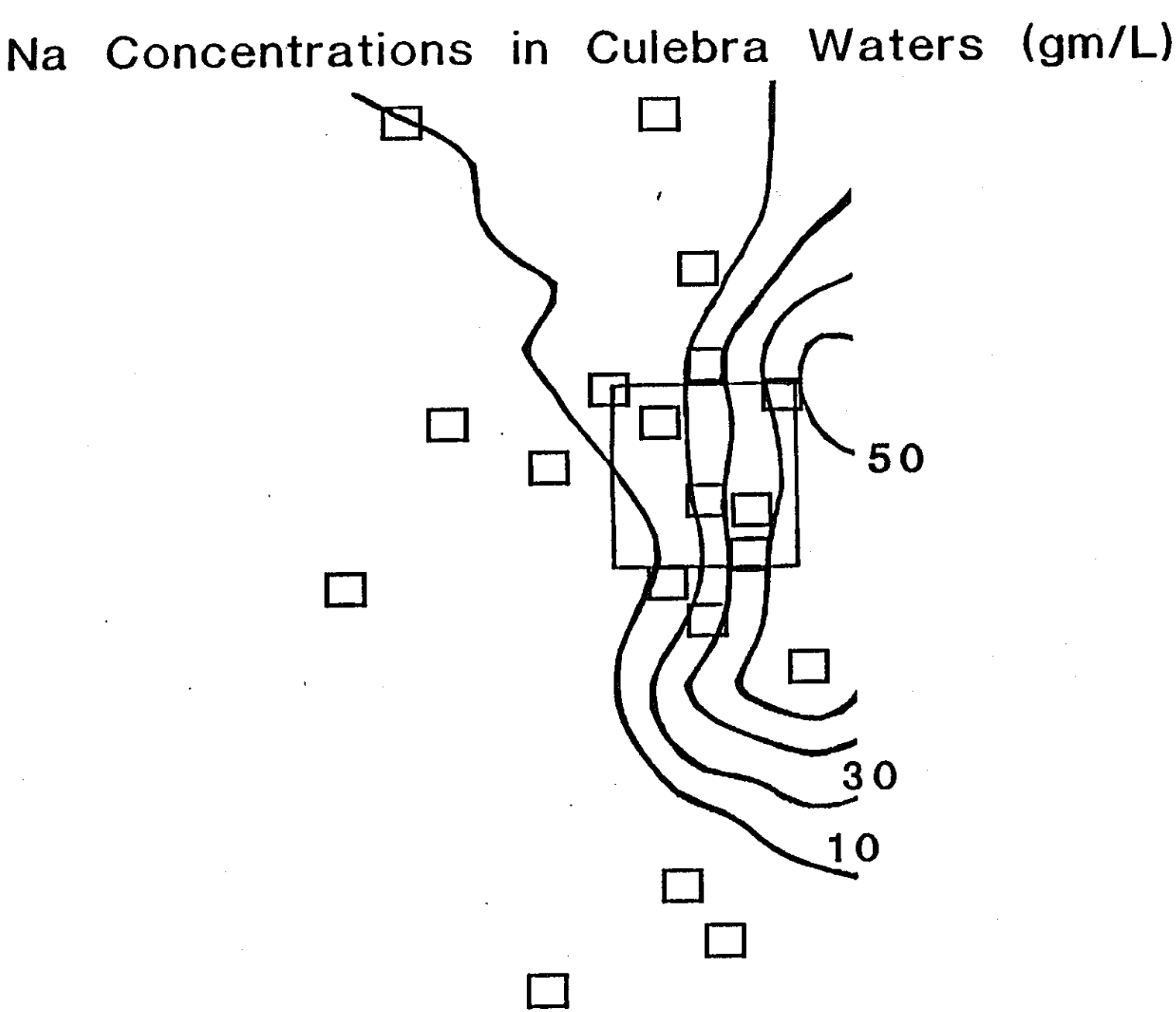


Figure 8. Concentrations of Na in Culebra Water.

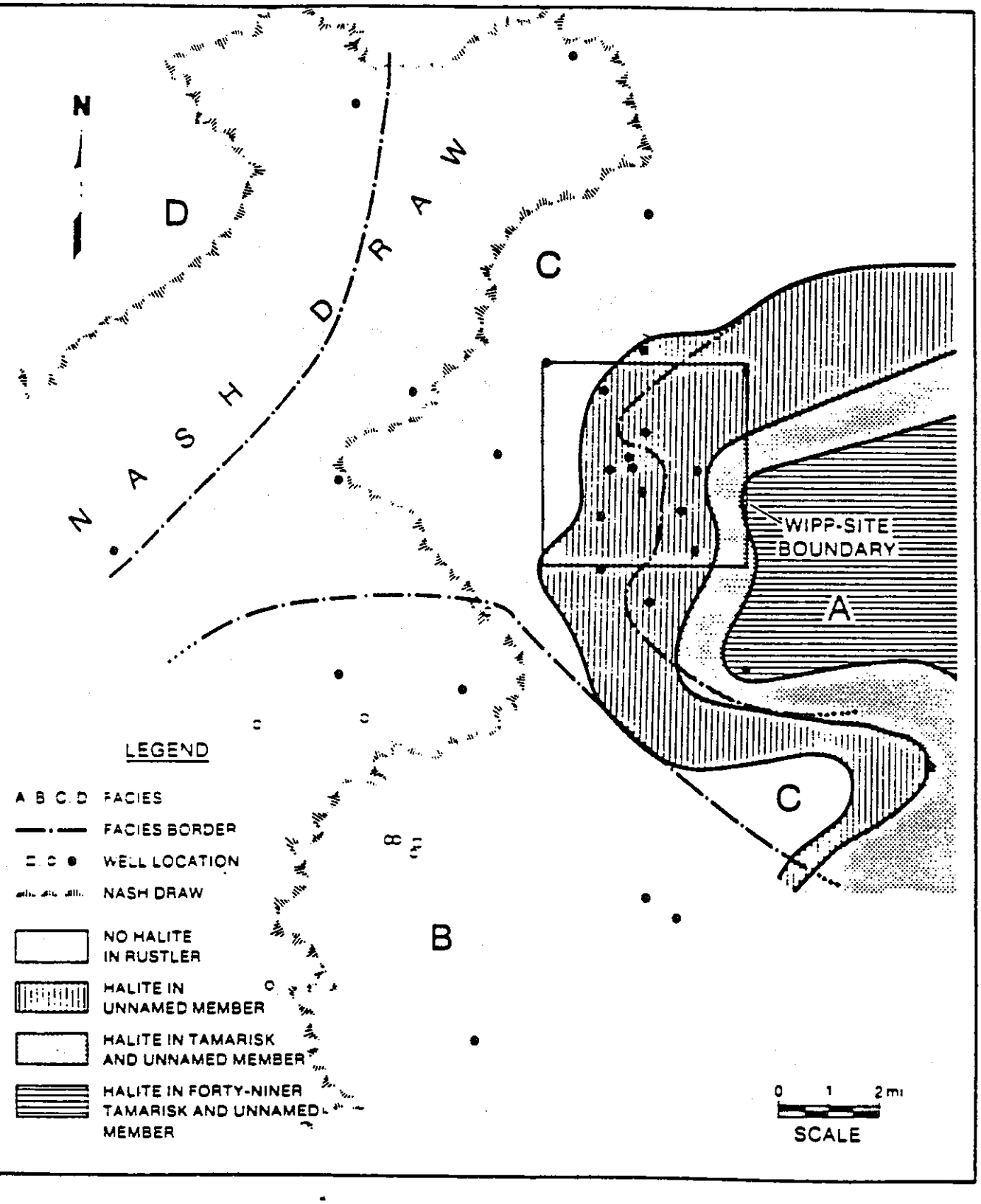


Figure 9. Regions Where Halite is Found in Water Bearing Strata.

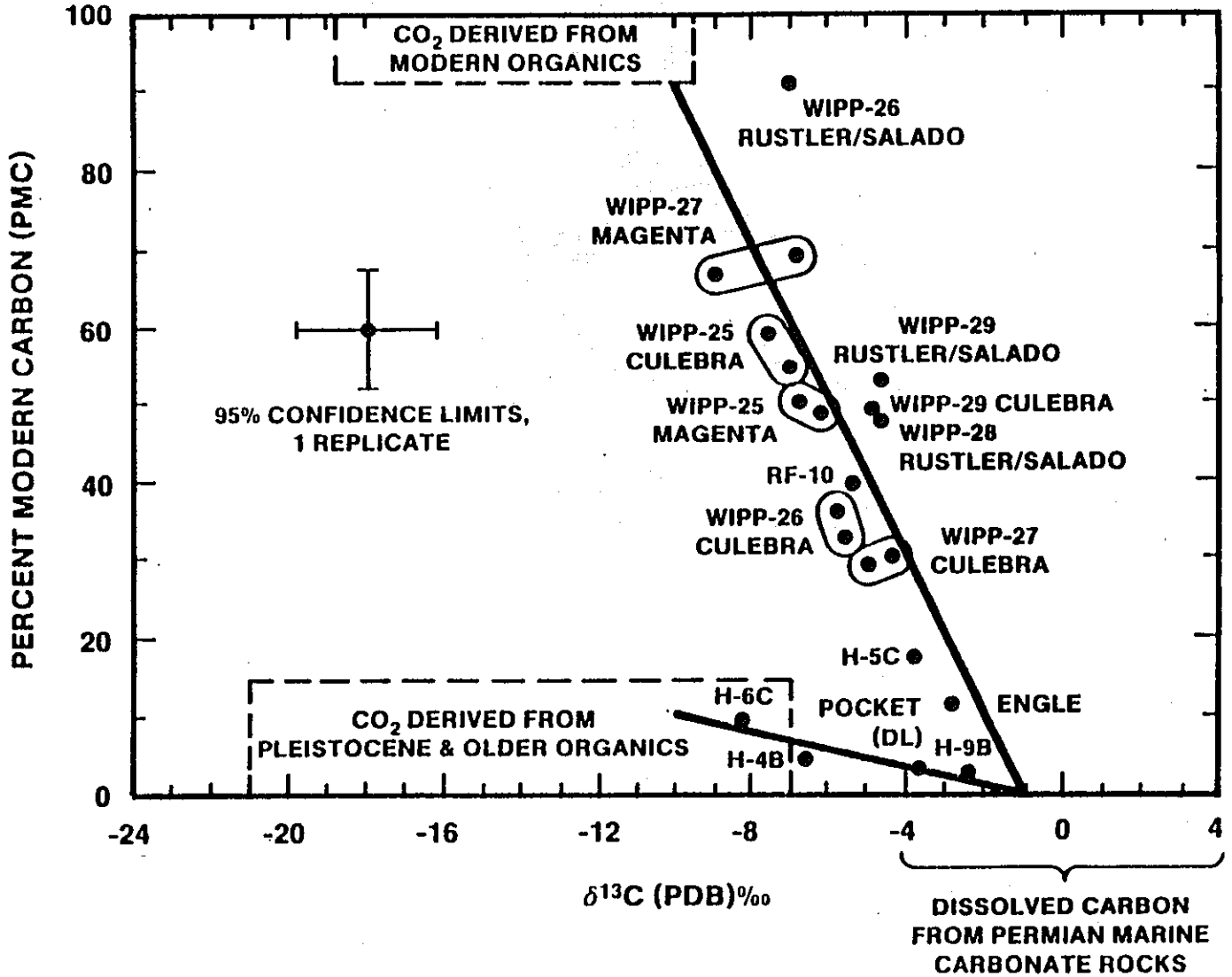
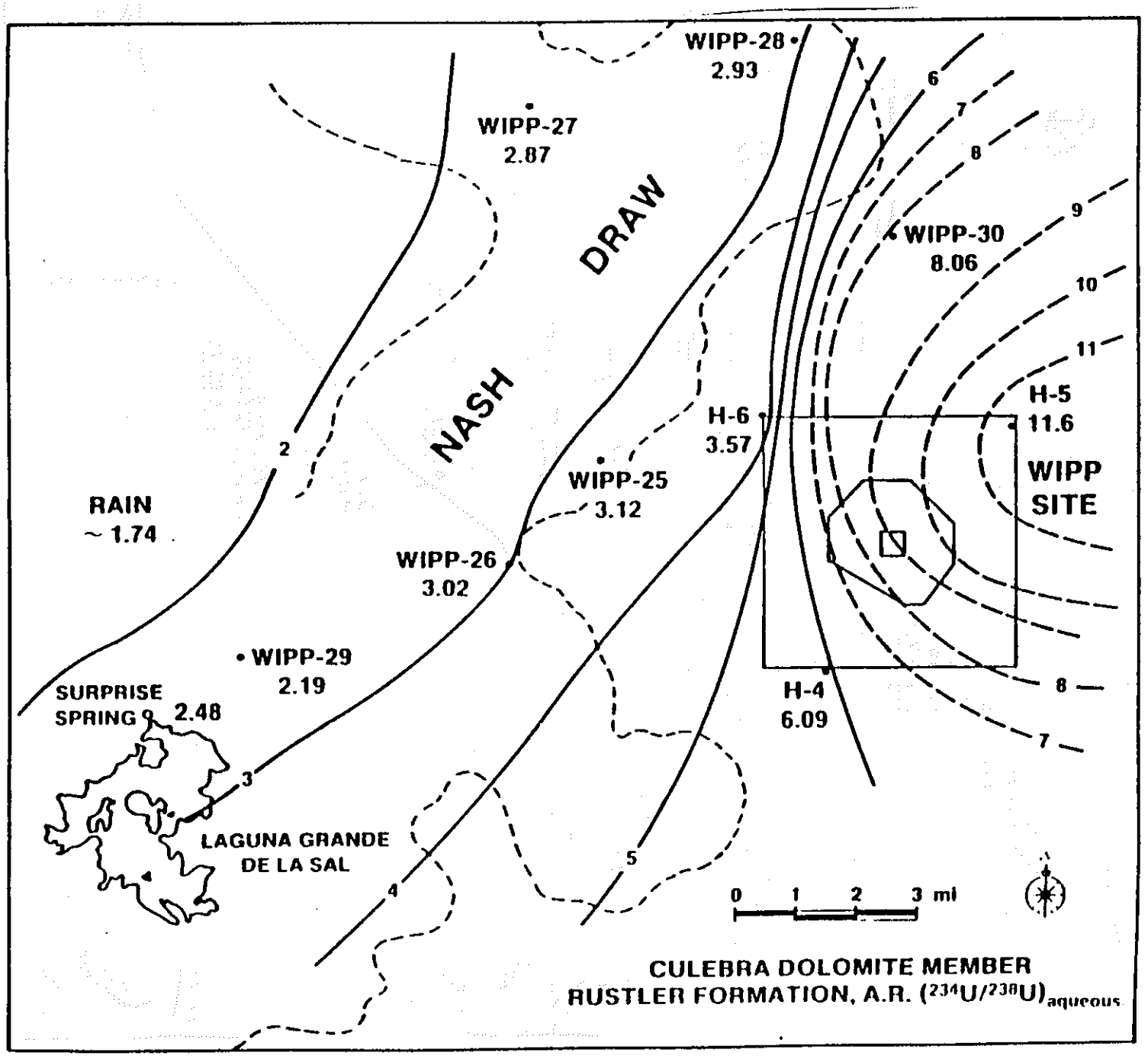


Figure 10. Percent Modern Carbon in WIPP Waters.

Figure 11. U_{234}/U_{238} Activity Ratios in Culebra Waters.



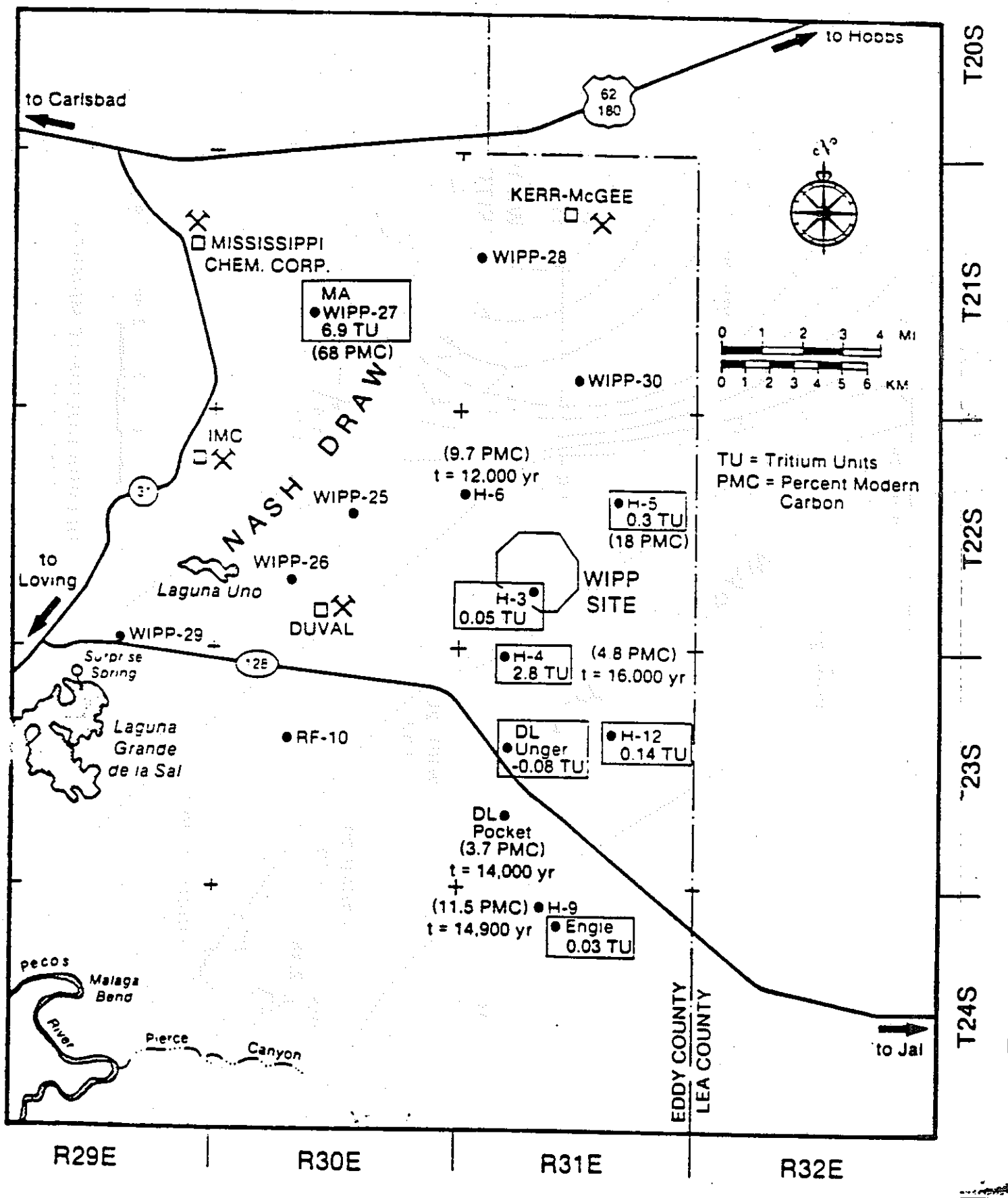


Figure 12. Summary of Carbon and Tritium Dating of Culebra Waters.

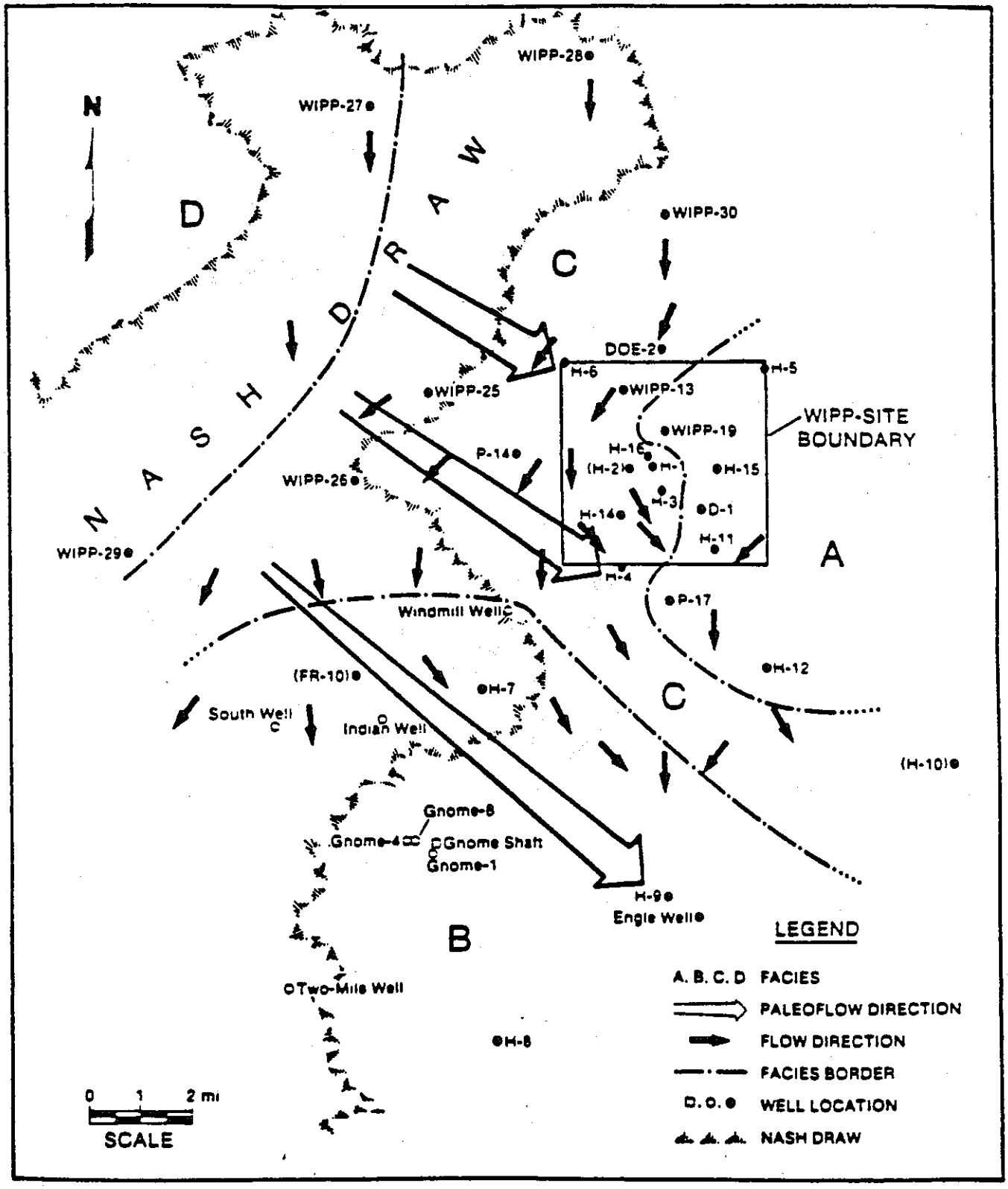


Figure 13. Current Flow Direction of Culebra Water and Inferred Paleoflow Direction of Culebra Water.

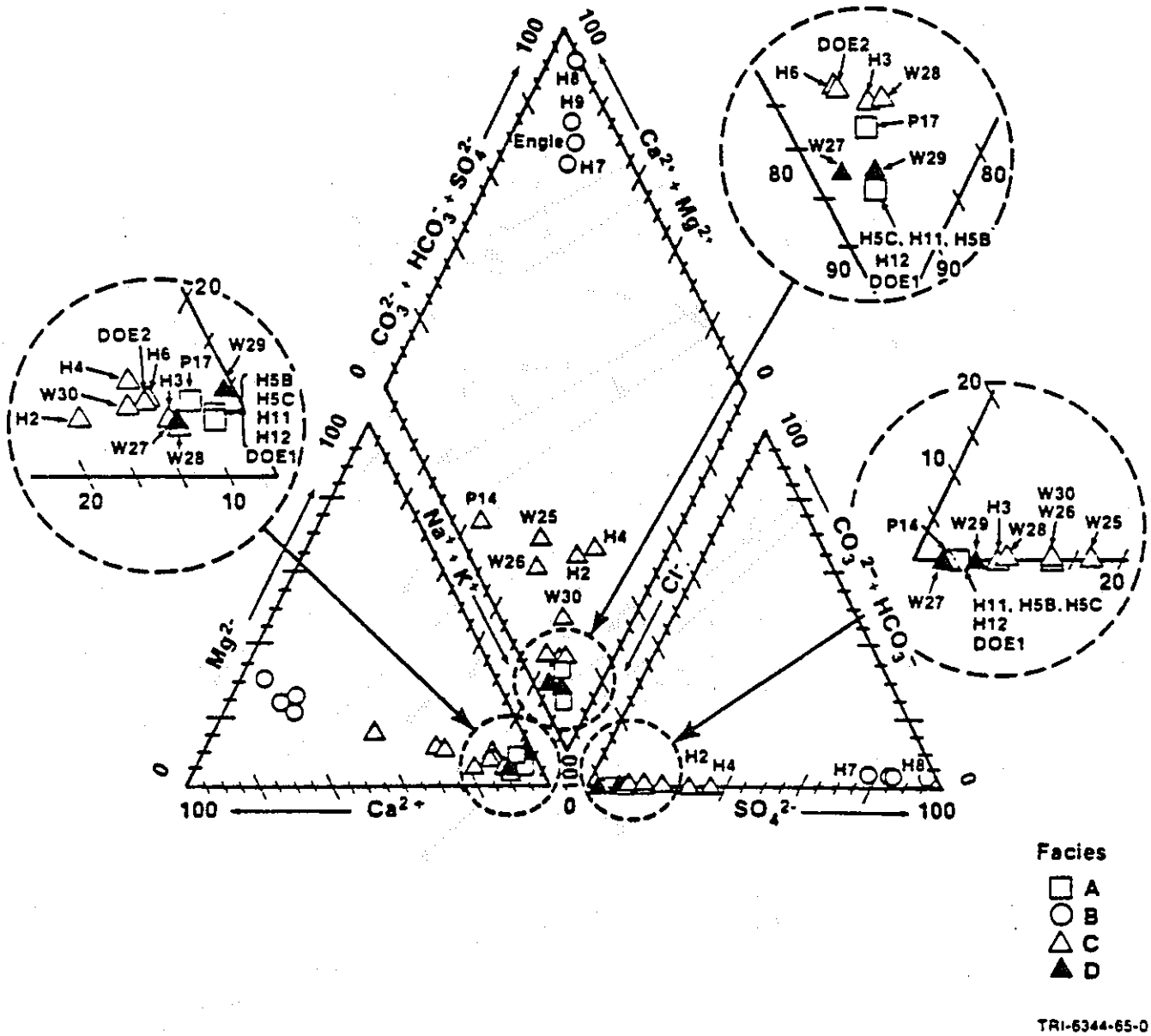


Figure 14. Definition of the Hydrochemical Facies Defined in Figure 13.

DRAFT

NSARP 55(91)R9 (IM1898-26)
Version 2

Flow Through Fractured Rock: What does the WIPP site Culebra data reveal?

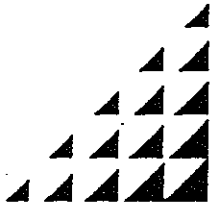
Peter Grindrod

Philip Capon

April 1991

This document is an informal note intended to promote the efficient exchange of information. It should not be used for any other purposes.

Intera Sciences
Chiltern House, 45 Station Road, Henley-on-Thames, Oxfordshire RG9 1AT, UK
Tel (0491) 410474 Fax (0491) 576916



INTERA

Contents

1 Introduction 1

2 The Conceptual Model 3

3 WIPP II: Preliminary Results 4

4 Mathematical Methods 10

5 Conclusions 11

Acknowledgement 12

References 12

1 Introduction

Given a limited set of field data points, conceptual models must be developed in order to interpolate the observed variable, filling-in realistic detail.

What does the field data tell us about spatial variability on scales from the inter-well distances downwards?

How can the transition from field data to a realistic full flow and tracer model simulation be facilitated?

What is the level of conceptual uncertainty, and what alternative methodologies are available to simulate parameter fields (permeabilities, porosities) which are sufficiently realistic to yield highly heterogeneous breakthrough and channelled flow?

Within Phase II of INTRAVAL, the UK Nirex Project Team are focusing their efforts upon such *inverse* problems, and the Wipp II Test Case in particular. The objective of the team is to develop and assess methodologies based on a variety of fundamental concepts, including conditional simulations based on kriging, for which there are a variety of codes available.

The data set available for the Culebra dolomite provides an opportunity to develop and validate new conceptual and mathematical models, and, in this report, we shall make use of the measured transmissivities in order to address the inverse problems for both flow and transport.

One of the main conclusions arising from Phase 1 of Intraval was the need to employ channelled flow conceptual models in analysing large scale flow infractured rock [4]. Discrete fracture networks, channelling models, and variable aperture fracture flow, all illustrate that dispersal and migration (even on very large scales) is fundamentally dependent upon the incorporation of small scale variability. Such detail is of course not necessarily measured in field experiments, but has a crucial *knock-on* effect, firstly in causing the flow model to become channelled, and secondly in the subsequent advection (fast channel dominated) tracer breakthrough and dispersal. This is precisely the problem which is addressed in deriving macroscopic parameters, such as dispersivities, or dispersion lengths, which are all too often found to be scale dependent (both theoretically and experimentally). Hence the current uncertainty regarding model concepts and their effect on the qualitative and quantitative migration and dispersal behaviour of tracers.

A conceptual model which starts out by asserting the existence of (non-linear) scaling effects is, therefore, potentially useful in seeking to translate the behaviour of flow and transport from the scale of the laboratory, through the scale of the field test, up to the scale of the repository. Indeed, the idea that experience (and data) gained from experiments over small spatial scales is relevant to large scale simulations is particularly important where the quantity of site data is limited.

Fractals have been used in a variety of applications in the natural sciences where scaling relationships have been found to hold for measurements made on scales differing by one or more orders of magnitude. In this report we present analysis using a conceptual rock-property model based on the **statistical self affinity of fractals**, which yields realizations of *measured* fields, conditioned by the data points. Simulated detail is generated on smaller and smaller scales by statistically scaling the spatial variability observed at the inter-well distances, down in a self consistent, nonlinear, manner [1].

The realization possesses the spatial structure inferred and extrapolated from the observed data. This approach contrasts with kriging, where a smooth surface is first fitted before a more variable field is simulated by the addition of a random components controlled by the estimated error in the initial fit. Here we proceed directly to a non-smooth realization based upon the scaling relationship observed in the spatial variability of the data.

The methodology is designed for implementation in the same spirit as discrete fracture network simulation: structure is calibrated and generated on the basis of the measured data. We anticipate channelling and non-Fickian dispersal, and an ensemble of simulations should be made for any single scenario.

The aim of this document is to demonstrate both the possibility and potential of such calculations. A full site analysis is outside of the scope of the Nirex Project team, whose objective is to consider a variety of conceptual approaches to inverse problems.

The code employed, AFFINITY [1], was developed by Intera Sciences for use on a variety of current and future national and international projects, where site data will be made available in both large and small measures.

In our example calculations for the WIPP II Test Case this results in a realized transmissivity field which has spatial variability at all scales down from that of the model region. When the derived field is sampled (producing a synthetic set of well data measurements), the observed spatial structure matches that originally obtained from the field data.

The realized transmissivity field varies over 12 orders of magnitude, and may be generated down a specified resolution.

Working on a square grid we solve the background flow problem (Darcy's Law assuming an incompressible fluid) along with a number of borehole simulations. In each case the flow is shown to be highly channelled.

We also solve subsequent tracer injection problems by tracking swarms of particles advected by the groundwater flow.

The numerical package, AFFINITY [1], solves all three problems interactively:

- the generation of a statistically self-affine transmissivity realization, interpolating well data;
- the solution of the associated flow problem;
- the solution of user-specified tracer injections/breakthrough problems.

2 The Conceptual Model

The spatial variability of a property z of a medium is represented by the behaviour of the quantity:

$$\gamma(h) = \frac{1}{2} < (z(\mathrm{x}+\mathrm{h}) - z(\mathrm{x}))^2 > .$$

where $h = |\mathrm{h}|$, and the brackets denote the *expected value* from a large number of samples at points x and $\mathrm{x}+\mathrm{h}$.

The behaviour of $\gamma(h)$ will be estimated from the data. Note that a similar estimate is made when choosing the variogram in kriging. However, in kriging, the variogram is theoretically the expected value of $(z(\mathrm{x}+\mathrm{h}) - z(\mathrm{x}))^2$, taken over all possible realizations of a random field z. In the current model z is treated simply as an unknown field, and all expected values are spatial averages over the model region.

It is assumed that the scaling rock properties may be represented by the form

$$\gamma(h) \propto h^{2H},$$

for some $H \in (0,1)$, for all h less than the measured inter-well distances; in particular as $h \to 0$. We assume that $\gamma(h) \to$ constant for large h.

A surface possessing such a scaling relationship is said to possess statistical self affinity [1], since the expected variation is nonlinearly scalable through successively smaller distances. Note that we do not require exact self affinity of the field, z, but rather that the statistical quantity γ is scalable. It turns out [1] than any field $z(x,y)$, defined on a two dimensional region, with the above scaling property holding, as $h \rightarrow 0$, defines a fractal (volume filling) surface, with dimension $3 - H$.

Using this model the site data is employed in order to obtain a fit for $\gamma(h)$, of the above form, which is subsequently used to generate a suitable realization, including spatial variability on any scale required.

In the example calculation below, the realization, $z(x,y)$, generated interpolates the observed data, possesses the desired self-affine scaling, and also matches the mean and variance of the available site observations:
$< z > \equiv \tilde{z}$ = the mean value of the well data,
$< (z - \tilde{z})^2 >$ = the variance of the well data.

This last conditions the sill ($\lim \gamma$ as $h \rightarrow \infty$). Thus both small and large scale structure is inferred from the data.

We discuss some of the technical details in section 4.

3 WIPP II: Preliminary Results

The transmissivities (precisely, the logarithmic values) from 39 of the wells within the WIPP II model region [3] were used in order to obtain the form of $\gamma(h)$, fitted in figure 1. The AFFINITY code [1] generated the realization of the transmissivity field matching this structure, interpolating all 39 measurements. A value of $H = 0.4$ was used (since the slope of the fitted curve in figure 1 is ≈ 0.8).

As a check we made 151 random samples from the realized field in order to generate a synthetic variogram, figure 2, which compares well with the original. Recall that a smooth interpolating surface will not possess such behaviour (for such a field γ behaves like h^2 as $h \rightarrow 0$).

The transmissivity field is depicted in figure 3. For the purpose of the subsequent calculations it has been generated on a 128 x 128 uniform grid over the whole model area, although further resolution could be output from the AFFINITY code.

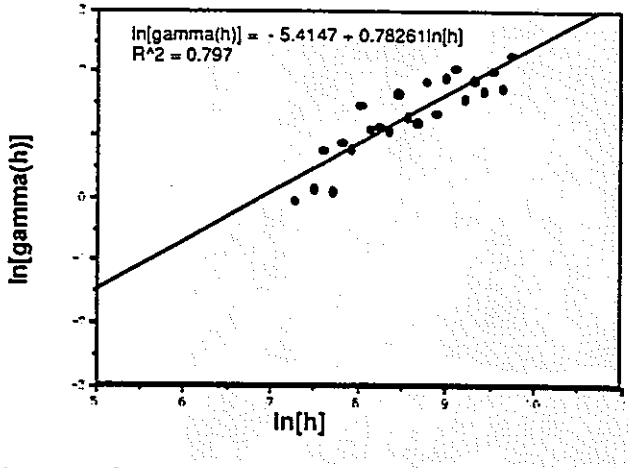


Figure 1: Variogram fitted from transmissivity data of 39 wells.

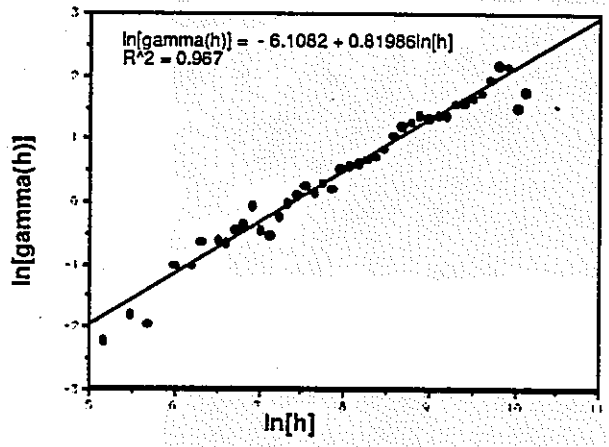


Figure 2: Synthetic variogram fitted from 151 random samples from the final realization.

In figure 4 we depict the pressure field obtained from the background flow calculation employing Darcy's Law for an incompressible fluid. In figure 5 we show the associated Darcy velocity field (coloured by modulus). Notice the highly channelled flow. Here the pressure boundary conditions were those given in [3].

In figure 6 we show a similar plot including a single borehole pump test. Again the flow is concentrated into a few discrete channels.

In figure 7 we show the results of a particle-tracking, simulated borehole injection test. Here 10,000 particles were tracked through the flow field, after being initially placed at a single location. In this example AFFINITY allows for complete mixing within each square grid cell, generating destinations and travel times for individual particles according to the relative outgoing flux across each cell boundary.

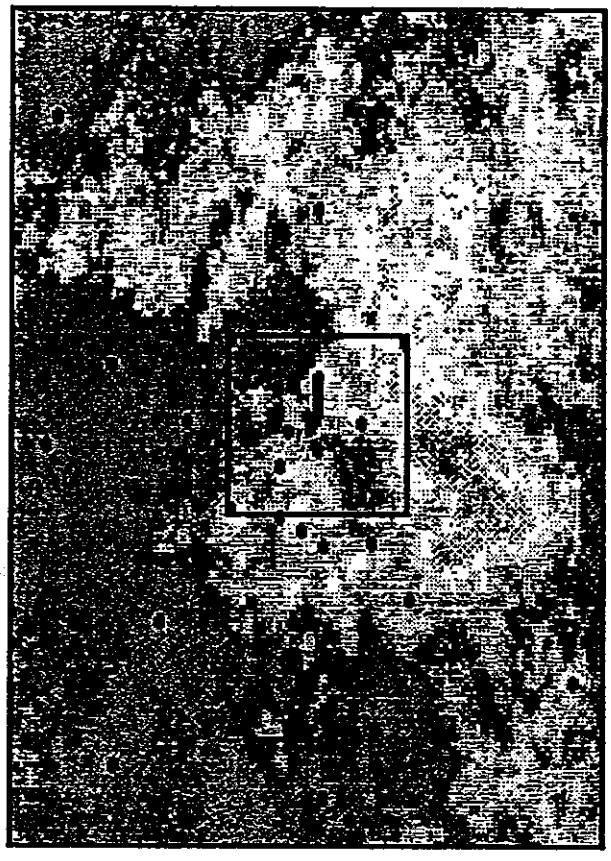


Figure 3: A plot of the realized transmissivity field (log values) for the WIPP site region. The transmissivities range from the highest values, $O(10^0)$ m^2/s, mapped in blue, through the green and yellow regions, down to the lowest values, $O(10^{-12})$ m^2/s, mapped in red. Dark points denote the positions of the Wipp site boreholes at which measured values are interpolated.



Figure 4: The pressure field (the equivalent fresh water head [3]) calculated using boundary data given in [3], and the transmissivity field depicted in Figure 3. Pressures are mapped via a continuous spectrum: blue (high), through green, through yellow, to red (low).



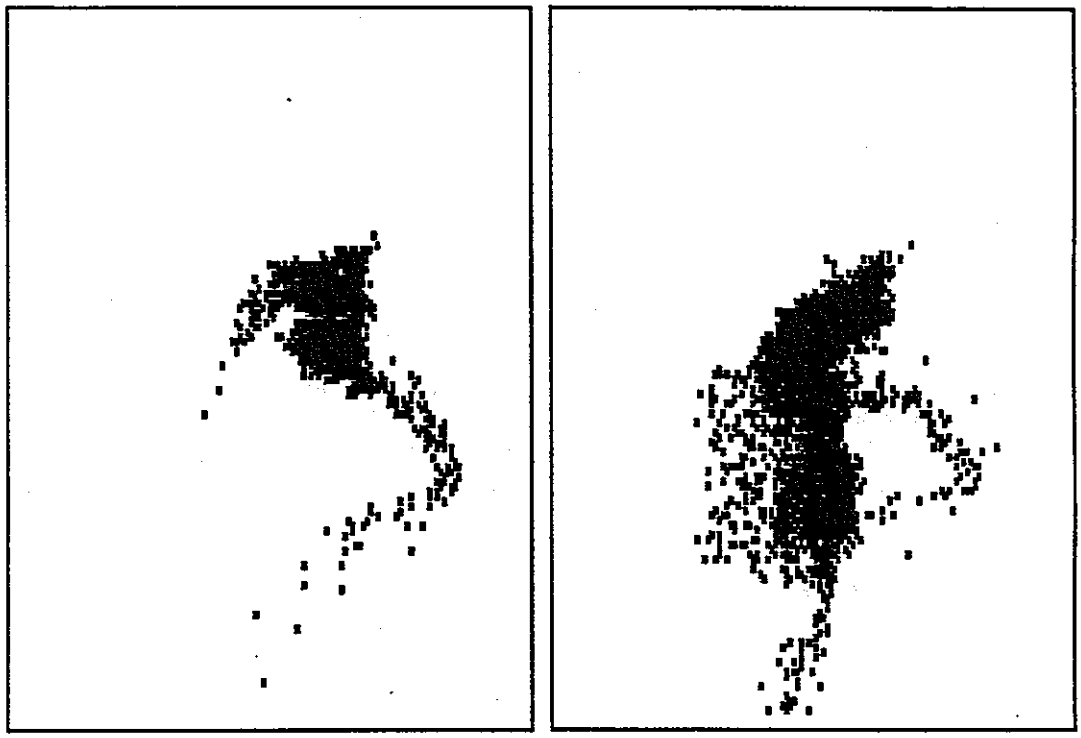
Figure 5: A plot of the modulus of the Darcy velocity for the groundwater consistent with the pressure field shown in Figure 4. $|\underline{v}|$ is mapped using a continuous spectrum: blue (high), through green, through yellow, to red (low).



Figure 6: A plot of the modulus of the Darcy velocity of groundwater, similar to Figure 5, incorporating a simulated pumping test, to the north-west of the centre of the model region.

Figure 7: Particle Tracking. Here the Darcy flow field is used to advect traced particles through the model region. Particle distributions are shown at six times.





9

4 Mathematical Methods

There are a number of methods for generating fractal fields (curves and surfaces, etc.). Of these, two approaches are available within AFFINITY. The first is based on spectral theory, while the second is an application of iterated function schemes.

There is a straightforward relationship between the spatially averaged quantity γ and the spectral density of the field z. In particular, the limiting behaviour of γ over small distances is directly related to the decay of the spectral density at infinity. Accordingly, once H is known, a suitable spectral density can be generated, and the corresponding field may be obtained efficiently by an application of the fast Fourier transform. A random number generator is employed to develop spectral realizations satisfying the required decay condition.

In order to condition the field with the observed data, one must impose linear constraints upon the spectral field. This reduces the number of degrees of freedom available in specifying the transformed field. In the example given above a more direct approach was used. A number, M, of suitable candidate fractal fields (all with $H = 0.4$) was first generated, and then a linear combination of these fields was chosen so as to interpolate the data, match the required spatial mean, and approximate the required spatial variance. This calculation was formulated as a linearly constrained quadratic optimization problem. The number of degrees of freedom, M, was varied so that variance of the resultant field was within a suitable tolerance of the desired value.

This technique could be used repeatedly to develop an ensemble of conditioned fields, each with the correct spatial structure (which may be verified $a-posteriori$).

The alternative method of field generation is based upon iterated function schemes. Here a function is constructed mapping three dimensional space onto itself, which is applied iteratively, starting from a simple set of points. The sequence of surfaces, successively obtained after each iteration, converges (uniformly) to an attracting set (a fixed point for the functional iteration). When the function has been suitably defined, this set is a fractal of the required dimensionality. This method is able trivially to condition on the data points, since these are used in defining a set of simple affine transformations from which the function to be iterated is composed. The higher the resolution required, the more iterates are made with the function. The importance of this technique may well be in defining fields efficiently to very high resolutions, or else in defining fields

over three dimensional domains, where even the fast Fourier transform is too slow. As an example we depict two curves, defined in this manner, which have been constructed from the same data set.

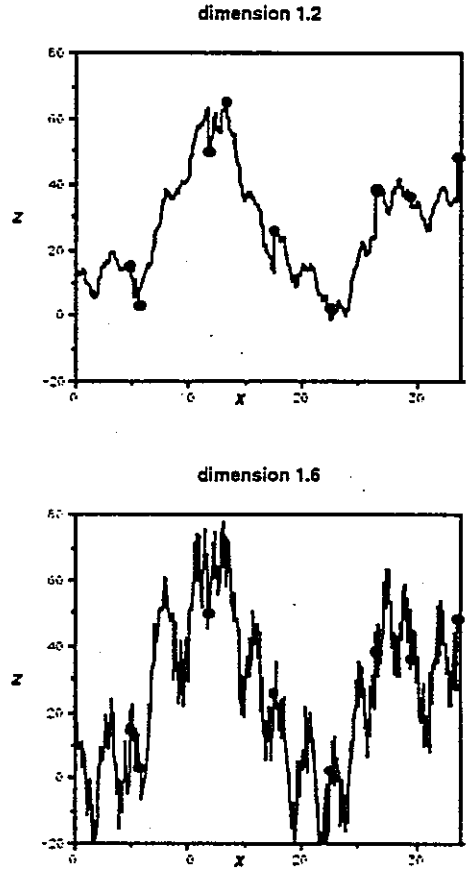


Figure 8: Conditioned curves using iterated function schemes.

5 Conclusions

We have employed a fractal-based methodology. The field data was used to generate a transmissivity field with spatial variability occurring on all scales according to a nonlinear statistical scaling law. The advantage is the specification of self consistent detail which is important in subsequent flow and transport calculations. The flow was shown to be highly channelled.

The AFFINITY package [1] is available to solve this inverse problem, passing in stages from the data analysis, through to transport stimulation calculations.

Although preliminary at present, we shall extend, improve, and validate

such predictions and analysis on the basis of the comparatively large WIPP II site data set [3].

Acknowledgement

The work described in this report was funded by UK Nirex Ltd through AEA Technology. We would like to thank our colleagues for useful discussions, and, in particular, Peter Robinson and Michael Williams for making the code available for the calculations. This is a preliminary draft and, at this stage, does not represent the views of the funding organizations.

References

[1] Peter Grindrod, Peter Robinson, Mike Williams, The Art of Noise: Self-affinity, flow and transport, Intera Sciences Internal Report, 1991.

[2] Ghislain de Marsily, Quantitative Hydrogeology, Academic Press, London, 1986

[3] T L Cauffman, A U La Venue, J P McCord, Ground-water Flow Modelling of the Culebra Dolomite, Volumes I and II. Sandia 89-7068/1, 7068/2, 1990.

[4] David Hodgkinson and Peter Grindrod, INTRAVAL Case 4: Draft Final Report, Intera Sciences Technical Report, 1898-21, January 1991.

D&R Internal Report NSARP 55(91)R8
Version 1

PRELIMINARY RESULTS FOR THE WIPP2 TEST CASE

K A Cliffe and C P Jackson

This document is an informal note containing unverified information, and is intended to promote efficient exchange of information. It should not be used for any other purpose.

Theoretical Studies Department
Radwaste Disposal Division
B 424.4
Harwell Laboratory
Didcot
Oxon OX11 0RA

Author:

Approved:

April 1991

1 Introduction

One of the options being considered for the long term disposal of low- and intermediate-level radioactive wastes is deep burial in stable geological formations. The most likely mechanism for the return of radionuclides to the biosphere is leaching from the repository followed by transport through the geosphere by groundwater flow. In order to assess the performance of a potential repository it is necessary to understand and be able to predict, amongst other things, the processes of groundwater flow and radionuclide transport in the relevant geological formations. Since transport by groundwater is very slow in regions that would be considered suitable for a repository these predictions must be made over very long timescales: far too long, in fact, to make direct experimental observations a viable method of establishing the safety of a repository. It is generally accepted that mathematical models of the physical processes must be constructed and used to make the necessary long-time predictions. It is clearly very important to establish that the models to be used constitute an adequate representation of the physical phenomena involved, and that the equations of the model can be solved with sufficient accuracy. The procedure for establishing the adequacy of a given model is called validation.

There are two aspects to validation. Firstly, the general laws governing the physical phenomena under consideration, in this case groundwater flow and radionuclide transport, need to be established. This aspect of validation is part of the general scientific process and a physical law can be considered to be validated if there is a concensus amongst the scientific community that it is an acceptable representation of the relevant physical phenomena. This part of the validation process involves making and testing hypotheses and careful comparison of model predictions with experimental data.

The second aspect to validation concerns the modelling of specific sites. Clearly the basic physical laws must be known and their relevance to the specific site must be established. In addition site-specific data for the models must be obtained. Once this data is known a complete model of the site can be constructed and reliable predictions of the groundwater flow and radionuclide transport can be made to establish the performance characteristics of the potential repository.

Thus validation of a site specific model involves an additional problem, namely that of obtaining the relevant data. It is clear that any experimental investigation can only yield relatively limited information on the geological and hydrogeological properties in the neighbourhood of the site. However,

groundwater flow and radionuclide transport models require, as input, values of various hydrogeological properties at each spatial point of the region to be considered in the predictions. Therefore, a procedure for infering the spatial variation of these properties, from a relatively small set of measurements, needs to be developed and validated. This is a particular example of the general class of scientific problems known as inverse problems. There is no general method available for solving such problems, rather specific methods have been developed to tackle each new situation.

A typical feature of inverse problems is that they do not have a unique solution. This means that, for example, several different transmissivity fields may be consistent with the measurements of transmissivity and head obtained during the site investigation. This merely reflects the uncertainty inherent in making limited measurements. It is important to consider the effects of this uncertainty on the results obtained with any model which depends on the data.

The international INTRAVAL project is aims to address issues arising from attempts to validate geosphere transport models. There are two phases to the project. Phase 1 was completed in 1990 and phase 2 has just started. Both phases are organised around various test cases based on experiments in geological media that might be used as host rocks for a radioactive waste repository. The emphasis of the project in phase two will be more on large scale and site specific experiments thus providing an opportunity for modellers to address the difficulties associated with inverse problems.

We are participating in the INTRAVAL project on behalf of UK Nirex Ltd. In phase 1 test cases 1a, 1b, 4 and 5 were studied as they were considered to be the ones of most relevance to UK Nirex Ltd. The proposed test cases for phase 2 were presented at a meeting in Cologne in September 1990. We have reviewed these cases and consider that WIPP-2 is the most appropriate one for the Nirex project team to tackle. This case is based on data available on the Culebra dolomite rock formation in the region around the WIPP-2 site. Extensive experimental investigations have been carried out over a number of years and data is available from some 60 boreholes and from hydrogeological tests carried out over a range of scales.

The purpose of this report is to outline our proposed programme of work on this test case and to present some preliminary results. In section 2 we shall describe the WIPP-2 test case including a summary of what is known about the local geology and a brief description of the hydrogeological modelling work that has already been done. In section 3 we describe the general approach that we intend to adopt in studying this case. In particular we discuss our strategy for

validation. Section 4 contains an outline of our proposed work programme. This is intended to facilitate interaction with the other project teams working on WIPP-2 and as such we expect that it will be modified as a result of discussion at the review meeting to be held in Seattle in April 1991. In section 5 we report on the progress we have made to date. These results are preliminary in nature and are intended to indicate the current status of our modelling capabilities that are of relevance to the WIPP-2 test case. Finally in section 6 we present our conclusions.

2 The WIPP-2 test case

2.1 Background

WIPP (Waste Isolation Pilot Plant) is the first underground repository for the disposal of radioactive wastes in the USA. As a result it is being subjected to rigorous scientific scrutiny. The investigation of the the site is being managed by Sandia National Laboratories for the US Department of Energy. The Department of Energy is expected to be committed to the validation of the various computer models to be used in the performance assessment for at least the duration of phase 2 of INTRAVAL. In particular they will provide data and modelling support from Sandia; they will make data available to the participating project teams and consider performing new experiments if they are needed to resolve issues that might arise during the course of phase 2.

The high level of support promised by the US Department of Energy for this test case together with the fact that the transmissivity of the rock (Culebra dolomite) is due to fracturing (as is the case for the host rocks at the two sites currently under investigation by UK Nirex Ltd.) make this the most suitable of the test cases for investigation by the Nirex project team.

2.2 Brief description of the geology

The WIPP site is near Carlsbad in New Mexico, USA. The site is part of the Delaware basin which is filled with 8000 m of sedimentary Phanerozoic rocks containing evaporites. The repository is located at a depth of 655 m within bedded evaporites, primarily halite, which are part of the Permian Salado formation. Above the Salado formation there is the Rustler formation. The most transmissive rock in the region is thought to be the Culebra dolomite member of the Rustler formation. This is a contiguous layer of rock, about 8 m thick. It is a vuggy dolomite and its relatively high transmissivity is due to fracturing which is considered to have been caused by dissolution of some of the underlying

highly soluble rock types such as halite, combined with the consequent displacement of the rock.

The Culebra Dolomite is considered to be the principal pathway for transport of radionuclides in the event of an accidental breach of the repository. As such its hydrogeology has been the subject of intensive investigation since about 1975. Some 60 wells at 41 different locations, which go as deep as the Culebra, have been constructed. Measurements of the Culebra transmissivity, thickness and elevation together with measurements of the hydraulic-heads, storativities and formation-fluid densities have been made at each of the 41 well sites. In addition a number of pumping and tracer tests have been carried out. An excellent summary of this data has recently been prepared by Cauffman, LaVenue and McCord [1].

2.3 Previous modelling work

A number of modelling studies of the hydrogeology of the Rustler formation and the Culebra dolomite member, in particular, have been carried out since 1979. The most recent and apparently most comprehensive is that of LaVenue, Cauffman and Pickens [2]. They have produced a model of the transmissivity field in the Culebra which they calibrated against measured steady-state and transient values of the hydraulic head at the well sites. A Kriging code, AKRIP, was used to interpolate the measured transmissivity field. This was then used in the finite-difference groundwater flow code SWIFT2 to produce calculated values of the hydraulic head at the wells. The initial or uncalibrated calculation led to discrepancies between the calculated and observed values of head which were systematically reduced to a level consistent with the uncertainties in the measurements. The technique used was to introduce pilot points into the region at which a value of the transmissivity was specified which led to a reduction in the difference between the observed and measured heads when the Kriging/groundwater flow calculation was repeated. The GRASP2 code was used to locate the areas in which the error in head was most sensitive to a change in the local value of transmissivity. A combination of GRASP2 calculations, expert judgment and trial and error was thus used to calibrate the transmissivity field against the known steady-state and transient behaviour of the Culebra dolomite. The details of this work are presented in the paper by LaVenue, Cauffman and Pickens [2]. LaVenue et al. also presented calculations of pathlines and travel times through model region and examined the sensitivity of various calculated quantities to the model transmissivities and boundary conditions.

The work of LaVenue et al. is a comprehensive and thorough study. Together with the report of Cauffman et al. it provides a reasonably complete statement of what is currently known about the hydrogeology of the Culebra Dolomite. Because of the techniques used in the study the problems of spatial variability and uncertainty were not directly addressed. Also the issue of the uniqueness of the calibrated transmissivity field was not considered in detail. The work we are proposing to do will attempt to address these issues and is thus intended to be complementary to that of LaVenue et al.

3 General approach

The aim of our participation in INTRAVAL is to improve our understanding of validation issues associated with groundwater flow and radionuclide transport in porous and fractured geological media. In this section we outline, in broad terms, our proposed approach to the WIPP2 test case. We treat, in turn, our ideas on validation and the methods we intend to employ.

3.1 Validation

The WIPP2 dataset on the Culebra hydrogeology is very large. This offers the opportunity to build models based on a subset of the data and then to use those models to make 'predictions' which can be tested against the already known data. This would provide a means of validating the models and of estimating how much information must be collected before one can have confidence in the model.

An important aspect of building a model is that it should be consistent with the original hypothesis which led to the formulation of the model. For instance a geostatistical model should be checked to see if is consistent with the original statistical hypothesis (eg. lognormality of the transmissivity field). We intend to examine these aspects of the validation process. We anticipate that the statistical inference problems will be quite difficult and are aware that it may well turn out that consistency cannot be demonstrated with the limited data available. An estimate of the amount of data necessary to establish the consistency of a given model would clearly be a valuable piece of knowledge.

Another aspect of the validation process which we think is important is that alternative models should be compared with one another where ever possible. With a number of project teams expected to work on this test case it should be feasible to do this.

As we mentioned in the introduction, peer review of methods and models is

fundamental to validation. Again with a number of project teams participating we expect our work to benefit from the constructive criticism of other experts.

The WIPP2 test case also offers the opportunity for us to suggest new experiments with the prospect that the US Department of Energy is willing to carry out any suitable new experimental work as part of its commitment to the test case.

Since the WIPP repository is scheduled to open in 1991 the implications of the models for the performance assessments will be of some importance to the US Department of Energy and Sandia National Laboratories. We think that this part of the validation process is of considerable importance. Validation is not just an interesting scientific exercise but also the means to establish confidence in repository performance assessments. We hope, therefore, that participating in the WIPP2 test case will not only lead to increased confidence in the particular models being developed for that site but to validation of the methodology which could then be applied elsewhere, in particular to the final assessment of the site ultimately chosen by UK Nirex Ltd. for the UK waste repository.

3.2 Geostatistical models

-58-

The methods we intend to apply to the WIPP2 test case are primarily geostatistical in nature. We feel that at present this type of model represents the best scientific approach to the problems of spatial variation and uncertainty. These problems are of crucial importance in simulating the groundwater flow and radionuclide transport in large scale heterogeneous media.

There are two basic types of geostatistical model. In the first type, which might be called deterministic, statistical methods, such as Kriging, are used to estimate hydrogeological parameters which are then fed into purely deterministic flow and transport calculations. The aim is to use the statistical methods to minimise the uncertainty in the results. The study of LaVenue is an excellent example of what can be achieved with these methods. One drawback of the deterministic approach based on Kriging is that it leads to a model in which spatial variation may not be treated very well. Kriged transmissivity fields have variograms which have quadratic behaviour near the origin. This is characteristic of very regular spatial variability. If the medium does not have this property, and the evidence is that porous and fractured heterogeneous media do not, then the Kriged transmissivity field will not represent certain aspects of the real transmissivity. There is also a potential problem of consistency since the Kriging process may well have been based on a model variogram which did not have quadratic behaviour near the origin and yet the field produced would have such

behavior. The impact of this inconsistency on the results of the model is not fully understood.

The second type of geostatistical model, and the type we are proposing to study, might be called stochastic. Here we attempt to produce a statistical model of the hydrogeology which incorporates both our knowledge of the system, obtained through measurements, and the effects of uncertainty. The groundwater flow and transport problems are then treated as stochastic differential equations to be solved by simulation or Monte Carlo methods. These are very powerful methods for solving stochastic differential equations, however, the drawback is that they are very demanding on computer resources. We are fortunate in having good access to the Cray2 at Harwell which is very well suited to this type of calculation. Also the necessary simulation techniques are being developed as part of a study of spatial variation in the Nirex Safety Assessment Research Programme.

The results produced by a stochastic model will include many realisations of the pressure or head field from which various statistics, such as the mean value of the field and the distribution in calculated head at the measurement points together with particle trajectories and travel times, may be obtained and compared with experimental data and also the output from other models.

4 Outline programme of work

In this section we outline a proposed programme of work on the WIPP2 test case. We anticipate that this will be modified as a result of feedback from the other project teams involved in the WIPP2 case.

4.1 Preliminary phase

In the first phase of our work we intend to demonstrate the feasibility of our general approach by producing a very simple stochastic model and performing a set of Monte-Carlo calculations with it. A best fit to an exponential variogram will be calculated from the available transmissivity data. The measured transmissivity values indicate that there is a definite spatial trend in the data. The western region has substantially higher transmissivities than the eastern region. The final statistical model will have to take this into account. However, in the preliminary phase this trend will be ignored as far as the calculation of the parameters for the variogram is concerned. The Turning Bands method will then be used to generate a set of realisations of the transmissivity, which will have a multivariate lognormal distribution and an exponential variogram with the

parameters obtained from the data as outlined above. These unconditional simulations will be conditioned on the known transmissivities and the resulting fields into the Monte-Carlo method. Particle paths and transit times times will be calculated from the computed pressure or head fields.

Although the spatial trend in the data will not be taken into account in the computation of the variogram (which will probably lead to an artificially high value for the variance) the fact that the simulations are to be conditioned on the known transmissivities means that the spatial trend will be taken into account in the calculations of the pressure field and the particle path and transit time calculations.

4.2 Detailed examination of possible statistical models

In the second phase of the work we intend to examine in detail a range of possible statistical models for the transmissivity data. It is at this stage that we will try to account for the effect of the observed spatial trend. We are also proposing to develop a methodology that could be applied to other situations.

An issue that we consider to be particularly important is that of consistency. A range of models, each of which will be based on a particular statistical hypothesis, will be constructed. At each stage the model will be subjected to suitably designed tests to check whether or not it is consistent with its underlying hypothesis. The aim is to arrive at a model which is both self-consistent and a good representation of the data.

We will start with a very simple model, which we know is almost certain to be inadequate, such as assuming the transmissivity field is pure nugget with no drift. This hypothesis would be very easy to test and presumably the test would indicate that the data is not consistent with the hypothesis. Models with spatial structure but no mean trend would be considered next and finally models taking into account the spatial trend would be considered. We think it worthwhile to go through this process in a systematic manner as it will illustrate a general method for tackling such problems and it will provide an indication of how much better the more sophisticated models are than the simpler ones.

4.3 Development of simulation techniques

Methods for simulating the statistical models referred to above will be developed. This work is already underway as part of the spatial variation studies in the NSARP programme. Any new techniques that are required specifically for the WIPP2 test case will be developed.

4.4 Pressure field and transport calculations

We will use the statistical models that we develop to carry out calculations of the flow and transport for the WIPP test case in much the same way as for the simple model described in the preliminary phase of the work. The results will be compared with experimental data and with those obtained by the other project teams.

4.5 Conclusion

The programme of work outlined above will be applied using both the full set of available data and randomly selected subsets. In this way we hope to be able to use the very large dataset for WIPP to test or validate our models by making predictions about known data on the basis of part of the dataset.

5 Progress to date

In this section we give a brief progress report on what has been achieved so far. This concerns work described mainly under the heading 'Preliminary phase' above.

We have computed the experimental variogram for the logarithm of the transmissivity based on the measurements summarised in Cauffman et al. [2]. We attempted to fit four different model variograms to this data, namely spherical, exponential, gaussian and cubic. We allowed each to include a nugget effect. We found that the spherical and exponential variogram gave the best fit and that in these cases no nugget effect was required. The gaussian and cubic variogram were both considerably worse and both required a significant nugget effect to obtain a best fit to the data. In the case of the gaussian variogram we interpret this as an indication that the quadratic behaviour near the origin is not a good model and that the transmissivity field is less regular than would be indicated by such quadratic behaviour. This is an indication that straightforward Kriging is likely to miss some of the features of the transmissivity. Whether these are significant or not remains to be seen.

The parameters calculated for the exponential variogram were used in a conditional simulation of the transmissivity field. The region modelled was the same as that used by LaVenue et al. [2]. Boundary conditions applied to the hydraulic head were taken from the calibrated values presented in [2].

Figure 1 shows a plot of the mean hydraulic head produced by our calculations. This is an average over 300 simulations. Figure 2 shows sample hydraulic heads taken at random from the 300 simulations. Figure 3 shows the mean

transmissivity field and figure 4 the transmissivity fields corresponding to the head plots shown in figure 2.

Finally, figure 5 shows sample particle paths, again corresponding to the head fields shown in figure 2,

These calculations demonstrate the feasibility of our general approach to the WIPP2 test case. They will, of course, be developed and refined as the project progresses and, in particular, we shall make detailed comparisons with the experimental data and the results obtained by other project teams.

6 Conclusion

We have described the WIPP2 test case which has been proposed as one of the cases to be studied as part of phase 2 of the INTRAVAL project. We consider WIPP2 to be an excellent case from the point of view of UK Nirex Ltd.

Our general approach to the validation issues relevant to the test case has been set out in section 2. We expect that our views will continue to evolve during the course of the project both as a result of our own work and that of the other project teams. We have also outlined a possible programme of work and presented preliminary results from our Monte-Carlo calculations.

7 Acknowledgment

The work described here was funded by UK Nirex Ltd.

8 References

1. Cauffman, T.L., LaVenue A.M. and McCord J.P. Ground-Water Flow Modeling of the Culebra Dolomite. Volume II: Data Base. Sandia National Laboratories Report no. SAND89-7068/2, (1990).

2. LaVenue, A.M., Cauffman, T.L. and Pickens J.F. Ground-Water Flow Modeling of the Culebra Dolomite. Volume I: Model Calibration. Sandia National Laboratories Report no. SAND89-7068/1, (1990).

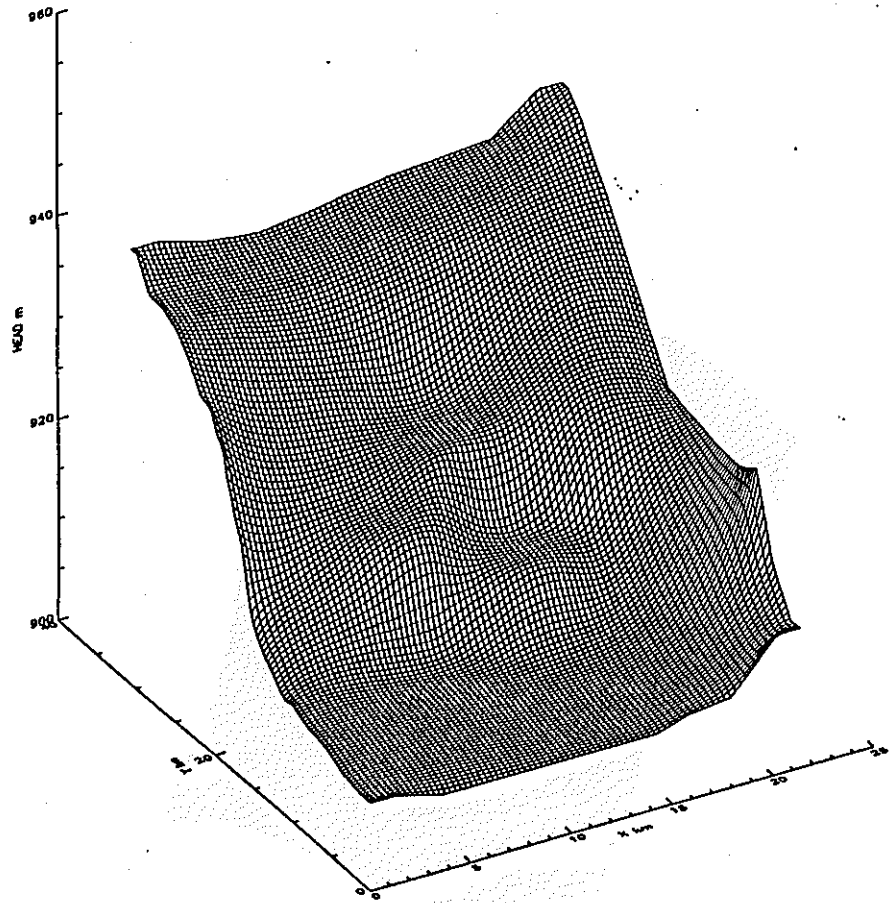


Figure 1. Mean hydraulic head.

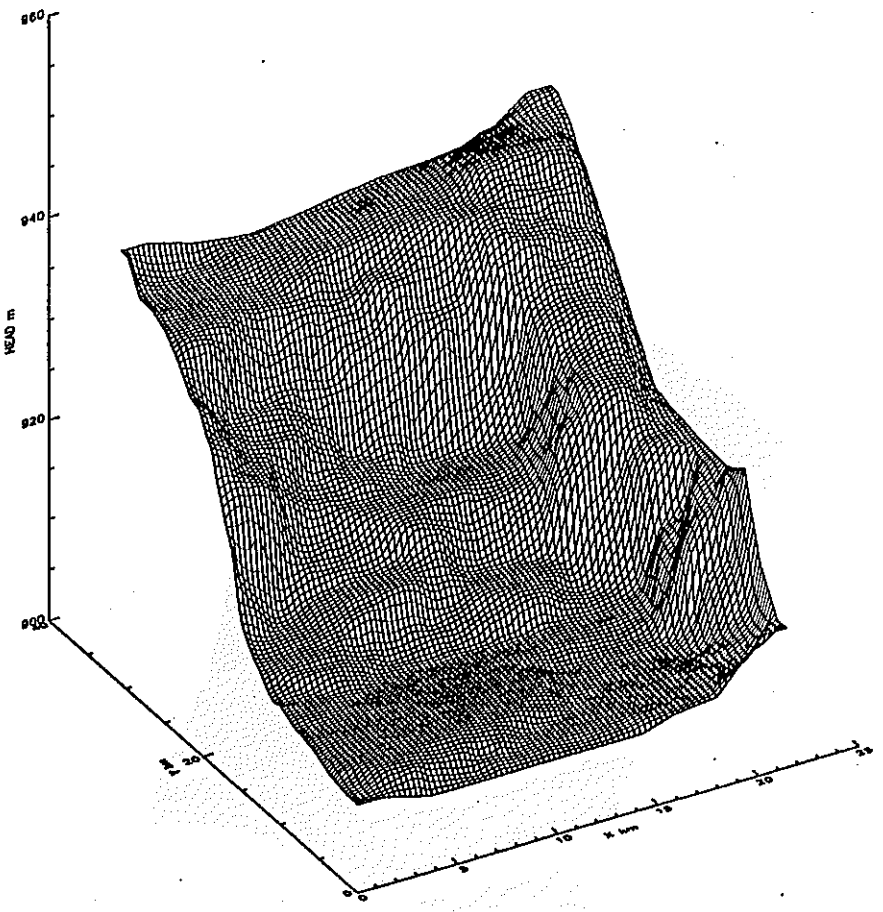


Figure 2a. Sample hydraulic head corresponding to the transmissivity shown in figure 4a.

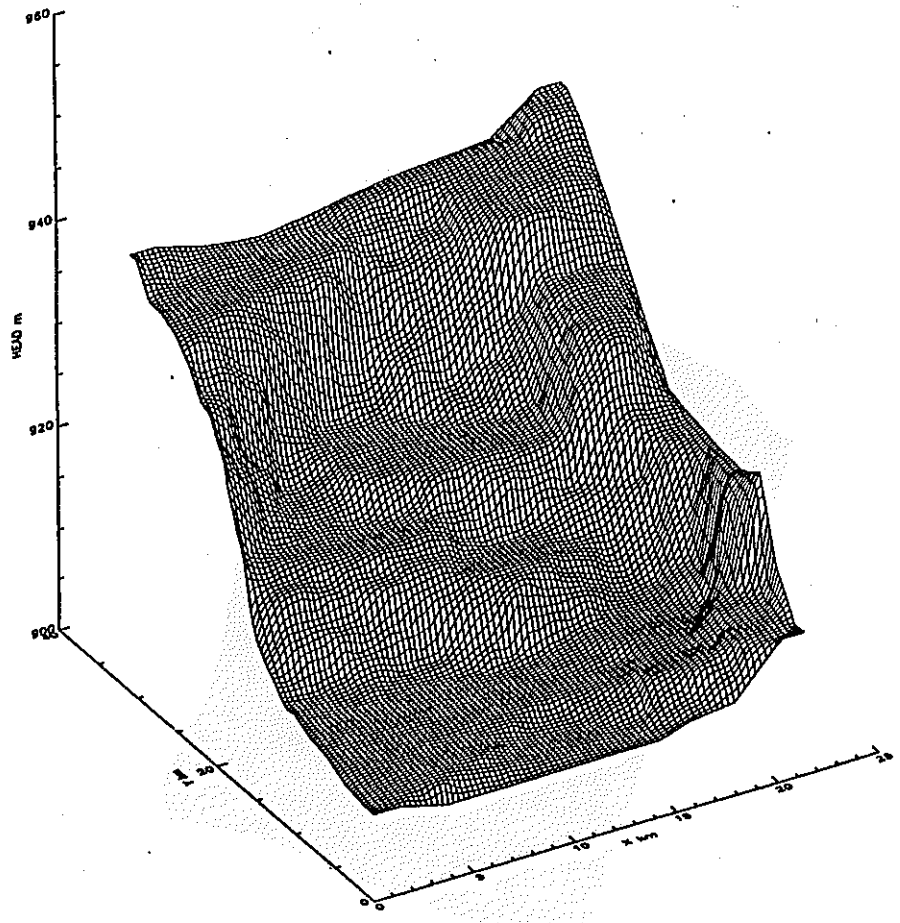


Figure 2b. Sample hydraulic head corresponding to the transmissivity shown in figure 4b.

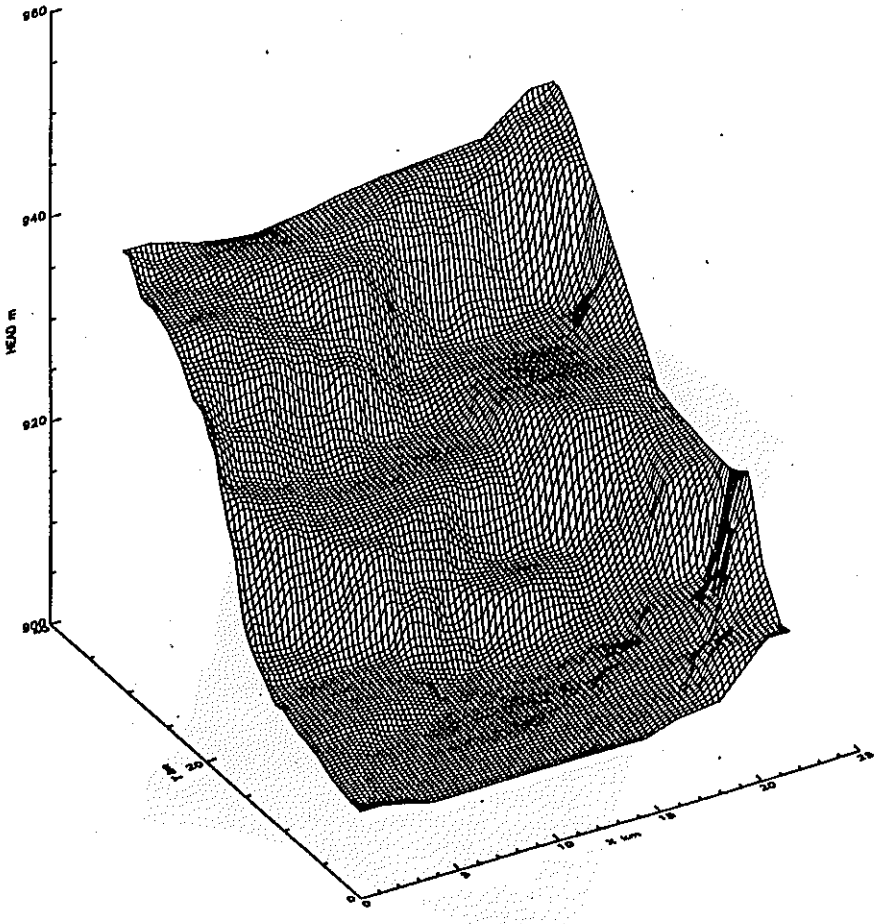


Figure 2c. Sample hydraulic head corresponding to the transmissivity shown in figure 4c.

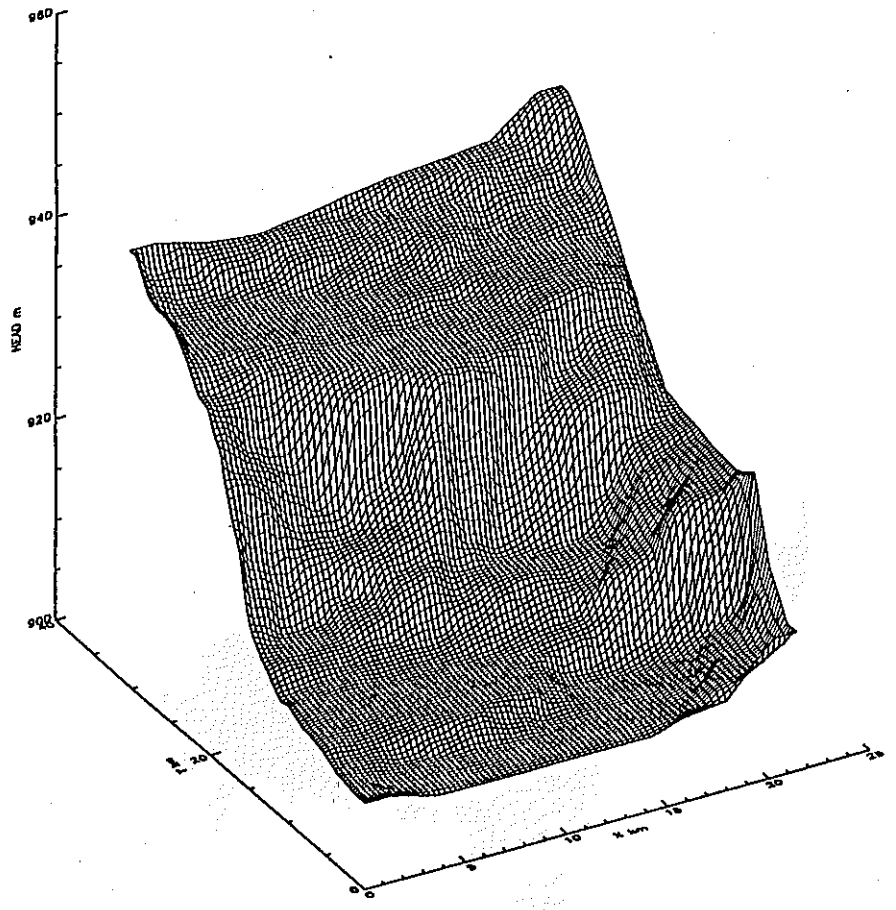


Figure 2d. Sample hydraulic head corresponding to the transmissivity shown in figure 4d.

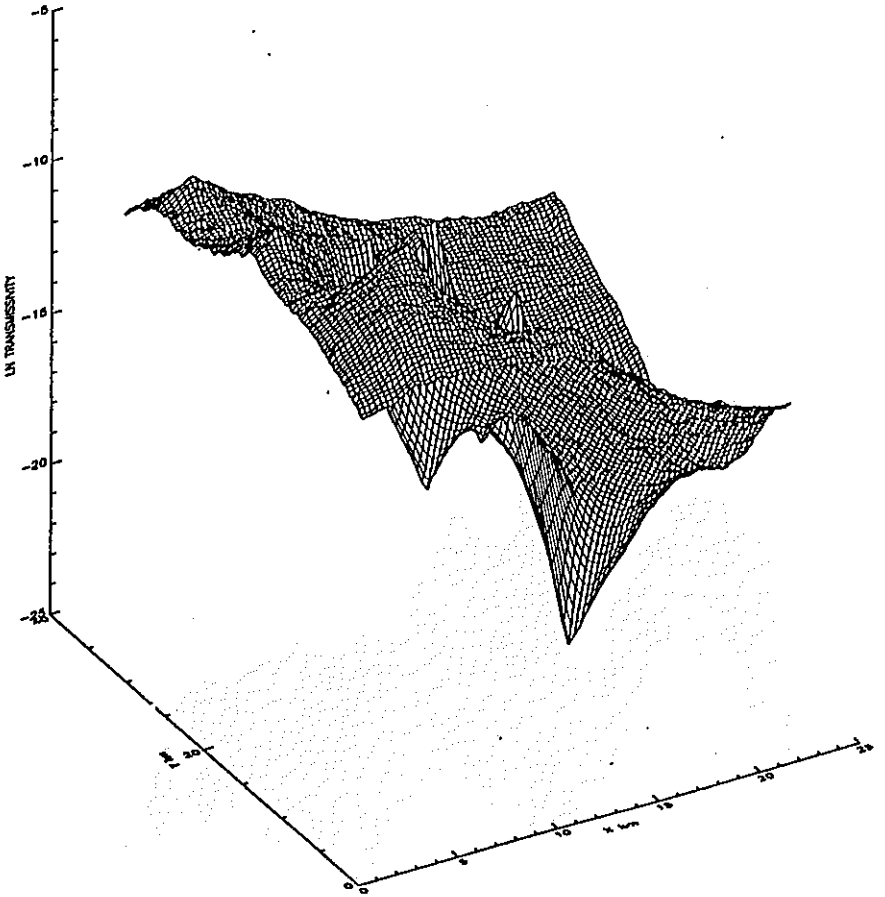


Figure 3. Mean transmissivity field.

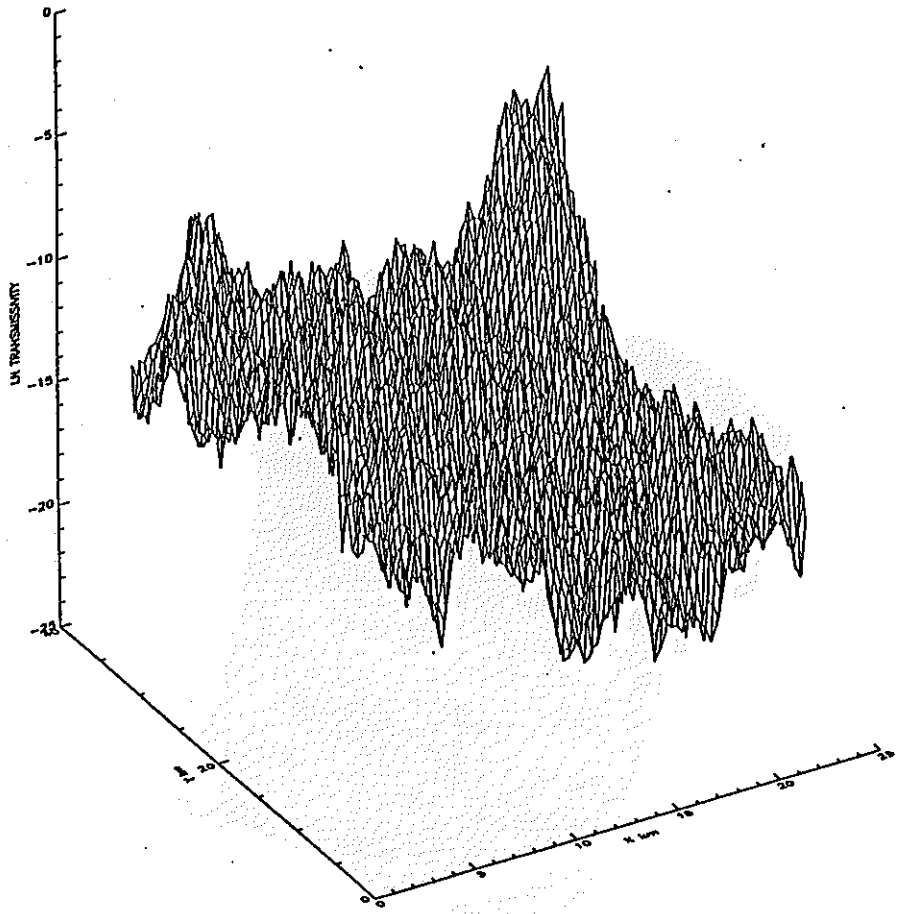


Figure 4a. Sample conditioned realisation of the transmissivity field.

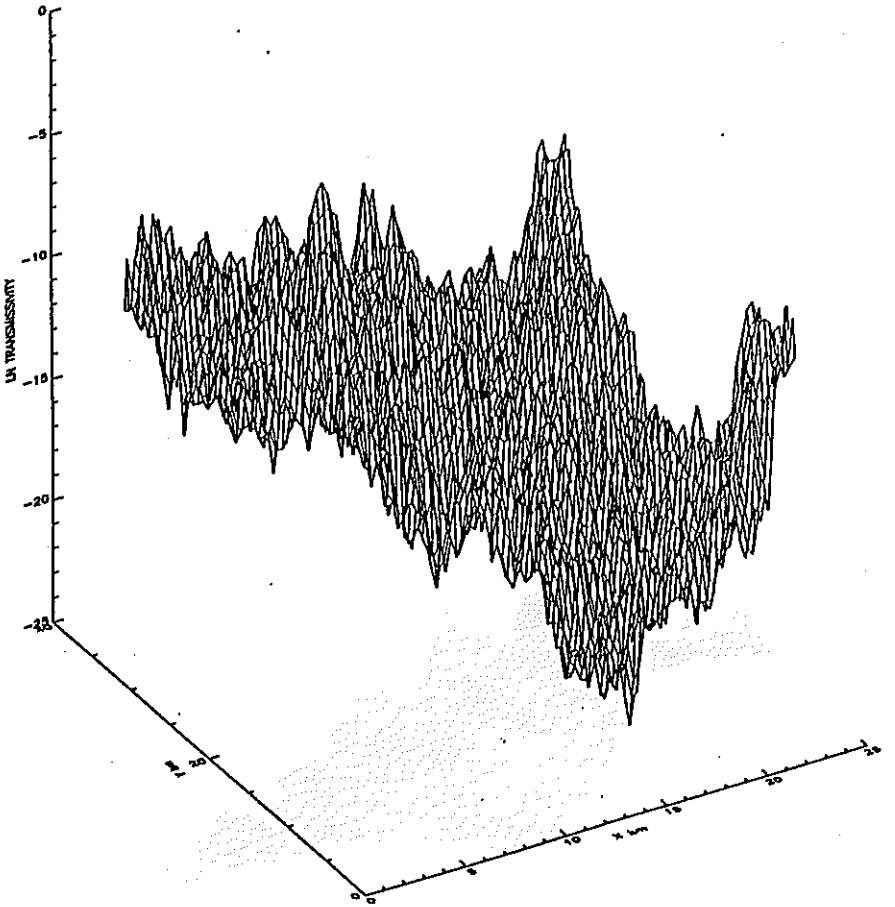


Figure 4b. Sample conditioned realisation of the transmissivity field.

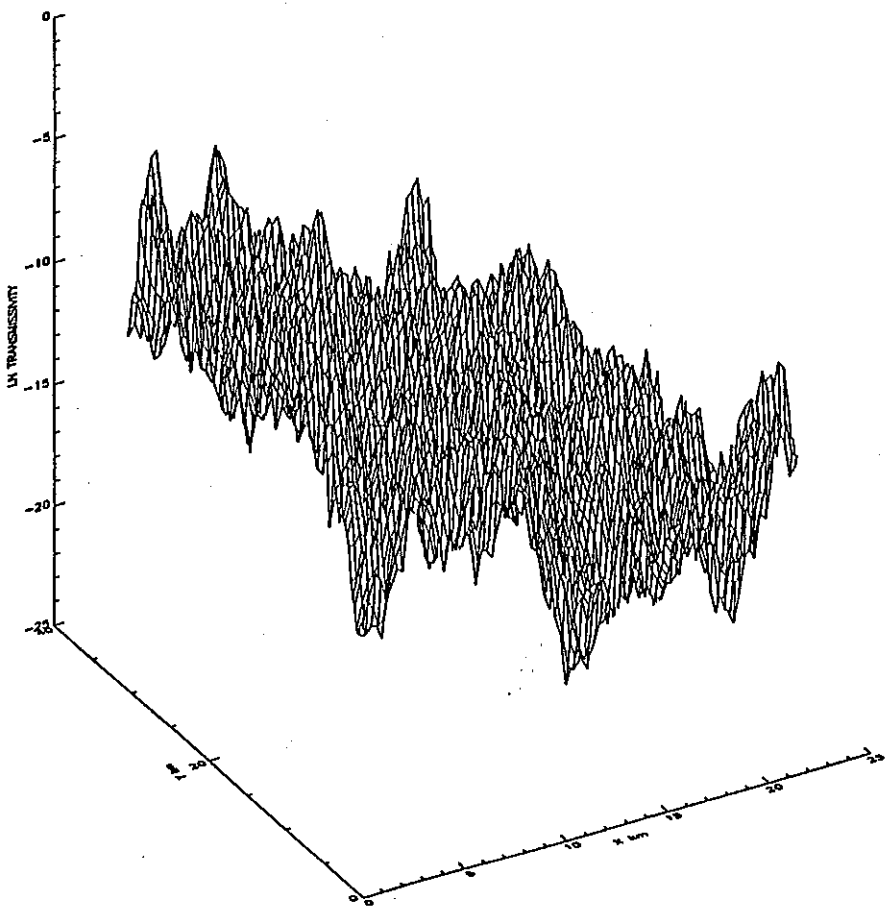


Figure 4c. Sample conditioned realisation of the transmissivity field.

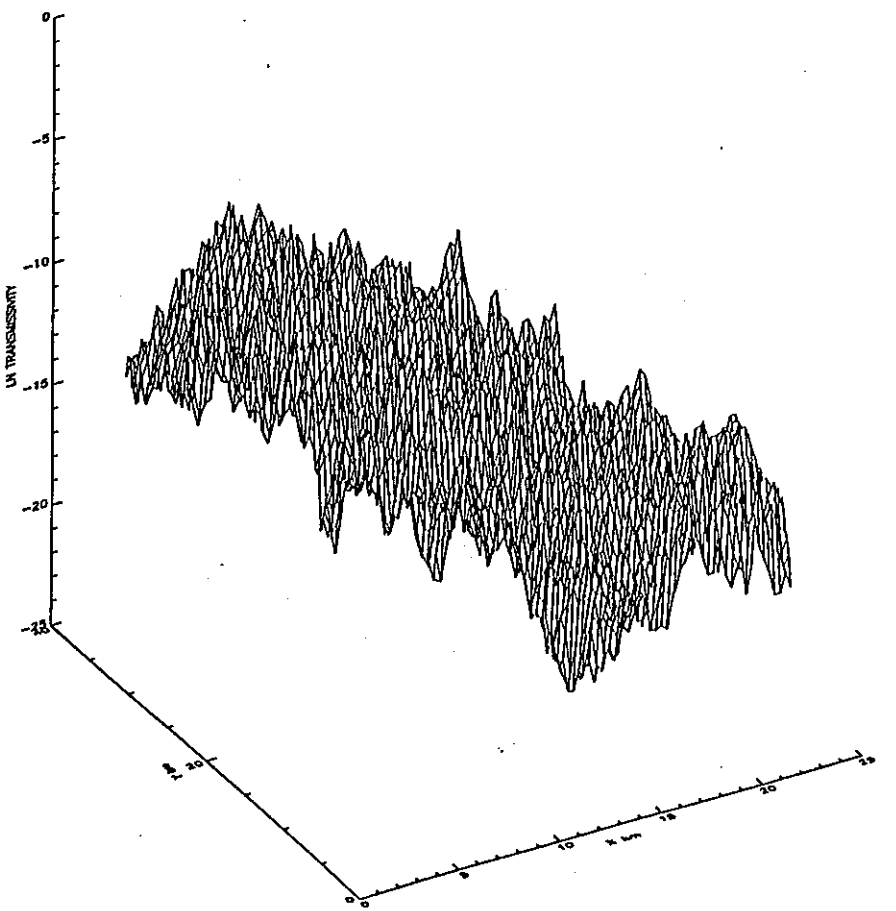


Figure 4d. Sample conditioned realisation of the transmissivity field.

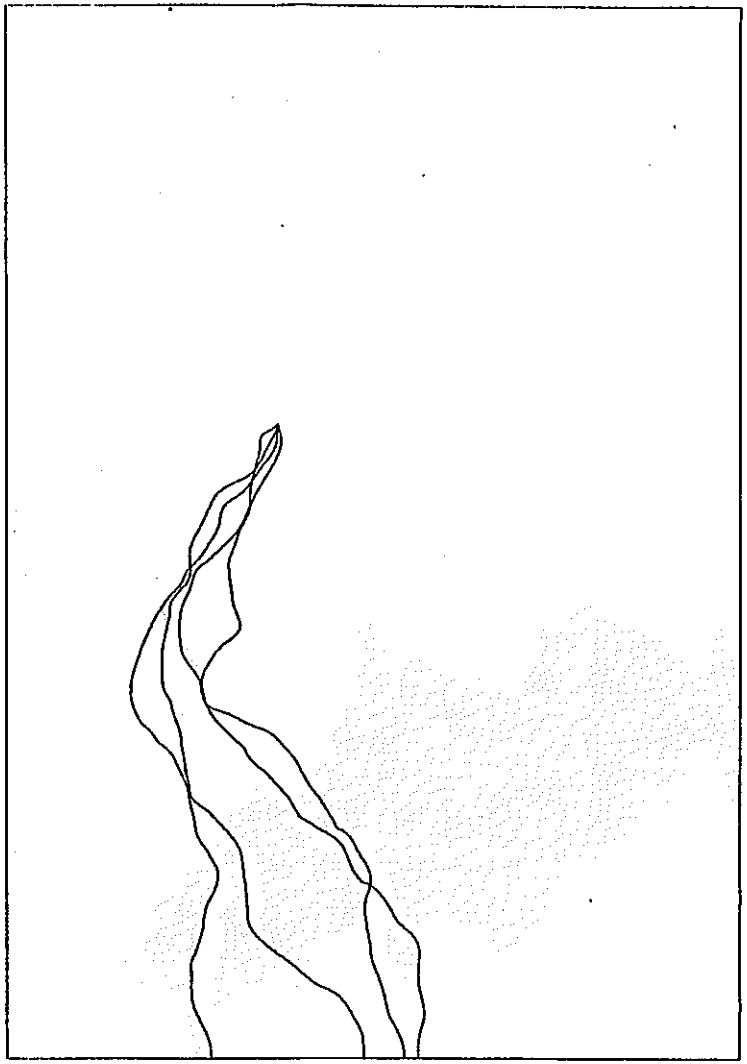


Figure 5a. Pathlines for the head fields shown in figure 2. The particles were released from well H-6.

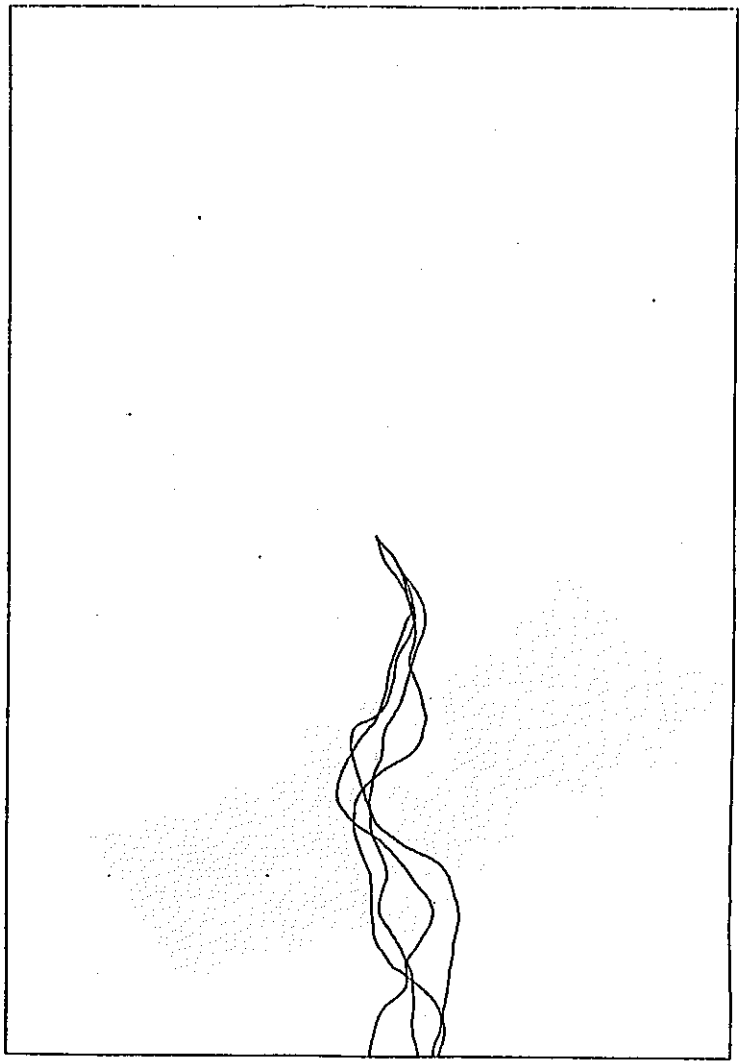


Figure 5b. Pathlines for the head fields shown in figure 2. The particles were released from well H-1.

11/21/1990

INTRAVAL Phase II TEST CASE:

LAS CRUCES TRENCH SITE

I. INTRODUCTION

A. Pilot Group Identification

The pilot group is comprised of the U.S. Nuclear Regulatory Commission (USNRC) Waste Management Branch, Washington, DC (Pilot Group Leader); the Center for Nuclear Waste Regulatory Analysis (CNWRA), San Antonio, TX; Massachusetts Institute of Technology (MIT), Cambridge, MA; New Mexico State University (NMSU), Las Cruces, NM; Pacific Northwest Laboratory (PNL), Richland, WA; Sandia National Laboratories (Sandia), Albuquerque, NM; and the University of Arizona (UA), Tucson, AZ. All participants are currently under contract with the USNRC. University of Arizona and New Mexico State University are currently under contract through September 1992 to do experimental work and to provide data acquisition, data analysis, and data support.

B. Experimental Location

The experiment is located at the New Mexico State University College Ranch, 40 km northeast of Las Cruces, NM, USA. Water and tracers are applied in a carefully controlled fashion to the surface of an experimental plot. The motion of water and the transport of various tracers through the vadose zone are monitored.

C. Original Purpose and Phase I Accomplishments

The original purpose of the Las Cruces Trench Site experiments was to test deterministic and stochastic flow theories by comparing model predictions with observed measured flow and transport parameters. To do this, a set of characterization experiments and two infiltration/redistribution experiments were designed and completed during Phase I of INTRAVAL.

During the characterization experiments, approximately 600 core and 600 disturbed soil samples were taken to the laboratory to determine soil-water retention and saturated hydraulic conductivity. In addition, the saturated hydraulic conductivity was determined in situ through borehole permeameter tests at a similar number of locations.

The purpose of the Plot 1 experiment was to test the feasibility of using tensiometers and solute samplers in very dry soils and to develop and test the data acquisition methods used in later experiments. Water containing tritium was applied at a rate of 1.76 cm/day to an area adjacent to the south side of the trench. Tritium

movement and tension were monitored during infiltration and water content was monitored during infiltration and redistribution.

The experience gained in performing the Plot 1 experiment was used to design and run the Plot 2a experiment. During this experiment, water was applied at 0.43 cm/day to an area north of the trench for 75.5 days. Tritium and bromide was applied with the first 11.5 days of water. The movement of tritium and bromide was monitored through approximately 50 solute samplers inserted through the north face of the trench wall during both infiltration and redistribution (Figure 1). The movement of water was monitored through approximately 50 tensiometers inserted through the north face of the trench wall (Figure 1) and through neutron probe readings taken at approximately 1000 locations in four different vertical planes (Figure 2). The data analysis for the Plot 1 and 2a experiments is complete and is presently in the Las Cruces Database. This data will be used for model calibration for the Phase II validation experiments.

D. Objectives of INTRAVAL Phase II Test Case

The objective of the Phase II test case is to test deterministic and stochastic water flow and transport theories by comparing model results with measured water flow and transport parameters. The emphasis of the testing is on natural soil systems that are heterogeneous but are well characterized hydrologically. Since the characterization and model calibration data have already been obtained, the emphasis will be placed on model testing and validation from the scientific and performance assessment perspective during Phase II rather than on data acquisition.

1. The scales of the experiments range from several cm (core and disturbed soil samples) to several tens of meters (field experiments). Temporal scales range from several hours to over a year.

2. Spatial scales for the soil heterogeneities range from less than a meter to several meters. Based on approximately 450 in situ and laboratory based measurements, the saturated hydraulic conductivity ranges over three orders of magnitude. The van Genuchten water retention parameters α and n range over three and one orders of magnitude respectively. There appear to be no complex discontinuities such as faults or fracture networks.

3. Water flow and transport of several tracers are monitored during infiltration and redistribution experiments to allow the coupling between these two phenomena to be investigated.

4. There has been little change in overall purpose of the experiment in moving from the Phase I to Phase II. Data for site characterization and model calibration were taken during Phase I. The first Phase II experiment, denoted as the Plot 2b experiment, utilizes the same experimental set-up as was used during the Plot 2a experiment. Water is applied over the same irrigated area

with different tracers (boron, chromium, pentafluorobenzoic acid, and 2,6-difluorobenzoic acid as well as tritium and bromide) and at an application rate approximately four times larger. During Phase II, models calibrated with the Phase I data will be used to predict the Plot 2b water flow and solute transport.

E. Validation Aspects

The ultimate goal of this work is to validate (or invalidate) stochastic and deterministic models for water flow and transport in spatially variable soils. To achieve this goal, mathematical and experimental methodologies required to unambiguously address model validation must be developed and tested. The Las Cruces Trench Experiments are designed by modelers and experimentalists to act as a catalyst in the development of validation methodologies and in the testing of water flow and transport models for spatially variable soils. The spatial variability of the important hydraulic parameters of the site has been carefully characterized on a fine scale and the experiments are run under very controlled conditions.

We plan to address model validation on two levels. On the first level, model predictions will simply be compared to field observations graphically and through simple statistical measures of correlation. While this level of model validation is not rigorous, it does allow the results of many models to be compared with relative little effort. Specifically we plan the following:

1. Using simple deterministic models, various scenarios for the Plot 2b experiment will be simulated by NMSU to help optimize the water/tracer application rates and the choice of tracers.

2. The Plot 2b experiment will then be run and the actual water/tracer application rates will be provided to the modelers.

3. Using the actual water/tracer applications, the Plot 2b experiment will be modeled.

4. After modeling is complete, the modelers will provide NMSU with ASCII files of the predicted water contents, tensions, and solute concentrations at the measurement locations and integrated fluxes through specified planes in a predetermined format. In addition, the stochastic modelers will provide NMSU with the predicted statistics of their models. NMSU will tabulate simple statistical measures of correlation between model prediction and observation and will include the predictive statistics provided by the stochastic modelers.

5. After receiving the model predictions, the observed water contents, tensions, solute concentrations, and integrated fluxes, as well as all of the model predictions, will be distributed in ASCII format to the participants (through the

Las Cruces Database). This will allow the individual participants to address the issues of model validation in more detail.

6. Presently, we anticipate using the following models:

   Sandia will utilize the VAM2D finite element code developed by Huyakorn et al. (1989). VAM2D can model water flow and transport in a variable saturated anisotropic soil as well as single-species and chained decay transport.

   MIT will use stochastic water flow models (Gelhar (1984), Mantoglou and Gelhar (1987a,b,c), Polmann et al. (1988), Yeh et al. (1985a, b, c)) to simulate the long term water movement in the Plot 1 experiment. These models generate effective media approximations to the important hydraulic parameters allowing non-Monte Carlo simulation of water flow in heterogeneous and anisotropic soils. The Plot 2b experiment may also be modeled by MIT later in Phase II if adequate funds become available.

   PNL will model transport of both inert and reactive tracers for the Plot 2b experiment. Initially, the transport analysis will be performed using one or more deterministic codes (e.g., TRACR3D, PORFLO3). Multiple realizations will be simulated using Monte Carlo methods to estimate the variation in the solute front due to spatially variable soil properties. Later, if chemically active tracers are used in the transport experiments, a coupled geochemical code (e.g., FASTCHEM) will be used to predict tracer plume movement in the trench soil profile.

   CNWRA will utilize the three-dimensional water flow code of Ababou (1988). This code models the nonlinear effects of partially saturated water flow in a randomly heterogeneous and anisotropic soil. The input parameters will be conditioned using the Las Cruces Database. The algorithm has been used to generate three-dimensional high resolution flow simulations, as described in Ababou and Gelhar (1988).

   NMSU will use the water content based algorithms of Hills et al. (1989a, 1990) to model water flow and transport using an isotropic uniform and layered soil model.

On the second level of model validation, MIT is presently developing statistically rigorous quantitative validation methodologies (under contract to the USNRC). Researchers at Sandia and NMSU are also investigating issues of model validation. If funds are available, MIT may demonstrate the model validation methodology using simple models for water flow and the Las Cruces Database for the Plot 1 experiment. Due to the extra effort required, it is not anticipated that the previously described models will be rigorously validated using this methodology during Phase II.

II. EXPERIMENTAL DESIGN

A. Parameters Measured - Key measurements include:

1. Saturated hydraulic conductivity (both in situ and laboratory measurements) and $\theta(h)$ data have been determined for approximately 600 locations in a vertical plane immediately adjacent to the test plots.

2. Measurements of θ_r and θ_s and estimates of the van Genuchten water retention parameters α and n have been determined for each of the 600 locations. Specific water capacity, C, can be estimated from the resulting van Genuchten curves.

3. Moisture content or moisture profiles as a function of time are monitored using downwell neutron-probe logging.

4. Tension data obtained from tensiometers placed on a two dimensional grid on the north trench wall are monitored as a function of time.

5. Concentrations of the tracers are sampled through the trench wall on a two dimensional grid as a function of time. Tracer concentration samples will also be taken at other locations from soil samples taken during and after the execution of the Plot 2b experiment. This destructive sampling will allow a three dimensional picture of the tracer concentration profiles to be generated.

B. Spatial and Temporal Scales

Temporal scales include sampling times for infiltration events ranging from hours (during early infiltration) to hundreds of days for later observations. The time interval for both infiltration tests and redistribution tests exceeds 70 days with measurements taken every several days during infiltration and less often during redistribution. The number of monitoring locations for tensions exceed 50. The number of monitoring locations for solute also exceeds 50. Over 1000 neutron probe monitoring locations are used to measure water content.

C. Experimental Set Up

A trench 16.5 m long, 4.8 m wide and 6.0 m deep was dug in undisturbed soil. Water containing tritium and bromide tracers was applied at a controlled rate of 0.43 cm/day on the surface of one side of the trench to generate data for model calibration. The movement of water below the soil surface has been monitored with neutron probes and tensiometers. Soil solution samples have been taken to determine the movement of tritium and bromide below the surface of the soil during the Plot 2a calibration experiment. During construction of the trench, the physical properties of the soil at the site were determined in sufficient detail to allow estimation of many of the statistical parameters needed in the stochastic and comparative

deterministic models.

An irrigated area measuring 1.2 m by 12 m is located adjacent to the trench. The walls of the trench were excavated vertically and reinforced to prevent cave-in. The trench and adjacent irrigated area have been covered to prevent surface runoff and recharge due to rainfall and to minimize evaporation.

The drip irrigation system consists of 80 irrigation lines placed parallel to the trench face with each irrigation line containing 4 drippers. The applied water is metered onto the plot to allow for water balance calculations. Water was applied at an rate of 0.43 cm/day during the model calibration experiment and will be applied at approximately 1.8 cm/day during the model validation experiment.

Laboratory and field uniformity tests of the drip irrigation system prior to the Plot 2a experiment indicated extremely small non uniformities and a random distribution to the non uniformities.

The water content in the soil is determined with neutron probes. Neutron access tubes were installed vertically in three rows parallel to the trench face (Figure 2). The first row is 2.0 m from the trench wall, the second row is 6.0 m from the trench wall, and the third row is 10.0 m from the trench wall. There are presently eleven neutron access tubes per row, spaced 1 m apart. Additional neutron access tubes are installed as the wetting front progresses horizontally. There is a fourth row of neutron access tubes positioned perpendicular to the trench wall and along the center of the irrigated area (Figure 2). These tubes are spaced at either 1 or 2 m intervals. Additional details of the experimental setup are given in Wierenga et al. (1986), in Nicholson et al. (1987), in Hills et al. (1990), and in Wierenga et al. (1990).

Tension is monitored through tensiometers installed in a two dimensional grid through the trench wall (Figure 1).

Tritium at a final concentration of 0.1mCi/l and bromide at a final concentration of 0.8 g/l were applied with the water during the first 11.5 days of irrigation for the Plot 2a calibration experiment. Tritium and bromide concentrations were sampled on a regular basis through solute samplers installed in a two dimensional grid through the trench wall (Figure 2). Tritium, bromide, boron, chromium, and the organic compounds pentafluorobenzoic acid (PFBA) and 2,6-difluorobenzoic acid (DFBA) will be added with the water during the Plot 2b experiment.

D. Sampling Strategy

Two sampling strategies are used.

Scheme 1: HYDROLOGIC PARAMETER CHARACTERIZATION.

From a total of 9 horizontal transects (25 m in length) and 3 vertical transects (6 m in length), sampled at intervals of 0.5 m in the horizontal direction, measurements of field saturated hydraulic conductivity have been made in situ with an unsaturated-borehole technique (borehole permeameter). Cores taken adjacent to these boreholes have been taken to the laboratory for analysis of a) water retention characteristics, b) particle-size analysis, c) bulk density, and d) soil chemical properties (e.g., $CaCO_3$ content, soil paste pH and soluble cations and anions). Over 600 measurements of field saturated hydraulic conductivity have been made to date. Similar numbers of water retention curves, particle-size analysis, bulk densities, and chemical properties have been measured in the laboratory from the core samples.

Scheme 2: INFILTRATION AND REDISTRIBUTION TESTING OF WATER AND SOLUTE MOVEMENT

The face of the experimental trench is monitored intensively with solution samples and tensiometers. The solution samplers are tensiometer cups that are connected to a vacuum line (sometimes called suction lysimeters). These units are used to collect small (2-10 ml) quantities of solution as the water infiltrates into the soil profile. Tracer pulses can be analyzed by periodic collection of samples. A 10 day pulse of tritium was used to trace the transport of water in a preliminary infiltration test performed on the south side of the trench face during the Plot 1 experiment. The Plot 1 experimental results indicated that the use of solution samplers is a viable technique for monitoring solute transport in unsaturated soils, particularly when the tensions were less than 150 cm. At higher suctions the water transmission rate is too low to obtain sufficient quantities of sample to monitor. These samplers were also used during the Plot 2a experiment and will be used during the Plot 2b experiment. Tensiometers placed adjacent to suction samplers (Figure 1) are used to monitor tensions (soil suction) and operated reasonably well after the wetting front had passed. These units do not work in the dry soil. Water tensions in dry soil must be inferred by the water retention characteristics taken from the characterization data of Scheme 1. Neutron probes are used to monitor water contents in three planes located parallel to the trench face and in 1 plane located perpendicular to the trench face (Figure 2). The neutron probe monitoring and tensiometer reading are done on the order of hours during initial infiltration, on the order of days as time progresses and infiltration moves water deep into the soil profile, and finally on the order of weeks during the later stages of redistribution. Higher flow rates require higher sampling rates. During and after the completion of the Plot 2b experiment, additional core samples will be taken from strategic locations throughout the experimental area to better define the three dimensional distribution of the tracers. The characterization methodologies developed by MIT will be used to help define core sample locations.

E. Independence Between Data Sets

The hydraulic characterization data are taken from an area adjacent to the Plot 1

and 2 infiltration and redistribution experiments. The results from the Plot 1 and 2 experiments were not used to calibrate or redefine the characterization data in any way. The characterization data are thus independent of the Plot 1 and 2 data.

The Plot 1 and Plot 2a data were taken from opposite sides of the trench and at different flow rates and are thus independent.

The neutron probe data, the tensiometer data, and the solute samples taken through the trench wall will be taken from the same locations during the Plot 2a and 2b experiments. However, additional solution samplers will be installed as the solute front moves through the soil profile. The experiments are at different flow rates with the Plot 2b experiment using additional tracers (boron, chromium, pentafluorobenzoic acid, and 2,6-difluorobenzoic acid). Thus, the Plot 2b data will be independent of the Plot 2a data in the sense that different experiments are run but dependent in the sense that the experiments are run at the same location using the same monitoring system.

The additional core samples taken during and after the Plot 2b experiment will be taken from locations not previously sampled. Thus this data will be independent of the solute concentration data obtained through the trench face during the Plot 2a and 2b experiments.

Water flow is monitored using both tensiometers and neutron probes. Since these methods are different, the corresponding data are independent.

F. Biases Inherent in the Design

1. The soil retention characteristics determined in the laboratory may not be a true representation of the water release characteristic in the field. Sampling and measurement techniques have not been developed to the point that the entire (wet to dry) range of the water retention curve can be measured in the field by a single instrument. Hence laboratory measurements are used to supplement field observations. Pressure plate techniques may tend to over estimate water contents at high tensions (1.0 to 1.5 MPa values).

2. Since tensiometers only operate in the wet range, the majority of the data will be in a range where tensions are not too large (< 150 cm H_2O). This will tend to bias the tensiometer readings toward wetter environments than are normally experienced in arid regions. In contrast, neutron probes can measure very small water contents. However, neutron probes are inherently poor at defining sharp wetting fronts due to the relatively large effective area of the probe measurement.

3. The unsaturated conductivity functions determined from pore-size models may inadequately describe the actual unsaturated conductivity values in the field. While these data are independent, they should be checked against

laboratory measurements of unsaturated conductivity and possibly with instantaneous profile observations using time dependent tension and moisture content profiles from the infiltration and redistribution tests that have been run at the trench site.

G. Complementary Experiments

A suite of experiments have been performed to evaluate stochastic model capabilities. The large lysimeter tests (described in Wierenga et al. (1986), Wierenga and van Genuchten (1989), and Hills et al. (1989b)) as well as the laboratory column tests were used to estimate transport parameters (i.e., Peclet number, dispersion coefficients, etc.) that are useful to understand field transport in soils of similar physical and chemical characteristics. These experiments consist of infiltration and redistribution tests in uniform soils and layered soils under similar flow conditions as those imposed in the field tests. The lysimeter tests are complete.

A Plot 3 experiment is planned at a different location. The purpose of the Plot 3 experiment is to further test validation methodologies and to validate stochastic and deterministic water flow and transport models on a larger field scale. Information gained during the Plot 2b experiment and suggestions from the INTRAVAL participants will be carefully considered during the Plot 3 experimental design.

H. Background Information

The field site is on a basin slope of Mount Summerford, which is at the north end of the Dona Ana Mountains. The Dona Ana Mountains form a domal uplift complex of the younger rhyolitic and the older andesitic volcanics intruded by monzonite (Gile, Hawley and Crossman (1970)). The sediments on the mid-piedmont have young soils (6500 to 4000 years B.C.) of the Dona Ana and Onite series (coarse-loamy Typic Haplargids). Sediments on the lower-piedmont slopes are older soils (mid-late Pleistocene) dominated by the Berino series (fine-loamy Typic Haplargids). The geologic features, Oeomorphic surfaces, soil series and vegetation types found in the area around the field test area are typical of many areas of southern New Mexico and are similar to arid and semiarid areas of the southwestern United States.

The climate in the region is characterized by an abundance of sunshine, low relative humidity, and an average Class A pan evaporation of 239 cm/yr. Average annual precipitation is 23 cm with 52% of the rainfall occurring between July 1 and September 30. The average monthly maximum air temperature is highest in June at 36 C and lowest in January at 13 C.

III. AVAILABLE EXPERIMENTAL RESULTS

A. Raw Data

Water retention data, density profiles, particle-size analysis data, and saturated

hydraulic conductivities measured through both laboratory and in situ techniques during the characterization experiments and water content data, tensiometer data, solute concentrations, and water applications rates measured during the Plot 1 and Plot 2a experiments are contained in the Las Cruces Database. The Plot 2b data will also be incorporated into the database using the same format. In addition, morphological mapping of the trench face, drip irrigation distribution tests, and outflow and inflow measurements from large and small column-support tests are on file at NMSU and at UA.

B. Processed Data

These data have been reported in two annual reports (NMSU to NRC 1985, 1986), in Wierenga et al. (1986), in Nicholson et al. (1987), and in Wierenga et al. (1989, 1990). These data consist of moisture profiles determined from neutron probe calibration curves; tension profiles from tensiometer data mapped as a function of time; tritium profiles and breakthrough curves (obtained from solute sample analysis); and wetting front observations from the first trench experiment from visual mapping of the wetting front advance with time. In addition, the van Genuchten water retention parameters α and n for each of the 600 core sample locations and the parameters for uniform and layered soil models are included in the Las Cruces Database and discussed in Wierenga et al. (1989, 1990).

C. Data Storage

Data are stored in Las Cruces in laboratory notebooks, on IBM (5 1/2" floppy) disks, and on 10 MByte Bernoulli disks. Redundant copies of the digital data are stored in Tucson on 20 MByte Bernoulli disks and in the Las Cruces Database. The Las Cruces Database is installed on a Digital VAX and is backed up regularly by computer center personnel. The database consists of 27 files in ASCII format, is in the public domain, and is accessible at no cost through the international computer networks using FTP. Copies of the database are also available on IBM compatible floppy disks.

IV. PREVIOUS MODELING

Early modeling of the Las Cruces Trench site using the field data sets are described in MIT reports (thesis, etc.), in Nicholson et al. (1987) , in Hills et al. (1989a, 1989b, 1990), and in Wierenga et al. (1990). More recently, scientists from the Center For Nuclear Waste Regulatory Analysis at the Southwest Research Institute; HydroGeoLogic, Inc.; KEMAKTA Consultants Co.; Massachusetts Institute of Technology, New Mexico State University; Pacific Northwest Laboratory; and Sandia National Laboratories have used the Las Cruces data to test transient models for water flow and solute transport through unsaturated soils. These models range from two-dimensional deterministic simulations of water flow and transport through uniform isotropic soils to three-dimensional simulations of water flow through fully hetero-

geneous, anisotropic soils. Stochastic models include one- and two-dimensional simulations of water flow using Monte-Carlo methods and two-dimensional simulations of water flow using the techniques of Mantoglou and Gelhar (1987a). Descriptions of the various models and model results are provided in the INTRAVAL Phase I Final Report on the unsaturated zone test cases (in preparation).

V. CURRENT STATUS AND EXPERIMENTAL SCHEDULE

The characterization, Plot 1, and Plot 2a experiments are complete. The infiltration phase of the Plot 2b experiment is complete as of November 1990 and redistribution is presently being monitored. The Plot 3 experiment will be planned during the next year and is expected to run through the summer of 1992.

VI. INFORMATION EXCHANGE

Addresses of Key Personnel

Name	Address	Phone No.
Dr. Rachid Ababou	Center for Nuclear Waste Regulatory Analyses, Southwest Research Institute San Antonio, TX 78228-0510 USA	512-522-2583
Evaristo Bonano	Sandia National Laboratories Org. 6416 P.O. Box 5800 Albuquerque, NM 87185 USA	505-844-5303
Dr. Glendon Gee	Pacific Northwest Laboratory Box 999 Richland, WA 99352 USA	509-376-8424
Dr. Lynn Gelhar	Dept. of Civil Engr. 48-329 Massachusetts Institute of Technology Cambridge, MA 02139 USA	617-253-7121
Dr. Richard Hills	Dept. of Mechanical Engr. New Mexico State University Las Cruces, NM 88003 USA	505-646-4342
Timothy McCartin	USNRC, MS NL/S-260 Washington, DC 20555 USA	301-492-3847
Dr. Dennis McLaughlin	Dept. of Civil Engr. 48-209 Massachusetts Institute of Technology Cambridge, MA 02139 USA	617-253-7176
Thomas Nicholson (Pilot Group Leader)	USNRC, MS NL/S-260 Washington, DC 20555 USA	301-492-3856
Dr. Peter Wierenga	Soil and Water Science University of Arizona Tucson, AZ 85721 USA	505-646-2028

VII. POSSIBILITIES FOR ADDITIONAL COMPLEMENTARY EXPERIMENTS AND DATA COLLECTION

As discussed above, an additional experiment is planned for the near future at a different location on the north side of the trench. The purpose of the Plot 3 experiment is to further test validation methodologies and to validate stochastic and deterministic water flow and transport models on a larger field scale. Information gained during the Plot 2b experiment and suggestions from the INTRAVAL participants will be carefully considered during the Plot 3 experimental design.

Additional site evaluations (infiltration and redistribution tests) using similar techniques have been discussed. Cooperation with other US experimentalists to obtain well-characterized data sets of hydrologic properties for multiple sites is desirable. These data sets are presently not available in the detail needed to adequately test stochastic models.

VIII. EXPECTED OUTPUT FROM PROJECT TEAMS

A. Experimental View

The criteria for validation and the requirements for precision in measurements will be aided by interchange with scientists who are running similar tests. We expect that much of the validation testing may well be aided by improved techniques that may be available and used by other countries but not currently being tested (because of budget constraints, etc.) in the USA. These ideas, discussed and shared, will be valuable for enhancement of the study. The development and testing of transport codes for unsaturated soil systems will aid the experimentalist in designing appropriate tests to evaluate the transport parameters needed in the modeling component of the study.

B. Modeler's View

The modeler's view is quite similar to that of the experimentalist in that the exchange of ideas and modeling techniques with INTRAVAL participants from the USA and other countries will be useful. For example, as stochastic codes become available from other countries, these codes could be used/tested against data available from this project. The geostatistical approaches can be enhanced by discussion with experts from INTERVAL projects that routinely use spectral analysis and other techniques to obtain the statistical parameters needed in the stochastic model(s). The information exchange will be very valuable during all stages of this project.

IX. REFERENCES

Ababou, R., "Three-Dimensional Flow in Random Porous Media", Ph.D. Thesis, Department of Civil Engineering, Massachusetts Institute of Technology, Cambridge, Massachusetts, January 1988, 2 volumes, (1988).

Ababou, R. and L.W. Gelhar, "A High-Resolution Finite Difference Simulator for 3D Unsaturated Flow in Heterogeneous Media," Computational Methods in Water Resources, Elsevier and Computational Mechanics Publications, Vol. 1, pp. 173-178, (1988).

Davis, L. A., and Shlomo P. Neuman, "Documentation and User's Guide: UNSAT2 - Variably Saturated Flow Model," NUREG/CR-3390, U.S. Nuclear Regulatory Commission, Washington, D.C., (1983).

Gelhar, L. W., "Stochastic Analysis of Flow in Heterogeneous Porous Media. In Fundamentals of Transport Phenomena in Porous Media, J. Bear and M. Corapcioglu, eds. Martinus Nijhoff Publ. Dordrecht, Netherlands, pp. 675-717, (1984).

Gile, L. U., J. H. Hawley, and R. B. Grossman, "Distribution and Genesis of Soils and Geomorphic Surfaces in a Desert Region of Southwestern New Mexico, Guidebook," pp. 156. Soil Sciences Society of America and New Mexico State University, Las Cruces, (1970).

Hills, R.G., I. Porro, D.B. Hudson and P.J. Wierenga, "Modelling One-Dimensional Infiltration into Very Dry Soils - Part 1: Model Development and Evaluation," Water Resources Research, Vol. 25, No. 6, pp. 1259-1269, (1989a).

Hills, R.G., D.B. Hudson, I. Porro, and P.J. Wierenga, "Modelling One-Dimensional Infiltration Into Very Dry Soils - Part 2: Estimation of the Soil-Water Parameters and Model Predictions," Water Resources Research, Vol. 25, No. 6, pp. 1271-1282, (1989b).

Hills, R.G., P.J. Wierenga, D.B. Hudson, M.R. Kirkland, "Site Description, Experimental Results, and Two-Dimensional Flow Predictions for the Las Cruces Trench Experiment 2," submitted to Water Resource Research for review, (1990).

Huyakorn, P.S., J.B. Kool, and J.B. Robertson, "VAM2D - Variable Saturated Analysis Model in Two Dimensions," NUREG/CR-5352, U.S. Nuclear Regulatory Commission, Washington, DC, (1989).

Mantoglou, Aristotelis, and Lynn W. Gelhar. "Stochastic Modeling of Large Scale Transient Unsaturated Flow Systems." Water Resources Research, Vol. 23, No. 1. pp. 37-46, (1987a).

Mantoglou, Aristotelis, and Lynn W. Gelhar. "Capillary Tension Head Variance, Mean Soil Moisture Context, and Effective Specific Soil Moisture Capacity of Transient Unsaturated Flow in Stratified Soils," Water Resources Research, Vol. 23, No. 1, pp. 47-56, (1987b).

Mantoglou, Aristotelis, and Lynn W. Gelhar. "Effective Hydraulic Conductivities of Transient Unsaturated Flow in Stratified Soils," Water Resources Research, Vol.

23, No. 1, pp.56-68, (1987c).

Nicholson, T. J., and others, "Validation of Stochastic Flow and Transport Models for Unsaturated Soils: A Comprehensive Field Study, "Proceedings of USDOE-AECL Symposium on Geostatistical Sensitivity and Uncertainty Methods for Groundwater Flow and Radionuclide Transport Modeling, San Francisco, CA, (1987).

Polmann, D.J., E.G. Vomvoris, D. McLaughlin, E.M. Hammick, and L.W. Gelhar, "Application of Stochastic Methods to the Simulation of Large-Scale Unsaturated Flow and Transport," NUREG/CR-5094, U.S. Nuclear Regulatory Commission, Washington, D.C., (1988).

Wierenga, P. J., and others, "Validation of Stochastic Flow and Transport Models for Unsaturated Soils: A Comprehensive Field Study," NUREG/CR-4622, U.S. Nuclear Regulatory Commission, Washington, DC, (1986).

Wierenga, P.J., and M. Th. van Genuchten, "Solute Transport through Small and Large Unsaturated Soil Columns," Groundwater, Vol. 27, No. 1, pp.35-42, (1989).

Wierenga, P. J., A. Toorman, D. Hudson, J. Vinson, M. Nash, and R.G. Hills, "Soil Physical Properties at the Las Cruces Trench Site," NUREG/CR-5441, U. S. Nuclear Regulatory Commission, Washington, DC, (1989).

Wierenga, P.J., D.B. Hudson, R.G. Hills, I. Porro, M.R. Kirkland, and J. Vinson, "Flow and Transport at the Las Cruces Trench Site," NUREG/CR-5607, U. S. Nuclear Regulatory Commission, Washington, DC, (1990).

Yeh, T.-C. Jim, Gelhar, L. W., and Gutjahr, A. L., "Stochastic Analysis of Unsaturated Flow in Heterogeneous Soils 1. Statistically Isotropic Media." Water Resour. Res., Vol. 21, No. 4, pp. 447-456, (1985a).

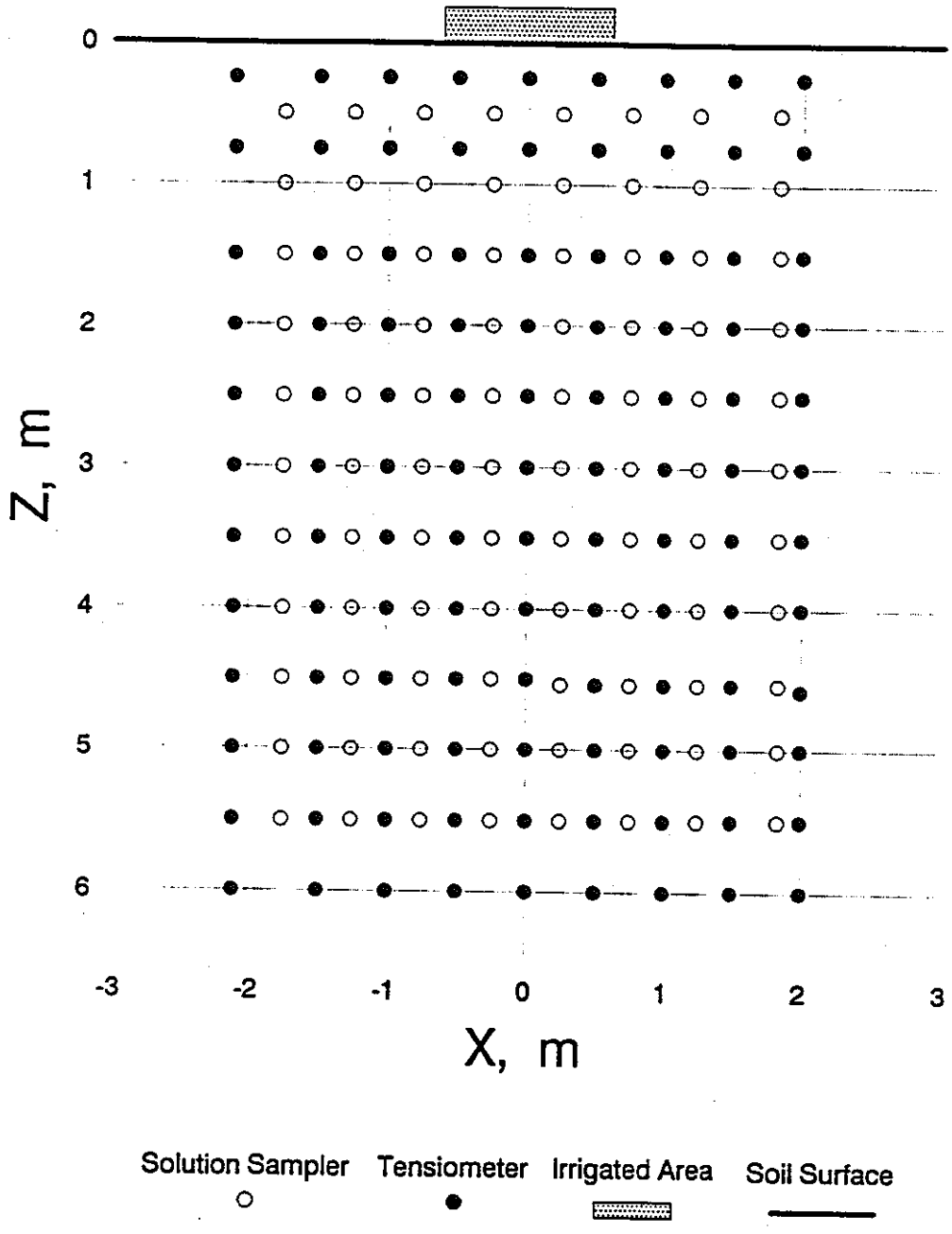
Yeh, T.-C. Jim, Gelhar, L. W., and Gutjahr, A. L., "Stochastic Analysis of Unsaturated Flow in Heterogeneous Soils 2. Statistically Anisotropic Media." Water Resour. Res., Vol. 21, No. 2, pp. 457-464, (1985b).

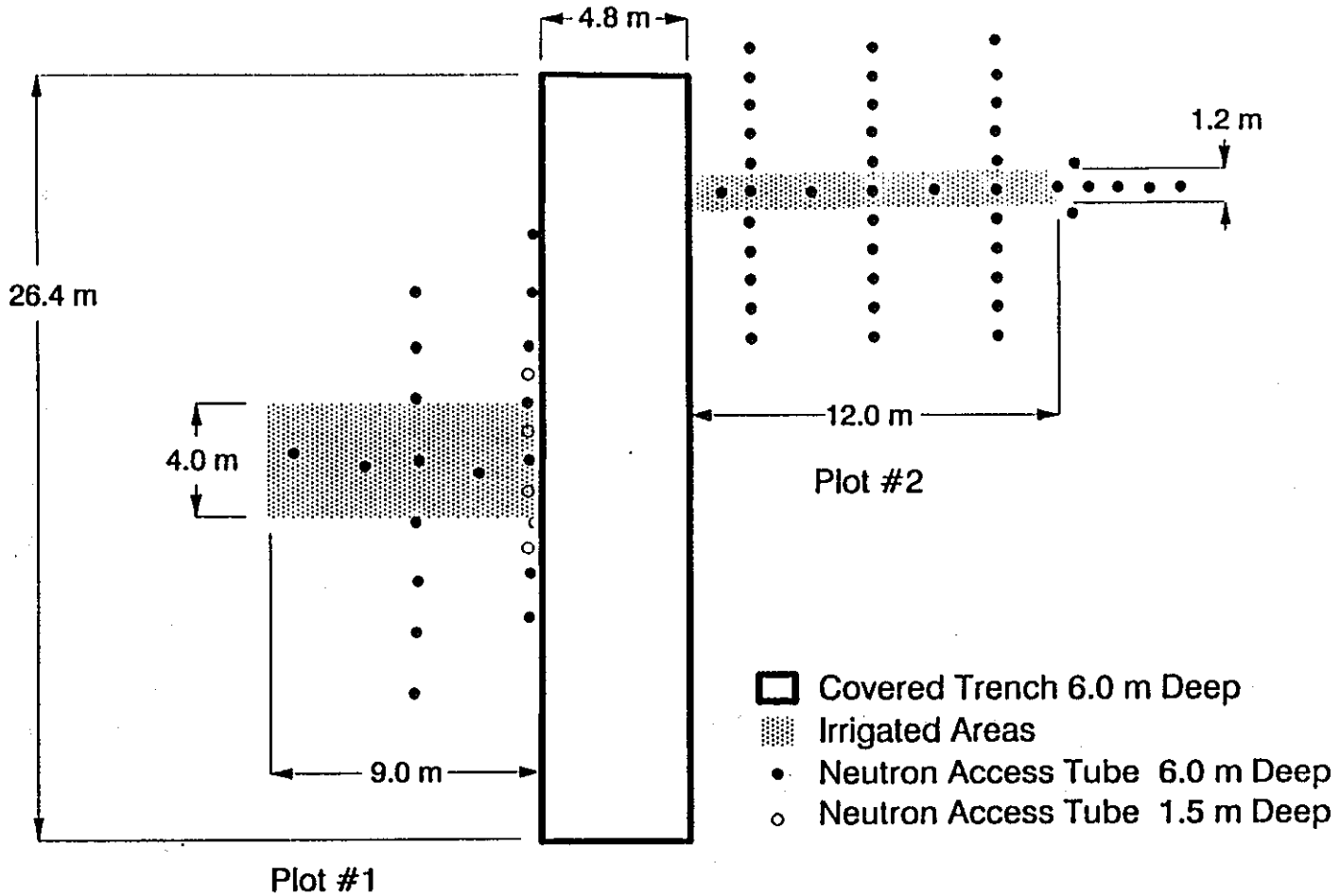
Yeh, T.-C. Jim, Gelhar. L.W., and Gutjahr, A . L., "Stochastic Analysis of Unsaturated Flow in Heterogeneous Soils 3. Observations and Applications." Water Resour. Res., Vol. 21, No. 4, pp. 465-471. (1985b).

LIST OF FIGURES

Figure 1. Location of the Tensiometers and Solution Samplers on the Trench Face for the Plot 2a Experiment.

Figure 2. Irrigated Areas and Neutron Probe Access Tube Locations for the Plots 1 and 2 Experiments.


0
1
2
3
4
5
6
Z, m
-3
-2
-1
0
1
2
3
X, m
Solution Sampler
Tensiometer
Irrigated Area
Soil Surface


4.8 m
1.2 m
26.4 m
4.0 m
12.0 m
Plot #2
9.0 m
Plot #1
Covered Trench 6.0 m Deep
Irrigated Areas
Neutron Access Tube 6.0 m Deep
Neutron Access Tube 1.5 m Deep

Bundesanstalt für Geowissenschaften und Rohstoffe

MENTE ET MALLEO

BUNDESANSTALT FÜR GEOWISSENSCHAFTEN UND ROHSTOFFE

HANNOVER

INTRAVAL PHASE II

Test Case : Saline Groundwater Movement in an Erosional Channel Crossing a Salt Dome

(Part 1)

1. Compiled by K. Schelkes
   R.-M. Knoop
   N.Geißler

2. Commissioned by Fed. Ministry of Science and Technology

3. Date November 1990

4. BGR File No. 107.849

5. BGR Record No. 13.106/90

Introductory remarks

In INTRAVAL Phase II it is planned to validate models taking into account the variable density of the groundwater with the test case "Saline Groundwater Movement in an Erosional Channel Crossing a Salt Dome". Basic work for the preparation of this test case was done during Phase I of the INTRAVAL project. Due to certain circumstances the data preparation was delayed and could just be finished now at the end of Phase I with the first part of the data sets. But this delay is more or less compatible with the time schedule of the salt working group, because the processing time for the INTRAVAL test case 13 " Experimental Study of Brine Transport in Porous Media" took much longer than planned.

This report contains the documents and data sets which may be used for the first part of the above-mentioned test case, the validation exercise "The Weisses Moor Pumping Test". Most of the material is also responsible for the second part "Saline Groundwater Movement in the Gorleben Erosion Channel". If data are missing, it has to be discussed in detail. There is the possibility to enlarge the data base to a certain extent.

The authors thank the BfS, Salzgitter, who is conducting the hydrogeological investigation program in the area of the Gorleben salt dome, for permission to use their data for this INTRAVAL test case.

Table of contents

Part I. Introduction

A. Pilot group
B. Experimental location and brief description
C. Original purpose
D. Objectives in INTRAVAL Phase II
E. Validation aspects

Part II. Background information

A. General remarks
B. The hydrogeology of the "Gorleben Erosion Channel"
C. Hydraulic conductivities and porosities
D. Groundwater densities and groundwater hydraulic
E. General information on salinometer data

Part III. Pumping test in highly saline groundwater

A. Description of the experiment
B. Available experimental results
C. Previous modelling
D. Current status, experimental schedule, complementary work
E. Expectations from project teams

Part IV. Introduction to the general case : Saline groundwater movement in the "Gorleben Erosion Channel"

A. Description of the case
B. Available experimental results
C. Possibilities for complementary experiments

Part V.

A. Information exchange
B. References
C. Table of contents (Appendixes)

Appendix 1 : Technical report "The Weisses Moor Pumping Test"

Appendix 2 : Description of the data sets

Appendix 3 : Figures and tables

Appendix 4 : Salinometer and temperature data (figures and tables)

Appendix 5 : Maps and cross sections

Appendix 6 : Data diskettes

Test Case :

Saline Groundwater Movement in an Erosional Channel Crossing a Salt Dome

(Part 1)

Part I. Introduction

A. Pilot group

The Pilot Group for this test case is the Bundesanstalt fuer Geowissenschaften und Rohstoffe (BGR), Hannover, in cooperation with the Bundesamt für Strahlenschutz (BfS), Salzgitter. The Pilot Group leader is Klaus Schelkes (BGR).

The BfS is conducting the hydrogeological investigation program in the area of the Gorleben salt dome, which is being carried out for site characterization and long-term safety assessment studies. The BGR is entrusted with the geoscientific direction and evaluation of the investigations carried out by contractors and the BGR itself.

The Pilot Group will provide the necessary information for evaluation of the Test Case on the basis of the existing data sets and continuing collection of field data. The performance of additional measurements will be possible to a certain extent in connection with the second phase of the Test Case.

B. Experimental location and brief description

The Gorleben salt dome, located in the northeastern part of Lower Saxony in the Fed. Rep. of Germany, is under investigation as a candidate site for final disposal of radioactive waste (Fig.3.1). This salt dome is approximately 14 km long, up to 4 km wide and its base is more than 3000 m below surface. Hydrogeological investigations were conducted in an area of about 300 km^2 around the salt dome to study the aquifer system in the sediments above the dome. A good picture of the hydrogeological situation has been obtained from these studies.

The Tertiary and Quaternary sequences form an aquifer system up to 300 m thick, normally divisible into two aquifers. The lower aquifer consists of Miocene lignite sands or Elsterian sands and gravels in subglacial erosion channels. One such channel, the so called "Gorleben channel", which is more than 10 km long and between 1 and 2 km wide, crosses the area of the salt dome from

south to north (Fig.3.2). Erosion along this channel extends down to the cap rock (a residue of the dissolution process of salt in groundwater) and in some places down to the salt itself. In the channel, fairly thick sandy sediments with interbedded lenses of till are overlain by a complex of silt and clay up to 110 m thick. Throughout the investigation area, the freshwater in the upper part of the aquifer system is underlain by saline groundwater. The salt content of the water usually increases with depth (Fig.3.3). Directly above the salt dome saturation may be reached at depths greater than 240 m below ground surface.

Pumping tests have been carried out at several locations within the " Gorleben channel" . One of these areas, located about 2 km southeast of the small village of Gorleben, is called " Weisses Moor" (Fig 3.5). Here, the lower aquifer was tested by withdrawing highly saline groundwater at a rate of 30 m^3/h for a period of three weeks. Responses were observed in all observation wells in the "Gorleben channel" which had screens in the lower aquifer.

C. Original purpose

The principal aim of the investigation is to understand and determine the groundwater movement in the strata surrounding a salt dome. Freshwater in the uppermost parts of the aquifer systems is in such situations commonly underlain by highly saline groundwater. The salt concentration usually increases with depth and reaches that of saturated brine near the top and the flanks of the salt dome. Here, dissolution of salt occurs, finally leading to formation of a cap rock. The groundwater movement in such an aquifer system depends to a large degree on its salinity, which influences the water density. Special experiments have been carried out to obtain information on hydrogeological structure, hydraulic parameters and groundwater movement.

D. Objectives in INTRAVAL Phase II

The objective of this test case is to calibrate and validate to a certain extent groundwater flow and transport models in which fluid-density variations depend on the salt content by comparing model results with measured field data. In INTRAVAL Phase I, a laboratory experiment simulating brine-front migration has been studied. The model simulation led to questions about the applicability of Fick's law under large density gradients. No consensus was reached.

The question was also raised whether this phenomenon is relevant in natural field situations, where usually only small density gradients occur. With this in mind, it was suggested simulating in

the next step a pumping test in which saline groundwater is in motion. In a pumping test, the natural groundwater flow field is masked by the flow field resulting from withdrawal of water. Therefore, detailed characterization of the regional flow field is not required. Under these conditions flow of the saline water is predominantly by advection. Dispersion and diffusion are of secondary importance.

After completion of the pumping test modelling, time and length scales will be extended in order to attempt to validate a model of regional ground water flow, salt dissolution and their interaction. For this reason, the flow situation in the whole channel will be considered. This should provide an opportunity to validate numerical modelling of a true field situation.

The hydrogeological system in the overburden of the Gorleben salt dome is very complex with heterogeneous hydraulic properties and complex boundary conditions. The groundwater density varies spatially, normally increasing with depth. At some locations in the aquifer system, however, rather high salinity is observed near the land surface. The geometric scale ranges over several km in length and 2 km in width. The time scale ranges from a few weeks for the evaluation of the density-influenced pumping test to several 10000 years for the calculation of the density-dependent groundwater movement for the natural flow system.

E. Validation aspects

This test case is intended to address the validation of models for complex, natural flow systems which are characterized by inhomogeneous geological settings and anisotropic geohydrological parameters.

So far, constant-density models have usually been used in order to simulate the natural groundwater system in the strata surrounding salt domes or bedded salt layers which are candidate sites for final disposal of radioactive wastes. From previous work (e.g. HYDROCOIN) it became obvious that the groundwater flow is very different when groundwater density variations are present. These variable-density models based on the concept of the classical coupled flow and transport equations need to be validated in field situations in which density variations have been observed. These validation goals may be approached in two different scales in this test case. The first phase of this study, a pumping test interpretation, will focus on a situation in which time scale effects and dissolution phenomena are of secondary importance. In this validation exercise, a model calibration should be carried out by using data from the first part of the drawdown measured in observation wells. Then the results of the full pumping test are used to check the model simulation.

In the second phase, a validation exercise will be attempted on a large spatial scale with long-term geohydrological effects such as the dissolution of rock salt. By use of the knowledge from site investigations a conceptual model will be constructed. Important assumptions will be the choice of the initial hydrological conditions, the description of the hydrogeological structure, the mathematical description of the lower boundary condition (salt dissolution), the initial groundwater density distribution, and the geological period for which modelling is done.

The model simulations should clarify the validity or invalidity of the underlying variable-density flow concepts. The ability of the models to simulate a dissolution boundary condition should, however, be tested. As validation criteria one can consider the present day water density distribution, measured flow velocities with deducible mass fluxes and measured or calculated pore water pressures.

The models for the regional-scale flow systems that take into account water density and processes such as dissolution are needed to improve confidence in geosphere migration modelling as part of safety assessment studies for repositories in salt structures. Furthermore, this type of model is necessary for site characterization. It will be applied to assess the quality of the strata surrounding the salt structures as a geohydrological and geochemical secondary barrier in case that radionuclides are released from the rock-salt formation.

Part II. Background information

A. General remarks

The Gorleben salt dome is situated in the northern part of LowerSaxony (Fig.3.1). Hydrogeological investigations were conducted in an area of about 300 km^2 around the salt dome to study the aquifer system in the sediments above the dome. During this geological and hydrogeological survey program, the basic information was obtained from

- drilling of exploratory boreholes with core sampling and geophysical logging;
- observation wells for geophysical logging, water level measurements, water sampling and special studies;
- seismic and geoelectrical measurements;
- extensive pumping tests.

Large quantities of data were acquired and stored on

- the geology;
- porosity, from geophysical log evaluation and core samples;
- permeability, from core samples and pumping tests (also providing values for storativity);
- chemical composition, density, electrical conductivity, isotopic composition of the groundwater;
- electrical conductivity distribution with depth around selected boreholes and vertical temperature profiles at all borehole locations;
- groundwater levels and the electrical conductivity distribution in the wells;
- pore water pressure in the screens of some of the observation wells, from direct pressure measurements; etc.

A short overview of the hydrogeological and hydraulic situation of the entire study area is given in Vierhuff (1984) and Fielitz et al. (1984) or in Jaritz et al. (1986), who also gives information on the salt dome itself.

B. The hydrogeology of the "Gorleben Erosion Channel"

A characteristic feature of the base of the Quaternary in North Germany is the presence of buried channels or overdeepened valleys, which are found as deep as 400 m below mean sea level (msl). They are probably erosion channels cut down into the then land surface by melt-waters beneath the ice sheet after the maximum of the Elsterian glaciation, i.e. after the Elsterian ice sheet had reached its most southerly extension.

The channels were partially filled by predominantly subglacial sand and gravel containing detached masses of till. During the melting of the Elsterian ice sheet, sediments known as the Lauenburg Clay Complex were deposited in unfilled hollows in the

channels. These sediments consist predominantly of silt and clay with minor layers of sand and rarely gravel, and in addition rare masses of till which slid into position or were transported from elsewhere. A few sand beds can be followed along the channels for several kilometres, but over a much shorter distance across the channels.

Since the Lauenburg Clay Complex sediments did not completely fill the channels, the distribution of the predominantly fine-grained sediments laid down during the subsequent Holsteinian Interglacial is largely determined by the positions of the channels. Re-inundation of the land by ice, this time the Saalian ice sheet, completely changed the Holsteinian landscape in North Germany. The subglacial channel sediments and the lower parts of the Lauenburg Clay Complex were mostly not affected by erosion during the Saalian. However, the Holsteinian sediments and the upper parts of the Lauenburg Clay Complex were removed from much of the area or were deformed and contorted by the ice.
The Gorleben erosion channel represents a small part of the branching north German Pleistocene channel system. This particular channel is 3 - 4 km wide where it traverses the Gorleben salt dome east of the line Vietze - Gorleben - Trebel. The channel probably continues its course northwards under the River Elbe. To the south it joins the less well developed Gartow channel (Fig.3.2).

The Gorleben channel reaches its deepest depth below sea level in the north between the boreholes GOHY 480 (E of Gorleben) and GOHY 650 (on the western edge of the Höhbeck hill). Here it is locally deeper than 275 m below msl. Above the salt dome, the shape of the channel bottom is particularly complicated and is very variable even on a small scale (see map of the base of Quaternary, Appendix 5.3.1)

The Gorleben channel is cut predominantly in Tertiary sediments; above the salt dome it has cut down into the cap rock over an area of about 4.5 km^2. Here, the sediments in the channel are in direct contact with the salt dome. Locally, the erosion has cut down through the cap rock as far as the salt itself over a few 100 m^2.

Within the channel, sedimentation began with basal sand and gravel in which masses and lenses of boulder clay are frequently intercalated. These basal Elsterian channel deposits are locally coarse. Some boreholes penetrated Elsterian basal sands and gravel containing angular fragments of rock salt. (This observation demonstrates that the pore spaces must have been exclusively filled with highly concentrated brine since the Elsterian sedimentation).

The sands and gravels locally interfinger over a depth of a few meters with sandy beds containing lenses of silt and clay; these sandy beds persist for several tens to hundreds of meters. The deposits in the channel constitute a permeable sequence, the channel aquifer. The channel aquifer is overlain by the Lauenburg Clay Complex, which has a maximum thickness of 110 m and is Elsterian in age. It has a relatively level lower boundary and consists primarily of clays and silts with minor layers of sand. The lower boundary of the Lauenburg Clay is gradational; it is mostly represented by a transition from predominantly sandy deposits below to silts and clays above, over a vertical thickness of several meters to a few tens of meters.

The Lauenburg Clay Complex (see structure contour-map of the Lauenburg Clay above the erosion channel, in Appendix 5.3.2) occurs above the Gorleben and Gartow channels and part of the northern marginal trough. It almost completely covers the so-called channel aquifer above the salt dome, thus nearly isolating it hydraulically from the shallower aquifers. The channel aquifer is therefore a confined aquifer. For further information see the cross sections in Appendix 5.4.

C. Hydraulic conductivities and porosities

Evaluations of short-term pumping tests supplied the values kfh for hydraulic conductivity in the horizontal direction, whereas those for the vertical direction, kfv, were mostly obtained from examination of samples. The hydraulic conductivity values, calculated from the grain size distribution of rock samples with the aid of the "Hazen formula", for the most part, lie between these two values. The ratio of vertical to horizontal hydraulic conductivity kfv : kfh is normally 1 : 10; for boulder clay and till 1 : 2.

The hydraulic conductivity values can be assigned to geological units:

a) Middle to coarse sands of the Quaternary:

upper aquifer	: kf	$< 1 * 10^{-3}$ m/s
lower aquifer	: kf	$5 * 10^{-5}$ to $5 * 10^{-4}$ m/s
mean	: kf	$5 * 10^{-4}$ m/s

b) Lignite sand of the Tertiary:

kf $5 * 10^{-5}$ to $5 * 10^{-4}$ m/s

c) Silt : kf is usually less in the Tertiary than in the Quaternary.

Hydraulic conductivity was measured directly on samples offine-grained and more cohesive material. Some of the material was compacted according to the German standard 18127 (DIN 18127). The results can be seen in Table 1 (Giesel et al, 1985).

Type of sediment	Hydraulic conductivity kf in m/s: mean value	lowest measured value	highest measured value	Number of measure-ments
fine sand	$1.3 * 10^{-8}$	$1.9 * 10^{-10}$	$9.9 * 10^{-7}$	40
silt	$1.2 * 10^{-9}$	$1.3 * 10^{-10}$	$1.5 * 10^{-8}$	22
clay	$8.3 * 10^{-10}$	$8.2 * 10^{-11}$	$4.8 * 10^{-9}$	16

Table 1: Measured hydraulic conductivities for unconsolidated rock samples

Long-term pumping tests were conducted from May of 1983 to April of 1985 at the three locations, "Weisses Moor", "Meetschow", and "Gorlebener Tannen" to determine the hydraulic characteristics of the rock overlying the salt dome. The values obtained are shown in Table 2. The kfv value refers here to the cover of the respective aquifer. The data were obtained from the evaluation of the pumping tests with a constant groundwater density approach (see also BGR 1983c).

	"Weisses Moor"		"Meetschow"	"Gorlebener Tannen"
	lower aquifer	upper aquifer		
T (10^{-3} m^2/s)	1 - 2	20	0.7 - 2	3 - 12
S (10^{-4})	3 - 9	5 - 8	1 - 8	2 - 8
kfh (10^{-5} m/s)	2 - 5	30 - 40	2 - 7	4 - 17
kfv (10^{-9} m/s)	5	200 - 300	-	-
aquifer thickness (m)	50	60	30	70

Table 2: Hydraulic characteristics of the overlying rock, determined from long-term pumping tests

Measurements of total porosity were mostly conducted on fine-grained and cohesive materials. The measured values generally indicate the fairly large variation of the porosity values within the individual unconsolidated sediments. Porosity was not recognized as dependent on the depth (Giesel et al, 1985). Table 3 shows the relationship between the total porosity and the major component for various sediment samples.

type of sediment	Total porosity (%) lowest measured value	highest measured value	mean value	number of measure-ments
fine-medium grain sand	21	46	32.3	7
fine sand	22	47	38.4	33
silt	22	46	38.3	17
clay	25	46	37.4	14

Table 3: Measured total porosity of unconsolidated rock samples

It is important to know the effective porosity of the unconsolidated rock when determining the pore velocity from the Darcy velocity. The effective porosity is always less than the total porosity, whereas the difference is small for coarse-grained sediments and rises with decreasing grain size (i.e. clay content). One way to approximately determine the effective porosity is to use borehole measurements. Porosity, as well as clay and silt content, was determined from geophysical borehole logs. The values obtained in this manner, graphically depicted as a continuous depth profile, provide an overview of these quantities for the different strata overlying the salt dome (BGR 1983a).

One of these values, the clay-corrected porosity, is an approximation of the effective porosity. The relationship between these two porosity concepts is discussed in more detail in BGR 1983a. From the figures shown in that report it is possible to approximately determine how large the portion of pore volume (excluding the clay and silt pore volumes) is and how large the volume portion of clay, fine-grained and medium-grained silt is at each depth. The calculated logs also show the finer classification of the strata which could not be further differentiated using the rinsing samples. Average clay-corrected porosity values were able to be given for strata with a certain major component (Table 4). It must be observed however, that some individual values that refer to certain strata can deviate relatively greatly from these mean values.

Major component	Mean value of the clay-corrected porosity
Coarse sand	approx. 32%
Medium to fine sand	approx. 28%
Silty sand	approx. 15%
Silt	approx. 10%
Clay	approx 7%

Table 4: Mean values for clay-corrected porosity

All the data on hydraulic parameters given up to now in this section, and data on its geological structure were used for the preparation of a provisional hydrogeological model. In this process, the following classes, each in summary form, were formed: gravel and sand, boulder clay and silt, clay and, divided into two classes, the cap rock. Characteristic hydraulic conductivity and effective porosity values are allocated to each class. These are listed in Table 5.

type of sediment/rock		hyd. conductivity [m/s] kfh	hyd. conductivity [m/s] kfv	eff. porosity [%]
gravel and sand	upper aquifer	$5 * 10^{-4}$	$5 * 10^{-5}$	30
	lower aquifer	$5 * 10^{-5}$	$5 * 10^{-6}$	30
boulder clay and silt		$5 * 10^{-6}$	$5 * 10^{-7}$	20
clay		$5 * 10^{-9}$	$5 * 10^{-10}$	10
cap rock	Karst	$1 * 10^{-5}$	$1 * 10^{-5}$	2
	Quaternary interstrat.	$5 * 10^{-5}$	$5 * 10^{-5}$	10

Table 5: Summary of hydraulic conductivity values horizontally and vertically to stratification, kfh and kfv, and effective porosity values

D. Groundwater densities and groundwater hydraulics

At each investigation borehole site, groundwater observation wells were drilled to various depths depending on the local aquifer system. In total, more than 300 observation wells have been installed in the area; these permit the piezometric head of groundwater to be monitored at different depths, water samples to be taken for chemical and isotope analysis, and various measurements made which enable the pressure distribution in the aquifer system and the velocity and direction of the groundwater flow to be determined.

The area is quite flat with differences in elevation of 5-15 m between gentle hills and the receiving streams. Below the higher elevations, the groundwater table (groundwater regeneration rate equal to 180 mm/yr maximum) is about 8 m higher than the level of the receiving streams. The water level contour map shows that the regional groundwater flow is predominantly from the southeast towards the northwest and that there is a local recharge mount south of the dome (Fig.3.1). The hydraulic gradient from the

higher elevations to the discharge areas in the uppermost aquifer is about 1-1.5 * 10^{-3}. If permeabilities of $1*10^{-4}$ to $5*10^{-3}$ m/s are assumed for this aquifer, the Darcy velocities are in the range of 5 - 250 m/yr, which is also found with direct flow measurements (see groundwater level contour maps, Appendix 5.2).

The groundwater flowing from the slightly elevated areas towards the surrounding lower areas penetrates the sediments almost to the salt dome at 200 - 250 m depth. Here saline water is found. Throughout the study area, the freshwater body is underlain by rather saline water. The boundary between fresh and saline water (10 ohm m line) is at a depth of more than 150 m in the northwestern and southeastern surroundings of the salt dome and rises to less than 50 m below sea level near the erosion channel above the salt dome. The salt content usually increases with depth. At depth greater than 240 m, saturated brines are found only directly above the salt dome. In some parts of the area, a comparatively high salinity is observed at shallow depths. At some places, saline water overlies fresh water. As an example, Figure 3.3 shows the density of water samples as a function of depth. At depths of 170 - 200 m below m.s.l., there is a very steep increase from 1020 to about 1170 kg/m^3. Below this transition zone, there is only a small increase in the density up to that of saturated brine (about 1200 kg/m^3).

The groundwater densities that were measured along a section of the quaternary channel have been entered in Figure 3.4. Groundwater observation wells, from which the data is used, are projected in the section. The lines of equal densities are based on density measurements made on water samples. The mean slope of the lines of equal densities and their vertical interval are, despite existing variations in the measured values, satisfactorily ensured for the given section course. The steepest density increase is in the above-mentioned transition zone with a thickness of about 30 m between 170 and 200 m below mean sea level. The isolines of equal densities slightly increase toward the north, i.e. in the flow direction of fresh water in the uppermost aquifer, with a gradient between 1.5 * 10^{-3} m/m and 3.5 * 10^{-3} m/m. But the positions of the inclined lines are not constant vertical to this cross-section and, especially for densities smaller than 1050 kg/m^3, the variation of the measured data is considerabely increasing.

Calculations of the flow velocity of salt water can be made from the information concerning the slope of these equal density lines using special approaches (BGR 1983b). Assuming the hydraulic conductivity values of fine sand the flow velocity is in the meters per year range, and it tends to decrease with depth from above to below (Fielitz et al. 1984, Giesel & Fielitz 1983). Corresponding values are also obtained from direct flow measurements in the screen sections of groundwater observation wells. The tendency of the flow velocity to decrease with depth is, although present, restricted.

E. General information on salinometer data

Electrical conductivity and temperature of the water within the casing were measured during geophysical well logging using a combined salinometer and temperature probe. This data was used to calculate approximate values of the groundwater densities at the depth of the screens and average densities of the water within the well. The latter is needed to calculate pore water pressure. Densities were calculated in three steps from the data measured at depth increments of 0.2 m.

Step (1): Calculation of a temperature-corrected electrical conductivity (reference temperature 20° C)

The following empirical formula is based on the results of the calibration of the probe with salt solutions of known concentration and temperature:

$$C20 = K * C / (1 + 0.0187 * (T - 20))$$

where

C : measured electrical conductivity [microS/cm],
C20 : electrical conductivity at 20°C [microS/cm],
T : measured temperature [20°C],
K : correction factor for the probe:
= 1.006 for salinometer probes TS1 and TS2,
= 1.0 for other salinometer probes.

Step (2): Calculation of the density at reference temperature

The following formula is based on data from the CRC Handbook of Chemistry and Physics (Weast, R. C. (ed.), 1974)) for pure NaCl solutions:

$$RHO20 = 998. + 10 * (3.981 * C20^1 + 5.558 * C20^2 - 12.76 * C20^3 + 14.67 * C20^4 - 7.397 * C20^5 + 1.377 * C20^6),$$

where

C20 : electrical conductivity at 20 °C [100 mS/cm]
RHO20 : fluid density at 20°C [kg/m^3].

Step (3): Calculation of the density at in-situ temperature

The following is an empirical formula based on BGR data:

$$
\begin{aligned}
RHO = {} & RHO20 + \\
& (0.16071 - 0.150464E{-}3 * RHO20) + \\
& (0.151134E{+}1 - 0.17298\ E{-}2 * RHO20) * (T - 20)^{1} + \\
& (-0.353166E{-}1 + 0.302242E{-}4 * RHO20) * (T - 20)^{2},
\end{aligned}
$$

where

RHO20 : fluid density at 20°C [kg/m³],
RHO : fluid density at in-situ temperature [kg/m³],
T : in-situ temperature [°C].

Results of the electrical conductivity and density calculations are shown in Appendixes 3.8 and 4.

Part III: Pumping test in highly saline groundwater

A. Description of the experiment

During the hydrogeological investigation program four pumping tests were carried out: one in fresh water and three in saline water. There were two reasons for doing the pumping tests. The first was more qualitative, namely to obtain information on boundaries, the hydrogeological structure of the area, connections between different aquifers, etc. The other important information we expected to receive from the tests was about hydraulic parameters, like permeability, storage and leakage coefficients, and their distribution in the pumped area.

One of the areas where a pumping test in saline water was carried out, the "Weisses Moor" area, is about 2 km southeast of Gorleben (Fig. 3.5). The pumped well penetrates the entire deeper aquifer in the erosion channel filled with saline water. The aquifer is between 20 and 100 m thick. The top of the aquifer consists of silty or clayey layers, sometimes boulder clay (marl). The base of the aquifer consists of gypsum or Tertiary clay and in some parts the salt itself (Fig. 3.6).

The connection of this lower aquifer with the upper aquifer was not observed during the pumping test. But there were observable connections with groundwater in the caprock.

The long-term pumping test was carried out with a pumping rate of 30 m^3/h over a period of 3 weeks. The electrical conductivity of the water was nearly 165 mS/cm, i.e. a density of approximately 1100 kg/m^3. The density ranges in the pumped aquifer from 1010 kg/m^3 up to 1200 kg/m^3. All of the relevant observation wells were monitored more than once a day for 5 weeks and after that time up to two times a week. (see also location map, Appendix 5.1) The measurements in the closest observation wells were made with an ultrasonic apparatus that measures levels with a precision of better than 1 mm. At the beginning and the end of the pumping test, electrical conductivity logs were made in all of the observation wells involved to obtain information on any changes in the salinity distribution in the wells themselves. How much water was extracted from each part of the sreen section of the well was determined from flow meter logs at the beginning and the end of the pumping phase. The density of the water was determined from electrical conductivity logs and measurements on water samples. The electrical conductivity and the amount of the water pumped were recorded continuously during the test.

A description of the pumping test including all information on its performance is given in the technical report (Appendix 1).

B. Available experimental results

The following data from the pumping test in the "Weisses Moor" area conducted in 1984 is available:

1. basic information

   - map of the borehole locations (App. 5.1)

2. hydrogeological data

   a) maps showing

      - base of the Quaternary (App. 5.3.1)
      - base of the Lauenburg clay complex (App. 5.3.2)
      - hydraulic contacts at the sides and bottom of the erosion channel (App. 5.3.3)
      - groundwater level contours (App. 5.2)

   b) hydrogeological cross sections : 3 N-S, 11 E-W profiles (App. 5.4)
   (3 permeability classes, precise representation of the lower aquifer, but that of the upper aquifer is simplified)

   c) geological description of the boreholes used for the maps and cross sections if they were needed to understand the hydrogeology of the erosion channel. The data sets include the locations, stratigraphy and petrography (only major component).
   If the borehole penetrates the caprock or the salt, the description ends with the statement "base of the aquifer" without further specification (App.3, Table 1).

3) pumping test data

   a) technical report of the "Weisses Moor" pumping test (App.1)

   b) basic data for observation wells (App.3, Table 2)

   c) hydrographs for the observation wells for the year 1984 (data measured with electric-tape gauges, ultrasonic probes, and pressure gauges)

   d) salinometer logs for the observation wells (App. 3.8.4) (with calculated water densities)

   e) pumping test data: pumping rates, electrical conductivity and temperature of the pumped water, rainfall, barometric pressure, flowmeter results (App. 3.7)

   f) density and electrical conductivity of the groundwater measured in the laboratory (App. 3, Fig.3 and Tab.3)

4) The data will be sent to the interested parties on diskettes and/or as tables, figures, texts etc.

   - data sets 2c, 3b, 3c, 3d, 3e, 3f
     (data sets for 2a, 2b as autocad files)

   - figures etc.: 2a, 2b, 3c, 3d, 3e

   - tables: 2c, 3b, 3c (selected data), 3d, 3e (selected data),3f

5) The formats and the structure of the data sets on the diskettes are given in Appendix 2. Appendixes 3 and 4 contain the tables and figures, Appendix 5 the maps and cross sections.

C. Previous modelling

The evaluation of the pumping test with the constant density approach was made at the end of 1985. The parameters were calculated using analytical and numerical models. The results of this work are also available. However, it is important to keep in mind that it is not possible to say exactly how large an error results from neglecting variations in density. To our knowledge, no one has done model simulations for pumping tests in highly saline groundwater.

D. Current status, experimental schedule, complementary work

The pumping test was conducted in 1984. There is no possibility for future experiments.

E. Expectations from project teams

This pumping test provided the opportunity to observe the behavior of a groundwater system filled with highly saline water under simplified conditions, i.e. a system with predominantly convective flow. These tests in the Gorleben area are probably the first tests involving such high salinities. The existing database should besufficient for a test case. It is not possible to expand it.

When this pumping test is simulated, the models should have the option of non-steady-state conditions and density variations, as well as having a 3-dimensional option or, at least as a first approximation, 2-dimensions with radial symmetry. (see also Part I, chapters D and E)

Part IV. Introduction to the general case: Saline groundwater movement in the Gorleben Erosion Channel

A. Description of the case

The erosion channel crossing the Gorleben salt dome is more than 10 km long and its width varies between 1 and 2 km. Highly saline water is found in the lower aquifer in this channel, which is overlain by a complex of silt and clay. The objective is to describe the complex groundwater flow system in this channel with models that include variable density.

A overall description of the system is given in part I, F: Background information. In addition, the following remarks refer to the determination of the model boundaries:

It is not possible to give simple boundary conditions for numerical modeling of this realistic field situation. Fig.10 shows a map of the area to be modelled. Some information on the boundaries is given below (see also App. 5.3.3). The southern boundary is defined by a groundwater divide. At this boundary the water is no more than brackish at depth. This water divide is also suggested as the southern boundary for the deeper aquifer.

In the upper aquifer, which contains fresh water, locally brackish water, two of the flow lines derived from the contour map of the groundwater table are suggested as the eastern and western boundaries. The definition of these boundaries for the lower aquifer, in which the groundwater is saline to concentrated brine, is not so easy. The erosion channel crosses the salt dome from NNE to SSW after leaving the recharge area south of the salt dome. In most parts, the lower aquifer is not present on either sides of the erosion channel and the boundary is formed by clayey layers. But there are some exceptions. On both sides of the southern end of the channel there is a good connection between the Quaternary sands of the channel and thick sandy Miocene layers surrounding the salt dome. On the western boundary further to the north, a side channel branches off from the main channel. The permeability where the side channel branches off is not as good as that of the sands in the channel itself. Moreover, on the western boundary in the northern part of the salt dome, it is not yet clear whether there is a connection, possibily via a thin sandy layer, with the Miocene sands north of the salt dome.

A special problem exists for the northern part of the area to be modelled. The hydrogeology of the Gorleben area and the erosion channel is well known on the south side of the River Elbe. There is little information available about the other side because the River Elbe formed the boundary between the Federal Republic of Germany and the former German Democratic Republic. But the discharge area for the groundwater in the lower aquifer is the topologically lowest part of the region, which is north of the River Elbe. Especially for this area, the data base will be enlarged in the near future. In addition to these difficulties, there are a few other problems of less importance, such as several areas mentioned above which have brackish water locally in the upper aquifer. These boundary problems, as well as the specific area to be modelled, should be discussed in detail.

B. Available experimental results

During the geological and hydrogeological survey program, large quantities of data were acquired and stored (see part I, background information). Now, first data sets are prepared for a validation exercise. The preparation is going ahead.

A number of borehole profiles, cross sections and maps are available as a database of the hydrogeology. Based on this data a generalized cross-section along the axis of the channel can be constructed, taking into account the hydrogeology of the whole channel as much as possible. In addition, the hydrogeological input data of a three-dimensional geohydraulic model developed by the BGR (1987) is also available. A current preparation of the hydrogeological data for automatical production of maps and cross sections in an rectangular net would provide the best basis for the implementation of the hydrogeology, if it will be completed in the next year.

The following documents and data sets are prepared (see part III):

1. basic information
   - map of the selected borehole locations

2. hydrogeological data
   a) maps showing
      - base of the Quaternary
      - base of the Lauenburg clay complex
      - hydraulic contactcs at the sides and bottom of the erosion channel
      - groundwater level contours
   b) hydrogeological cross sections: 3 N-S, 11 E-W profiles
   c) geological description of the boreholes used for the maps and cross sections if they were needed to understand the hydrogeology of the erosion channel.

3. pumping test data usuable for this exercise:
   a) basic data for the selected observation wells
   c) hydrographs for these observation wells for the year 1984
   d) selected salinometer logs for these observation wells (with calculated water densities)
   e) density and electrical conductivity of the groundwater measured in the laboratory

4. Information on the kinds, formats and structures of the data sets is given in part III.

C. Possibilities for complementary experiments and data collection -

The data base can be enlarged to a certain extent by field work to obtain special information like pore water pressure or electrical conductivity and density of the groundwater. But most oft the geological and hydrogeological field work has been completed and most of the data has been prepared for processing. Preparation of the data for the part 2 of the test case is in progress.

BUNDESANSTALT FÜR GEOWISSENSCHAFTEN UND ROHSTOFFE

HANNOVER

For the BGR:

(Dr. H. Venzlaff)
-Ltd. Direktor und Professor-

For the authors:

(K. Schelkes)
-Wiss. Rat-

Part V.

A. Information exchange

Klaus Schelkes
Bundesanstalt für Geowissenschaften und Rohstoffe
Stilleweg 2
Postfach 51 01 53
D-3000 Hannover 51
Federal Republic of Germany

Tel.: xx49-511-643-2820
Telex: 923730 bgrha d
Telefax: xx49-511-643-2304

B. REFERENCES

BfS (1990):
Fortschreibung des Zusammenfassenden Zwischenberichtes ueber bisherige Ergebnisse der Standortuntersuchung Gorleben vom Mai 1983, ET-2/90, Salzgitter.

BGR (1981):
Ermittlung von Boden- und nutzungsspezifischen Jahreswerten der Grundwasserneubildung mit Hilfe von Boden- und Klimadaten sowie deren flaechenhafte Darstellung fuer den Raum Luechow - Gartow - Schnackenburg. - Report, File -No. 89714; Hannover.

BGR (1983a):
Berechnung von Tiefenprofilen des Tongehalts und der Porositaet aus Bohrlochmessungen in Lockersedimenten. - Report, File -No. 94447; Hannover.

BGR (1983b):
Das horizontale hydraulische Potentialgefaelle im hochversalzenen Grundwasser eines Teilbereichs der Gorlebener Rinne. - Report, File -No. 95495; Hannover.

BGR (1983c):
Diskussionsbeitrag zum 1. Pumpversuch im hydrogeologischen Untersuchungsprogramm Gorleben. - Report, File -No. 95510; Hannover.

BGR (1985):
Hydrogeologische Untersuchungen an geplanten Standorten fuer die Endlagerung radioaktiver Abfaelle.- KWA 5108/4 - Final report, File -No. 97314; Hannover.

BGR (1987):
Die Bewegung des Grundwassers im Deckgebirge ueber dem Salzstock Gorleben- Untersuchungen mit einem numerischen Modell. - Report, File -No. 102396, Hannover.

BGR (1988):
Dokumentation der Grundwasser-Standrohrspiegelhoehen aus dem Untersuchungsgebiet Gorleben in Ganglinien fuer den Zeitraum 1980 - 1986. - Report, File -No. 103494, Hannover.

Boehme, J., & Ludwig, R. (1989):
Isotope studies of the hydrology of the Gorleben area. - Proc. 10-th Salt-Water Intrusion Meeting (SWIM), Gent, 16 - 20 May 1988, Naturrw. Tijdschr., 70: 256 - 262, 3 figs., 3 tab.; Gent.

Delisle, G. & Schelkes, K. (1981):
Assessment of the Flow Regime of Fresh and Salinar Ground Waters in the Sedimentary Cover of a Salt Dome - Problems and Methods. - Proc. Seventh Salt Water Intrusion Meeting (SWIM), Uppsala, 14. - 17. Sept. 1981, Sverig. geol. Undersoekn., Rapporter och meddelanden, 27: 172 - 192; Stockholm.

Fielitz, K., Giesel, W., Schelkes, K. & Schmidt, G. (1984):
Calculations of Groundwater Movement and Salt Transport in the Groundwater of the Sedimentary Cover of the "Gorleben" Salt Dome.- Proc. Int. Symp. on Groundwater Resources Utilization and Contaminant Hydrogeology, Vol. II, p. 383-392, May 1984, Montreal, Canada.

Giesel, W. et.al.(1985):
Grundwasserbewegung im Deckgebirge ueber dem Salzstock Gorleben - Datenermittlung, Interpretation und Modellrechnungen. - Technical report 17 of the PSE - final report. Project management (ed.); Berlin.

Giesel, W. & Fielitz, K. (1983):
Evaluation of Groundwater Salinity from Well Logs and Conclusions on Flow of Highly Saline Water.- Geologia Applicata E Idrogeologia, Vol. XVIII - Parte II, p. 107-116, Bari.

Jaritz, W., Bornemann, O., Giesel, W. & Vierhuff, H. (1986):
Geoscientific Investigation of the Gorleben Site.- Proc. Int. Symp. on the Siting, Design and Construction of Underground Repositories for Radioactive Wastes, IAEA, Wien, p. 371-384.

PTB (1983):
Zusammenfassender Zwischenbericht ueber bisherige Ergebnisse der Standortuntersuchung in Gorleben; Braunschweig.

Schelkes, K., & Vierhuff, H. (1983):
Ueber den Einfluss undichter Aufsatzverrohrungen bei Grundwasser-Messstellen auf hydrogeologische Untersuchungen. -Z. dt. geol. Ges., 134: 789 - 805, 11 figs., 1 tab.; Hannover.

Vierhuff, H. (1984):
Hydrogeological Investigations in the Area of the Gorleben Salt Dome.- Proc. Int. Symp. on Groundwater Resources Utilization and Contaminant Hydrogeology, Vol.II, p. 357-579, May 1984, Montreal, Canada.

C. Table of contents (Appendices)

Appendix 1: Technical report: The Weisses Moor pumping test

Appendix 2: Description of the data sets

1. File name: BOREHOLE.DAT (with list of abbreviations)
2. File name: WELLS.DAT
3. File name: WELL2120.DAT
4. File name: DENSITY.DAT
5. File name: GWL_xxxx.DAT
6. File name: GOHYxxxx.Sy (with an example of a data file and a subroutine to read the data files)
7. Hydrogeological maps and cross-sections

Appendix 3: Figures and tables

a. List of figures

1. Location of the Gorleben salt dome
2. The Gorleben and Gartow erosion channels
3. El. conductivity and density measured on water samples
4. Density distribution in a cross section
5. Pumping test area "Weisses Moor"
6. Hydrogeological cross section

7. Pumping test data
7.1 Inflow rates calculated from flowmeter logs
7.2 Pumping rates
7.3 Water level fluctuations in the pumped well
7.4 Detail of fig. 7.3
7.5 El. conductivity of the pumped water
7.6 Temperature of the pumped water
7.7 Barometric pressure
7.8 Detail of fig. 7.7

8. El. conductivity profiles in the screens of the pumped well and selected observation wells
8.1 Pumped Well 2120
8.2 Observation well 2121
8.3 Observation well 2122
8.4 Observation well 2123
8.5 Observation well 2124
8.6 Observation well 2125
8.7 Observation well 2127
8.8 Observation well 514

9. Hydrographs for the observation wells for the year 1984
   - 9.1 GOHY 11,12,13,21,22,23
   - 9.2 GOHY 41,42,43,51,52,53,54
   - 9.3 GOHY 61,81,82,83,91,92,93
   - 9.4 GOHY 481,482,491,492,493,501,641,642
   - 9.5 GOHY 511,512,513,521,522,523,541
   - 9.6 GOHY 551,554,561,562,573,613
   - 9.7 GOHY 651,652,741,742,951,952,971,1023
   - 9.8 GOHY 1142,1162,1212,1321
   - 9.9 GOHY 2111,2112,2113,2114
   - 9.10 GOHY 2115,2116,2117
   - 9.11 GOHY 2121,2122,2123,2124,2125
   - 9.12 GOHY 14,953,1143,1163,1182
   - 9.13 GOHY 24,55,193,862,972
   - 9.14 GOHY 84,851,853,861,871,942,943,2127
   - 9.15 GOHY 483,504,514,552,563
   - 9.16 GOHY 502,622,653,674,944,1024

10. Map with information on model boundaries

b. List of tables

1. Stratigraphic and petrographic information
2. Basic data for the observation wells and the pumped well
3. Measured el. conductivities and densities of water samples
4. Example of the file structure of a GWL_xxxx.DAT data set
5. Example of the file structure of the WELL2120.DAT data set

Appendix 4: Figures and tables of salinometer and temperature data

- 4.1 Figures of the salinometer and temperature logs
- 4.2 Tables of the masured el. conductivities and water temperatures together with calculated el. conductivities and densities in the screen section of the pumped well and the observation wells

Appendix 5: Maps and cross sections

5.1 Borehole location map (1:25000)

5.2 Groundwater level (GWL) contour maps
5.2.1 GWL contour map averaged over the year 1982 (1:50000)
5.2.2 GWL contour map averaged over the year 1986 (1:50000)
5.2.3 Detail of map 5.2.2 (1:25000)

5.3 Hydrogeological maps
5.3.1 Base of Quaternary (1:50000)
5.3.2 Structure contour map of Lauenburg clay (1:50000)
5.3.3 Marginal hydraulic contact of the erosion channel (1:50000)

5.4 Hydrogeological cross sections
5.4.1 Positions of cross sections (1:50000)
5.4.2 Legend for cross sections
5.4.3 Schematic hydrogeological cross section AR - AR'
5.4.4 Schematic hydrogeological cross section BR - BR'
5.4.5 Schematic hydrogeological cross section CR - CR'
5.4.6 Schematic hydrogeological cross section DR - DR'
5.4.7 Schematic hydrogeological cross section ER - ER'
5.4.8 Schematic hydrogeological cross section FR - FR'
5.4.9 Schematic hydrogeological cross section GR - GR'
5.4.10 Schematic hydrogeological cross section HR - HR'
5.4.11 Schematic hydrogeological cross section IR - IR'
5.4.12 Schematic hydrogeological cross section KR - KR'
5.4.13 Schematic hydrogeological cross section LR - LR'
5.4.14 Schematic hydrogeological cross section MR - MR'
5.4.15 Schematic hydrogeological cross section NR - NR'
5.4.16 Schematic hydrogeological cross section OR - OR'

Appendix 6: Diskettes

1. Hydrogeological maps and cross sections (2 diskettes, autocad)
2. Text file and basic data sets (1 diskette)
   data files: APPEND_2.DAT, BOREHOLE.DAT, WELLS.DAT, WELL2120.DAT,DENSITY.DAT
3. Water level measurements in observation wells (1 diskette)
   data files: GWL_xxxx.DAT
4. Measured el. conductivity and temperature data, calculated density values (2 diskettes)
   data files: GOHYxxxx.Sy

INTRAVAL Phase 2
Seattle, April 22-25, 1991
Party TVO
Project Team VTT

DRAFT

Comments on tracer tests and data interpretation

Aimo Hautojärvi and Seppo Vuori

Technical Research Centre of Finland

Nuclear Engineering Laboratory

General remarks

There are not many means to study water flow paths, transport processes and phenomena in crystalline rock. Tracer tests are very useful in determining transport properties of rocks. The importance of well performed break-through measurements should be emphasized because there might be no other methods to study water flow and migration in fissures without destructing the rock volume in question.

To learn more about the transport with ground water than just a general velocity and perhaps some dispersion, carefully planned and performed experiments are needed. Some of the main questions to be answered are:

- which phenomena are to be studied
- what is the transport path geometry (which may depend on flow situation)
- how should the tracer be injected (spatially and temporally)
- how should the sampling and monitoring be arranged.

Some thoughts and arguments are given here.

About the phenomena

The first phenomena to be studied is hydrodynamic dispersion because it is unavoidable encountered in any experiments. Before any other phenomena can be reliably studied the dispersion must be very well controlled. Dispersion cannot be controlled just by one measurement because it is time and length dependent. Dispersion cannot apriori be characterized by the "dispersion coefficient" or "dispersion length" already from the simple reason that dispersion is mostly not symmetrical or "Fickian" (it may be in some time and spatial domain). The time and/or length dependence of dispersion has to be determined which means that more than one measurement has to be done.

Actually dispersion as such is not a phenomenon of primary interest for nuclear waste repository performance assessment. With rather slow flow velocities in the repository conditions matrix diffusion will disperse transported pulses much more than the hydrodynamic dispersion which probably will become negligible compared to the dispersion due to the matrix diffusion. To study matrix diffusion properly, however, the hydrodynamic dispersion should be made as small as practically possible and of course controllable which means very small flow rates in experiments. Also geometrical spreading of injection pulses causes disturbing dispersion. (At this point we disagree with Chin-Fu Tsangs point of view to use line sources).

Retardation due to sorption should be studied in addition to batch type of experiments also in transport experiments. It is clear that the transport of sorbing species should be compared with non-sorbing ones in identical conditions and well specified fractures. Repeated short injections should be used to study possible nonlinear effects possibly together with a continuous release of the same chemical specie but detectable separately (e.g radioactive vs. stable isotopes).

Transport path geometry

Transport paths are thought to be very narrow channels which probably are formed differently in different potential fields. There might be a risk that channels are somewhat unstable and small (unobserved, uncontrolled) variations in the experimental environment change channel properties even during performed tests. Thus the potential field used in the experiment should be established to be stable against small variations in the experimental environment. It should be remembered also that e.g. injection arrangements might introduce major disturbances and changes in flow patterns. Natural, linear, and radial potential fields correspond perhaps closest to the actual situation to be analyzed in a performance assessment. Transport paths should be studied one by one because it is easy to make a superposition if desired but very difficult or impossible to decompose one. Several tests between different locations of injection and sampling are needed to characterize flow paths and geometries. The injections or rather very gentle releases should be point releases (cf. the dispersion discussion).

In safety analysis the properties of the flow channels are of major interest. Release of materials from the disposed waste may not be direct to a channel but has some kind of coupling (slower flow, diffusion) into the channel. To study both of these factors "pure" separated measurement results are much more easier to interprete than results with mixed effects. This means again a statistical sampling of the flow paths and their surroundings point by point.

Injections, sampling, and monitoring

These items have been discussed already partly above. Some points are discussed here further. The injection should be as short as practically possible taking into account that concentrations of injected solutions should not be so high that the properties of injected solution deviates too much from the properties of the carrier flow. The detecting accuracies should be also taken into account. This problem is illustrated in the following.

It is assumed that two flow channels with different velocities contribute to the tracer break-through. The break-through curves through the two channel system with with constant release pulses of different lengths are plotted in figure 1. It is seen that a very short pulse (A) may cause difficulties in detection. As the injection time increases the break-through curves (B) and (C) are higher but still reflect directly the properties of the transport system. At the same time more and more tails from the earlier released portion of the injected solution overlaps with the first fronts of the later released portions and the direct system behavior is smeared out.

The system response function could of course be in principle be derivated from the integrated results but due to experimental errors and possible instabilities the result is more and more inaccurate. For example it would be impossible to say from the result (E) if there are two channels contributing or has there been some change in the experimental conditions (injection variations, instabilities in flow, changes in the coupling of the injection into the flow channel, ...). It can be concluded that in this hypothetical case the tracer should be injected for 1000...2000 h. Compared to the injection til end of the experiment the result is much easier to interprete more accurately and in an unambigious way not to speak about the costs of the tracer solution.

The break-through curves of short duration release pulses are compared in figure 2. It is seen that some flattening and broadening occurs with increasing injection duration. When the release pulse is not "broader" than say 10 % of the width of the break-through curve the system response is "ideal" as in case (A). To increase the level of output concentration longer pulses might, however, be desirable. The injection should be stopped at latest when the first rise of concentration at the sampling site is observed (at 2000...2500 h).

When the transport properties of the channels are studied it is obvious that the channels should be first found and the tracer should be released directly into them. Injection into areas around would cause a slow and possibly time dependent transport into the channel. The effects of this kind of source term would be impossible to distinguish from e.g. transport along different flow paths, dispersion in channels, and matrix diffusion. Injection with overpressure cause unavoidably such source term effects. The same applies also to dipole experiments where the charging disturbes badly the natural channeling. It could be argued that also the withdrawal in radial tests causes disturbances but the situation is somewhat better because flow and tracers scan most of the time transport properties in areas that are far away from the disturbance.

The time dependence of the injection should be monitored very exactly because it is important to distinguish between source term effects and transport effects. Even relatively short injection pulses have an effect on the shape of break-through curves as is shown in figure 2.

INTRAVAL phase 2 test cases

Finnsjön

Our project team has modelled the radial and dipole experiments earlier using a concept of channeled flow in two dimensions and tracer transport in varying aperture two dimensional channel with a linear velocity profile across a characteristic width (e.g. half of the channel width). Transport times were calculated from the measured transmissivities in boreholes employing a factor to take into account the difference between volume and hydraulic apertures. A fixed value (5 cm) of the characteristic width was used for the characteristic width of velocity profile in calculations. The measured break-through curves were influenced much on varying injections which were not measured very accurately. The injections were in radial experiments mostly long injections. It was therefore difficult to assess in detail the forms of the various break-through curves. An overall agreement between the calculations and measurements was obtained both in the radial and dipole experiments using consistently same parameters in calculations.

A preparatory tracer test was performed before the actual experiments. Short injection pulses were used in the test. The injection technique was, however, not the same as in the actual experiments. Due to the short injection period this might not have affected the results too much. Very interesting in addition to the short injection duration is that the test was performed using a four times higher withdrawal pumping rate than the radial experiment. This gives a possibility to really evaluate the model behavior to the experiments.

Fits of the generalized Taylor dispersion model to the data of the preparatory tracer experiment are shown in figures 3 to 6. The obtained fit parameter, the characteristic width of the velocity profile, varied between 3.1 cm ... 6.6 cm. The theory may in some cases not

give unique values but rather two possibilities. In the case of Uranine as a tracer from BFi 01 to BFi 02 also a characteristic width of 1.7 cm could explain the results. It can be concluded that break-through curves from preparatory, radial, and dipole tests can be consistently described using a single parameter value describing the dispersion. Due to the generalization of Taylor type of dispersion also asymmetric pulses can be considered to be entirely due to hydrodynamic dispersion. In the hydraulic conditions in the fracture zone 2 at Finnsjön the hydraulic dispersion dominates and there is no possibility to assess the effects of matrix diffusion in these tests.

Stripa 3-D

In the Stripa 3-D experiment long injection pulses were used but they were measured accurately. An overpressure was used in injection. This causes some uncertainty to a "real" source term for the transport in channels. The recoveries were also typically rather low. If tracer has escaped to unknown areas there has been a division into the observed part and into the unobserved part. The best that can be done is to assume that there has been a constant division factor but some uncertainty should be attributed to the division factor.

The effects of the long and varying injection rates can be in principle taken into account e.g. by deconvolution technique. A thorough sensitivity and error analysis should be made before final conclusions can be drawn from these tests. Chin-Fu Tsang et al. have used deconvolution technique to study the transport properties of the channels. Using their deconvoluted data we have fitted our generalized Taylor dispersion model into these curves. The results are shown in figures 7 to 11 using 2...4 independent channels. The characteristic width of the velocity profile varies from 2 cm to 15 cm being in many cases 4...6 cm. This kind of result would indicate a domination of hydraulic dispersion over matrix diffusion. Actually the observed break-through curves could be explained entirely by hydrodynamic dispersion alone. To see a possible contribution of matrix diffusion to the results a two channel matrix diffusion model was fitted to the uranine data. The result is shown in figure 12. It can be seen that there is very little agreement with the calculated and measured/deconvoluted data. It should be born in mind that there are certain errors in the deconvoluted data and hydrodynamic dispersion mixes with pure matrix diffusion. In any case it is almost impossible to extract reliable parameter values for matrix diffusion.

Some preliminary sensitivity studies have been made for the Stripa 3-D data deconvolution. The tracer injection and break-through curves presented in figure 13 have been used to extract the "delta-pulse response" (without using the positivity condition). The result is shown in figure 14 together a fitted curve of our generalized Taylor dispersion model. The fitted curve is then convolved with the tracer injection curve and compared with the measured break-through curve in figure 15. The overall fit is reasonable but the modelled curve shows kinks that are not observed in the measured values. The reason might be that the "delta-pulse response" does not really have such "sharp and peaky" behavior as is given by the deconvolution.

Synthetic data was prepared to assess the effects of systematic changes instead of random changes. The model data in figure 15 was considered to be the actual data. The curve was distorted slightly by an exponential decrease from 9000 hours on. The deconvolution of the distorted synthetic data is shown in figure 16 together with the non-distorted data. It i seen that peak behavior is remained but negative output values are produced. From this it is

concluded that one reason to give negative values in the deconvolution of the actual data as in figure 14 might be a systematic decrease in the input curve.

The deconvolution result is not very sensitive to random errors as shown by Tsang et al. but it seems to be surprisingly sensitive to the sharp peaks in the input (tracer injection + coupling into the channels). If the tracer injection data is rounded off to be somewhat "broader" (this could be an effect of a coupling term) there is a dramatic effect on the deconvolution (this is a very preliminary result not shown here but will be studied further).

WIPP 2

Three tracer break-through curves from the WIPP site (tracer test H-11) have been analyzed preliminary. The break-through curves show a very asymmetric behavior and first parts arrive extremely fast. There are several explanations for that kind of behavior. Very many channels could be involved. There might be an enormous matrix diffusion like diffusion into stagnant areas of water with porosity of the order of 1. There might be also a time dependent source term just releasing tracer over several hundreds of hours giving the observed long tails. A sketch how this may happen is presented in figure 17.

There is only one channel in this model but the injection procedure spreads the tracer in the surrounding. The tracer is recovered slowly from the surrounding and transported then further in the channel. The model calculations are shown in figures 18 to 23. The exponential source term together with the dispersive transport would reproduce the observed curves. In order to study the transport properties of the flowpathways the injections should be located as near as possible to the highly conductive structures and no overpressure should be used to avoid difficulties and ambiguities in the interpretation.

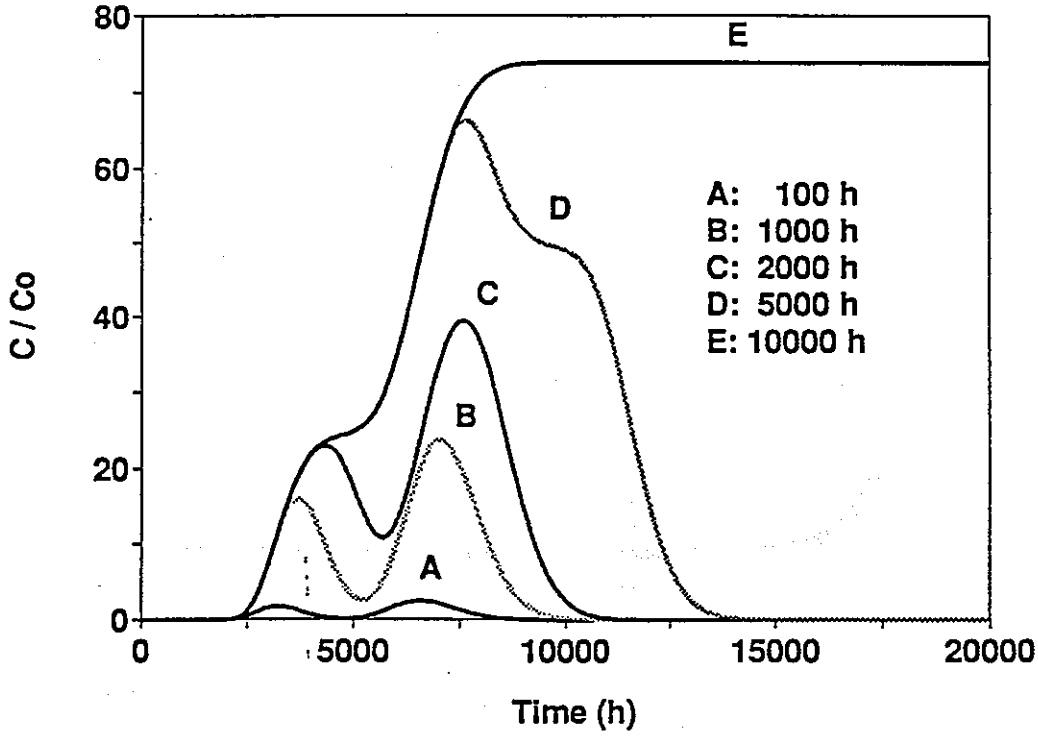

80
60
40
20
0
C / Co
0
5000
10000
15000
20000
Time (h)
E
D
C
B
A
A: 100 h
B: 1000 h
C: 2000 h
D: 5000 h
E: 10000 h

Fig. 1.

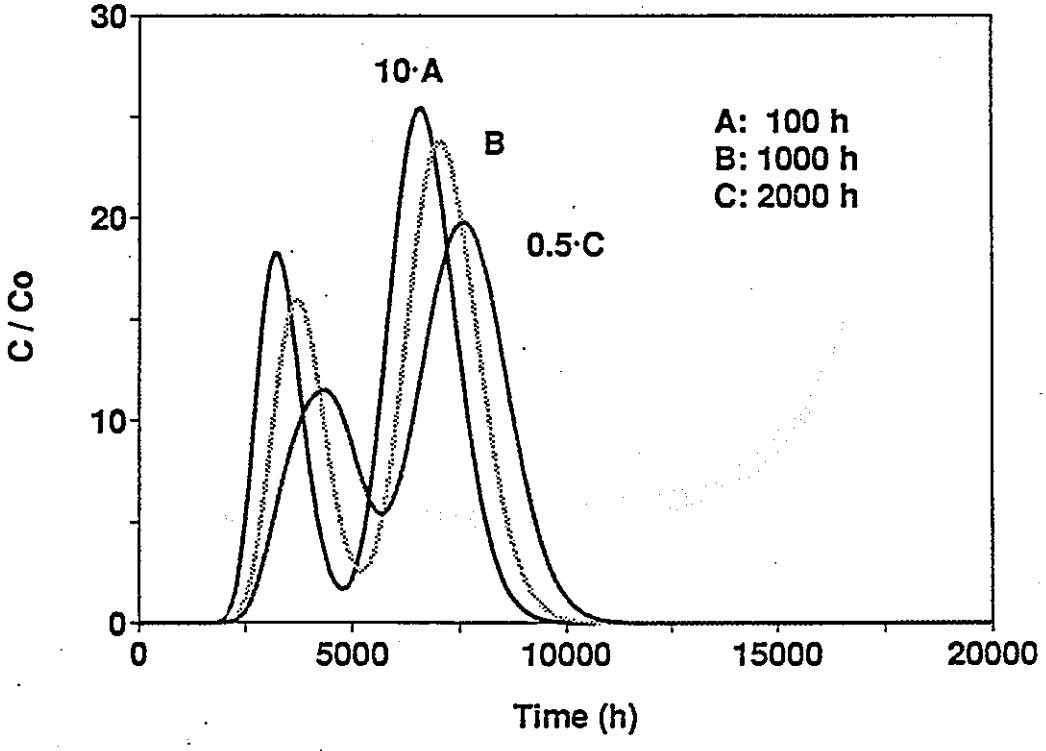

30
20
10
0
C / Co
0
5000
10000
15000
20000
Time (h)
10·A
B
0.5·C
A: 100 h
B: 1000 h
C: 2000 h

Fig.

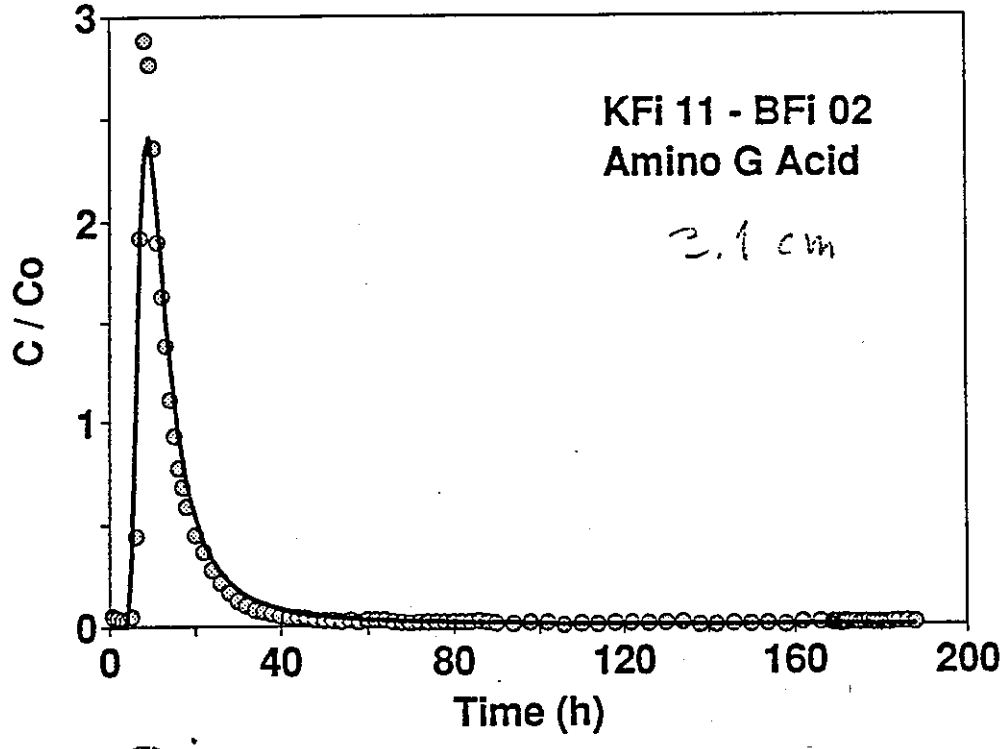

KFi 11 - BFi 02
Amino G Acid
2.1 cm
C / Co
Time (h)
0
1
2
3
0
40
80
120
160
200

Fig. 3

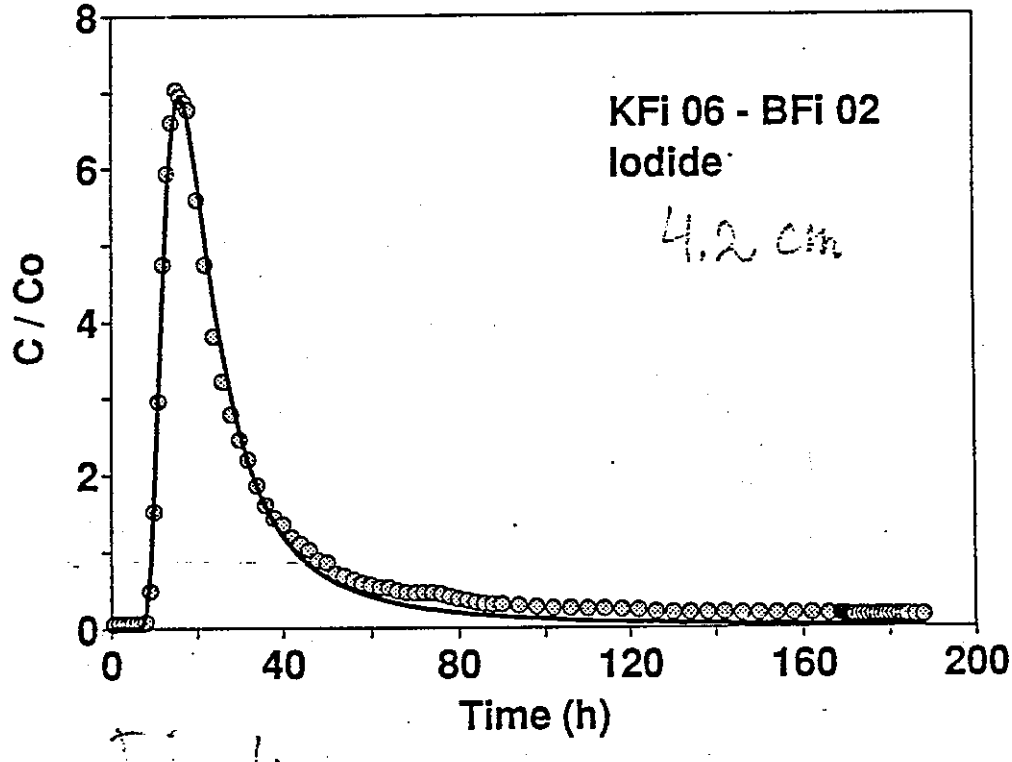

KFi 06 - BFi 02
Iodide
4.2 cm
C / Co
Time (h)
0
2
4
6
8
0
40
80
120
160
200

Fig. 4

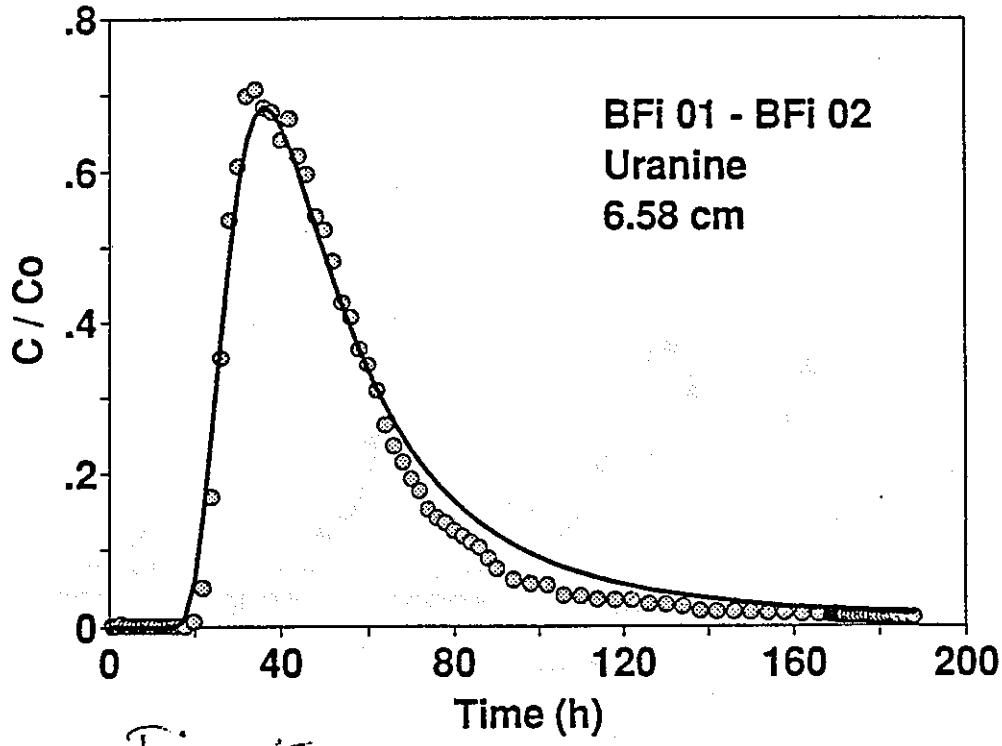

BFi 01 - BFi 02
Uranine
6.58 cm
C / Co
.8
.6
.4
.2
0
0
40
80
120
160
200
Time (h)

Fig. 5

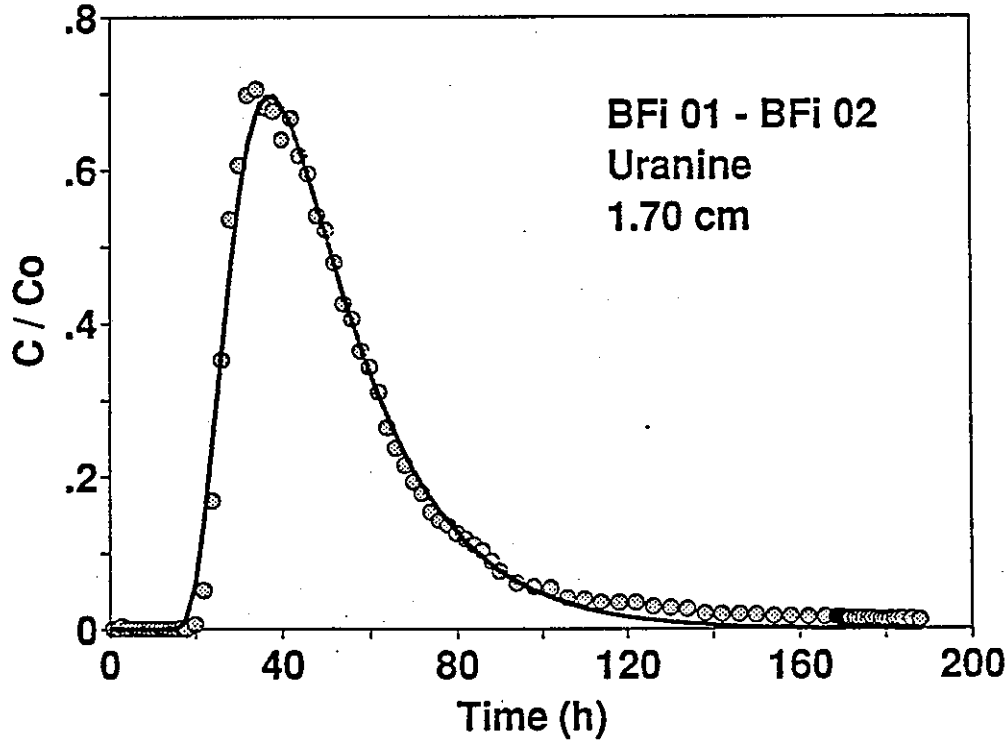

BFi 01 - BFi 02
Uranine
1.70 cm
C / Co
.8
.6
.4
.2
0
0
40
80
120
160
200
Time (h)

Fig. 6

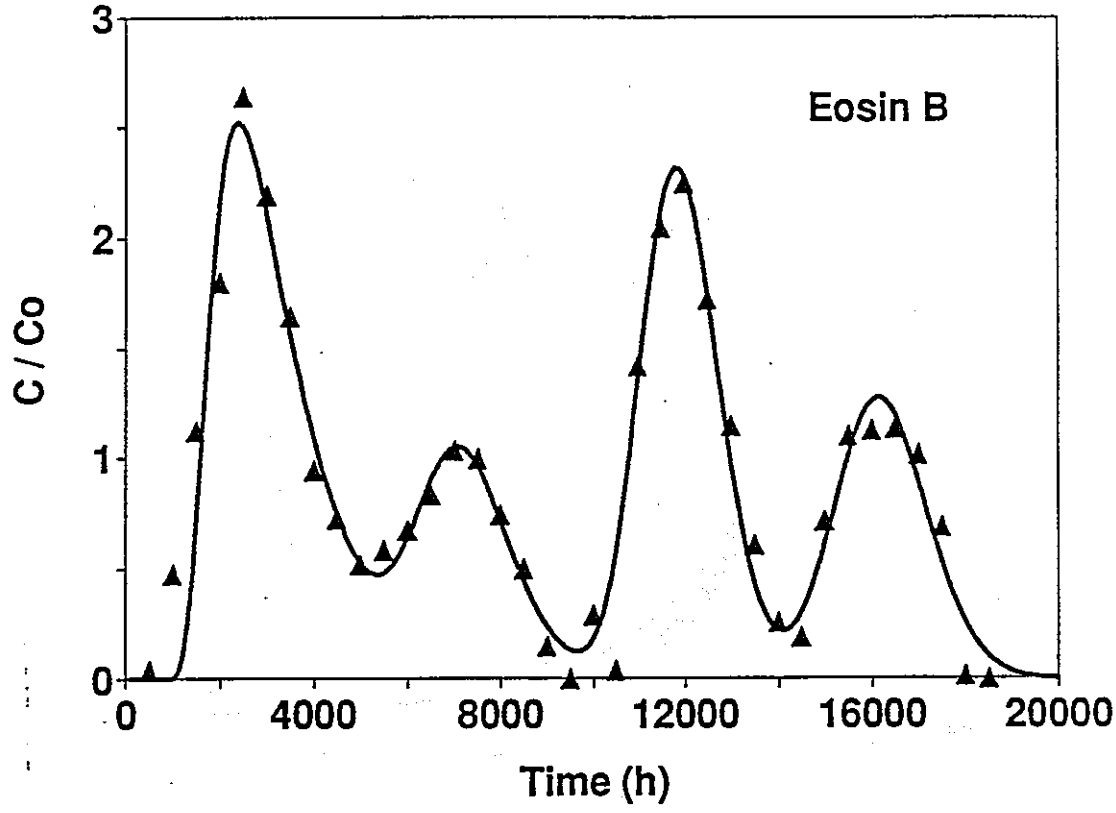


Fig. 7

a_1 = 13.2 cm

a_2 = 6.3 cm

a_3 = 4.0 cm

a_4 = 4.0 cm

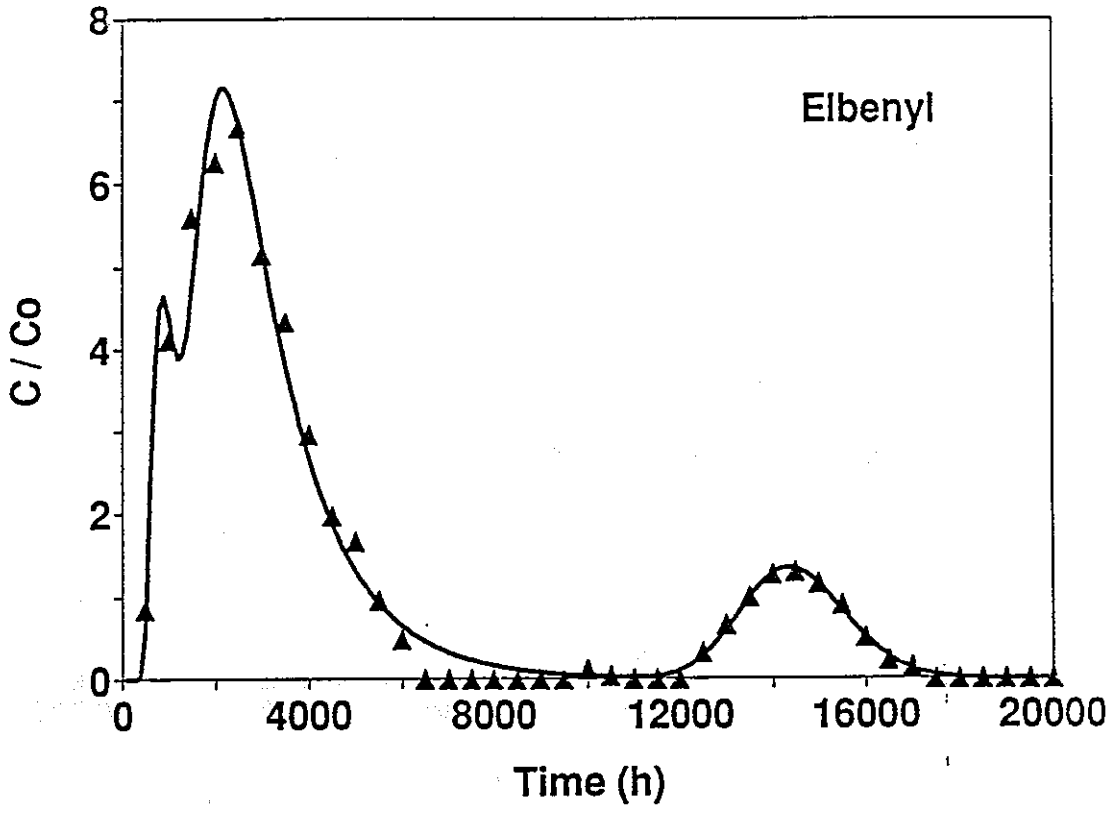


Fig. 8

a_1 = 15.5 cm

a_2 = 15.0 cm

a_3 = 4.9 cm

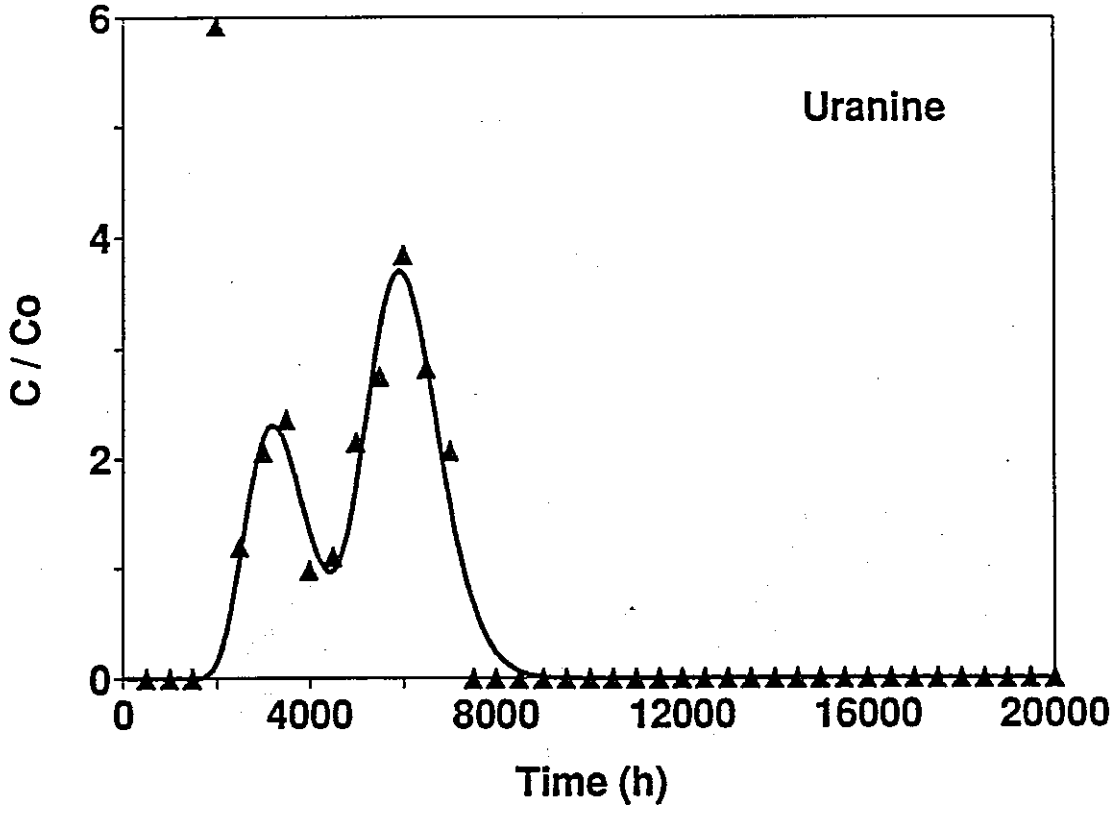


Fig. 9

Q_1 = 6.5 l/h

Q_2 = 5.2 l/h

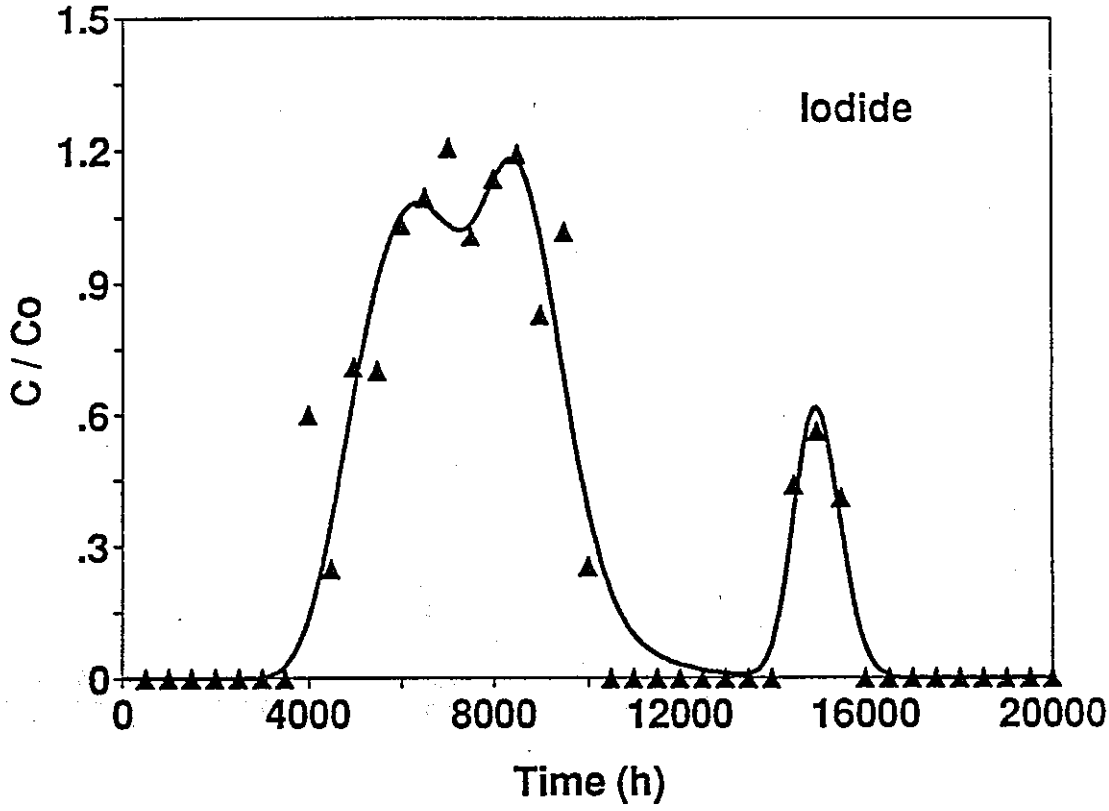


Fig. 10

a_1 = 10.6 cm

a_2 = 4.5 cm

a_3 = 2.0 cm

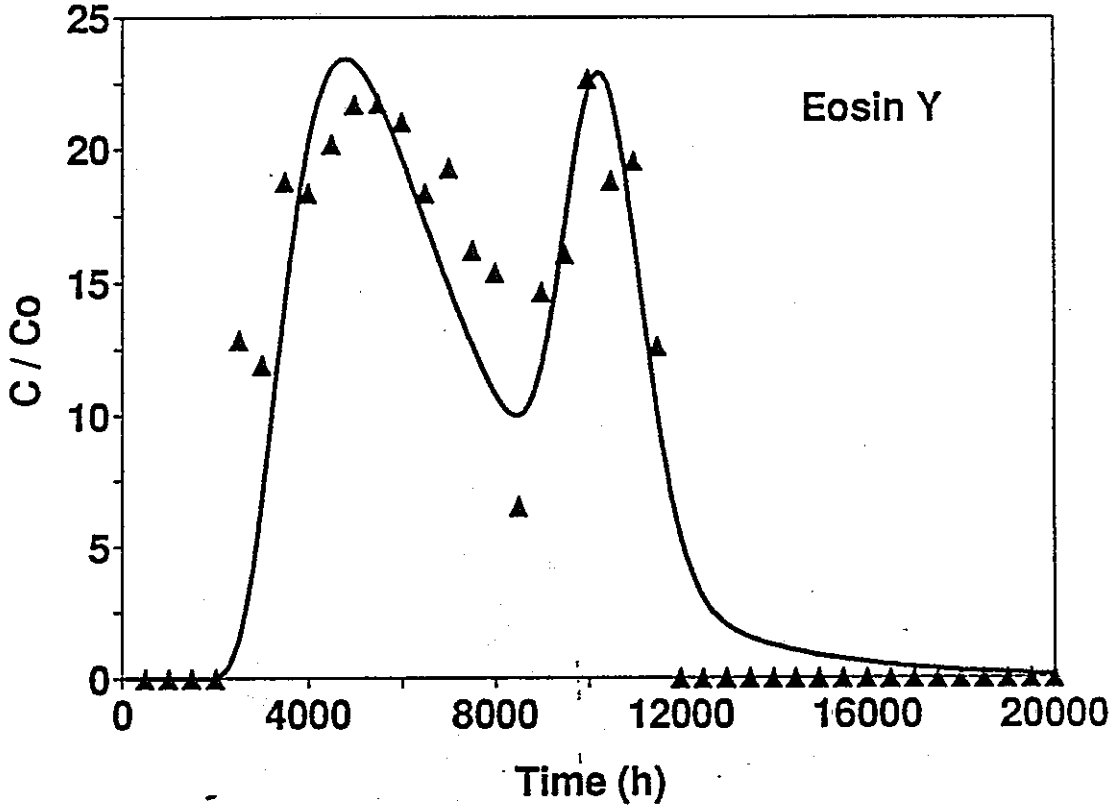


Fig. 11

a_1 = 20.6 cm

a_2 = 4.2 cm

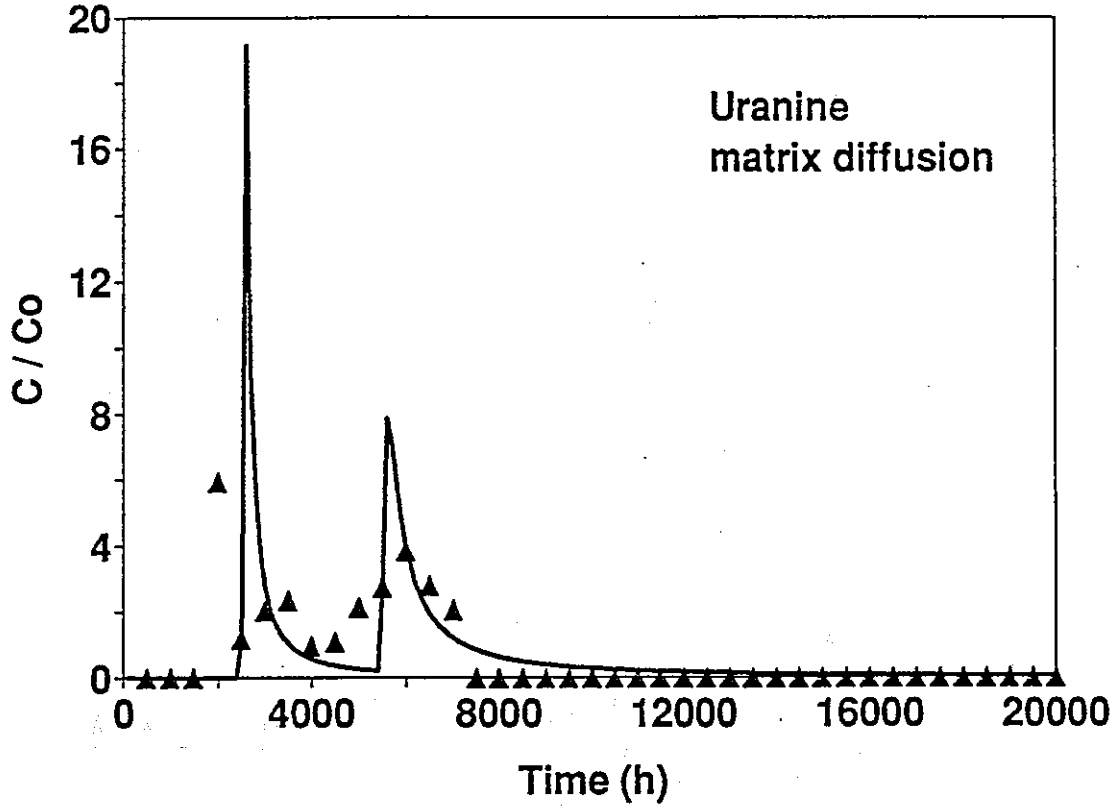


Fig. 12

$D_e = 5 \cdot 10^{-14}\ m^2/s$

$\varepsilon_p = 0.002$

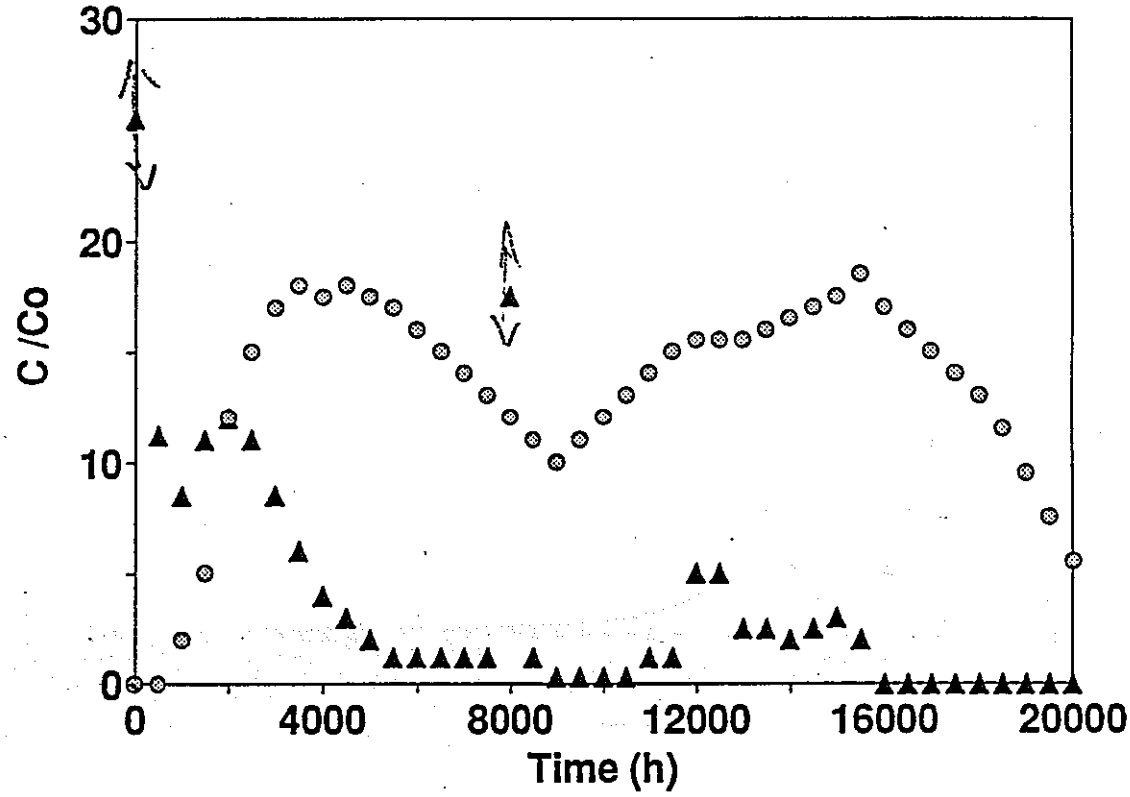


Fig. 13

ENOSINE INPUT ▲

OUTPUT ⊗

(Hidden Data Area)

for i = 2:k

mm(:,i) = [zeros(i-1,1); m(1:k+1-i)];

end

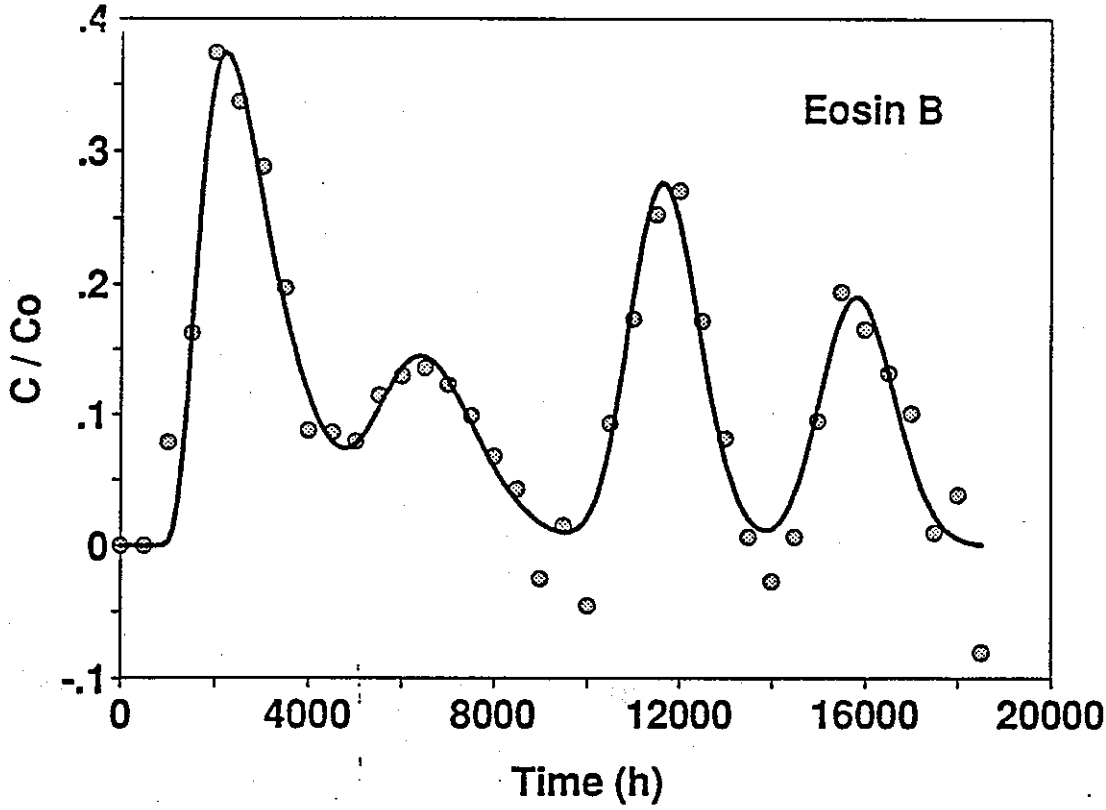


Fig. 14

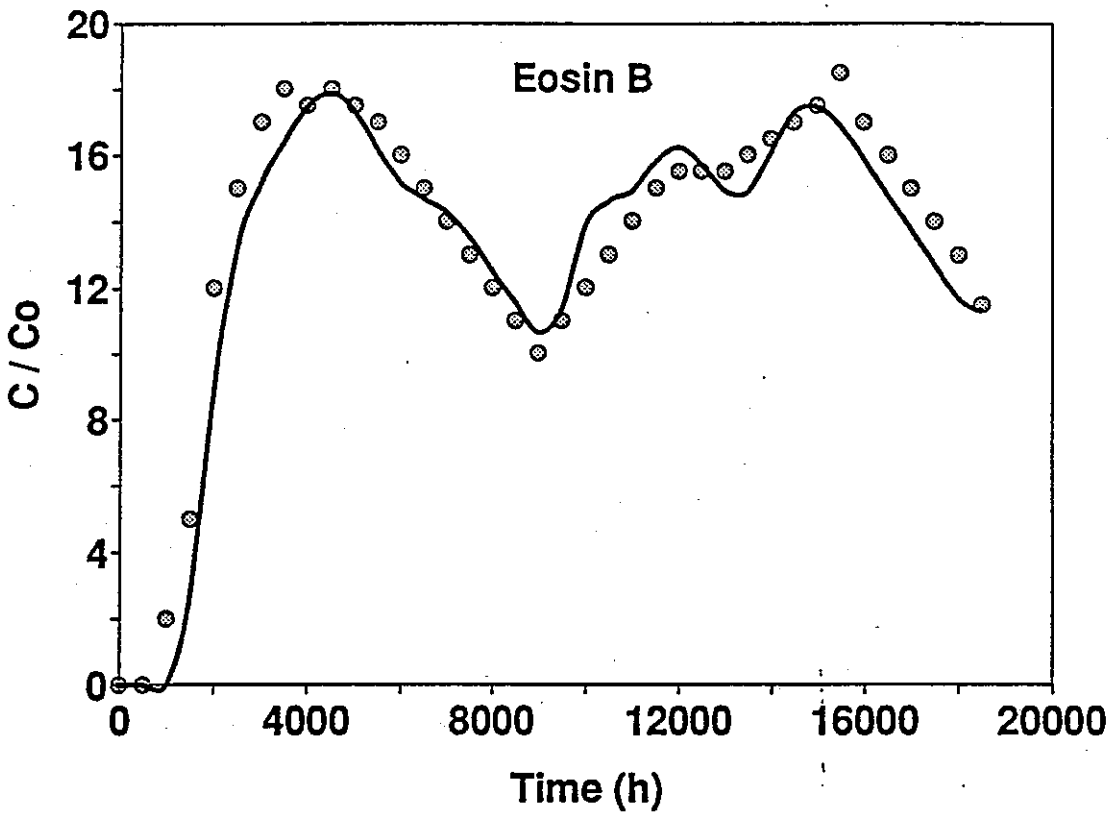


Fig. 15

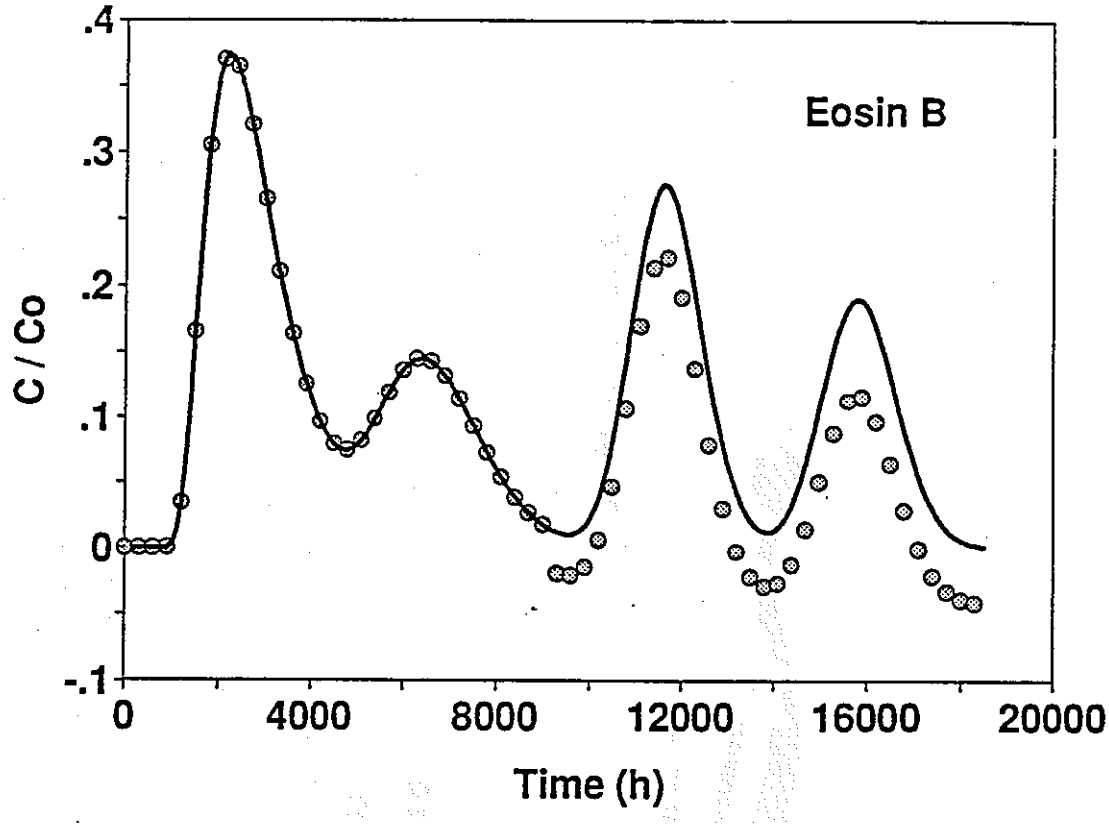
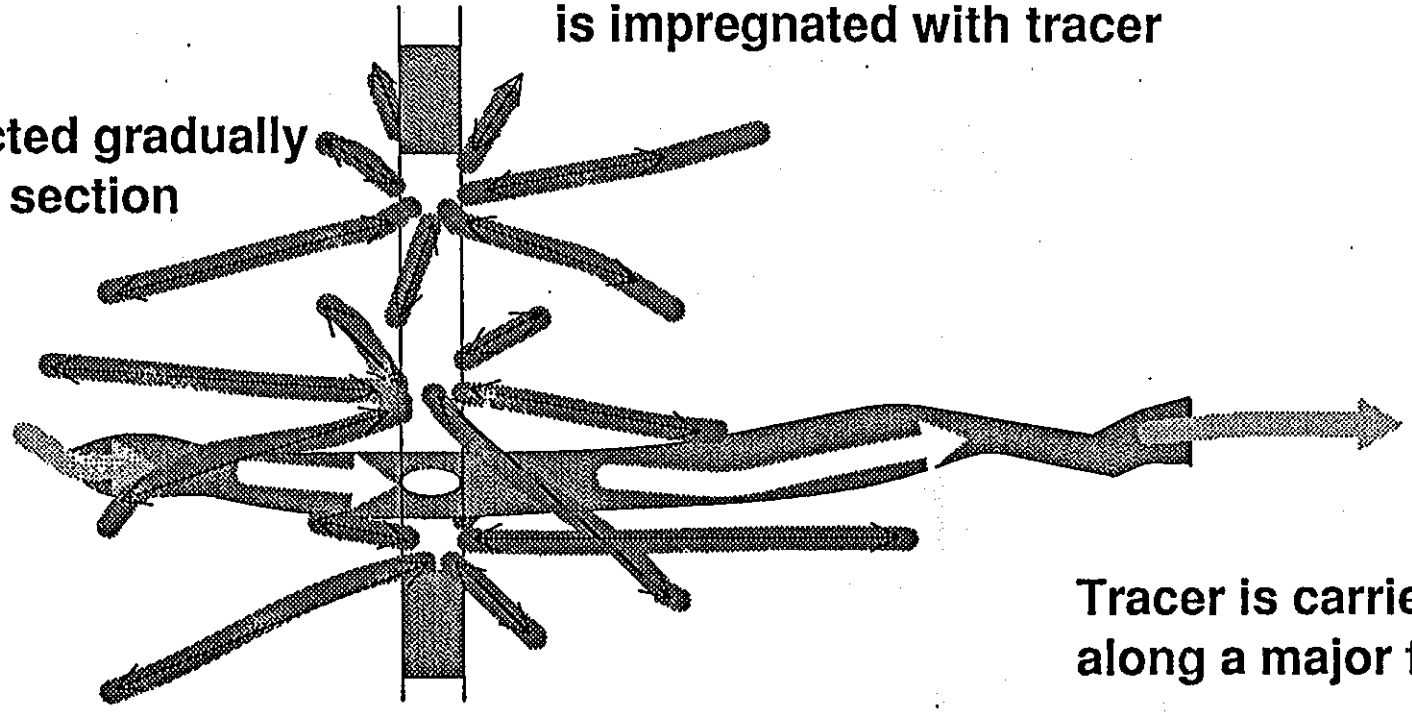


Fig. 16.

Syntheticmen

Surrounding of injection section
is impregnated with tracer

acer is recollected gradually
to the injection section



Tracer is carried away
along a major flow path

The tracer concentration lasts
for long times in the injection
section (decaying exponentially)

Fig. 17

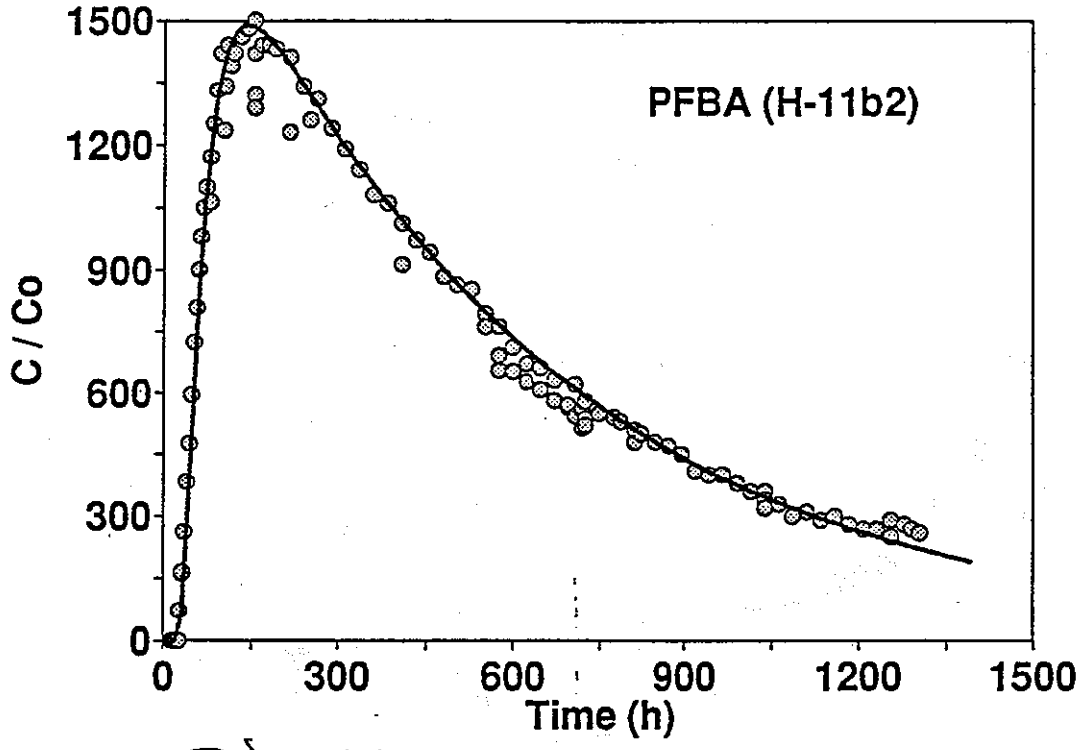

PFBA (H-11b2)
C / Co
1500
1200
900
600
300
0
0
300
600
900
1200
1500
Time (h)

Fig. 18

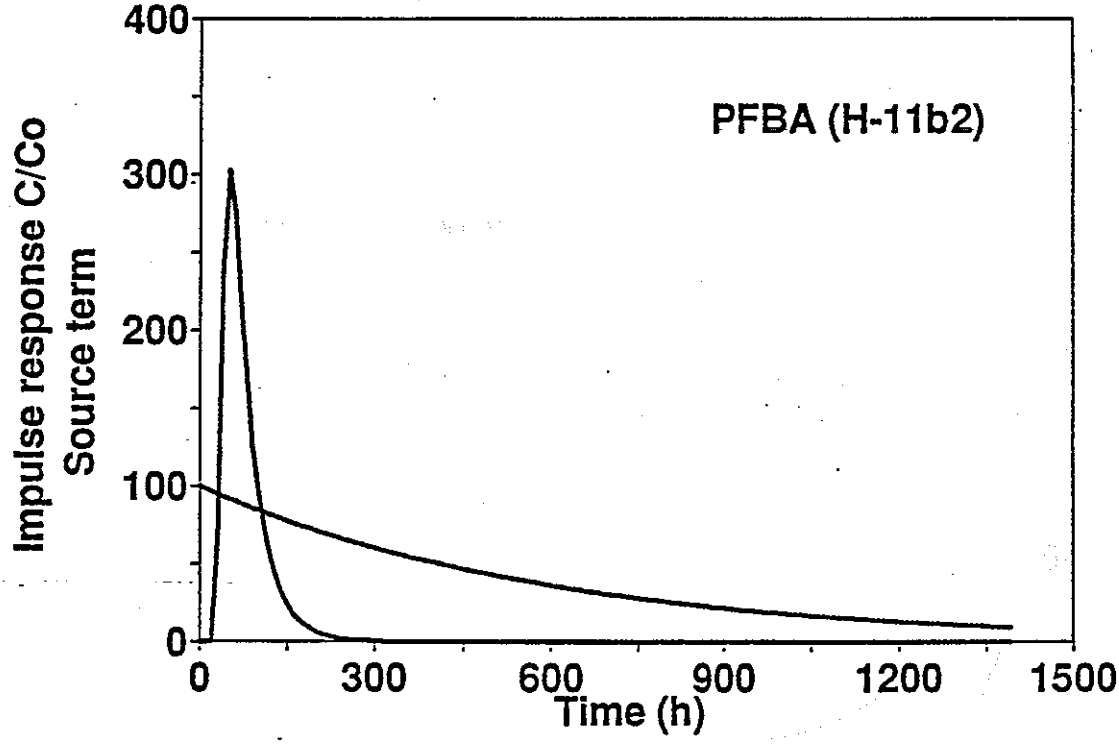

PFBA (H-11b2)
Impulse response C/Co
Source term
400
300
200
100
0
0
300
600
900
1200
1500
Time (h)

Fig. 19

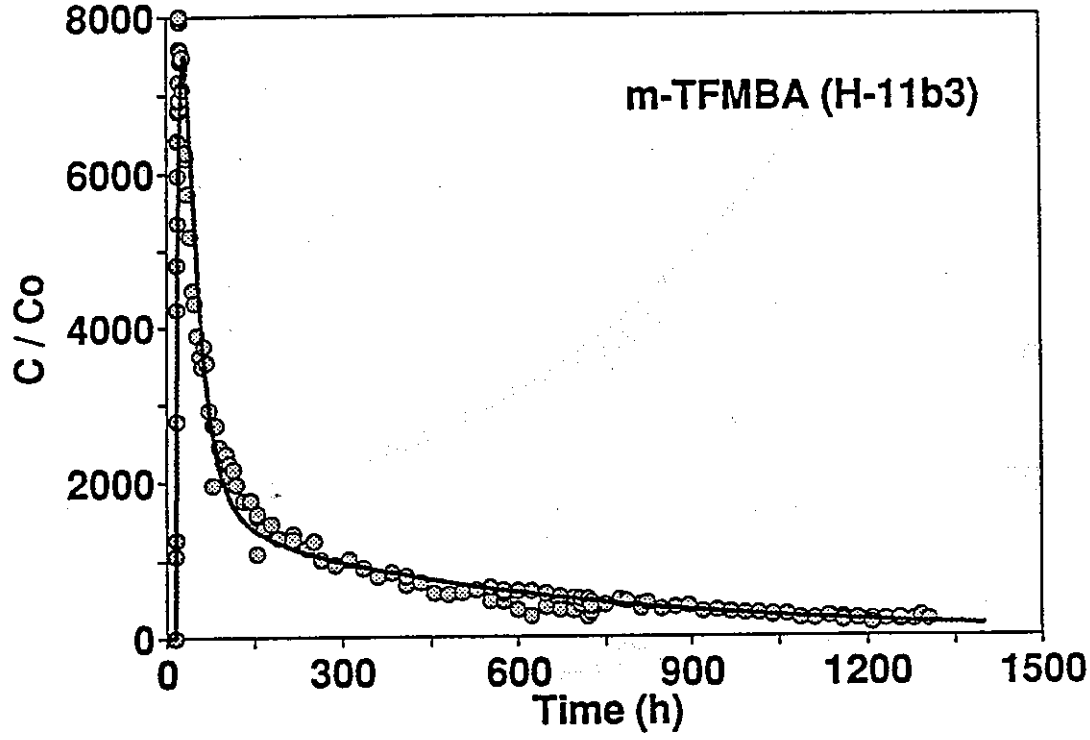

m-TFMBA (H-11b3)
C / Co
8000
6000
4000
2000
0
0
300
600
900
1200
1500
Time (h)

Fig. 20

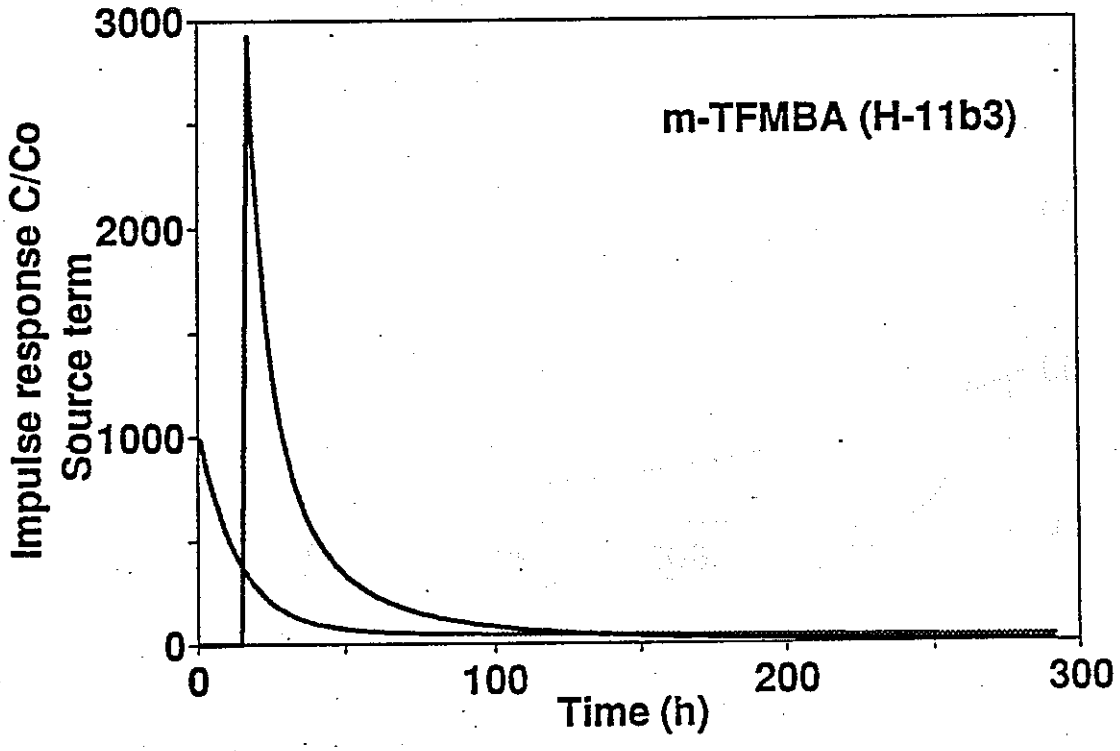

m-TFMBA (H-11b3)
Impulse response C/Co
Source term
3000
2000
1000
0
0
100
200
300
Time (h)

Fig. 21

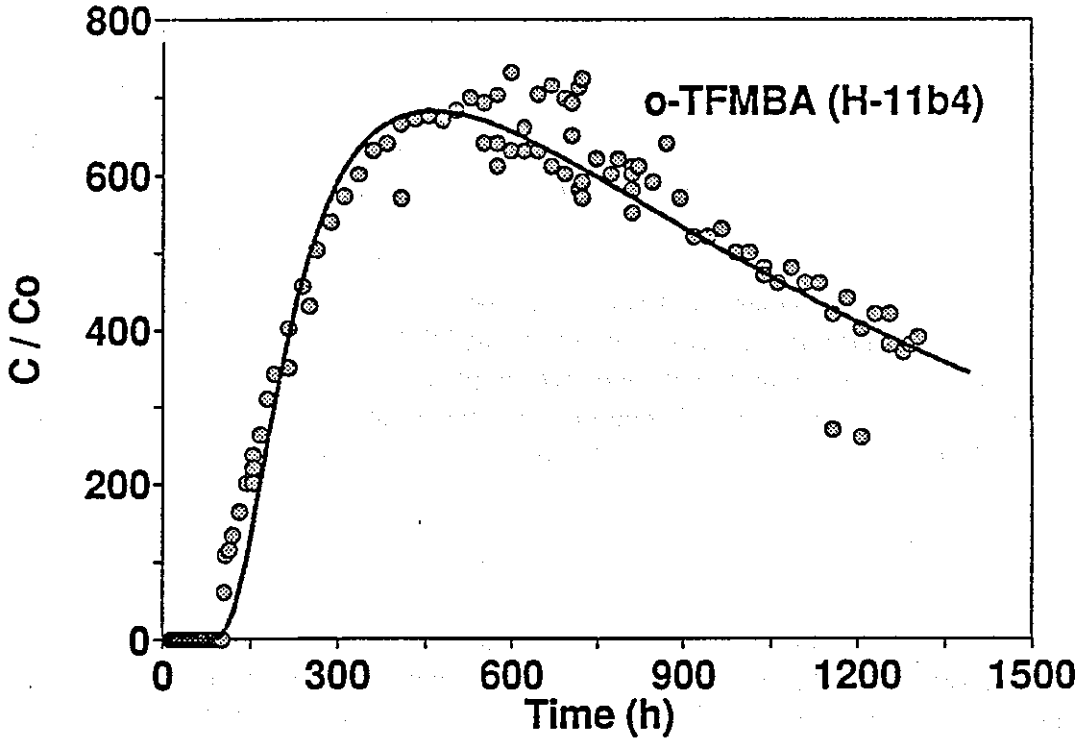

o-TFMBA (H-11b4)
C / Co
Time (h)
800
600
400
200
0
0
300
600
900
1200
1500

Fig. 22

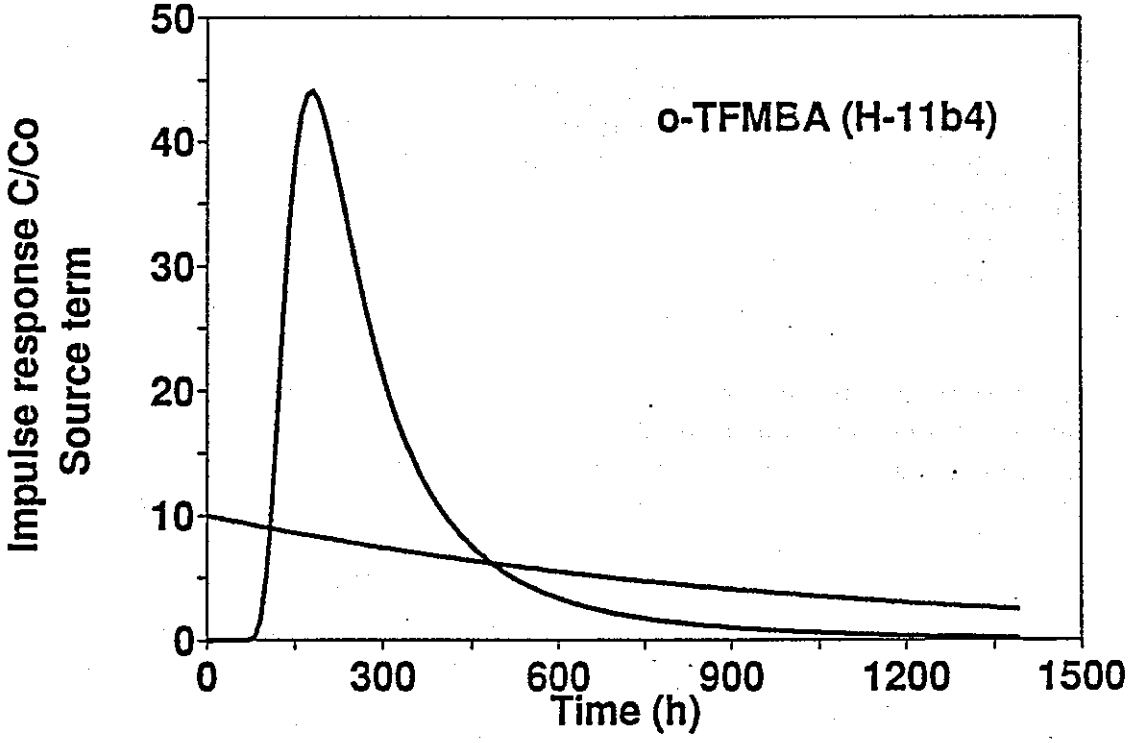

o-TFMBA (H-11b4)
Impulse response C/Co
Source term
Time (h)
50
40
30
20
10
0
0
300
600
900
1200
1500

Fig. 23

Summary of the VTT contribution

In the first part of the work e.g. geological and hydraulic base information was given to the project teams as part of a thorough description of the test site. At this stage the hydraulic interference test data were not yet, however, available. The teams were given an opportunity to predict head differences, flow through the injection sections, tracer transport times and other transport properties for the planned radial experiment.

A conceptual model of flow channels in fractures has been employed to predict and interprete the results of hydraulic and tracer transport results of the INTRAVAL test case 5. Also a two-dimensional model of three separate subzones was applied to predict the relevant data. The fracture aperture heterogeneity and channeling was taken into account by introducing a coefficient which was estimated to have a value of 5 for the Finnsjön case. The factor is the ratio of the real volume aperture and the ideal parallel plate hydraulic aperture. The transmissivities of the separate subzones were estimated based on the given transmissivities in single boreholes.

The conceptual transport model is a logical continuation of the hydraulic channel concept. It is assumed that velocity differences exist within each channel. Due to lack of data on the velocity field in detail we have assumed a simple linear variation across the channel width (or several cycles of such variation). The parabolic like velocity distribution across the channel aperture smooths much sooner out due to the molecular diffusion. The molecular diffusion combined to the larger scale velocity variation causes, however, non-Fickian dispersion. Analytical approximative calculations have been worked through in order to calculate the dispersion behavior. A value of 5 cm was estimated for the characteristic width over which the velocity varies from zero to its maximum value. Two identical parallel channels (upper and lower boundary of a subzone) were assumed to

It was also commented to the test pilot group prior to the test that short injection pulses would give the best information on the transport phenomena. The test was planned to be run using mainly long injection pulses but short pulses were also considered. Predictions based on the available data on that time were calculated and reported before knowing the results. A minor misunderstanding of the injection arrangement causes the predicted absolute values of concentrations not to be directly comparable to the experimental results. Otherwise the predictions were reasonably succesful.

When the experimental results were reported and also the hydraulic interference data were available new calculations were done using the same concepts as in the predictive modeling but this time taking into account injection variations and only one transport route (to see the effect of the fastest and presumable the route with largest contribution). The model agreement with the experimental results appeared to be good. It was noticed that it is very difficult or practically impossible to distinguish between the effects of a second (slower) route and variations in the injection and ground water flow system. The flow rates through the injection sections especially in the upper subzone were initially extremely high compared to the geometrically deduced flow rate. Dilution tests in the injection sections showed, however, a much smaller flow rate at the end of the radial experiment but without any slow down of the transport velocities.

The break-through curves in the dipole experiment were predicted using the data of the radial

experiment and the assumption of isotropy and homogeneity of the upper subzone (except that the flow is highly channelized). This gave a reasonable agreement with experimental results but first after a modification of the flow division between the three active transport routes resulted a good agreement. The concentrations of the circulating tracers in the pumping borehole as well as in the observation boreholes at the "sides of the dipole field".

It could be concluded that the employed conceptual model agrees consistently and with same parameters with all the analyzed tracer tests. Also a simple two-dimensional hydraulic model agrees reasonably well with the hydraulic data. The dominating transport process is a non-Fickian dispersion and it is impossible to see the effects of matrix diffusion in the test case 5 if the applied conceptual model has some validity.

The first phenomenon to be seen when slowing down the transport velocities would be diffusion into stagnant areas of ground water. This would be very much like matrix diffusion the difference being that it is faster than the diffusion into the rock matrix but approaches a steady state rather quickly. The result at the end is only a slower transport with the mean flow velocity (integrated over areas reachable by diffusion). The diffusion into the rock matrix can be seen in these kind of experiments only after the above mentioned processes approach a steady state and do not contribute very much to the broadening and skewness of the break-through curves.

The flow in the fracture zone 2 at the Finnsjön test site seems to be highly channelized and borehole sections happen to be well connected to the channels at least in the upper subzone.

Studies of Tracer Experiments in a Fracture Zone at the Finnsjön Research Area — INTRAVAL Test Case 5

Edited by

Chin-Fu Tsang
Lawrence Berkeley Laboratory, USA
and
Shlomo Neuman
University of Arizona, USA

Contents by

P. Andersson and Coworkers
Swedish Geological Company AB, Sweden

L. Moreno and I. Neretnieks
Royal Institute of Technology, Sweden

P. Grindrod and D.J. Worth
Intera-ECL, United Kingdom

A. Hautojärvi and Coworkers
Technical Research Centre of Finland

Hideo Kimura and Masahiro Munakata
Japan Atomic Energy Research Institute, Japan

R. Yamashita and A. Kobayashi
Hazama Corporation, Japan

Patrick Goblet
Ecole des Mines de Paris, France

CONTENTS

1. Introduction
   Chin-Fu Tsang and Shlomo Neuman 1-1

2. Description of Experiments and Available Data
   P. Andersson and Coworkers 2-1

3. Hydrologic Investigation and Groundwater Flow Modeling—SGAB/SKB
   P. Andersson and Coworkers 3-1

4. SGAB/SKB Analysis of Tracer Data
   P. Andersson and Coworkers 4-1

5. KTH Analysis of Tracer Data
   L. Moreno and I. Neretnieks 5-1

6. INTERA-ECL Analysis of Tracer Data
   P. Grindrod and D.J. Worth 6-1

7. VTT Analysis of Tracer Data
   A. Hautojärvi and Coworkers 7-1

8. JAERI Analysis of Tracer Test Data
   Hideo Kimura and Masahiro Munakata 8-1

9. HAZAMA Analysis of Tracer Data
   R. Yamashita and A. Kobayashi 9-1

10. EMP Evaluation and Comments
    Patrick Goblet 10-1

11. Overall Comments and Discussions
    Chin-Fu Tsang and Shlomo Neuman 11-1

12. References 12-1

1. INTRODUCTION

Chin-Fu Tsang
Lawrence Berkeley Laboratory, USA
and
Shlomo Neuman
University of Arizona, USA

Test case 5 is based on a set of tracer tests in a fracture zone in crystalline rock at the Finnsjön research area in Sweden. The experiments are confined to a sub-horizontal fracture zone at approximately 300 m depth. The thickness of the zone is approximately 100 m and its horizontal extent is in the order of kilometers.

It appears that the zone contains three highly permeable sub-layers. The transmissivity of the upper layer is estimated to be 10^{-4} $m^2 \cdot s^{-1}$, the middle 10^{-7}–10^{-6} $m^2 \cdot s^{-1}$ and the lower 10^{-4} $m^{-2} \cdot s^{-1}$. The middle layer is not continuous. An interface between fresh water and salt water exists in the fracture zone relatively close to the upper pervious layer. The salt content of the groundwater is higher below the zone than above. The natural hydraulic head gradient is estimated at 1/300 in the horizontal direction.

The fracture zone and the surrounding rock are penetrated by several core drilled (and some percussion drilled) boreholes. Packer tests for hydraulic conductivity have been performed in all boreholes in 2 m and 20 m section intervals. A regional pumping test has been conducted by pumping water from the full length of one borehole and observing the drawdown in 11 wells totalling 40 intervals.

Two sets of tracer test have been completed: a radially convergent test and a dipole test. The radially convergent test was conducted by pumping one well from a packer interval covering the full width of the fracture zone and injecting 11 different non-sorbed tracers at 9 different intervals in three wells surrounding the production well, with more than one tracer injected at some points. The dipole test was conducted by pumping in one well and injecting in another. A total of 20 different tracers were introduced at the upper layer of the injection well. The tracer discharge points at the discharge well were estimated by sampling the tracers in different layers. Both the radially convergent and the dipole test showed that tracers could move between the layers in the fracture zone.

Seven project teams, including the Pilot Group who developed this test case, studied and analyzed the data to various degrees. They are:

1. Swedish Geological Company (SGAB) and Swedish Nuclear Fuel and Waste Management Company (SKB)
2. Technical Research Centre of Finland (VTT)
3. Royal Institute of Technology (KTH), Sweden
4. Hazama-Gumi, Japan
5. Japan Atomic Energy Research Institute (JAERI), Japan
6. Intera and Nirex Ltd., UK
7. Ecole des Mines de Paris (EMP), France

Among the seven groups, SGAB/SKB made a detailed study of the hydrological data and established a groundwater flow model before analyzing tracer test data. All the other groups started with the flow data and hydrologic properties, and studied tracer data using a variety of conceptual models.

The conceptual models used range from one-dimensional channel model, two-dimensional porous medium model, to two-dimensional fracture network model.

SGAB/SKB considered a vertical cross section of porous medium with multiple layers as well as a horizontal cross section with regions of different hydrologic properties. A finite element method was used to solve for both the flow and transport. They also used a one-dimensional transport model to analyze some of the data, especially to account for the effects of variable injection and the occurrence of multiple flow paths. Conservative, sorptive, and radioactive tracer tests are all analyzed.

The VTT group interpreted both the radially convergent and dipole tracer test data based on a channel model, characterized by a number of channels, each with its own properties. The VTT and the SGAB groups are the only groups so far that have addressed not only the convergent test, but also the dipole tests.

The KTH group interpreted the radially convergent tracer tests data with two linear transport models, one with advection and dispersion and the other with advection, dispersion and matrix diffusion.

The Intera group utilized a two-dimensional (r,ϕ) flow field and solved the advection-dispersion problem with an off-center tracer input. They also tried to fit the data that exhibit double peaks with a two-fracture model.

The project team from Hazama-Gumi analyzed the radially convergent tracer test by a two-dimensional fracture network model in a vertical cross-section. Matrix diffusion was taken into account and its effect studied.

The JAERI group used a two-dimensional variable-aperture channeling model to represent the fracture zone. Data were studied to relate to the mean aperture and the variance of the aperture density distribution.

The EMP team calibrated a multiple flow path model on the radially convergent test. The model was then used to predict the dipole test.

Key features and other factors included in the conceptual models used by the six groups so far are presented in a comparative table, Table 1.1.

In the next chapter, the experimental test case will be described together with the hydrogeological setting. Types of data available will also be described. In Chapter 3, the hydrological analyses and the establishment of a groundwater flow model by the only one group so far who has completed such a study is presented. From Chapters 4–10, the seven groups' efforts in the evaluation of tracer test data are given, including the goal and motivation of the work, the conceptual and mathematical models used, the calculational results and a discussion of these results in comparison to field data.

A final chapter will give a general discussion of the test case and lessons learned from the work by the seven groups as well as retrospective comments on the experimental design and measurements.

Table 1.1. Summary of conceptual models used by project teams.

	Representation	Dimension	Some of the effects considered
SGAB/SKB	Porous medium with subregions	2D	Dispersion Sorption Matrix diffusion Radioactive decay
	Linear advective dispersive system	1D	
Intera	Horizontal constant aperture fracture	2D	Dispersion Two parallel fractures
KTH	Linear advective dispersive system	1D	Dispersion
	Linear advective dispersive system with matrix diffusion	1D	Dispersion Matrix diffusion
VTT	Channels	Multiple 1D	Advective dispersion Taylor diffusion Multiple flow paths
JAERI	Variable-aperture fracture with channeling effect	2D	Advective dispersion Local dispersion Multiple flow paths
Hazama	Fracture network (3 subregions)	2D	Advective dispersion Matrix diffusion Multiple flowpaths
EMP	Multiple channels		

(To be updated or corrected by the project team.)

2. Description of Experiments and Available Data

P. Andersson and Coworkers
Swedish Geological Company AB, Sweden

2.1 Purpose

This test case is based on three hydraulic interference tests and two tracer experiments performed at the Finnsjön research area located in northern Upland in central Sweden (Figure 2.1) [Andersson, 1987; Andersson et al., 1988c; Gustafsson et al., 1989; Andersson et al., 1990]. The main objectives with the experiments were to determine parameters important for the understanding of radionuclide transport in major fracture zones and to utilize the results for calibration and verification of radionuclide transport models. An additional objective was to develop and improve equipment and experimental methods for application in future field experiments.

These experiments were selected as a test case in the INTRAVAL project since they were designed to study phenomena important in geosphere transport such as advection, dispersion, channeling, dilution, matrix diffusion, heterogeneity in a rather large geometrical scale. Another important aspect of the experiments was that at the start of the INTRAVAL project the tracer tests were still in a planning stage, which made it possible for INTRAVAL participants to comment on the design of the experiments and also to carry out predictive modelling of the tracer tests.

2.2 Overview

These experiments form Phase 3 of the Fracture Zone Project which was started 1984. Phase 1 and 2 of the project were devoted to a detailed characterization of the major fracture zones in the area. The fracture zone chosen for the tracer experiments, Zone 2, is located in granodioritic rock in the Brandaul area at the Finnsjön study site. In the area where the tracer tests were performed the zone is almost planar with the upper surface located between 100 to 240 m below ground. In general the zone has a thickness of about 100 m, but most of the flow appears to take place in three subzones.

Two tracer experiments have been carried out, one in a radially converging flow geometry and one in a dipole flow geometry. In the radially converging experiment tracer injections were made in three peripheral boreholes situated in different directions from a withdrawal hole. The distance from the injection holes to the withdrawal hole is in the order of 150 to 200 m. Tracers were injected in 9 different intervals of the zone for 5-7 weeks, and first arrivals in the withdrawal hole ranged from 22 to 3500 hours.

The dipole experiment was performed after the radially converging experiment using the same hole for withdrawal and one of the other holes for injection. The two other holes used for injection in the radially converging test were used as observation holes in the dipole experiment. During a 7 week period pulse injection of tracers were made and the first breakthrough in the withdrawal hole was registered after about 20 to 25 hours. The water pumped from the withdrawal hole was recirculated to the injection hole.

Prior to the start of the radially converging test a series of hydraulic interference tests was performed in order to determine the hydraulic properties of Zone 2. Pressure responses were registered in packed-off sections in all bore holes in the Brandan area during pumping of the hole later used as withdrawal hole in the tracer experiments. In conjunction with the interference tests

a preliminary tracer test was performed in order to optimize the design and performance of the planned radially converging tracer experiment.

In addition to the results from the interference test and tracer tests performed during Phase 3 of the Fracture Zone Project, a lot of background information on geology, hydrology and geochemistry from investigations of the Brandan area have been available. Laboratory measurements of porosities and diffusivities on drill core samples from the site have also been performed.

2.3 Description of the Site

The general geological, geophysical and hydrological characteristics of the Finnsjön study site have been summarized by Ahlbom et al., [1986, 1987]. At the main investigation site two major fracture zones have been identified, the Brandan fracture zone, Zone 1, and a low-angle zone, Zone 2 (Figures 2.2, 2.3). The geohydrology of the site is dominated by these two highly conductive zones. Zone 1 has a NNE strike with a dip of about 75° to the east, and the thickness of the zone is about 20 m. The hydraulic conductivity varies between $1 \cdot 10^{-6}$ to $5 \cdot 10^{-5}$ m/s as compared to $1 \cdot 10^{-7}$ m/s in the country rock (2m test intervals).

Zone 2, which is the zone utilized for the tracer tests, is trending north with a dip of about 16° to the west and consists of sections with high fracture frequency and tectonisation. The zone is well defined in 7 boreholes (Figure 2.4) located within an area of about 500×500 m. In this area the fracture zone is almost planar with the upper surface located between 100 to 240 m below ground. The zone is about 100 m wide and seems to consist of three subzones with hydraulic conductivities of $2 \cdot 10^{-4}$, $1 \cdot 10^{-4}$ and $1 \cdot 10^{-5}$ m/s (2m test intervals) going from the uppermost zone downwards. The parts in between the sub zones have hydraulic conductivities similar to the country rock. Within the fracture zone the mean value is $5 \cdot 10^{-6}$ m/s. The direction of the groundwater gradient in Zone 2 is towards ENE, and varies in magnitude from 1m/350m to 1m/150m.

The rock where Zone 2 is located is dominated by granodiorite. The rock is medium-grained and red in color. The fracture infillings are dominated by calcite. Other minerals present are hematite, laumontite, asphaltite and clay minerals.

The composition of the groundwater above Zone 2 differs from that in Zone 2 and below Zone 2. The water above Zone 2 is a younger near-surface water, and the water below Zone 2 is an old saline water characterized by a high content of species in solution such as Na, Ca and Cl. The water in Zone 2 is a mixture of these two waters which indicates the appearance of two circulating groundwater systems, one above and one below Zone 2. Both are drained into Zone 2 in the area where Zone 2 is most deeply located and the water is discharged from the shallow parts of Zone 2 into the Brandan zone, Zone 1.

2.4 Experimental Design

2.4.1 Hydraulic interference tests and preliminary tracer test

Three hydraulic interference tests were carried out by withdrawal from different isolated intervals in borehole BFI02 within Zone 2 (Figures 2.2 and 2.4), i.e. the lower and upper parts (test 1 and 2, respectively) and from the entire zone (test 3B) [Andersson et al., 1988c]. In tests 1 and 2, a double packer assembly with a packer spacing of 24 m was isolating the respective subzones from the above and below lying rock. In test 3B a single packer isolated the interval between 193 m and the borehole bottom (288.69 m). The flow rate during tests 1 and 2 was

approximately 500 l/min and in test 3B approximately 700 l/min. The drawdown phases of the tests had a duration of 4-8 days.

The pressure responses were registered in 3-6 intervals in all boreholes in the Brandan area and also in 6 boreholes outside the Brandan area up to 1500 m from the pumping well. During the tests, the flow rate of the discharged water during pumping, electrical conductivity and temperature of the discharged water and the atmospheric pressure were also measured. Registrations of the groundwater table in the observation holes were also undertaken.

During interference test 2 a preliminary tracer test was performed in order to optimize the design and performance of the planned radially converging experiment. Tracers were injected as pulses in the upper highly conductive subzone of Zone 2 in boreholes BFI01 (Uranine), KFI06 (Amino G Acid) and KFI1 1 (Iodide). Tracer breakthroughs were monitored in the pumping well BFI02. Before injection of tracer slugs (50-125 1) the natural piezometric head in the borehole section was registered. In order to force the tracer some distance into the fractures flushing with groundwater and distilled water (50-1251) was done after injection. When natural piezometric head was reached in all sections pumping in borehole BFI02 was started.

2.4.2 Radially converging experiment

In the radially converging experiment hole BFI02 was used as a withdrawal hole and injection of tracers into Zone 2 was made in three peripheral holes, BFIO1, KFI06 and KFI1 1 (Figures 2.2, 2.4) [Gustafsson et al., 1989]. The distances along Zone 2 between the withdrawal hole and BFI01, KFI06 and KFI11 are 168, 189 and 155 m, respectively. In each injection hole three sections were packed off, one in the upper highly conductive part of Zone 2, one at the lower boundary of Zone 2 and one at the most highly conductive part in between. In the withdrawal hole the packed-off section enclosed the whole thickness of Zone 2.

In total 11 different tracers were injected, 8 of them continuously for 5-7 weeks, and three as pulses. The injection intervals in each injection hole and the tracers injected are given in Table 2.1. The tracers selected, DTPA- and EDTA complexes, fluorescent dyes and anions, are stable and non-sorbing.

The injection of tracer was carried out by injecting tracer solution with a constant flow rate into a closed system circulating water from a packed-off section to the ground and back to the packed-off section (Figure 2.5). At the same time, water was discharged from the system with a constant flow rate to avoid pressure build up in the system.In order to obtain good initial mixing of the tracer in the injection section, the volume of concentrated tracer solution necessary to get the desired tracer concentration in the injection section was added during the first circulation cycle of the system. After that, the tracer solution was added with the constant flow rate chosen for the continuous injection, about 2 ml/min.

In order to determine the initial concentration of tracer solution to be added for obtaining the desired concentration in the injection section in the borehole, information about the groundwater flow rate through the injection section is needed. This flow rate was estimated by introducing a tracer pulse into the circulation system and measure the dilution of the tracer versus time. This measurement was performed one week before start of the continuous injection.

During the continuous pulse injection the injection flow rate was registered as injected volume of tracer solution versus time. The water volumes discharged from the injection system was also measured and sampled in order to determine the tracer concentration in the injection section.

Table 2.1. Injection Intervals and Tracers in the radially converging test.

Hole	Interval [m]	Tracer	Type of Injection
BFI01	Upper; 241.5 – 246.5	In-EDTA	Continuous
	Middle; 263.5 – 266.5	Uranine	Continuous
	Lower; 351.5 – 356.5	Ho-EDTA	Continuous
KFI06	Upper; 212.0 – 212.0	Iodide	Pulse
	Middle; 236.5 – 239.5	Yb-EDTA	Continuous
	Lower; 252.5 – 271.5	REO_4	Continuous
KFI11	Upper; 221.5 – 226.5	Gd-DTPA	Continuous
		TM-EDTA	Pulsed
		Amino G	Pulsed
	Middle; 282.5 – 294.5	Er-EDTA	Continuous
	Lower; 329.5 – 338.5	Dy-EDTA	Continuous

Pulse injections of tracers were performed after the continuous injection of tracers had been terminated except in the case of Iodide which started as a continuous injection but ended up as a pulse injection due to equipment failure. The pulse injection was carried out by simultaneously discharging water from the top of the packed-off section and injecting tracer solution at the bottom with the same flow rates. When the section was filled with tracer solution, the solution was circulated in the same manner as in the continuous injections to maintain a homogeneously distributed tracer solution. The circulating solution was sampled in order to determine the decay of tracer concentration versus time.

The tracer withdrawal was made by pumping at a rate of 2.0 l/s in hole BFI02 from a packed-off section covering the whole thickness of Zone 2. In order to obtain steady state prior to the tracer injection, pumping in the withdrawal hole started approximately 6 weeks before the start of the tracer injection. The water discharged from the hole was continuously sampled for tracer analysis during the time period of tracer injection (Figure 2.6). The hydraulic head in the pumped section and also the groundwater level was registered. After the end of tracer injection a detailed sampling of the withdrawal hole was made in order to determine possible interconnections between highly conductive intervals of Zone 2. This sampling was made 52 days after the start of injection by using a double packer system to stepwise discharge and sample water from 7 sections of Zone 2, each time covering 2 m of the zone. After the detailed sampling, the withdrawal and sampling of water from the entire thickness of Zone 2 was continued.

2.4.3 Dipole tracer experiment

The dipole experiment was performed in a recirculating system between BFI01 (injection) and BFI02 (withdrawal) [Andersson et al., 1990]. The high flow rates needed to create a dipole flow field in the scale of 168 m made it necessary to recirculate the water. Holes KFI06 and KFI11 were used as observation holes.

In the dipole experiment only the upper highly conductive part of Zone 2 was used for tracer injection in hole BFI01, the same upper section as was used in the radially converging experiment. The two observation holes were packed-off in the same manner as in the radially converging test. Water from the packed-off section in the withdrawal hole BFI02 was

recirculated to the injection section in BFI01 through a pipe system and tracers were injected into the system were the pipe entered the injection hole (Figure 2.7). Two tracer injections were also made in the upper section of the observation hole KFI11.

In total 15 injections of tracers were made during 7 weeks. Both radioactive and nonradioactive tracers were used. The radiotracers included both non-sorbing and sorbing species. The combination of tracers used in the injections and the sequence of the injections are presented in Table 2.2. The tracer injections in hole BFI01 were made with a duration of approximately 4 minutes. The duration of the two injections performed in hole KFI11 was approximately 60 minutes.

The tracers were sampled in the upper part of Zone 2 in holes BFI02 and KFI1 1 with automatic samplers in the same way as in the radially converging test. Occasionally samples were also taken in the water from the lower intervals of hole KFI11 and in the water from the sections in hole KFI06.

For the sorbing tracers the chemistry of the circulating water is of importance and therefore a comprehensive chemical analysis of the sampled water was made at the end of the dipole experiment. During the experiment the temperature of the water entering the injection hole BFI01 was measured, and also the oxidation-reduction potential showing that the conditions were stable and reducing (-200 mV). The electrical conductivity and the temperature of the water discharged from the withdrawal hole BFI02 were registered every day during the experiment.

During the pumping period the pumping rate was measured once a day. Hydraulic heads in 9 different boreholes in the area were measured almost every day during the pumping period and measurements were also made prior to the staff of the dipole pumping and one week after terminating the pumping.

2.4.4 Complementary experiments

Laboratory measurements of the porosity and diffusivity were performed on drillcore samples from boreholes KFI06 and KFI11 [Gidlund et al., 1988]. The samples were taken at different distances from a fracture surface. The porosity was determined from the difference in dry and wet weight of the sample. The diffusivity was determined by placing a sample between two reservoirs, one containing a tracer solution (iodide or Uranine) and the other initially free from tracer, and measuring the concentration increase of the tracer in the low concentration reservoir.

2.5 Available Results

2.5.1 Interference tests and preliminary tracer test

Results from the hydraulic interference tests [Andersson et al., 1989c] have been given as primary drawdown responses in the boreholes within Zone 2 during the time of pumping in hole BFI02. Graphs of the recovery of the groundwater head in the boreholes after stop of pumping have also been available. In addition, graphs of the flow rate, electrical conductivity and temperature of the water discharged from BFI02 have been given as well as the barometric pressure.

Drawdown of the primary responses have also been given as a function of distance from the pumping hole BFI02. The drawdown curves, both time-dependent and distance dependent have been used to evaluate hydraulic parameters such as transmissivities and storativities. These data have also been available and they indicate that the upper and lower subzones of Zone 2 have a

Table 2.2. Tracers and injection schedule in the dipole experiment.

Injection	Day after pump start	Tracer	Half-life
A	14	Rhodamine WT	Dye tracer
1	23	$^{82}Br(I)^-$	1.47 d
2	24	$^{99m}Tc(VII)O_4^-$	6.01 h
		$^{186}Re(VII)O_4^-$	3.78 d
3	26	$^{131}I(I)^-$	8.04 d
4	31	$^{99m}Tc(VII)O_4^-$	6.01 h
5	32	$^{58}Co(II)^+$	70.92 d
		$^{86}Rb(I)^+$	18.66 d
6	35	$^{24}Na(I)^+$	14.66 h
		$^{82}BR(I)^-$	1.47 d
		$^{99m}Tc(VII)O_4^-$	6.01 h
		$^{131}I(I)^-$	8.04 d
		$^{186}Re(VII)O_4^-$	3.78 d
		$^{201}Tl(I)^+$	3.05 d
7	39	$^{51}Cr(III)$-EDTA	22.70 d
		$^{111}In(III)$-EDTA	2.81 d
		$^{140}La(III)$-DOTA	1.68 d
		$^{160}Tb(III)$-EDTA	72.1 d
		$^{169}Yb(III)$-EDTA	32.0 d
		$^{177}Lu(III)$-EDTA	6.71 d
8	43	$^{58}Co(III)$-EDTA	70.92 d
B	44	Blue Dextran 2000	Macro molecule
9*	46	$^{131}I(I)^-$	8.04 d
10*	47	$^{131}I(I)^-$	8.04 d
C	48	In-EDTA	Metal complex
D	49	Gd-DTPA	Metal complex
		Tm-EDTA	Metal complex
E	54	Rhodamine WT	Dye Tracer

*Injection in hole KFI11, upper section.

high hydraulic diffusivity (high transmissivity and low storativity) and that a vertical leakage between the subzones and between Zone 2 and the surrounding rock occurs.

Primary data available from the tracer test performed in conjunction with interference test 2 are concentration and volumes of tracers injected, volumes of borehole sections and tubing, duration of tracer injection, pumping capacity and duration of pumping in BFI02 and tracer concentration versus time in BFI02. The tracer breakthrough curves have been used to evaluate hydraulic parameters such as hydraulic fracture conductivity, fracture aperture, flow porosity and dispersivity, which also have been given.

2.5.2 Radially converging experiment

Breakthrough curves monitored in the withdrawal hole BFI02 for all eleven tracers injected at nine locations, three in each injection hole, have been available as tracer concentration versus time from start of injection [Gustafsson et al., 1989]. Also the tracer concentrations in the injection sections during the time of continuous injection have been available. An example is given in Figure 2.8 showing the breakthrough curve for In-EDTA in the withdrawal hole BFI02 and the injection concentration of In-EDTA in the upper section of hole BFI01.

Other data available from the radially converging test are:

- volumes of the injection sections and the tubing in the injection systems,
- initial concentration of the tracers injected,
- volumes of tracer solution in the storage tanks versus time and calculated mean injection flow rates,
- mean discharge rate of water from the injection system,
- first arrival of the tracers in the withdrawal hole (Table 2.3),
- total mass of tracers injected and the tracer recovery (Table 2.3),
- groundwater levels in the boreholes as a function of elapsed time,
- relative hydraulic head differences versus elapsed time between the pumped interval in the withdrawal hole and the injection sections in the injection holes, and calculated mean head differences before and after the detailed sampling in the withdrawal hole BFI02,
- pump capacity in hole BFI02, and temperature and hydraulic conductivity in the pumped water as a function of time,
- groundwater flow rates versus time in the injection intervals during injection, and calculated mean values,
- groundwater flow rates in the injection intervals prior to and after the injection of tracers, log of events.

Results from the detailed sampling in hole BFI02 have been given as tracer concentration in samples from all seven sections pumped, four samples from each section taken during a time period of four to seven hours. An example is given in Figure 2.9 showing the concentration of In-EDTA in the different section of hole BFI02. Decreasing concentration versus time in a section indicates contamination from the previous sampled section while increasing or a high, constant concentration indicates that the sampled section contains a main flow path.

Table 2.3. First arrival and recovery of tracers in BFI02, radially converging experiment.

Tracer	First arrival hours	Recovery [%]	Elapsed time [hours]
In-EDTA	75	97.6	4510
Uranine	700	18.0	4510
Ho-EDTA	1250*	6.1	4510
Iodide	106	69.7	3119
Yb-EDTA	1250*	11.8	4510
ReO_4^-	194	65.3	4510
Gd-DTPA	24	88.6	4510
Tm-EDTA**	23	72.1	860
Amino G**	23	86.7	600
Er-EDTA	850	1.9	4510
Dy-EDTA	3600*	0.7	4510

*First arrival after the detailed sampling of BFI02
**Pulsed injection.

2.5.3 Dipole experiment

In the dipole experiment tracers were detected in both the withdrawal hole BFI02 and in the two observation holes KFI06 and KFI11. Breakthrough curves for the 19 injected tracers have been available as concentration normalized to injection concentration versus elapsed time after injection [Andersson et al., 1990]. Figure 2.10 shows the breakthrough curve for 131I (injection 3) in the withdrawal hole BFI02 and in the observation hole KFI11.

Other data from the experiment that have been available are:

- initial tracer concentration in the injected solution and volume of that solution injected, duration of injected tracer pulse,
- tracer first arrivals, mean residence time and peak concentrations for breakthrough in the withdrawal hole BFI02 and in the observation holes KFI06 and KFI11 (Table 2.4), the recovery of tracers in the three holes at different times,
- hydraulic heads and groundwater levels in 9 different boreholes as a function of time since the start of pumping in hole BFI02, and hydraulic head differences between the different holes and the pumped section in BFI02, pumping rate in BFI02 versus time, and the mean value over the period 0–1485 hours which was 120.2 l/min,
- electrical conductivity, temperature and redox-potential of the pumped water during the experiment.

Table 2.4. First arrival, mean residence time and peak concentration for breakthrough in the withdrawal hole BFI02 and in the observation hole KFI11.

Inj.	Tracer	First arrival [hours]	Mean residence time [hours]	Peak concentration C/C_o
		Withdrawal hole BFI02		
1	^{82}Br	FD	FD	FD
2	^{186}Re	(24)	(24)	$(6.3 \cdot 10^{-4})$
3	^{131}I	20	45	$8.2 \cdot 10^{-4}$
6	^{82}Br	20	46	$8.6 \cdot 10^{-4}$
	^{131}I	20	44	$8.2 \cdot 10^{-4}$
	^{186}Re	20	45	$6.6 \cdot 10^{-4}$
7	^{51}Cr	20	42	$6.0 \cdot 10^{-4}$
	^{111}In	20	45	$7.0 \cdot 10^{-4}$
	^{140}La	(34)	FD	$(6.4 \cdot 10^{-4})$
	^{160}Tb	(24)	(36)	$2.5 \cdot 10^{-4}$
	^{169}Yb	(24)	(40)	$8.6 \cdot 10^{-4}$
	^{177}Lu	30	49	$3.8 \cdot 10^{-4}$
8	^{58}Co	20	(37)	$5.3 \cdot 10^{-4}$
A	Rhodamine	WT22	50	$5.3 \cdot 10^{-4}$
C	In-EDTA	20	45	$1.4 \cdot 10^{-4}$
D	Gd-DTPA	20	41	$2.0 \cdot 10^{-4}$
	TM-EDTA	20	41	$2.8 \cdot 10^{-4}$
E	Rhodamine	WT22		
		Observation hole KFI11		
1	^{82}Br	FD	FD	FD
2	^{186}Re	10	21	$2.9 \cdot 10^{-3}$
3	^{131}I	20	20	$4.7 \cdot 10^{-3}$
6	^{24}Na	12	21	$2.6 \cdot 10^{-3}$
	^{82}Br	11	20	$4.5 \cdot 10^{-3}$
	^{131}I	10	19	$4.0 \cdot 10^{-3}$
	^{186}Re	10	19	$4.1 \cdot 10^{-3}$
7	^{51}Cr	(10)	20	$2.9 \cdot 10^{-3}$
	^{111}In	(10)	22	$3.6 \cdot 10^{-3}$
	^{140}La	13	22	$2.2 \cdot 10^{-3}$
	^{160}Tb	(10)	18	$1.9 \cdot 10^{-3}$
	^{169}Yb	(10)	20	$4.5 \cdot 10^{-3}$
	^{177}Lu	12	30	$1.2 \cdot 10^{-3}$
8	^{58}Co	(10)	20	$2.6 \cdot 10^{-3}$
A	Rhodamine	WTFD	FD	FD
C	In-EDTA	11	21	$0.7 \cdot 10^{-3}$
D	Tm-EDTA	10	19	$1.6 \cdot 10^{-3}$
	Gd-DTPA	10	19	$1.5 \cdot 10^{-3}$
E	Rhodamine	WT12	26	$1.7 \cdot 10^{-3}$

FD = Few Data points ( ) = Uncertain values

Breakthrough curves in the withdrawal hole from two tracer injections in the observation hole KFI11 have also been available as well as results from a tracer dilution test performed in hole KFI11. The dilution measurement showed that the groundwater flow rate through the packed off section in KFI11 was 519 ml/min.

2.6 Supporting Data

Geological data from a surface survey of the Brandan area as well as from borehole investigations have been reported by Ahlbom et al. [1986, 1987]. The type of data recorded in these investigations are; rock type, rock alteration, fracture frequency, fracture orientation, fracture infillings etc.

Hydraulic data resulting from comprehensive hydraulic testing of the Brandan area have been available. The hydraulic conductivity has been determined by means of a large number of hydraulic single hole tests, and a statistical analysis of the hydraulic conductivity data based on the concept of conductive fracture frequency has been made [Andersson et al., 1988a and 1988b]. A first series of interference tests were performed during the drilling of borehole BFI01 using the air-flush system of the drilling rig as a high capacity pump, and measuring the pressure response in all boreholes within the Brandan area [Ahlbom et al., 1987]. These tests provided data on storativities and transmissivities in Zone 2.

Results from analyses of surface water, drilling water and deep hole groundwater have also been reported [Ahlbom et al., 1986] as well as results from ground geophysical investigations and geophysical logging in all boreholes within the Brandan area [Ahlbom et al., 1986 and 1987]. Examples of the geophysical information available are; resistivity, borehole deviation, temperature, natural gamma radiation.

Data on porosities and diffusivities determined in the laboratory on samples from boreholes KFI06 and KFI11 have been available [Gidlund et al., 1988]. Measured porosities ranged from 1.5–5.4%, and effective diffusivities varied between 10^{-13} and $2 \cdot 10^{-2}$ m^2/s for iodide and between 10^{-14} and $4 \cdot 10^{-13}$ m^2/s for Uranine.

3. Hydrologic Investigation and Groundwater Flow Modeling — SGAB/SKB

P. Andersson and Coworkers
Swedish Geological Company AB, Sweden

3.1 Modeling Purpose

The flow and transport modeling in connection with case 5 was carried out as parts of the sequence of field experiments: the hydraulic interference tests, the radially converging tracer test and the dipole tracer test. Figure 3.1 illustrates the general flow of field experiments and related modeling. Thus, there were several separate modeling efforts. The general purpose for all the modeling described here was to predict each field experiment based on all available information and compare the results with the actual outcome of the experiment. As each experiment was completed, new information could be added to the model in order to improve the predictive ability for the prediction of the following experiment. It was emphasized during the this whole sequence that groundwater flow should be predicted as well as solute transport.

In addition to the general modeling purpose described above, model simulations were also performed in order to assist in the design of all the different experiments.

Finally, considerable effort was placed on using models to evaluate and interpret the experimental data with respect to injection schedules, observed occurrence of multiple flow paths, etc.

3.2 Conceptual Model

The low angle fracture zone is generally modelled as a porous medium, where flow and transport can be described using averaged properties of the medium. Figure 3.2 shows a conceptual model of the fracture zone. The total thickness of the zone is about 100 metres. It consists of highly fractured sub-zones, of which the dominating ones are located at the upper and lower limitations of the zone. Vertical connections between the subzones exist as indicated in Figure 3.2. However, the variability of media properties is much larger in the vertical direction than in the horizontal, and with the lower hydraulic connectivity in the vertical direction.

Most of the transport modeling was performed for the upper, 0.5 m thick highly conductive, part of the fracture zone. Some of the flow modeling was also carried out with the fracture zone represented as the equivalent to a multilayered aquifer.

Considered transport processes are advection/dispersion, radioactive decay and linear equilibrium sorption.

Prior to the interference tests, transient flow modeling was carried out in order to predict the interference tests and to assist in the design of the tests. The available information was somewhat limited, and consisted mainly of singlehole transmissivity measurements between packed off sections in a number of boreholes. Thus, no averaged properties or boundary conditions were known. In this case a vertical profile with radial symmetry was used, with the fracture zone being represented as a layered aquifer. This conceptual model is shown in Figure 3.3. The understanding at this time of the fracture zone was that it consisted of three highly conductive sub-zones, separated by layers of relatively low hydraulic conductivity.

The results of the interference tests provided an extensive amount of drawdown data, with which the predictions could be evaluated and the flow model be calibrated and updated. These calibrations were made in order to be able to predict the flow conditions during the radially

converging test, which was to be performed with a different pumping rate than during the interference tests. One of the interpretations of the interference test results was that the prediction model geometry was too simplified. Accordingly, the geometrical structure of the model was updated by adding more recent geological analyses, which resulted in the model geometry shown in Figure 3.4. In this case the entire 100 m thick fracture zone is represented as a horizontal plane. The calibration of the model was done using the last of the three interference tests, pumping of the entire thickness of the fracture zone. This was the same test geometry as was to be used during the radially converging tracer experiment.

Using the updated model, calibrated with transient pumping test data from eight different boreholes, the steady state flow field for the radially converging test was predicted. Using the flow field (hydraulic head distribution), tracer breakthrough curves were predicted prior to the start of the tracer test. Although information about hydraulic parameters and boundary conditions now was available, very little was known about the transport parameters that were required.

Lastly, the dipole test was predicted. An evaluation of the radially converging test yielded transport parameters that could be used for predicting the dipole test. In this case the model geometry was simplified considerably, since some preliminary flow modelling indicated that the influence of hydraulic boundaries would be relatively small. However, these flow simulations indicated that the existing natural gradient may affect the flow field, and therefore it was included in the transport simulations.

The above described sequence concerns the two-dimensional modeling. In addition, one-dimensional models were used for evaluation of the tracer tests. In this case, very little consideration is given to the flow hydraulics and only water residence times are of interest. The purpose of these models were primarily to be able to make some interpretations about the transport connectivity between the different injection sections and the sampled borehole. It is here emphasized that information from all the experiments provided a basis for these interpretations.

The different modelling steps are published in a number of reports. The interference test modeling is described in Nordqvist and Andersson (1987), Andersson et al. (1988), and Ahlbom and Smellie (1989). Predictions and evaluation of the radially converging experiment is contained in Gustafsson et al. (1989). The dipole tracer test predictions are reported in Nordqvist (1988), and a preliminary evaluation of the dipole predictions are given in Andersson et al. (1990).

3.3 Mathematical/Numerical Model

3.3.1 Governing equations

The groundwater flow is assumed to take place in a porous medium, and is in two dimensions governed by the equation (Freeze and Cherry, 1979):

$$\frac{\partial}{\partial x}\left(T\frac{\partial h}{\partial x}\right)+\frac{\partial}{\partial y}\left(T\frac{\partial h}{\partial y}\right)Q=S\frac{\partial h}{\partial t} \qquad (3\text{-}1)$$

where T = transmissivity (m^2/s)
h = piezometric head (m)
S = storage coefficient
Q = fluid mass sources or sinks (volume fluid/(volume aquifer · time))

Equation (3-1) is based on Darcy's law and a continuity equation. Constant density of fluid, saturated flow and an isotropic medium is assumed.

The transport simulations were all performed for a single solute. The transport mechanisms considered in the simulations are:

— advection, governed by the general flow field

— hydrodynamic dispersion, originating from variations in the average velocity field

— radioactive decay

— equilibrium linear adsorption

The governing equation for the solute transport model in two dimensions applied in this work can be written as:

$$\nabla(D\nabla C) - \nabla(\underline{v}C) - \Gamma = R\frac{\partial C}{\partial t} \tag{3-2}$$

where C = concentration of solute (kg/m^3)
$\underline{v}$ = average linear velocity (m/s)
D = dispersion tensor
R = retardation factor due to adsorption
Γ = solute sink due to decay (kg/m3 s)

The average linear velocity is given by Darcys' law:

$$\underline{v} = K/\phi \cdot \nabla h \tag{3-3}$$

where ϕ is the flow porosity and h is obtained from solving equation (3-1).

The dispersion tensor, D, is defined as

$$D = \begin{bmatrix} D_{xx} & D_{xy} \\ D_{yx} & D_{yy} \end{bmatrix} \tag{3-4}$$

and

$$D_{xx} = (1/v^2)(d^1v^2_x + d_Tv^2_y) \tag{3-5}$$

$$D_{yy} = (1/v^2)(d_Tv^2_x + d_Lv^2_y) \tag{3-6}$$

$$D_{ij} = (1/v^2)(d_L - d_T)(v_i v_j) \qquad (3\text{-}7)$$

$$i \neq j \ , \ i = x,y$$

$$j = x,y$$

where v = magnitude of the average linear velocity vector (m/s)
v_x = magnitude of x-component of v (m/s)
V_y = magnitude of y-component of v (m/s)
d_L = longitudinal dispersion coefficient (m^2/s)
d_T = transverse dispersion coefficient (m^2/s)

The size of the dispersion coefficients are dependent upon the local magnitude of average velocity in a flowing system:

$$d_L = a_L V \qquad (3\text{-}8)$$

$$d_T = a_T V \qquad (3\text{-}9)$$

where a_L = longitudinal dispersivity of solid matrix (m)
a_T = transverse dispersivity of solid matrix (m)

The dispersivities a_L and a_T may be considered as fundamental transport properties, when applied to a particular field situation. However, they may not be representative if scales of transport vary or in cases where large heterogeneities exist.

Radioactive decay is treated as a first order mass production process defined as:

$$\Gamma = \lambda C R \qquad (3\text{-}10)$$

where λ = radioactive decay constant (s^{-1})

The decay constant, λ, is equal to In 2/half-life for the radioactive solute. For conservative solutes, λ is set to zero.

The retardation factor, R, is defined as:

$$R = 1 + \rho_b K_d/\phi \qquad (3\text{-}11)$$

where ρ_b = bulk mass density of the porous medium (kg/m^3)
K_d = distribution coefficient (m^3/kg)

For a non-sorbing solute, R is set to 1. The distribution coefficient, K_d, is assumed to describe the adsorption characteristics of the system. For linear, reversible, equilibrium adsorption it is related to the adsorption density as:

$$C_s = K_d C \qquad (3\text{-}12)$$

where C_s = mass adsorbate/mass solid grains plus adsorbate.

Equation (3-1) for transport in unconsolidated deposits, the adsorption per mass concept is usually sufficiently accurate. However, when dealing with transport in fractured rocks adsorption isotherms need to be expressed in terms of adsorption per available surface area.

As a final remark regarding adsorption, it should be pointed out that only adsorption on external fracture rock surfaces is considered in this work. A related mechanism that may be important, but not considered here, is inner adsorption of tracers wi. For transport in unconsolidated deposits, the adsorption per mass concept is usually sufficiently accurate. However, when dealing with transport in fractured rocks adsorption isotherms need to be expressed in terms of adsorption per available surface area.

As a final remark regarding adsorption, it should be pointed out that only adsorption on external fracture rock surfaces is considered in this work. A related mechanism that may be important, but not considered here, is inner adsorption of tracers within the rock matrix caused by diffusion of solute into the rock matrix.

The transport equations in two dimensions were solved numerically by a two-dimensional finite element code, SUTRA, version 1284-2D, (Voss, 1984).

In addition to the two-dimensional model described above, one-dimensional modeling was performed, mainly in the evaluation part of the tracer tests. The mathematical description is in this case analogous to the two-dimensional case. The fluid velocity is assumed to be a constant, and transversal dispersivity is ignored. The governing equation for the one-dimensional case is:

$$D\frac{\partial^2 C}{\partial x^2} - v\frac{\partial C}{\partial x} - \lambda RC = R\frac{\partial C}{\partial t} \qquad (3\text{-}14)$$

where x = distance from injection point (m)

This model was applied in the evaluation of the radially converging tracer test. Although a linear flow model (constant velocity) is used for a radial flow field, it can be demonstrated that breakthrough curves and parameter estimates are very similar for Peclet numbers of the order 10 and higher.

Mixing in the sampled borehole of tracers travelling through several different major flowpaths is considered. The concentration in the sampled section is assumed to be a volume-averaged concentration:

$$C_i = \Sigma f_i C_i \qquad (3\text{-}15)$$

where C = tracer concentration in borehole
f_i = fractional volume parameter
C_i = tracer concentration from flowpath i

As independent measurements (other than the breakthrough curves) indicated the existence of such multiple-path transport, this approach proved particularly useful.

The one-dimensional models were solved using analytical solutions as given by Van Genuchten and Alves (1984). Variable injection schemes were simulated by superposition of these solutions.

3.3.2 Boundary and Initial Conditions

When solving the flow equations with SUTRA, the required boundary conditions are either specified hydraulic head or constant flow. In cases where flow crosses a boundary, solute concentration of fluid entering the flow domain has to be specified.

For the tracer injections, boundary conditions for a step input can be defined as so called first type boundary conditions:

$$C = C_a \tag{3-16}$$

where C is the solute concentrations in the injection well, and C_a is a constant. A so called third type boundary condition for a step input is defined as:

$$-D\frac{\partial C}{\partial x} + vC = vC_a \tag{3-17}$$

The latter boundary condition represent a convected input of solute at the upstream boundary. In this report, a third type boundary conditions is assumed in most cases for the injection well.

In some of the one-dimensional models, a slightly different kind of third type boundary is used, where a decaying injection concentration is considered (Javandel et al., 1984):

$$-D\frac{\partial C}{\partial x} + vC = vf(t) \tag{3-18}$$

with

$$f(t) = C_a\exp(-\alpha t) \tag{3-19}$$

where α = source decay parameter (s^{-1})

Boundary condition (3-16) was used for evaluation of some pulse injections, in order to account for any storage of tracer in the packed off tracer injection volume.

In addition, pulse injections were also evaluated assuming an instantaneous unit pulse (Zuber, 1974)

Initial conditions are given as hydraulic head and solute concentration over the region. When solving the equations for steady-state flow, initial head distribution is rather arbitrary. Calculations involving transient solute transport require specification of initial concentrations across the computational domain.

3.3.3 Parameter estimation methods

Two methods were used for estimating flow and transport parameters. A rather informal approach was taken to the calibration of the two-dimensional models (SUTRA), where trial-and-error was employed to update model parameters between experiments.

For the one-dimensional analysis, non-linear least squares regression was used. The technique that was used for regression is sometimes referred to as the Marquardt method (Marquardt, 1963) and is in this report formulated as, in an iterative form (see also Cooley, 1985):

$$B_{r+1} = B_r + p_{r+1}(X_r^T W X_r + u_{r+1})^{-1} X_r^T W(C_r^0 - C_r^m) \qquad (3\text{-}20)$$

where B_r = vector of parameter estimates
X = vector of parameter sensitivities
W = reliability weight matrix
C_{ro} = vector of observed concentrations
C_r^m = vector of model concentrations
p = damping parameter (≤ 1)
u = Marquardt parameter

Equation (3-20) gives the updated parameter estimate at the (r+1)th iteration. The parameter sensitivity vector is obtained by taking partial derivatives of the dependent variable with respect to each parameter. Thus, for an element in the X matrix:

$$X_{ij} = \partial C_j^m / \partial B_i \qquad (3\text{-}21)$$

The parameter sensitivities are obtained by taking analytical derivatives.

The reliability weight matrix, W, usually reflects the error structure of the observed data. However, it may also be used investigator to emphasize/de-emphasize certain components of the data. If the observations are assumed to be random (no correlation between observations) and have a common variance W reduces to an identity matrix, and that is what is assumed in this work.

Standard errors of the parameters and linear correlation between parameters were obtained from the variance-covariance matrix, $s^2(X^TWX)^{-1}$, where s^2 is the error variance. Details of the statistical analysis procedures of regression results are also given by Cooley, 1979.

3.4 Model Selection Criteria

An objective of the modeling was that both hydraulic heads and tracer transport should be described essentially by the same model. Further, this model should be based on physical processes.

A general approach for the selection of model(s) in this case was that they should be relatively simple, as this should be seen as an initial effort to model the flow and tracer tests in Finnsjön. Thus, for reasons of simplicity, a more or less traditional porous media approach was taken where the flow domain can be assigned averaged flow and transport properties on the scale of the performed experiments. As the fracture density is high in the zone, this assumption should be entirely reasonable.

The fracture zone is a fairly well defined horizontal plane, bounded by more or less impermeable boundaries. Thus, a 2-D confined aquifer model was selected, in order to account for effects of hydraulic boundaries on the flow field, especially during the radially converging tracer test.

The reasons for applying the 1-D models were slightly different. In this case the flow conditions were more or less neglected and only water residence times were considered. The desire was to use some simple models as a tool to support the interpretation of the experimental data, especially with respect to variable injection schemes, different inlet boundary conditions, multiple flow paths, retardation, etc.

The radially converging flow field was in this case approximated with a linear flow field, which is a reasonable approximation at moderately high Peclet numbers. This approximation was used for reasons of simplicity, since simple analytical solutions exist and parameters can be estimated with a relatively small computational effort.

In summary, the 1-D modelling can be seen as a natural extension of the analysis of the experiment(s), where the effects of injection stops, multiple flow paths, etc, can be checked with a minimum of computational effort. The 2-D model, on the other hand, was used to predict the outcome of each experiment.

3.5 Results

In this section all the modeling steps, including predictions, comparison with results and calibrations, will be described for each of the three experiments considered.

3.5.1 Predictions of the hydraulic interference tests

The hydraulic interference tests were predicted based on somewhat limited data. The outer boundaries of the fracture zone were uncertain, and only local transmissivity values from single hole packer measurements were available. Thus, a very simple geometry was used, as shown in Figure 3.3. As transient drawdown data already existed from measurements during drilling of borehole BFI02 (Ahlbom et al., 1987), some limited calibration of the model could be carried out. However, only short time series were available in this case and this calibration could at best yield very approximate values of the hydraulic parameters. The parameter distribution that was actually used for the predictions are presented in Figure 3.3. The fracture zone is represented as a horizontal band of more or less permeable layers. Radial symmetry is assumed, with the pumping section located along the left border. The zone of relatively lower hydraulic conductivity values to the far right in the model is a somewhat artificial feature. It was introduced with the purpose of simulating a mixed boundary, since neither a constant head or a no flow boundary seemed reasonable.

Four different scenarios were predicted; pumping in subzone 1 (corresponding to test 2), pumping in subzone 2, pumping in subzone 3 (corresponding to test 1), and pumping in the entire fracture zone (corresponding to test 3B). The comparisons for test 3B are presented in Figures 3.5 to 3.8, with the interference test results plotted together with the predicted primary responses and predicted groundwater level responses (or the uppermost section). The predicted primary responses should be compared to the uppermost observed curve, while the predicted groundwater level responses should be compared to the lowermost observed drawdown curve. The remainder of the predicted sections are here omitted for clarity, and only the predicted extremes are plotted. The predictions of tests 1 and 2 are not presented as the results are very similar to test 3B.

Comparisons of predicted versus observed results from the interference tests show that the predictions generally are not accurate. It is apparent that accurate predictions of the interference tests are difficult to make based on the actual information that was available. However, by analyzing the discrepancies between predicted and measured results, some valuable information can be gained about the zone.

Both the model predictions as well as analytical interpretations (Andersson et al., 1988) indicate that the previously assumed transmissivity of Zone 2 is somewhat low. Further, the different subzones are not isolated units, but are hydraulically interconnected. This is indicated by the fact that measured drawdowns from different observation sections within the zone for a particular observation borehole in most case merge to similar values of drawdown as steady state is approached. The validity of this interpretation is also supported by some parameter sensitivity tests performed during the predictive modeling (Nordqvist and Andersson, 1987). In one of those tests the layers separating the subzones were assigned a significantly lower hydraulic conductivity than those given in Figure 3.3. The result was a significant vertical difference in drawdowns between different subzones within the zone, which was generally not observed during the interference tests. However, it should be pointed out that since certain (but small) drawdown differences between different sections actually were observed, this may indicate a somewhat lower hydraulic conductivity in the vertical direction (see also Andersson et al., 1988). An additional important interpretation is that hydraulic boundaries are not accounted for correctly, which is indicated by the shape of the drawdown curves obtained from the interference tests.

In order to obtain an improved model that would describe flow in the Brandan area, some additional data needs were recognized. The most important was a better description of the geometrical framework, with respect to the extent of the fracture zone and the nature of its boundaries. Further, values of transmissivity of the zone would have to be refined. In the following section an attempt to update the groundwater flow model is described.

3.5.2 Calibration of the model

* Model Geometry

The flow domain chosen was based on updated interpretations of the geology of the Brandan area (Andersson et al., 1988), and is considerably larger than in any of the previous modeling efforts in this area (Andersson and Andersson 1987, Nordqvist and Andersson 1987). The main justification for this was that data from the interference test were available from boreholes outside Zone 2, such as KFI01 and KFI04. Thus, modeling results outside the fracture zone could be verified, although in a somewhat qualitative manner. The computational flow domain used for the simulations is shown in Figure 3.4 with the boreholes of interest marked.

Figure 3.4 describes the zone in a horizontal plane as a triangle lined by the vertically oriented Brandan zone along one edge. Along the left edge of the computational domain another vertical fracture zone is included, the Gåvastbo zone. Each rock unit is assumed to be homogeneous.

The flow domain was discretisized into a finite element mesh in order to provide input to the numerical model. The element mesh is shown in Figure 3.9, and consists of 1404 nodes and 1326 quadrilateral elements.

The modeling was performed only in a horizontal plane representing the entire thickness of Zone 2. The zone was modeled as one hydraulic unit with boundary conditions as specified below. It was not considered relevant to attempt to model any of the subzones separately (test 1

and test 2), since the interference test results indicated that a significant part of the flow originated from vertical flows within Zone 2, when pumping only in one of the subzones. Thus, the test actually simulated is test 3B, pumping in the entire Zone 2. Further, the radially converging tracer test was to be performed by pumping the entire thickness of the zone.

* Boundary Conditions

One of the main obstacles when attempting to model the fracture zone is to define the hydrogeological boundaries of the zone in the horizontal direction. In the simulations described here, boundaries were defined based on interpretations of the interference test data and geological information. The boundary conditions imposed on the modeled domain are shown in Figure 3.10. No natural gradient was considered, since it is inadequately defined for the model geometry and is judged not to influence the drawdown distribution significantly when pumping from the fracture zone. A constant head was assigned to one end of the Brandan zone in order to account for regional inflow of groundwater. Flow was also allowed in the model to originate from the Gåvastbo Zone, thus entering the fracture zone close to the boreholes HFI01, KFI05, KFI09 and KFI10. The location and hydraulic description of all boundaries should be considered to be approximate.

As initial conditions for the transient conditions the hydraulic head was set to zero for the entire flow domain. Groundwater withdrawal rate was set to 700 l/min, corresponding to the pumping rate for test 3B.

* Calibration Strategy and Criteria

The approach chosen for calibration of the present flow model was to utilize as much geological and hydrogeological information as possible, in order to obtain an accurate description of the flow conditions in the Brändan area. This involved in addition to the detailed geological interpretations indicated earlier, the measured responses from the actual interference tests.

The general procedure was to simulate transient flow, using the assumed geometry of the flow domain, in such a way that an agreement between simulated and measured drawdowns of the primary responses would be achieved.

One very important point is that although data of high quality from the interference tests are available for calibration of the flow model, there is at this point no way to verify that a calibrated model is a unique solution to this particular system. In order to verify a calibrated model data from a different hydraulic event, for example pumping of a different borehole, would be required.

The term calibration criteria here refers to the measure used in order to judge whether a calibration is satisfactory or not. The criterium employed here was simply to visually compare measured and simulated transient drawdown behaviour in all the monitored boreholes. Differences in drawdown between boreholes were also used to some extent, but in a somewhat more qualitative manner.

The "tuning" parameters for the calibration were transmissivity and storage values, and to some extent the boundary conditions. Boundary effects are detected in the transient drawdown curves as deviations from corresponding type curves for infinite aquifers. A combination of transmissivities, storage coefficients and boundaries that would yield a good fit between measured and simulated primary responses, was considered as an indication that these parameters were correctly estimated. The storage coefficients were basically tuned using the initial stages of the compared curves, while transmissivity values entirely govern steady state drawdowns.

* Results of Calibrations

The calibrated flow model was arrived at by adjusting hydraulic parameters and boundary conditions until a satisfactory fit between observed and simulated drawdown behaviour was obtained. During this process, extensive interaction between modeling results and analytical aquifer analysis was maintained.

Using the assumed geometry, the parameter distribution yielding the best fit is shown in Figure 3.11. All the separate rock units in are here assumed to be homogeneous and isotropic. The separate section at the top of the triangular shape representing Zone 2, was introduced to eliminate undesired effects on flow in the zone of the assigned constant head in the direction of Lake Finnsjon. The simulated and observed transient drawdown curves, for the boreholes within zone, are shown in Figures 3.12 to 3.15. The hydraulic head distribution near steady state, presented in Figure 3.16, shows a relatively low hydraulic head gradient within the zone due to the high transmissivity, while steep gradients prevail in the rock outside Zone 2. Budget calculations carried out by SUTRA indicate that approximately 60% of the discharged fluid in the model originates from the constant head boundary at the upper part of the Brandan Zone.

The transient curves show a relatively good agreement between simulated and observed primary responses. The main exception consists of borehole BFI01, where simulated drawdowns are significantly higher than the observed as steady state is approached. As is discussed in Andersson et al. (1988), measured responses in BFI01 (and to some extent in KFI11) are not consistent with those observed in other boreholes. The behaviour of BFI01 is not possible to model using the assumptions of the flow geometry and an isotropic medium.

As a qualitative check of the calibrated model, measured responses outside Zone 2 were also compared with the model results. Figure 3.17 shows an example of this, where data from borehole KFI04 are compared to model calculations. The slopes of the measured and modeled transient curves are similar, while they differ somewhat timewise. The time discrepancy may be due to open-borehole effects in KFI04 (no packers) not accounted for in the numerical model.

* Parameter Sensitivity

The term parameter sensitivity refers in this case to how flow conditions in the computational domain changes as hydraulic parameters are changed, and is not used as a measure of parameter uncertainty. The effects of parameter changes on the simulation results were not examined systematically, but during the calibration process two main features of the flow system became apparent:

— total drawdown within the fracture zone is generally governed by the nature of surrounding boundaries. In Figure 3.18 the transmissivity within is increased by approximately one order of magnitude compared to Figure 3.16. Changes in transmissivity within Zone 2 have very little effect on the magnitude of the drawdowns in the different boreholes.

— hydraulic gradients within the zone are entirely governed by the transmissivity. This is also noted in Figure 3.18, where drawdowns approaching steady state are almost identical in all the boreholes within the zone for the case of high transmissivity.

Figures 3.16 and 3.18 also demonstrates the "bathtub" effect that is a result of a bounded system such as this. This means that the drawdown behaviour in general is very similar between the boreholes within the fracture zone. Thus, to explain the observed inconsistencies in observed responses in BFI01 one must include properties not accounted for in the present flow model.

These may be local heterogeneities close to the borehole. Another possibility would be a general anisotropy within the zone.

Some simulations were carried out in order to study the effects of anisotropic transmissivities. The aim was was to investigate whether the inconsistent behaviour of the near-region boreholes (KFI06, KFI11, and BFI01) could be explained, while simultaneously simulating responses in the other boreholes. The results indicated that by accounting for anisotropy it may be possible to improve the calibrated model for the boreholes close to the pumped hole, BFI01, KFI06 and KFI11. However, the fits obtained for the observation holes KFIOS, KFIO9, KFI10 and HFIO1 are not entirely satisfactory. The implications of the anisotropy modeling were essentially that more questions were raised than answered. With the assumptions of this particular flow geometry, a general anisotropy in the fracture zone may partly explain the observed inconsistencies for the boreholes close to the pumping hole, but will not improve the calibrated model over the whole flow domain in general. This would suggest that local heterogeneities rather than a general anisotropy cause the inconsistent drawdown behaviour in BFI01 (and to some extent KFI11).

3.5.3 Summary

To summarize, the numerical simulations have proven to be very useful when analyzing the hydraulic properties of the fracture zone. It has been shown that using the assumed geometry of the flow domain, it is possible to simulate the observed responses of the interference test in the boreholes within Zone 2. However, in the boreholes closest to BFI02 the agreement between measured and simulated responses was not entirely satisfactory.

A comparison of the results from these simulations with previous modeling efforts indicates that a considerably better understanding of the flow conditions has been gained through the interference tests. The improvements are mainly due to the more detailed description of the flow geometry, which enables a better description of the hydraulic boundaries.

Some comments should be made regarding the certainty of the parameter distribution obtained during the calibration. Using trial and error as a parameter estimation procedure based on data from a single event, one gets essentially no information about the uniqueness of the obtained parameters. More sophisticated parameter estimation schemes may reveal that other parameter distributions also would explain the observed data. One implication of this is that confidence in predictive ability of the model has to be somewhat restricted. Only data from a different hydraulic event (pumping in a different borehole) would enable this particular calibration to be verified.

The transmissivity arrived at in Zone 2, and used in the model, is 3.0E-03 m^2/s, and the storage coefficient 2.0E-OS. The limited sensitivity studies shows that the magnitude of the drawdown within Zone 2 is not very sensitive to changes in transmissivity in Zone 2, while hydraulic gradients within Zone 2 are entirely governed by the transmissivity (given the specified boundary conditions).

Applying anisotropic properties to Zone 2 may partly account for the inconsistencies observed in boreholes adjacent to BFI02. However, these calculations were of a somewhat hypothetical character and do not necessarily represent a physical reality.

4. SGAB/SKB Analysis of Tracer Data

P. Andersson and Coworkers
Swedish Geological Company AB, Sweden

4.1 Conceptual Model

Based on the calibrated flow model described in the previous section, the steady state hydraulic distribution during the radially converging head distribution was predicted. The steady state flow field was in turn used to calculate transient solute transport by adding transport parameters. The predictive simulations were oriented towards predicting tracer behaviour in horizontal planes representing the different subzones. All the subzones were assigned the same thickness. Variations between them consisted of different hydraulic conductivities.

The results of the predictions were obtained in the form of concentration versus time in the pumped borehole. In addition, areal plots of tracer distribution were produced.

The flow domain for the solute transport predictions in the horizontal plane was chosen as small as possible, enclosing only the boreholes included in the radially converging tracer test ,BFI02, BFI01, KFI06, KFI11. A small model domain provides for reducing numerical difficulties and maintaining computational efficiency, by enabling the construction of finer finite element meshes. Separate meshes for the three injection boreholes were used, to further enhance computational efficiency. By using separate meshes, element directions can be readily designed to optimize numerical efficiency when solving the advection-dispersion equation. The finite element meshes are shown in Figure 4.1.

The boundary conditions for the transport domains were constant hydraulic head along all boundaries. Boundary conditions for the flow domains in Figure 4.1 were obtained by running the calibrated flow model at steady state and appropriate groundwater withdrawal schemes. The resulting hydraulic head distribution was interpolated from the flow model onto the boundaries for the transport domain. The simulated steady state hydraulic head distribution at a pumping rate of 2 vs in BFI02 is shown in Figure 4.2.

A constant value of solute concentration, C = 1.0, was defined at the node representing the injection borehole. At all other nodes, solute concentration was initially set to zero.

Hydraulic parameters were estimated from previous hydraulic interference tests. The results from the interference test did not clearly indicate any differences between subzone 1 and subzone 3 in responses to pumping. Thus, subzone 1 and 3 were represented using high hydraulic conductivities, while subzone 2 was assigned significantly lower values. The values used for hydraulic conductivities were estimated from the evaluation of the interference test in combination with results from detailed water injection tests in 0.1 m sections in borehole BFI02 (Andersson et al., 1988). The latter tests, in combination with core mapping in boreholes KFI06 and KFI11 (Andersson et al., 1989), provided information about thicknesses of the different subzones. However, if the thicknesses obtained are not representative for the flow domain involved in the tracer test, estimated hydraulic conductivities may be in error.

The following parameters were used for simulations in the horizontal plane (each subzone is assumed to have a thickness of 0.5 m):

— high conductivity zones (subzones 1 and 3):

K = 3.5 E-03 m/s	(hydraulic conductivity)
ϕ = 3 E-04	(porosity)
a_L = 10.0 m	(transverse dispersivity)
a_T = 3.0 m	(longitudinal dispersivity)

— low conductivity zones (subzone 2):

K = 7.0 E-05
ϕ = 3 E-04
a_L = 10.0 m
a_T = 3.0 m

The values used for the porosity was taken from previous tracer tests in the Brändan area (Ahlbom et al., 1987). Dispersivity values were chosen somewhat arbitrarily. Earlier investigations (Gustafsson and Klockars, 1981), indicated values of the order of 1 m on a scale of approximately 30 m. However, due to scale effects, dispersivity values may be expected to be larger for the radially converging tracer test.

The actual breakthrough curves were obtained by scaling the simulated observations at the point of observation (BFI02) according to some assumptions about the dilution effects in the sampling sections. In this case, a flux-averaging of sample concentration was assumed, with fluxes assigned according to the assumed transmissivities for each layer.

In the following the predictions will be compared with the actual outcome of the tracer experiment. The discussion will only include processes and parameters associated with the model as described above. It is emphasized that both hydraulic gradients and breakthrough curves should be predicted satisfactorily. Obtaining an accurate breakthrough curve but failing to predict hydraulic head gradients is considered a rather dubious result.

4.2 Results and Comparison with Observed Data

Table 4.1 summarizes the observed head differences for all the nine injection intervals as well as the predicted head differences. The measured values were estimated from plotted time series of head differences calculated from manually leveled (generally once a day) hydraulic heads.

It can be seen from Table 4.1 that head differences measured prior to the detailed sampling differ significantly from the ones measured after the detailed sampling. No apparent explanation exists for these discrepancies. However, in order to compare predicted and measured hydraulic head differences between pumping and injection intervals, the leveled values prior to the detailed sampling were chosen. The reason for this was that those values are somewhat more consistent between intervals.

Table 3.1 again confirms that the groundwater flow model does not explain hydraulic heads in borehole BFI01. For boreholes KFI06 and KFI11 the agreement is significantly better, although also here a disturbing discrepancy can be noted. Considering the large differences in manually leveled gradients between before and after the detailed sampling, it is difficult to say whether this discrepancy represent a true model error. However, it should be kept in mind when analyzing the predicted tracer breakthrough curves.

Table 4.1. Comparison of measured and predicted head differences (units in metres). Measured values in parentheses denote leveling after the detailed sampling.

Borehole	Section	Measured	Average	Predicted
KFI06				
	Lower	0.62(–0.15)		
	Middle	0.64(0.28)	0.62(–0.07)	0.42
	Upper	0.59(–0.34)		
KFI11				
	Lower	0.81(0.42)		
	Middle	0.74(0.33)	0.77(0.0)	0.47
	Upper	0.77(–0.74)		
BFI01				
	Lower	1.14(0.80)		
	Middle	1.25(0.84)	1.27(0.73)	0.46
	Upper	1.41(0.55)		

Table 4.2 presents a comparison between measured and predicted first arrival times, as obtained for the measured and predicted breakthrough curves. It may have been more desirable to compare average travel times as the time of 50 % of the steady-state concentration, but those were not well defined in all breakthrough curves. In general, the middle section is considered to be part of a low conductivity zone, while the upper and lower are consider to be located in high conductivity zones. Regarding the predicted first arrival times, the high conductivity zones are considered more accurate with respect to the actual hydraulic conductivities given as input.

The comparison between measured and predicted travel times reveal several interesting features. Firstly, predicted arrival times are significantly underestimated for all sections. Secondly, the assumption that both the upper and lower intervals essentially represent layers with high fluid velocity (during the tracer experiment) is not correct. The only case where this assumption holds is for borehole KFI06. Thirdly, the differences between boreholes in measured first arrival times do not correspond to the prevailing hydraulic gradients.

Predicted steady state concentrations, as sampled in BFI02, were significantly overestimated. It was evident that the modeled mass injection into the aquifer is too large compared to the actual. However, this simply illustrates the impact of the type of boundary condition applied. In this case, a constant concentration was specified at a finite element node, and the injected mass into the flow domain is the influenced by the surrounding element sizes.

4.3 Calibration

In order to analyze the discrepancies between measured and predicted tracer transport, it is important to recognize which aspects of the flow and transport processes are influenced by the various parameters used in the model.

Table 4.2. Comparison of measured and predicted first arrival times (units in hours).

Borehole	Section	Measured t_0	Predicted t_0
KFI06			
	Lower	194	1
	Middle	1250-1350	50
	Upper	106	1
KFI11			
	Lower	3600	1
	Middle	850	50
	Upper	24	1
BFI01			
	Lower	1250	1
	Middle	700	50
	Upper	75	1

• Hydraulic gradient

The hydraulic gradient was predicted using a calibrated model from hydraulic interference tests. It is important to note that an accurate description of the hydraulic gradient is a necessary requirement in order to predict groundwater velocities and solute transport. The flow and transport model assumed in this work, will loose its physical meaning if the accuracy of hydraulic head predictions is neglected or ignored.

The hydraulic head distribution is governed by the transmissivities as well as the physical geometry of the modeled region. The latter feature represents a principle advantage of employing a two-dimensional model rather than a one-dimensional when determining the groundwater flow pattern. The fracture zone appears to be a bounded system surrounded by more or less impermeable boundaries (Andersson et al., 1989), and the hydraulic heads in such a system can only be computed with a two-dimensional model. In this case, it may be argued that sufficient data is not available for the fracture zone for such a description. However, the principle should be clear that an accurate prediction of hydraulic heads should form a foundation on which solute transport can be simulated. Otherwise, the assumed groundwater flow and transport model is not correct.

The observed hydraulic heads from the radially converging tracer experiment indicated that the predictive model is relatively accurate with regard to transmissivities and boundary configuration. As expected, borehole BFI01 was not predicted satisfactorily, which confirms that there are heterogeneities or anisotropic conditions within the fracture zone not accounted for in the model. Another possibility is the presence of a natural gradient having considerably larger influence than assumed. Some simulation experiments incorporating anisotropy are described in Section 3, which may partly explain the deviant behaviour of BFI01. In addition, complete

verification of the calibrated flow model could not be made, as observations during the tracer test were not obtained from all the boreholes within the fracture zone.

Any natural hydraulic gradients have been neglected during the predictive modeling, since the gradients are not well defined over the entire area. However, the measurements that are available indicate a gradient directed from BFI01 to BFI02. If this gradient is large, it may (at least partly) explain the different behaviour of BFI01.

A summary of the discussion of hydraulic gradients is that based on the observations made during the tracer test, large prediction errors of groundwater velocities and solute transport would not arise from ill-defined geometry, incorrectly estimated transmissivities or neglected gradients. At the most, predicted velocities would differ with a factor 2-3 for BFI01.

• Groundwater velocity

In the previous section, it was clear that the predicted residence times were significantly shorter than the observed. Given that the hydraulic gradients apparently were predicted relatively accurately (except for BFI01), the reason for the discrepancy is to be found in either the hydraulic conductivities or the

Hydraulic conductivities have been measured extensively by single hole injection tests. The conductivities from these agrees reasonably well with values estimated from the interference test, and subsequently used in the predictive modeling. Thus, only relatively small errors in predicted travel times can be attributed to erroneously assumed hydraulic conductivities.

The flow porosity for the fracture zone is essentially unknown, and it appears that the prediction error regarding travel times can be explained by this lack of information. The value used for the predictions, 3.0 E-04, was obtained from measurements over 75 m large section (Ahlbom et al., 1986). However, the flow porosity would be greater in the fracture zone than for the surrounding rockmass. Thus, the value obtained from the 75 m section may significantly underestimate the porosity in the fracture zone. By scaling the porosity valued used in the predictions to a fracture zone with a width of 1.0 m, one obtains a flow porosity of 2.25 E-02.

Using a flow porosity of 2.25 E-02 and with other parameters as before, new breakthrough curves were simulated. These are compared to the observed breakthrough curves in Figure 4.3. In addition to changing the porosity, the concentration boundary condition for the injection well (BFI02) is changed according to measured injection rates of tracers. The latter will be explained further below.

• Tracer distribution

Given the average groundwater velocity distribution, the actual tracer distribution is then governed by dispersive and/or diffusive effects. Steady state concentrations, as measured in samples obtained from the pumping hole, is influenced by the general flow pattern as well as dilution effects in the sampling section. As for the shape of the breakthrough curve, longitudinal and transversal dispersivities are important.

Figure 4.3 shows simulated breakthrough curves using a revised injection boundary condition, compared to the predictive modeling. For the predictive simulations, knowledge about injection rates was very limited, and the injection was modelled as a point of fixed concentration. In order to be able to compare the predicted and observed steady state levels, the boundary condition was changed to a constant mass injection into the aquifer.

Mass injection rates were measured carefully during the entire injection periods, and was consequently used for the modified upstream boundary condition. Thus, a specified mass injection rate rather than specified solute concentration was used, although it may be argued that the difference between the two types of boundary conditions is mainly a scaling effect.

By comparison of the general shape of the simulated curves and observed breakthrough curves (Figure 4.3), one can conclude that the dispersive effects are reasonably well predicted. It is important to note that it is not realistic to assess the correctness of the individual dispersion parameters (longitudinal and transversal dispersivities) with only one observation location.

In summary, the calibration of the model after the radially converging experiment mainly concerned adjustment of the flow porosity, and some minor adjustment of the hydraulic conductivity. These updated parameters were then used for the prediction of the dipole tracer test.

4.4 Dipole Tracer Experiment

The model geometry for the dipole test was somewhat different than for the previously described tests. In this case pumping (with re-circulation) was performed only in the uppermost, 0.5 m thick layer of the fracture zone. Based on the fact that there would be no net changes in fluid storage in this layer, it was assumed that also this thin layer could be modelled with a two-dimensional model.

Some preliminary flow modeling was carried out in order to investigate the influence of hydraulic boundaries and natural gradients on the flow field (Nordqvist, 1988). It was found that the assumed hydraulic boundaries were not important, while the natural gradient (measured in a limited number of boreholes) had an influence on the dipole flow field.

4.4.1 Modelled cases

The solute transport predictions are all based on the relatively simple flow geometry arrived at during the preliminary calculations of the flow field configuration. Thus, a natural gradient of 1/300 is assumed and no particular boundary conditions are applied. The various parameters applied are generally derived from previous pumping and tracer tests in the fracture zone and from literature data. The modelled cases can be divided into three main categories:

1. Conservative tracers (no reactions).
2. Radioactive tracers.
3. Sorbing tracers.

The computational domain for the flow and transport simulations is relatively simple and is illustrated in Figure 4.4, where the superimposed grid represents the applied finite element mesh. The flow and transport domain includes the injection borehole, BFI01, the pumped borehole, BFI01, as well as boreholes KFI06 and KFI11. Homogeneous and isotropic conditions are assumed. It should be pointed out here that the latter assumption may not be valid for the entire fracture zone, which has been indicated by previous pumping and tracer tests. However, it is at present not possible to in detail account for such heterogeneities and/or anisotropies. In other words, it is not expected that the groundwater velocity distribution will be correctly simulated across the entire computational domain. This lack of a detailed description of the velocity field will instead show up as a dispersive effect. Thus, lacking a detailed description of significant heterogeneities across the flow domain, the dispersivity values can not really be regarded as fundamental material properties that are scale invariant. Instead, the dispersive effects is likely to be of a macroscopic nature, reflecting the scale of any heterogeneities present.

Given the lack of a detailed description of the geometrical features, parameters have been estimated so that solute transport between BFI01 and BFI02 is expected to be modelled as accurately as possible. Any observed responses in KFI06 and KFI11 will be checked for further indications of heterogeneities and anisotropic conditions.

The transport predictions are generally presented as breakthrough curves in the sampled borehole, BFI02. Injection of tracer mass in borehole BFI01 is accomplished by letting the injection fluid have a unit concentration during the four first minutes of pumping, as is the case in the field experiment as well. Thereafter the concentration of the injection fluid is equal to the concentration of the pumped fluid at all timesteps, thereby simulating the re-circulating dipole tracer test. However, the numerical simulations uses for practical reasons the concentration from the previous time step as injection concentration. Thus, a certain time lag is introduced which do not correspond to the actual time lag during the tracer test. In the field experiment, the time lag is of the order of a few minutes, while the simulations generally assumes a time lag of 30 minutes (time step used in simulations). This will introduce a certain error in the breakthrough curves, especially in the steep regions of the curves. However, these errors are relatively small.

Below the various parameters used for the different cases will be defined. It should again be mentioned that these parameters only pertain to the particular flow and transport model assumed in this work. That is, flow and transport processes are assumed to take place in a fractured medium that approaches a porous medium at this geometrical scale.

• Flow parameters

The flow parameters used are based on previous pumping and tracer tests. A transmissivity of 1.0E-03 m^2/s is assumed for the fracture zone. Further, the fracture zone is assumed to have a thickness of 0.5 m, which is consistent with previous transport modelling (Gustafsson et al., 1989) and also with single hole injection tests in 0.11 m sections (Andersson et al., 1988). The assumed transmissivity and thickness imply a hydraulic conductivity of 2.0E-03 m/s. This value is slightly lower than was used for the simulations of the radially converging tracer test, as the predicted hydraulic gradients for the radially converging test were somewhat lower than the measured.

The flow porosity is estimated based on the results from the radially converging tracer test, and is chosen so that transport times between BFI01 and BFI02 are expected to be modelled relatively accurate. The assumed porosity is 2.5E-02.

• Transport parameters

The modelled physical processes in this work are advection/dispersion, radioactive decay and adsorption. For the three main cases, the assumed parameters are as follows:

Conservative substances are in this work only affected by advective/dispersive mechanisms. The dispersivity values are consistent with previous modelling in this fracture zone. The longitudinal dispersivity is set to 10.0 m, while the transversal dispersivity is set to 3.0 m.

Radioactive substances are in addition to advection/dispersion processes subjected to radioactive decay. Three of the used radioactive tracers are simulated, with the following half-lives:

Br-82 1.47 days
I-131 8.04 days
Na-24 14.66 hours

Simulation of sorbing tracers requires characterization of the equilibrium relationships for the sorption processes. In this case a linear relationship between sorption density and solute concentration in the fluid is generally assumed. Literature data are usually expressed as linear relationships. However, since the solute concentrations is expected to vary significantly in magnitude during the dipole tracer test, it may be questionable if a linear relationship is appropriate. As adsorption density on the rock surface increases, it is reasonable to expect that adsorption characteristics will change. However, the simplest possible approach was taken here and linear isotherms are assumed.

As been explained earlier, the usual way of expressing K_d-values (adsorption equilibrium constants) as sorption per mass solid is inappropriate for flow in fractures. Instead, adsorption density should be related to the available surface area of the rock. However, this requires data on available surface for adsorption in the fracture zone rather than the density of the rock. Lacking such data, a formation factor, f, is used. This concept was adapted in Gustafsson and Klockars, 1984, in order to account for the inadequacy of applying adsorption per mass relations rather than adsorption per surface area. Thus, lacking information on surface area available for sorption, an f-value is selected such that a range of retardation factors, R, is simulated. The f-value is in a general way thought to be related to the flow porosity, but is here somewhat arbitrarily set to 0.001. In other words, R-values rather than K_d-values are simulated here.

With the rock porosity set to 2700 kg/m^3, the following retardation factors (with corresponding K_d-values) are simulated:

Table 4.3. Simulated R-values and representative tracers.

R	K_d	Tracer
1.0	0	non-sorbing
1.1	0.001	Na-24
2.2	0.01	Na-24
13.2	0.1	Rb-86,Co-58
121.6	1.0	Co-58,Tc-99
1081.0	10.0	Tc-99

Na-24 is assumed to undergo ion exchange rather than pure adsorption (Andersson, 1989), and is therefore assigned a relative retardation factor. Other values are obtained from Andersson (1983), Andersson and Allard (1983), and Allard et al (1979).

4.5 Results

• Conservative tracers

The predicted tracer response in BFI02 for conservative substances is presented in Figure 4.5. For illustrative purposes, a predicted breakthrough curve resulting from a non-recirculating dipole experiment is shown, as well as for a recirculating test. Figure 4.5 shows typical theoretical responses for a dipole tracer test. The concentration peak resulting from the pulse input occurs

after approximately 45 hours. It can be noted that the breakthrough curve does not reach a steady state due to the hydraulic gradient imposed on the flow field, and the numerical calculations indicate that approximately 10 percent of injected mass is lost out of the system. The predicted steady state hydraulic head difference between BFI01 and BFI02 was approximately 2.9 m.

• Radioactive tracers

The resulting breakthrough curve for Na-24 is shown in Figure 4.6. The breakthrough curve for a conservative tracer is also shown for comparison. The effect of radioactive decay is generally to reduce the magnitudes of the resulting breakthrough curve. An additional effect is that the peak occurs somewhat earlier. For example, a concentration peak occurring at approximately 30 hours is predicted for Na-24, compared to 45 hours for a conservative tracer. In the case of Na-24 one can also note that a considerable amount of decay will have occurred by the time of the arrival in borehole BFI02, and that a concentration of practically zero will have been reached already after approximately 125 hours.

• Sorbing tracers

The calculations involving sorbing tracers were performed on a range of different degrees of retardation, rather than for specific tracers. The reason for this is that some of the relevant data needed is missing, and it is judged to be more reasonable to assess sorption of specific tracers during the evaluation following the completion of the dipole tracer test. However, some examples of typical tracers for each retardation factor has been given in Table 3.3.

Figure 4.7 illustrates the effect of applying different sorption properties on the predicted breakthrough curves in BFI02. Applying different K_d-values have a significant effect on tracer transport. For very weakly sorbing tracers ($K_d = 0.001$), the effect is hardly noticeable. In this case, estimation of sorption parameters from the tracer test results will be very difficult. The same can of course also be said for strongly sorbing tracers ($K_d = 1.0$, $K_d = 10.0$ is omitted), where practically no tracer will be possible to detect. This is especially true if such tracers are radioactive as well. However, for intermediate tracers it is evident that sorption parameters can be readily estimated. One can note that the informative region (the area formed by the difference of two breakthrough curves) for estimating sorption parameters is relatively large in this case.

A number of the sorbing tracers used in the dipole experiment are radioactive as well. The combined effect of radioactive decay and sorption is not presented here. For predictive purposes, modelling of each process separately is sufficient.

4.5.1 Comparison with observed data

The results from the dipole tracer test has been published very recently (Andersson et al., 1990), and no thorough evaluation has been undertaken yet. However, a preliminary comparison with observed data can be done. Figure 4.8 shows predicted and observed breakthrough curves for a conservative tracer. Average travel time and peak level is predicted relatively well, but it is evident that more than the predicted 10 percent of the injected tracer mass is lost. Based on measurements of salinity during the experiment, it is indicated that some of the discharged water originates from below, where the salinity increases sharply. Thus, the dipole field, which is assumed to be two-dimensional, would have a three-dimensional component. A simple mass balance gives a preliminary estimate of the contribution of high-salinity water to the discharged water, indicating that possibly as much as 30 percent of the injected tracer mass would be lost (or delayed) due to this effect. However, it is difficult to interpret the apparently high salinity since this may be a transient effect developed during the initial stages of pumping.

As far as predicting the flow field, it can be mentioned that the observed head difference between the injection hole and the discharge hole was almost identical to the predicted.

Most of the results from the dipole tracer test have not been evaluated (compared with predictions) by the completion of this report. For example, data from two other observation holes other than the pumped borehole is available.

4.6 One-Dimensional Modeling of the Radially Converging Tracer Test

The one-dimensional transport modeling was carried out with a slightly different purpose than the two-dimensional flow and transport modelling. In this case the purpose was to evaluate the breakthrough curves from the radially converging test, in order to be able to make some interpretations primarily about the transport connectivity between the different injection sections and the sampled borehole. It is emphasized that supplementary information from all the experiments provided a basis for these interpretations. The analysis generally assumed steady-state flow, but accounted for variable injection schemes. An important difference, compared to the 2-D modelling, is that mixing in the sampled borehole of tracers travelling through several different major flow-paths is considered as described in section 3.3. As independent measurements (other than the breakthrough curves) indicated the existence of such multiple-path transport, this approach proved particularly useful.

The general approach was to estimate transport parameters by a non-linear regression procedure, using various analytical one-dimensional models as given by Van Genuchten and Alves, 1984. The regression method was in this case used as a tool to answer the question: What model and what parameters explain observed data? Thus, it is also an exercise in model discrimination, although only advection-dispersion transport models were considered in this case.

Some examples of this evaluation will be given below. This analysis is still under way, and only a few remarks about each breakthrough curve is given.

• In-EDTA

In - EDTA was injected as a step input, in borehole BFI01 in the uppermost highly conductive layer of the fracture zone. From detailed sampling at different levels in the fracture zone during the radially converging test, it was evident that at least two major flow paths was contributing to tracer arrival in the sampled section (Gustafsson et al., 1989). Similar indications were also found from the interference tests, by analysis of primary and secondary pressure responses (Andersson et al., 1989). Figure 4.9 demonstrates the breakthrough curve for In-EDTA and a model estimate assuming two main flowpaths.

It should be noted that whenever two or more flowpaths were considered for an injection in the upper 0.5 m part of the fracture zone, this was interpreted as most of the transport were taking place in the upper part as spreading in a plane, while the other flowpath(s) may just be "channels" of preferential flow. The understanding of the fracture zone had at this stage of the investigations changed somewhat, meaning that the fracture zone did not really consist of separate sub-layers as was thought prior to the interference tests. Only the upper, 0.5 m thick, highly conductive part was considered with certainty to be a well-defined plane, with the possibility of a similar plane at the bottom delimitation of the zone as well. In between, there would be patches of more or less vertical connections within the fracture zone (see also Figure 3.2).

• Amino G Acid

Amino G Acid was injected as a pulse in borehole KFI11 in the upper part of the fracture zone. Figure 4.10 shows the regression results, assuming one flow path. In this case the injection boundary condition was an instantaneous pulse. As this was an undisturbed pulse injection, as described in Gustafsson et al (1989), one might expect that the appropriate upper boundary condition would be that of a decaying pulse injection (Equation 3-18). For a comparison, a regression estimate using the latter boundary condition is shown in Figure 4.11. As can be seen, there is almost no difference between the two. Thus, in this case, explanation of observed data is not improved by accounting for a decaying inlet concentration.

As the case was for In-EDTA, there were observational evidence for the occurrence of more than one major flow path. Thus, a model assuming an instantaneous pulse was fitted to the breakthrough curve, which is shown in Figure 4.12. At a first glance, one can see that observed data is explained extremely well by this model. The bulk of the transport appears to take place in the upper plane with relatively large dispersivity, while there is a second preferential flow path with very low dispersivity. However, although the statistical analysis of the regression results showed that the fitted parameters were unique, this model was rejected. The reason was that the second flow part in this case had a Peclet number of 0.5, which was regarded as unreasonably low. Instead, a more careful analysis of the injection data was undertaken, showing that tracer mass was not leaving the injection section as an exponential function. Accordingly, a variable injection scheme was considered, estimated from the tracer injection data. This was tried for one and two flow paths, of which the latter is shown in Figure 4.13. Considering that the injection tracer data only allowed for an approximate estimate of the injection scheme, it can be seen that the second peak in the breakthrough curve is explained very well by using the injection data in more detail. In addition, the assumption of two flow paths (which was observed) explains the complete breakthrough curve very well. The correlations between parameters were low, so it was judged that none of the fitted parameters were redundant in this case.

This should be seen as a demonstration of the importance of accounting for the tracer injection. In this case, an erroneous interpretation of the breakthrough curve was avoided due to the monitoring of injection concentrations.

Iodide was injected as a step injection in borehole KFI06 in the upper part of the fracture zone. However, after 125 hours of injection the entire volume accidentally was released during a three hour period. In this case, the resulting pulse was "forced" so that no tracer remained in the injection section after the injection. Regression was carried out for one and two flow paths models and is shown in Figures 4.14 and 4.15. It is obvious that the two path models does significantly better of the two. However, in this case only one significant flow path was observed and the two path model is in this case not supported by independent observations. A more likely explanation is, again, the injection configuration. As tracer in this case became "forced" out of the injection section, an injection ring around the borehole may have formed in the initial stages. This could very well explain the occurrence of the "second" peak in the breakthrough curve for Iodide (Guvanasen and Guvanasen, 1987).

• ReO_4

ReO_4 was injected as a step injection in borehole KFI06 in the lower part of the fracture zone. In this case the tracer mass injection varied significantly with time, and at least two main flow paths were observed. The bulk of the tracer arrived in the lower part of the fracture zone, while as smaller part arrived in the upper part. Regression with a two path model, accounting for the

variable mass injection, is presented in Figure 4.16. Data is explained by the model very well up to around 2000 hours. The remaining tailing beyond this point is not explained. Regression runs using three flow paths did improve the model fits but could not be supported by independent observations.

4.6.1 Summary

The regression analysis using simple one dimensional advection/dispersion models have proven to be very useful as a starting point of evaluating experimental data. Especially the effects of variable injection and occurrence of multiple flow paths can be evaluated readily. Such effects are important to understand in order to analyze the breakthrough curves further, where additional transport processes may be needed to account for the unexplained parts of the observed data. It should be pointed again that supporting field data (other than the breakthrough curve) is essential to the analyses presented for the tracers above.

Actual parameter values and statistical analyses of the non-linear regression are in preparation. The parameters that were optimized were basically residence times, dispersion coefficients and borehole mixing parameters. Similar analyses is planned for the dipole experiment, where also sorption parameters can be estimated. One possibility that will be considered is parameter estimation from both experiments simultaneously.

4.7 Model Adequacy and Validation

The primary objective of this modeling effort has been to determine transport parameters of the fracture zone. Hence, the modeling should not be seen as an attempt to validate any specific model~ or process but merely as an initial modeling for the purpose of evaluating transport parameters such as flow porosity, hydraulic fracture conductivity and dispersivity.

The sequence of tests and the use of predictive modeling as a design tool has served as a catalyst for the interaction between the modellers and experimentalists involved in the project. The predictive modeling with he 2-D porous media model has also showed that it is possible to predict the head distribution of the system fairly well in the scale beyond 3-500 meters while in the near-region one has to include local heterogeneities in order to make good predictions. The transport could also be predicted fairly well after the first calibration process. However, the local heterogeneities still need to be better accounted for.

5. Evaluation of Tracer Test in Finnsjön Radial Convergent Experiment

Luis Moreno and Ivars Neretnieks
Royal Institute of Technology, Sweden

5.1 Conceptual Model

In the radial convergent experiment, tracers were injected in 3 boreholes, and water was pumped from a packed-off interval including the whole thickness of the highly conductive zone. The geometry and other details are found in Gustafsson et al. (1989)

When radionuclides are carried by water flowing through a porous or fractured medium, they are influenced by several mechanisms:

— Molecular diffusion

— Mechanical dispersion

— Channeling

— Matrix diffusion

— Chemical or physical interactions.

For a one dimensional flow, the movement of tracers, which do not react with the rock, may be described by

$$\frac{\partial C_f}{\partial t} + U_f \frac{\partial C_f}{\partial x} - D_L \frac{\partial^2 C_f}{\partial x^2} = D_e \frac{2}{\delta} \left. \frac{\partial C_p}{\partial z} \right|_{z=0} \qquad (5\text{-}1)$$

The diffusion into the rock matrix may be written as:

$$\frac{\partial C_p}{\partial t} - D_p \frac{\partial^2 C_p}{\partial z^2} = 0 \qquad (5\text{-}2)$$

Equations for one dimensional transport may be used for radial convergent system if the Peclet number is large. For the initial and boundary conditions used in these tracer tests there exist analytical solution for one dimensional transport.

The initial conditions are: zero concentration in the water in fracture and within the rock matrix. The boundary conditions are, given flux at the injection hole and finite concentration at long distance.

For tracer test with short contact time or rock with very low porosity (effective diffusion) the effect of matrix diffusion is negligible.

In the first evaluation we use the Advection-Dispersion model. In this case we neglect the effect of matrix diffusion, and the right hand term in equation (1) is zero.

a) The Advection-Dispersion Model

For pulse injection the analytical solution by Lenda and Zuber (1970) may be used. For continuous injection the solution by Lapidus and Amundsen (1952) is used. For variable injection, the injection is approximated by a series of square pulses.

In both cases the effluent concentration may be expressed as a function of the Peclet number and the residence time. The tracer is diluted by water which flows into the pumping hole from other directions and in other levels. To take into account this effect a proportionality factor is defined, P_f, (1/dilution factor)

$$C(t) = C_0 P_f f(Pe, t_w, t) \tag{5-3}$$

where Pe is the Peclet number, defined as $U_f L/D_L$, t_w the water residence time, and P_f the proportionality factor.

b) The Advection-Dispersion-Matrix Diffusion Model

In this case equations (1) and (2) are considered. For the initial and boundary conditions used in the tests, analytical solutions are available. The solution by Tang et al. (1980) for a continuous injection is used.

In this case the concentration is determined for the Peclet number, water residence time and a parameter which takes into account the diffusion into the rock matrix.

$$C(t) = C_0 P_f f(Pe, t_w, A, t) \tag{5-4}$$

where the A-parameter for a nonsorbing tracer is defined as:

$$A = \frac{\delta}{2(D_e \varepsilon_p)^{0.5}} \tag{5-5}$$

Equation (5) shows that the same effect of matrix diffusion may be obtained with different values of the fracture aperture, effective diffusion coefficient, and rock porosity. The diffusion into the rock matrix is also influenced by the residence time of the tracer.

The importance of matrix diffusion may be studied by evaluation of the ratio

$$F = \frac{t_w^{0.5}}{A} \tag{5-6}$$

If the F-parameter is introduced in the analytical solution, the effluent concentration becomes only a function of Peclet number, relative residence time, and the F-parameter.

An estimation of F-parameter may be done from water residence time, fracture aperture, diffusion coefficient, and rock porosity. The two last entities have been measured in the laboratory (Gidlund et al., 1988).

Runs with step injection for Peclet numbers of 10 were performed to determine when matrix diffusion becomes important. It was found that for an F-parameter of 0.3, the time to reach 50 % the maximum concentration is increased by 25 % compared to the case without diffusion. For an F-parameter of 1.0 the time is increased by a factor 2. We choose here the criterion that diffusion into the rock matrix is important if the F-parameter is larger than 0.3.

5.2 Results

Two models were used in the evaluation of the tracer tests: The Advection-Dispersion model (ADM) and the Advection-Dispersion-Diffusion model (ADDM). The experimental data (about 350 points) were reduced to about half. A smoothing routine was used first, then every second point was selected to represent the experimental data in the fitting process.

5.2.1 Evaluation of the Tracer Test Using the ADM Model

For the first model we selected seven curves. Three curves were not used because the recovery was very small (less than 10 % of the injected tracer). The tracer test with Yb-Edta was also not used because the breakthrough curve can not be explain for the ADM model.

When the experimental data presented two or more peaks, the model was used to fit two paths. The use of models which may fit several paths is dubious because of the large number of parameters which must be determined. With 2 pathways we need to calculate 6 parameters, 3 for each pathway. This number may be reduced if some assumptions are made. The assumption that the dispersivity is the same may be used, but in a fractured medium we do not have any evidence that this is true. Another alternative is to set the sum of the dilution factors to 1.0. This also may be applied to the model with one pathway. For recoveries much smaller than 100 % this is not possible.

The results are shown in Table 1. Some fitted breakthrough curves are shown in Figures 1 - 3. The dispersion of the tracer in most of the cases is large, the Peclet number is about 4 - 5. In the cases in which the breakthrough curves clearly present two peaks, a model for two pathways is used (Tests with ReO_4, Amino G and Tm-Edta). The water residence times vary from about 100 to 2000 hours. The tracers which show a very low recovery (not analysed with this model) present long water residence times.

The fracture aperture can not be calculated from the mass balance, in this case, because the flow of water in the fracture used by the tracer is unknown.

The proportionality factor used in this model takes into account the initial concentration of the tracer in the injection hole and the dilution in the fracture and in the pumping hole. This parameter may be calculated independently from the injection and pumping data.

3.2 Evaluation of the tracer test using the ADDM model.

The effective diffusion coefficient for samples from Finnsjön was determined using Uranin and Iodide. For Uranin (a large molecule) the values varied from 1.2 to $36.4 \cdot 10^{-14}$ m^2/s. For Iodide (a relative small molecule) these values were between 12.6 and $236 \cdot 10^{-14}$ m^2/s. The rock porosity was found to be 0.02 - 0.03.

Using these values the F-parameter was calculated for different effective diffusion coefficients and different water residence times. The values of the F-parameter are shown in Table 2. A fracture aperture of 0.25 mm is assumed. The rock porosity used in these calculations is 0.025

Table 1. Results of the fitting process using the Advection-Dispersion Model.

Tracer	Injection point*	Pe	t_w (h)	Pf.	S.D., %	Exp. Recov.
In-Edta	H01-U	4.4	339	16.4	5.6	0.98
Uranin	H01-M	4.9	1935	52.5	6.5	0.18
Iodide	H06-U	5.6	369	2800	6.6	0.70
ReO_4 (1 path)	H06-L	1.6	1180	6.8	8.8	0.65
ReO_4 (2 paths)		9.0	422	3.5		
		85.4	1095	1.8	4.8	
Gd-Dtpa	H11-U	1.4	131	43.6	6.8	0.89
		2.6	108	45.0	4.4	
Amino G (1 path)	H11-U	3.8	152	66.8	2.2	0.87
Amino G (2 paths)		3.9	151	66.5		
		4.6	169	7.6	2.9	
Tm-Edta (1 path)	H11-U	4.2	146	4571	1.9	0.72
Tm-Edta (2 paths)		3.8	155	4798		
		600	175	366	2.2	

*) U = Upper part, M = Middle, and L = Lower

Table 2. Values of the F-parameter for different effective diffusion coefficients and different water residence times.

Eff. Diffusion Coef, m^2/s	Water Residence time, hours 30	100	300	1000
$1.0 \cdot 10^{-14}$	0.042	0.076	0.131	0.240
$1.0 \cdot 10^{-13}$	0.131	0.240	***0.416***	***0.759***
$1.0 \cdot 10^{-12}$	***0.416***	***0.759***	***1.315***	***2.400***

For the tracer tests with large molecules the diffusion into the rock matrix is important if the residence time is longer than 100-200 hours. For small molecules the diffusion into the matrix is important in all the cases studied.

The residence times may be obtained from Table 1. From these values the diffusion into the rock matrix can be seen to be important for the tracer tests with In-Edta and Uranin. For the relatively small molecules both cases are important, ReO_4 and Iodide, matrix diffusion will considerably influence the breakthrough curves.

The results of fitting these tracer tests using the Advection-Dispersion-Diffusion model are shown in Table 3.

In most of the cases, the tracer tests with large molecules show smaller values of the F-parameter.

The residence times calculated using the ADDM model are, in all cases, less than for the ADM model. This is because the effect of matrix diffusion has been accounted for.

In these fitting processes we have used a large Peclet number, 100, to test if the dispersion in the breakthrough curve can be explained by the diffusion into the rock matrix only. In the ADM model the dispersion of the curve accounts only for mechanical dispersion. For some tests we have fitted the Peclet number and the A-parameter, this means that the dispersion in the breakthrough curve is explain by two mechanism simultaneously. A large Peclet number is compensated by a large F-parameter (Large diffusion into the rock matrix).

Table 3. Results of the fitting process using the Advection-Dispersion-Diffusion Model.

Tracer	Pe (–)	t_w h	A $s^{0.5}$	Pf. (–)	F	S.D., %
In-Edta	18.5	199	1432	19.0	0.59	5.3
	100	159	879	19.9	0.86	5.6
	21.8	190	1272	19.2	0.65	5.3
	100	167	1008	19.2	0.77	5.6
Gd-Dtpa	3.4	91.4	3035	47.4	0.19	4.6
	100	41.6	547	47.4	7.07	7.5
ReO_4 (1 peak)	100	161	403	6.71	1.89	2.9
	100	96.6	181	8.86	3.26	5.6
	14.3	289	1078	5.55	0.95	2.5
(2 peaks)	100	129	250	8.86	2.73	9.0
Iodide	100	120	335	4615	1.96	4.4
	100	125	364	4360	1.84	4.5
Uranin	100	657	1135	41.7	1.36	4.0

– The underlined values for Peclet number has been chosen so that dispersion is neglected.

– The underlined values of the proportionality are calculated from data on injection and pumping flowrates.

The proportionality factor may be calculated directly from the injection flowrate and the pumping flowrate. If this value of the proportionality factor is used in the fits, then we impose that the tracer is recovered 100 % if the experiment is run for very long time. The small recovery of the tracer Uranin can not be explained by diffusion into the rock matrix. If the condition of 100% recovery is imposed the parameters obtained have not physical meaning.

5.2.3 Fracture Aperture

Tracer tests with nonsorbing tracers are performed to get information on the volume of the rock mass which may be used by the water flow. In tracer tests the fracture apertures may be calculated from the water residence time and the flowrate.

In these tests the flowrate in the fracture can not be clearly determined. Some tracers have arrived at two or more locations in the pumping hole. We do not know in which fractures or pathways the tracers have moved from the injection location to the pumping hole.

Some estimations may be done for the fracture apertures. Different approaches may be used:

— Determination of the total aperture of the fractures which are in a 2-m section using the residence time obtained from the ADM.

— Determination of the total aperture of the fractures which are in a 2-m section, using the residence time obtained from the ADDM. This and the first methods are based on the conservation of mass.

— Determination of the aperture of individual fractures calculated from the A-parameter in the ADDM. This method utilizes information on the effect of matrix diffusion.

— Determination of the total aperture of fractures which are in a given section, using hydraulic heads and the cubic law. It assumes that there is parallel plate flow.

For the two first cases, the possible pathways to be considered are those that are at about the same level in the injection and the pumping holes. The pathway with the larger flow in a 2-m section is chosen. The residence times are taken from the ADM and ADDM respectively. The flow in each section is calculated from the respective values of the transmissivity.

In these both cases we may only estimate the total aperture in a 2-m section, no the aperture of an individual fracture.

The aperture in the third case is calculated using equation (5). The values for D_e and ρ_p independently determined in the laboratory are used.

The apertures calculated using these different approaches are shown in Table 4.

5.3 Dsicussion and Conclusions

Above we have shown that the interpreted results of tracer tests strongly depend on the model used. This means that the properties of the medium, calculated by using tracer tests, are determined by the processes which are included in a certain model.

The dispersion of the tracer may be accounted for mechanical dispersion (Peclet number) or by diffusion into the rock matrix. In our calculations we have used these two extreme cases. In practice, both mechanisms work simultaneously, and it is difficult to determine from tracer tests the relative effect of each of these mechanisms. When these two parameters (Pe and A) are simultaneously fitted, similar results (Standard deviation in the least square method) may be obtained with very different values of these parameters, in some situations.

6. INTERA Analysis of Tracer Data

P. Grindrod and D.J. Worth
Intera, United Kingdom

6.1 Conceptual Model

Radially convergent tracer experiments have been carried out for INTRAVAL Case 5 at the Finnsjön research area in central Sweden. The objective is to determine the parameters governing the transport of solutes in a major fracture area.

The fracture is assumed to be oriented on a two dimensional plane. In radial geometry, a central withdrawal (pumping) borehole and three injection boreholes at round 150m distance were utilized, see figure 6-1. In all, there were nine continuous injection tests, where tracer was continually supplied at a fixed concentration, and three pulse injection tests. To date, there has been relatively little discussion of the pulse injection tests, but here, we shall concentrate on them for two major reasons. First, pulse breakthrough is likely to be more sensitive to the assumed geometry of the fracture, since there is both a wave-front and a wave-back to be considered. Second, in the two tests carried out simultaneously from borehole KI11, there is evidence of a double pulse breakthrough, where only one pulse was injected. This subtle behaviour may be lost in the continuous breakthrough data; hence we expect that disparities between the model and the experiment should be most apparent in the pulse injection case.

It is usually argued that radially convergent test data may be fitted by a one dimensional fracture model with constant advection term. This rules out *a priori* any effects of the radial convergence of the groundwater flow. Here, we consider the two dimensional radial flow problem. We are able to develop an analytical solution for a simple advection-dispersion problem. If molecular diffusion of the solute is considered, then we show that the Laplace transform of the solution is available, although the inversion would generally require a numerical algorithm.

When data from the pulse and continuous injection tests at Finnsjön is employed, various formats are analyzed elsewhere employing one dimensional models: diffusion, dispersion, rock matrix diffusion, sorption. Similar considerations may be included in the present context. We begin with a simple model for pulse tracer injection and generalize later.

6.2 Mathematical/Numerical Model

We consider two transport processes: the advection and the dispersion of a solute within the fracture fluid.

Let $c(r,\theta,t)$ denote the distribution of tracer within the fracture with respect to spherical coordinates in the fracture plane.

We have

$$c_t = \frac{1}{r}(rD_{(r)}\, c_r)_r + D_{(\theta)}\frac{c_{\theta\theta}}{r^2} + \frac{Q}{r}c_r \qquad (6\text{-}1)$$

for $t > 0$, and

$$c(r,\theta,0) = M\delta(r-R,\ \theta-0) \quad . \tag{6-2}$$

Here, Q/r is the radial velocity of the fluid flow, and $D_{(r)}$ and $D_{(\theta)}$ denote the consequent dispersion-diffusion terms in the radial and azimuthal directions.

The classical theory for dispersion of solutes in (slow) fracture flow yields

$$D_{(r)}(r) = \frac{h^2Q^2}{r^2} \times \text{constant}$$

where h is half the cross fracture width. Moreover, the constant Q is itself $O(h^{-1})$ if the pumping rate is fixed, since

$$\begin{bmatrix} \text{flux} & \text{out} \\ \text{at} & \text{centre} \\ \text{pumping} & \text{hole} \end{bmatrix} = 4\pi Qh \quad .$$

We shall assume that dispersion dominates any molecular diffusion in the radial direction and hence we shall write

$$D_{(r)} = \frac{\tilde{D}}{r^2} \quad .$$

For $t > 0$, c is a continuously differentiable, classical solution. Let p(r,t) denote the azimuthal average

$$p = \int_0^{2\pi} c(r,\theta,t)\, d\theta/2\pi \quad .$$

This problem for p has an explicit solution for which

$$p(0,t) = \frac{M}{\pi}\left\{\frac{\exp\{R^2Q/4\tilde{D} - R^4/16\tilde{D}t - Q^2t/4\tilde{D}\}}{\sqrt{4\pi\tilde{D}t}}\right.$$

$$\left. - \frac{Q\exp\{R^2Q/2\tilde{D}\}}{4\tilde{D}}\operatorname{erfc}\left\{\sqrt{tQ^2/4\tilde{D}} + R^2/\sqrt{16\tilde{D}t}\right\}\right\} \quad . \tag{6-3}$$

Notice that the initial value problem for p is far simpler than that for c.

Rescaling the problem so that

$$\rho = r/R$$
$$m = M/R^2$$
$$q = Q/R^2$$
$$d = \tilde{D}/R^4 \ ,$$

we obtain from (6-3)

$$p(0,t) = \frac{m}{\pi}\left\{\frac{\exp\left\{\frac{q}{4d} - \frac{1}{16td} - \frac{q^2 t}{4d}\right\}}{\sqrt{4\pi dt}} - \frac{q}{4d}\exp\frac{q}{2d}\,\mathrm{erfc}\left\{\sqrt{\frac{tq^2}{4d}} + \frac{1}{\sqrt{16dt}}\right\}\right\} \ . \qquad (6\text{-}4)$$

Notice that we only require the form of the concentration at the central borehole:

$$p(0,t) = c(0,.,t)$$

in order to analyze the injection data.

As an alternative to the above approach, let us reconsider the model (1) and (2), where hydrodynamic dispersion is ignored, so that $D_{(r)}$ and $D_{(\theta)}$ are simply regarded as constant = D (modelling the molecular diffusivity of the tracer in fracture water).

With p defined as before, we obtain

$$p_t = \frac{1}{r}(rDp_r)_r + \frac{Q}{r}p_r \quad t > 0$$

together with

$$p(r,0) = M\frac{\delta(r-R)}{2\pi R} \quad t = 0 \ .$$

Taking the Laplace transform $\hat{p}(r,s)$ of p(r,t), we obtain

$$\hat{p}(r,s) = \begin{cases} Ar^{\frac{1-n}{2}} I_{\left(\frac{n-1}{2}\right)}\left(r\sqrt{\frac{s}{D}}\right) & r < R \\ Br^{\frac{1-n}{2}}\left\{I_{\left(\frac{n-1}{2}\right)}\left(r\sqrt{\frac{s}{D}}\right) - I_{-\left(\frac{n-1}{2}\right)}\left(r\sqrt{\frac{s}{D}}\right)\right\} & r > R \end{cases}$$

where I_q denotes the Modified Bessel function of the first kind of order q, $\eta = 1 + Q/D$, and A and B are constant with respect to r, chosen so that

$$\hat{p}(R,s)\Big|_{-}^{+} = 0$$

$$\hat{p}_r(R,s)\Big|_{-}^{+} = -MQ/2\pi\, DR \quad .$$

Some algebra shows that

$$A = \frac{M}{2\pi R^{\frac{3-\alpha}{2}}\sqrt{sD}} \frac{\left(I_{-\left(\frac{\alpha-1}{2}\right)}\left(R\sqrt{\frac{s}{D}}\right) - I_{\left(\frac{\alpha-1}{2}\right)}\left(R\sqrt{\frac{s}{D}}\right)\right)}{\left(I_{-\left(\frac{\alpha-1}{2}\right)}\left(R\sqrt{\frac{s}{D}}\right) I_{\left(\frac{\alpha-1}{2}\right)}\left(R\sqrt{\frac{s}{D}}\right) - \dot{I}_{-\left(\frac{\alpha-1}{2}\right)}\left(R\sqrt{\frac{s}{D}}\right) I_{\left(\frac{\alpha-1}{2}\right)}\left(R\sqrt{\frac{s}{D}}\right)\right)}$$

where $\dot{I}_q(w)$ denotes $\frac{d}{dw} I_q(w)$, etc. Importantly, we have

$$\hat{p}(r,s) \to \frac{A(s)}{2^{\frac{\alpha-1}{2}}} \left(\frac{s}{D}\right)^{\frac{\alpha-1}{4}} \frac{1}{\Gamma\left(\frac{\alpha+1}{2}\right)}$$

as $r \to 0$.

Hence c(0,.,t) may be determined (= p(0,t)) once this last transform is inverted. However, an analytical inversion is beyond our scope, so a numerical method would be required.

6.3 Results

Using the Case 5 data and breakthrough pulses of the form given by (6-4) in Section 6-2, we sought numerical best fit curves by minimizing the sums of squares of the residuals over the time frame of the experiments.

The fitted breakthrough pulses are shown in Figures 2–4. The values for d and q [c.f., (6-4)] are given in Table 6.1. Following Gustafsson et al. (1989), we make the following remark about the experimentally observed data for c(0,.,t).

Table 6-1. Values for d and q.

	d	q
KFI11:U Amino G acid	0.00046	0.0054
KFI11:U TM EDTA	0.000566	0.00518
KFI06: U Iodide	0.00009	0.0021

The apparent double peaks in Figures 6-2 and 6-3 are not artifacts caused by withdrawal stop or inconsistencies in the tracer release. Indeed, the tracer release data is available (Gustafsson et al., 1989), and the duration is so short as to rule out the superposition of two pulses (each of the form given in (6-3) differing only in the values set for m, one shifted by an appropriate time difference.

In the Amino G. Acid experiment, a background concentration is evident due to the use of the same tracer in a previous test.

Both the above points were considered. The double peaks must be a consequence of flow path geometry, but there is no unique way to determine this from the available data. If the single fracture plane is replaced by a pair of parallel fractures connecting the packed-off boreholes (as depicted in Figure 6-1), then the solution takes the form of two pulses (given by 6-3)) having distinct values for D and Q. Ignoring gravity, the pressure gradient is the same in each fracture, depending only on r. We have

$$\begin{bmatrix}\text{flux} & \text{out} \\ \text{at} & \text{centre} \\ \text{of} & \text{fracture}\end{bmatrix} = 4\pi Qh = \frac{4\pi h^3}{3\mu}\{rP_r\}$$

where P(r) is the pressure and must be such that $\{rP_r\}$ is constant (ΔP vanishes for slow incompressible flow), μ is the viscosity.

Thus if two parallel fractures A and B yield values of Q_B and Q_s, the fracture widths are in the ratio

$$h_A/h_B = \sqrt{Q_A}/\sqrt{Q_B} \ .$$

Note here it is the pressure drop that remains the same through both fractures, not the pumping rate. Similarly, the dispersion constants ($\tilde{D} = O(h^2Q^2)$) $\tilde{D}_A$ and $\tilde{D}_B$ must be so that

$$\frac{\tilde{D}_A}{\tilde{D}_S} = \frac{h_A^4}{h_B^4} \ .$$

Thus we must have

$$\frac{\tilde{D}_A}{\tilde{D}_S} = \frac{Q_A^2}{Q_B^2} = \frac{h_A^4}{h_B^4}$$

if both fractures are subject to the same pressure differences between the injection and extraction holes.

Accordingly, we tried to fit the *twin peak* breakthrough curves via two terms of the form of (6-3) where coefficients satisfied (6-5). The results are shown for one case in Figure 6-5.

Although a number of ways of weighting the residuals in our fitting routine were tried, it is clear that there is not a good fit in Figure 6-5 — rather less of an improvement on Figure 6-3 than might have been hoped for. However, this result is revealing in that it suggests that just one or two parallel fractures subject to radially convergent flow are inadequate to model the observed pulse breakthrough.

6.4 Discussions and Conclusions

A number of ideas suggest themselves as worthwhile extensions of the approach represented in this paper.

Firstly, for two dimensional radially convergent flow models, we could repeat the analysis including, for example, matrix diffusion into the rock, perpendicular to the fracture plane. Similarly, a more detailed consideration of the flow parameters may be possible given the hydrological data available. Having concentrated upon Taylor dispersion, it would perhaps be wise to include a molecular diffusion term.

Secondly, and more fundamentally, what can be said about the use of two dimensional flow models (fluid velocity O(1/r)), and how can we assess the effective flow regime from the data?

One method we have in mind for future analysis is as follows. Following [4], we consider radially convergent flow in d-dimensions (where d is not necessarily an integer). We shall aim to locate the best fit d (along with other parameters) and take the difference [2–d] to be a qualitative measure of the non-uniformity or channeling behavior of the flow.

With a fracture of constant (one dimensional) cross-section located on a d-dimensional subspace of R^3 ($d \in (0,2)$), we obtain the analogue of (6-1):

$$c_t = (r^{d-1} D_{(r)} C_r)_r / r^{d-1} + \frac{Q}{r^{d-1}} C_r$$

where $D_{(r)} = O(1/r^{2(d-1)})$ in the case of Taylor dispersion.

This transport model has been used elsewhere, without dispersion (Shaw et al., 1989) and could be of use in identifying which flow models are appropriate. For example, a result of $d \approx 1$ would indicate a high degree of channeling and would immediately add to the utility of the closed form analytical solutions to the one dimensional transport models.

Given the results of section 6-3, we suggest that, at the current stage, there are sufficient grounds to question our basic flow model; that is, given the information available concerning the fracture zone, do we wish to continue with idealized uniform, plane fractures? In view of our results, it is perhaps not surprising that one dimensional transport models are employed as effectively on the continuous injection problems: the whole question as to whether the tests are in reality subject to radially convergent flow remains open.

Importantly, it seems that, given the data of the kind supplied here, the modellers must have some means of validating the groundwater flow model, rather than making approximations. It may be that channeling effectively restricts these problems to become one dimensional in nature. If this is so, it should be identified rather than incidental.

7. VTT Analysis of Tracer Data

A. Hautojärvi and Coworkers
Technical Research Centre of Finland

7.1 Conceptual Model

There is a need to have an increasingly better realistic picture of the migration phenomena and properties of the bedrock as a basis for the performance assessment of a repository. One part of the migration is migration in fracture zones. Dispersion may lower the maxima of the release pulses and the nature of dispersion should be studied thoroughly.

Many tests and direct observations indicate that the flow in rock fractures is concentrated in a limited part of the whole fracture. These conductive parts of fractures are called channels. It is also observed that there is a discrepancy between the apertures deduced from water injection tests and apertures evaluated from tracer tests e.g., (4,5). One probable explanation for this discrepancy is the inapplicability of the parallel plate approximation for the evaluation. A strong variation of the aperture explains more consistently the observed data.

A concept of varying aperture channels has been developed and applied to calculate flow times in radial tests. The drawback of the concept is that more parameters have to be introduced. These new parameters could be determined by observing them directly from geometrical measurements or by some other more indirect means.

Dispersion in one channel is due to velocity differences in the channel but these differences may be counteracted by the transverse diffusion in the channel. This leads to a decreasing dispersion. The diffusional convection in confined channels has been studied by many authors since the classical work by Taylor (refs. elsewhere, 1). Taylor (6) showed that after a sufficient long time the dispersion in a tube can be described by a constant dispersion coefficient relative to a plane moving with the mean flow velocity.

The time to reach the stationary dispersion depends on the tube diameter and diffusion coefficient. The molecules of the solute have to diffuse across the channel and experience effectively all the convective velocities of the flow field before approaching the steady state.

In the case of molecule thermal diffusion the steady state is reached in small diameter tubes rather quickly. In very flat flow channels the steady state is obtained in a short time across the aperture dimension and the dispersion follows Taylor dispersion. In the other transversal direction it takes however a much longer time to reach the steady state and transient analysis is needed. The two dimensions can be treated independently when the measures of the channel dimensions are markedly different.

Water flow in a fracture is assumed to be concentrated in channels. The actually tortuous channels in three dimensions are flattened and straightened to give a two-dimensional channel network in a fracture plane. The already idealized picture of the channels being the basis of the conceptual model is presented in Figure 1 in Ref. (3).

Boreholes, for injection and pumping, penetrate this plane and the channel network connects the planar borehole sections. Channels with different flow resistances exist and the borehole may hit a channel or there might be an additional resistance to couple the borehole section to the channel. Hydraulic measurements are performed in each borehole to evaluate the transmissivity of the fracture plane. The coupling resistance may influence the measurement remarkably.

The apertures as well as the widths of the channels may vary strongly along the channel lengths. The aperture variation is taken into account in the model as described later and a mean effective width is assumed to describe the possibly varying width of each channel. The number of the channels is taken to be high enough in the fracture plane so that radial symmetry is obtained in pumping tests reasonably well in average.

The channels in a rock fracture have usually very small apertures compared to the widths of the channels and thus the transport of a tracer can be described by a two-dimensional geometry in the fracture flow. This follows from the fact that diffusion mixes the tracer much faster across the aperture than across the width and the transverse directions may thus be decoupled. A dispersion theory for a flat channel is developed according to the method used by Gill and Sankarasubramanian for the tube flow (7,8).

The flow field in a flat fissure depends very strongly on the possible variations of the aperture across the channel width and a wide range of different flow velocity distributions certainly exist. A linear flow velocity field is analyzed in this paper as a first approximation.

Other flow velocity distributions might be considered in principle as well but because of rather tedious mathematics and lack of actual velocity data the treatment has been omitted. The linear flow velocity field approximation is thought, however, to reveal most of the essential features of the coupling of velocity field and diffusion.

The linear flow velocity distribution over the channel implies that the velocity should have its maximum at the other side of the channel which is an unphysical condition with stationary boundaries. The flow may have its maximum velocity, however, very near one side of the channel and the narrow region where velocity drops from the maximum to zero does probably not contribute as much to the dispersion as the broader part of the velocity distribution. The velocity maximum might also be near the center of the channel and for symmetry reasons the channel center could be considered as a reflective boundary.

The conceptual model for the convective diffusion of a tracer in a fracture channel is illustrated in Figure 2 in Hautojärvi et al. (1988).

7.2 Mathematical Model

A good description of the hydraulic properties is needed as a base in order to solve the tracer transport problem. Essential parameters in addition to the geometrical description of the transport routes are flow rates through the injection sections and flow velocities. These have to be determined from the hydraulic information gathered in site investigations. Based on the presented concept the following terminology and definitions are used. The mathematical model has been presented in more detail in Hautojärvi et al. (1988)..

7.2.1 Mean flow time

The mean flow time t_p due to pumping is

$$t_p = \frac{V}{Q} , \qquad (7\text{-}1)$$

where Q is the pumping rate and V is the water conducting volume of the fracture plane which has to be pumped until a tracer from an injection point reaches the pumping site. In radial flow

$$V = (2b)_{fr}^{V}\pi(r_2^2 - r_1^2) \quad , \tag{7-2}$$

where $(2b)_{fr}^{V}$ is the average aperture of the fracture, r_2 is the distance between the boreholes and r_1 is the radius of the observation hole.

The volume to be pumped can be expressed by using a definition for the degree of channeling ϕ_{ch}

$$\phi_{ch} = \frac{A_{ch}}{A_{fr}} \approx \frac{\lambda}{d} \quad , \tag{7-3}$$

where d stands for the average distance between channels and λ for the average width of the channel.

Denoting the mean (volume) aperture of the channel by $(2b)_{ch}^{V}$ it is obtained that

$$(2b)_{fr}^{V} = \phi_{ch}(2b)_{ch}^{V} \quad , \tag{7-4}$$

The flow resistance depends strongly on the channel aperture and the water injection tests are sensitive to the smallest apertures in the channels. However, the tracer tests scan the whole volume of the channels due to diffusional mixing across the channel aperture. The relation between channel apertures determined in two different ways can be written using a factor C_v:

$$(2b)_{ch}^{V} = C_v(2b)_{ch}^{H} \quad , \tag{7-5}$$

where $(2b)_{ch}^{H}$ is the aperture determined from the hydraulic transmissivity measurements. Assuming the cubic law the apparent hydraulic aperture of the channels can be calculated from

$$(2b)_{ch}^{H} = \sqrt[3]{\frac{12\mu}{\rho g}T_{ch}} \tag{7-6}$$

where ρ, μ, and g is the water density, water viscosity and gravitational acceleration, respectively, and T_{ch} is the transmissivity of the channel.

As the transmissivity of the whole fracture plane is actually concentrated in channels, the transmissivity of the channels is given by

$$T_{ch} = \frac{T_{fr}}{\phi_{ch}} \quad , \tag{7-7}$$

The mean flow time is obtained from equations (7-2)–(7-7) to be

$$tp = \sqrt[3]{\frac{12\mu}{\rho g}} \frac{\pi\left(r_2^2 - r_1^2\right)}{Q} T_{fr}^{1/3} Cv \phi_{ch}^{2/3} \quad , \tag{7-8}$$

In order to calculate flow time it is necessary to evaluate the factor $C_v\phi_{ch}^{2/3}$. From the concept of parallel plates and equations (7-6) and (7-7) it follows that

$$Cv \phi_{ch}^{2/3} = \frac{(2b)_{fr}^{V}}{(2b)_{fr}^{H}} \tag{7-9}$$

Values found in the literature for this factor $C_v\phi_{ch}^{2/3}$ vary typically between 5–20 (Gelhar, 1987). Simplified theoretical calculations using a sine function to describe the variation of the aperture illuminates also this factor as shown in Hautojärvi et al. (1988). Direct measurements of apertures also show large variations with small minima and large maxima compared to the minima (Gale et al., 1987).

The effect of pumping might be divided by several fracture planes separated from each other by a tighter layer of rock. In this case the transport time would be

$$t_P = \sqrt[3]{\frac{12\mu}{\rho g}} \frac{\pi(r_2^2 - r_1^2)}{Q} T_{total}^{1/3} Cv \phi_{ch}^{2/3} \sum_i \sqrt[3]{\frac{T_{fr}^i}{T_{total}}} \tag{7-10}$$

where T_{fr}^i is the transmissivity of the fracture i and T_{total} is the sum of the transmissivities of the pumped fractures.

If there were n_{fr} identical fractures, the transport time would be

$$tp = \sqrt[3]{\frac{12\mu}{\rho g}} \frac{\pi(r_2^2 - r_1^2)}{Q} T_{total}^{1/3} Cv \phi_{ch}^{2/3} n_{fr}^{2/3} \quad , \tag{7-11}$$

7.2.2 Tracer transport

The convective diffusion in a flow field with a linear velocity distribution across the channel width is described by the partial differential equation for tracer concentration C

$$\frac{\partial C}{\partial t} - D\left[\frac{\partial^2 C}{\partial y^2} + \frac{\partial^2 C}{\partial x^2}\right] + u_0\left(1 - \frac{y}{a}\right)\frac{\partial C}{\partial x} = 0 \quad , \tag{7-12}$$

where D is the molecular diffusion coefficient, u_o is the maximum velocity in the channel and a is the width over which the velocity varies from zero to its maximum value.

Defining dimensionless variables and the Peclet number Pe

$$\begin{aligned} X &= Dx/a^2u_0 \\ X_s &= Dx_s/a^2u_0 \\ r &= Dt/a^2 \\ \eta &= y/a \\ Pe &= au_0/D \end{aligned} \tag{7-13}$$

Equation (7-12) can be written in the following way

$$\frac{\partial C}{\partial r} - \left[\frac{\partial^2 C}{\partial \eta^2} + \frac{1}{(Pe)^2}\frac{\partial^2 C}{\partial X^2}\right] + (1 - \eta)\frac{\partial C}{\partial X} = 0 \quad . \tag{7-14}$$

The solution is sought in a series form

$$C = \sum_{k=0}^{\infty} f_k(\tau,\eta)\frac{\partial^k C_m}{\partial X^k} \quad , \tag{7-15}$$

where C_m is the mean concentration across the channel.

Then the problem can be solved in terms of C_m as shown in Hautojärvi et al. (1988).

$$C_m = \frac{1}{2}\left\{\mathrm{erf}\left[\frac{\frac{1}{2}X_s + X + \xi_1}{2\sqrt{\xi_2}}\right] + \mathrm{erf}\left[\frac{\frac{1}{2}X_s - X - \xi_1}{2\sqrt{\xi_2}}\right]\right\} \quad , \tag{7-16}$$

where

$$\xi_1 = -\frac{1}{2}\tau$$

$$\xi_2 = \left(\frac{1}{(Pe)^2} + \frac{1}{120}\right)\tau - 8\sum_{n=0}^{\infty}\frac{1}{(2n+1)^8\pi^8}(1 - e^{-(2n+1)^2\pi^2\tau}) \ , \qquad (7\text{-}17)$$

It is worthwhile to notice that the time dependent part of the series in the expression of ξ_2 converges very fast at positive time values and a good approximation for ξ_2 having the right behaviour at zero and infinite times is

$$\xi_2 = \left(\frac{1}{(Pe)^2} + \frac{1}{120}\right)\tau - \frac{17}{20160} + \frac{17}{20160}e^{-\pi^2\tau} \ , \qquad (7\text{-}18)$$

The mean flux across the channel is then calculated using the formula

$$\begin{aligned} \phi &= \int_0^1 uC\, d\eta \\ &= u_0 C_m(-K_1) + u_0\frac{\partial C_m}{\partial X}\left(\frac{1}{(Pe)^2} - K_2\right) + \cdots \\ &= \frac{1}{2}u_0 C_m + u_0\frac{\partial C_m}{\partial X}\left(-\frac{1}{120} + \frac{1}{120}e^{-\pi^2\tau}\right) \ . \end{aligned} \qquad (7\text{-}19)$$

The analytical expressions have been verified by comparing them independently with Monte Carlo simulations as shown in Hautojärvi et al. (1988).

It may be possible to describe dispersion in a limited range of parameter values as a one-dimensional phenomena but extrapolating from one set of parameters to another range might be erroneous. Velocity differences exist in fractures over different length scales (apertures, widths, distances between neighboring channels). It depends on the time scale and dimensions of the source which features are dominating. By measuring in a certain scale and especially with only one time domain (with one velocity) only that scale is studied. It is almost impossible to extrapolate the results to other scales.

The dispersion due to velocity differences over the aperture is eliminated in time scales of minutes, but experiments over short distances and with high velocities would give a high dispersion. This result and especially the "dispersion coefficient" derived from it could, however, not be applied in slower flows and longer distances. A similar situation is possible when extrapolating results from field tests to performance assessment.

It is important therefore to study the reason for observed dispersion. This is possible only by applying models that take into account some of the physical phenomena causing dispersion (hopefully the most important ones). With a one dimensional model it is possible only to fit and perhaps select the type of the "dispersion coefficient" (constant, dispersion length or some other behavior).

The time $0.5 \cdot a^2/D$ characterize the approaching of the steady state. Here a means the measure of the dimension under consideration, i.e., the aperture or the channel width and D is the

molecular diffusion coefficient. The unsteady convective diffusion analysis should be applied especially in the case of ground water flow in a flat rock fissure which might have a considerable width while the aperture is very small. The characteristic time to reach the steady state dispersion in a channel having a width of 1 mm, 1 cm and 10 cm with a diffusion coefficient of $3 \cdot 10^{-9}$ m^2/s is 170 s, 4.6 h and 19 d, respectively.

We consider that the coupling of diffusion and the velocity field affects so much the experiment that it should be taken into account. On the other hand if the concept could be proved to be valid, it would offer a mean to determine some of the basic migration characteristics also for extrapolation to time and space scales appropriate to repository performance assessment. Matrix diffusion is considered to have a minor effect in the time scale of the performed experiments.

7.3 Results

7.3.1 Hydraulic conceptual model and interpretation of hydraulic data

- Predictions

The zone 2 has been modelled as three separate parallel subzones, although some flow routes from middle and lower subzones come via the upper subzone.

At the time pf predictive modeling the results of the interference tests (Andersson et al., 1988b) were not available and the average transmissivities between the injection sections and the pumping borehole were estimated using the transmissivity measurements in each borehole (Andersson et al., 1987; Andersson et al., 1988a; Ahlbom et al., 1987; Andersson et al., 1988b). Arithmetic averages were used as guidelines when giving transmissivity values for the subzones. Some measured high values in the middle and lower subzones led us to assign relatively high transmissivities to the subzones. In the borehole KFi06 there was a section with a high value but it was not included finally in the middle injection section.

The conceptual hydraulic model and the chosen transmissivity values for the subzones are presented in Figure 6 and Table 2 in Hautojärvi et al. (1988).

- Recalculations and comparisons

After getting the results of interference tests and also measured flow rates through the injection sections, some transmissivity values were slightly revised. The head differences and transport times were recalculated using still the same concepts and methods as in original predictions.

We call these recalculations also predictions (we think that we would have got these same results already in the first phase if the data had been available).

Predicted and measured head differences between the injection sections and the pumping section in the borehole BFi02 are presented in Table 1 in Hautojärvi et al. (1990). No anisotropy in the transmissivity of the Zone 2 and its subzones was assumed. Head differences due to natural undisturbed potential field have not been reported to our knowledge. The natural gradient may dominate far away from the pumping borehole and some values were guessed for the natural head differences.

The relatively good agreement between the head values indicate that the total transmissivity of the Zone 2 was evaluated quite well. The total transmissivity was assumed to be the average of the sums of transmissivities measured in individual boreholes (10^{-3} m^2/s). On the other hand, the measured head differences indicate total transmissivity of $4 \cdot 10^{-3} \cdots 20 \cdot 10^{-3}$ m^2/s (assuming

that the guessed natural head gradient in Table 1 in Hautojärvi et al. (1990) is valid). From the results of the interference tests the total transmissivity of the Zone 2 was determined to about $3 \cdot 10^{-3}$ m^2/s (Andersson et al., 1988b).

According to the conceptual channel model as shown in Figure 1 in Hautojärvi et al (1990) the total, average transmissivity of the Zone 2 is due to several very conductive channels. However, the boreholes are connected to the most conductive channel network by smaller, less transmissive channels.

The predicted and measured transport times are compared in Table 2 and in Figure 2 in Hautojärvi et al (1990). The short transport times especially in the upper subzone were predicted quite successfully. The discrepancies are explained, in our opinion, with local heterogeneities of the channel properties and especially at the first part of the transport route.

The effective transmissivities of the flow routes from the injection sections to the pumped borehole were evaluated from the transmissivity of the conducting channel network and the most conductive fractures intersecting the injection and pumping sections in the boreholes. The transmissivities of the flow routes were evaluated like the total resistivity of resistances in series would be calculated. The effective transmissivities are given in Table 3 and the measured transport times are presented in Figure 3 in Hautojärvi et al (1990) as a function of the effective transmissivity of the tracer routes. There exist a relation between the transport time and the transmissivity but an unknown constant, including the number of parallel transport routes, degree of channeling and factor from aperture variability, is present. In Figure 3 in Hautojärvi et al (1990) the line represents a value of 7 used in the predictive modelling for the constant in question.

7.3.2 Tracer transport

- Predictions

In the predictive tracer break-through calculations the source terms were not known in detail and the break-through curves presented in Hautojärvi et al. (1988) show a general behavior but they should not be compared directly with the experimental results.

- Recalculations and interpretations

One transport route between the injection borehole section and the pumping borehole has been assumed in recalculations (instead of 2 parallel routes in first predictive calculations). This transport route represents the fastest connection between the injection and collection sites and it may contribute to the total flow several tens of percents. Any slower routes would contribute later parts of the break-through curves. In order to see to what extent the fastest route could explain the break-through curves the calculations were carried out by taking into account just one route and normalizing the mass flux to the experimental value. It is thought that the route might be a flat channel in the rock having an aperture of about 1 mm or less and a width of 10 cm. A velocity gradient is supposed to exist in this channel more or less symmetrically over half of the channel width i.e., the velocity varies from a minimum (zero) to maximum velocity over 5 cm.

The injection sections were assumed to be well mixed volumes with a ground water flow Q_w interacting and mixing with the volume. The analysis was performed with constant ground water flows but time dependent tracer concentrations taking into account also possible injection stops or other changes in the tracer injections. The ground water flows through injection sections were adjusted to give a good overall agreement with the measured concentrations in the injection sections. Break-through curves were calculated adjusting the ground water velocity and a

normalization factor (representing the one channel contribution) for the transported mass in order to compare the break-through curve shapes in detail and especially the front of the curves. The calculated results for the concentrations in injection sections and break-through curves together with experimental results are given in Figures 5–14 in Hautojärvi et al. (1990).

Some comments and remarks concerning the results are given in also the following. A general remark is that it is obvious that the ground water flow through the injection sections has not been constant. This does not affect the break-through curves drastically if the ground water flow rates are high, because then the tracer mass flow rate is anyhow almost constant (this is true when the steady state of the tracer concentration has been reached in the injection section). However, if the ground water flow rate is low, then the concentration in the injection section varies slowly with time and a varying ground water flow affects the tracer mass flow and may thus be not very well known.

• BFi01 Upper

The concentration in the injection section decays fast, when the injection is stopped. This break-through curve shows also a fast response to changes in the injection concentration. This indicates a high ground water flow rate. The increase in the injection concentration at 400 h might be due to real tracer injection increase which is reflected in the break-through curve. The experimental decay of the break-through curve is somewhat slower than calculated being perhaps due to a slightly reduced Q_w. During the first injection pulse (0–22 h) q_{inj} has been lower than in average (see In-EDTA tank volume).

• BFi01 Lower

The measured concentration in the injection section seems to follow rather well the theoretical one with $Q_w = 6$ ml/min, although the decay after the injection stop indicates a slightly higher flow rate. Large amounts of the tracer are lost. The rather low head difference especially at the lower section after the detailed sampling could be partly responsible for the loss.

• KFi06 Upper

From the interpretation of the tracer being transported essentially via one route it follows that Q_w is rather small and the tracer is diluted slowly in the injection section. If Q_w would be higher only more routes or a heterogeneous system could explain the slow decay of the break-through curve. The second hump in the break-through curve is due to the first pump stop in BFi02.

• KFi06 Middle

The concentration in the injection hole reaches slowly C_{00} indicating nearly vanishing Q_w. The break-through curve has an exceptionally sharp front edge. The velocity gradient is modelled here to stretch only over 2 cm instead of 5 cm to reflect the apparently small dispersion. The detailed sampling might have affected although the edge.

• KFi06 Lower

Strong variations in the tracer injections are washed out due to dispersion during transport. The second hump in the experimental break-through curve might be due to the pump stop during the detailed sampling.

• KFi11 Upper

Tracer injection stops are reflected very sharply in the break-through curve. Initially q_{inj} has been assumed to have been somewhat lower than in average and some fitting of injection stop times has been done because the given data is also slightly uncertain. Assumed injection time intervals are given in the table in Ref. (3). It seems very plausible that further changes in q_{inj} would explain the break-through curve variations also after 220 h.

• KFi11 Middle

The injection section concentration increases slowly almost to the value C_{00} and decays also very slowly. Loss of collected tracer occurs after 1500 h. In the ground water level curves there is some increase about at this time and thus a small hydraulic potential change might have caused the rest of the tracer to be transported to elsewhere.

• KFi11 Lower

A rather fast rise of the experimental concentration in the injection section is seen but a slow decay. By subtracting carefully a constant background a very small net response might be observed rather quickly in the pumping hole. The tracer should in this case be transported mainly probably to the fracture zone 1 and only a small portion of it would then be directed towards the hole BFi02.

• KFi11 Upper pulse injections

Both tracers injected at the same time show a similar behavior. A single channel could explain break-through curves. The normalization factors are somewhat uncertain because a detailed injection description has not been available. The second hump is probably due to some changes in the injection section conditions which are reflected also in the ln C/C_0 data at 120–150 h. It should be noted that the concentrations decay rather slowly in the injection section contradictory to the stop of the continuous injection case. The Q_w values differ by a factor of 70. The transit times are, however, exactly the same in either cases.

• Flow rates through the injection sections

The measured and predicted flow rates through the injection sections are presented in Table 4 in Ref. (3). The measured values are obtained from the time dependent modeling of the concentrations in the injection sections as discussed above. It was observed in the dilution experiments performed before and after the tracer test that the flow rate through the injection sections had changed dramatically. It should be noted, however, that the transport times did apparently not change due to the flow rate change as seen most clearly in the case of KFi11 upper section for Gd-DTPA (continuous) and Amino-G (pulse) injections.

7.4 Discussion and Conclusions From Radially Convergent Test Data

The experimental results have been explained satisfactorily consistent, in our opinion. This could indicate some degree of validity, but more checks should be needed to test the conceptual hydraulic and transport model adequacy. We regret that we have not had time to test our modeling for the pulse injections during the high (8 l/s) pumping flow rate. In assessing the obtained model parameter values the experimental difficulties in field tests should be taken into account. It has been difficult to control the source term, to keep the hydraulic situation stable and to measure hydraulic boundary conditions and natural gradients extensively.

There is no reason, in our opinion, to perform tracer tests with long (continuous type) injection pulses. Some 10% injection width from the estimated break-through width might be optimal. For validation purposes experiments with different pumping rates (flow velocities) would be very valuable. Flow routes should be studied one by one (as is done in the radial experiment if the injection sections are short enough) and not mixed (dipole experiment or large overpressure in the injection section). The necessary statistics should be gathered then by hard work with several injections.

Implications from the experiments to the performance assessment are that there are hardly any remarkable effects of retardation or dispersion that could be taken into account when assessing the migration in such highly conductive fracture zones. If the flow velocities would be for some reason much lower (small hydraulic gradients) the dominating effect would be matrix diffusion, which could not be studied in these experiments. Actually the studied migration phenomen, dispersion, is relatively uninteresting in the case of repository assessment and its role should not be emphasized too much. The most interesting things learned from these experiments were perhaps the relations between measured transmissivities and transport times and the possibly (hopefully) somewhat adequate picture of the flow situation and fracture properties.

7.5 Analysis of Dipole Experiment

The conceptual model used by the VTT team has been presented in the INTRAVAL workshop in Helsinki 12. - 16.6.1989 [1]. Some model calculations were also presented assuring that the tracer injection would last 10 min with a concentration of 1000 ppm. These results may be translated to correspond the actual experimental situation and results (C/Co) by dividing by a factor of 1000 (1/1000 ppm) and by 2.5 (10 min/4 min). In these calculations the recirculation was not taken into account. At the time of the Las Vegas workshop in February 1990 the modeling was improved to take into account the recirculation, but unfortunately the results could not be presented yet in the workshop. A letter was sent to the test pilot group 6.2.1990 as a reference of the predictive modeling (a copy is enclosed)

After getting the results of the dipole experiment from the test pilot group [2], recalculations were performed and are presented in this short report. This report should be considered as a continuation to the radially converging experiment report (VTT, 1990).

The conceptual model for the subzone in the dipole experiment is the same as the concept used in the modeling of the radial experiment i.e. flow in flat channels from the injection borehole to the withdrawal borehole. The channel network is thought to be so dense, that an ideal dipole field is established for the potential. The flow, however, takes place in confined channels. As soon as the number of the channels, their lengths and velocities in the channels are defined, the problem reduces to a problem of parallel flow routes between two locations. Each of the flow routes has a response function of its own and contributes additively to the whole system response.

The lengths of different flow routes are calculated from the field line lengths of the dipole field given by the expression

$$L = 2a\,\theta/\sin\theta \quad ,$$

where 2a is the distance between the injection and withdrawal borehole sections and θ is the departure angle of the field line relative to the interconnecting line.

The flow resistance is proportional to the length of the flow route and the ratio of its resistance to the total resistance determines the flow rate at the route. Transport times are handled as free parameters reflecting possible variations in the flow route volumes for equal lengths. Transport times were calibrated using the results of the radial experiment taking into account the higher potential gradient. The velocity should be a factor of 3 higher in the dipole test if the effects of natural gradients are neglected.

7.6 Results

In the predictive modeling the number of the flow routes was guessed to be 4 with departure angles θ, 90, 180 and 270 degrees. Three active routes were modeled because the route with 180 degree departure is "infinite" long. The predicted relative concentration as a function of time is compared to a measured curve in Figure 7-1. The overall agreement is fair but some deviation from the ideal four channel behavior is obvious.

In order to "explain" or fit the measured curves the relative flow rates of the three flow routes were varied as well as the velocities. The lengths of the flow routes were taken from the distances between boreholes BFi01 - KFi11 - BFi02 and BFi01 - KFi06 - BFi02, respectively. The parameters of the predictive modeling and of the fitted modeling are presented in Table 1 and the concept is illustrated in Figure 7-2. A loss of 35% of the tracer per each cycle is modeled but the first arrival is without any losses.

Table 7.1. Parameters used in the predictive and final modeling of the dipole experiment.

	PREDICTED			FITTED		
Flow route	Relative flow rate (%)	Velocity (m/s)	Relative length	Relative flow rate (%)	Velocity (m/s)	Relative length
via KFi11	25.6	$7.16 \cdot 10^{-4}$	1.57	45.0	$3.30 \cdot 10^{-3}$	1.9
straight	48.8	$1.37 \cdot 10^{-3}$	1.0	50.0	$1.25 \cdot 10^{-3}$	1.0
via KFi06	25.6	$7.16 \cdot 10^{-4}$	1.57	5.0	$8.50 \cdot 10^{-4}$	2.0

The calculated results for the relative I-131 concentrations (Run N:o 3, A.3) in the borehole BFi02 are presented in Figure 7-3 together with experimental results. No artificial normalization factor was used. The outlet concentration was calculated as mean concentration over the channel width and not as flux weighted concentration as in the radial experiment. The width of the peak indicates a contribution of more than one channel. It can be seen from Table 7.1 that the straight route and the route via KFi11 contribute both at the peak value.

Many different tracers were injected but there are some discrepancies between the results. Some conservative tracers show clearly a much lower breakthrough concentration than I-131. The relative concentrations of some of the tracers were normalized at the peak value in order to compare the dispersion and breakthrough behavior and to get an idea of a possible experimental scatter in the breakthrough curves. The comparison is presented in Figure 7-4 together with the calculated curve.

The flow route via KFi11 appears to be much faster and contributing much more than an "ideal" route. This was partly seen in the radial experiment and in the interference tests. The modeling is somewhat more complicated than just in the case of withdrawal borehole. The first arrival of the tracer is just due to the response of the channel between BFi01 and KFi11 but after recirculation occurs the whole response of all of the routes affects the source term for the channel at later times. In Figure 7-5 the calculated breakthrough curve is presented together with two of the measured curves (I-131 B.3 and Br-82 B.6). The second peak is mainly due to the recirculating concentration from the whole system. The calculated peak concentration does not reach the experimental one fully. This may be due to the very convective nature of the fast flow which can not be modeled with the used diffusive convection model accurately at short times.

The flow via the observation borehole KFi06 is slower and has a minor contribution to the total flow and tracer transport. The calculated result is shown in Figure 7-6 together with three tracers (I-131 C.1, Cr-51 C.2 and YB-169 C.4). The calculated curve is normalized by a factor of 0.5 to have a better overlap for the front of the measured curve and the small kink which is thought to be near the actual maximum value. The rise of the I-131 concentrations after 400 hours is due to the second injection 9 days (216 h) later (it is not known if this part of data has been corrected for radioactive decay according to the appropriate injection time). The reason to the discrepancy between the measured and modeled values by a factor of 2 may be a dilution in the observation borehole sampling or two parallel routes with somewhat different velocities (causes also dilution at early times). The Cr-51 and Yb-169 EDTA complexes seem to have a lower recovery also here and for comparison purposes the data has been normalized by a factor of 2.

7.7 Conclusions for Dipole Test Data

The presented conceptual model seems to explain well the overall features of the dipole experiment. Some normalization factors has to be used in order to fit all the data using consistently same parameters in the modeling. The calculated results could be reproduced with different sets of parameters but the approach has been here to minimize the number of parameters (number of channels and channel property variations). The presented parameter values should therefore be taken as representative values giving roughly the right picture of the flow and tracer transport situation. The concentration measurements in the withdrawal borehole and observation boreholes are actually very different kind of measurements giving information from the whole flow area or from "one channel", respectively. The fair agreement with these both type of measurements with the same conceptual model and model parameters (same parameters as also in the radial case) enhances the confidence to the employed concept and modeling procedure.

8. JAERI Analysis of Tracer Test Data

Hideo Kimura and Masahiro Munakate
Japan Atomic Energy Research Institute, Japan

8.1 Conceptual Model

The most attractive point of this experiment for the modeller is to get informations about "large-scale" nuclide transport in a deep fracture zone. We have applied two different conceptual models for this tracer test. One is a equivalent single fracture approach where the fracture aperture is constant in two-dimensional plane, and the other is a variable aperture channeling model (Moreno, L. et al., 1988, and Tsang, Y.W. et al., 1988). We are interested in which model is suitable for describing the tracer movements in the fracture zone.

In this study, the upper highly conductive part of Zone 2 is modelled by the two conceptual models. The assumptions used for the equivalent single fracture approach are;

- Steady state flow field is established.
- The groundwater flus from aquifer (Zone 2) into other layers is negligible (two-dimensional flow).
- The aquifer (Zone 2) is modelled as the porous and homogeneous medium, or the dual porosity medium.
- Channeling is ignored, the fracture aperture is constant in two-dimensional plane.
- Matrix diffusion is considered in the dual porosity approach.

The assumptions used for the variable aperture channeling model are;

- Steady state flow field is established.
- The groundwater flow field of the fracture is two-dimension.
- Probability distribution of channel aperture is given by lognormal distribution, and the channel apertures are correlated each other.
- Each channel is modelled as one-dimension. (The flow between two adjacent nodes is determined by both aperture.)
- Effective volume of groundwater in the channel related to the flow is not always equal to the volume of the fracture (porosity of fracture $\phi \leq 1.0$)
- Effects of matrix diffusion and sorption are taken into accounts.

8.2 Mathematical/Numerical Model

8.2.1 Groundwater flow

The groundwater flow field is given by analytical solutions in the case of equivalent single fracture approach. In the variable aperture channeling model, the fracture plane is divided by a rectangular grid into nodes with different apertures. Considering two adjacent nodes with apertures bi and bj, the flow from node i to node j, Qij, is given by the following equations.

$$Q_{ij} = k_{ij}(P_i - P_j) \tag{8-1}$$

$$k_{ij} = \frac{\phi g}{6\mu} \frac{\Delta y}{\Delta x} \left(\frac{1}{b_i^3} + \frac{1}{b_j^3} \right)^{-1} \tag{8-2}$$

where P_i: pressure at note i
k_{ij}: transmissivity node i to j
μ: viscosity
Δx: grid size in the direction of flow
Δy: grid size in the direction perpendicular to flow

Boundary conditions are

$$P = P_0 \quad \text{(outside boundary)} \tag{8-3}$$

$$Q = Q_p \quad \text{(pumping or injection well)} \tag{8-4}$$

where P_0: analytical pressure
Q_p: pumping or injection rate.

Lognormal distribution is given by the following function.

$$f(b) = \frac{1}{\sqrt{2\pi}\, b \sigma_b \ln 10} \exp\left(- \frac{(\log b - \log b_0)^2}{2\sigma_b^2} \right) \tag{8-5}$$

$$b_0 = \overline{be}^{-(\sigma_o \ln 10)^2} \tag{8-6}$$

where σ_b: standard deviation in the lognormal distribution
b_0: mean log aperture
$\overline{b}$: mean aperture

The correlation strength A between point i and j is considered as follows:

$$A = \exp\left(- \frac{\Delta x_{ij}}{\lambda_x} - \frac{\Delta y_{ij}}{\lambda_y} \right) \tag{8-7}$$

where Δx_{ij} : x-component of distance between point i and j
Δy_{ij} : y-component of distance between point i and j
λ_x : correlation length in x-direction
λ_y : correlation length in y-direction

A system of equations about the pressures P is solved using SOR or CG method.

8.2.2 Nuclide transport

Two-dimensional advection-dispersion-sorption-matrix diffusion model has been applied for the equivalent single fracture approach. The mass balance equation for a solute transport can be written as:

$$R_f \frac{\partial c}{\partial t} = \nabla(D\nabla c) - \bar{v}\nabla c - R_f \lambda c - \Gamma \tag{8-8}$$

$$D_{ij} = D_T |\vec{v}| \delta_{ij} + (D_L - D_T) \cdot \frac{v_i v_j}{|\vec{v}|} + \phi D_d \tau \delta_{ij} \tag{8-9}$$

where R_f: retardation factor of nuclide (–)
c: concentration of nuclide (kg/m^3)
D: dispersion coefficient tensor (m^2/s)
λ: decay constant (1/s)
D_T: transverse dispersion length (m)
D_L: longitudinal dispersion length (m)
τ: tortuosity (–)

Γ is the mass flux between fracture and rock matrix, and is zero for the porous medium approach. The mass flux Γ is obtained by the following mass equations in the rock matrix.

$$R_m \frac{\partial c'}{\partial t} = D_m \frac{\partial^2 c'}{\partial z^2} - R_m \lambda c' \tag{8-10}$$

$$\Gamma = \frac{\varepsilon D_m}{\delta} \left. \frac{\partial c'}{\partial z} \right|_{x=0} \tag{8-11}$$

$$c'(x,y,0) = c(x,y) \tag{8-12}$$

where R_m: retardation factor of nuclide in the rock matrix (–)
c': concentration of nuclide in the rock matrix (kg/m^3)
D_m: diffusion coefficient in the rock matrix (m^2/s)
ε: porosity of the rock matrix (–)
δ: aperture of the fracture (m)

The z-axis denotes the normal direction of fracture plane. The equations (8-8)–(8-12) are discretized by Galerkin finite element method, and are solved for the following boundary conditions.

$$c = c_0[1 - \theta(t - t_b)] \quad \text{at injection well} \tag{8-13}$$

$$(\nabla c)_n = 0 \quad \text{at pumping well} \tag{8-14}$$

where c_0: initial concentration at injection well (kg/m^3)
$\theta(t)$: step function (–)
t_b: duration of band release (s)

In the variable aperture channeling model, nuclide transport through the fracture is calculated using the particle-tracking method (Yamashita R. and Kimura H. 1989). In this simulation, the fracture plane is modelled as a rectangular network system. The travel time of particle in each channel is given by one-dimensional solution, and particles coming to an intersection of network are distributed in the outlet branches with a probability proportional to the flow rates.

8.3 Model Selection Criteria

Phenomena expected to occur in this test area should be taken into account in the conceptual model. However, detailed simulations are not necessary for the preliminary calculations. Because, detailed simulations require lots of man-power and main features of tracer test can be drawn out from simple model. In this case, the assumptions of steady state and two-dimensional flow condition reduce computational costs, and advection-dispersion-sorption model is the most preliminary one. After comparison between experimental and calculated breakthrough-curves, the conceptual model will be refined considering other mechanisms if discrepancies are seen among them.

8.4 Results

8.4.1 Radially converging tracer experiments

Pulse injected breakthroughs from the upper parts of boreholes KFI11 and KFI06 and continuous injected breakthrough from the upper part of borehole BFI01 are analyzed by the variable aperture model. The resulting breakthrough curves of non-sorbing tracers Tm-EDTA, Iodide and In-EDTA are given as absolute concentration (ppb or ppm). Nevertheless, the shapes of breakthrough curves (arrival time, peak time, etc.) were only compared with those of numerical breakthrough, because it is difficult to estimate the dilution factors of tracers at sampling borehole BFI02 and mass-losses of tracers from the upper part of Zone 2 into other parts.

Flow and solute transport calculations were carried out with two-dimensional model for different realizations of the variable apertures in a single fracture. Fractures with specified aperture parameters were generated, and the head differences between injection and sampling hole and breakthrough curves of tracers were studied. We used the grid of 100 × 100 and $\Delta x = \Delta y = 5.0$ m. The standard deviation in the aperture density distribution, mean aperture and spatial correlation length were obtained so that the averaged numerical breakthrough curve and heads of different realizations fit those of experiment. The particle-tracking calculations were performed

by considering advection, sorption and matrix diffusion. In these simulations, local dispersion was neglected. The pumping and injecting boreholes in the modelled area are shown in Fig. 8.1. The pumping hole BFI02 is located at the center of modelled area, and borehole BFI01 is located at the y-direction of BFI02 considering the dipole tracer test. Breakthrough curves of pulse injected tracers were calculated by 2500 particles, and that of continuous injected tracer was 4300 particles in each realization. In the continuous injection, number of released particles is proportional to the concentration of borehole BFI01.

Table 8.1 shows calculated and measured head differences between the injection sections and the pumping section in the borehole BFI02. The calculated head differences are averaged values of 28

Table 8.1. Calculated and measured head differences between the injection sections and the pumping section in the borehole BFI02.

	BFI01(U)	KFI06(U)	KFI11(U)
Measured	1.14	0.62	0.81
Calculated	1.13	0.97	1.00

runs. In the averaging process, the realization such that head difference is larger than 11.4 m (10 times of measured value) is not included. Because it may be resulted from the numerical error and introduce short travel time, Figures 8.2a, 8.2b, and 8.2c show calculated (average of 28 runs) and observed breakthrough curves at the borehole BFI02(U). These results were obtained by assuming conductive area where the mean apertures are 2.00 and 1.52 times larger than other area (shadow area in Fig. 8.1). This assumption is resulted from short travel time from the borehole BFI11 to BFI02 and small head differences between the pumping hole BFI02 and injection holes KFI06 and KFI11. This assumption is not consistent with the measured transmissivities of upper part of Zone 2. The input pumping rate of this simulation was 40% less than experimental value considering the distribution of transmissivities in the pumping hole BFI02 (Gustafsson E. et al. 1989). The best-fit parameters in this simulation are summarized in Table 8.2. The effects of matrix diffusion are weak in these simulations because of high velocities. Obtained average fluid flow distribution is shown in Fig. 8.3.

8.4.2 Dipole tracer experiments

The breakthrough curve for non-sorbing tracer ^{131}I with pulse input was analyzed by the equivalent single aperture model (MIG2DF) and the variable aperture model. In the equivalent single aperture model, the finite element grid is composed of 1120 four-node isoparametric elements. In order to reduce numerical dispersion, the grid size was chosen so as to be smaller than the longitudinal dispersion length 8.4 m which is expected from the result in a deep basalt flow (Leonhart L.S. et al. 1985). The observed breakthrough curve is reflected from the effect of tracer recirculation and radioactive decay, where at least 4 recirculation of tracer might be occurred.

Calculated and measured breakthrough curves are shown in Fig. 8.4a and 8.4b. In this calculation, we assumed that 89% of the collected tracer at the borehole BFI02 is re-injected at BFI01. Best-fit parameters in this simulation are summarized in Table 8.3.

Table 8.2. Best-fit parameters for radially converging test.

Parameters	Values
Correlation length (x-direction)	5.0 m
Correlation length (y-direction)	2.5 m
Input Standard deviation	0.5
Input Mean aperture	0.000955 m
Obtained Standard deviation	0.554
Obtained Mean aperture	0.00111 m
Effective diffusion constant in rock mass	5.0E-12 m^2/sec

Table 8.3. Best-fit parameters for dipole test.

Parameters	Values
Longitudinal dispersion length	8.0 m
Transverse dispersion length	4.0 m
Effective thickness of aquifer	0.015 m

Table 8.4. Measured and calculated head differences between BFI01 and BFI02 hole.

	Head differences
Measured	2.9 m
Case1 calculation	2.73 m
Case2 calculation	2.37 m

In the variable aperture model, we used the grid of 100 × 140 and $\Delta x = \Delta y = 5.0$ m. Modelled area is expanded in the y-direction than the radially converging test case to consider large-dipole flow field. The simulations were performed by using the same parameters obtained from radially converging test except the mean aperture. Two sets of calculations were performed, one is based on the assumption that pumping and injection rates are 40% less than real values (case1), the other is that injection rate is 40% less than experimental value (case2). This reduction of injection rate is arised from the results of radially converging tracer test. The fitted breakthrough curves were obtained by mean aperture = 0.00158 (case1) and 0.00198 m (case2) which are larger than that of radially converging test case. Averaged breakthrough curves of case1 and case2 are shown in Fig. 8.5a and 8.5b together with the measured curve. In these

breakthrough curves, the effect of tracer recirculation is not so important because of channeling effect compared with the equivalent single aperture model. Obtained averaged fluid flow distributions of case1 and case2 are shown in Fig. 8.6a and 8.6b. Water flux distributions across the line specified in Fig. 8.6a are also shown in Fig. 8.7a and 8.7b. These flux distributions are classified into 3 sections: path related to KFI11 hole, direct path and path related to KFI06 hole. Accumulated flow rates related to KFI06 are almost same in the both simulations, but there are differences of 5% in those related to KFI11 and direct path.

8.5 Conclusions

Our conceptual model seems to explain the experimental results of radially converging and dipole tests. The variable aperture model is basically a generic model, but some assumptions are necessary for the calibrations of breakthrough curves in the large scale flow field. More experimental data related to the assumptions and geostatistics should be needed for the validation of flow and transport model.

The result of radially converging test show that there are multiple flow paths from injection holes to pumping hole. The results of dipole test BFI01 to BFI02 hole) show the applicabilities of both model, but breakthrough data from KFI11 and KFI06 will not be explained by the equivalent single aperture model. It means that dipole data obtained from 2-holes are insufficient for the analysis of the transport medium. The simulations of dipole breakthrough data from KFI11 and KFI06 should be needed in the variable aperture model, and the results based on these best-fit parameters may be different from the observed curves. The simulations will be helpful if the pulse injected data from borehole BFI01 are obtained, because pulse data are more sensitive to the flow paths of fracture zone than continuous data.

The differences of obtained mean aperture between radially converging and dipole test may be arised from the effects of stagnant portion of the fracture water. The stagnant portion of the fracture water will be decreased according to the flow rates. Another reason may be leakage to other layers. We have already considered the 40% loss of pumping rate, therefore more large loss will be necessary.

9. HAZAMA Analysis of Tracer Test Data

R. Yamashita and A. Kobayashi
Hazama Corporation, Japan

9.1 Conceptual Model

In crystalline rocks, fractures are expected to be major flow paths of underground water. It is very important to model fractures and understand mechanisms of solute transport through a fracture network for performance assessment of high level radioactive waste disposal. The state of the art seems to be a stage to investigate and deduce mechanisms of phenomena. On such a stage, a modeling method is needed to understand results of field and laboratory experiments. The breakthrough curves measured at the radially converging tracer test in Finnsjön area have some features, which are long tailings and sharp concentration fronts. The authors tried to simulate these features and to examine what are the important physical mechanisms for solute transport in this area.

According to the borehole observations, Zone-2 is divided into three regions which are upper, middle and lower subzones.

The model is based on a fracture network approach, in which fractures are generated using the statistical parameters of their directions, extensions and positions. The parameters of the statistical approach should be determined by using the observed data. However the available data is not enough to characterize the fracture network.

Thus, the following assumptions are made to generate a fracture network for simplicity.

1. All fractures have the same aperture (b) and the same length (L).
2. The positions of the fractures are random in each subzone.
3. The density of the fractures is bigger in the upper and the lower subzones than in the middle subzone.
4. The dips of the fractures have the average value of 30° and the standard deviation of 30° in all subzones.

The groundwater flow during the tracer test was considered to be caused mainly by pumping at BFI-02, and the natural potential gradient is assumed to be negligible. In our analyses, the water flow is assumed to flow symmetrically with the pumping borehole BFI-02. By using this model, it can be simulated that the flow velocity in the vicinity of BFI-02 is faster than the velocity in the far portion. The seepage analyses are carried out for the steady state flow.

Solute is assumed to transport through the fractures mainly by advection because the measured breakthrough curves showed solute moved fairly fast. The major assumptions in our transport model are that complete mixing occurs at the intersections of the fractures and hydrodynamic dispersion including molecular diffusion in the fractures are negligible.

9.2 Mathematical and Numerical Model

Parallel plate model is used for the flow in each fracture element and the conductivity(k) of each fracture is calculated using the following equation.

$$k = \frac{b^2 \rho g}{12\mu} \tag{9-1}$$

where b is the fracture aperture, ρ is the bulk density of water, ,μ is the viscosity of water. Flow rate (q) in each fracture is given by

$$q = 2\pi b k \frac{\partial h}{\partial r} \tag{9-2}$$

where h is the total head in the fracture and r is the radial co-ordinate.

Boundary conditions are shown in the Fig.9.1. Total heads along the injection borehole and the pumping section were prescribed to be h_1 and h_2, respectively. The other boundaries are set to be no flux. According to the field measurement, difference between h_1 and h_2 is set to be 4 m.

Using one dimensional finite elements, total heads at all intersections of the fractures were calculated under the above stated boundary conditions.

In the solute transport analyses, advection and matrix diffusion are assumed as physical transport mechanisms in the fractures. To calculate the solute transport, a particle tracking method was developed so that the effect of matrix diffusion on advective transport could be considered.

The basic idea of the particle tracking method is that the residence time of each particle within the fracture is determined by using a proper probability density function(P.D.F.). If advection is the only mechanism considered in the transport analysis, the residence time of the particle through a fracture element is calculated deterministically by the flow velocity and the fracture length. However, due to local dispersion, each particle may have different residence time. In order to consider local dispersion, it is possible to treat the mass flux at the outlet of each fracture as the P.D.F of a particle residence time as shown in Fig. 9.2. Since advection and matrix diffusion are considered as the transport mechanisms, the flux can be given by an analytical solution for impulse injection at the inlet of the fracture element.

The governing equation for solute transport in the fracture element is given by

$$\frac{\partial c}{\partial t} = -v \frac{\partial c}{\partial x} + \frac{2\delta D_m}{b} \left. \frac{\partial c'}{\partial z} \right|_{z=b/2} , \tag{9-3}$$

where x is a local co-ordinate along the fracture, z is a local co-ordinate vertical to the fracture, c is the concentration in the fracture, c' is the concentration in the adjoined rock matrix, ϕ is the porosity of the rock matrix, D_m is the diffusion co-efficient of the rock matrix.

The governing equation in the rock matrix is given by the following equation.

$$\frac{\partial c'}{\partial t} = D_m \frac{\partial^2 c'}{\partial z^2} \quad z > \frac{b}{2} \tag{9-4}$$

Following initial and boundary conditions are introduced for the above equations.

$$c = c' = 0 \quad (t = 0) \tag{9-5}$$

$$c = \frac{1}{bv}\delta(t) \quad x = 0 \tag{9-6}$$

$$c = c'|_{z=b/2} \tag{9-7}$$

$$c' = 0 \quad (z = +\infty) \tag{9-8}$$

where $\delta(t)$ is the Dirac impulse function which represents impulse release at $z = O$. The analytical solution is given by the following equation.

$$c(x,t) = \frac{u}{bv\sqrt{\pi}(t - t_w)^{3/2}} \exp\left(\frac{-u^2}{t - t_w}\right)\theta(t - t_w) \tag{9-9}$$

$$\theta(t) = \begin{cases} 0 & t<0 \\ 1 & t\geq 0 \end{cases} \tag{9-10}$$

$$t_w = x/v \tag{9-11}$$

$$u = \frac{\phi\sqrt{D_m}\, t_w}{b} \tag{9-12}$$

The outlet flux of the fracture at $x = L$ is

$$Flux(L,t) = bvc(L,t) \tag{9-13}$$

The residence time (t') of the particle is determined from the above probability density function (= Flux) by using a uniform random number $[R]_0^1$ generated by the computer program.

$$[R]_0^1 = \int_0^{t'} Flux(x,t)\, dt \tag{9-14}$$

The particles, introduced at the injection section in the injection boreholes, are followed until they arrive at the pumping section in BFI-02.

9.4 Model selection criteria

In fractured media, some fractures may be highly conductive and some may be not. Past experiences show fractured media exhibit strong heterogeneity and groundwater flows through a limited portion of the fractures. Fracture network approach has the possibility to simulate heterogeneous solute distribution in fractured media.

9.5 Results

Three different fracture networks were generated stochastically, which are shown in Fig. 9.3. In these cases, the length of the fractures is set to be 50 m and the densities in the upper,middle and lower regions are 0.004, 0.001 and 0.002 (m^2) respectively. Velocity distributions calculated by flow analyses using the fracture networks are shown in Fig. 9.4.

In the tracer test, Uranine,Iodide, Amino G Acid were used as tracers and injected into BFI01, KFI06, KFI11, respectively. The injection sections in these boreholes are the subzone 1 which is the highly conductive part in the zone-2. The measured breakthrough curves are shown in Fig. 9.5. In the figure,the vertical axis represents the normalized mass flux F(t) at the pumping borehole which is given by the following equation

$$F(t) = M(t)/M_0$$

where M(t) is the mass flux of the tracer at the pumping borehole and M_0 is the total mass of the injected tracer. It is obvious from the measured breakthrough curves that the lower peak concentration c_p and the larger apparent dispersion occur as t_p becomes later, where c_p and t_p are defined in Fig. 9.5.

Transport analyses were carried out by the proposed particle tracking technique using 5000 particles. For each flow field (Fig. 9.4(a),(b),(c)), three transport calculations were executed using different parameters (D_m,ϕ). Calculated breakthrough curves are shown in Fig. 9.6, Fig. 9.7, Fig. 9.8. The parameters used in the calculations and calculated total flow rate Q at the injection borehole are summarized in Table 9.1.

The calculated results shows that multipeak breakthrough curves are likely to be produced if matrix diffusion is not considered (RUN-4, RUN-7). This means that there exist multiple major flow paths in the model. On the other hand, the tendency of the calculated curves considering matrix diffusion agree with the measured ones quantitatively. Those are RUN-2, RUN-5 and RUN-9 which agree with the breakthrough curves of Amino G Acid,Iodide and Uranine respectively. Both steep rises and long tails of the breakthrough curves, which are considered to be important features, are simulated very well in these runs. It is found from the parameters used in these runs that the fracture aperture b ranges from 0.4×10^{-3} to 0.5×10^{-3} and the porosity of the rock matrix ranges from 0.015 to 0.03 .

The major results of our work are as follows:

1. Comparing calculated results with measured data, it can be concluded that matrix diffusion has significant influences on the breakthrough curves in Finnsjön site.
2. Total flow rates obtained in the flow calculations are smaller than the field data. The reason for this may be that the generated fracture networks are not adequate to represent the whole fracture system in zone-2.

3. Despite of the inadequacy of fracture network modeling, the calculated results agree well with the measured breakthrough curves. It is found from this that solute transfers through limited fractures among all fractures.

Table 9.1. Parameters used in the calculations.

Run		b(m)	Q(m^3/sec)	D_m(m^2/sec)	ϕ
RUN 1	:	0.4×10^{-3}	0.0017	0.0	0.0
RUN 2	:	0.4×10^{-3}	0.0017	1.0×10^{-9}	0.015
RUN 3	:	0.4×10^{-3}	0.0017	1.0×10^{-9}	0.03
RUN 4	:	0.5×10^{-3}	0.019	0.0	0.0
RUN 5	:	0.5×10^{-3}	0.019	1.0×10^{-9}	0.015
RUN 6	:	0.5×10^{-3}	0.019	1.0×10^{-9}	0.03
RUN 7	:	0.45×10^{-3}	0.023	0.0	0.0
RUN 8	:	0.45×10^{-3}	0.023	1.0×10^{-9}	0.015
RUN 9	:	0.45×10^{-3}	0.023	1.0×10^{-9}	0.03

10. EMP Evaluation and Comments

Patrick Goblet
Ecole des Mines de Paris, France

10.1 Introduction

This report is a short version of Goblet (1990).

An interpretation of the radially converging test is first proposed and, based on this interpretation, the two-well test is predicted. Comparison of this prediction to the experimental results leads to a refinement of the model. Finally, comments and proposals for future experiments are made.

10.2 Model Description for Radially Converging Tracer Test

As it travels from the storage tank to the measuring device, the tracer encounters three subsystems, each of which plays a particular role:

- Injection loop
- Fracture system
- Recovery well

For each of these subsystems we will propose a schematic model.

10.2.1 Injection loop

The injection loop may be described as a mixing box (see Fig. 10.1).

The mass balance equation for this system writes:

$$V_0 \frac{dC_0}{dt} = Q_w C_b + qC_{00} - qC_0 - Q_w C_0 \qquad (10\text{-}1)$$

with V_0 : total volume of the mixing loop

C_0 : concentration resulting from the mixing

Q_w : aquifer flowrate through the loop

C_b : background concentration. It will from now on be neglected : $C_b = 0$

q : injection rate into the loop

C_{00} : concentration of the tracer injected into the loop

It is worth noting that the storage term on the left-hand side, generally negligible when the Q_w flow rate is high (upper level of Zone 2), may be significative for zones of smaller Darcy velocity. For this reason, the proportionality relationship between C_0 and C_{00}:

$$C_0 = \frac{q\, C_{00}}{q + Q_w} \qquad (10\text{-}2)$$

is not valid in all injection intervals.

C_0 was regularly measured in the injection loop during the experiments.

We tried systematically to use relation (10-1) to deduce the flow rate Q_w for each injection interval:

$$Q_w(t) + \frac{1}{C_0}\left(q\,C_{00} - q\,C_0(t)\;V_0\frac{d\,C_0}{dt}\right) \qquad (10\text{-}3)$$

The purpose of this model was to check for flow anisotropy by comparing different injection intervals.

It appeared however that this formulation was too sensitive to oscillations in C_0 measurements, and produced unrealistic variations of Q_w (negative values). These results will not be detailed here.

10.2.2 Flow through the fractured zone

The tracer movement through the fractured medium is described by a model relying on the following assumptions:

- Equivalent porous medium
- transport by advection and dispersion (conservative tracers) described by the classical "dispersion equation":

$$\nabla\cdot(\alpha\,|\,U_D\,|\,\nabla C - U_D C) + \varepsilon_C\frac{\partial C}{\partial t}$$

with α : dispersivity tensor, defined by its longitudinal and transverse components α_L and α_T. Molecular diffusion is neglected

U_D : Darcy velocity

C : mass of tracer per unit volume of water

ε_C : kinematic porosity

The following initial and boundary conditions were used:

- Initial concentration equals zero
- Prescribed concentration at injection borehole
- Zero concentration gradient at pumping borehole.

- If necessary, independent channels are considered. They describe either different structures in the medium, or different types of porosities without interconnection.

The source term should ideally be the output of the injection loop model. However, the analysis of the injection loop model revealed a questionable reliability of these measurements. Furthermore, the flow rate through the injection sections shows a continuous decrease with time, which is not consistent with the assumption of a steady state flow field.

For these reasons, the following schematization was adopted:

- The flow rate through the entire system is considered steady state, representing conditions averaged on time.
- The injected mass of tracer is deduced from the product $q \times C_{00}$. This value is more reliably known, as the tracer level in the storage tanks is regularly measured.

10.2.3 Recovery well

At the pumping well, the producing layers are mixed together. If the tracer moves through a set of channels carrying a total flow rate Q_1, the equation describing the dilution in the pumping well writes in steady state:

$$C_p = C_{is} \times \frac{Q_1}{Q_p} \qquad (10\text{-}4)$$

with C_{is} : flux-weighted average of the in-situ concentration across the channels

Q_p : withdrawal flow rate

C_p : measured concentration

If we write the dilution equation, in steady state, inside the set of channels, we have:

$$C_{is} = \frac{q\, C_{00}}{Q_1} \qquad (10\text{-}5)$$

This equation describes the geometric dilution inside the set of channels, due to the converging flow pattern.

The concentration in steady state is therefore independent of the flow rate through the channels used by the tracer:

$$C_p = \frac{q\, C_{00}}{Q_p} \qquad (10\text{-}6)$$

This equation represnts the global dilution of the tracer in the converging flow, independently of the particular routes used by the tracer.

10.2.4 Multichannel model

It is, however, interesting to elaborate a little on the fate of the tracer through the channels. Let us assume a purely convective transport through three independent channels (see Fig. 10.2). Each channel is characterized by its volume and the flow rate flowing through it.

The resulting concentration curve will look as in Fig. 10.3, assuming $V_1/Q_1 < V_2/Q_2 < V_3/Q_3$.

The transit times t_j and plateau values C_j are given by:

$$t_j = V_j/Q_j \quad , \quad j = 1,3$$

and

$$C_1 = \frac{Q_1 C_{1,is}}{Q_p} \; ; \; C_2 = \frac{Q_1 C_{1,is} + Q_2 C_{2,is}}{Q_p} \; ; \; C_3 = \frac{Q_1 C_{1,is} + Q_2 C_{2,is} + Q_3 C_{3,is}}{Q_p}$$

with $C_{j,is}$: average in situ concentration at the outlet of channel j.

The recovery curve depends therefore on three types of parameters:

- The dilution rate inside each channel, function of the geometry of the flow in this channel. This rate is related to the concentration decrease along the channel.
- The flow rate inside each channel.
- The global dilution rate between the tracer conducting channels and the total flow rate $(\Sigma Q_j)/Q_p$.

To reduce the number of free parameters, we have to use more hypotheses. Let us for instance postulate that the dilution rate inside each channel, essentially due to the radial nature of the flow, is the same for all channels. Then, since the concentration at the inlet is the same, C_0, for all channels, we have: $C_{1,is} = C_{2,is} = C_{3,is}$.

With this hypothesis, it is possible to tell what proportion of the total tracer-carrying flow goes through each channel:

$$\frac{Q_1}{\Sigma Q_j} = \frac{C_{1,is}}{C_{3,is}} \quad ; \quad \frac{Q_1 + Q_2}{\Sigma Q_j} = \frac{C_{2,is}}{C_{3,is}}$$

If we assume that the repartition, found on a localized radial test, between different classes of channels, or different classes of porosities, is valid all over the conducting layer, then we can attribute a global flow to each porosity class, and determine this porosity. This procedure will be illustrated later.

10.3 Interpretation of the In-EDTA Injection (BFI01:U)

10.3.1 Interpretation of the tracer injection curve

The curve showing the variation od C_0 (concentration inside the injection section) with time has a rather irregular shape which calls for several comments:

The general shape of the curve indicates a decrease with time of the flow rate through the injection section.

This is in good qualitative agreement with the measurements realized by point dilution [E. Gustafsson, et al., 1989]. However, there is a discrepancy between the values deduced from the C_0 curve and the values obtained by point dilution:

Q_w initial (point dilution) = 268 ml/min

Q_w initial (from C_0) = 900 to 1800 ml/min

Q_w final (from C_0) = 400 ml/min

Q_w final (point dilution) = 45 ml/min

This discrepancy seems difficult to understand since both types of measurements rely on the same principle.

At times 800 and 915 hours, the pumping stops for about 39 hours. According to Eq. (10-1), one should observe an increase of C_0 at a rate:

$$\frac{dC_0}{dt} = \frac{q}{V_0}(C_{00} - C_0)$$

with $q = 2.35$ ml/m

$V_0 = 138$ l

$C_{00} = 985$ ppm

$C_0 = 5$ ppm

C_0 should initially increase of 1 ppm per hour. After 39 hours, the increase rate would be practically the same, and C_0 would have reached a value of more than 40 ppm. No such increase appears in the curve, except maybe a little hump near 800 hours. This is probably due to 3 factors:

- The flow rate through the injection section does not drop immediately to zero when the pumping stops.
- The concentration drops back very quickly when pumping is restarted.
- The sampling of C_0 is not sufficiently frequent to see, except in a random way, this type of perturbation.

After the detailed sampling, the pumping starts again, and concentration should decrease according to the equation:

$$\frac{dC_0}{dt} = -\frac{Q_w}{V_0} C_0 \Rightarrow C_0 = C_{0,init}\, e^{-Q_w t/V_0}$$

The concentration must therefore decrease of 50% within a time of $V_0 \text{ Log } 2/Q_w = 4$ hours if $Q_w = 400$ ml/min, and about 40 hours if $Q_w = 45$ ml/min, and decrease of 90% within 13 to 120 hours. This is consistent with the few measurement points available. A more refined sampling would have been useful to obtain a better estimation.

10.3.2 Interpretation of the recovery curve

From the preceding observations we conclude that the C_0 curve in the injection borehole is difficult to use. Moreover, a model taking into account a progressive clogging of the injection sections would be too complex. We choose therefore, as indicated before, to treat the source as a continuous injection of a concentration equal to 985 ppm in a flowrate of 2,35 ml/min (average values from Gustafsson, et al. (1989)). The steady state concentration to be expected at the pumping well is then:

$$\frac{2.35\ 10^{-3} \times 985}{120} = 19 \text{ ppb}$$

The recovery curve for In-EDTA increases rather sharply after 200 hours (from which an injection stop of 40 hours must be deduced), then exhibits a plateau around 11 ppb for 200 hours

before increasing again. We choose arbitrarily to simplify the curve into 2 steps according to Fig. 10.4. The concentration value before the injection stop is close to 19 ppb, which seems to show that all important pathways have been completely invaded. However, the concentration curve in this period is somewhat uncertain due to the withdrawal stop. If the total flow rate through these pathways is Q_p, then the flow through the fastest pathway is $Q_p \times 11/19$. If we further assume that the ratio between "fast" porosity and total porosity is uniform in the upper part of Zone 2, the flow rate flowing through this "fast" porosity is $120 \times 11/19 = 70$ l/min.

We simulated the In-EDTA with the METIS code, with the following assumptions:

- The flow geometry is radially symmetric.
- The conductive thickness is 5 m.
- The flow rate is 70 l/min.
- The prescribed concentration is 11 ppb.
- The history of injection stops is exactly reproduced.

The purpose of this model is to calibrate the porosity, assuming this parameter to be uniform.

The best fit is obtained for a kinematic porosity of 1.6% and a dispersivity of 10 m.

We simulate then the second flow path, aiming to obtain at 550 hours an increase of 5 ppb. For this purpose, the flow rate through this "secondary porosity" is $120 \times 5/19 = 31$ l/min, and the calibrated porosity is 2.5%. The sharp aspect of the measured curve is not reproduced because a rather high dispersivity (10 m) is considered. This could indicate the need for a smaller dispersivity for this path.

Figure 10.5 shows the comparison between the 2-paths model and the measurements.

Finally, a third set of paths accounts for the fact that tracer concentration has not reached the theoretical value of 19 ppb. The flow rate in these paths is equal to 19 l/min, and the hydrodispersive properties are unknown since no tracer has reached the production well.

10.3.3 Summary and discussion

The recovery curve of In-EDTA can be modelled with a multiple-path model having the following characteristics:

- Path 1: Flow rate = 70 l/min
  Porosity = 1.6%
  Dispersivity = 10 m
- Path 2: Flow rate = 31 l/min
  Porosity = 2.5%
  Dispersivity = 10 m
- Path 3: Flow rate = 19 l/min
  Porosity = unknown
  Dispersivity = unknown

The multiple path model may be rightfully subject to critics when the physical evidence of these paths does not exist. We believe that in the present case, the in-situ measurements do show different routes for the tracer, one in the upper part of Zone 2 (level 203-212 in BFI02), and one in the intermediate part (level 238 m). Moreover, this scheme seems consistent on the three

investigated directions, BFI01-BFI02 traced with In-EDTA, KFI06-BFI02 with Iodide and KFI11-BFI02 with Bd-DTPA.

Finally, the Tm-EDTA and Amino-G pulse injections realized in section KFI11: upper both show a distinct two-peak behaviour, with a second peak showing practically no dispersion, as will be seen later.

A certain mode of tracer circulation seems therefore to be a general feature of the investigated domain:

- Flow through a "fast" structure carrying most of the flow rate.
- Secondary flow through several structures with lower velocity.

At the present stage it is not clear whether these structures correspond to different overlapping porosities (different fracture families) or to different subregions of Zone 2.

10.4 Interpretation of the Gd-DTPA Injection (KFI11:U)

10.4.1 Tracer injection curve

Unlike the In-EDTA curve, the C_0 curve for Gd-DTPA decreases with time. At the end of the injection period, the ratio between C_{00} (in the tracer tank) and C_0 (in the injection section) is approximately: 2350/12 = 196.

The average value of this ratio during the injection period is: 2400/18 = 130.

In the case of In-EDTA, we have an initial ratio of 1000/1.3 = 770, and a final ratio of 1000/7 = 142, with an average value of 250.

These ratios do not show in a convincing manner any anisotropy of flow. But it is difficult to draw final conclusions from the rather erratic behaviour of the C_0 values.

10.4.2 Tracer recovery

The mass flux of Gd-DTPA into the medium is equal to $2.51\ 10^{-3}$ l/mn × 2274 ppm. The theoretical steady state concentration should therefore be:

$$\frac{2274 \times 2.51\ 10^{-3}}{120} = 47.5 \text{ ppb}$$

This prediction is in good agreement with the measurements. This result is also in agreement with the very good recovery rate obtained after 4500 hours (89%).

The recovery curve shows two successive arrivals, one between 30 and 170 hours, and one after 220 hours. This discontinuity is probably due to an injection stop between 168 and 213 hours.

The very sharp peaks between 800 and 1000 hours are due to the accumulation of tracer during withdrawal stops.

We have tried to model the general shape of this curve with a single path, radial model. We produced exactly the injection sequence, with three injection stops between 30 and 46 hours, between 80 and 96 hours and between 168 and 213 hours.

The purpose of this model is to determine values of dispersivity and kinematic porosity, and to see if the discontinuities in the recovery curve (multipeak behaviour between 0 and 200 hours, and large decrease after 200 hours) can be explained by the injection history.

Figure 10.6 shows the fit we obtain for the following values of the parameters:

- Dispersivity = 10 m
- Porosity = 1.4 10^{-3}

This exercise is essentially qualitative, and no attempt has been made to obtain a very good fit. However, some lessons can be learned:

- The first two injection stops are perfectly reflected on the measured curve, while they are smoothed in the modelled curve. The radial scheme with a dispersivity of 10 m is therefore more smoothing than reality.
- If one tries to model the experiment with a smaller dispersivity to try and see the peaks in the recovery curves, the obtained model is much more contrasted than the measurements.

The most appropriate model would therefore be a multichannel model with a small dispersivity in each channel. But we do not think that the detailed analysis of the curve under this angle is justified, because the "channels" are much less clearly visible than in the case of In-EDTA.

10.5 Analysis of the Pulse Injections in KFI11:U

After the detailed sampling of borehole BFI02 had been performed, two short injections were simultaneously performed in the upper section of borehole KFI11. The tracers used are Tm-EDTA and AminoG Acid. These experiments are interesting in that they duplicate the Gd-DTPA experiment, but with a different type of injection.

10.5.1 Tracer injection curves

The short injections were performed with the same mixing procedure as the step injections, and the C_0 concentration was regularly measured. According to Eq. (10-1), with q = 0, this concentration must follow an exponential curve, with a "half-life" of (V Log 2)/Q. Alternately, the flow rate Q can be determined from the half-life $T_{1/2}$ by Q = (V Log 2)/T. The exponential behaviour is clear on the measured curves after a few homogenizing cycles, with the same half-life of 50 hours. The flow rate through the injection section is therefore, at the end of the injection period:

$$Q = \frac{27.1 \text{ Log } 2}{50 \times 60} = 6.3\ 10^{-3}\ \text{l/min}$$

This value is roughly consistent with the value obtained by point dilution at the end of the experiment (2 ml/min), but totally inconsistent with the value obtained from the Gd-DTPA C_0 concentrations (around 350 ml/min).

10.5.2 Recovery curves

The recovery curves for these tracers both show the same behaviour, i.e., two peaks, the second being much sharper than the first one. This behaviour is rather unusual, because one generally expects that a later peak be more spread than the previous ones. It has been stated by

the authors of the test that this second peak was not a measurement artefact. The first peak follows the dispersion equation in radially converging flow with the following parameters:

Flow rate = 120 l/min

Dispersivity = 25 m for Tm-EDTA

Dispersivity - 25 m for AminoG Acid

Porosity = 0,002 for Tm-EDTA

Porosity = 0.002 for AminoG Acid

Since this peak accounts for most of the mass transported, it has been assigned in a first approach the total flow rate.

The second peak can be described either by a radial, or by a 1D model, since the very low value of dispersivity does not permit to discriminate between both models.

The ratio between the mass contained in the two peaks may be obtained approximately from the recovery curves:

$$\frac{\text{Mass in peak 2}}{\text{Mass in peak 1}} = 0.10 \text{ for Tm-EDTA}$$
$$= 0.125 \text{ for AminoG Acid}$$

One must note that the maximum recovery rate for Tm-EDTA is slightly worse than for AminoG Acid (72% against 87%). If the first undergoes some sort of interaction, its effect might be more pronounced on a late peak, hence the smaller ratio between the two peaks.

Taking the value from AminoG Acid as the best estimate, we conclude that the "slow" channel carries approximately 11% of the total flowrate of tracer labelled water when the two main channels separate. If this repartition was characteristic of a general structure of the domain, the flow rate in the "fast" structure would then be $120 \times 0.89 = 107$ l/min, and in the "slow" structure, 13 l/min.

The porosity estimate for the fast zone should then be revised to account for this new flow rate:

$$\text{Porosity in the first path} = 0.002 \times 0.89 = 0.0018$$

The best fit for the "slow" structure is then obtained (in radial geometry) for:

Flow rate = 13 l/min

Porosity = 0.0003

Dispersivity = 0.3 m

Introducing these characteristics in the model for Gd-DTPA, one obtains the curve of Fig. 10.7. The effect of the fast path is visible on the modelled curve, but could not be distinguished among the oscillations of the measured curve.

10.6 Analysis of the Short Injection of Iodine in KFI06:U

In the upper section of borehole KFI06, a continuous injection of Iodine degenerated into a short injection due to a pump failure. Since no measurements of C_0 concentration in the injection section are available, the analysis is limited to the recovery curve.

This test has been modelled using a radial geometry, and a 125 hours injection period. The flow rate is 120 l/min. The best fit is obtained for the following set of parameters:

Dispersivity = 25 m

Porosity = 0.0015

10.7 Summary of Results

We can summarize the structures and parameters identified on the interpreted tests as follows:

– BFI01 – BFI02 direction:

The In-EDTA test gives the following structure:

- Flow path 1: Flow rate = 70 l/mn
  Porosity = 1.6 10^{-3}
  dispersivity = 10 m
- Flow path 2: Flow rate = 31 l/mn
  Porosity = 2.5 10^{-3}
  dispersivity = 10 m

All the porosities are estimated for a thickness of 5 m.

– KFI11 – BFI02 direction:

The Gd-DTPA test gives the following structure:

- Single flow path: Flow rate = 120 l/mn
  Porosity = 1.4 10^{-3}
  dispersivity = 10 m

The AminoG Acid test gives slightly different results.

- Flow path 1: Flow rate = 107 l/mn
  Porosity = 1.8 10^{-3}
  dispersivity = 25 m
- Flow path 2: Flow rate = 13 l/mn
  Porosity = 0.3 10^{-3}
  dispersivity = 0.3 m

– KFI06 – BFI02 direction:

The Iodine test gives the following structure:

- Single flow path: Flow rate = 120 l/mn
  Porosity = 1.5 10^{-3}
  dispersivity = 25 m

10.8 Two Well Tracer Test

10.8.1 Qualitative analysis of the recovery curves

In line with the general objective of INTRAVAL project, our main purpose was to assess the possibility of predicting the two-well tracer test on the basis of the results of the RCT. To this effect we selected among the rich collection of tracers available those who met at best two criteria:

- Recovery rate as close as possible to 100%. Any retardation mechanism was avoided in order to focus on hydrodispersive parameters. From this viewpoint, 5 tracers with recovery rates higher than 75%, were worth considering: I-131, BR-82, Re-186, In-111, Yb-EDTA.
- Good definition of the curves: this criterium is related to the background level of the considered tracer as well as to the detection limit. From this viewpoint the best tracers are I-131, Re-186 (Run 6), Rhodamine WT, EDTA complexes of In, Tm, and Gd-DTPA complex.

Finally the best tracer in these experimental conditions seems to be I-131.

Sujrprisingly, In-EDTA has a low recovery rate, while it behaved as a conservative tracer during RCT.

We shall therefore use the results obtained with In-EDTA during RCT to predict the behaviour of I-131 during the two-well test.

10.8.2 Model description

The interpretation of the RCT has shown that a porous medium model is appropriate at the scale of the experiments performed in Zone 2.

Our model relies therefore on the same hypotheses as for RCT:

- Equivalent porous medium.

Transport by advection and dispersion.

The principle of our predictive model is to test the validity of the "model structure" defined as a result of the interpretation of RCT. This model structure is based on the concept of "channeling," with the general meaning of distinct structures carrying the tracer in more or less independent fashion, each structure having its own flow rate, porosity and dispersivity. The physical interpretation of these structures is not completely clear with the available experimental results: they can be viewed either as components of a dual porosity system, or as different units of the medium. One of the objectives of the present interpretation will be to clarify this structure.

10.9 Prediction and Analysis of I-131 Test (Run 3)

10.9.1 First prediction of I-131 test

In a first step the I-131 test was predicted using a model which incorporates the principal features of the model obtained for RCT:

- A "principal structure" is assumed to carry a flow rate equal to 70 l/min, with a porosity of 1.6% and a dispersivity of 10 m. A secondary structure carries 31 l/min, in a porosity of 2.5%. For this experiment the interpretation is restricted to the first 200 hours.
- The medium is supposed to be horizontally homogeneous. The flow pattern is that of a two-well system in an infinite medium.
- Tracer injection is done in each structure proportionnally to its flow rate, and the resulting recovery curves are cumulated.

Figure 10.8 shows the simulated recovery curve, together with the measured curve.

Although the peak time is roughly reproduced, the general shape of the curves is different.

The "model structure" obtained from RCT does not seem appropriate to simulate the two-well test.

10.9.2 Analysis of the withdrawal scheme

As mentioned in the experiment description, the equipment in the pumping borehole has been modified between RCT and two-well test: the whole thickness of the zone 2 is pumped in the first case, and only the 25 uppermost meters in the second case (see Fig. 10.9).

Transmissivity profiles measured in BFI02 show (see Table 10.1) that only 70% of the total transmissivity of Zone 2 is situated in the 25 topmost meters.

Table 10.1. Main conductive intervals in BFI02 (from Gustafsson (1989)).

Interval	Transmissivity (m^2/s)
203-205	$1.9\ 10^{-3}$
208-210	$1.9\ 10^{-6}$
212-214	$1.4\ 10^{-5}$
238-240	$1.6\ 10^{-6}$
257.1-259.1	$3.0\ 10^{-5}$
260-262	$8.2\ 10^{-4}$
276-278	$2.0\ 10^{-6}$

It seems therefore realistic for the RCT to attribute the 70 l/min of the "fast zone" to the top of Zone 2, and the remaining 50 l/min to the lower part.

In the case of the two-well test, only the upper part is pumped, and therefore the "two-channel" model is inappropriate.

10.9.3 Refined prediction of I-131 test

10.9.3.1 Single structure model

Based on these considerations, we have simulated the I-131 injection in a single, plane infinite structure, with a flow rate equal to 120 l/min. Some modification of porosity is to be expected, since the reference thickness has changed between the two tests.

The modelled curve obtained for a porosity equal to $2.5\ 10^{-3}$ is shown on Fig. 10.10. The peak date and level are much more satisfactory than for the first model.

Three additional mechanisms must be taken into account in order to reproduce more correctly the experimental conditions:

- Recirculation of the tracer.
- Regional gradient.
- Leakage from lower levels.

10.9.3.2 Modelling of the recirculation

Recirculation is modelled in the numerical code METIS by introducing at each time step the concentration at the producing borehole from the previous time step in a mixed boundary bondition:

Mass flux at injection node = flow rate × concentration

A delay equal to the duration of a time step is thus introduced instead of the 20 minutes actually necessary to flow through the total tubing and pipe system. This approximation is sufficient considering the smooth influence of recirculation.

Simulation of the I-131 curve with recirculation gives the result shown in Fig. 10.11.

10.9.3.3 Influence of the regional gradient

The piezometric head maps indicate a regional groundwater flow oriented rouhly in the direction BFI01-BFI02, with a gradient of $3\ 10^{-3}$.

However, since no measurement of natural flow exists, we have to rely on transmissivity values measured in the borehole to estimate the flux. The average conductivities measured in boreholes BFI01 and BFI02 differ up to a factor 3:

- $k = 2.6\ 10^{-4}$ m/s in BFI01
- $k = 8\ \ 10^{-5}$ m/s in BFI02

If we introduce each value in a simulation of I-131 with a $3\ 10^{-3}$ regional gradient, we obtain the curves shown on Figs. 10.12 and 10.13.

These figures show the important effect of the regional flow, and demonstrate the need to estimate this parameter prior to a two-well experiment.

10.9.3.4 Influence of leakage

During the two-well experiment, an increasing leakage is found to occur into borehole BFI02 from the more saline deeper horizons. This is clearly demonstrated by the evolution of pumped water electrical conductivity with time: during RCT, the conductivity is constantly equal to 750 ms/m, while during the two-well test it increases from a value of 350 mS/m to about 600 mS/m. This suggests a progressive mixing of water of the top horizon with water from the rest of Zone 2, until a final composition almost representative of the whole thickness of Zone 2 is reached.

We have described this dilution by a very crude model: the concentration at time t is reduced by a factor proportional to t. The slope of this dilution curve is chosen to adjust the final level of the curve. The best fit was obtained for a final dilution of 40%, and is shown on Fig. 10.14.

10.9.3.5 Summary and discussion

The I-131 curve has been roughly reproduced with a model taking into account advective-dispersive flux in a flowfield influenced both by the two-well system and by regional flow, recirculation and leakage from lower levels in Zone 2.

We do not consider the reproduction of the curve obtained on Fig. 10.14 as totally satisfactory, but a rather large number of free parameters has been introduced:

- Aquifer thickness

- Average porosity
- Dispersivity
- Regional flow
- Leakage

Furthermore, the hypothesis of horizontal homogeneity is incorrect, as is fully demonstrated by the comparison of calculated and measured curves in borehole KFI11 (Fig. 10.15).

From these parameters, some are roughly consistent with the interpretation of RCT (porosity, dispersivity, "model structure"). Some can only be estimated from independent measurements, but are subject to large variations (regional flow). Finally some are fitted without other cross checking than qualitative (leakage).

It is therefore pointless to go into a curve fitting procedure which without any doubt would lead to a perfect fit but would not be sustained by independent estimations.

Our global interpretation of RCT and two-well test seem to show a general feature of the "model structure" which can be described in the following manner:

- Most of the flow rate (up to 70%) takes place in the topmost 15 meters of Zone 2, and probably in a much narrower interval.
- Flow is discharged through ill-defined paths towards at least one secondary structure, situated about 30 m below (238 m level).

The apparently general character of this behaviour would justify the use of independent measurements to try and confirm it. The most important of the available measurements are the results of the interference tests.

10.10 Summary and Conclusions

Our comments will cover four topics:

- Evaluation of the experiment.
- Evaluation of the model we propose to describe this experiment.
- Discussion of some unexplained mechanisms.
- Comments on the contribution of this exercise to the general goal of validation of geosphere models.

10.11 Comments on the Experiment

As a first comment it must be stressed that the Finnsjön data set is to our knowledge the best available at this scale in a fractured medium. This must be emphasized before any further remark which might tend to diminish its merits.

10.11.1 Experimental setup

The radially converging test has several advantages:

- The flow pattern is well controlled, and in particular, the effect of a poorly known natural gradient may be cancelled.

- The horizontal isotropy of the medium can be assessed with injections from varying directions.
- The recovery is in principle complete for a perfect tracer. Any interaction can therefore be detected.

The main inconvenience of this type of test is the high dilution due to the converging flow, which imposes rather high injection concentration.

The two-well, or doublet, system has some specific advantages:

- Large volume of investigation.
- Easy control of injection.
- Finally, the restitution, as for the radial test, is normally complete.

It also has some disadvantages:

- The recovery curves show very long tails, and the experiments must last sufficiently long to sample these tails, on which the precision may be poor, close to the detection limit.
- Tracer losses are therefore difficult to explain with certainty: insufficiently long sampling or existence of pathways which do not converge to the production well?
- This experimental set up is more sensitive to regional flow, unless a sufficiently high flow rate is used. For instance the contribution of regional flow may be shown to be quite significant in the Finnsjön case.
- Very high dilution of the tracer.

As a general conclusion, it was evidently of primary interest to have both geometries available at the same location, since they do not investigate the same volume.

- Injection localization

Injecting tracer in zones isolated by packers has the advantage of precisely delimiting the investigated zone. It is the most promising way to investigate the scale effect: each injection section leads to a specific value of porosity and injectivity (defined as the fraction of the total flow entering this section). It is thus possible to estimate the heterogeneity of the medium. One can then increase the height of the injection chambers and try to look for an asymptotic behaviour characterized by a convergence of the average porosities and dispersivities. This is of course extremely costly on a 100 meter-scale.

The present experiment has the more limited ambition of investigating typical subzones of a larger volume. But while the injection sections have been kept identical in both experiments, the withdrawal sections have been modified: all the thickness of Zone 2 is sampled in the radial test, and only the 25 top most meters in the double test. We think that this modification brings a supplementary information, but without the possibility of cross-checking. For this reason we think that either the withdrawal device should have been kept the same, or both devices should have been used in both geometries, maybe for limited tests with dyes for instance, to investigate the influence of this modification.

- Injection device

The homogeneization loop used to mix the tracer inside the injection sections permits a better control of the source-term, since the concentration in the section may be continuously measured.

Furthermore, this device constitutes a kind of long duration indirect measurement of the flow through the sections. This information is of primary importance to assess the heterogeneity and anisotropy of the flow.

In the Finnsjön experiments, the use of this device revealed three problems:

- Irregular variation of the injected concentration: the general trend is an increase with time, but some variations are difficult to explain. A more frequent sampling would have been appreciable.
- Progressive decrease of the flow through the injection sections, not related to any change in piezometry, and indicating possibly a clogging of the injection section. Without the continuous monitoring of the injected concentration, this phenomenon would not have been detected.
- Finally, the estimations of flow rate obtained from the injection curves are inconsistent with the point dilution measurements, except qualitatively. We have no explanation for this discrepancy.

Fortunately, the measurements of tracer level in the tracer tanks give another way of estimating the source term. This shows the interest of redundancy in the measurements.

- Type of injection

Generally continuous injections were used in the radial test. We think that they give a more reliable information and are generally less prone to artifacts. However, the coexistence of this injection form with pulse tests gives an appreciable possibility of cross-checking.

In the two-well test, it is not possible to maintain a continuous injection with a high flow rate. But we think that the pulse test may be more appropriate anyway in this case, because the effect of the channel length distribution is very important, and would probably be less visible in a continuous injection. Moreover, the necessity of recirculating the water gives even more interest to a short injection, because the recirculated tracer is easier to detect.

10.11.2 Available measurements

As stated before, the measurement set is very complete. In particular, one must emphasize the interest of detailed logs of events to explain irregularities in the measurements.

The in-situ measurements obtained during the detailed sampling seem very difficult to use: the concentrations obtained are generally lower than those measured in the pumped borehole, while the dilution rate due to foreign water might be expected to be lower.

Moreover, it seems difficult to distinguish between measurements which do show a local pathway and measurements contaminated by other zones.

However, the qualitative information given by these measurements, if used with care, may be interesting.

10.11.3 Type of tracers used

For the radially converging test, 11 tracers were used in 9 injection sections and 19 tracers in one section for the doublet test. The interpretation of the results shows the primary interest of tracers with high recovery rate: they give the best information on porosity. The interacting tracers have presently no other interest than methodological: what is the best tracer in a given context? Since there is no model for their behaviour, they do not bring at the present stage any

supplementary information on the medium. However, as this type of interaction model develops and is validated in the lab, multitracing will take more interest provided that, as in the two-well tests, different tracers are injected simultaneously and in the same locations.

When heterogeneity and isotropy are to be investigated, the same tracer, preferably non sorbed, should be used in all sections. This was not the case in the radial test, and for this reason the information on anisotropy and heterogeneity is not fully reliable.

Some tracers showed a good behaviour in the radial test, and some retardation in the doublet test (In-EDTA). This has not been explained, and shows the importance of not relying on only one presumably good tracer: in the case of the doublet I-131 was an appropriate substitute for In-EDTA.

Finally the repetition of tests with the same tracer is a rather unique feature of the two-well experiment and brings much more confidence as to the reproducibility of the experiments.

10.12 Comments on the Model

- The relative regularity of the curves measured in the observation as well as in the withdrawal boreholes suggests that an Equivalent Porous Medium model is appropriate at the scale of 150–200 m characteristic of the experiment.
- We have introduced in our model the notion of multiple pathways. Qualitative considerations on the position of the packer in the production borehole as well as the results of the detailed in-situ sampling seem to suggest that these pathways correspond to different routes between injection and recovery well rather than to multiple porosity. Large and well correlated fractured structures seem to play an important role in the transfer. It would of course be of great interest to try and correlate these results with those of the interference hydraulic tests. This has not been possible within the time constraints of this study, but would constitute a valuable project within Phase 2 of INTRAVAL.
- The model we have built relies on large simplifications. For instance, the variation of flow rate in the injection sections with time is neglected. The emphasis has been put on the individual modelling of each route. Once again, a synthetic model is a goal to have in mind for Phase 2.
- The prediction of I-131 tracing in the doublet system from the results of In-EDTA in the radial test did not succeed fully at first. However, a single iteration, taking into account the differences in the withdrawal devices, led to a rather satisfactory reproduction of the two-well test data without excessive data manipulation. This gives us confidence that our interpretation of the transport in the BFI01-BFI02 direction has a certain robustness.

10.13 Unexplained Mechanisms

Below are discussed a series of mechanisms and observations, which either were not taken into account at all, or were taken into account without enough data to cross-check them. Most of these phenomena have to do with the flow geometry, and might find an explanation in a synthetic flow model.

10.13.1 Variation of hydraulic head with time (radial test)

The measurements of hydraulic head show a generally stable flow. However, after the pumping stop for the detailed sampling, the piezometric head never resumes its value before the stop.

The explanation of this observation can probably only be found in a detailed interpretation of the interference tests, unless it is due, as stated in the case definition, to a modification of the borehole skin. This phenomenon has anyway no consequence on the tracer test, except maybe on the descending part of the curves.

10.13.2 Influence of regional flow

Our simulations of the two-well test show that the influence of a regional flow is very important. We have shown that a "realistic" regional flow, i.e., consistent with the transmissivity and porosity values, gives a correct reproduction of the data. However this free parameter should be investigated separately, by means of natural gradient tests.

10.13.3 Injection sections behaviour

We have not been able to model satisfactorily the evolution of concentration in these sections. This raises some questions concerning the exact rate at which tracer is introduced into the system. Fortunately an alternative measurement exists (tracer tank level). However the modification with time of the flow around the injection points remains uncertain.

A question must also be raised as to the reliability of the point dilution technique, which gives results inconsistent with the measurements inside the injection sections.

10.13.4 Transit time heterogeneity

The transit time between boreholes BFI01 and KFI11 during the two-well test is inconsistent with an homogeneous system. Although our model reproduces rather well the fastest pathways between BFI01 and BFI02, it is therefore inadequate for the modelling of the global system. Once again this heterogeneity in mass transfer properties should be checked against the results of the hydraulic tests.

10.13.5 Non-conservative behaviour of In-EDTA

This tracer is recovered up to 100% during the radial test, and only 30% during the doublet test. This behaviour is surprising since in the same time I-131 is fully recovered. Further work is probably necessary on the stability of EDTA complexes.

10.14 Validation

Our work shows a possibility of partial validation of the mass transfer processes in the upper section of Zone 2. Starting from the interpretation of the radial test, hydrodispersive parameters are identified, and the second test is correctly predicted. However, the parameters identified are characteristic of a specific domain between boreholes BFI01 and BFI02. It means that process and parameter identification are correct in this domain. But the prediction capability of our model fails for boreholes KFI11 and KFI06. This shows that the horizontal heterogeneity of the medium is not correctly introduced in our model.

A way to improve our model might be to interpret the hydraulic tests, and to see whether they give an information about heterogeneity usable for mass transfer modelling.

Moreover, a global model of flow would permit to see if our flow path model is consistent with the injectivity of the different borehole sections.

The objective to look for is a global model of mass transfer for all boreholes. This could be the basis for the prediction of a natural gradient test on a larger scale.

11. Overall Comments and Discussions

Chin-Fu Tsang
Lawrence Berkeley Laboratory, USA
and
Shlomo Neuman
University of Arizona, USA

11.1 Comments on Experiments and Data

The Finnsjön experiment includes major tracer tests in a highly conductive fracture zone with transport distance up to 400 m. Both continuous injection and pulse tests were made. Two types of transport patterns were studied: (1) radially convergent tests and (2) dipole recirculation tests. A large number of tracers, including conservative, sorptive and radioactive (with relatively short decay times), were used. Not only are these data available, but there are also substantial pressure transient data from both single well tests and interference tests from a number of wells. Thus the data base is comprehensive and provides a good opportunity for studies covering different scales.

The possibilities to predict results of the tracer tests were reduced by several uncertainties regarding the characterization of the zone. For example, little is known about the vertical leakage into and out from the zone and the regional flow is not well established. Furthermore, the zone is highly heterogeneous with regard to the transmissivity values obtained from the boreholes intersecting the zone. In addition, the correlation structure along the zone is difficult to determine from the vertical boreholes. The tracer tests did not reveal the transport characteristics of the individual subzones because all tracers emerged into the pumped borehole through the top subzone. System heterogeneity is a major problem for such a large-scale experiment. The experiment will stimulate efforts in evaluating heterogeneity and determining the optimal measurement requirement to characterize such a flow and transport system.

11.2 Comments on Analysis Efforts

Analysis efforts from the project teams cover a wide range of conceptual models (see Table 1.1). These range from porous medium model, to fracture network model, to channel models. Processes studied include advective dispersion, local dispersion, matrix diffusion, sorption and radioactive decay. Except for modeling effort of the pilot group, SGAB/SKB, most of the other efforts are still in an early stage. There is room for substantial additional work, such as complete analysis of all data based on one conceptual model to evaluate the extent of the model's applicability, quantitative calculation of the effects of variable injection rates, and comparative evaluation of conservative, sorptive and radioactive tracer transport. One area of great uncertainty is the lack of knowledge of the geometric structure of the transport paths. Models with too many requirements on input parameters, such as the fracture network model, are especially in difficulties, since many of the needed parameters may not be available.

As emphasized by SGAB/SKB, there is a need to evaluate the flow field before analysis of tracer transport data. Both the single well pumping tests and the multiple well interference tests provide information on system structure and heterogeneity. It may be useful for the project teams to study and understand these data. On the other hand, pressure transients smooth out certain heterogeneity scales, depending on test ranges and periods, and may not be able to bring out the medium geometric structures that strongly influence tracer transport. The simultaneous study of pressure and tracer tests is an important subject.

11.3 Relevance to Model Validation and Recommendation for Further Work

The state-of-the-art of the field is not yet suitable for a systematic validation procedure during INTRAVAL Phase 1. The project teams have chosen their own conceptual models somewhat arbitrarily and tried to reproduce field data. Good discussions are given of discrepancies between model predictions and observed data. A number of interesting suggestions for further investigation have resulted. New understanding has been gained on tracer transport based on the various conceptual and calculational models used. We believe that it is appropriate now for the different project teams to initiate a new study of the substantial data base again, based on their best model, in a logical validation procedure that is established a priori. Much benefit will emerge from such a renewed effort. Thus it is recommended that this test case be included in Phase 2 of the INTRAVAL project.

12. REFERENCES

Chapter 2

Ahlbom K, Andersson P, Ekman L, Gustafsson E, Smellie J and E-L Tullborg (1986): *Preliminary Investigations of Fracture Zones in the Brandan Area, Finnsjön Study Site*, SKB Technical Report 86-05.

Ahlbom K, Andersson P, Ekman L and S Tiren (1987): *Characterization of Fracture Zones in the Brandan Area, Finnsjön Study Site*, Swedish Geological Co, Uppsala, Internal Report IRAP 87354

Andersson P (1987): *Tracer Experiments in a Fracture Zone at Finnsjön Research Area - INTRAVAL Test Case Description*, Swedish Geological Co, Uppsala, Internal Report IRAP 87400.

Andersson J-E, Ekman L and A Winberg (1988a): *Detailed Investigations of Fracture Zones in the Brandan Area, Finnsjön Study Site Single Hole Water Injectlon Tests* in *Detailed Sections - Analysis of the Conductive Fracture Frequency, SKB* Progress Report 88-08, Swedish Geological Co, Uppsala, Internal Report IRAP 87362.

Andersson J-E, Ekman L and K Hansson (1988b): Single Hole Water Injection Tests in Borehole BF102 Within the Brdndan Area, Finnsjön Study Site. The Fracture Zone Project – Phase 3, Swedish Geological Co, Uppsala, Internal Report IRAP 88208.

Andersson J-E, Ekman L, Gustafsson E, Nordqvist R and S Tiren (1988c): *Hydraulic Interference Tests and Tracer Tests within the Brandan Area, Finnsjön Study Site. The Fracture Zone Project – Phase 3, SKB* Technical Report 89-12.

Andersson P, Eriksson C-O, C88ustafssQn E and T Ittner (188088: *Dipole Tracer Experiment in a Low-Angle Fracture Zone at the Finnsjön Site, Central Sweden – Experimental Design and Preliminary Results. The Fracture Zone Project – Phase 3*, Swedish Geological Co, Uppsala, Internal Report IRAP 90206.

Gidlund J, Moreno M and I Neretnieks (1988): *Porosity and Diffusivity Measurements of Samples from Finnsjön*, Dep. of Chem. Engin., Royal Inst. of Technology, Stockholm, KAT 88/13.

Gustafsson E, Andersson P, Eriksson C-O and R Nordqvist (1989): *Radially Converging Tracer Experiment in a Low-Angle Fracture Zone at the Finnsjon Site, Central Sweden. The Fracture Zone Project – Phase 3*, Swedish Geological Co, Uppsala, Internal Report IRAP 88313.

Chapters 3 and 4

Ahlbom K, Andersson P, Ekman L, Gustafsson E, Smellie J, and E-L Tullborg (1986). Preliminary Investigations of Fracture Zones in the Brändan Area, Finnsjön Study Site. SKB Technical Report 86-05.

Ahlbom K, Andersson P, Ekman L, and S Tiren S (1987). Characterization of Fracture Zones in the Brändan Area, Finnsjön Study Site. SKB Progress Report 88-09.

Ahlbom K, and J A T Smellie (editors) (1989). Characterization of Fracture Zone 2, Finnsjön Study \Site, Part 1-6. SKB Technical Report 89-

Allard B, Kipatsi H, and B Torstenfelt (1979). Technetium: Reduction and Sorption in Granite Bedrock. Radiochem. Radioanal. Letters 37 (4-5), 222-230.

Andersson K, and B Allard (1983). Sorption of Radionuclides on Geologic Media- A Literature Survey. I: Fission Products. KBS Technical Report 83-07.

Andersson K (1989). Personal Communication.

Andersson J, and P Andersson (1987). Flow Simulations in a Fracture Zone in the Brändan Area, Finnsjön. SKB Progress Report 87-26.

Andersson J-E, Ekman L, and A Winberg (1988a). Detailed Investigations of Fracture Zones in the Brändan Area, Finnsjön Study Site. Single Hole Water Injection Tests in Detailed Sections. Analysis of Conductive Fracture Frequency. SKB Progress Report 88-08.

Andersson J-E, Ekman L, Gustafsson E, Nordqvist R, and S Tiren (1988b). Hydraulic Interference Tests Within the Brändan Area, Finnsjön Study Site. The Fracture Zone Project Phase 3. SKB Technical Report 89-12.

Andersson J-E, Nordqvist R, Nyberg G, Smellie J, and S Tiren (1989). Hydrogeological Conditions in the Finnsjön Area. Compilation of Data and Conceptual Model. SKB Progress Report 89-24.

Andersson P, Eriksson C-O, Gustafsson E, and T Ittner (1990). Dipole Tracer Experiment in a Low-Angle Fracture Zone at the Finnsjön Site, Central Sweden- Experimental Design and Preliminary Results. SKB Progress Report 90-24.

Cooley R L (1979). A method for estimating parameters and assessing reliability for models of steady state ground-water flow. 2. Application of statistical analysis. Water Resources Research, vol. 15, no.

Cooley R L (1985). A comparison of several methods of solving nonlinear regression groundwater flow problems. Water Resources Research, vol. 21, no. 10.

Ekman L, Andersson J-E, Andersson P, Carlsten S, Eriksson C-O, Gustafsson E, Hansson K, and L Stenberg (1989). Documentation of Borehole BFI02 within the Brändan Area, Finnsjön Study Site. The Fracture Zone Project- Phase 3. SKB Progress Report 89-21.

Freeze R A, and J A Cherry (1979). Groundwater. Prentice Hall.

Gustafsson E, and C-E Klockars (1981). Studies on Groundwater Transport in Fractured Crystalline Rock Under Controlled Conditions Using Non-Radioactive tracers. SKB Technical Report 81-07.

Gustafsson E, and C-E Klockars (1984). Study of Strontium and Cesium Migration in Fractured Crystalline Rock. SKB Technical Report 84-07.

Gustafsson E, Andersson P, Eriksson C-O, and R Nordqvist (1989). Radially Converging Tracer Experiment in a Low Angle Fracture Zone at the Finnsjön Site, Central Sweden. The Fracture Zone Project Phase 3. SKB Progress Report 90-27.

Guvanasen V, and V M Guvanasen (1987). An approximate semianalytical solution for tracer injection tests in a confined aquifer with a radially converging flow field and finite volume of tracer and chase fluid. Water Resources Research, vol. 23, no. 8.

Javandel I, Doughty C, and C-F Tsang (1984). Groundwater Transport: Handbook of Mathematical Models. American Geophysical Union, Washington D.C.

Marquardht D W (1963). An algorithm for least squares estimation of nonlinear parameters. J. Soc. Ind. Appl. Math., 11(2).

Nordquist R, and Andersson J-E (1987). Transient Flow Simulations in a Fracture Zone in the Brändan Area, Finnsjön. SKB Progress Report 88-11.

Nordquist R (1988). Numerical Predictions of a Radially Converging Tracer Test in a Fracture one in the Brändan Area, Finnsjön. SGAB Internal Report IRAP 88 235.

Nordqvist R (1989). Numerical Predictions of a Dipole Tracer Test in a Fracture Zone in the Brändan Area, Finnsjön. SKB Progress Report 89-34.

Van Genuchten M Th, and Alves W J (1982). Analytical solutions of the one-dimensional convective-dispersive solute transport equation, U. S. Dep. Agric. Tech. Bull., 1661.

Voss C (1984). A Finite-Element Simulation Model for Saturated-Unsaturated Fluid-Density-Dependent Groundwater Flow with Energy transport or Chemically Reactive Single Species Solute Transport. U.S. Geological Survey Water Resources Investigations Report 84-4369.

Zuber A (1974). Theoretical Possibilities of the Two-Well Pulse Method. Isotope Techniques in Groundwater Hydrology. Proc. Symp. IAEA Vienna.

Chapter 5.old

Gidlund, J., L. Moreno, and I. Neretnieks, "Porosity and diffusivity measurements of samples from Finnsjön," KAT 88- 31, Department of Chemical Engineering, Royal Institute of Technology, Stockholm, 1988.

Gustafsson, E., P. Andersson, C. Eriksson, and R. Nordqvist, "Radially converging tracer experiment in a low-angle fracture zone at the Finnsjön site, Central Sweden — The Fracture Zone Project — Phase 3., Swedish Geological Co. IRAP 88313, 1989.

Lapidus, L. and N. Amundsen, "Mathematics of adsorption in beds," J. Phys. Chem., *56*, 984, 1952.

Lenda, A. and A. Zuber, "Tracer dispersion in groundwater experiments," Proceedings of a symposium organized by IAEA, Vienna, 1970.

Tang, G.H., E.O. Frind, and E.A. Sudicky, "Contaminant transport in fractured porous media. An analytical solution for a single fracture," Water Resour. Res. *17*, 555, 1980.

Moreno, L., Y.W. Tsang, C.F. Tsang, F.V. Hale, and I. Neretnieks, "Flow and tracer transport in a single fracture: a stochastic model and its relation to some field observations," Water Resour. Res. *24*, 2033–2048, 1988.

Chapter 5.new

Gidlund, J., L. Moreno, and I. Neretnieks, "Porosity and diffusivity measurements of samples from Finnsjön," KAT 88-31, Department of Chemical Engineering, Royal Institute of Technology, Stockholm, 1988.

Gustafsson, E., P. Andersson, C. Eriksson, and R. Nordqvist, "Radially converging tracer experiment in a low-angle fracture zone at the Finnsjön site, Central Sweden - The Fracture Zone Project - Phase 3., Swedish Geological Co. IRAP 88313, 1989

Lapidus, L. and N. Amundsen, "Mathematics of adsoprtion in beds," J. Phys. Chem., 56, 984, 1952.

Lenda, A. and A. Zuber, "Tracer dispersion in groundwater experiments," Proceedings of a symposium organized by IAEA, Vienna, 1970.

Tang, G.H., E.O. Frind, and E.A. Sudicky, "Contaminant transport in fractured porous media. An analytical solution for a single fracture," Water Resour. Res. 17, 555, 1980.

Moreno, L., Y.W. Tsang, C.F. Tsang, F.V. Hale, and I. Neretnieks, "Flow and tracer transport in a single fracture: a stochastic model and its relation to some field observations, Water Resour. Res. 24, 2033-2048, 1988.

Chapter 6

E. Gustafsson, P. Andersson, C.O. Eriksson and R. Nordqvist. Radially converging tracer experiment in a low angled fracture zone at Finnsjön, Central Sweden. Swedish Geological Co., Uppsala, Sweden, 1989.

L. Moreno and I. Neretnieks. Prediction of tracer tests at Finnsjön. Department of Chemical Engineering, Royal Institute of Technology, Stockholm, Sweden, 1989.

D.P. Hodgkinson and D.A. Lever. Interpretation of a field experiment onthe transport of sorbed and non-sorbed tracers through a fracture in crystalline rock. Radioactive Waste Management and Nuclear Fueld cycle, Volume 4(2), 129–159, 1983.

W.T. Shaw, D.P. Hodgkinson, P. Grindrod. Preliminary fractural analysis of the Stripa 3D migration experiment: Case 4 of the INTRAVAL project, INTRA-ECL I1898-8, Version 1, June 1989.

Chapter 7

K. Ahlbom, P. Andersson, L. Ekman and S. Tiren, Characterization of Fracture Zones in the Brändan Area, Finnsjön Study Site, B. Hydrogeology, ITAP87354, Swedish Geological Co, (1987).

J.-E. Andersson, L. Ekman, and K. Hansson, Single Hole Water Injection Tests in Borehole BFi2 within the Brändan Area, Finnsjön Study Site, IRAP 88208, Swedish Geological Co, (1988a).

J.-E. Andersson, L. Ekman, and A. Winberg, Detailed Investigations of Fracture Zones in the Brändan Area, Finnsjön Study Site, IRAP 87367, Swedish Geological Co., (1987).

J.-E. Andersson et al., Hydraulic interference tests and tracer tests within the Brändan Area, Finnsjön study site, The Fracture Zone Project — Phase 3, SKB TR 83-12 (1988b).

P. Andersson, C.O. Eriksson, E. Gustafsson and T. Ittner, Dipole tracer experiment in a lowangle fracture zone at the Finnsjön site, Central Sweden, Experimental design and preliminary results, Report IRAP 90 206, The Fracture Zone Project - Phase 3, Swedish Geological Co., Uppsala, Sweden, March 1990

J. Gale, R. Macleod, J. Welhan, C. Cole and L. Vail, Hydrogeological Characterization of the Stripa Site, Stripa Project, Technical Report 87-15.

L.W. Gelhar, Applications of stochastic models to solute transport in fractured rocks, SKB – Technical Report 87-05.

W.N. Gill and R. Sankarasubramanian, Proc. Roy. Soc. Lond. A316 (1970) 341–350.

W.N. Gill and R. Sankarasubramanian, Proc. Roy. Soc. Lond. A322 (1971) 101–117.

A. Hautojärvi and V. Taivassalo, Test case 5: Tracer tests at Finnsjön. Predictive modelling of the radially converging experiment. Report YJT-88-13.

A. Hautojärvi and V. Taivassalo, and S. Vuori, Case 5 (Finnsjön experiments). Interpretation of results of the radially converging test. Intraval Workshop 12.-16.6. 1989 Helsinki.

A. Hautojärvi, V. Taivassalo and S. Vuori, Case 5 (Finnsjön experiments), Preliminary predictive modelling of the dipole experiment, INTRAVAL Workshop 12.-16.6.1989, Helsinki, Technical Research Centre of Finland, Nuclear Engineering Laboratory.

A. Hautojärvi and V. Taivassalo, and S. Vuori, Interpretation of test case 5: Radially converging experiment. Intraval Workshop 5.-10.2. 1990 Las Vegas.

K.S. Novakowski, Comparison of fracture aperture widths determined from hydraulic measurements and tracer experiments, Presentation in the Fourth Canadian/American Conference on Hydrogeology—Fluid Flow, Heat Transfer and Mass Transport in Fractured Rocks, June 21–24, 1988, Banff, Alberta, Canada.

G.I. Taylor, Proc. Roy. Soc. Lond. A219 (1953) 186–203.

VTT Contribution to the Intraval Phase 1 Reporting, Test case 5, Radially converging experiment, Project team VTT, Finland, Draft 8.5.1990.

Chapter 8

Moreno, L. et al., Flow and tracer transport in a single fracture: A stochastic model and its relation to some field observations, W.R.R. 24(12), 2033-2048, 1988.

Tsang, Y.W. et al., Flow and tracer transport in Fractured media: A variable aperture channel model and its properties, W.R.R. 24(12), 2049-2060, 1988.

Yamashita, R., and Kimura, H., Mass transport analysis for fracture networks considering matrix diffusion (in Japanese); Proc. of JSCE, No. 412/III12, 1989.12.

Gustafsson, E. et al., Radially converging tracer experiment in a low-angle fracture zone at the Finnsjön site, central Sweden; The fracture zone project.

Leonhart, L.S. et al., Analysis and interpretation of a recirculating tracer experiment performed on a deep basalt flow top, Bulletin of the Association of Engineering Geologists, vol. XXII, No. 3. pp. 259-274, 1985.

Chapter 9

Andersson, J.E. et al.: Hydraulic interference tests and tracer tests within the Brandan area,Finnsjön study site; SKB-TR 89-12, Sweden 1988.

Ryo Yamashita and Hideo Kimura: Mass transport analysis for fracture networks considering matrix diffusion (in Japanese); Proceedings of JSCE, No.412/III12, 1989.12.

Chapter 10

Goblet, P., Interpretation of two sets of tracer tests in a fracture zone (Finnsjön Site, Sweden)—INTRAVAL Project, Phase 1, Case 5—CIG/Ecole des Mines Report LHM/RD/90/75 (1990).

Gustafsson, E., Andersson, P., Eriksson, C.O., Nordqvist, R., Radially converging tracer experiment in a low-angle fracture zone at the Finnsjön Site, Central Sweden (1989).

Andersson, P., Eriksson, C.O., Gustafsson, E., Ittner, T., Dipole tracer experiment in a low-angle fracture zone at the Finnsjön Site, Central Sweden – Experimental design and preliminary results (1990).

FIGURE CAPTIONS

Chapter 2

Figure 2.1 Location of the Brändan area, Finnsjön study site.

Figure 2.2 Borehole location in the Brändan area.

Figure 2.3 Block diagram of fracture zones in the Brändan area.

Figure 2.4 Cross section through the Brändan area showing Zone 2.

Figure 2.5 Injection and circulation system, radially converging experiment.

Figure 2.6 Withdrawal equipment, radially converging experiment.

Figure 2.7 Experimental design of the dipole experiment.

Figure 2.8 Breakthrough curve for In-EDTA (top) and concentration in the injection section as a function of time (bottom).

Figure 2.9 Results from detailed sampling in BFI02 during the radially converging experiment. Concentration of In-EDTA.

Figure 2.10 Breakthrough curves for ^{131}I in the withdrawal hole BFI02 (top) and in the observation hole KFI11 (bottom).

Chapter 3

Figure 3.1 General flow of field experiments and related modeling.

Figure 3.2 Conceptual model of the fracture zone (from Andersson et al., 1988).

Figure 3.3 Conceptual model and parameter distribution used for the predictive modeling of the interference tests.

Figure 3.4 Conceptual model used for the calibration of the interference tests and for predictions of the radially converging tracer test.

Figure 3.5 Comparison of predicted (solid line) and measured transient drawdown responses during interference test 3B for boreholes BFI02 and BFI01.

Figure 3.6 Comparison of predicted (solid line) and measured transient drawdown responses during interference test 3B for boreholes KFI05 and KFI06.

Figure 3.7 Comparison of predicted (solid line) and measured transient drawdown responses during interference test 3B for boreholes KFI09 and KFI10.

Figure 3.8 Comparison of predicted (solid line) and measured transient drawdown responses during interference test 3B for boreholes KFI11 and HFI01.

Figure 3.9 Finite element mesh for the modelled region.

Figure 3.10 Boundary conditions for the modelled region.

Figure 3.11 Parameter distribution for the calibrated model.

Figure 3.12 Simulated (solid line) and observed drawdown responses in boreholes BFI01 and BFI02.

Figure 3.13 Simulated (solid line) and observed drawdown responses in boreholes HFI01 and KFI05.

Figure 3.14 Simulated (solid line) and observed drawdown responses in boreholes KFI06 and KFI09.

Figure 3.15 Simulated (solid line) and observed drawdown responses in boreholes KFI10 and KFI11.

Figure 3.16 Hydraulic head distribution near steady state for the calibrated model.

Figure 3.17 Simulated (solid line) and observed transient responses in bore-hole KFI04.

Figure 3.18 Hydraulic head distribution near steady state assuming a transmissivity in the fracture zone one order of magnitude higher than for the calibrated model.

Chapter 4

Figure 4.1 Finite element meshes used for the transport simulations representing injection boreholes BFI01, KFI06 and KFI11.

Figure 4.2 Predicted steady state hydraulic head distribution for the region of interest for the radially converging tracer test.

Figure 4.3 Simulated versus observed breakthrough data after adjustment of porosity.

Figure 4.4 Finite element mesh for transport predictions of the dipole test.

Figure 4.5 Predicted breakthrough curve of a conservative tracer in borehole BFI02. For comparison the results obtained both with and without recirculation are illustrated.

Figure 4.6 Predicted breakthrough curve of ^{24}Na with decay and recirculation.

Figure 4.7 Predicted breakthrough curves for a range of R-values.

Figure 4.8 Comparison of model predictions and experimental results from the dipole tracer test.

Figure 4.9 Regression estimate for In-EDTA with a two-path model.

Figure 4.10 Regression estimate for Amino G Acid assuming an instantaneous pulse input.

Figure 4.11 Regression estimate for Amino G Acid assuming a decaying pulse injection.

Figure 4.12 Regression estimate for Amino G Acid assuming an instantaneous pulse input and two main flow paths.

Figure 4.13 Regression estimate for Amino G Acid assuming two flow paths and applying a variable injection scheme, estimated from tracer injection data.

Figure 4.14 Regression estimate for Iodide assuming one major flow path.

Figure 4.15 Regression estimate for Iodide assuming two major flow paths.

Figure 4.16 Regression estimate for ReO_4 assuming two major flow paths and applying a variable injection scheme.

Chapter 5

Figure 5.1 Results of fitting with Advection-Dispersion model (ADM) for the tracer In-EDTA.

Figure 5.2 Results of fitting with Advection-Dispersion model (ADM) for the tracer Gd-DTPA.

Figure 5.3 Results of fitting with Advection-Dispersion model (ADM) for the tracer Iodide.

Figure 5.4 Results of fitting with Advection-Dispersion-Matrix Diffusion model (ADDM) for the tracer In-EDTA. Pf calculated from experimental data.

Figure 5.5 Results of fitting with Advection-Dispersion-Matrix Diffusion model (ADDM) for the tracer In-EDTA. Pf calculated from experimental data and Pe assumed to be 100 (low dispersion).

Figure 5.6 Results of fitting with Advection-Dispersion-Matrix Diffusion model (ADDM) for the tracer Gd-DTPA. Pf calculated from experimental data and Pe assumed to be 100 (low dispersion).

Figure 5.7 Results of fitting with Advection-Dispersion-Matrix Diffusion model (ADDM) for the tracer Iodide. Pf calculated from experimental data and Pe assumed to be 100 (low dispersion).

Chapter 6

Figure 6.1 The fracture zone.

Figure 6.2 Pulse breakthrough for tracer Tm-EDTA, borehole KFI11.

Figure 6.3 Pulse breakthrough for tracer Amino G Acid, borehole KFI11.

Figure 6.4 Pulse breakthrough for tracer iodide, borehole KFI06.

Figure 6.5 Borehole KFI11, tracer Amino G Acid.

Chapter 7

Figure 7.1 Comparison of the predicted breakthrough curve with a measured curve (I-131, A.3). The predicted curve is calculated using four transport routes in 90 degree angles. The side routes are identical and there is no flow to the 180 degree route. Recirculation and a loss of 25% per cycle is taken into account. Figure 2. The applied conceptual model for the dipole experiment with three flow routes having different relative flow rates than in the predicted ideal case. The losses per cycle are taken to be 35%. The flow routes are modeled to go via or very near the observation boreholes and only a small fraction of the modeled flows are sampled actually in the observation boreholes.

Figure 7.2 The applied conceptual model for the dipole experiment with three flow routes having different relative flow rates than in the predicted ideal case. The losses per cycle are taken to be 35%. The flow routes are modeled to go via or very near the observation boreholes and only a small fraction of the modeled flows are sampled actually in the observation boreholes.

Figure 7.3 Comparison of the calculated breakthrough curve with a measured curve (A.3). The used concept is shown in Fig. 2 and model parameters are presented in Table 1.

Figure 7.4 Comparison of the breakthrough curves of different tracers and the calculated curve. The smooth line is the calculated curve and wiggling lines are Rhodamine WT data (A.14 and A.18). All other data are presented as points (A.3, A.4, A.5, A.6, A.12, A.16 and A.17) but normalized roughly to the peak concentration value of I-131 (A.3) by factors 1.1 - 2.0. The Rhodamine WT curves show a somewhat different shape which could be explained within the used model surprisingly by a higher molecular diffusion coefficient (a higher dispersion and slower arrival of the front edge and perhaps a faster arrival of the tail).

Figure 7.5 Modeled and measured breakthrough curves (I-131 B.3 and Br-82 B.6) in the observation borehole KFi11. The too low peak value of the modeled concentration may be due to the very convective nature of the fast transport which cannot be modeled very accurately at short times.

Figure 7.6 Modeled and measured breakthrough curves (I-131 C.1, Cr-51 C.2 and Yb-169 C.4) in the observation borehole KFi06. The calculated curve is normalized by a factor of 0.5 and the Cr- and Yb-EDTA complex values by a factor of 2 in order to compare the curve shapes better. A second injection 216 h later causes the rise of the I-131 concentration values after 400 h.

Chapter 8

Figure 8.1

Figure 8.2

Figure 8.3

Figure 8.4

Figure 8.5

Figure 8.6

Figure 8.7

Chapter 9

Figure 9.1 Modeled region and boundary conditions.

Figure 9.2 Local co-ordinates system and schematic figure of local dispersion.

Figure 9.3 Generated fracture networks. (a) Fracture network-1; (b) fracture network-2; (c) fracture network-3.

Figure 9.4 flow vectors in fracture networks. (a) Fracture network-1; (b) fracture network-2; (c) fracture network-3.

Figure 9.5 Measured Breakthrough curves.

Figure 9.6 Calculated breakthrough curves (network-2).

Figure 9.7 Calculated breakthrough curves (network-1).

Figure 9.8 Calculated breakthrough curves (network-3).

Chapter 10

Figure 10.1 Schematization of the injection loop.

Figure 10.2 Schematization of a multichannel system.

Figure 10.3 Recovery curve of a multichannel system.

Figure 10.4 Decomposition of In-EDTA recovery curve into two flow paths.

Figure 10.5 Modelling of In-EDTA curve with a two-paths model.

Figure 10.6 Modelling of Gd-DTPA curve with a 10 m dispersivity.

Figure 10.7 Modelling of Gd-DTPA curve with a two-path model.

Figure 10.8 Prediction of the Iodine curve during the two-well test with a two-path model.

Figure 10.9 Comparison of the Injection-Recovery systems for Radially Converging Test and two-well test.

Figure 10.10 Prediction of Iodine curve with a single-path model.

Figure 10.11 Prediction of Iodine curve with a single-path model and recirculation.

Figure 10.12 Prediction of Iodine Curve with a single path model, recirculation and regional flow (second value of hydraulic conductivity).

Figure 10.13 Prediction of Iodine Curve with a single path model, recirculation and regional flow (second value of hydraulic conductivity).

Figure 10.14 Prediction of Iodine Curve with a single path model, recirculation, regional flow and leakage.

Figure 10.15 Comparison of modelled and measured curves in borehole KFI11 during two-well test.

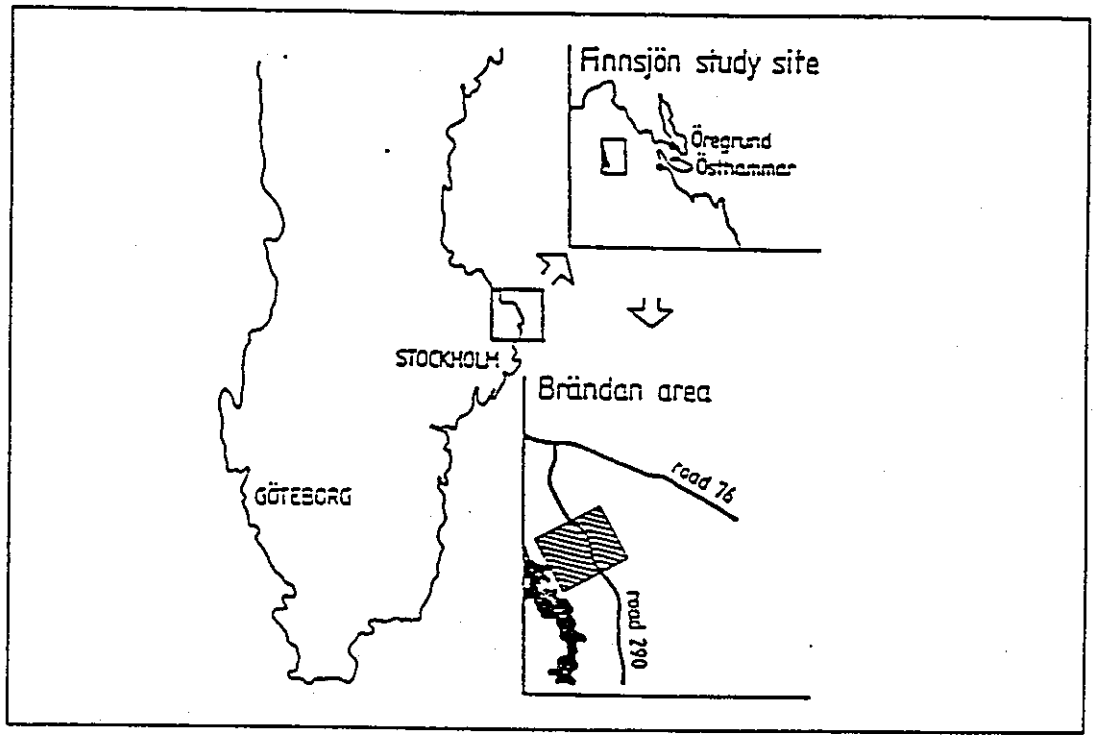


Figure 2.1 Location of the Brändan area, Finnsjön study site.

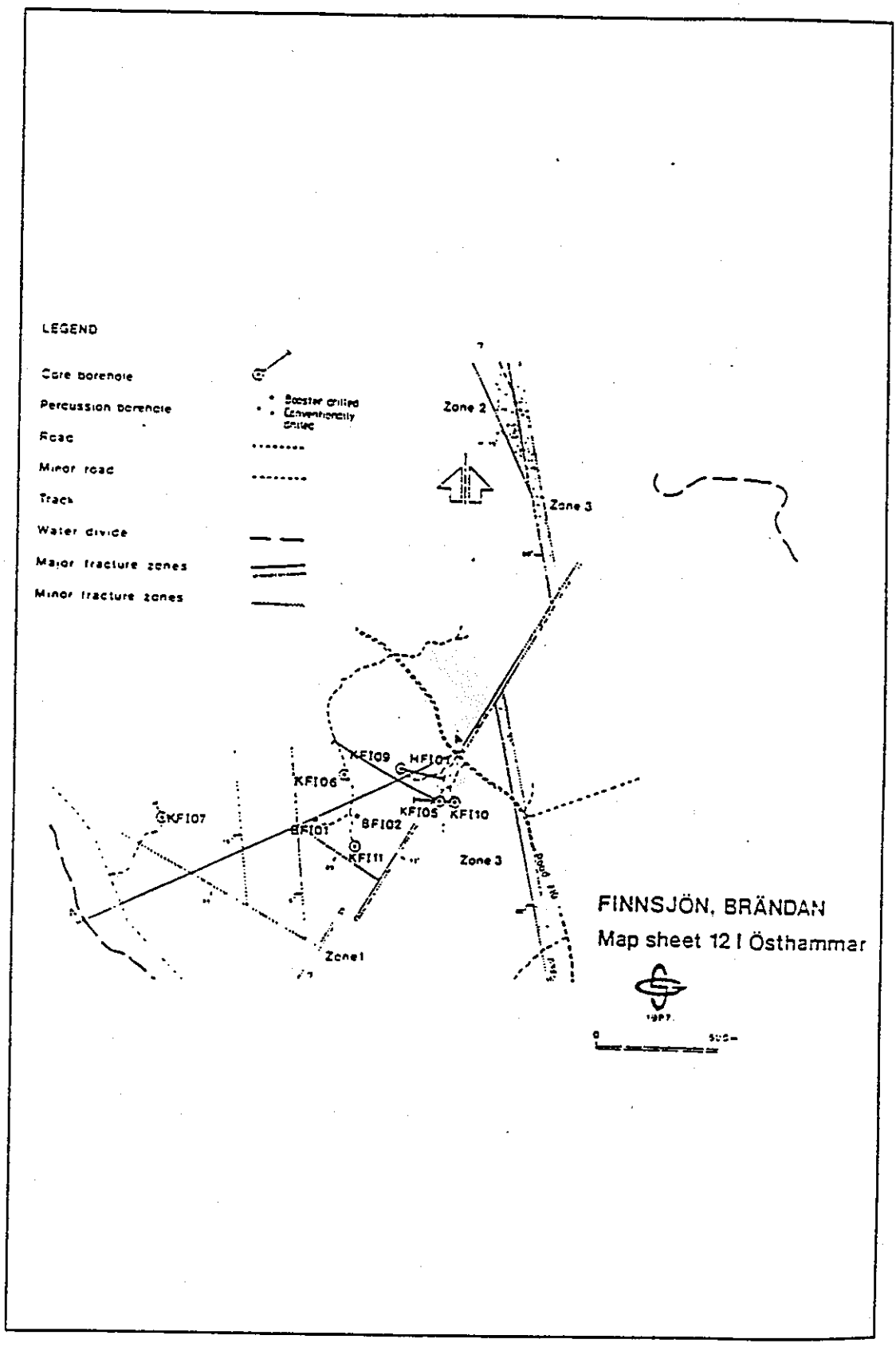


Figure 2.2 Borehole location in the Brändan area.

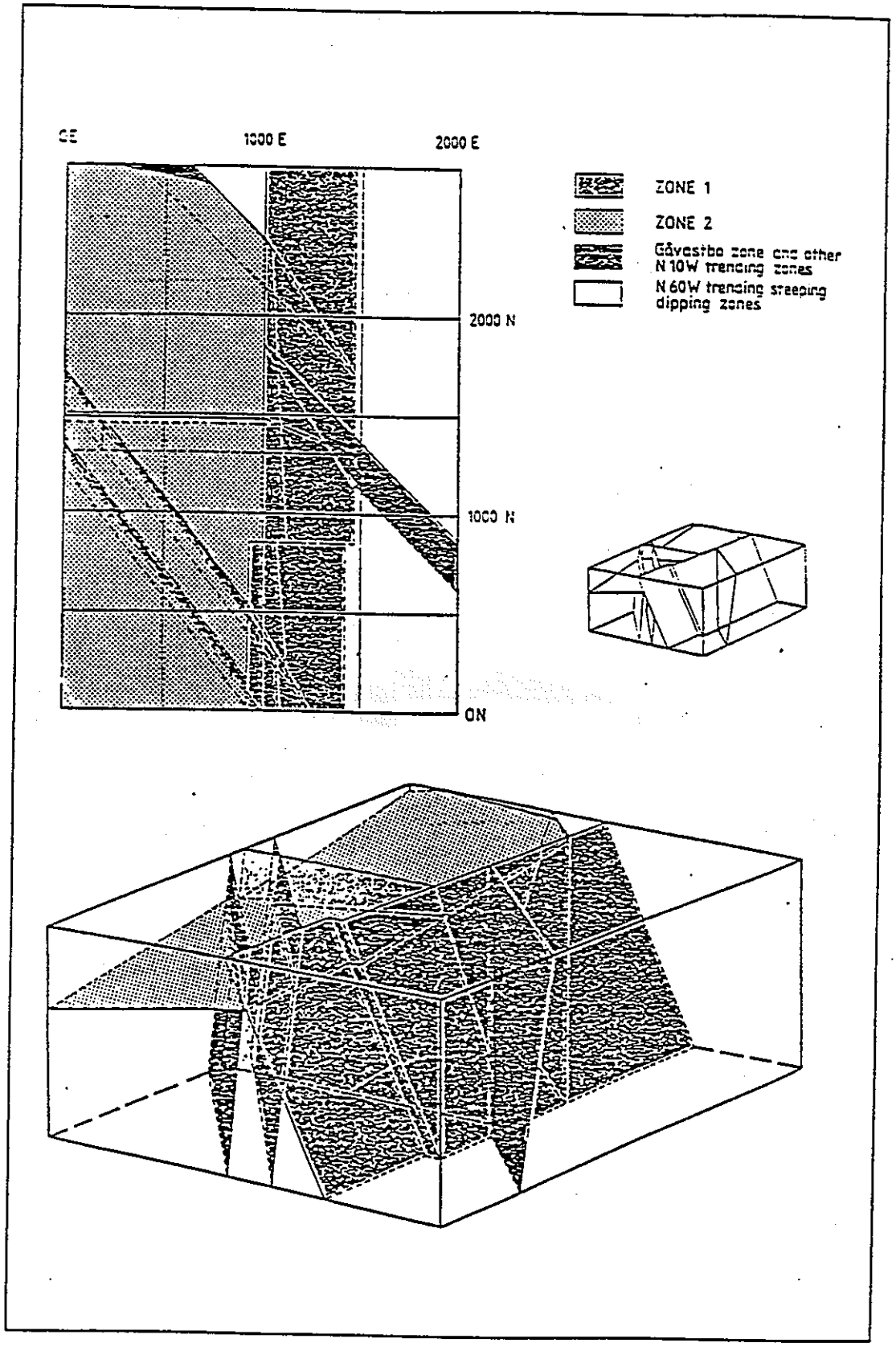


Figure 2.3 Block diagram of fracture zones in the Brändan area.

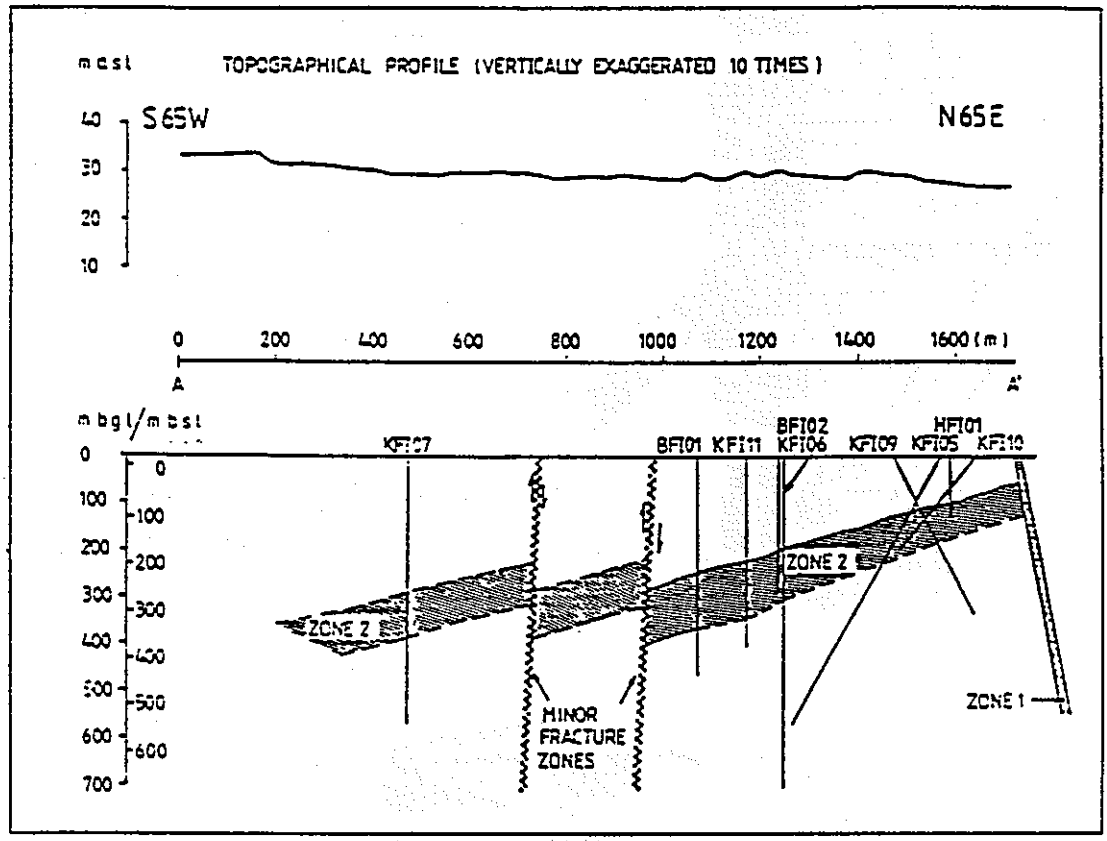


Figure 2.4 Cross section through the Brändan area showing Zone 2.

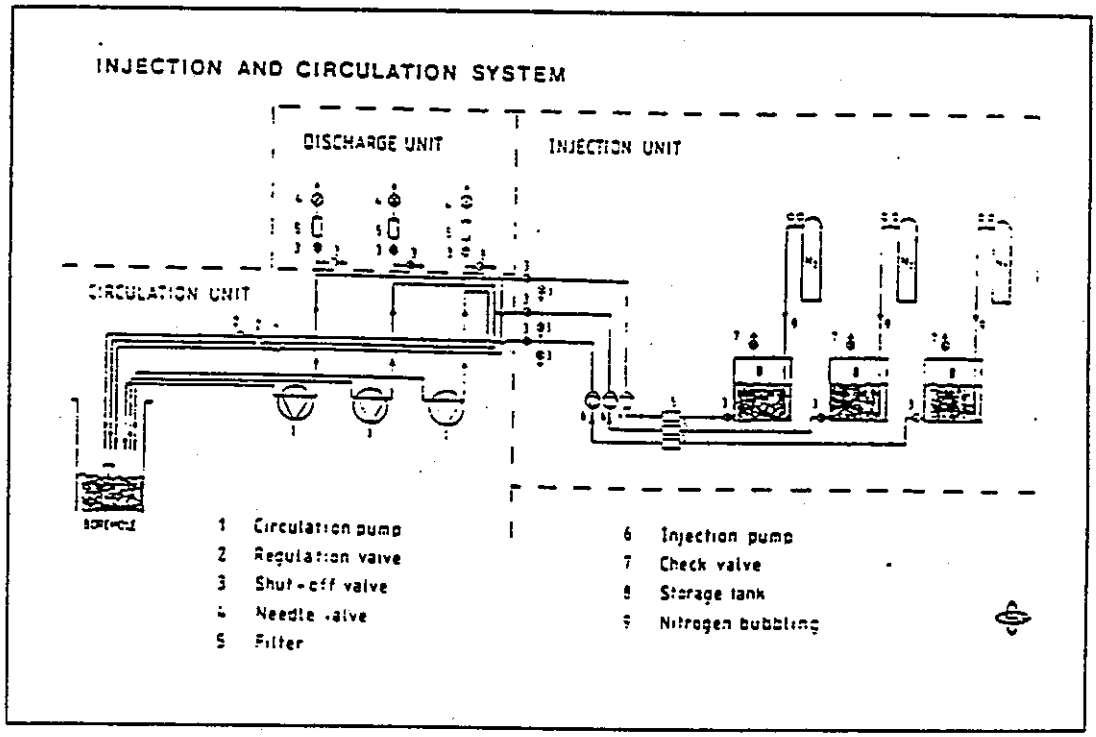


Figure 2.5 Injection and circulation system, radially converging experiment.

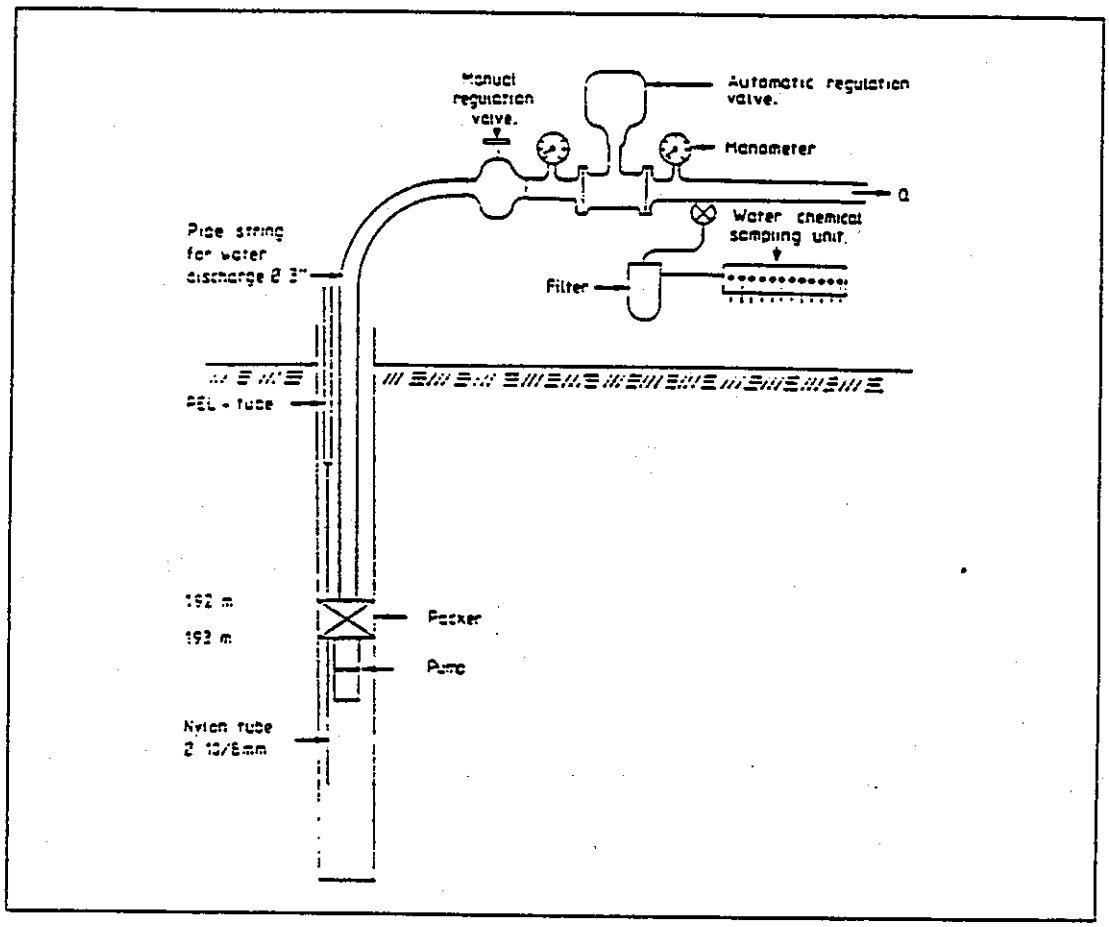


Figure 2.6 Withdrawal equipment, radially converging experiment.

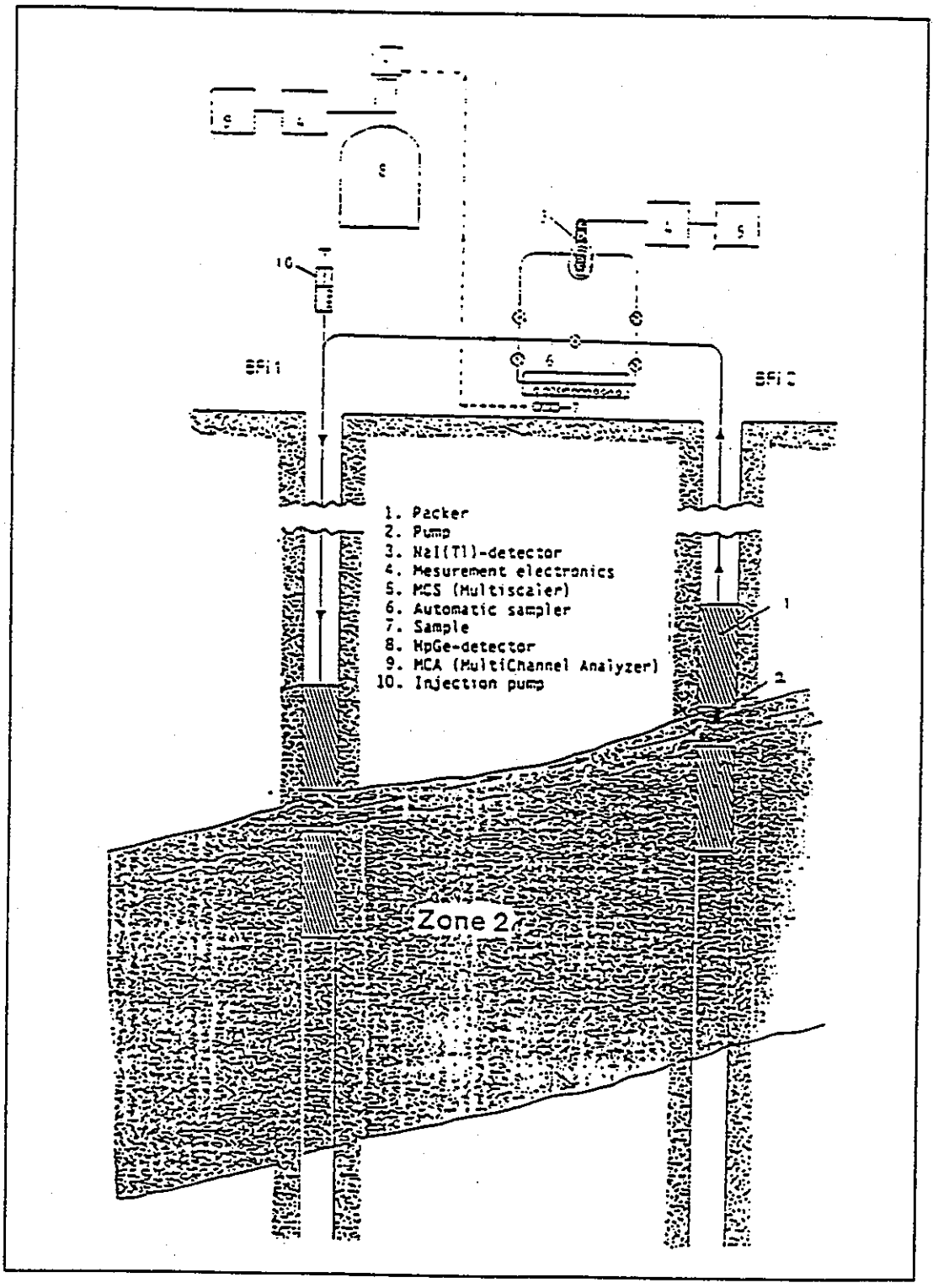


Figure 2.7 Experimental design of the dipole experiment.

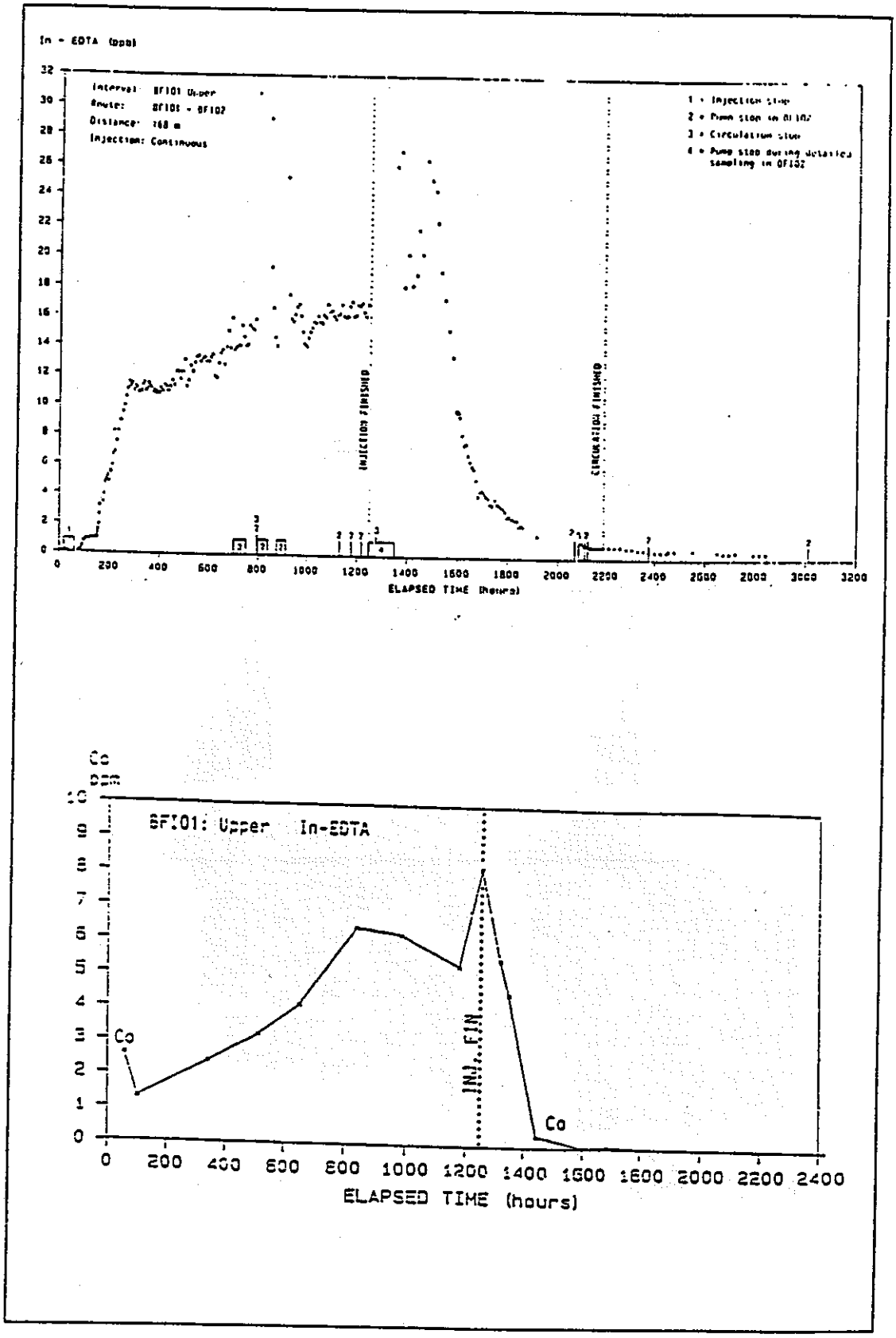


Figure 2.8 Breakthrough curve for In-EDTA (top) and concentration in the injection section as a function of time (bottom).

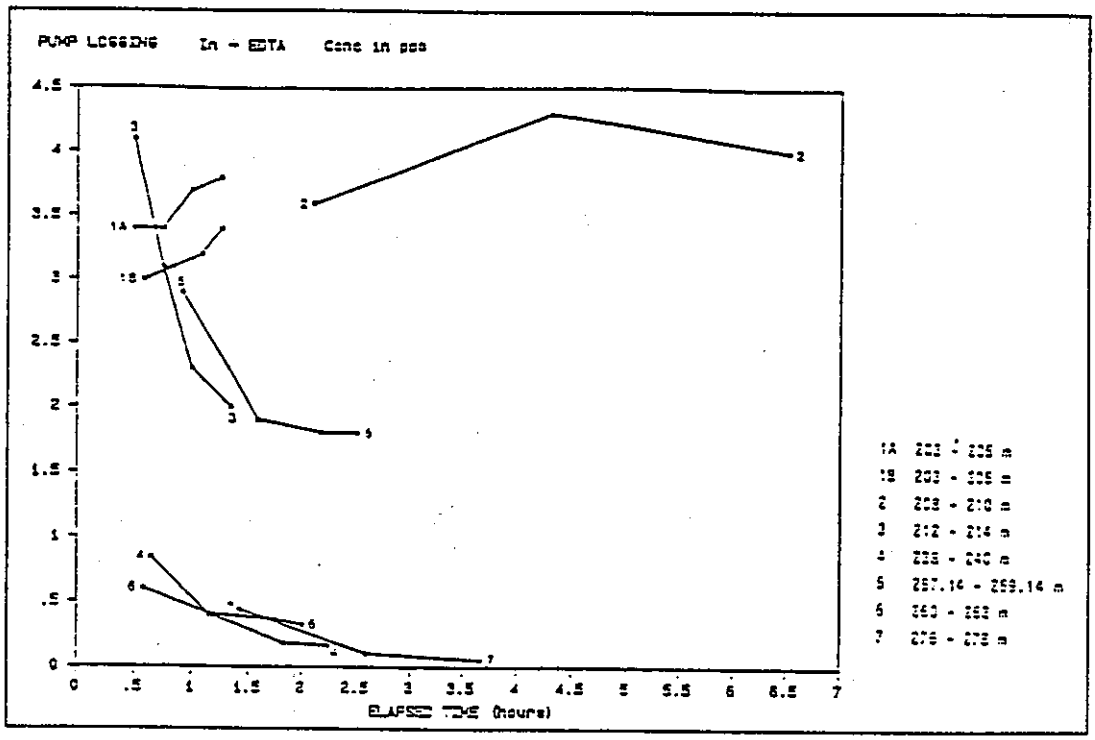


Figure 2.9 Results from detailed sampling in BFI02 during the radially converging experiment. Concentration of In-EDTA.

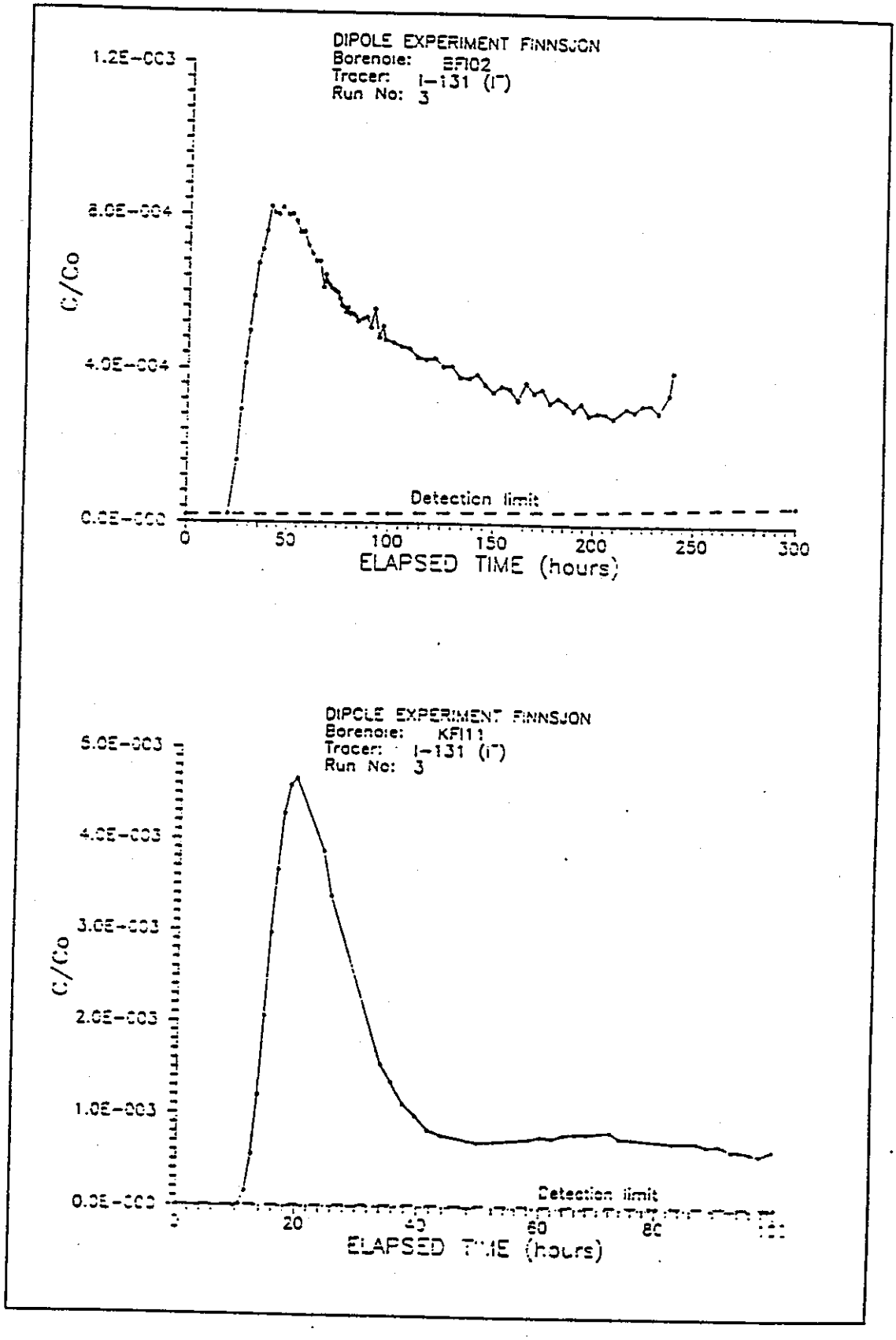


Figure 2.10 Breakthrough curves for ^{131}I in the withdrawal hole BFI02 (top) and in the observation hole KFI11 (bottom).

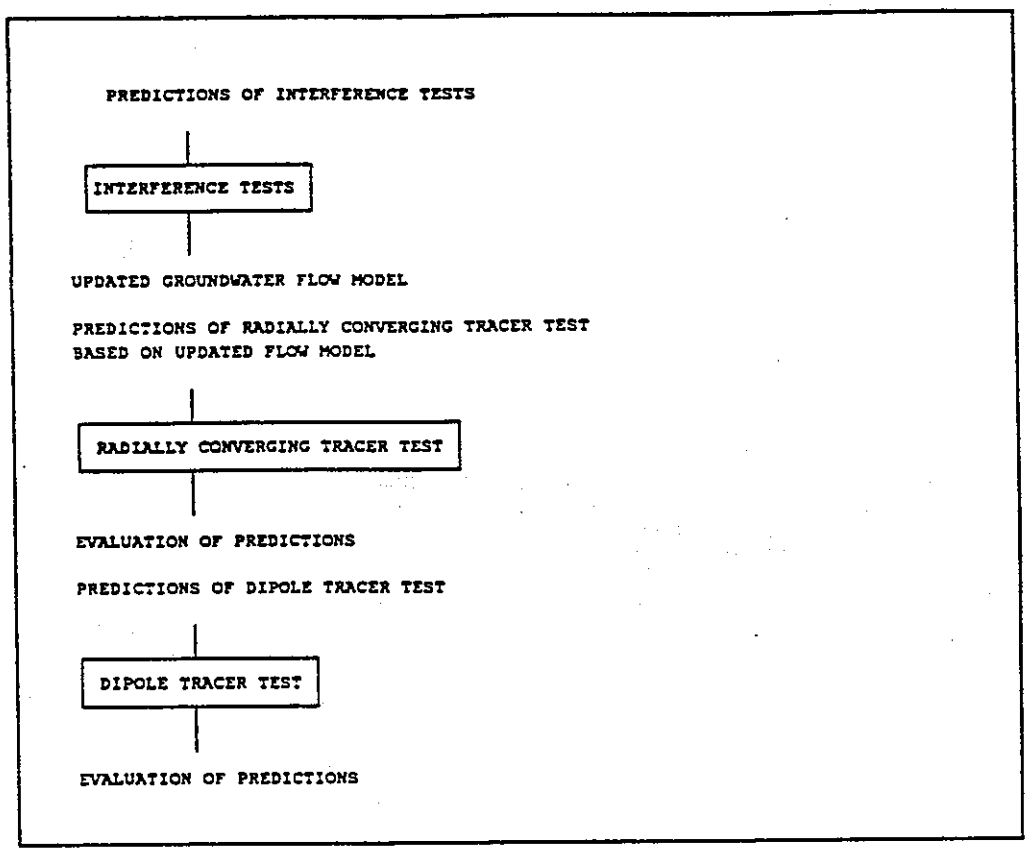


Figure 3.1 General flow of field experiments and related modeling.

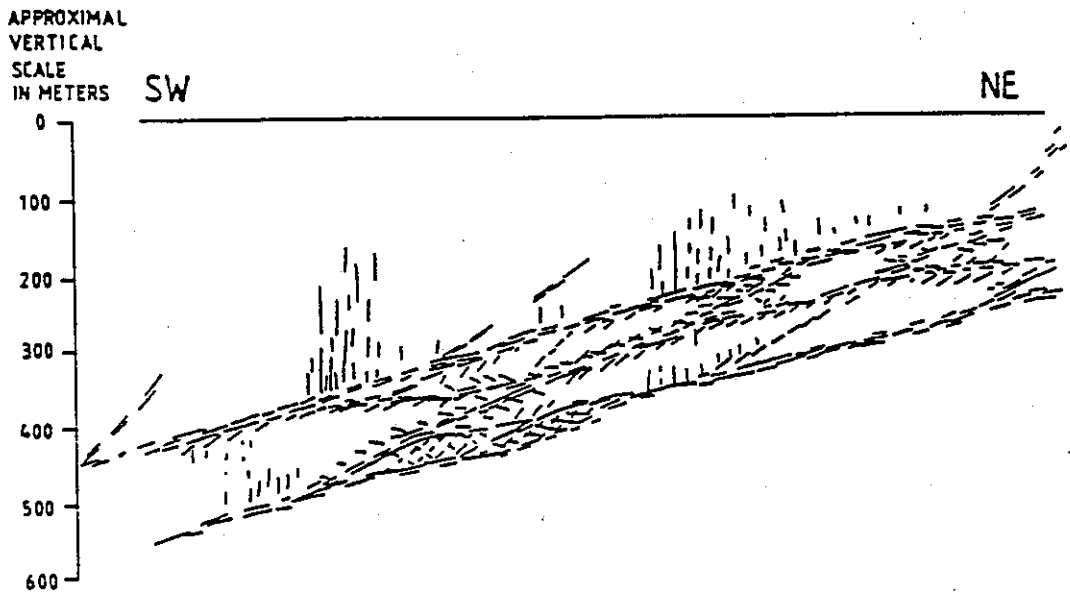


Figure 3.2 Conceptual model of the fracture zone (from Andersson et al, 1988)

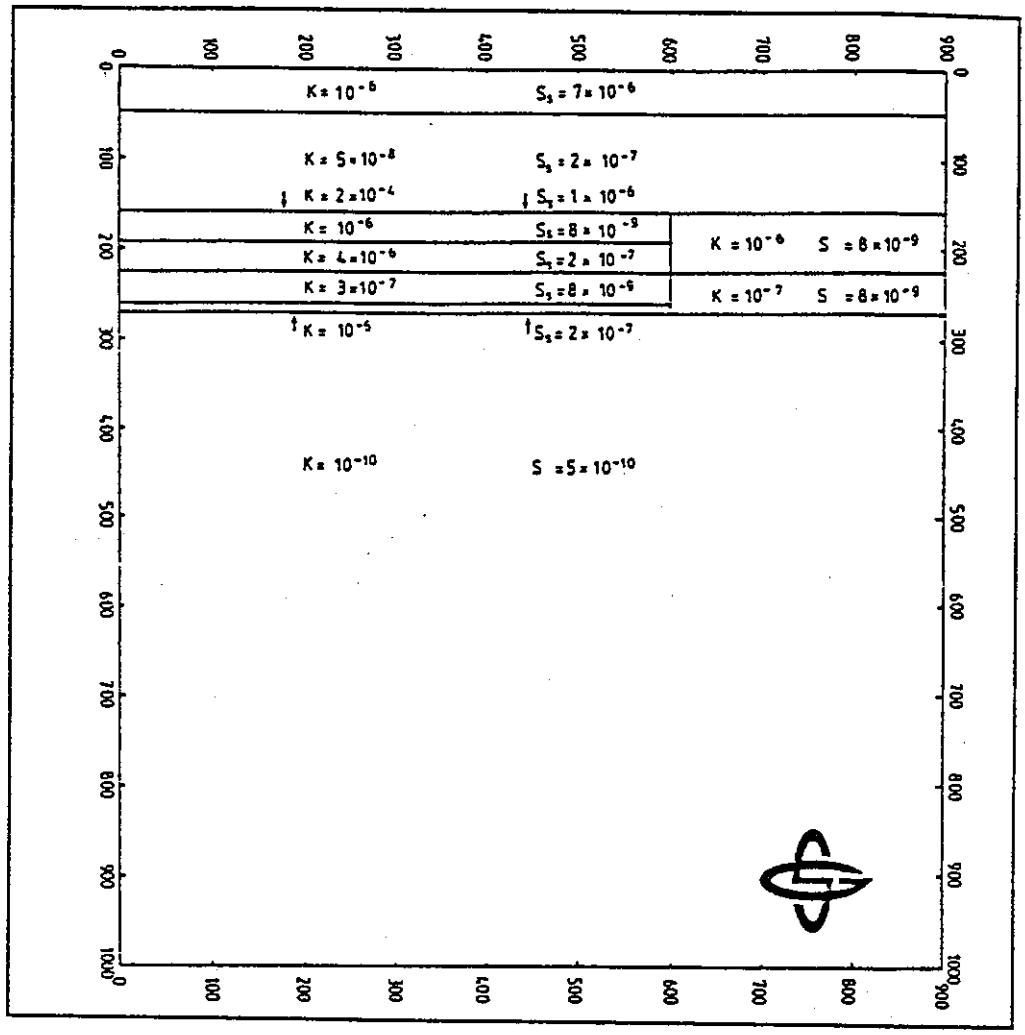


Figure 3.3 Conceptual model and parameter distribution uesd for the predictive modeling of the interfverence tests.

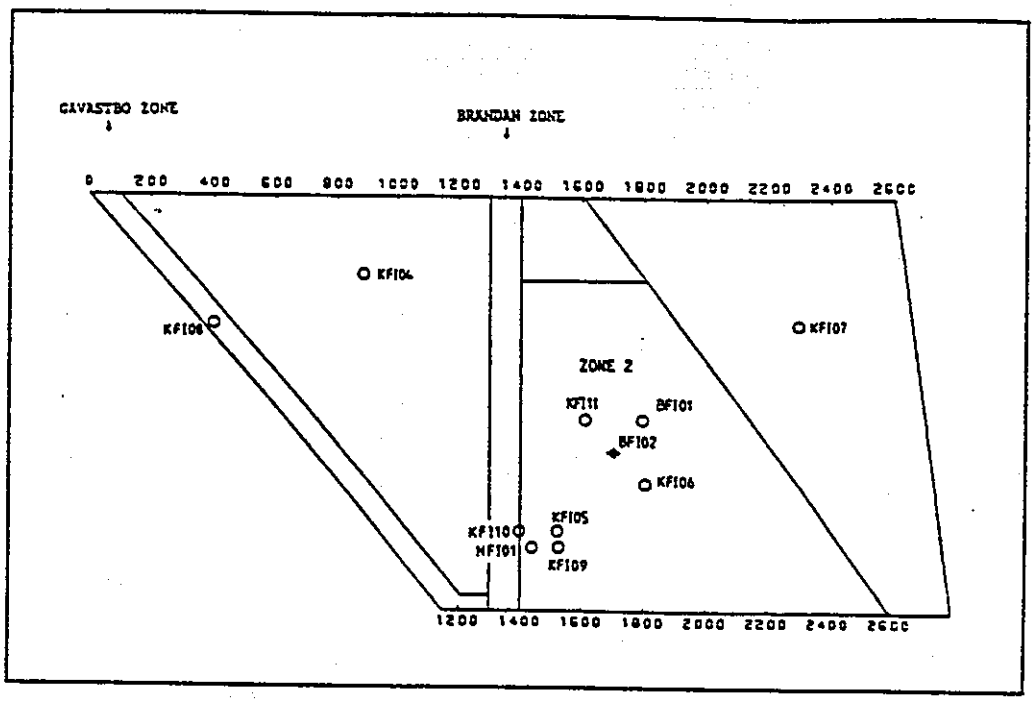


Figure 3.4 Conceptual model used for the calibration of the interference tests and for predictions of the radially converging tracer test.

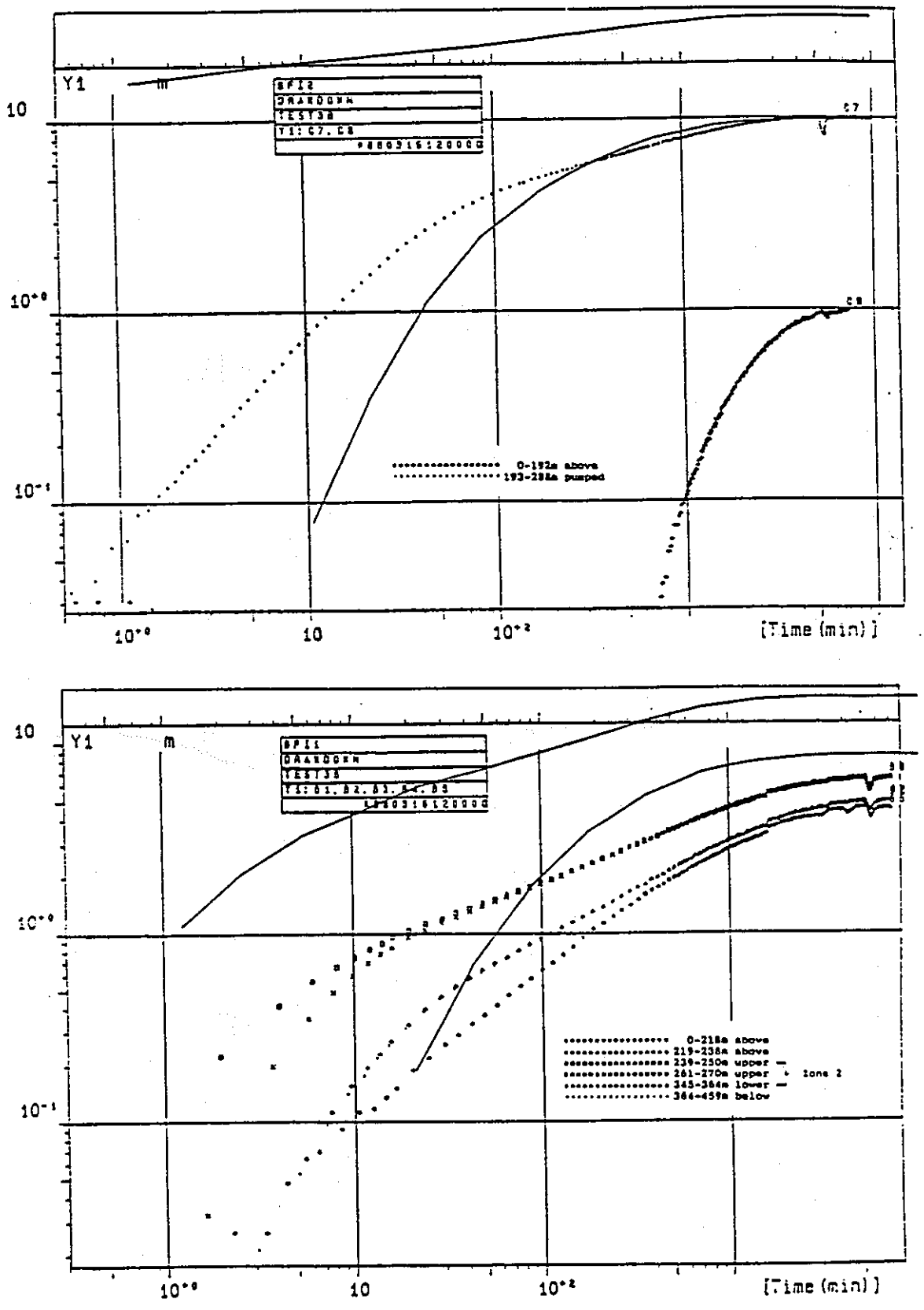


Figure 3.5 Comparison of predicted (solid line) and measured transient drawdown responses during interference test 3B for boreholes BFI02 and BFI01.

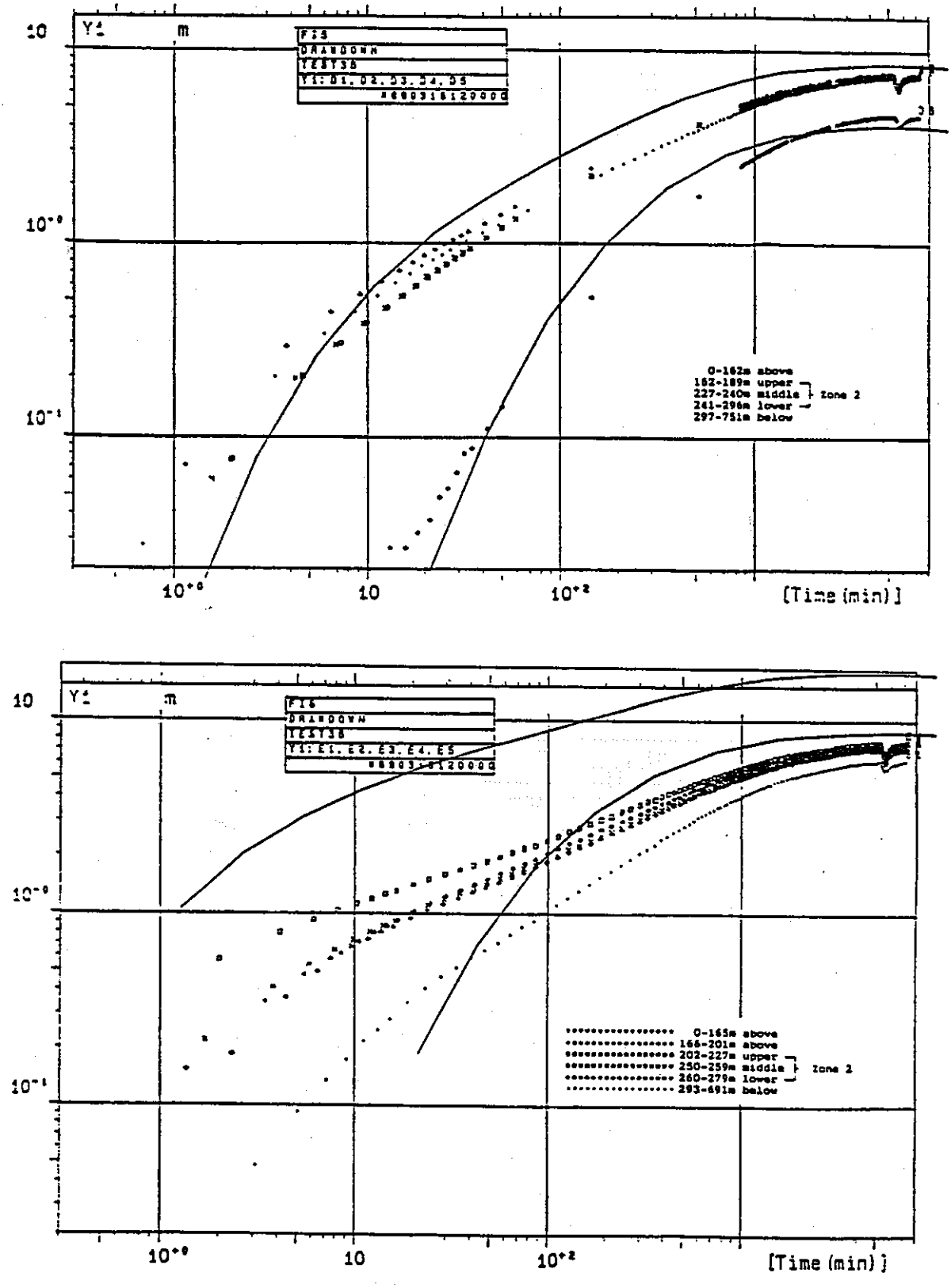


Figure 3.6 Comparison of predicted (solid line) and measured transient drawdown responses during interference test 3B for boreholes KFI05 and KFI06.

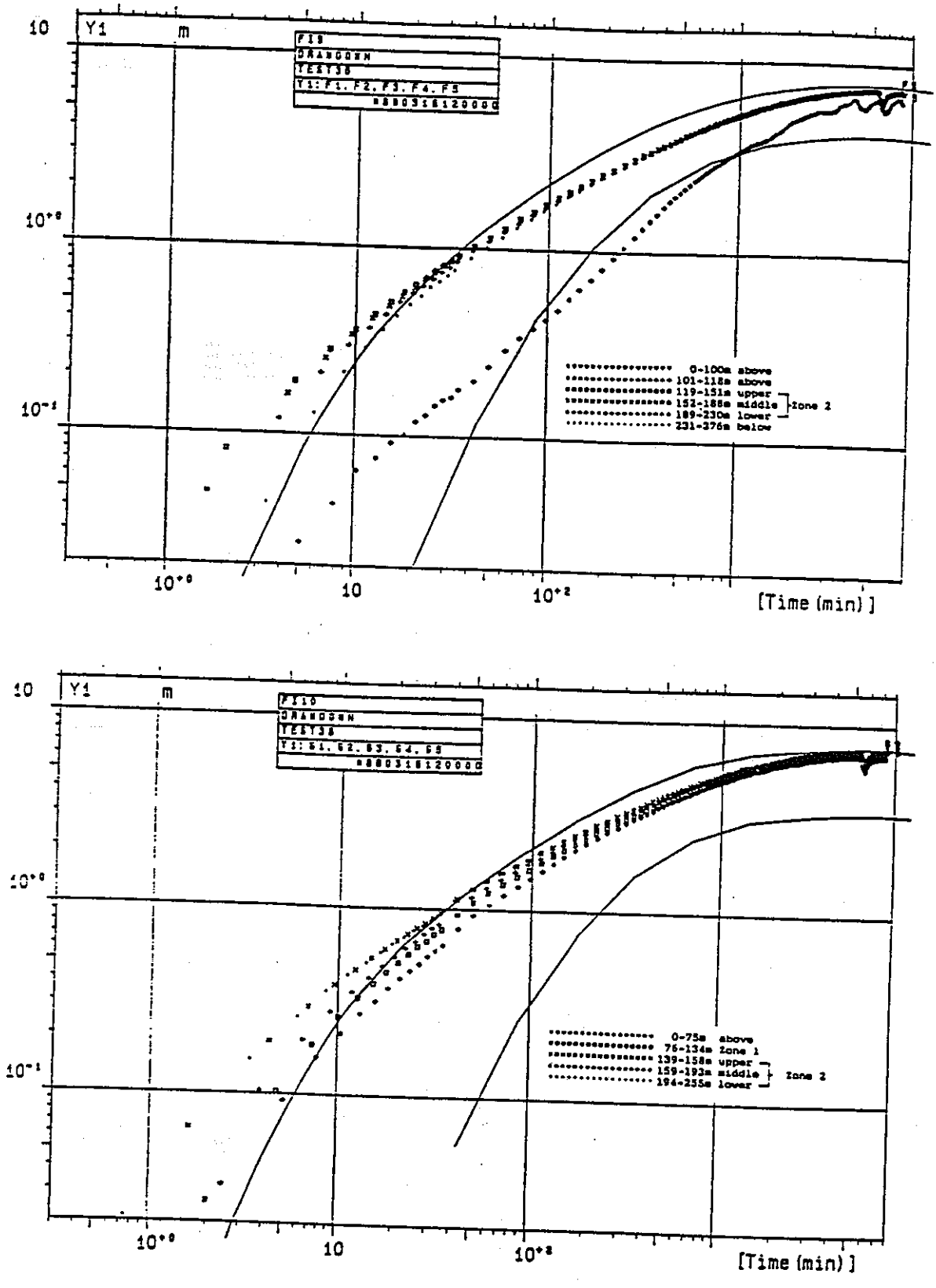


Figure 3.7 Comparison of predicted (solid line) and measured transient drawdown responses during interference test 3B for boreholes KFI09 and KFI10.

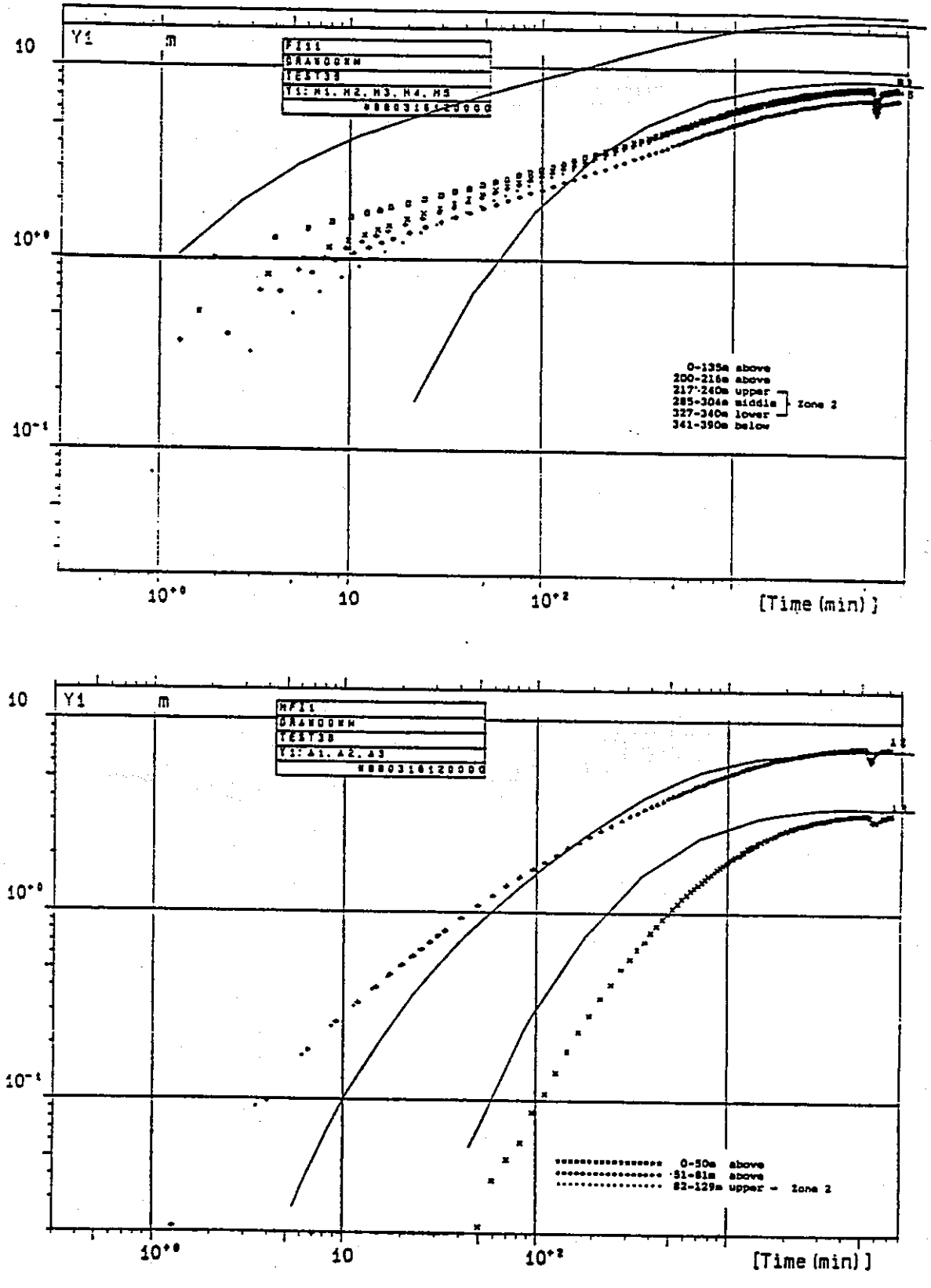


Figure 3.8 Comparison of predicted (solid line) and measured transient drawdown responses during interference test 3B for boreholes KFI11 and HFI01.

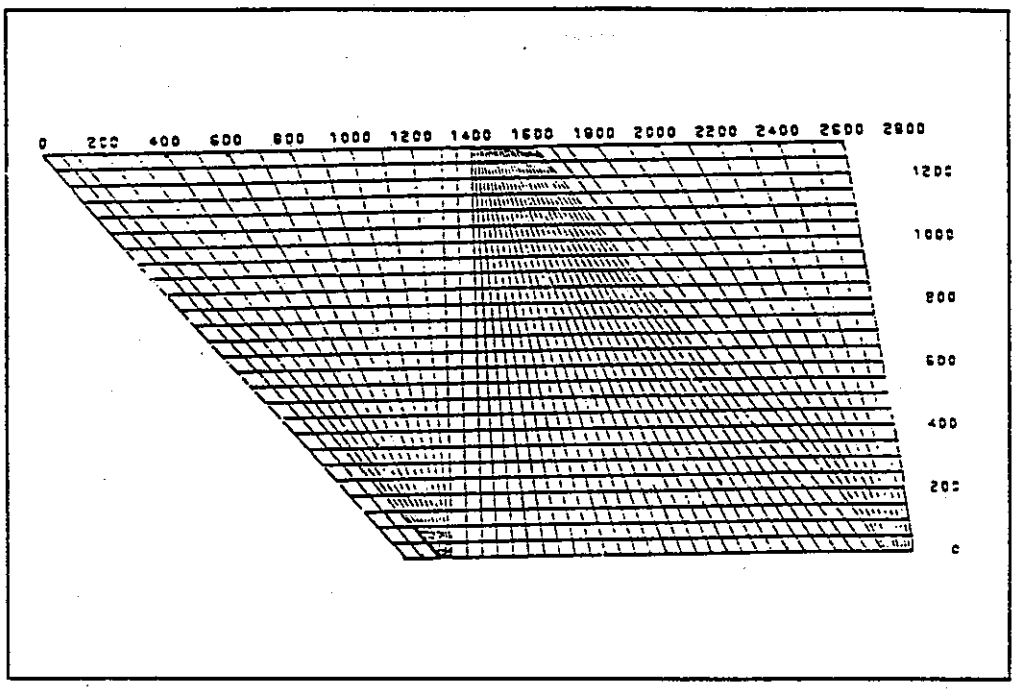


Figure 3.9 Finite element mesh for the modelled region.

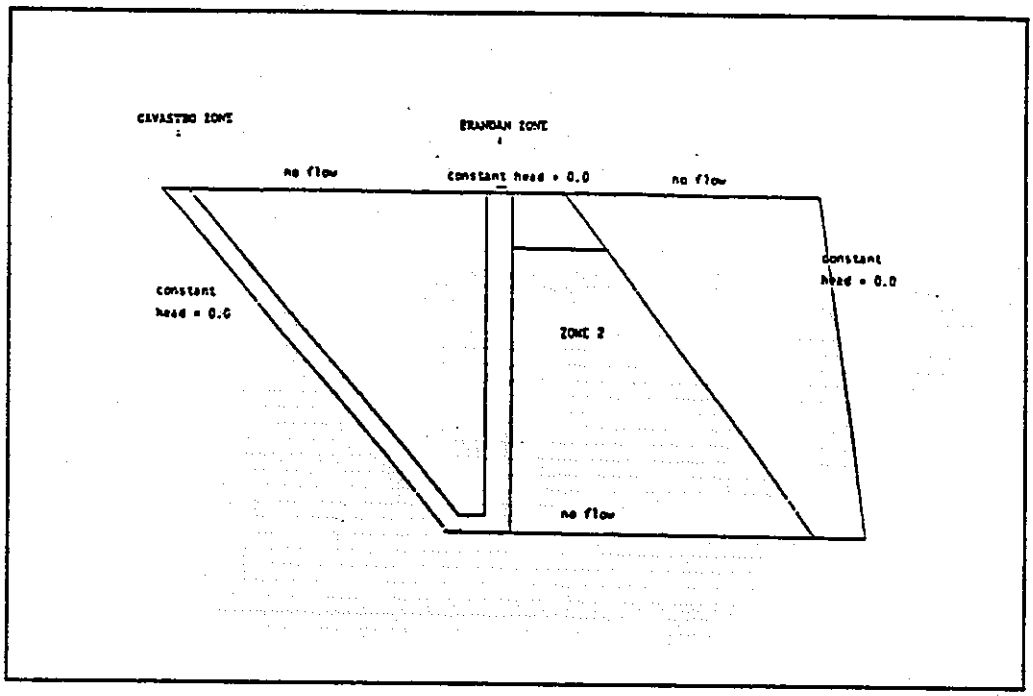


Figure 3.10 Boundary conditions for the modelled region.

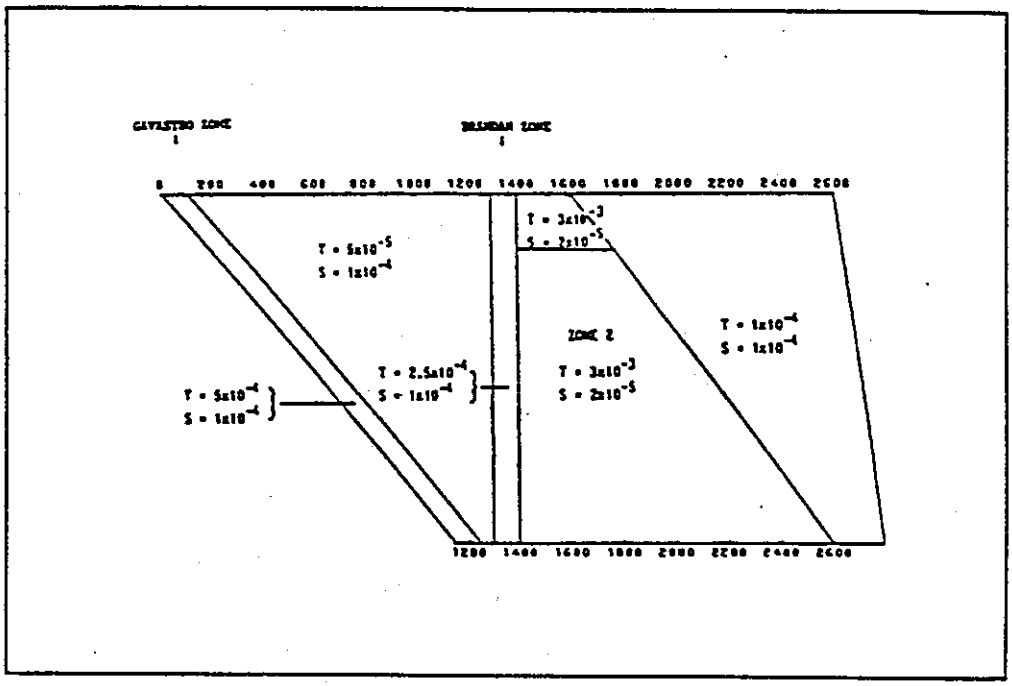


Figure 3.11 Parameter distribution for the calibrated model.

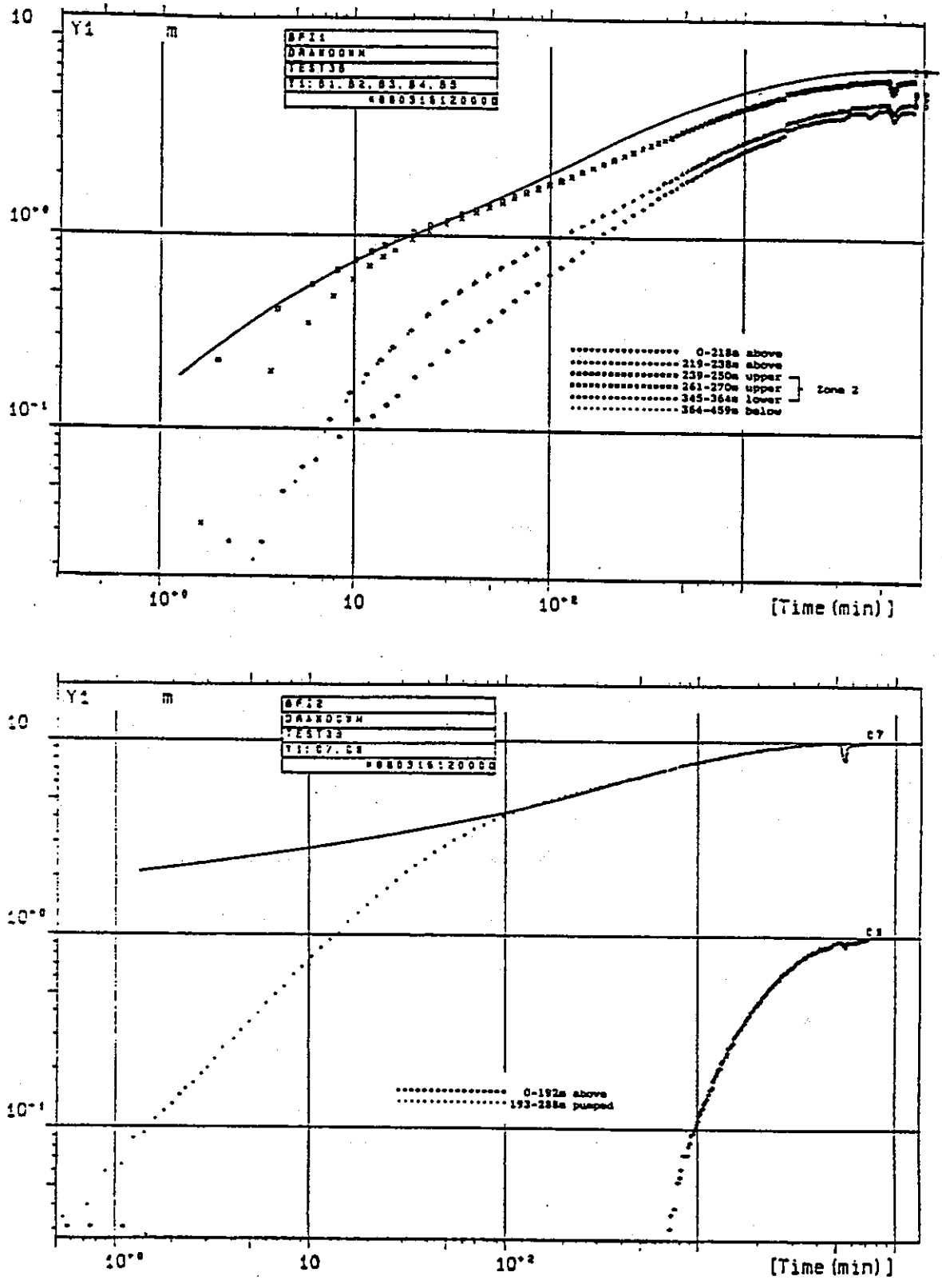


Figure 3.12 Simulated (solid line) and observed drawdown responses in boreholes BFI01 and BFI02.

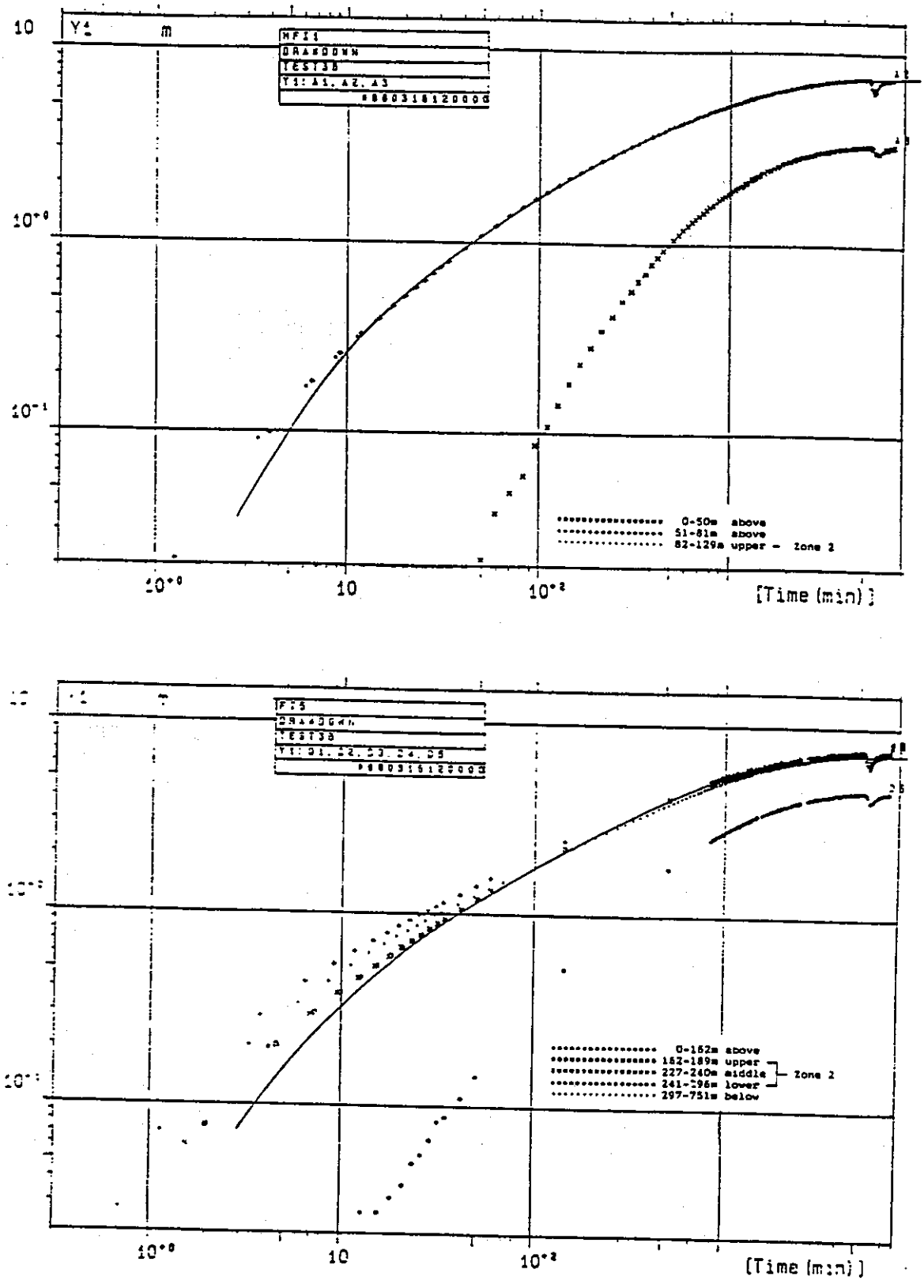
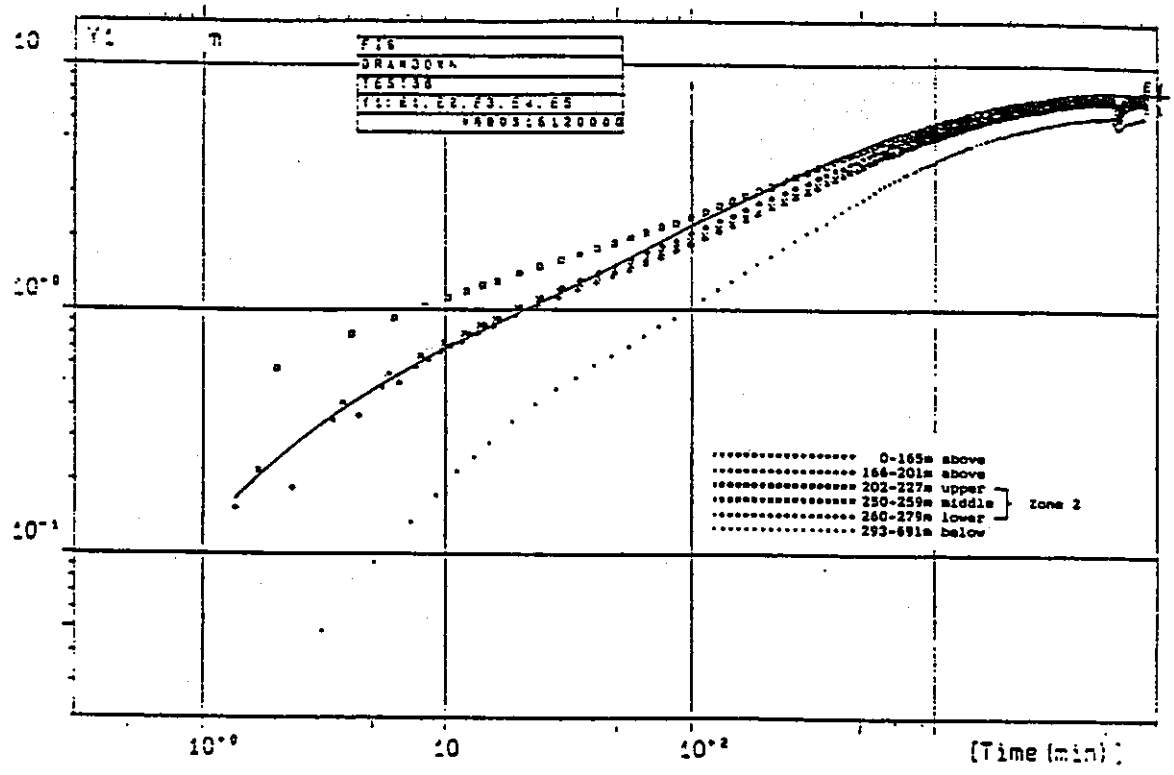


Figure 3.13 Simulated (solid line) and observed drawdown responses in boreholes HFI01 and KFI05



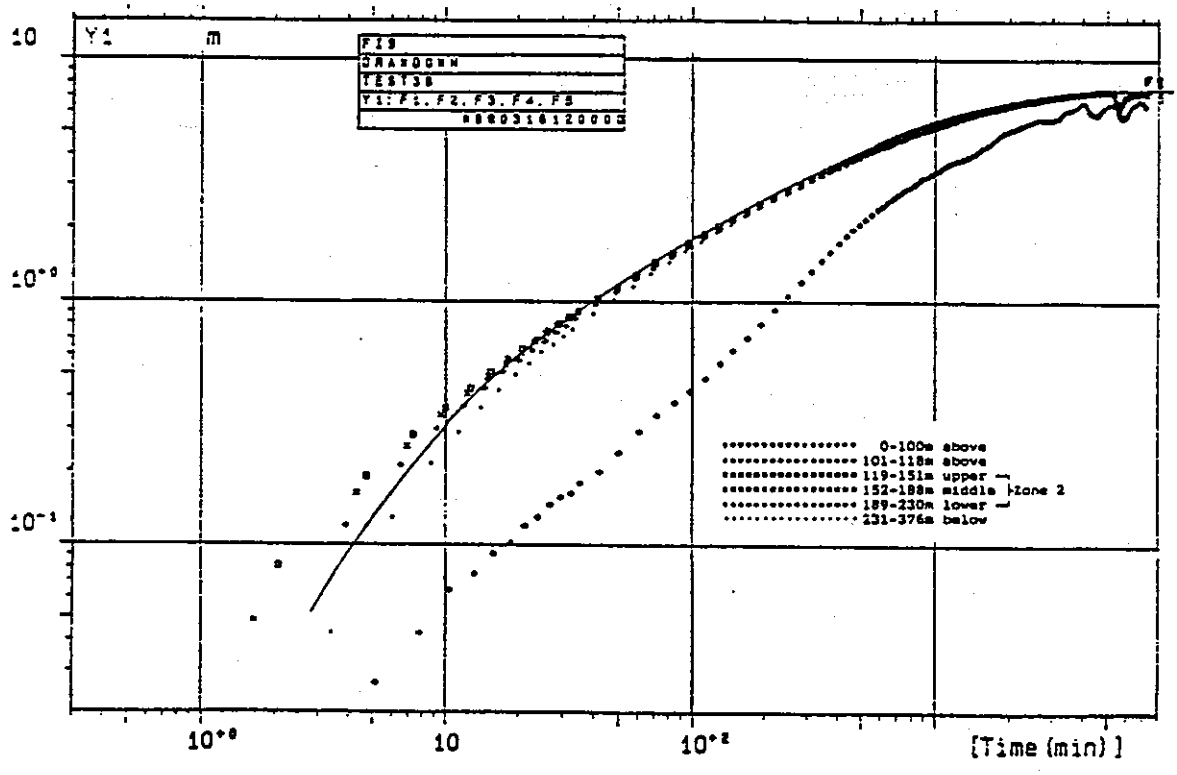


Figure 3.14 Simulated (solid line) and observed drawdown responses in boreholes KFI06 and KFI09.

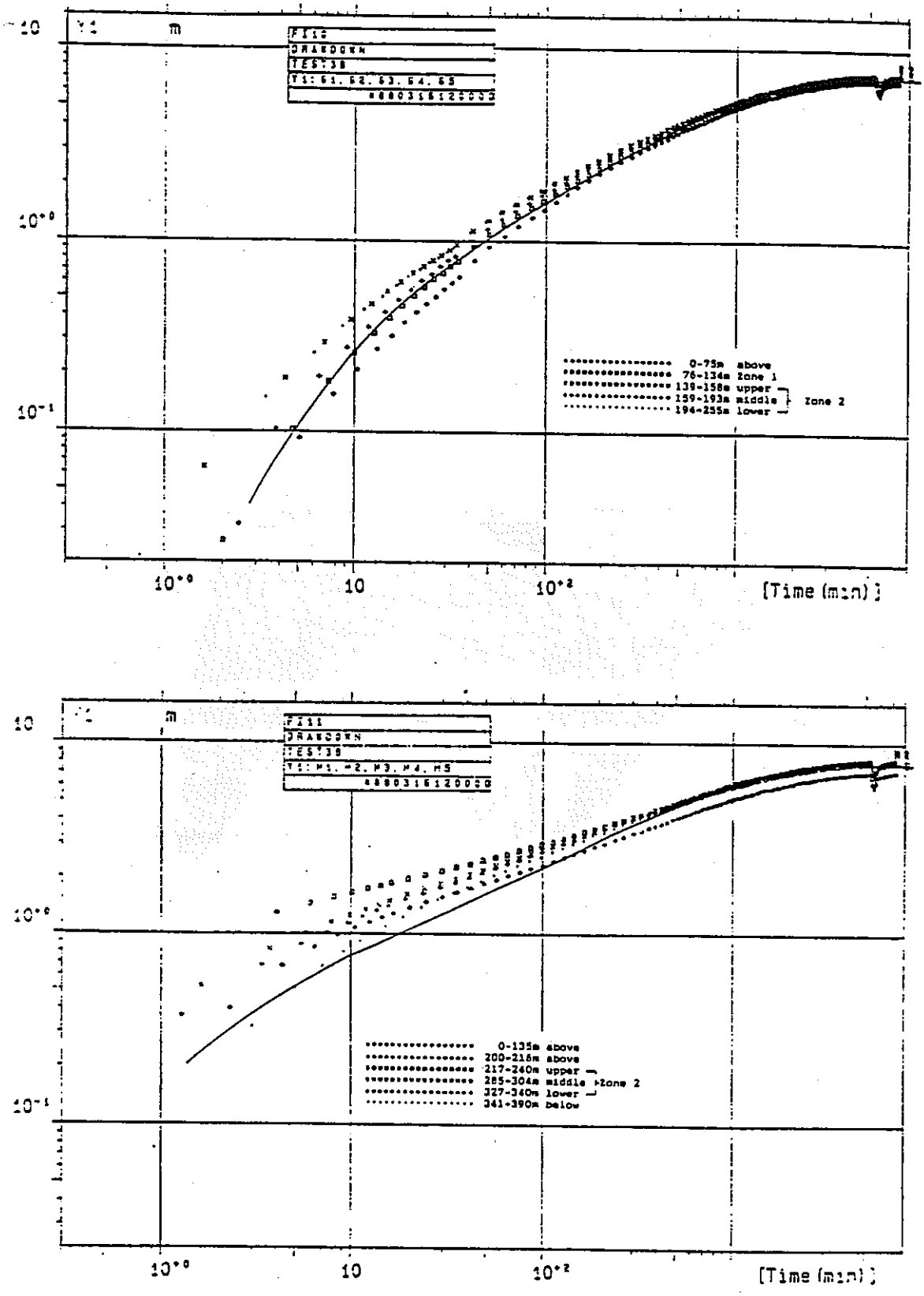


Figure 3.15 Simulated (solid line) and observed drawdown responses in boreholes KFI10 and KFI11.

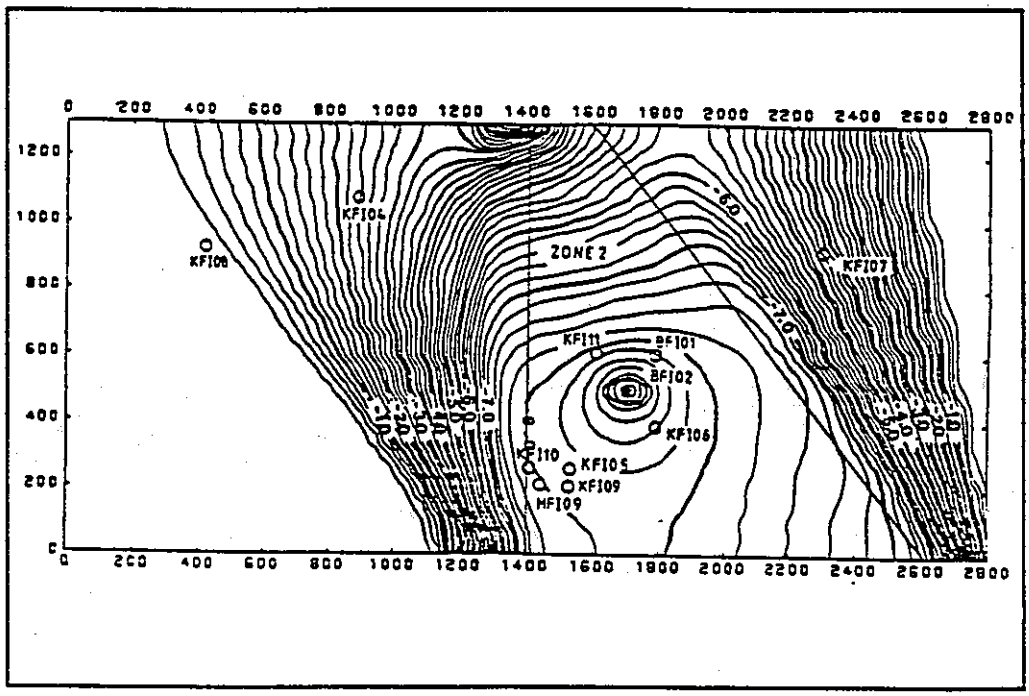


Figure 3.16 Hydraulic head distribution near steady state for the calibrated model.

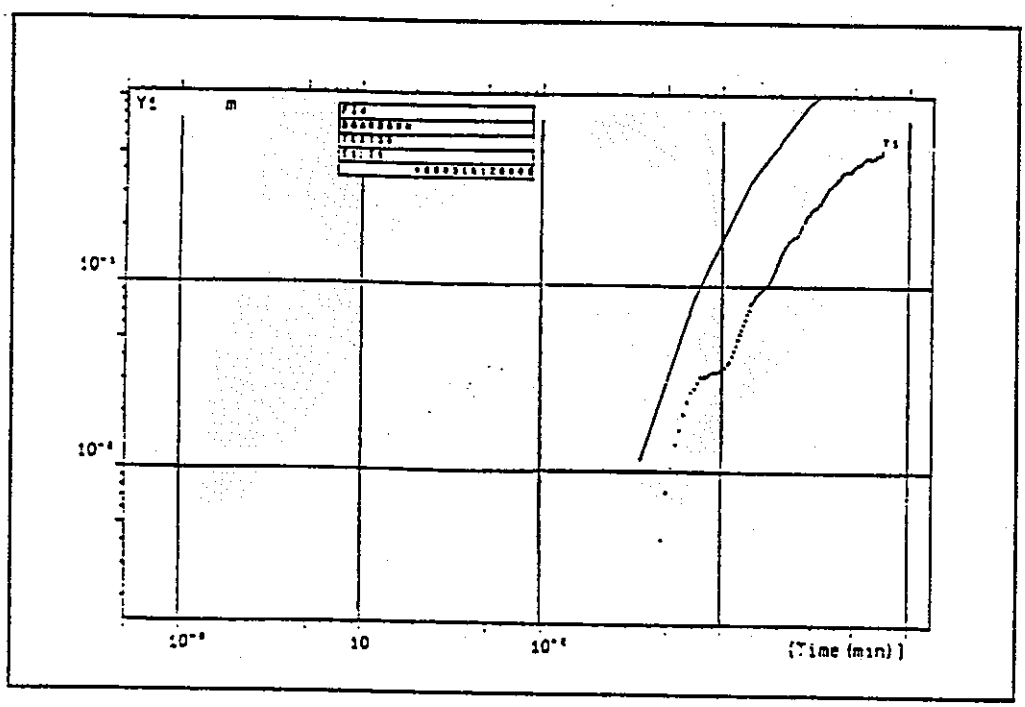


Figure 3.17 Simulated (solid line) and observed transient responses in borehole KFI04.

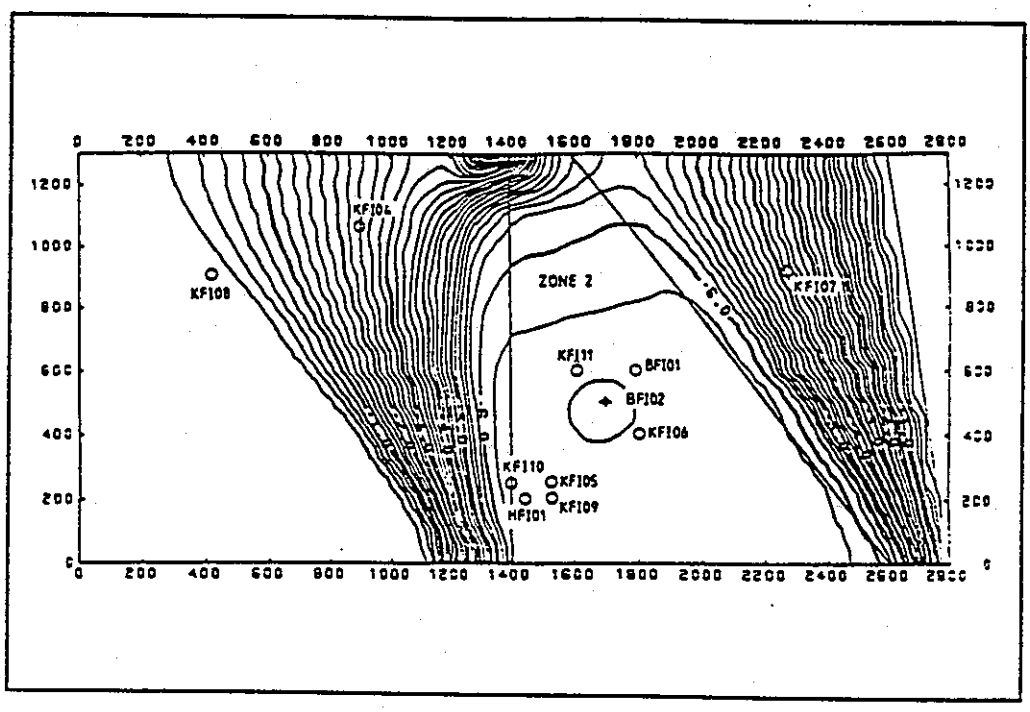


Figure 3.18 Hydraulic head distribution near steady state assuming a transmissivity in the fracture zone one order of magnitude higher than for the calibrated model.

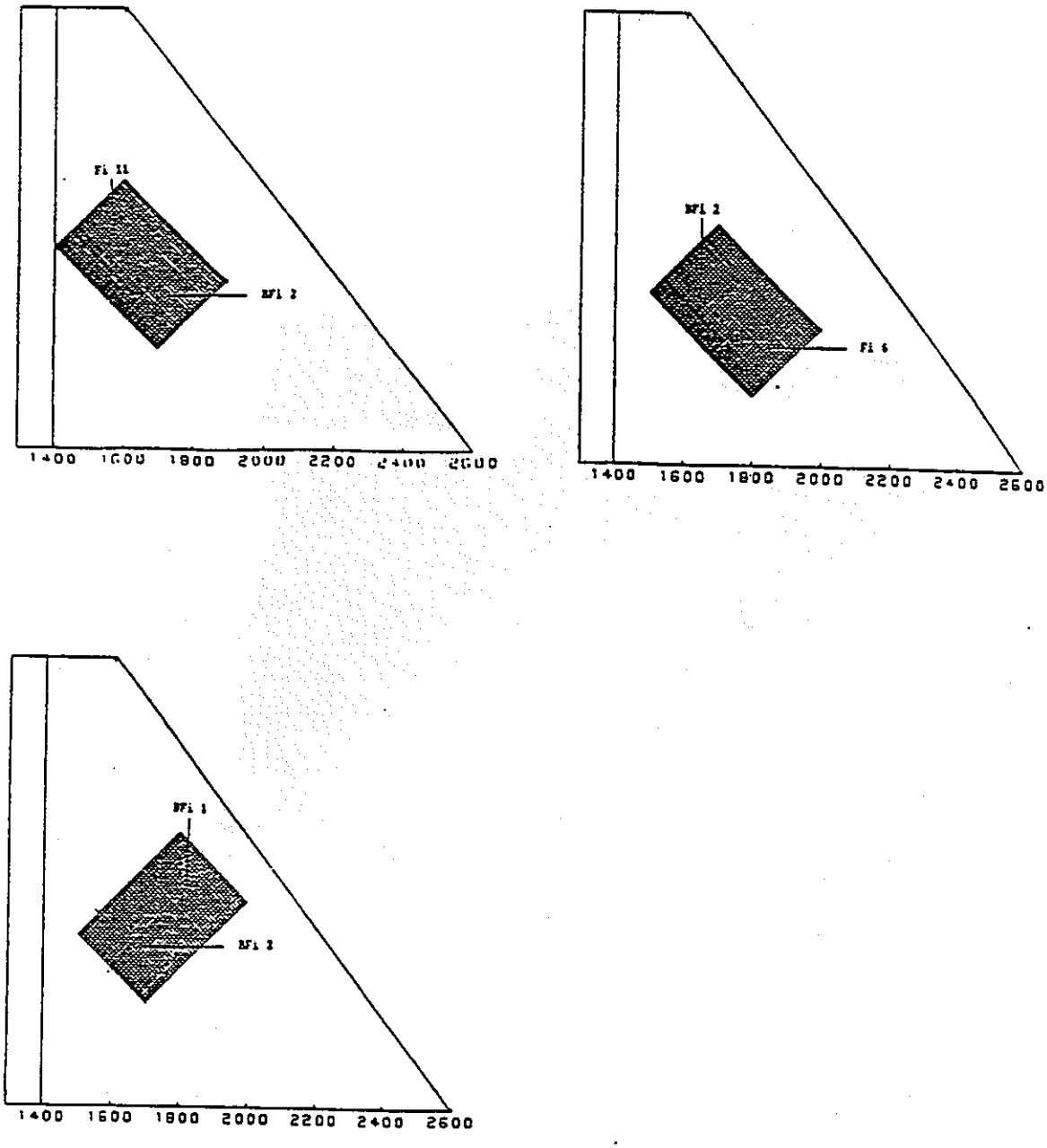


Figure 4.1 Finite element meshes used for the transport simulations representin injection boreholes BFI01, KFI06 and KFI11.

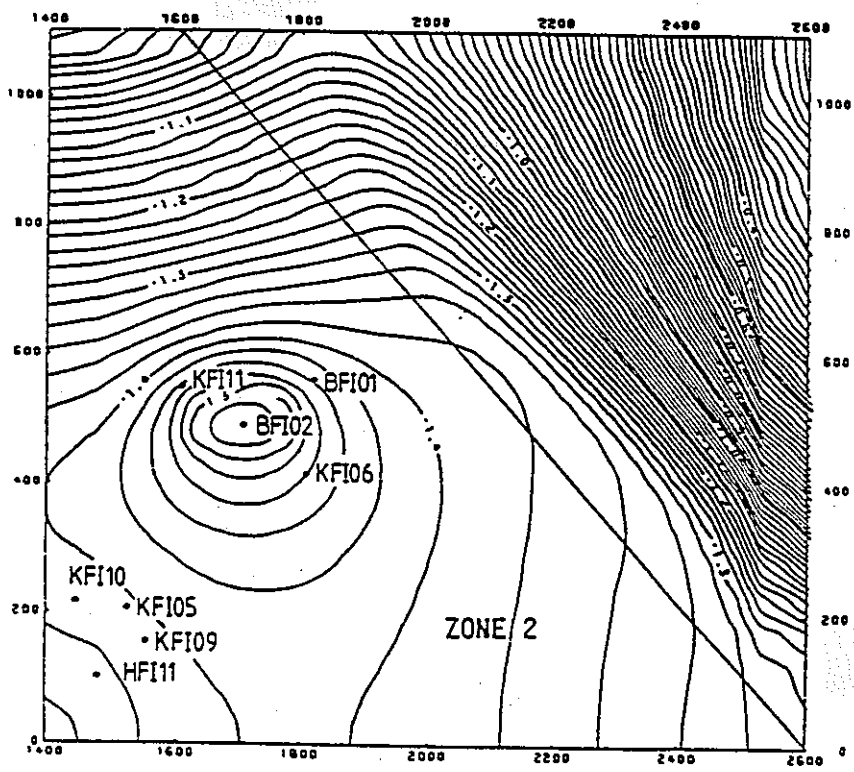


Figure 4.2 Predicted steady state hydraulic head distribution for the region of interest for the radially converging tracer test.

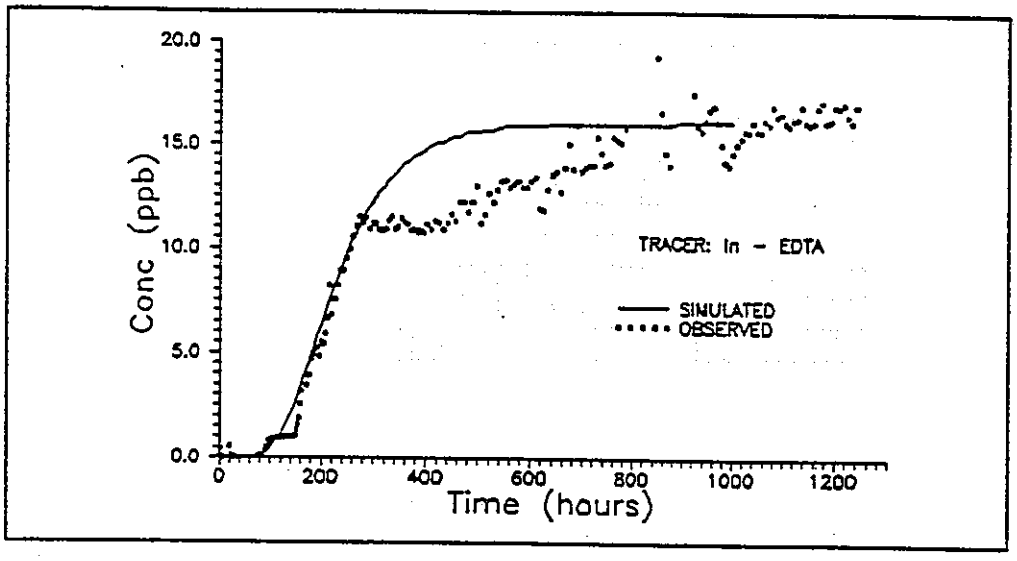


Figure 4.3 Simulated versus observed breakthrough data after adjustment of porosity.

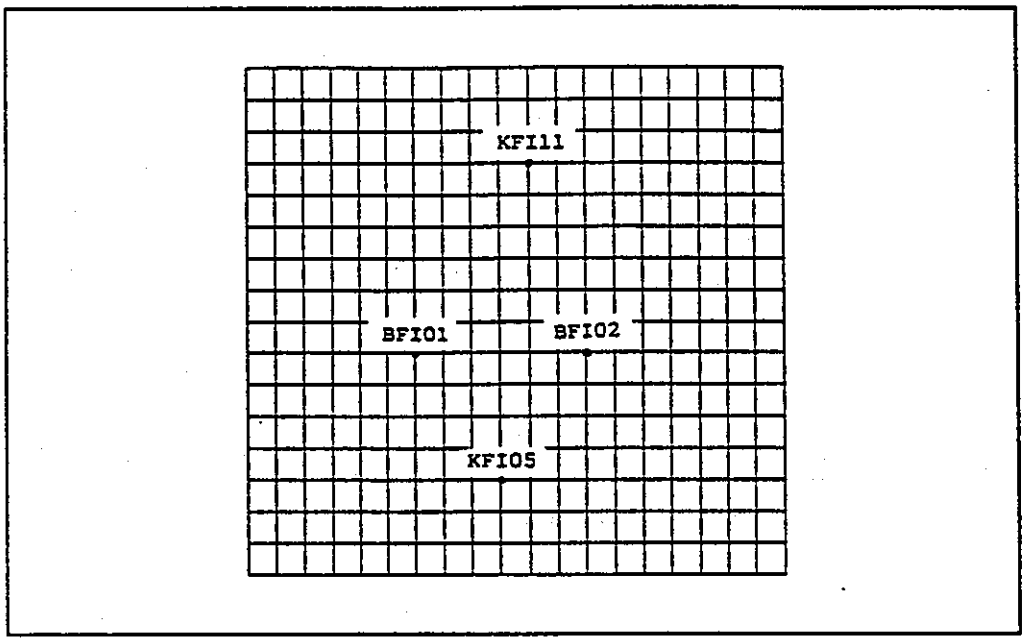


Figure 4.4 Finite element mesh for transport predictions of the dipole test.

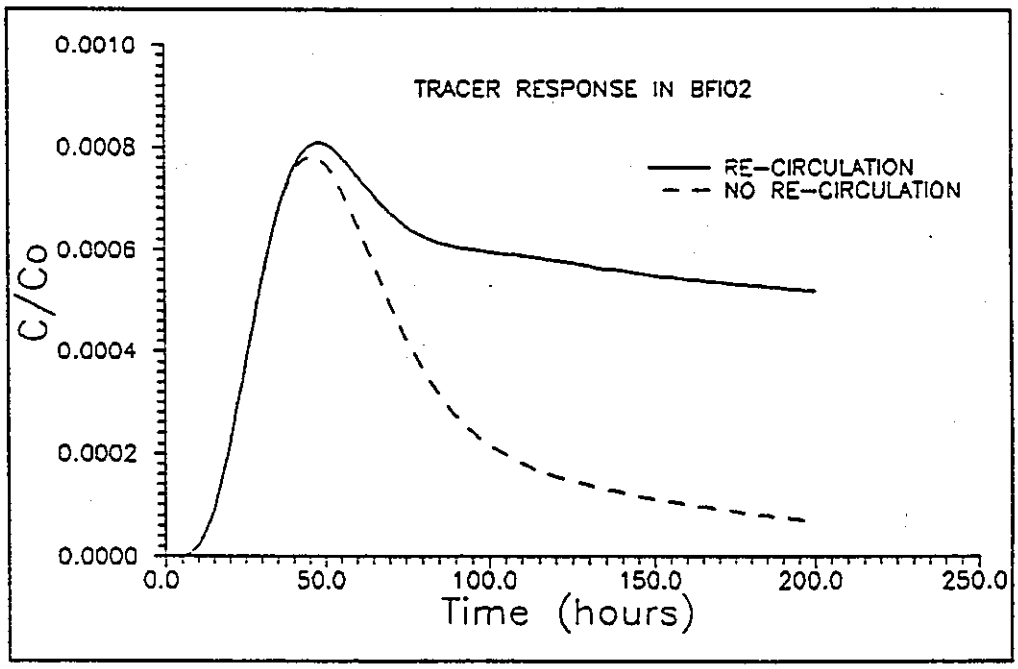


Figure 4.5 Predicted breakthrough curve of a conservative tracer in borehole BFI02. For comparison the results obtained both with and without recirculation are illustrated.

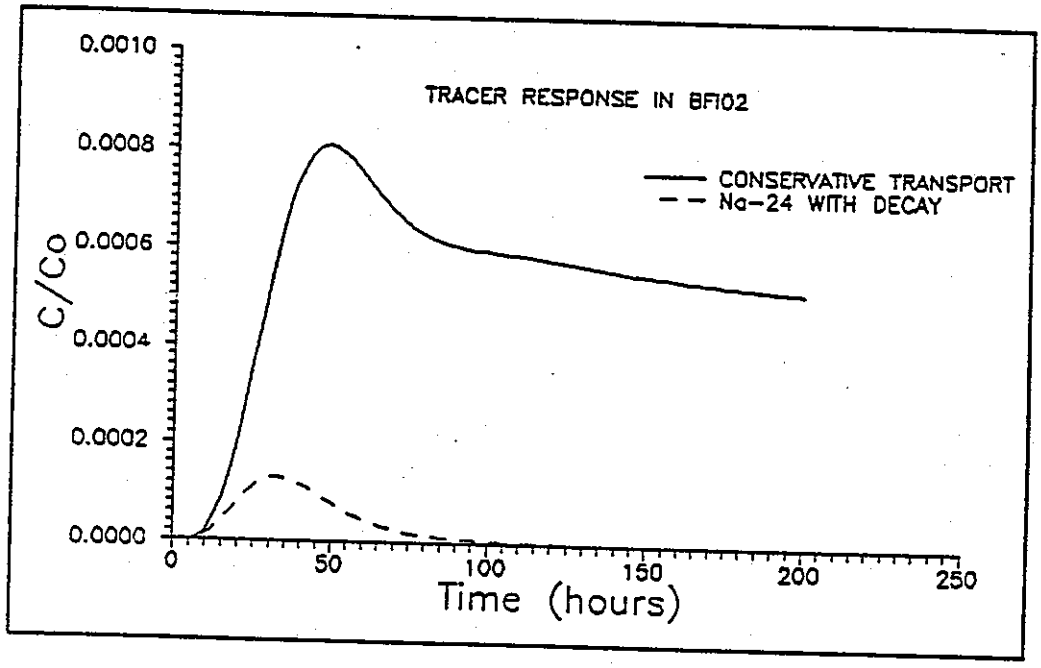


Figure 4.6 Predicted breakthrough curve of ^{24}Na with decay and recirculation.

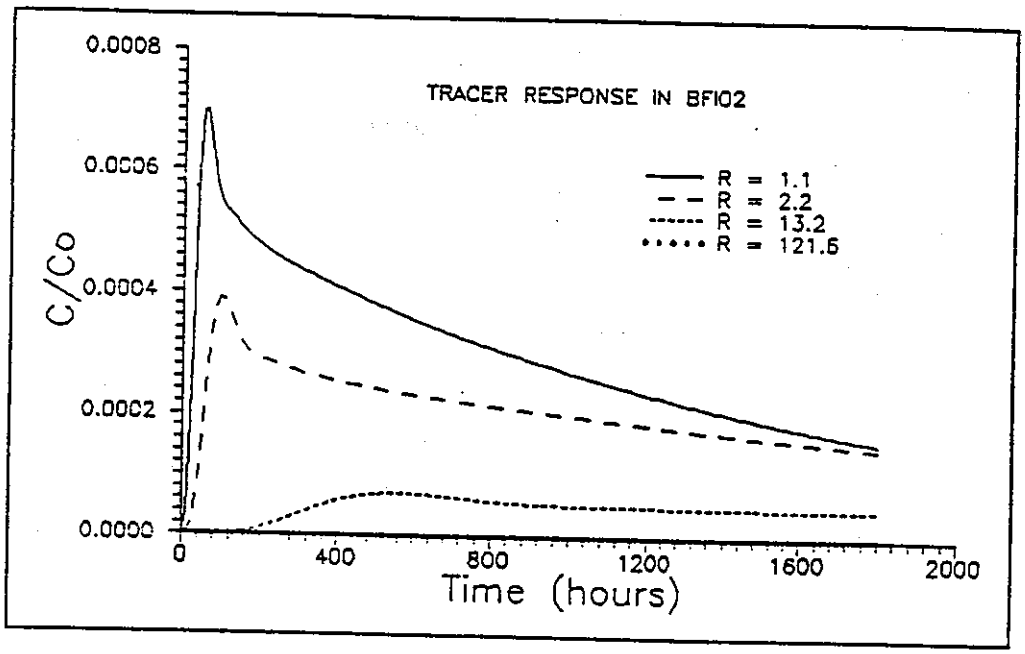


Figure 4.7 Predicted breakthrough curves for a range of R-values.

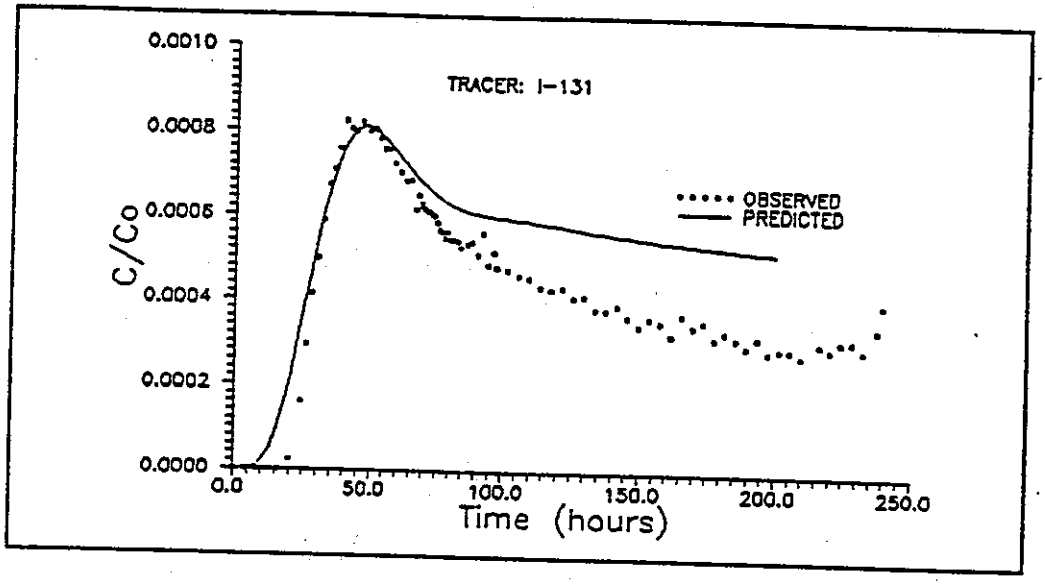


Figure 4.8 Comparison of model predictions and experimental results from the dipole trracer test.

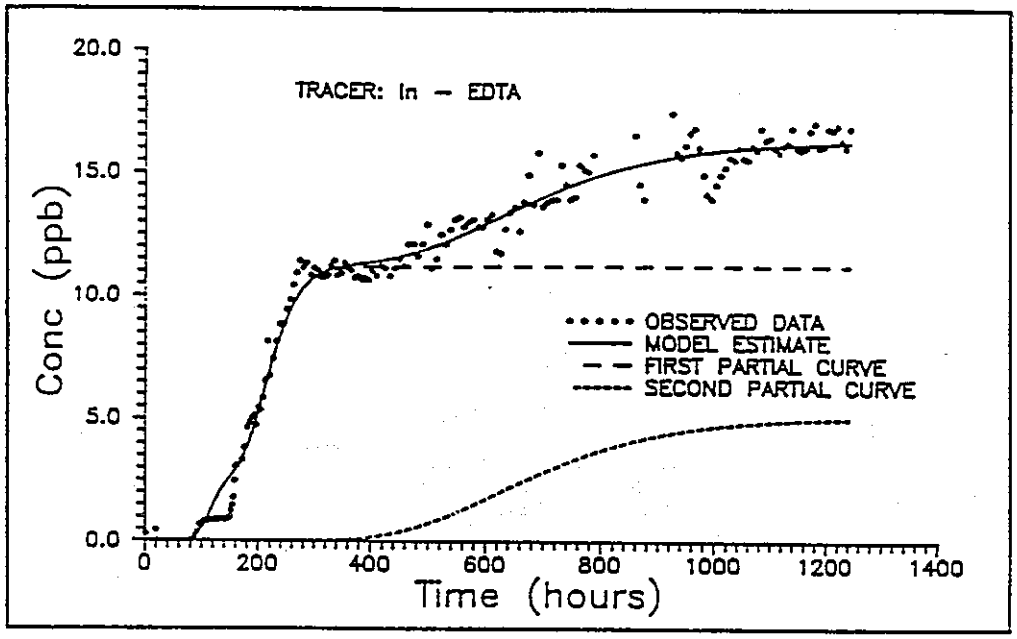


Figure 4.9 Regression estimate for In–EDTA with a two–path model.

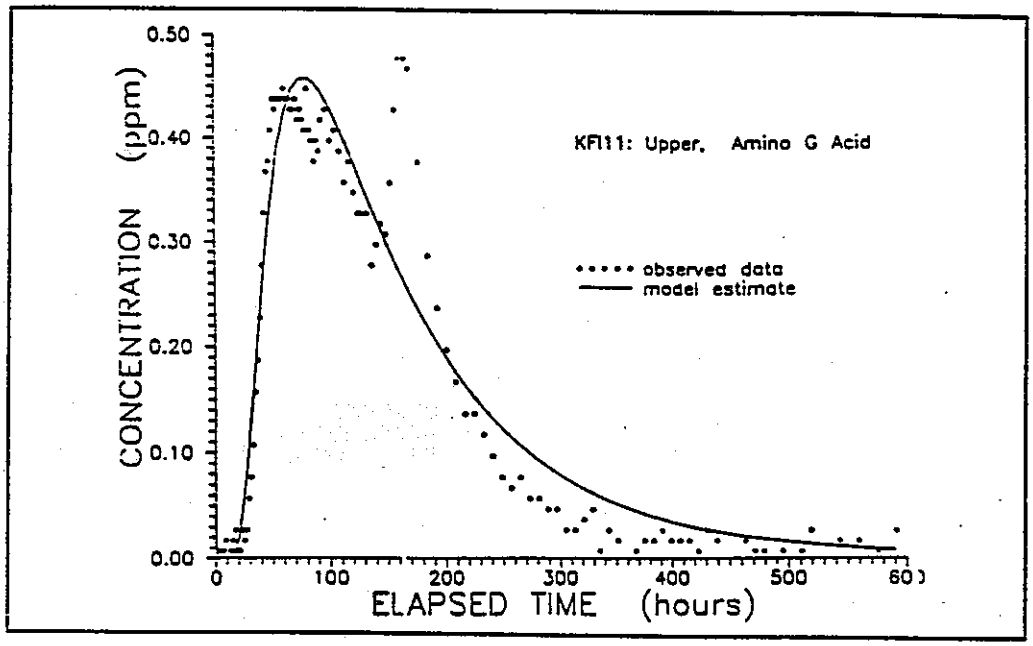


Figure 4.10 Regression estimate for Amino G Acid assuming an instantaneous pulse input.

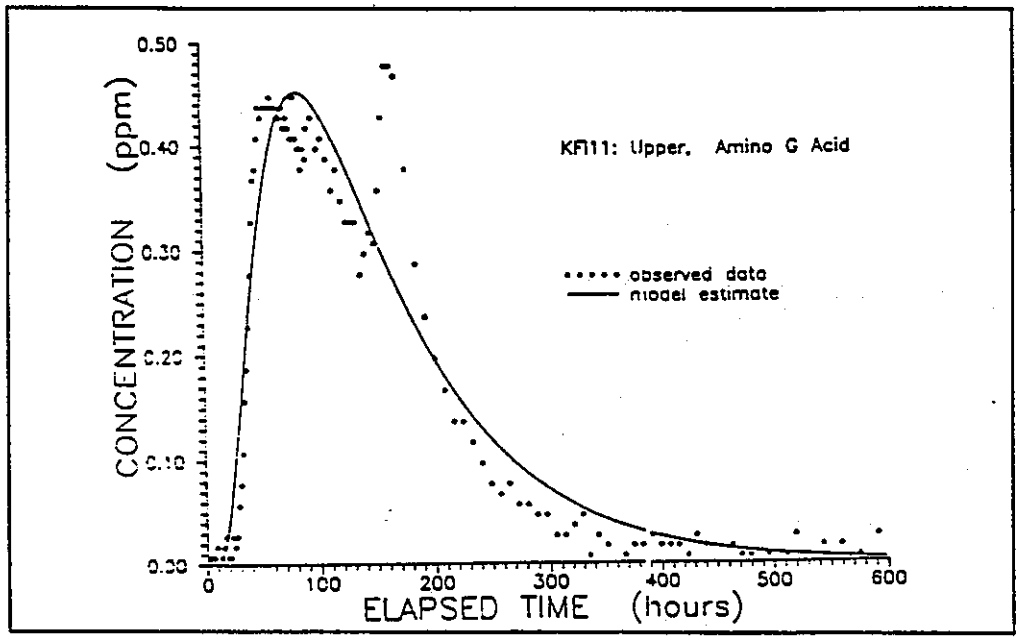


Figure 4.11 Regression estimate for Amono G Acid assuming a decaying pulse injection.

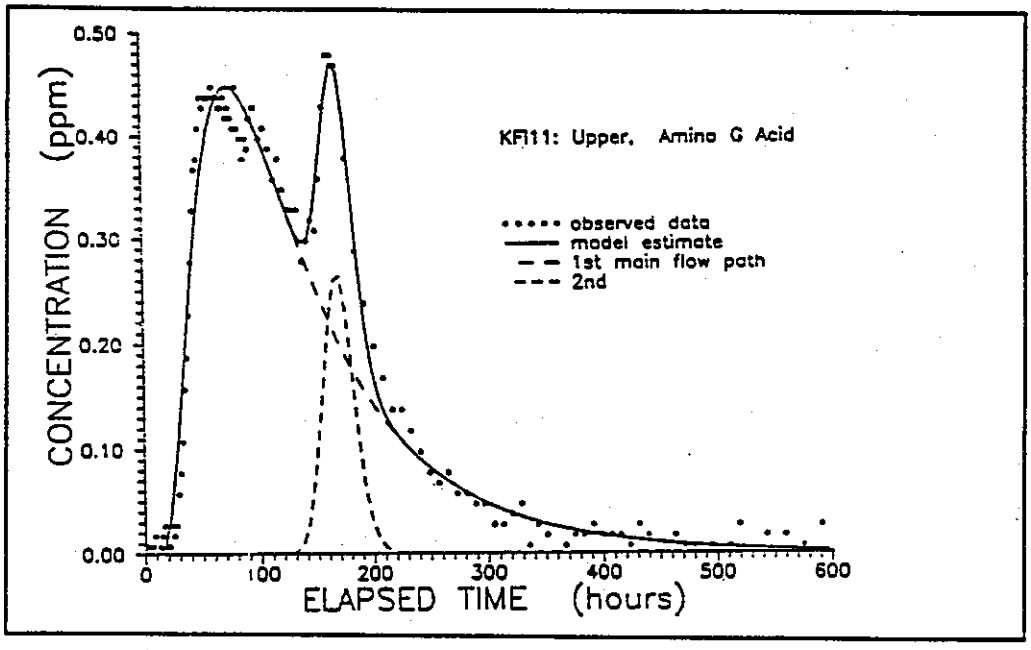


Figure 4.12 Regression estimate for Amino G Acid assuming an instantaneous pulse input and two main flow paths.

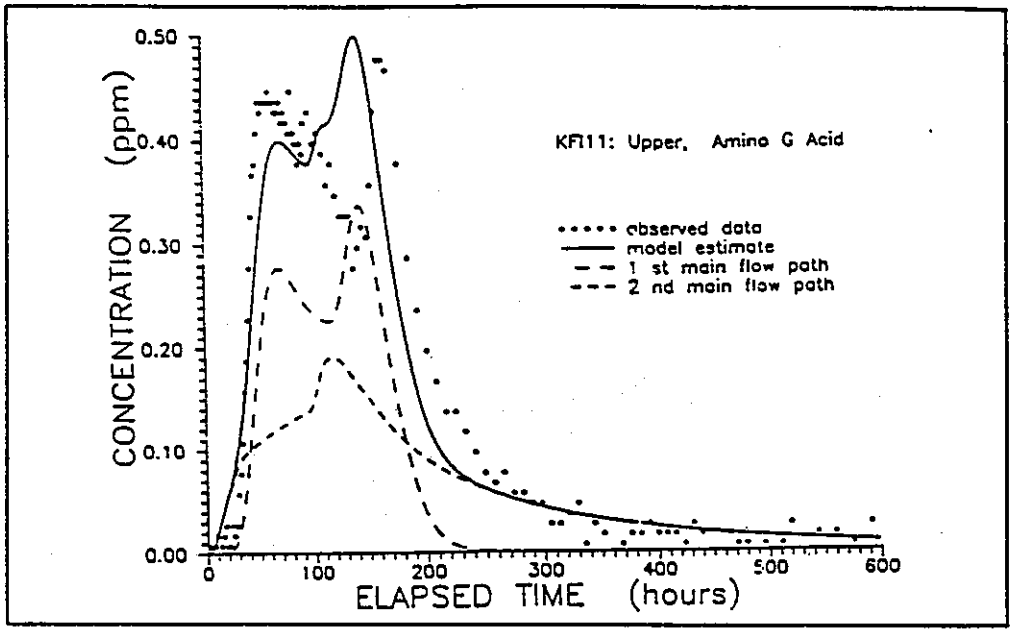


Figure 4.13 Regression estimate for Amino G Acid assuming two flow paths and applying a variable injection scheme, estimated from tracer injection data.

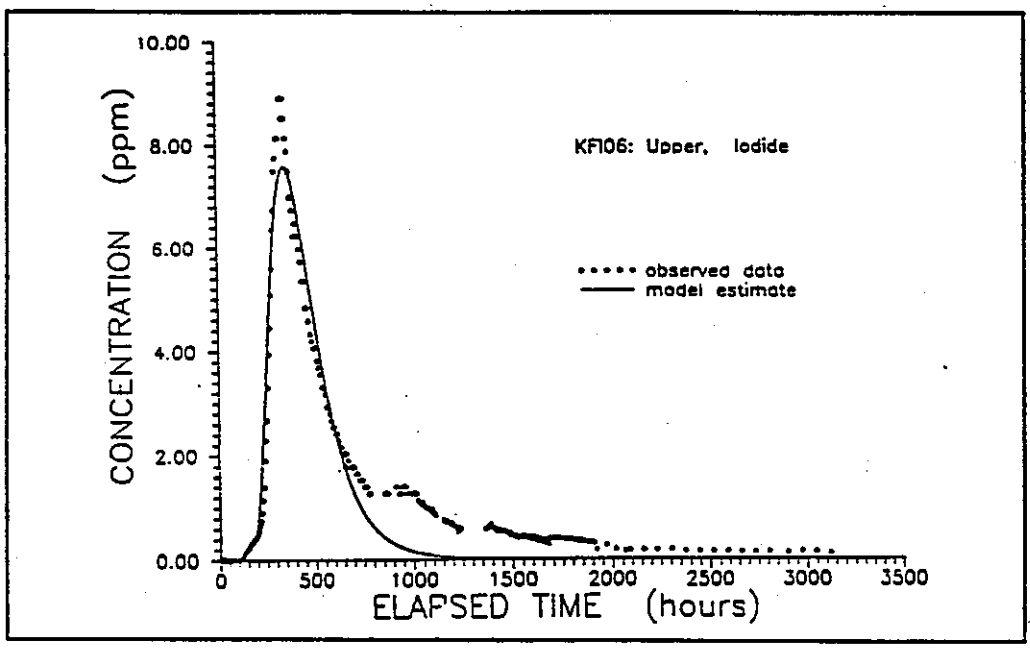


Figure 4.14 Regression estimate for Iodide assuming one major flow path.

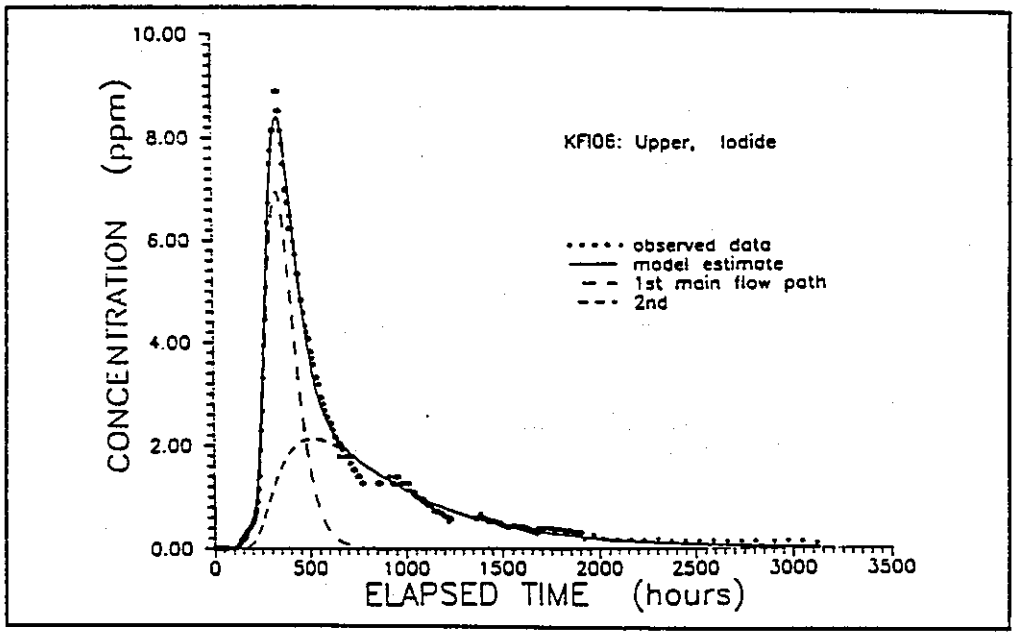


Figure 4.15 Regression estimate for Iodide assuming two major flow paths.

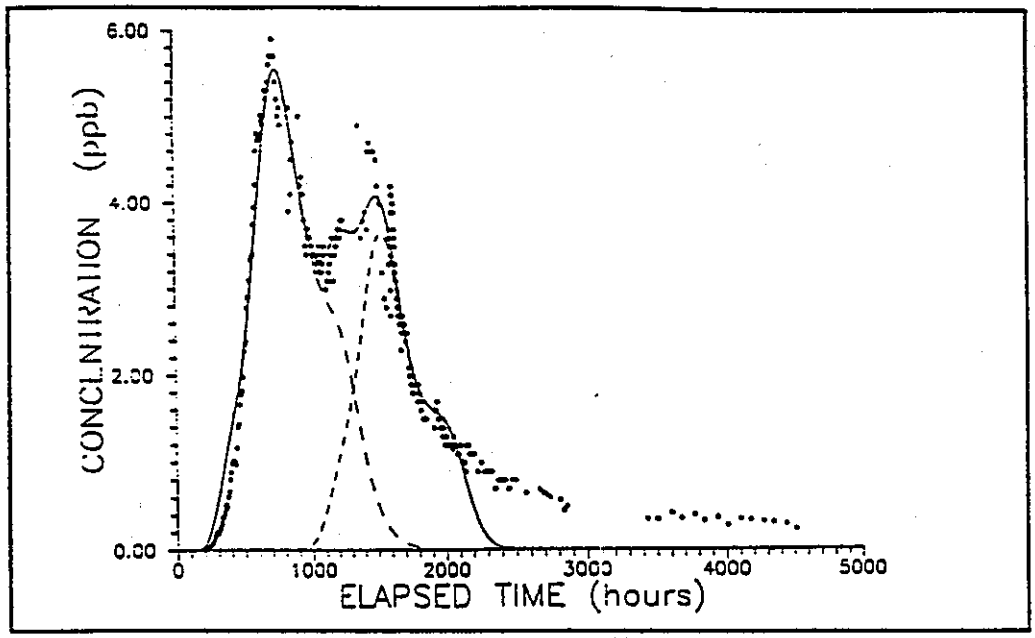


Figure 4.16 Regression estimate for ReO_4 assuming two major flow paths and applying a variable injection scheme.

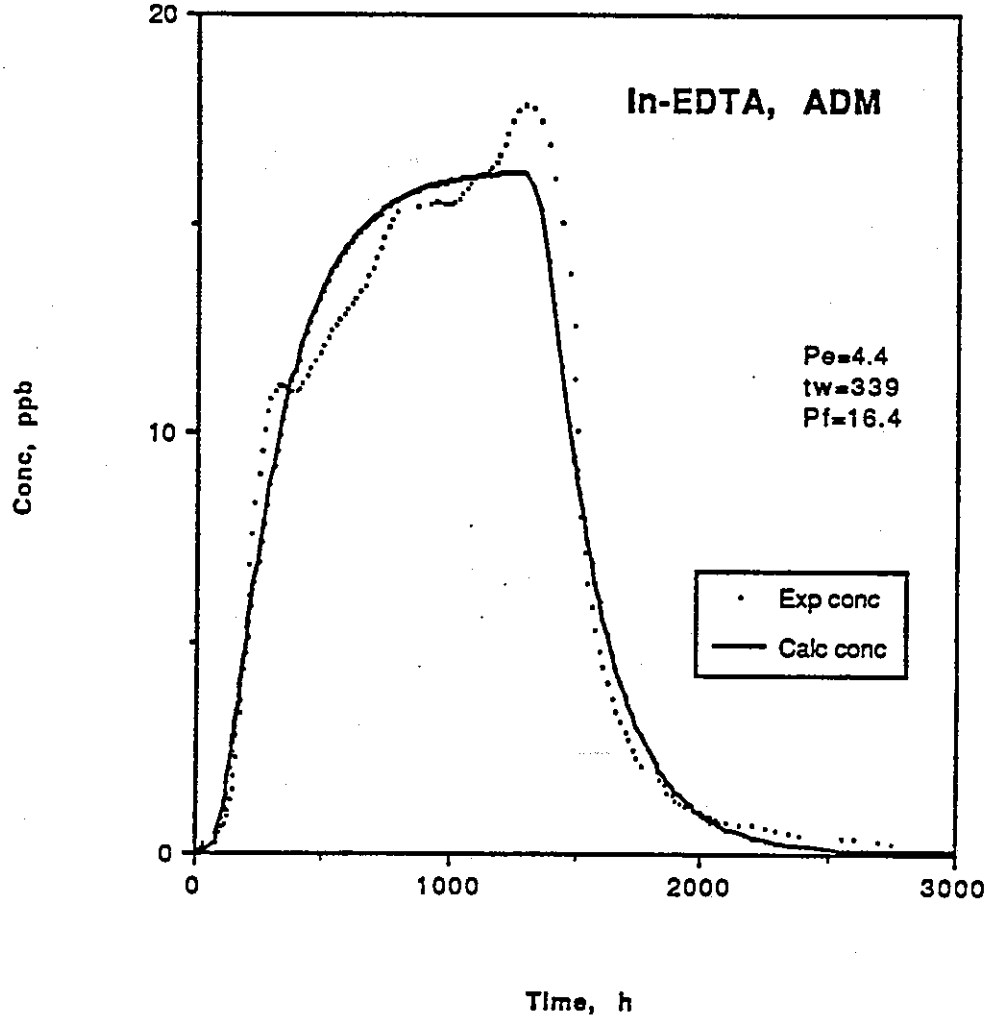


Figure 5.1 Results of fitting with Advection-Dispersion model (ADM) for the tracer In-EDTA.

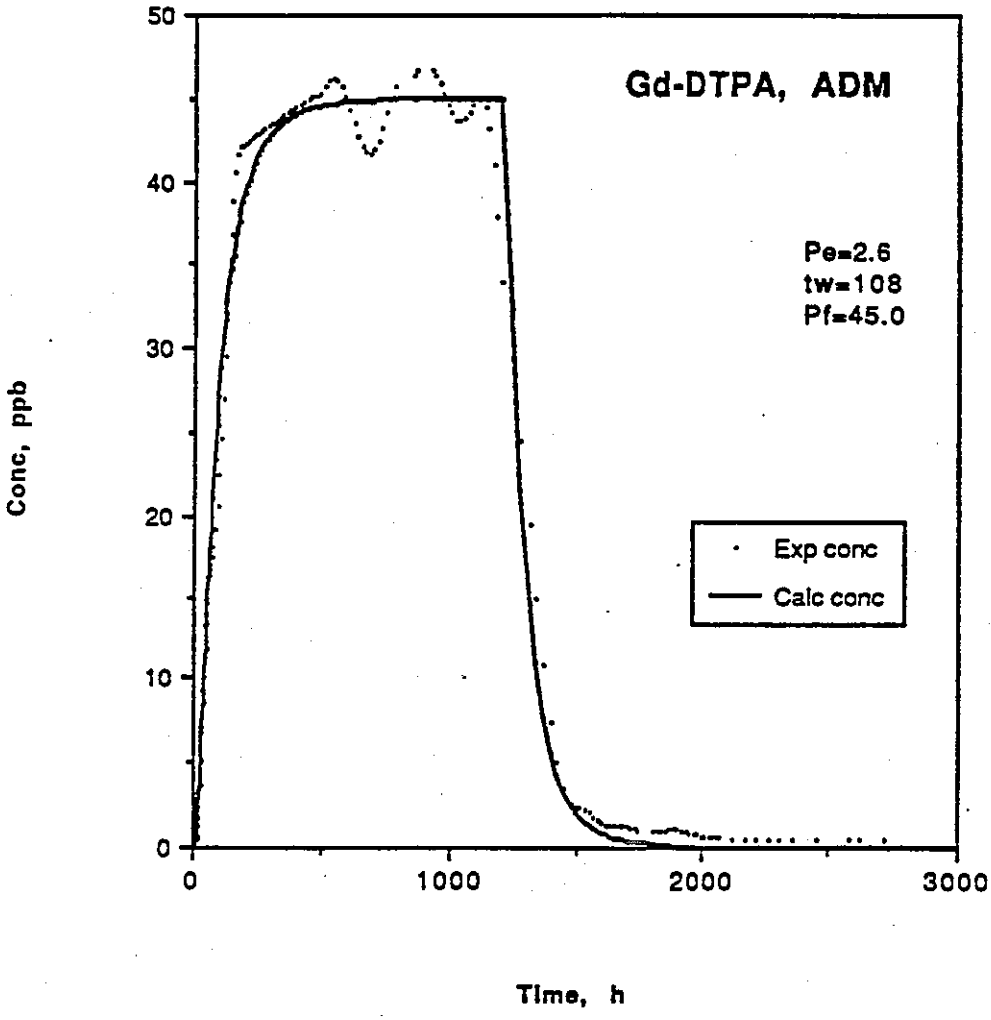


Figure 5.2 Results of fitting with Advection-Dispersion model (ADM) for the tracer Gd-DTPA.

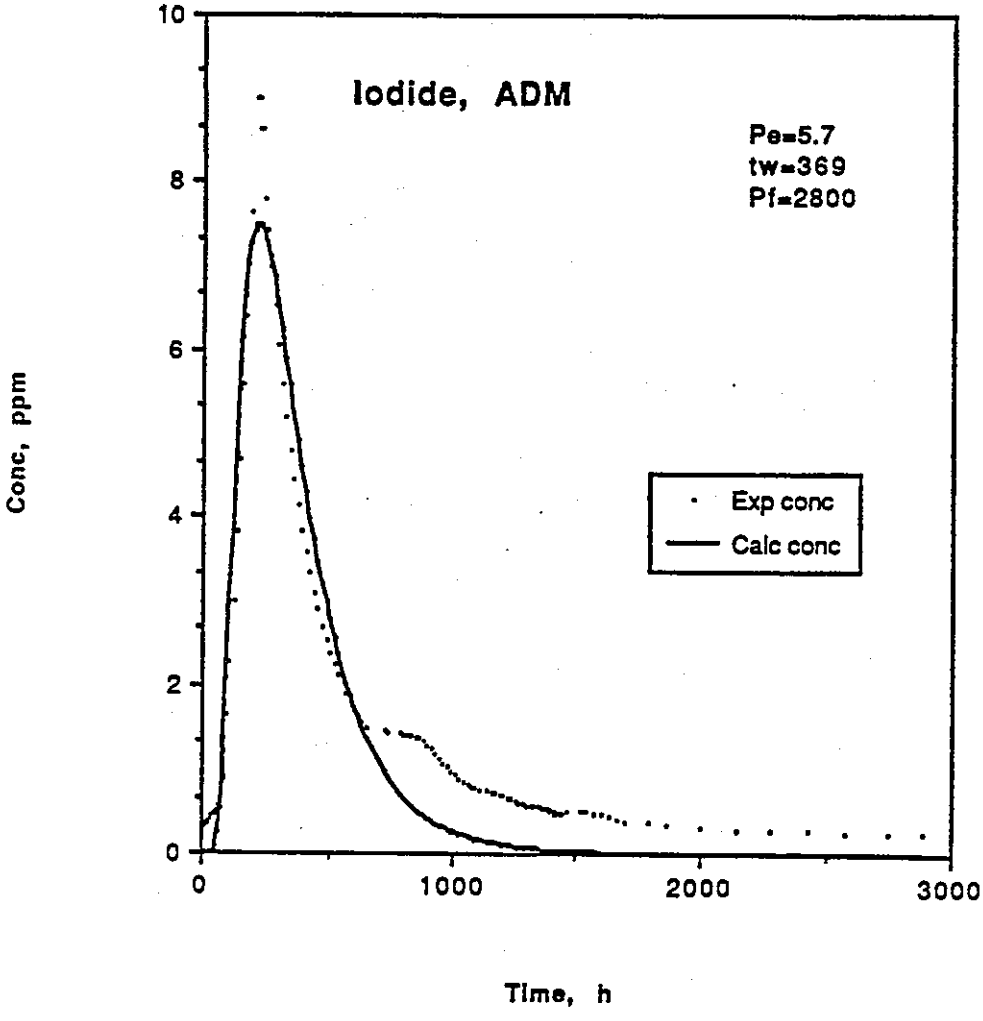


Figure 5.3 Results of fitting with Advection-Dispersion model (ADM) for the tracer Iodide.

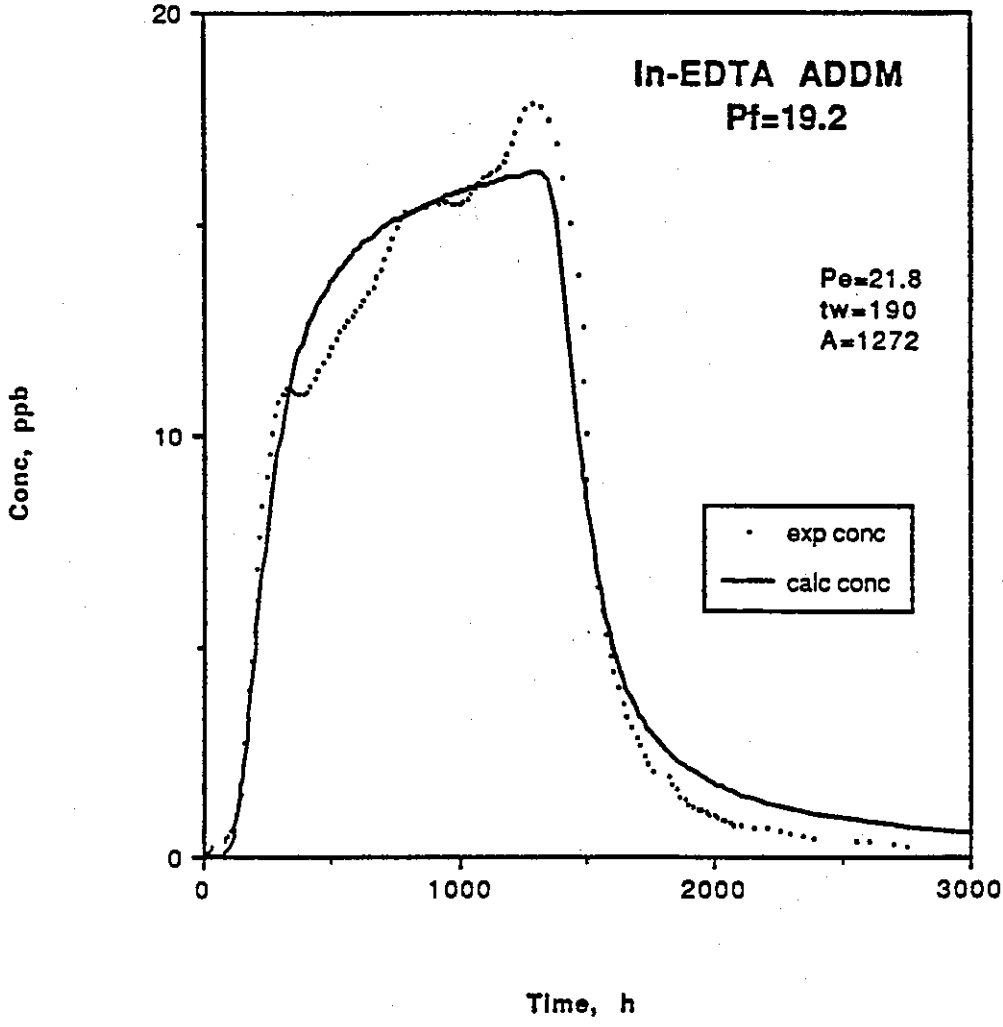


Figure 5.4 Results of fitting with Advection-Dispersion-Matrix Diffusion model (ADDM) for the tracer In-EDTA. Pf calculated from experimental data.

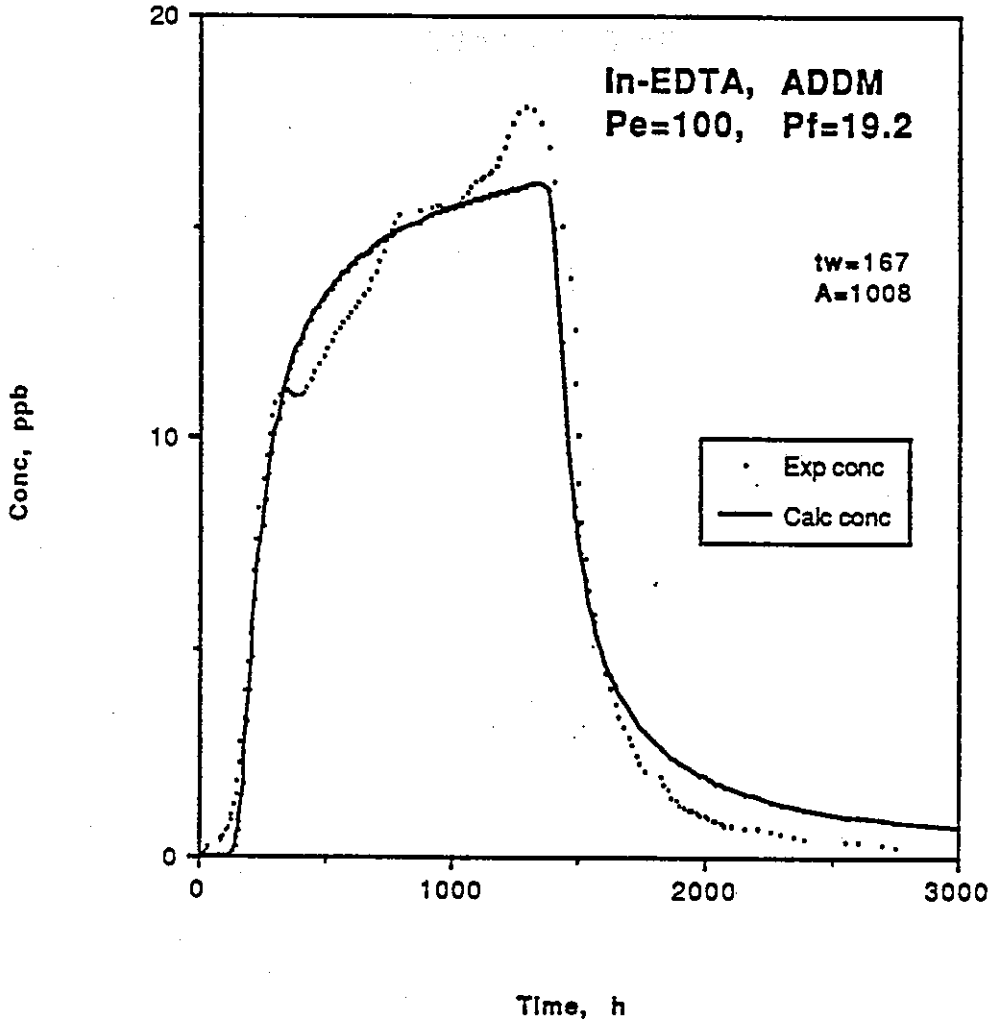


Figure 5.5 Results of fitting with Advection-Dispersion-Matrix Diffusion model (ADDM) for the tracer In-EDTA. Pf calculated from experimental data and Pe assumed to be 100 (low dispersion).

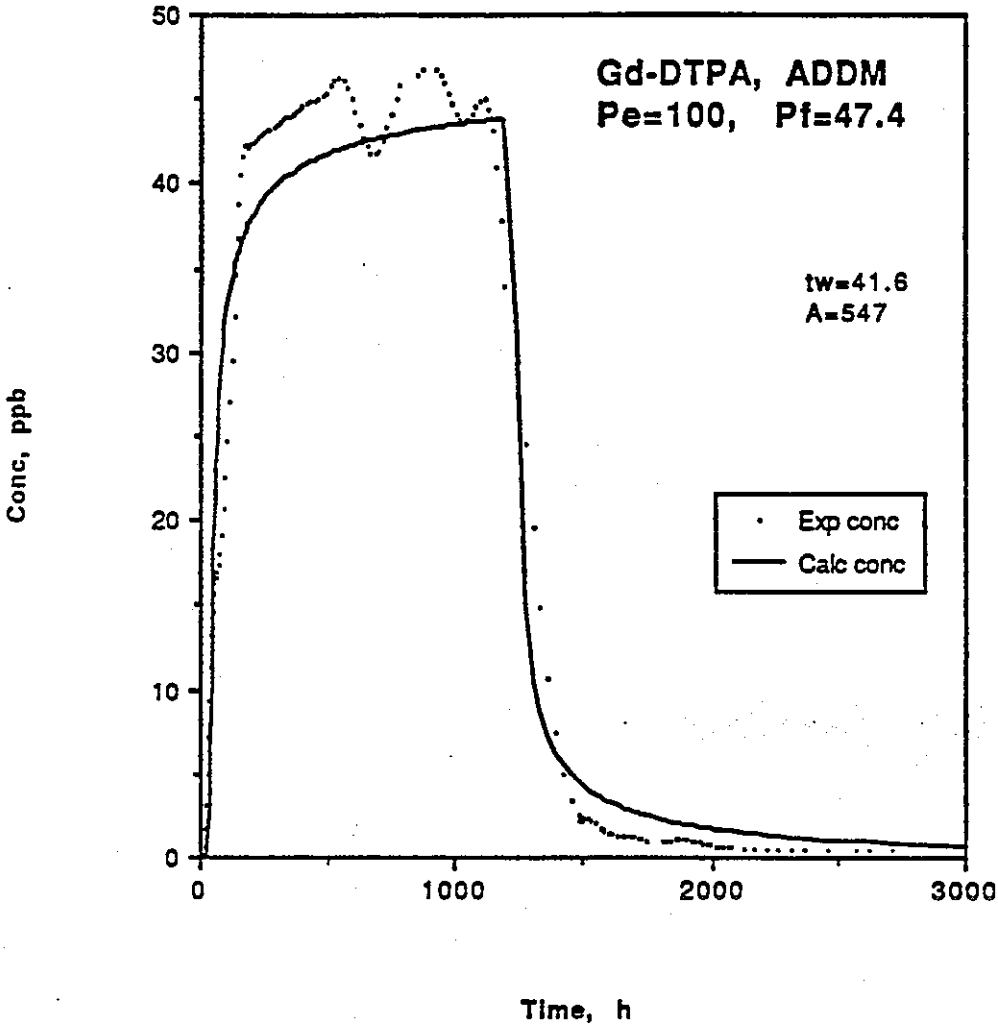


Figure 5.6 Results of fitting with Advection-Dispersion-Matrix Diffusion model (ADDM) for the tracer Gd-DTPA. Pf calculated from experimental data and Pe assumed to be 100 (low dispersion).

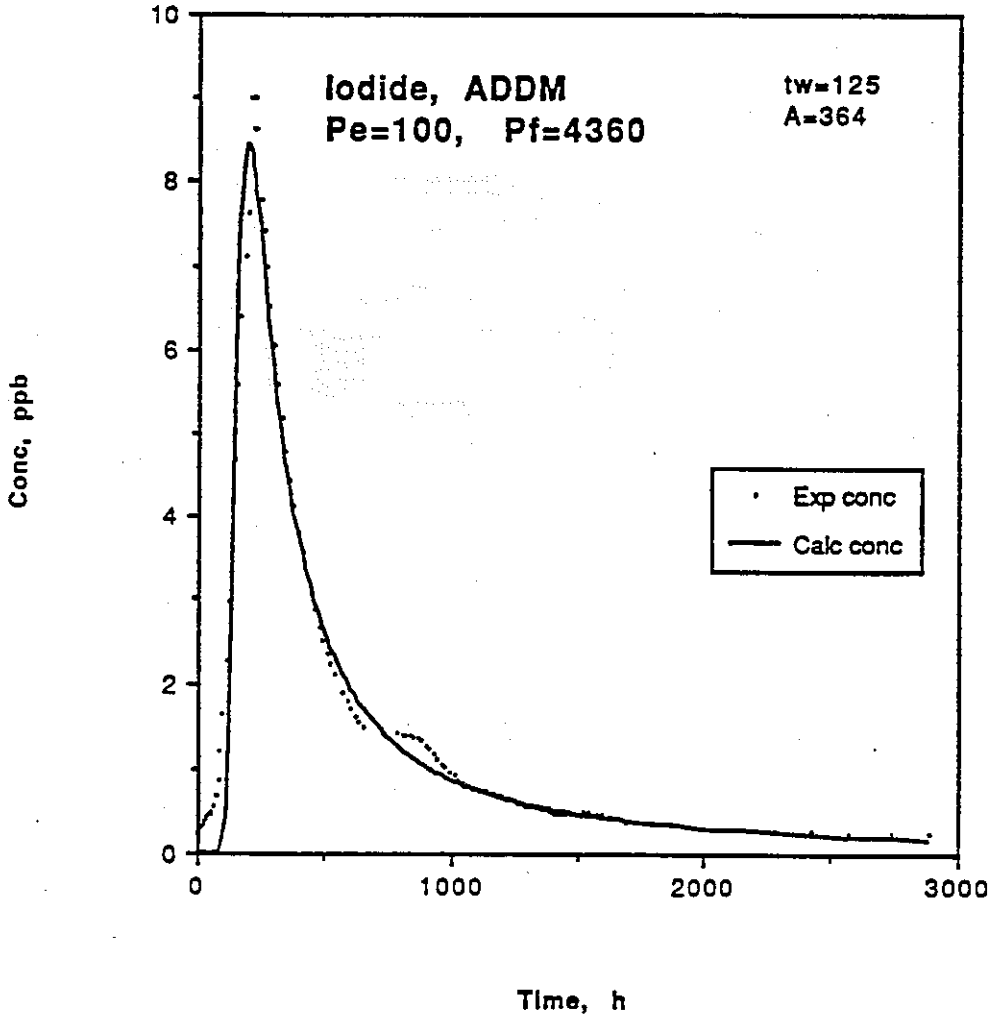


Figure 5.7 Results of fitting with Advection-Dispersion-Matrix Diffusion model (ADDM) for the tracer Iodide. Pf calculated from experimental data and Pe assumed to be 100 (low dispersion).

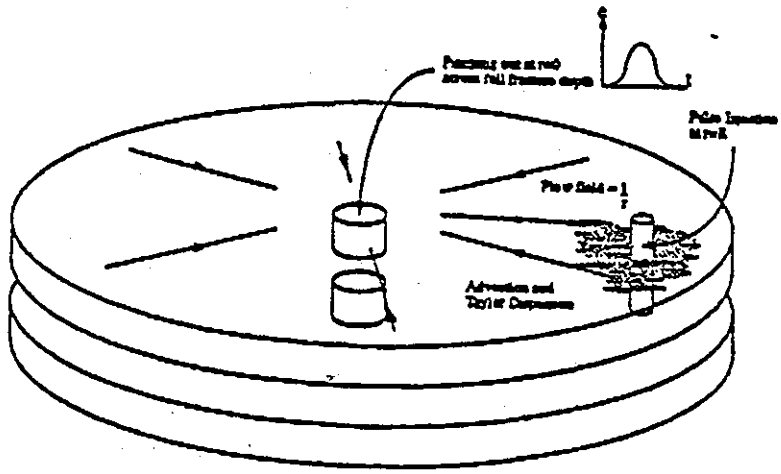


Figure 6.1 The fracture zone.

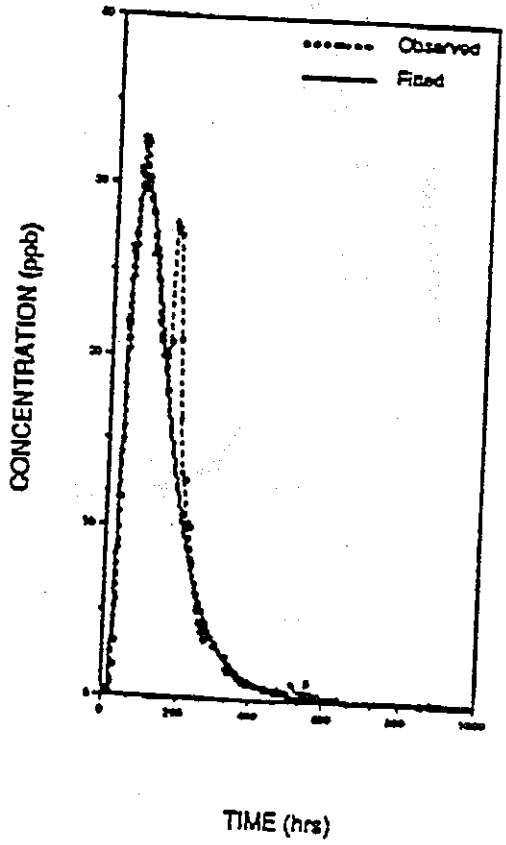


Figure 6.2 Pulse breakthrough for tracer Tm-EDTA, borehole KFI11.

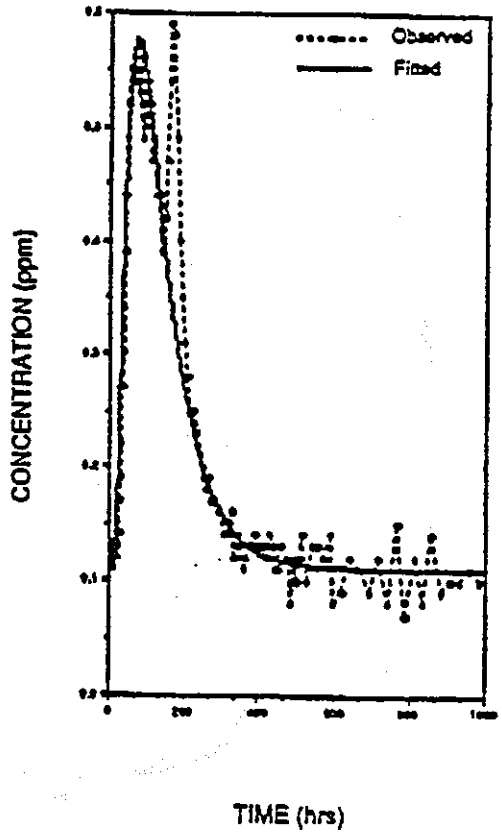


Figure 6.3 Pulse breakthrough for tracer Amino G Acid, borehole KFI11.

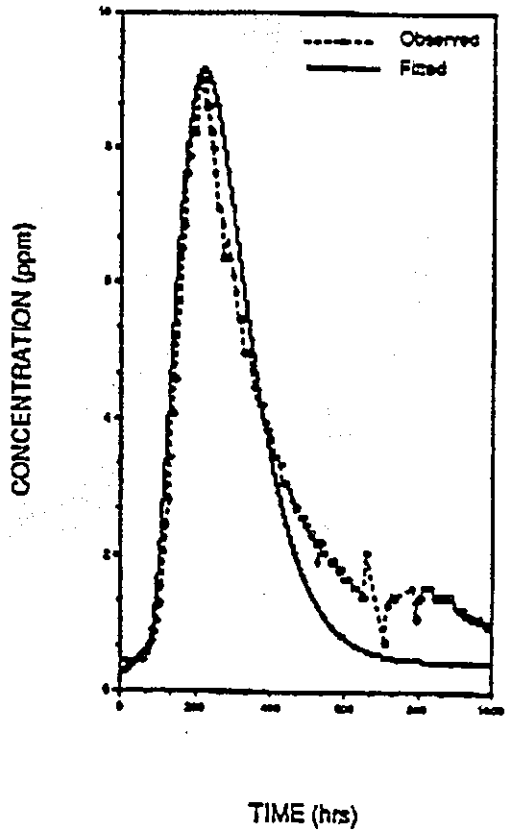


Figure 6.4 Pulse breakthrough for tracer iodide, borehole KFI06.

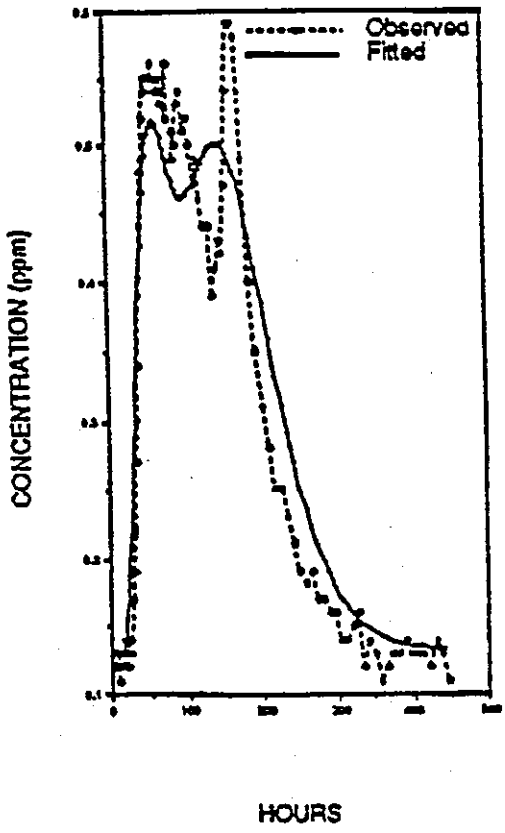


Figure 6.5 Borehole KFI11, tracer Amino G Acid.

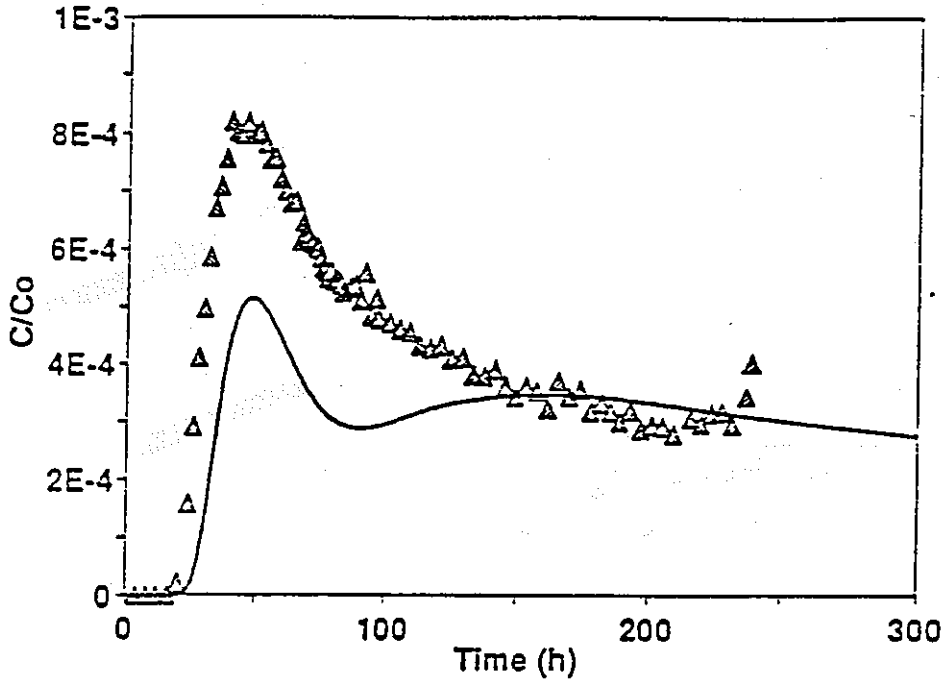


Figure 7.1 Comparison of the predicted breakthrough curve with a measured curve (I-131, A.3). The predicted curve is calculated using four transport routes in 90 degree angles. The side routes are identical and there is no flow to the 180 degree route. Recirculation and a loss of 25% per cycle is taken into account. Figure 2. The applied conceptual model for the dipole experiment with three flow routes having different relative flow rates than in the predicted ideal case. The losses per cycle are taken to be 35%. The flow routes are modeled to go via or very near the observation boreholes and only a small fraction of the modeled flows are sampled actually in the observation boreholes.

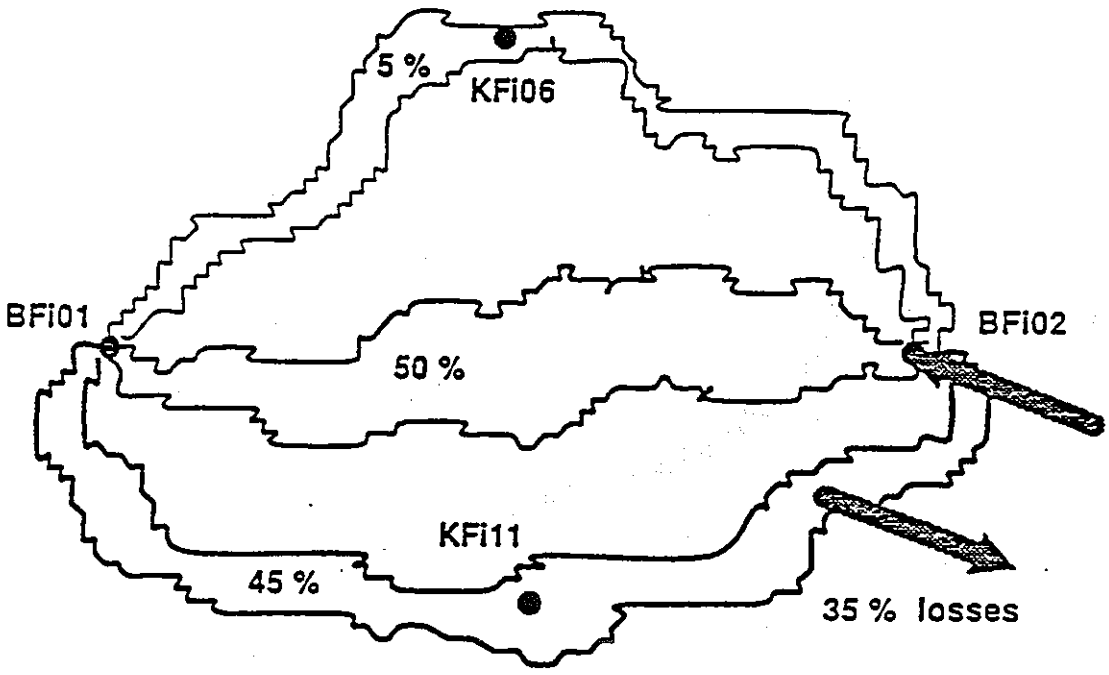


Figure 7.2 The applied conceptual model for the dipole experiment with three flow routes having different relative flow rates than in the predicted ideal case. The losses per cycle are taken to be 35%. The flow routes are modeled to go via or very near the observation boreholes and only a small fraction of the modeled flows are sampled actually in the observation boreholes.

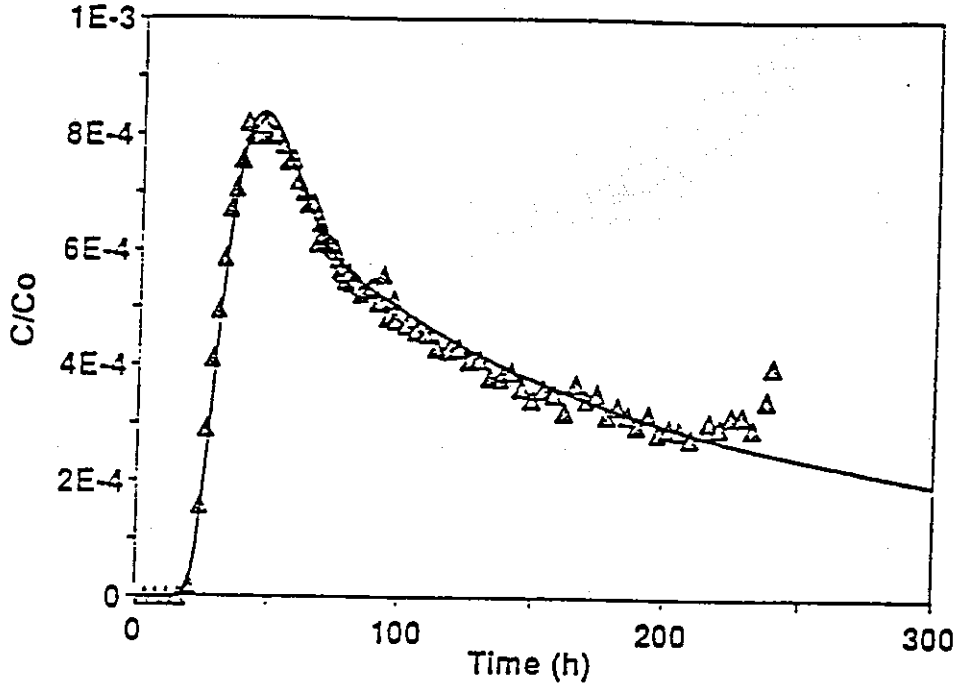


Figure 7.3 Comparison of the calculated breakthrough curve with a measured curve (A.3). The used concept is shown in Fig. 2 and model parameters are presented in Table 1.

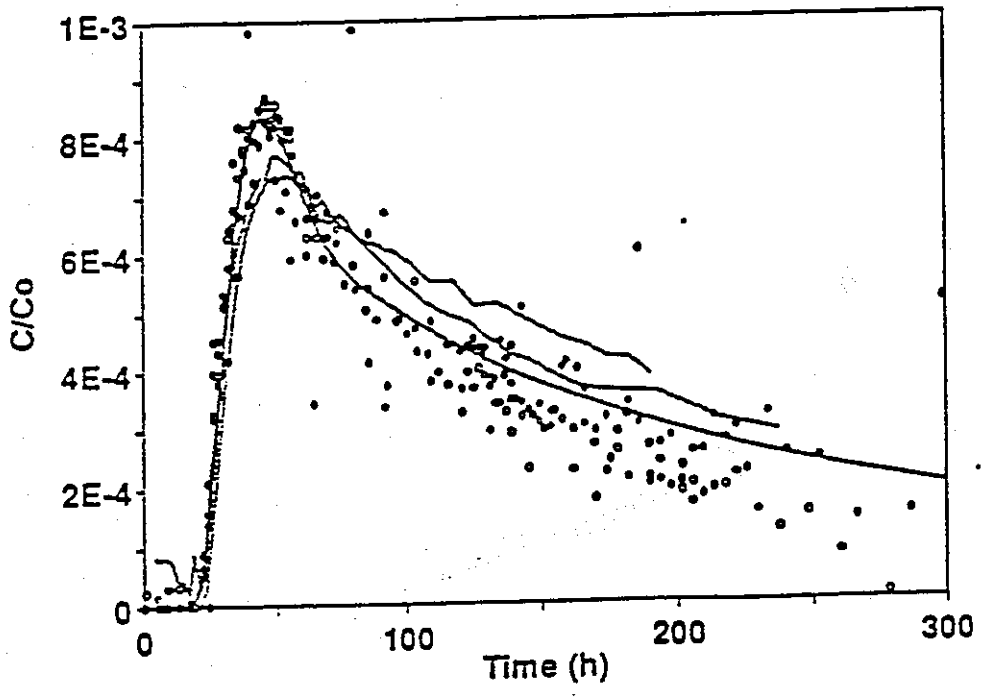


Figure 7.4 Comparison of the breakthrough curves of different tracers and the calculated curve. The smooth line is the calculated curve and wiggling lines are Rhodamine WT data (A.14 and A.18). All other data are presented as points (A.3, A.4, A.5, A.6, A.12, A.16 and A.17) but normalized roughly to the peak concentration value of I-131 (A.3) by factors 1.1 - 2.0. The Rhodamine WT curves show a somewhat different shape which could be explained within the used model surprisingly by a higher molecular diffusion coefficient (a higher dispersion and slower arrival of the front edge and perhaps a faster arrival of the tail).

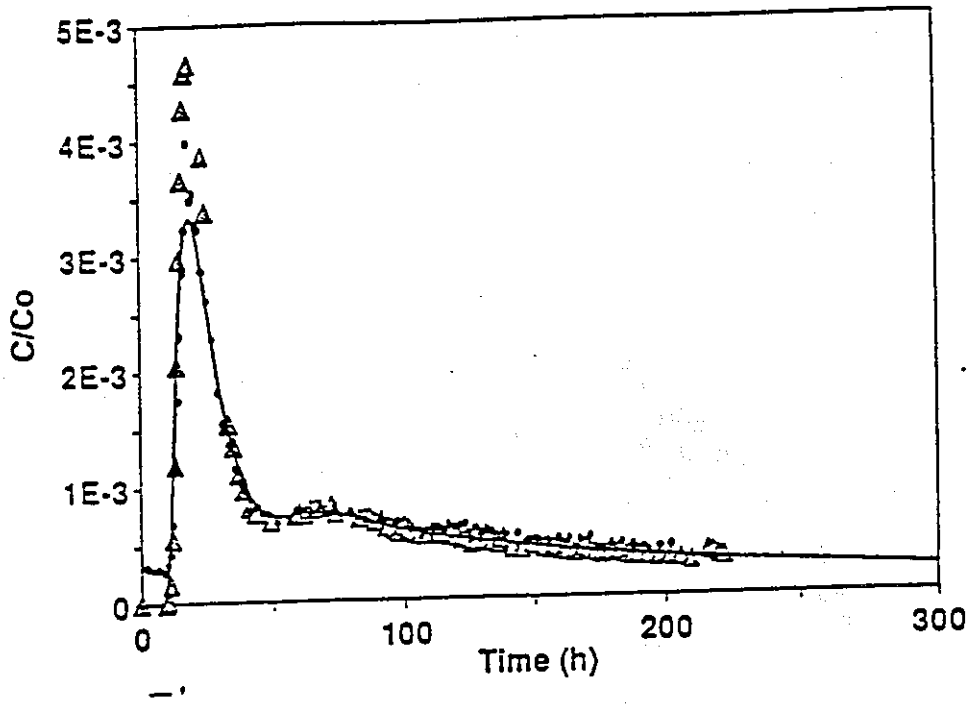


Figure 7.5 Modeled and measured breakthrough curves (I-131 B.3 and Br-82 B.6) in the observation borehole KFi11. The too low peak value of the modeled concentration may be due to the very convective nature of the fast transport which cannot be modeled very accurately at short times.

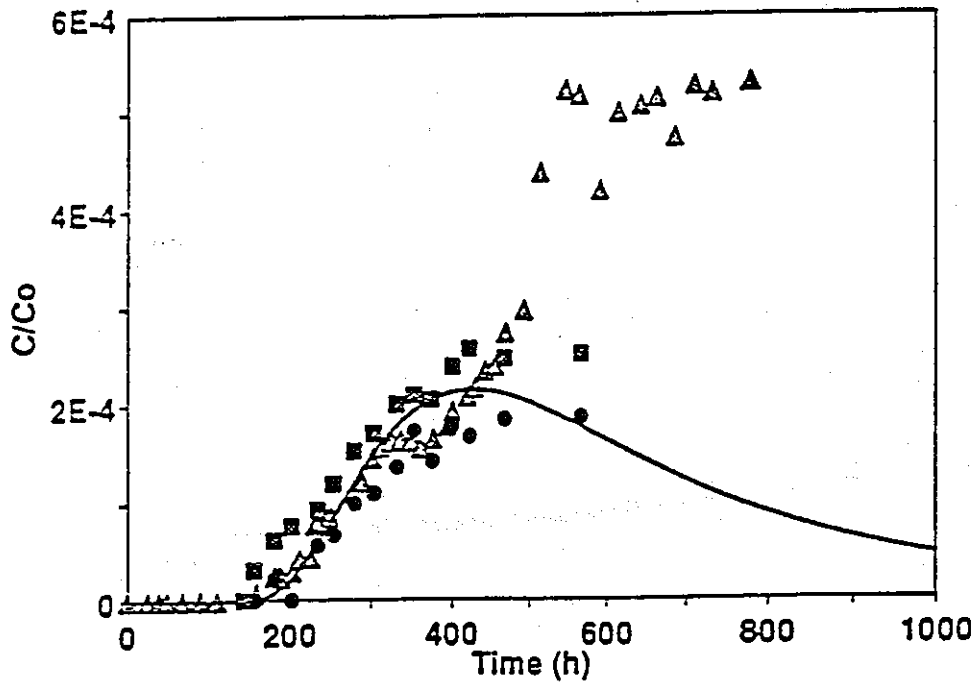


Figure 7.6 Modeled and measured breakthrough curves (I-131 C.1, Cr-51 C.2 and Yb-169 C.4) in the observation borehole KFi06. The calculated curve is normalized by a factor of 0.5 and the Cr- and Yb-EDTA complex values by a factor of 2 in order to compare the curve shapes better. A second injection 216 h later causes the rise of the I-131 concentration values after 400 h.

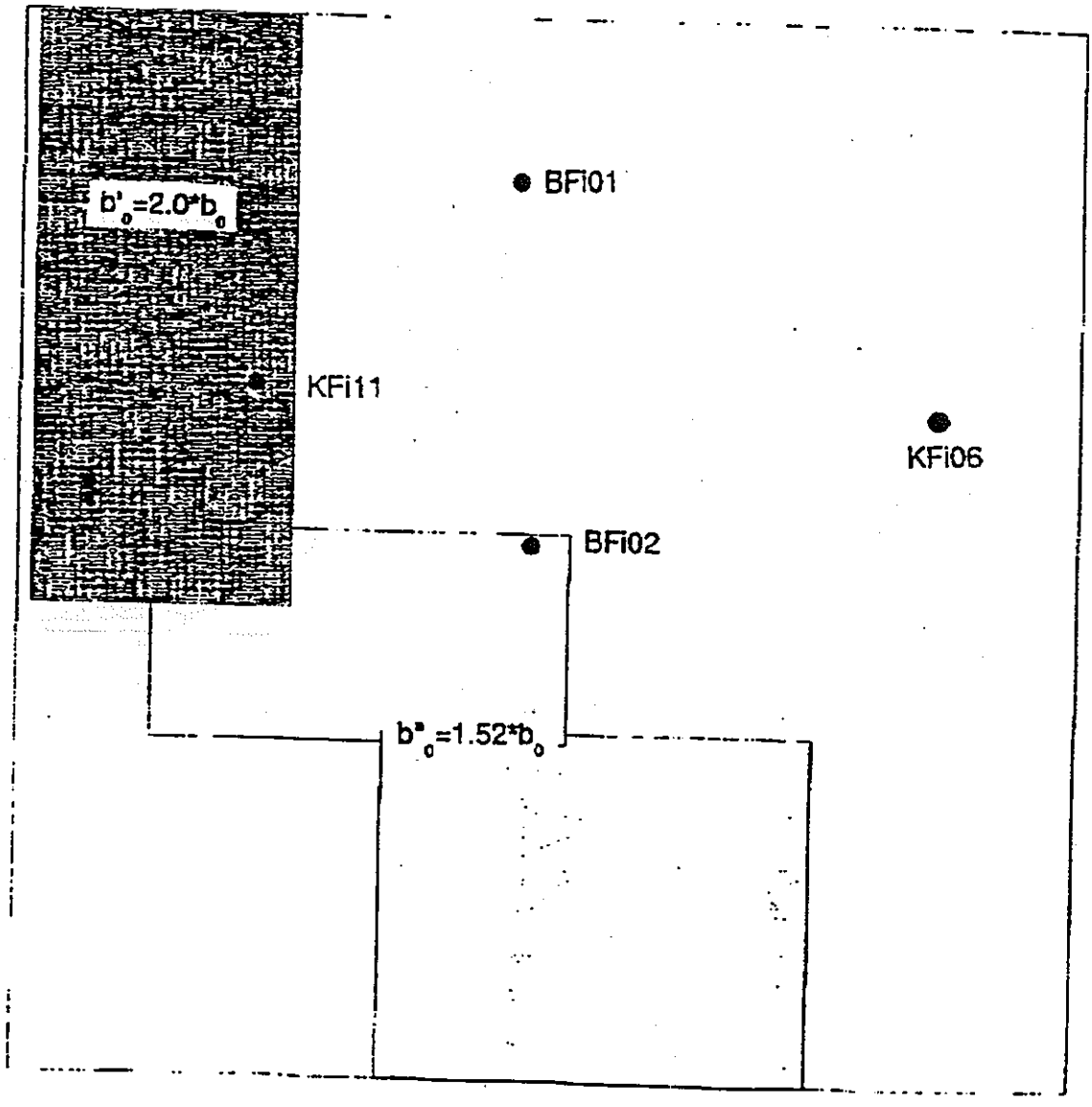
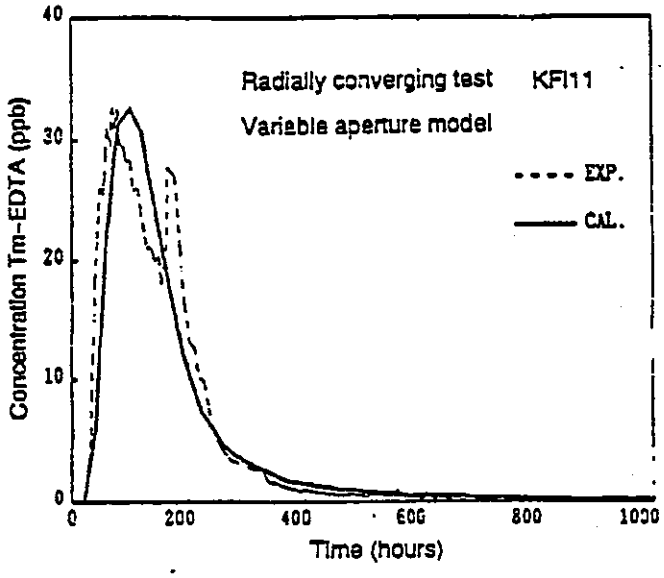
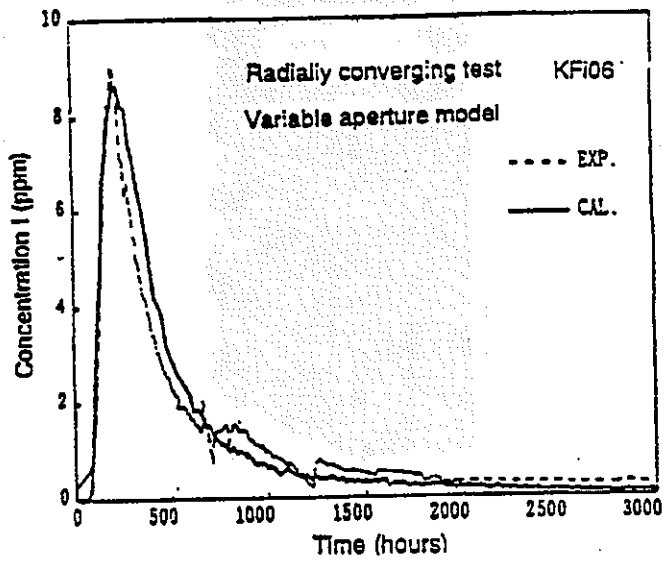


Figure 8.1


Radially converging test KFI11
Variable aperture model
EXP.
CAL.
Concentration Tm-EDTA (ppb)
Time (hours)
0
10
20
30
40
200
400
600
800
1000


Radially converging test KFi06
Variable aperture model
EXP.
CAL.
Concentration I (ppm)
Time (hours)
0
2
4
6
8
10
500
1000
1500
2000
2500
3000

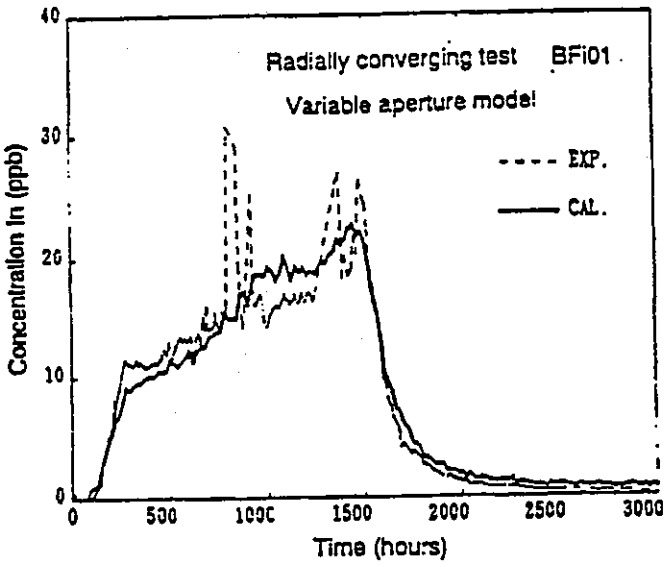

Radially converging test BFi01
Variable aperture model
EXP.
CAL.
Concentration In (ppb)
Time (hours)
0
10
20
30
40
500
1000
1500
2000
2500
3000

Figure 8.2

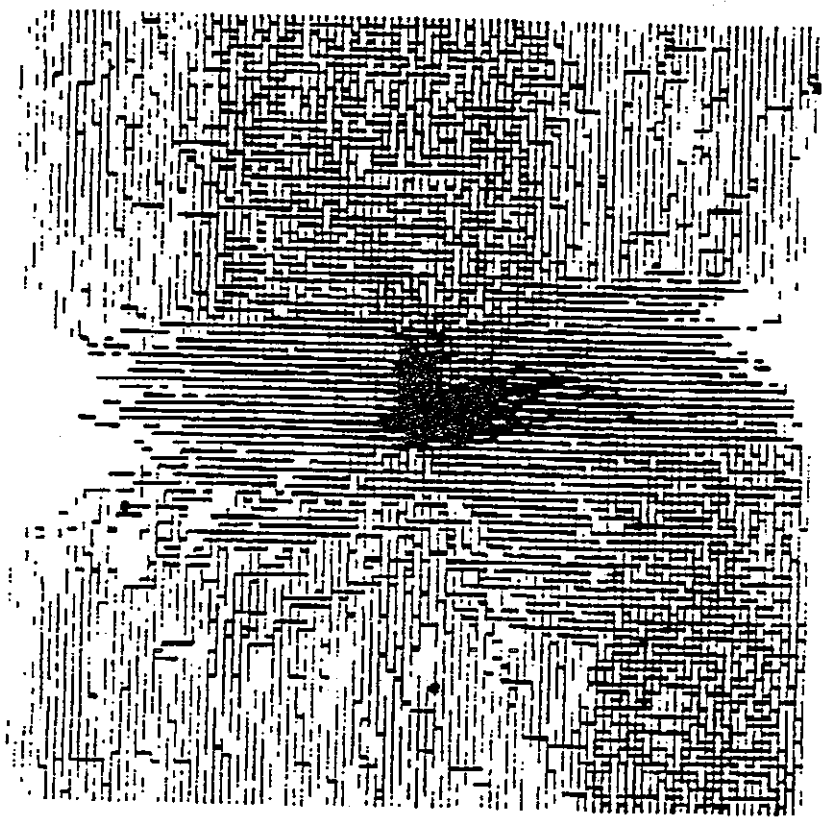
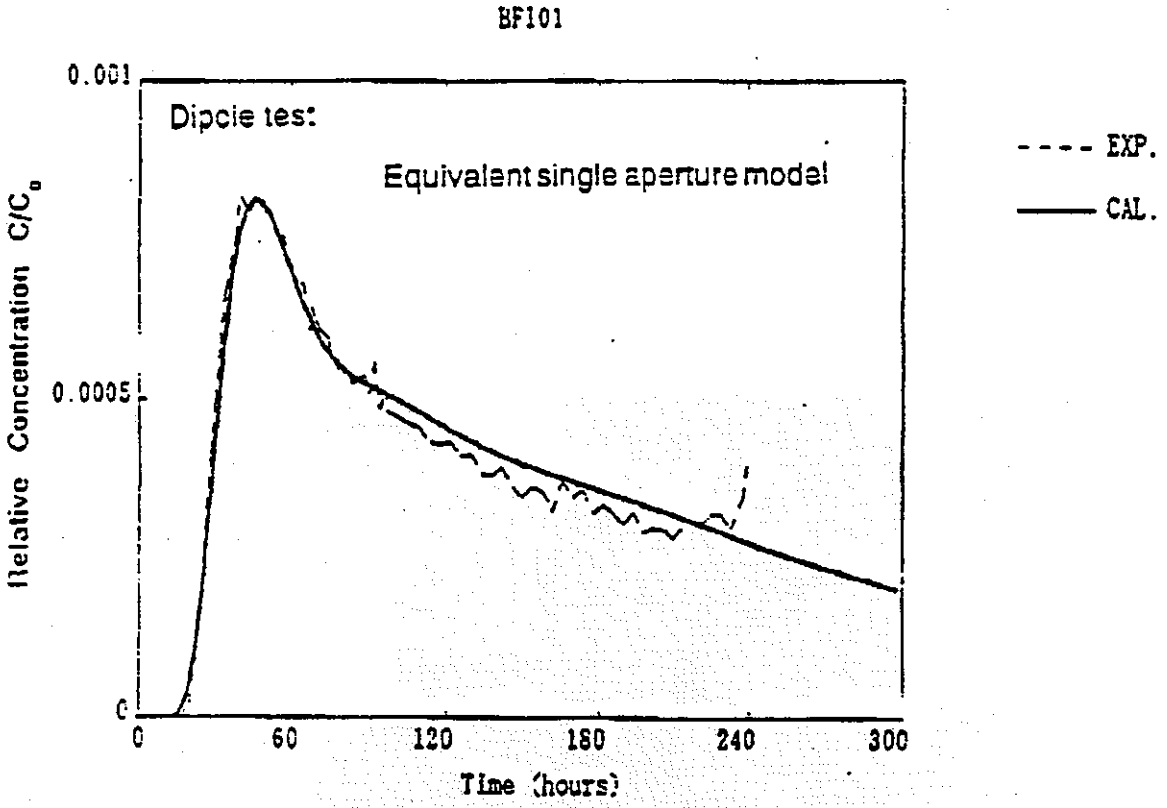


Figure 8.3


BF101
0.001
Dipole test
Equivalent single aperture model
EXP.
CAL.
Relative Concentration C/C₀
0.0005
0
0
60
120
180
240
300
Time (hours)

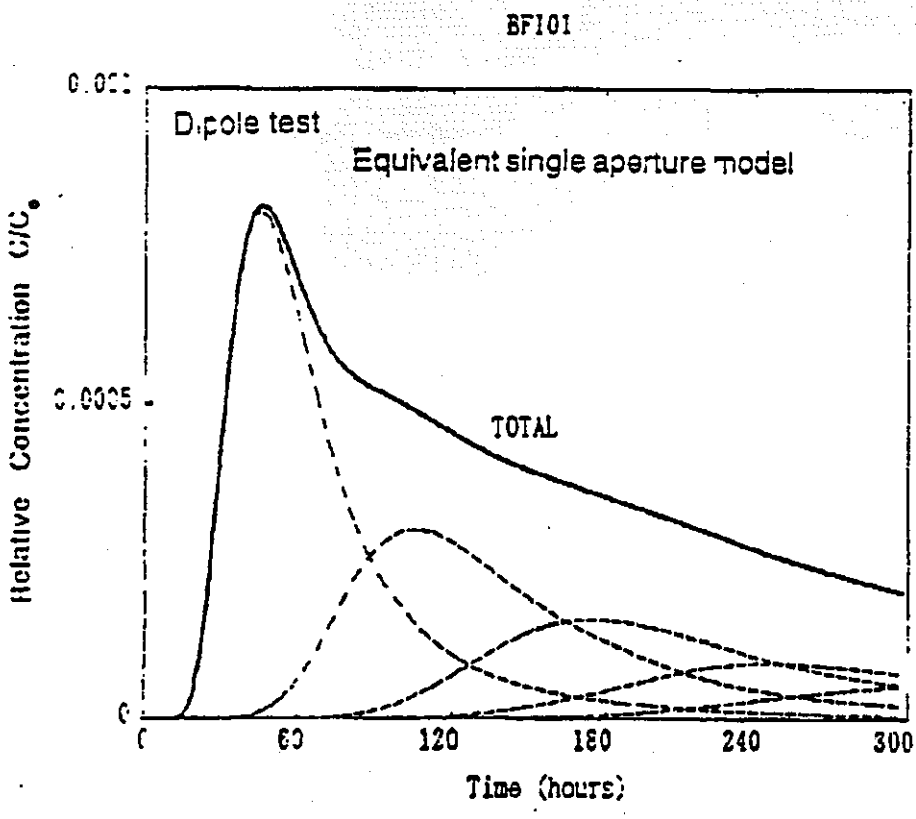
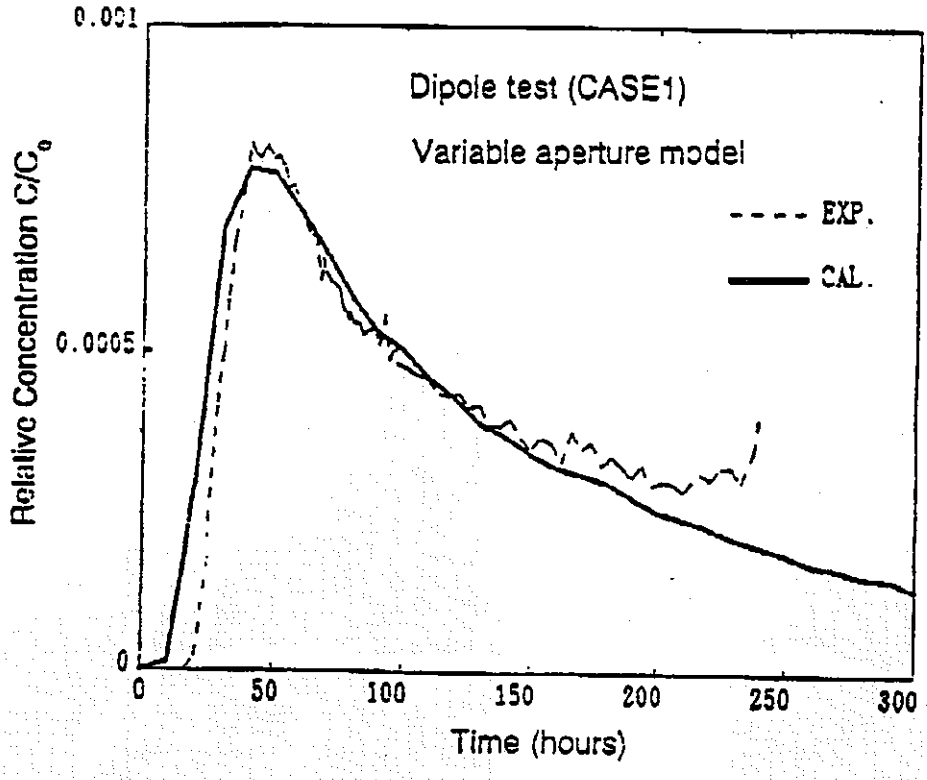

BF101
Dipole test
Equivalent single aperture model
TOTAL
Relative Concentration C/C₀
0.0005
0
60
120
180
240
300
Time (hours)

Figure 8.4


0.001
0.0005
0
Relative Concentration C/C$_0$
Dipole test (CASE1)
Variable aperture model
EXP.
CAL.
0
50
100
150
200
250
300
Time (hours)

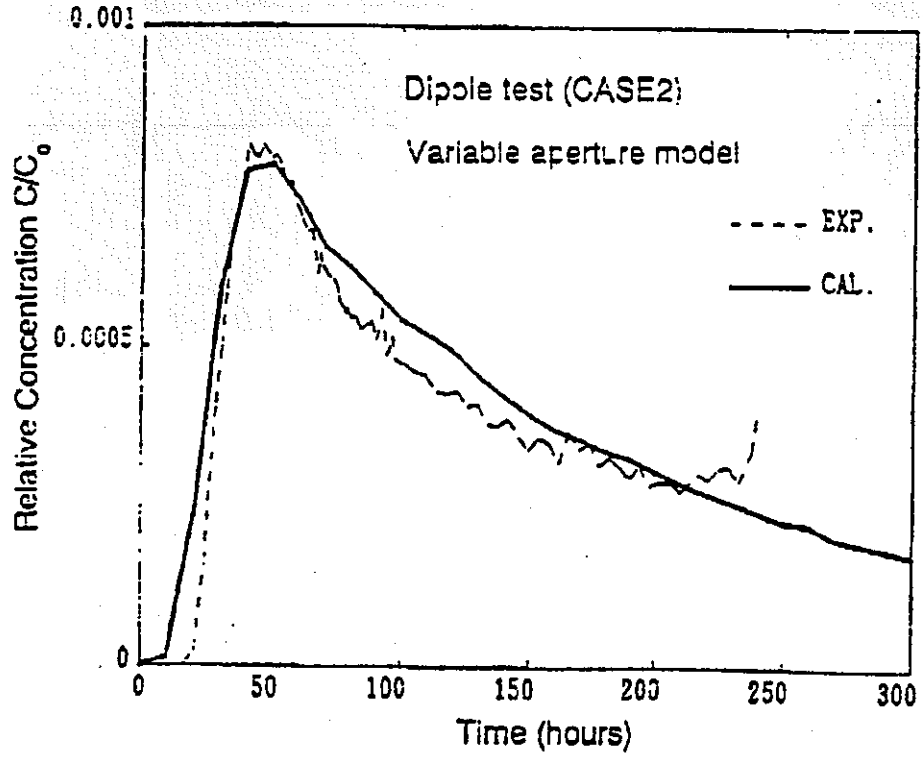

0.001
0.0005
0
Relative Concentration C/C$_0$
Dipole test (CASE2)
Variable aperture model
EXP.
CAL.
0
50
100
150
200
250
300
Time (hours)

Figure 8.5

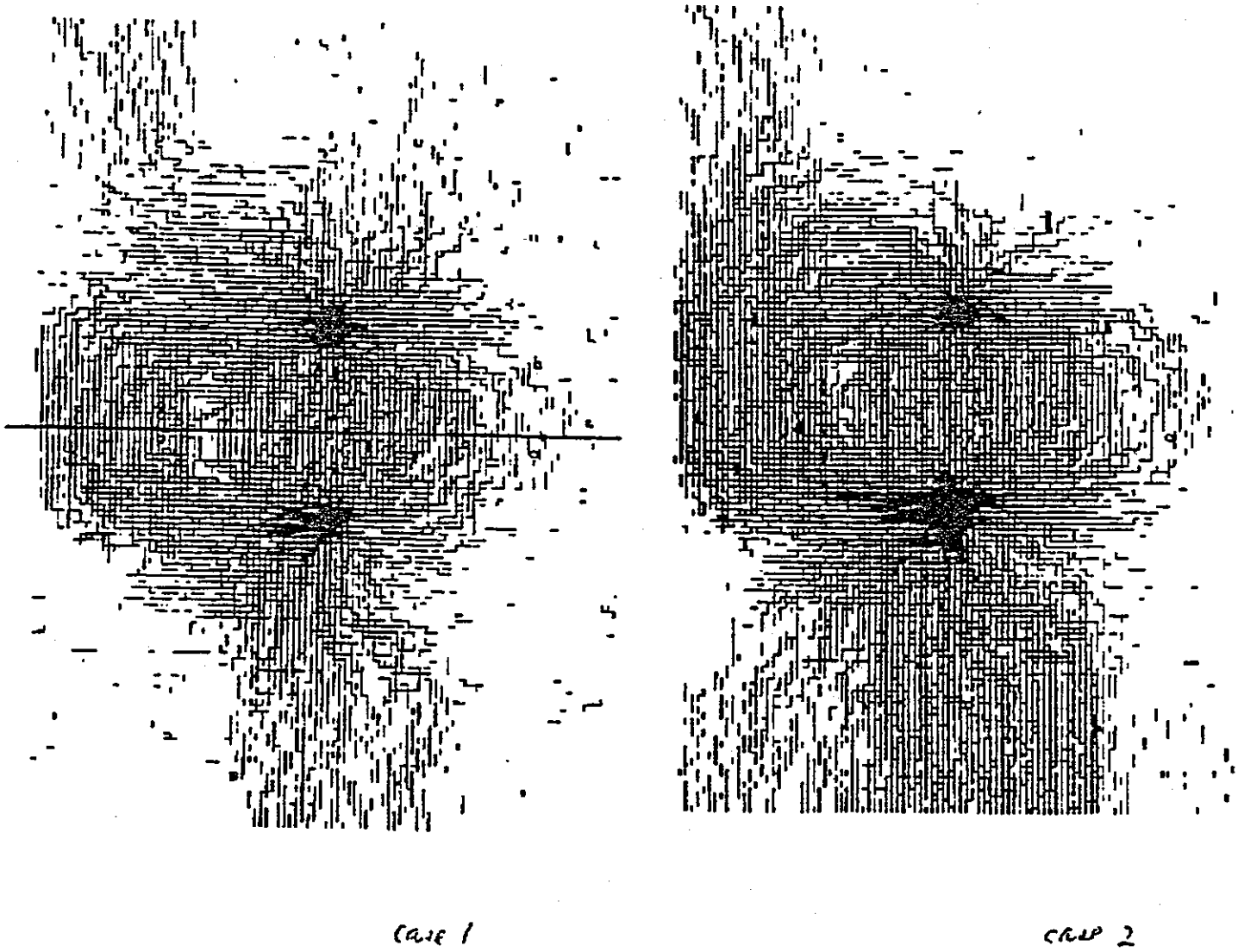


Figure 8.6

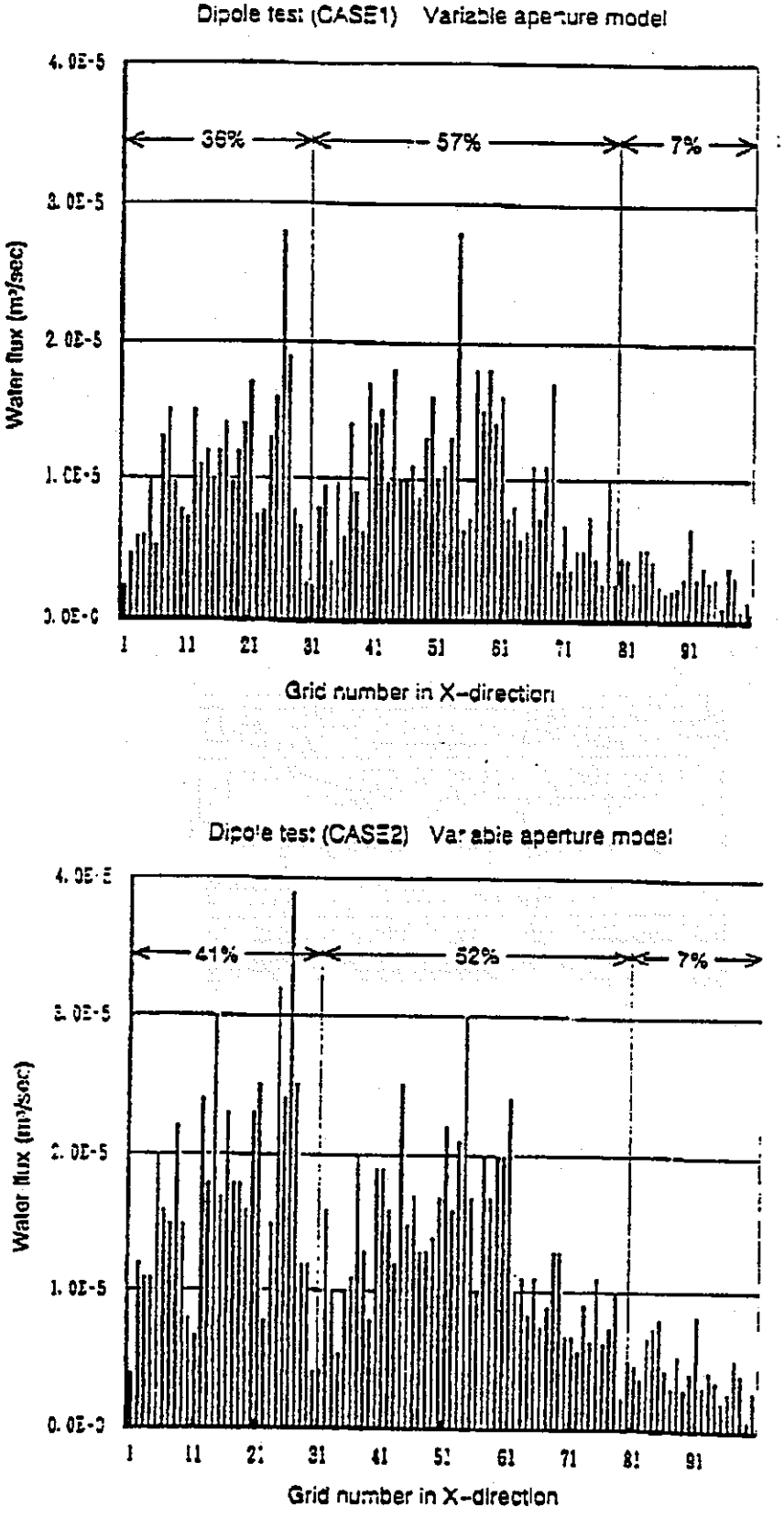

Dipole test (CASE1) Variable aperture model
4.0E-5
3.0E-5
2.0E-5
1.0E-5
0.0E-0
Water flux (m³/sec)
36%
57%
7%
1
11
21
31
41
51
61
71
81
91
Grid number in X-direction
Dipole test (CASE2) Variable aperture model
4.0E-5
3.0E-5
2.0E-5
1.0E-5
0.0E-0
Water flux (m³/sec)
41%
52%
7%
1
11
21
31
41
51
61
71
81
91
Grid number in X-direction

Figure 8.7

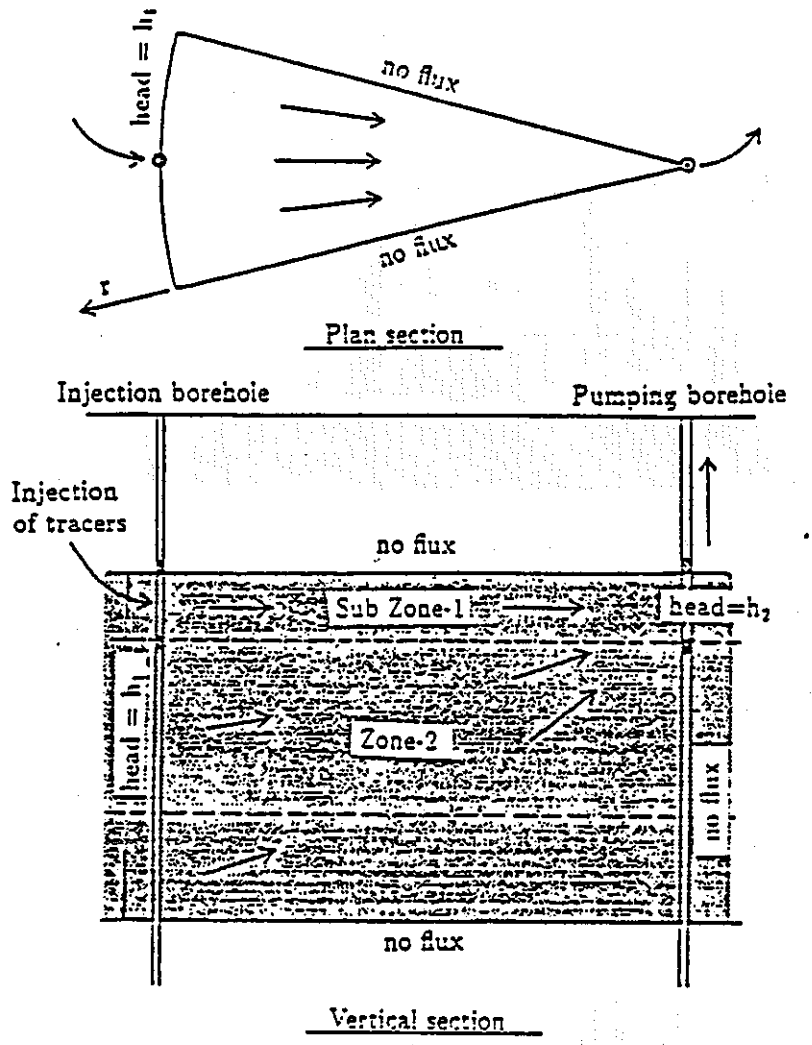


Figure 9.1 Modeled region and boundary conditions.

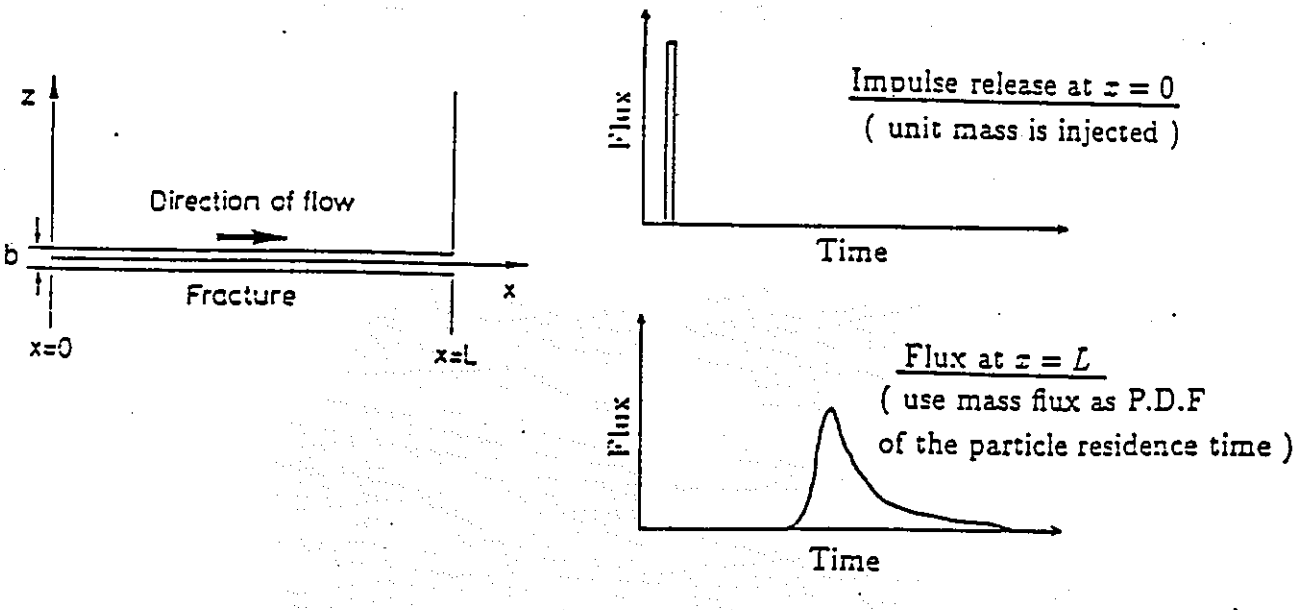
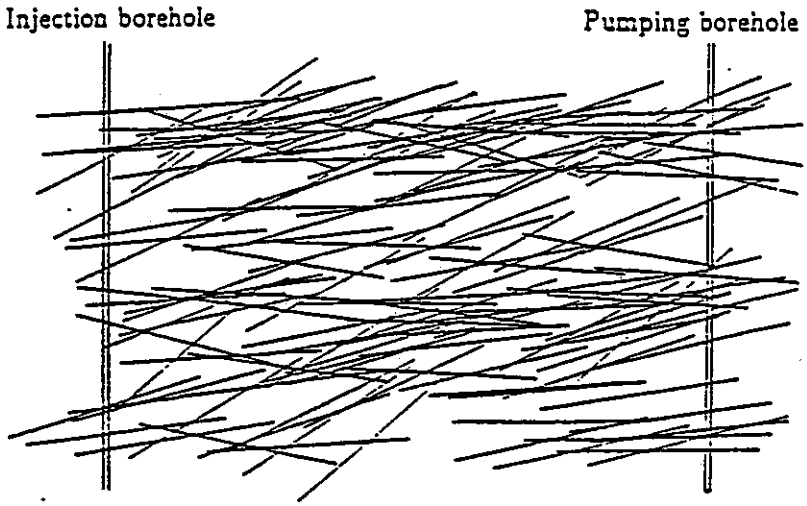
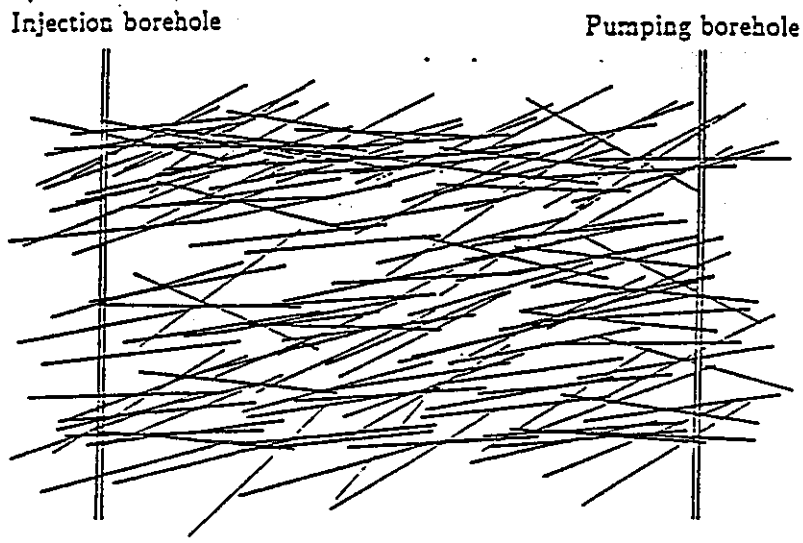


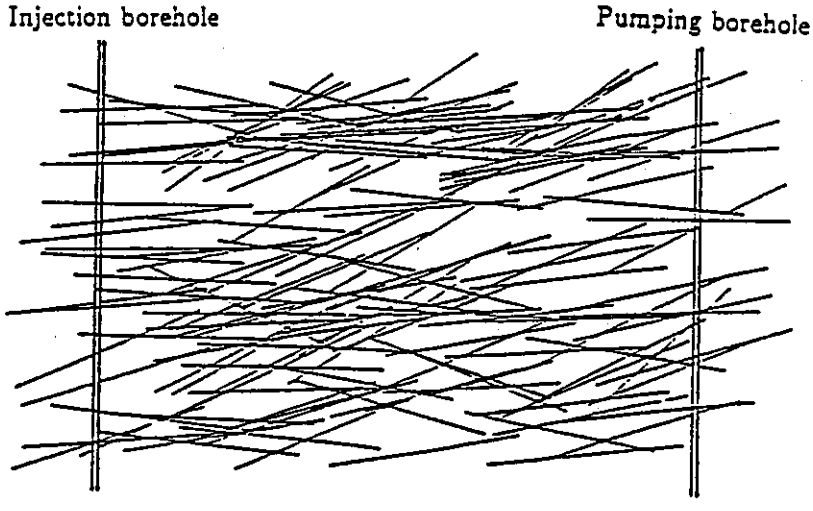
Figure 9.2 Local coordinates system and schematic figure of local dispersion.



(a) fracture network-1

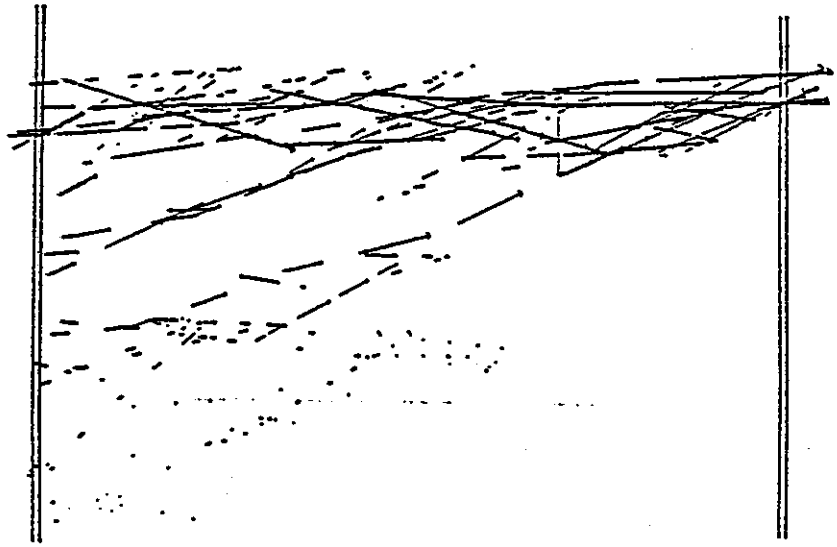


(b) fracture network-2



(c) fracture network-3

Figure 9.3 Generated fracture networks. (a) Fracture network-1; (b) fracture network-2; (c) fracture network-3.



(a) fracture network-1



(b) fracture network-2



(c) fracture network-3

Figure 9.4 Flow vectors in fracture networks. (a) Fracture network-1; (b) fracture network-2; (c) fracture network-3.

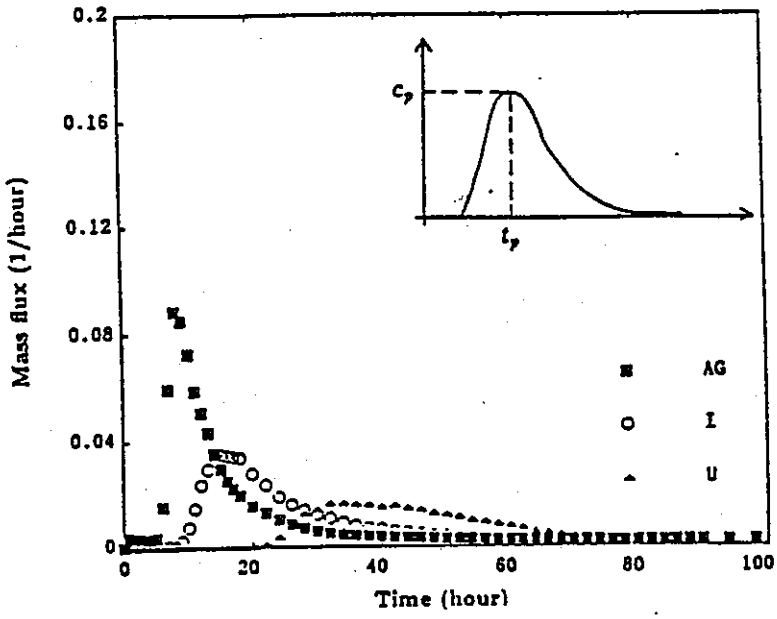


Figure 9.5 Measured Breakthrough curves.

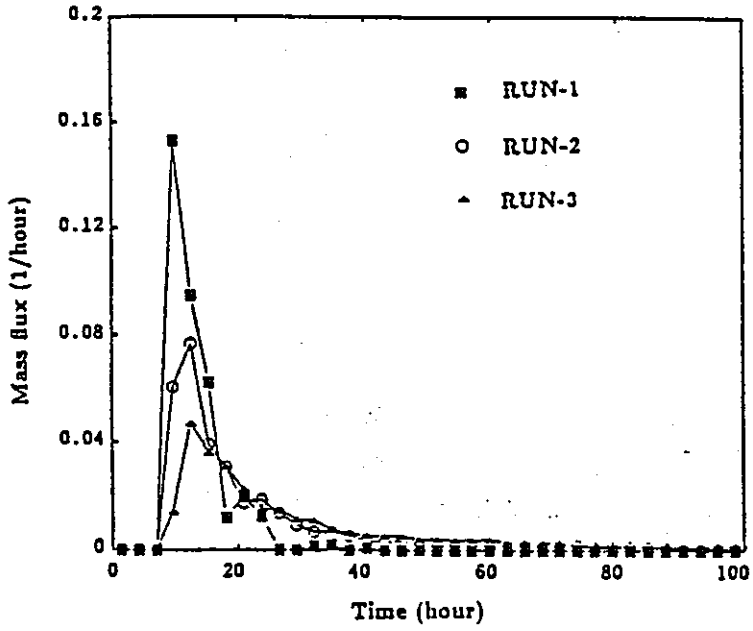


Figure 9.6 Calculated breakthrough curves (network-1).

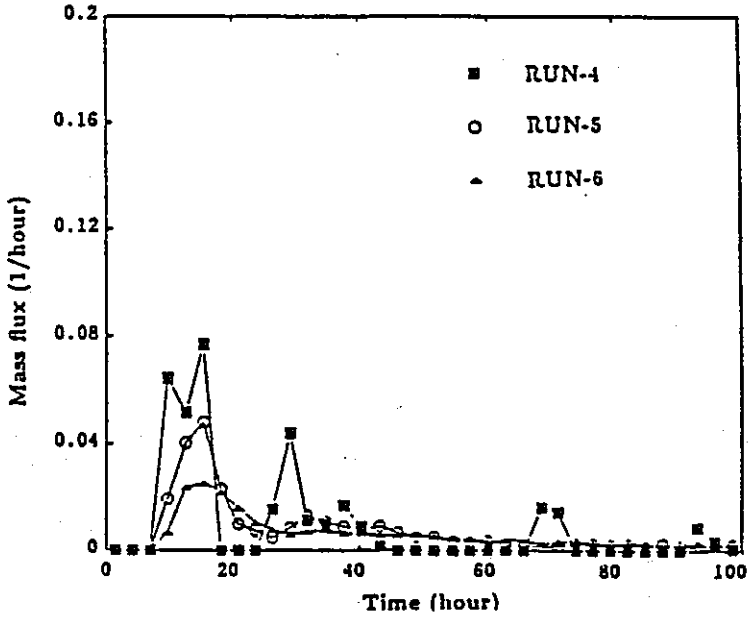


Figure 9.7 Calculated breakthrough curves (network-2).

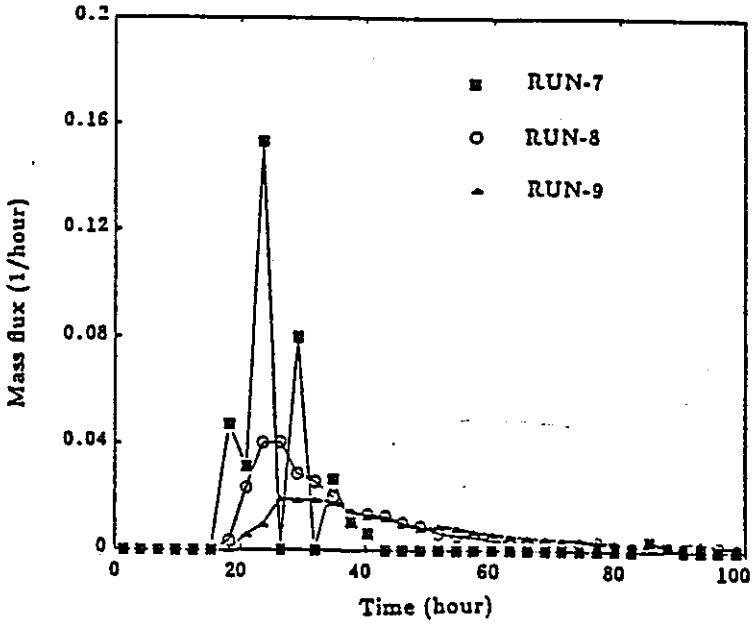


Figure 9.8 Calculated breakthrough curves (network-3).

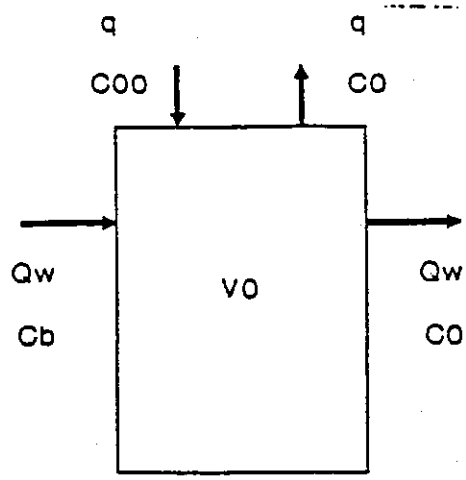


Figure 10.1 Schematization of the injection loop.

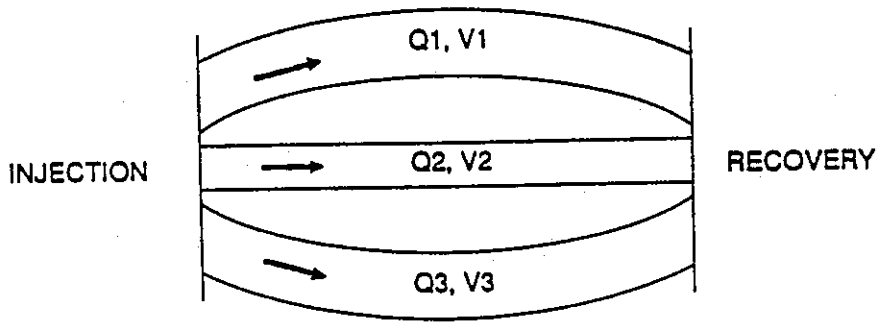


Figure 10.2 Schematization of a multichannel system.

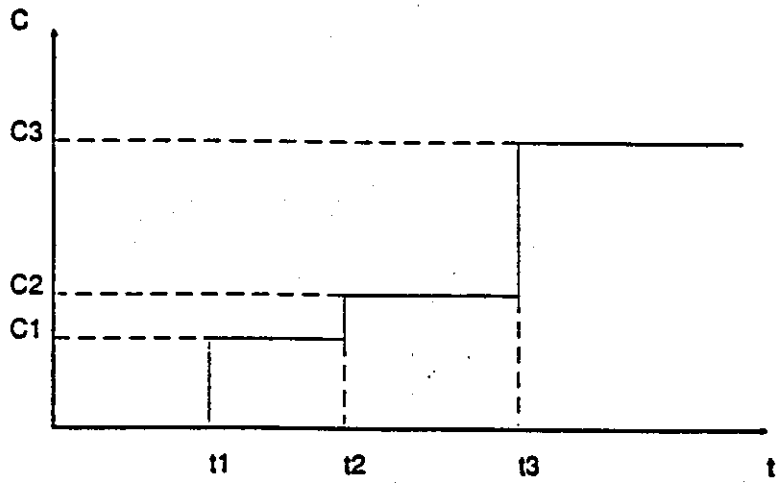


Figure 10.3 Recovery curve of a multichannel system.

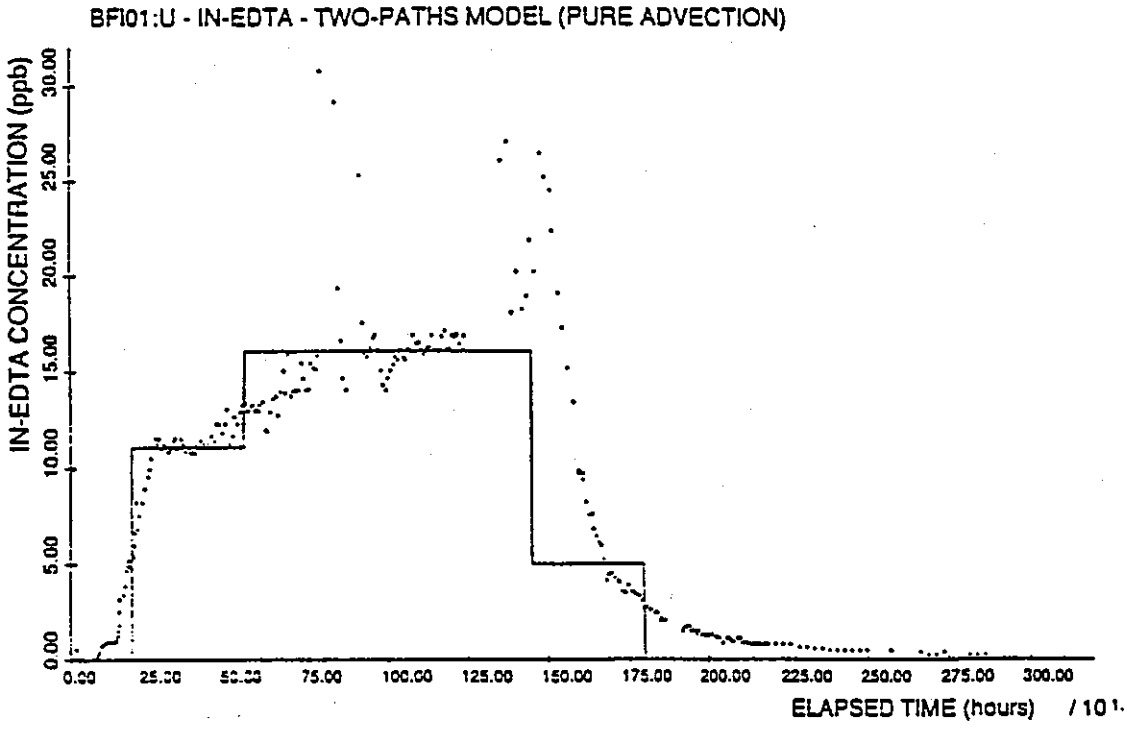


Figure 10.4 Decomposition of In-EDTA recovery curve into two flow paths.

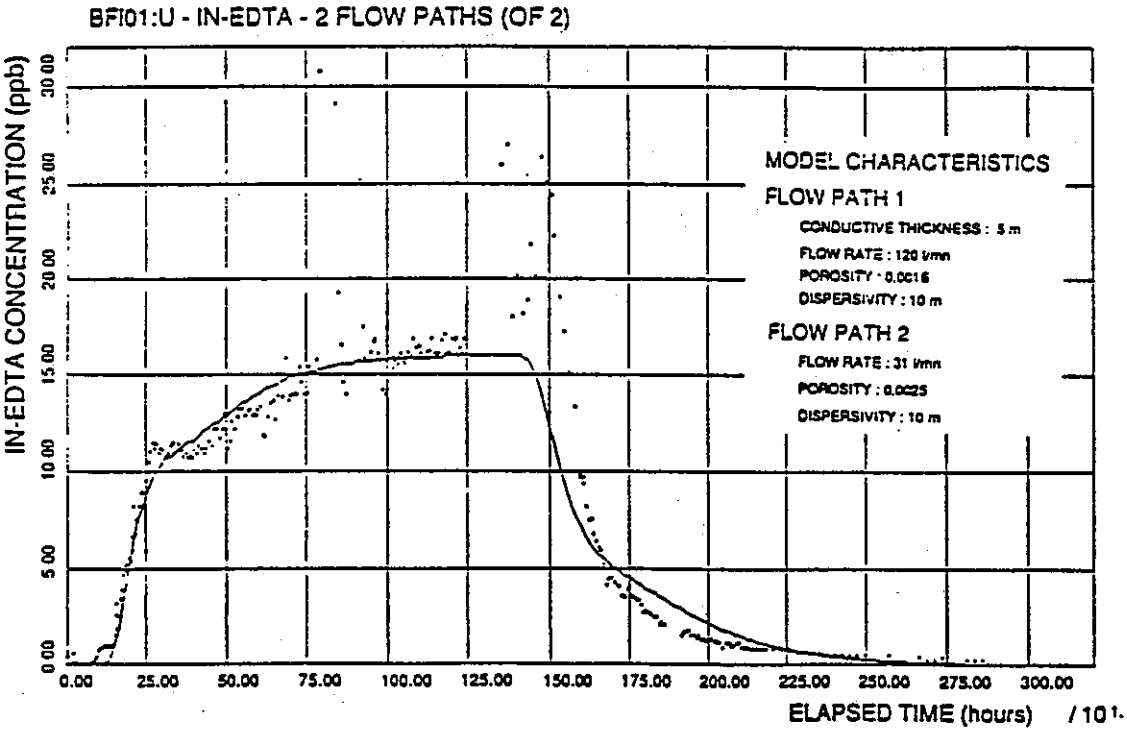


Figure 10.5 Modelling of In-EDTA curve with a two-paths model.

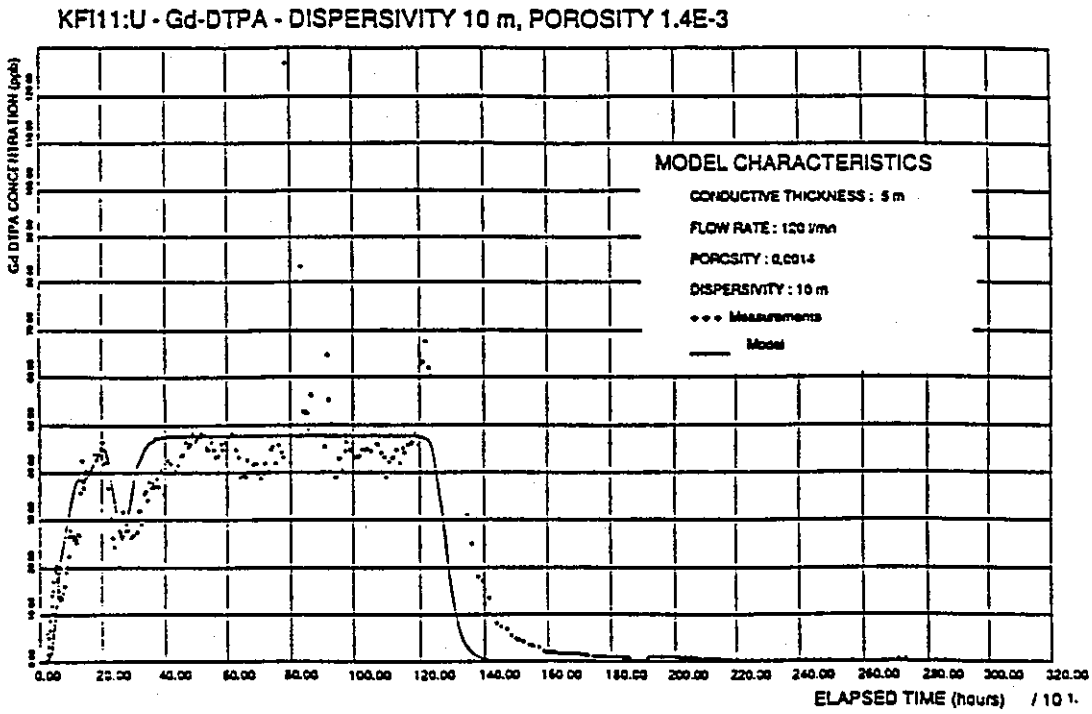


Figure 10.6 Modelling of Gd-DTPA curve with a 10 m dispersivity.

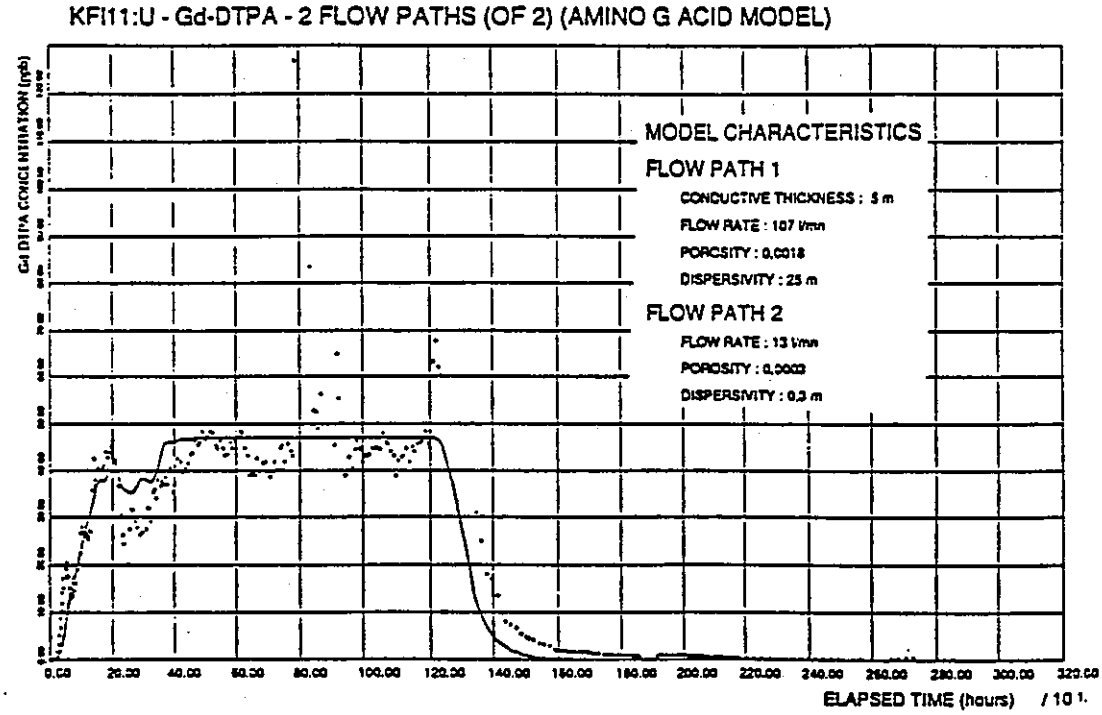


Figure 10.7 Modelling of Gd-DTPA curve with a two-path model.

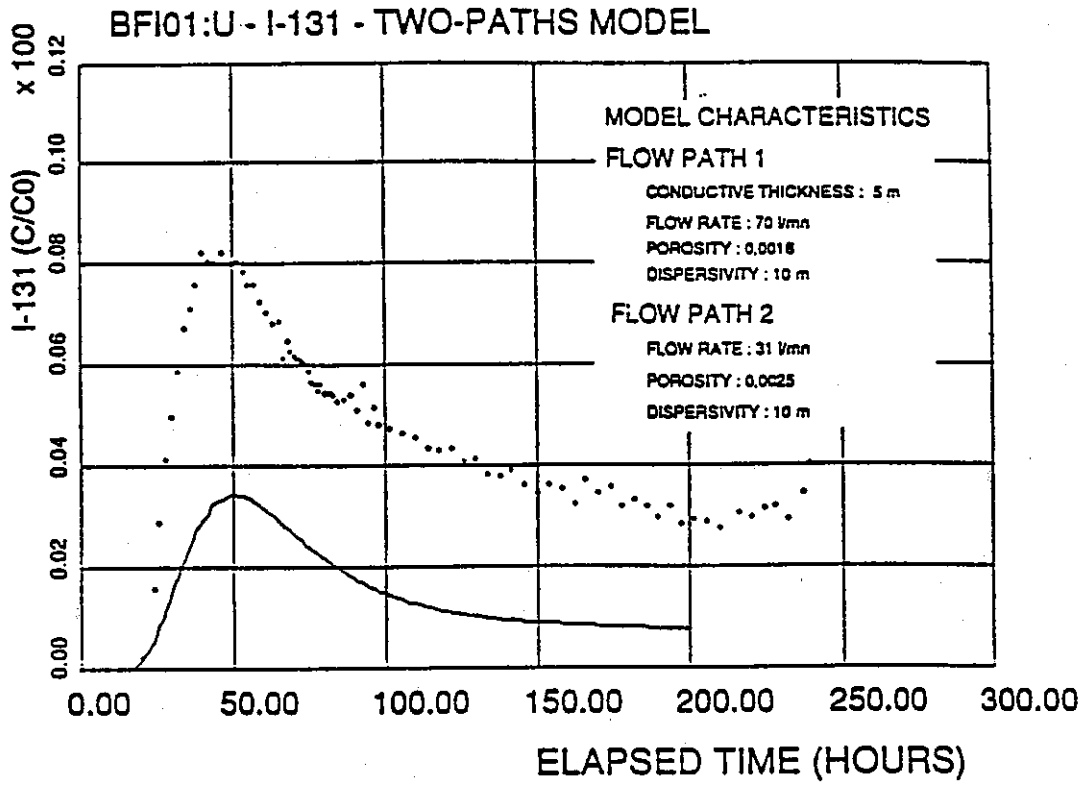


Figure 10.8 Prediction of the Iodine curve during the two-well test with a two-path model.

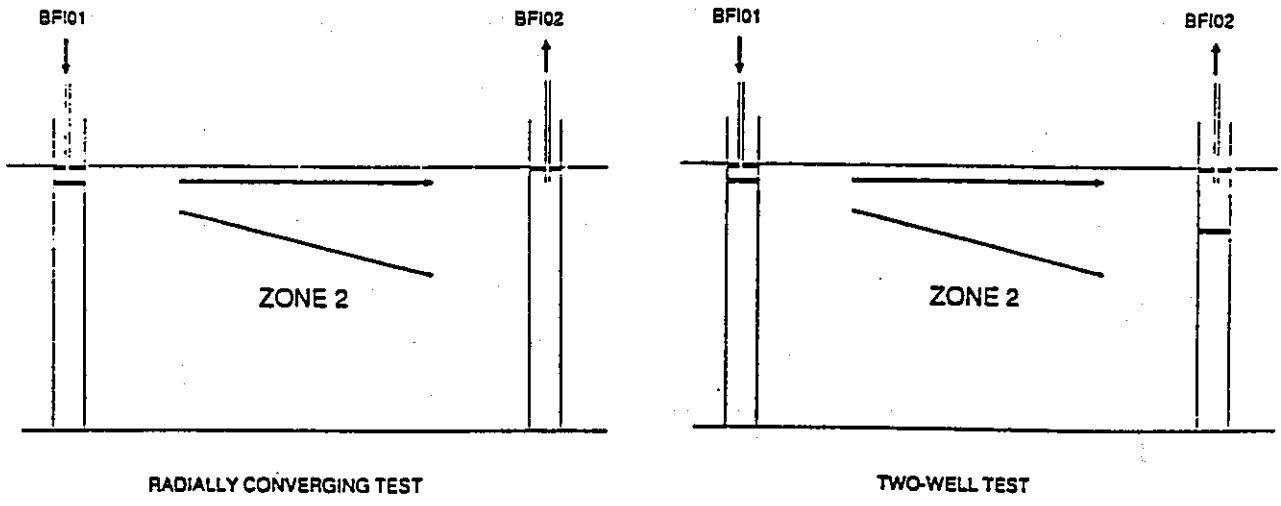


Figure 10.9 Comparison of the Injection-Recovery systems for Radially Converging Test and two-well test.

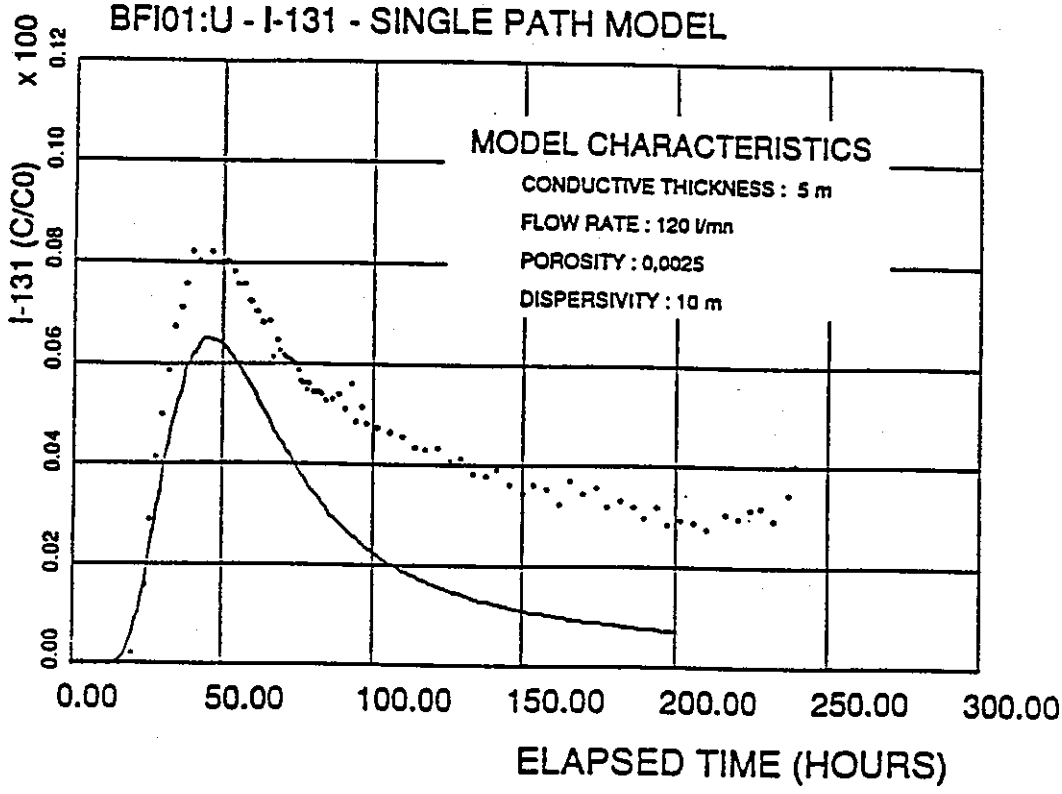


Figure 10.10 Prediction of Iodine curve with a single-path model.

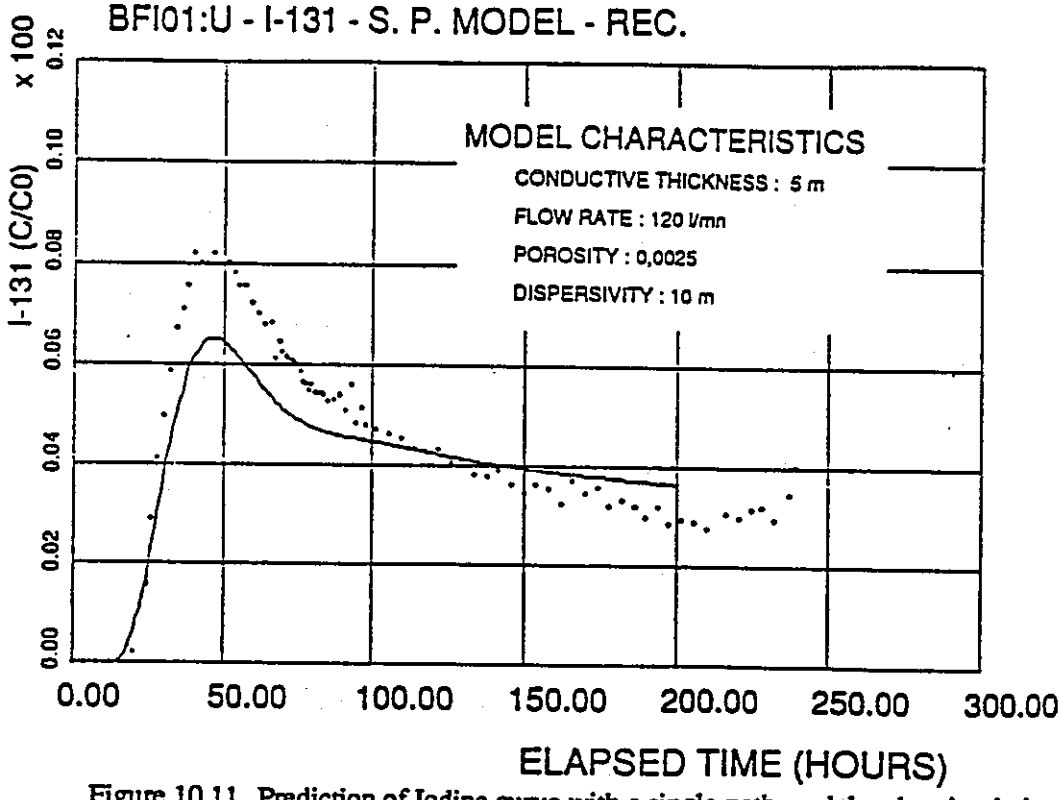


Figure 10.11 Prediction of Iodine curve with a single-path model and recirculation.

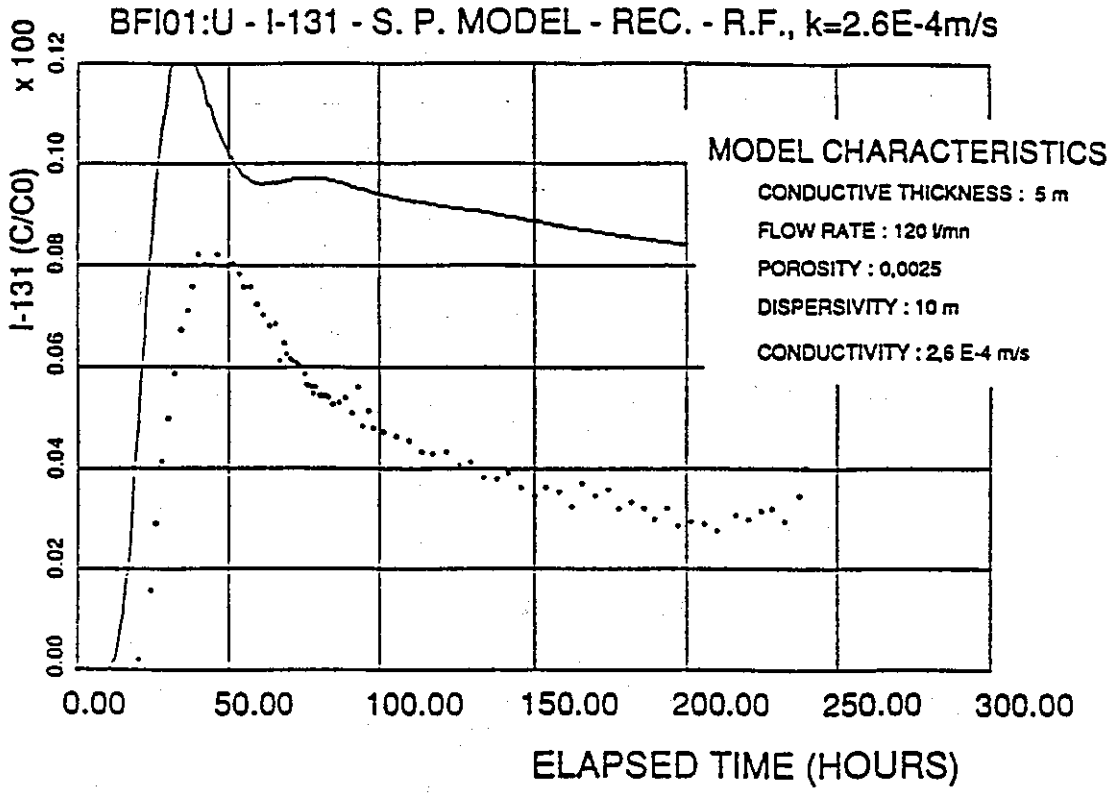


Figure 10.12 Prediction of Iodine Curve with a single path model, recirculation and regional flow (second value of hydraulic conductivity).

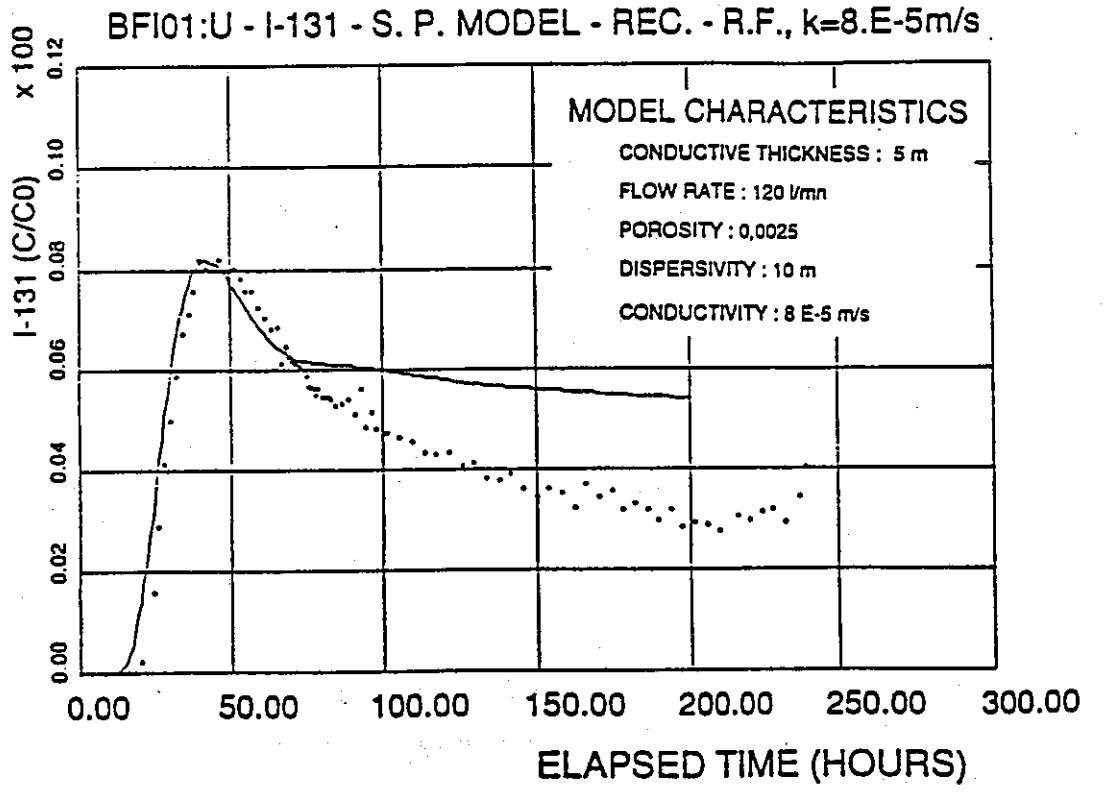


Figure 10.13 Prediction of Iodine Curve with a single path model, recirculation and regional flow (second value of hydraulic conductivity).

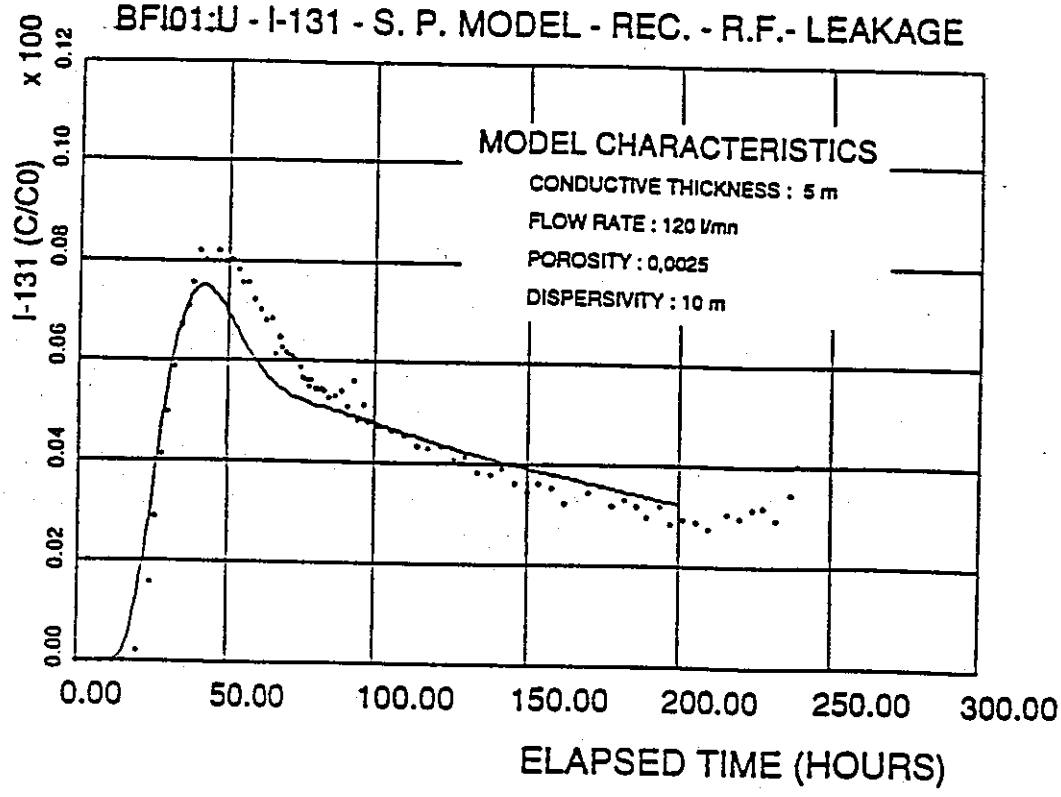


Figure 10.14 Prediction of Iodine Curve with a single path model, recirculation, regional flow and leakage.

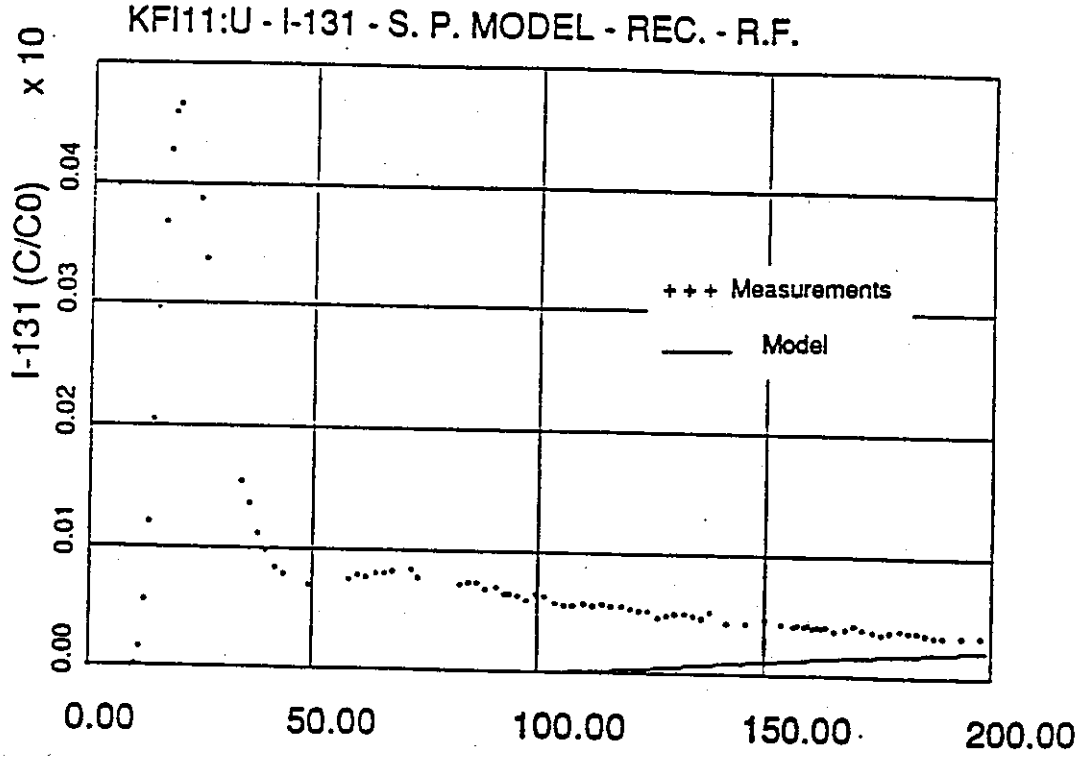


Figure 10.15 Comparison of modelled and measured curves in borehole KFI11 during two-well test.

PNC ZJ1214 91−003(3)

限定資料

地層処分性能評価用解析システムの統合化研究(Ⅱ)

(動力炉・核燃料開発事業団　委託研究成果報告書)

1991 年 5 月



三菱原子力工業株式会社

この資料は，動燃事業団の開発業務を進めるため，特に限られた関係者だけに開示するものです。ついては，複製，転載，引用等を行わないよう，また第三者への開示又は内容漏洩がないよう管理して下さい。また今回の開示目的以外のことには使用しないよう特に注意して下さい。

本資料についての問合せは下記に願います。

〒107　東京都港区赤坂１－９－13

動力炉・核燃料開発事業団

技術協力部　技術管理室

限 定 資 料
PNC ZJ1214 91-003
1991年 5 月

地層処分性能評価用解析システムの統合化研究(Ⅱ)

池田康博* ・石原義尚*
中原 豊* ・杉崎敬良*
土井英雄**・浜本 浩*
向井 悟**・蜂谷尚之**

要 旨

本研究は，地層処分システムの性能評価システムを体系的に開発していくために，以下に示す研究を実施した。

(1) Site-genericな観点から地層処分システムを包括的に性能評価するための統合モデルの全プロセス構成を体系付け，開発アプローチ法を総括した。

(2) 統合モデル体系を構成するためのプロセスモデル候補及びその検証／確証のステータスをレビューした。

(3) 統合モデル体系を成立させるために必要なプロセス連成関係を同定し，その課題，実行方法を総括した。

(4) 統合モデル体系を構成するためのプロセスモデル候補のモデル信頼性を評価する（確証）方法を確立させるため，INTRAVALフェーズ２の確証ケースの応用を検討した。

(5) 統合 モデル体系を構成するためのプロセスモデル候補のコード信頼性を評価する（検証）方法を確立させるため，FEMWATERを使って検証を実施した。

本報告書は，三菱原子力工業株式会社が動力炉・核燃料開発事業団の委託により実施した研究の成果である。

契約番号：020D0151

事業団担当部課室および担当者：環境開発部地層処分開発室（梅木博之）

* ：系統設計部系統計画チーム

** ：大宮研究所評価・解析チーム

COMMERCIAL PROPRIETARY
PNC ZJ1214 91-003
MAY, 1991

Integration Study (Ⅱ) for Performance Assessment System of Geological Disposal

Yasuhiro Ikeda* ・Yoshinao Ishihara *
Yutaka Nakahara * ・Takayoshi Sugisaki*
Hideo Doi ** ・Hiroshi Hamamoto*
Satoru Mukai** ・Naoyuki Hachiya **

Abstract

In the study, we have performed the following tasks in order to develop a systematic, comprehensive approach and a reliable, integrated computational system for performance assessment of a geologic disposal system.

(1) Develop system integration model concept including an integrated computational approach and a complete set of processes to performance assessment site-generically.
(2) Review candidate models based system integration model, including the status of verification and validation activities.
(3) Identify coupled processes based system integration model and review methodology for models of coupled processes.
(4) Apply test cases in INTRAVAL Phase 2 to develop methodology and techniques to validate candidate conceptual models.
(5) Verify FEMWATER to develop methodology and techniques to assure the numerical accuracy of computer codes.

Work performed by Mitsubishi Atomic Power Industries, Inc. under contract with Power Reactor and Nuclear Fuel Development Corporation.
PNC Liaison:Waste Technology Development Division, Geological Isolation Section, Hiroyuki Umeki.
* : System Engineering Department, System Planning Team.
**: Omiya Technical Institute, Analytical Evaluation Team.

目　　次

1. まえがき ・・・・・・・・・・・・・・・・・・・・・・・・・・・・・・・・ 1-1
2. PRELIMINARY SYSTEM MODEL CONCEPT ・・・・・・・・・・・・・・・・・・・・ 2-1
2.1 INFORMATION ON PRELIMINARY CONCEPTUAL SITES ・・・・・・・・・・・・ 2-7
2.2 INFORMATION ON PRELIMINARY BASE CASE SCENARIO ・・・・・・・・・・・ 2-7
2.3 SCHEMATIC OF THE SYSTEM INTEGRATION MODEL ・・・・・・・・・・・・・ 2-19
2.4 STRATEGY FOR DEVELOPMENT OF SYSTEM INTEGRATION MODEL ・・・・・・・ 2-23
2.4.1 Introduction ・・・・・・・・・・・・・・・・・・・・・・・・・・ 2-23
2.4.2 Developmental Phases ・・・・・・・・・・・・・・・・・・・・・・ 2-23
2.4.3 Code Configuration and Integrity Control ・・・・・・・・・・・・ 2-26
3. REVIEW OF CANDIDATE COMPONENT PROCESS MODELS ・・・・・・・・・・・・・ 3-1
3.1 CODE SURVEY ・・・・・・・・・・・・・・・・・・・・・・・・・・・・ 3-1
3.2 TABLE DESCRIPTION ・・・・・・・・・・・・・・・・・・・・・・・・・ 3-1
4. STRATEGY FOR COUPLING ・・・・・・・・・・・・・・・・・・・・・・・・ 4-1
4.1 REVIEW OF COUPLING STUDIES ・・・・・・・・・・・・・・・・・・・・ 4-1
4.1.1 Transport Coupling at Subsystem Boundaries ・・・・・・・・・・ 4-1
4.1.2 Mechanical Coupling at Subsystem Boundaries ・・・・・・・・・・ 4-1
4.1.3 Thermal Coupling at Subsystem Boundaries ・・・・・・・・・・・・ 4-1
4.1.4 Thermal and Chemical Coupling ・・・・・・・・・・・・・・・・・ 4-1
4.1.5 Thermal and Mechanical Coupling ・・・・・・・・・・・・・・・・ 4-2
4.1.6 Chemical and Mechanical Coupling ・・・・・・・・・・・・・・・・ 4-3
4.1.7 Chemical and Transport Coupling ・・・・・・・・・・・・・・・・ 4-4
4.1.8 Mechanical and Transport Coupling ・・・・・・・・・・・・・・・ 4-7
4.1.9 Geothermal and Hydrological Coupling ・・・・・・・・・・・・・・ 4-7
4.1.10 Geomechanical and Hydrological Coupling ・・・・・・・・・・・・ 4-8
4.1.11 Flow-Transport-Climate Coupling ・・・・・・・・・・・・・・・・ 4-8
4.1.12 Modification of Flow Field and Transport Process in Rock Mass ・・・・・・・・・・・・・・・・・・・・・・・・・・・・ 4-9
4.2 IMPLEMENTATION OF COUPLING ・・・・・・・・・・・・・・・・・・・・ 4-9
4.2.1 Waste Package ・・・・・・・・・・・・・・・・・・・・・・・・・・ 4-10
4.2.2 Mined Facility ・・・・・・・・・・・・・・・・・・・・・・・・・ 4-19
4.2.3 Repository Rock Mass ・・・・・・・・・・・・・・・・・・・・・・ 4-23
4.2.4 Regional Rock Mass ・・・・・・・・・・・・・・・・・・・・・・・ 4-27

4.2.5 Waste Package - Repository Rock Mass ・・・・・・・・・・・・・ 4-31
4.2.6 Waste Package - Mined Facility ・・・・・・・・・・・・・・・・ 4-35
4.2.7 Mined Facility - Repository Rock Mass ・・・・・・・・・・・・ 4-39
4.2.8 Repository Rock Mass - Regional Rock Mass ・・・・・・・・・・ 4-43
5. SUMMARY OF MODEL INTEGRATION STUDY ・・・・・・・・・・・・・・・・・・ 5-1
6. プロセスモデルの確証 ・・・・・・・・・・・・・・・・・・・・・・・・ 6-1
6.1 INTRAVALフェーズ２のテストケース ・・・・・・・・・・・・・・・・ 6-1
6.2 テストケースの取り組み方針 ・・・・・・・・・・・・・・・・・・・・ 6-1
6.2.1 確証について ・・・・・・・・・・・・・・・・・・・・・・・・・ 6-1
6.2.2 Finnsjönに対する取組み方針 ・・・・・・・・・・・・・・・・・・ 6-3
6.2.3 Molに対する取組み方針 ・・・・・・・・・・・・・・・・・・・・ 6-9
6.3 引用文献 ・・・・・・・・・・・・・・・・・・・・・・・・・・・・・ 6-12
7. プロセスコードの検証 ・・・・・・・・・・・・・・・・・・・・・・・・ 7-1
7.1 検証実施範囲の選定 ・・・・・・・・・・・・・・・・・・・・・・・・ 7-1
7.1.1 概要 ・・・・・・・・・・・・・・・・・・・・・・・・・・・・・ 7-1
7.1.2 問題の内容 ・・・・・・・・・・・・・・・・・・・・・・・・・・ 7-1
7.2 検証計算と評価 ・・・・・・・・・・・・・・・・・・・・・・・・・・ 7-3
7.2.1 計算パラメータ ・・・・・・・・・・・・・・・・・・・・・・・・ 7-3
7.2.2 メッシュ ・・・・・・・・・・・・・・・・・・・・・・・・・・・ 7-4
7.2.3 計算ケース ・・・・・・・・・・・・・・・・・・・・・・・・・・ 7-8
7.2.4 計算結果 ・・・・・・・・・・・・・・・・・・・・・・・・・・・ 7-9
7.2.5 検証計算のまとめ ・・・・・・・・・・・・・・・・・・・・・・・ 7-51
7.3 検証のためのユーザ・インターフェイス ・・・・・・・・・・・・・・・ 7-52
7.4 まとめ ・・・・・・・・・・・・・・・・・・・・・・・・・・・・・・ 7-54
8. あとがき ・・・・・・・・・・・・・・・・・・・・・・・・・・・・・・ 8-1

図 目 次

Figure 1 Size Scales in Performance Assessment ・・・・・・・・ 2-4
Figure 2 Computational Sequence for System Performance ・・・・ 2-5
Figure 3 Crystalline Rock Model ・・・・・・・・・・・・・・・・ 2-8
Figure 4 Simple Sedimentary Rock Model ・・・・・・・・・・・・ 2-9
Figure 5 Complex Sedimentary Rock Model ・・・・・・・・・・・ 2-10
Figure 6 Schematic of the System Integration Model ・・・・・・ 2-21
Figure 7 Development Process of the System Integration Model ・ 2-24
Figure 8 Principal Process Coupling ・・・・・・・・・・・・・・ 2-24
Figure 9 Schematic of the Coupling Diagrams for the Entire System ・・・・・・・・・・・・・・・・・・・・・・・・・・ 4-12
Figure 10 Waste Package Coupling ・・・・・・・・・・・・・・・ 4-13
Figure 11 Mined Facility Coupling ・・・・・・・・・・・・・・・ 4-21
Figure 12 Repository Rock Mass Coupling ・・・・・・・・・・・・ 4-25
Figure 13 Regional Rock Mass Coupling ・・・・・・・・・・・・・ 4-29
Figure 14 Waste Package - Repository Coupling ・・・・・・・・・ 4-33
Figure 15 Waste Package - Mined Facility Coupling ・・・・・・・ 4-37
Figure 16 Mined Facility - Repository Coupling ・・・・・・・・・ 4-41
Figure 17 Repository Rock Mass - Regional Rock Mass Coupling ・ 4-44
図－18 トレーサ注入の概念図 ・・・・・・・・・・・・・・・・・ 6-47
図－19 トレーサ注入装置 ・・・・・・・・・・・・・・・・・・・ 6-47
図－20 揚水装置 ・・・・・・・・・・・・・・・・・・・・・・・ 6-49
図－21 Finnsjönテストケースの体系 ・・・・・・・・・・・・・・ 6-105
図－22 トレーサの移行 ・・・・・・・・・・・・・・・・・・・・ 6-109
図－23 出口濃度の測定値と計算値の比較(トレーサI^-) ・・・・・ 6-109
図－24 CP1における圧力分布 ・・・・・・・・・・・・・・・・・ 6-111
図－25 試料No.9の試料量とトリチウム濃度との関係 ・・・・・・ 6-112
図－26 フィルタNo.4とNo.6のトリチウム濃度 ・・・・・・・・・ 6-113
図－27 Molテストケースの評価体系 ・・・・・・・・・・・・・・ 6-117
図－28 解析領域 ・・・・・・・・・・・・・・・・・・・・・・・ 7-1
図－29 要素分割図(メッシュ1) ・・・・・・・・・・・・・・・・ 7-5
図－30 要素分割図(メッシュ2) ・・・・・・・・・・・・・・・・ 7-5
図－31 要素分割図(メッシュ3) ・・・・・・・・・・・・・・・・ 7-6
図－32 要素分割図(メッシュ4) ・・・・・・・・・・・・・・・・ 7-6
図－33 要素分割図(メッシュ5) ・・・・・・・・・・・・・・・・ 7-7
図－34 要素分割図(メッシュ6) ・・・・・・・・・・・・・・・・ 7-7
図－35 等水頭線図(ケース1) ・・・・・・・・・・・・・・・・・ 7-10
図－36 等水頭線図(ケース4) ・・・・・・・・・・・・・・・・・ 7-10

図－37　等水頭線図(ケース7)　・・・

表 目 次

Table 1 List of Events and Processes on Significance in Japan ・ 2-11
Table 2 Mechanical Process and Thermal Process Modeling Codes ・ 3-3
Table 3 Chemical Process Modeling Codes ・・・・・・・・・・・・ 3-5
Table 4 Transport Process Modeling Codes ・・・・・・・・・・・ 3-7
Table 5 Dose Process Modeling Codes ・・・・・・・・・・・・・・ 3-11
表－ 6 INTRAVALプロジェクトでの試験ケース ・・・・・・・・・・ 6-13
表－ 7 INTRAVALフェーズ２のテストケース ・・・・・・・・・・・ 6-15
表－ 8 INTRAVALフェーズ２テストケースの試験内容 ・・・・・・・ 6-17
表－ 9 放射性核種の移行のプロセスモデル例 ・・・・・・・・・・ 6-45
表－10 トレーサの注入位置と使用したトレーサ ・・・・・・・・・ 6-46
表－11 BFI02における揚水に関するデータ ・・・・・・・・・・・ 6-48
表－12 ダイポール試験におけるトレーサ注入状況 ・・・・・・・・ 6-50
表－13 揚水および水頭に関するデータ ・・・・・・・・・・・・・ 6-51
表－14 トレーサ注入に関するデータ ・・・・・・・・・・・・・・ 6-59
表－15 BFI02におけるトレーサ相対濃度 ・・・・・・・・・・・・ 6-73
表－16 KFI11におけるトレーサ相対濃度 ・・・・・・・・・・・・ 6-79
表－17 BFI02,KFI11におけるトレーサ濃度 ・・・・・・・・・・・ 6-85
表－18 KFI06におけるトレーサ相対濃度 ・・・・・・・・・・・・ 6-87
表－19 井戸中の地下水レベル ・・・・・・・・・・・・・・・・・ 6-89
表－20 ゾーン２中の水頭 ・・・・・・・・・・・・・・・・・・・ 6-93
表－21 BFI02の揚水部分との水頭差 ・・・・・・・・・・・・・・ 6-97
表－22 揚水に関するデータ ・・・・・・・・・・・・・・・・・・ 6-103
表－23 Finnsjon揚水試験に関する検討方針 ・・・・・・・・・・・ 6-107
表－24 各フィルタに接続したパイプの内容積 ・・・・・・・・・・ 6-110
表－25 Molテストケースに関する検討方針(案) ・・・・・・・・・ 6-115
表－26 要素数及び節点数 ・・・・・・・・・・・・・・・・・・・ 7-4
表－27 計算ケース ・・・・・・・・・・・・・・・・・・・・・・ 7-8
表－28 水頭最大誤差 ・・・・・・・・・・・・・・・・・・・・・ 7-21
表－29 流出境界節点でのV_zの比較 ・・・・・・・・・・・・・・・ 7-48

1. まえがき

高レベル放射性廃棄物の地層処分における性能評価の複雑さは、考慮すべき現象が腐食、溶解、地球化学、伝熱、岩力学、地下水流、物質移動等多岐にわたり、それらが相互に作用しながら複雑に組み合わさった複合現象を取り扱う必要があること、更に複雑な広域地層を対象に1万年以上にわたる超長期間の挙動を予測解析することにある。このため各現象を扱う多岐にわたった多数のモデル／コードを統合して計算するシステムの構築ならびに各モデル／コード及び全体システムの妥当性を十分に保証する手段の開発が必要である。

元年度研究は、第一段階として

- 個別の解析コードについてその妥当性を保証するために、各種の検証／確証の応用事例を調べ各々の特徴や適用範囲等を整理し、コードを広く検証／確証するための概念、方法を構築した。そして、調査した検証手法の応用として、地下水による核種移動解析コードFEMWASTE-PNCの移流、分散及び崩壊の計算についてパラメータを変化させて数学的厳密解との比較を行ない、ほぼ正しい計算結果が得られることを確認した。また、調査した確証手法の応用として、国際プロジェクトINTRAVALフェーズ1のケース1a，1bを一次元核種移動モデルで評価したが、十分な確信を得るまでには至らなかった。
- 現象の理解促進とデータを自由に扱えるシミュレーションシステムの対話環境を構築していくために、FEMWATER／FEMWASTE-PNCの計算結果を画像出力するプログラムの開発とユーザ・インターフェイスの概念を実証するためのプロトタイプ・ユーザ・インターフェースの開発を行なった。

本研究は、元年度の研究成果を踏まえ、更に性能評価全体にわたる解析システムの開発を円滑に進めるためには、解析システムの体系的理論モデル構造の具体化とそれに基づいた開発方策が不可欠であるので、Top-down的アプローチとBottom-up的アプローチを組み合わせて

a. 開発の全体モデルを構築してそのモデルの立場から必要な個別モデルと個別モデル統合の方法論の検討

b. 現実にあるモデル／コードの妥当性を示すニーズからの検証／確証

を行なう。a項の作業に当たっては、三菱商事株式会社の協力を得て行なう。

2. PRELIMINARY SYSTEM MODEL CONCEPT

Quantitative analysis of the long-term performance of a mined geologic disposal system for high-level nuclear waste is a very challenging task from several viewpoints. First, a large number of complex physical processes must be simulated. Second, the natural variability of the geologic environment, which is inhomogeneous and often discontinuous, must be accurately represented. And third, long-term performance predictions are very difficult to validate because experiments are conducted over time scales that are brief compared to geologic time scales.

The development of computer programs (also called codes) for repository performance assessment has usually followed one of two approaches: the development of large research codes or the development of simplified system-level codes. The large research codes generally contain detailed models of selected physical processes and retain a high degree of geometric detail. These codes are useful for detailed studies of the response of repository components and subsystems, such as the waste package; however, these codes cannot simulate the response of the total repository system because disparate size scales and the number and complexity of physical processes results in impractical long computational time, even for the fastest computers. The total system codes, on the other hand, approximate the response of major repository subsystems. These models achieve practical computational times by sacrificing detailed geometric and process modeling. Accurate system-level modeling must therefore depend upon reliable approximations for repository components and subsystems. These approximations will be based on a large base of information from performance assessment calculations, laboratory experiments, and in situ experiments.

Since the data base for system-level modeling is not currently available within the Japanese repository program, our initial efforts during this study have focussed on a conceptual approach to integrate large research codes into useful computational tools for the engineer and analyst. Our conceptual approach is structured around four size scales: regional, repository, mined facility, and waste package. The size scales are illustrated in Figure 1 and defined as follows:

- Regional Scale. This scale represents the overall geologic and hydrologic environment for the repository. At the regional scale, the rock mass is the main geologic barrier to the migration of radionuclides; typical dimensions of a regional scale model will be on the order of 100 kilometers.

- Repository Scale. This scale represents the rock mass that is directly adjacent to the repository. This rock mass provides a local geologic barrier to radionuclide migration; typical dimensions will be on the order of 10 kilometers.

- Mined Facility Scale. The mined facility is the underground excavation for the repository facility, including shafts, access tunnels, rooms, and boreholes for waste packages. The seals, backfill, and other man-made structures or materials that are installed during construction or decommissioning provide engineered barriers against the migration of radionuclides. Typical dimensions for the mined facility are 1 to 5 kilometers on a side; the height of a typical room is 5 to 10 meters.

- Waste Package Scale. The waste package includes the vitrified waste, steel canister, carbon steel overpack, and buffer material directly surrounding the overpack. The waste package is the primary engineered barrier that prevents the escape of radionuclides into the geologic environment. The typical dimension of the waste package is approximately 1 to 2 meters in diameter.

The different size scales are useful because they allow a very large and complex computational problem to be broken into simpler pieces. These simplifications occur on several levels: geometric, process, coupling, and computational sequence.

From a geometric point of view, it is very difficult to simulate the fine details of a waste package, with a size scale of ~1 meter, in a regional model with a size scale of 100 km. In fact, the computational cell in the regional model usually spans hundreds of waste packages in order to be practical and efficient. It is therefore necessary to use separate models, each of which can capture the appropriate level of geometric detail for the specific analysis and size scale of interest. (As an aside, it is possible to maintain disparate size scales in a single model through a technique called subcycling; however, the other considerations in this section [process and coupling] tend to drive the computational approach to separate models.)

A similar simplification is also possible for processes. For example, processes that are important at the waste package scale may be unimportant for the mined facility, repository, or regional scale, and vice versa. In addition, gradients and coupling are strongest near the waste package, and decrease as the size scale of the model increases. These facts mean that the model for each size scale is generally simpler than a model used to simulate the total system simultaneously.

The four size scales were therefore used as a framework to identify and list the important phenomena for the repository. In developing the list, we have classified the processes into five major types: thermal, mechanical, hydrological, geochemical, and dose assessment. We have also chosen to be comprehensive, rather than to make simplifying assumptions during this initial study. The list and hierarchy of processes is presented in Section 2.3 of this report.

Coupling is also simplified by the size scales because process coupling can usually be described within a given size scale, rather than across size scales. Again, the size scales and the process hierarchy serve as a framework for describing coupled phenomena, the details of which are presented in Section 3.

Finally, from the point of view of computational sequence, the four size scales streamline the performance assessment for the total repository system because the various size scales couple primarily through boundary conditions. For example, the recommended conceptual approach for a base case (or nominal) scenario, where all systems function as designed or anticipated, is as follows:

1. Determine the flow into the repository and waste package,
2. Determine the source term from the waste package, and
3. Determine the fate and migration of radionuclides away from the waste package.

In terms of the size scales, the conceptual approach becomes the computational sequence illustrated schematically in Figure 2:

- A regional hydrological model determines the regional heads and flow field, which will be used to derive the hydrologic boundary conditions for the repository scale model.
- A repository hydrological model determines the flow field into the mined facility and to the waste package. The flow to the waste package is then a boundary condition for the waste package model.

- A waste package model evaluates the long-term stability of the vitrified waste, overpack, and buffer material to determine the release and migration of radionuclides from the waste package to the edge of the borehole. This is often referred to as the source term in performance assessment.

- A repository scale model determines the fate and transport of radionuclides released by the waste package. The transport through the repository scale model becomes a source term for the regional scale model.

- A regional scale model determines the fate and transport of radionuclides into the accessible environment. Other computer models can then perform dose and health effects calculations to determine the impacts from the repository on the biosphere and the public.

This sequence is a bit simplified because the mined facility is also a potential path to the accessible environment; however, the utility of multiple size scales in breaking a complex calculation into simpler components is clearly evident. It is also worth noting that this computational sequence may change substantially for disruptive scenarios, where the geologic or engineered barriers perform in an "off-normal" manner.

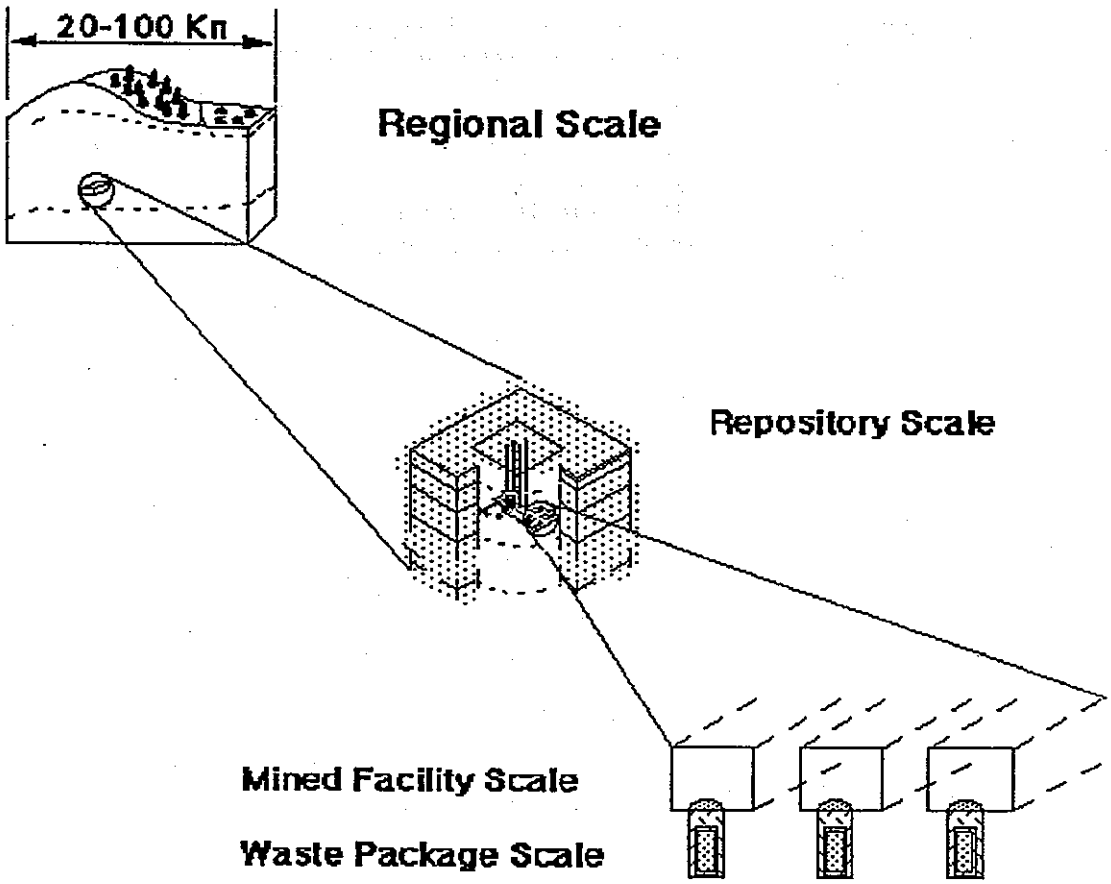


Figure 1. Size Scales in Performance Assessment

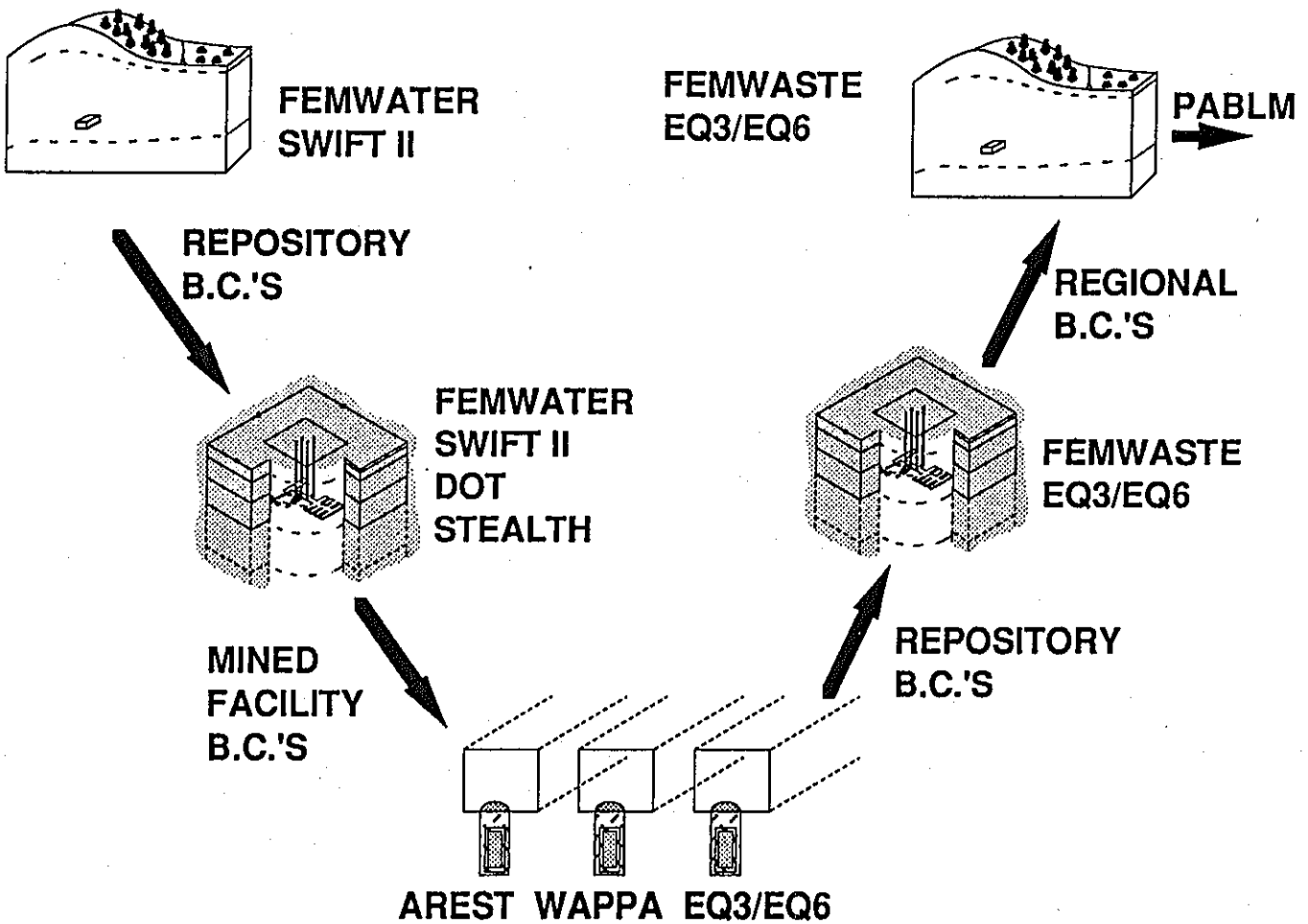


Figure 2. Computational Sequence for System Performance

2.1 INFORMATION ON PRELIMINARY CONCEPTUAL SITES

In Japan it is recommended that feasibility study should be carried out for many potential geological conditions as possible so that the range of availability of future candidate site can be extended. Therefore we have carried out site-generic approach in order to achieve activities focussed on integration of performance assessment system for HLW disporsal system in Japan.

As the approach is largely conceptual and preliminary at present, we set up preliminary conceptual sites for crystalline rock, simple sedimentary rock and complex sedimentary rock. Figures 2～4 show these diagrams. We are using these site concepts in developing system integration schematic and studies of process coupling. Although these diagrams are useful for preliminary studies of scenarios, processes and codes, detailed features of conceptual site's models would be necessary as it is developed.

2.2 INFORMATION ON PRELIMINARY BASE CASE SCENARIO

As scenario and performance assessment are interactive, it needs scenarios specification for performance analysis of geological disposal system. This study is an initial step in developing an efficient, integrated computational system for performance assessment. As the first step, we have focussed on the overall framework of performance analysis for base case scenario, that is groundwater scenario in which nuclide is transported to biosphere indirectly.

According to site-generic approach, PNC has tried to identify potentially significant processes and events by taking into account of variety of geological, hydrological and geochemical conditions in Japan. Table 1 shows a list of processes and events identified. The list is helpful in forming a comprehensive list of processes in the regional, repository, mined facility and waste package scale. We are using it as input of preliminary base case scenario in order to show how we have organized processes and examined the couplings between them.

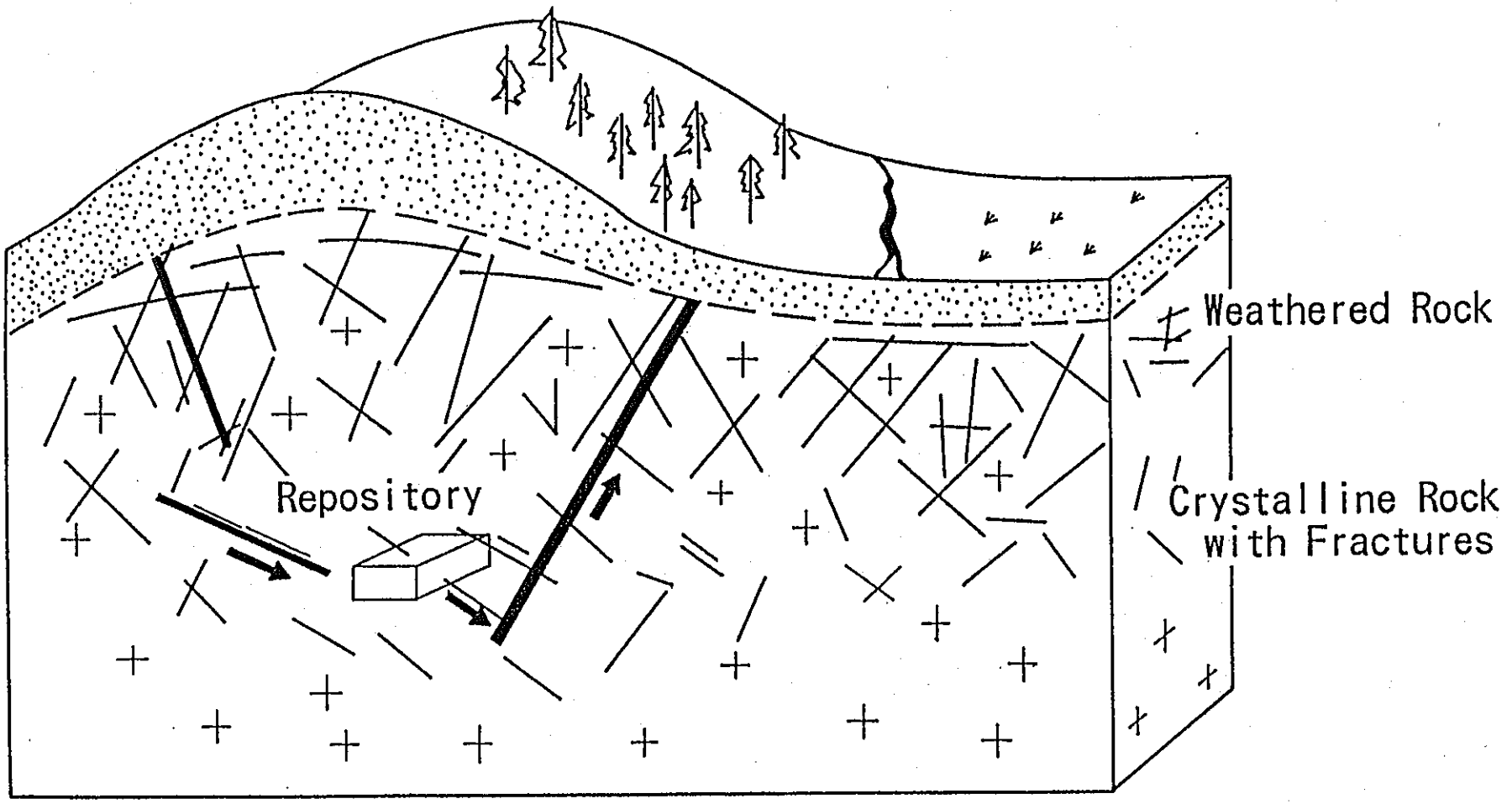


Figure 3 Crystalline Rock Model

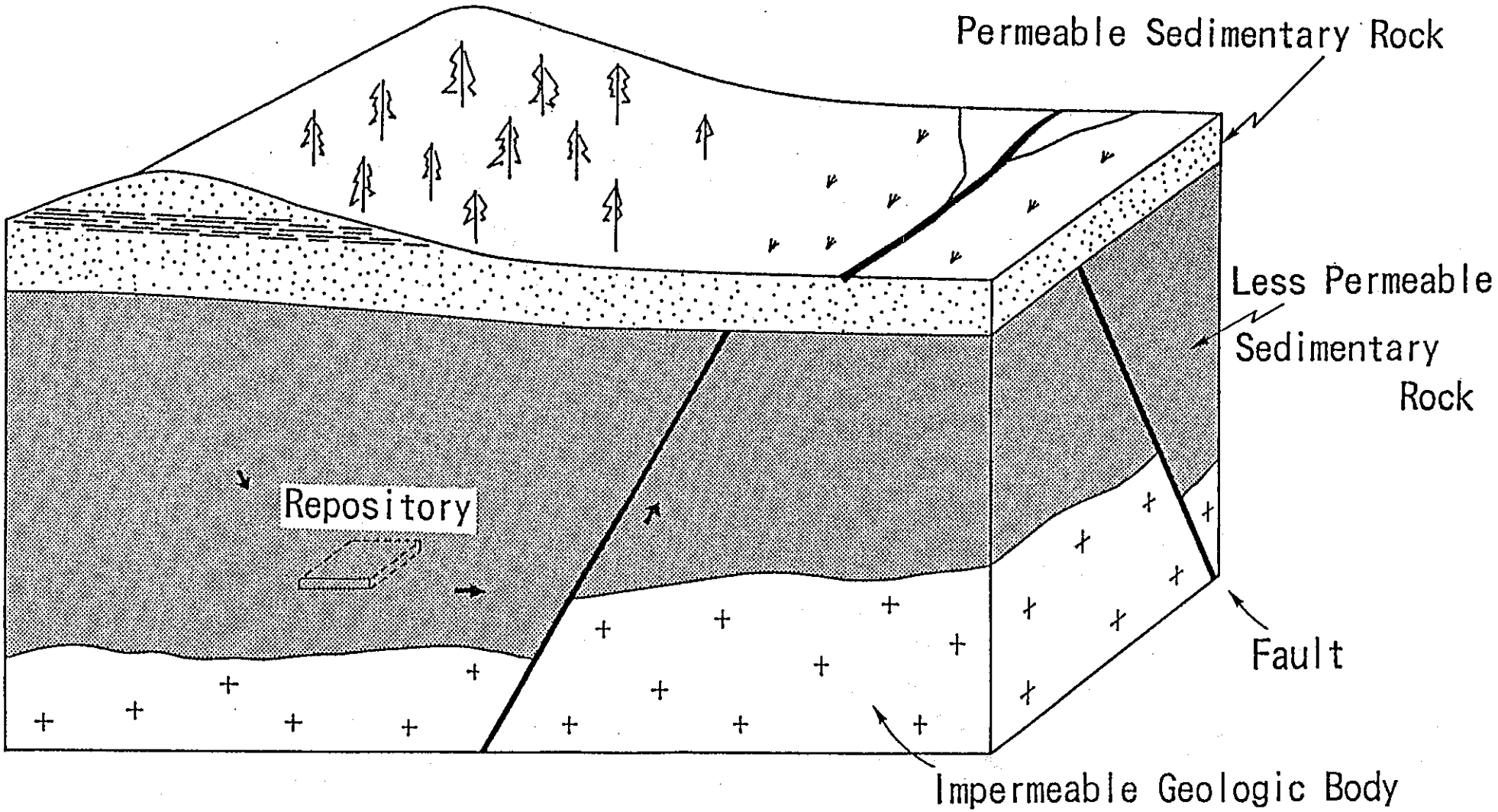


Figure 4 Simple Sedimentary Rock Model

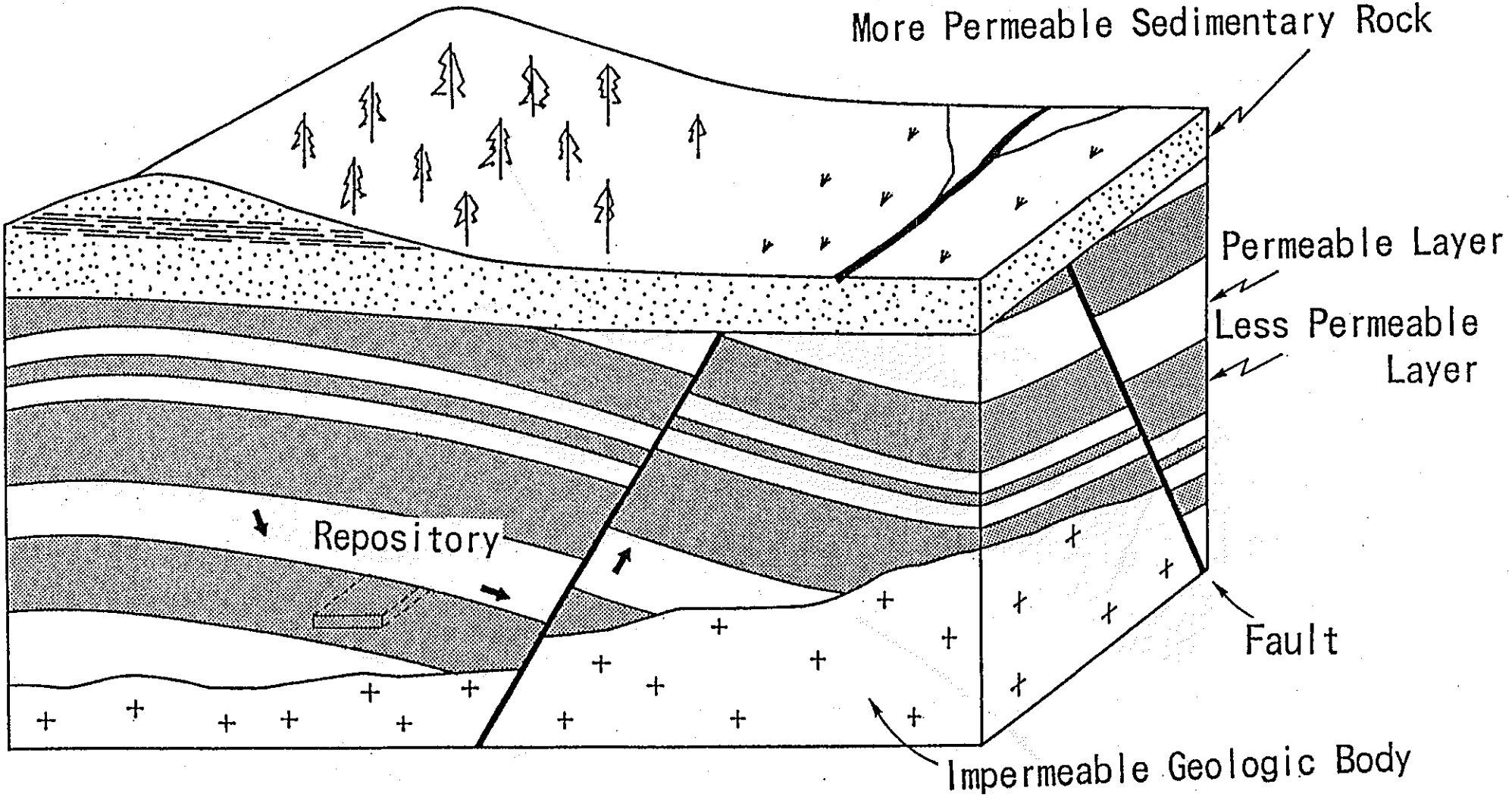


Figure 5 Complex Sedimentary Rock Model

Table 1 List of Events and Processes on Significance in Japan

(Remarks) D : Description only
Ql : Qualitative analysis will be made.
Qt : Quantitative analysis will be made.
In : Initial events
◎ : Important events or processes considered to be important in Japan

A. Natural Processes and Events

1. Climate change (D,Ql,Qt,In,◎)
2. Hydrology change (D,Ql,Qt)
3. Sea Level change (D,Ql,Qt)
4. Denudation (D,Ql,Qt)
5. Stream erosion (D,Ql)
6. Glacial erosion (D)
7. Subsurface erosion (D)
8. Flooding (D,Ql)
9. Sedimentation (D,Ql)
10. Diagenesis (D,Ql)
11. Diapirism (D)
12. Faulting/seismicity (D,Ql,Qt,In,◎)
13. Geochemical changes (D,Ql,Qt)
14. Fluid interaction
    - Groundwater flow (D,Ql,Qt)
    - Dissolution (D,Ql)
    - Brine pockets (D,Ql)
15. Uplift/subsidence (D,Ql,Qt,In,◎)
    - Orogenic (D,Ql)

Table 1 (continued)

- Epeirogenic (D,Ql)
- Isostatic (D,Ql)

16.Undetected features

- Faults,shear zones (D,Ql)
- Breccia pipes (D,Ql)
- Lava tubes (D,Ql)
- Intrusive dykes (D,Ql)
- Gas oil or brine pockets (D,Ql)

17.Magmatic activity (D,Ql,Qt,In,◎)

- Intrusive
- Extrusive

18.Meteorite impact (D,Ql,Qt,In)

19.Weathering

20.Alteration

21.Hydrothermal activity

22.Marine erosion

B.Human activities

1.Undetected past intrusion

- Undiscovered boreholes (D)
- Mine shafts (D)

2.Improper design

- Shaft seal failure (D)
- Exploration borehole seal failure (D)

3.Improper operation

- Improper waste emplacement (D)

4.Transport agent introduction

- Irrigation (D)
- Reservoirs (D)

Table 1 (continued)

- International artificial groundwater recharge or withdrawal (D)
- Chemical liquid waste disposal (D)

5.Climate change(including climate control) (D)

6.Large-scale alterations of hydrogy (D)

7.International intrusion

- War (D)
- Sabotage (D)
- Waste recovery (D)

8.Inadvertent future intrusion

- Exploratory drilling (D,Ql,In,◎)
- Archelolgical exhumation (D)
- Resource mining (D,Ql,In,◎)

C.Multibarrier Performance(Waste/Repository/Geological environment Interactions)

(This list does not include processes relevant to biosphere analysis.)

1.Near-field phenomena

1-1 Processes relevant to near-field conditions

(1)Thermal conditions

a)Radioactive decay;Heat generation (D,Ql,Qt)

b)Heat transfer

- Conduction (D,Ql,Qt)
- Convection (D,Ql)
- Radiation (D,Ql)

c)Geothermal effects (D,Ql,Qt)

(2)Mechanical conditions

a)Swelling of bentonite (D,Ql,Qt)

b)Effects of rock pressure & pore water pressure (D,Ql,Qt)

c)Rock deformation (D,Ql)

(3)Radiological conditions

Table 1 (continued)

a)Radiation (D,Q1,Qt)

b)Attenuation (D,Q1,Qt)

(4)Geochemical conditions

a)Rock/groundwater chemical interactions (D,Q1,Qt)

b)Groundwater radiolysis (D,Q1)

(5)Hydrological conditions (D,Q1,Qt)

(6)Coupled thermal-mechanical-hydrological processes (D,Q1)

1-2 Processes relevant to nuclides release from near-field

(1)Groundwater ingress

a)Water saturation of bentonite (D,Q1)

b)Alteration of engineered materials during resaturation (D,Q1)

c)Change of groundwater chemical property during resaturation (D,Q1)

(2)Degradation of overpack

a)Corrosion

- Corrosion of carbon steel (D,Q1,Qt)

i)Uniform corrosion

- O_2 consumption control (D,Q1,Qt)
- H_2 production control (D,Q1,Qt)

ii)Local corrosion

- Microbial corrosion (D)
- Stress corrosion cracking (D,Q1)
- Macro-cell formation (D)
- Pitting corrosion
  - O_2 consumption control (D,Q1,Qt)
  - H_2 production control (D,Q1,Qt)

- Corrosion of titanium (D,Q1,Qt)
- Corrosion of copper (D,Q1,Qt)

b)Change of groundwater chemical property by corrosion of overpack (D,Q1,Qt)

Table 1 (continued)

c)Microbial effects on corrosion (D)

d)Organic effects on corrosion (D)

f)Gas production (D,Ql)

- H_2 gas production (D,Ql,Qt)
- Effects of H_2 gas

i)Accumulation and release of H_2 gas (D,Ql)

ii)Effect on corrosion (D,Ql)

iii)Effects near-field hydrological conditions (D,Ql)

(3)Nuclide release from waste form

a)Glass dissolution

- Selective nuclides release (D,Ql,Qt)
- Glass matrix dissolution (D,Ql,Qt)
- Precipitation of glass constituents (D,Ql,Qt)
- Mass-transport of glass constituents (D,Ql,Qt)
- Change of groundwater chemical property by glass dissolution (D,Ql,Qt)

b)Nuclides dissolution

- Dissolution of major actinides

i)Pu dissolution

- Effects of chemical form in solid phase (D,Ql)
- Effects of ligands in aqueous phase (D,Ql,Qt)
- Effects of Eh (D,Ql,Qt)
- Effects of pH (D,Ql,Qt)
- Effects of ionic strength (D,Ql,Qt)

ii)Np dissolution

(the same as Pu dissolution)

iii)Am dissolution

(the same as Pu dissolution)

iv)Th dissolution

Table 1 (continued)

(the same as Pu dissolution)

v)U dissolution

(the same as Pu dissolution)

- Dissolution of other actinides and their daughters

i)Cm dissolution (D,Ql,Qt)

ii)Pa dissolution (D,Ql,Qt)

iii)Ac dissolution (D,Ql,Qt)

iv)Ra dissolution (D,Ql,Qt)

v)Po dissolution (D,Ql,Qt)

vi)Pb dissolution (D,Ql,Qt)

vii)Bi dissolution (D,Ql,Qt)

- Dissolution of fission products

i)Cs dissolution (D,Ql,Qt)

ii)Sn dissolution (D,Ql,Qt)

iii)Tc dissolution (D,Ql,Qt)

iv)Se dissolution (D,Ql,Qt)

v)Zr dissolution (D,Ql,Qt)

vi)Pd dissolution (D,Ql,Qt)

vii)Sb dissolution (D,Ql,Qt)

c)Colloid formation (D,Ql)

d)Microbial & organic effects on nuclides dissolution (D)

(4)Nuclides migration through engineered barriers

a)Overpack settlement (D,Ql,Qt)

b)Advection & dispersion in buffer material (D,Ql,Qt)

c)Nuclide diffusion in buffer material

- Diffusion of actinides and their daughters (D,Ql,Qt)

- Diffusion of fission products (D,Ql,Qt)

d)Surface diffusion (D)

e)Nuclides sorption to buffer material

Table 1 (continued)

- Sorption of major actinides (D,Q1,Qt)
- Sorption of other actinides and their daughters (D,Q1,Qt)
- Sorption of fission products (D,Q1,Qt)

f)Nuclides migration through rock in near-field

- Advection (D,Q1,Qt)
- Dispersion (D,Q1,Qt)
- Matrix diffusion (D,Q1)
- Sorption/precipitation (D,Q1)

g)Microbial/organic effects (D)

2.Far-field phenomina

2-1 Processes relevant to far-field conditions

(1)Regional hydrogy

a)Water supply

- Rainfall (D,Q1,Qt)
- Water supply from adjacent hydrogeological systems (D,Q1,Qt)

b)Seepage

- Seepage through fractured media (D,Q1,Qt)
- Seepage through porous media (D,Q1,Qt)

c)Discharge

- Discharge to surface water systems (D.Q1,Qt)
- Discharge to adjacent groundwater systems (D,Q1,Qt)
- Evapolation (D,Q1,Qt)

(2)Geochemistry

a)Rock/groundwater chemcal interactions (D,Q1,Qt)

b)Effects of groundwater flow (D,Q1)

2-2 Nuclides migration through far-field

(1)Nuclides migration through dual continuum(fractured porous media)

a)Advection and dispersion (channeling) of nuclides in single fracture (D,Q1,Qt)

Table 1 (continued)

b)Advection and dispersion (channeling) of nuclides in fractured network (D,Ql,Qt)

c)Sorption

- Sorption to fracture surface (D,Ql)
- Sorption to fracture filling materals (D,Ql,Qt)
- Crystallization (D)
- Irreversible sorption (D)

d)Colloid transtort (D,Ql)

e)Nuclides migration in rock matrix

- Advection and dispersion (D,Ql,Qt)
- Matrix diffusion (D,Ql,Qt)
- Sorption to rock matrix (D,Ql,Qt)
- Crystallization (D)
- Irreversible sorption (D)
- Colloid transport (D,Ql)

(2)Nuclides migration through single continuum (porous media) (D,Ql,Qt)

(3)Nuclides migration in surface water systems (D,Ql,Qt)

2.3 SCHEMATIC OF THE SYSTEM INTEGRATION MODEL

Figure 6, a schematic of the System Integration Model, indicates the hierarchy of all processes to be considered in the repository. Proceeding from left to right, this figure identifies the major systems and subsystems for the repository, and then classifies the relevant processes and subprocesses for each physical component. The mined geologic disposal system is divided into the four size scales (waste package, mined facility, repository, and region), two of which are further split into subsystems such as entry, backfill, or vitrified waste. For each of these physical components, the relevant thermal, mechanical, chemical, transport, geologic, climatic, and dose assessment processes are identified. In some areas, the basic processes are further split into specific subprocesses. Reading from right to left, this figure shows how the processes contribute to the response of the four scales, which then roll up to the performance of the total geologic disposal system.

Each of the processes in Figure 6 will require a model to represent it. Existing codes relate many of these processes and include coupling between them. Capabilities of existing codes are discussed under Section 3. Figure 6 only shows the hierarchy and relationship between the individual mechanistic models. The necessary coupling of these processes is shown in Figure 10 through Figure 13 and discussed in Section 4.

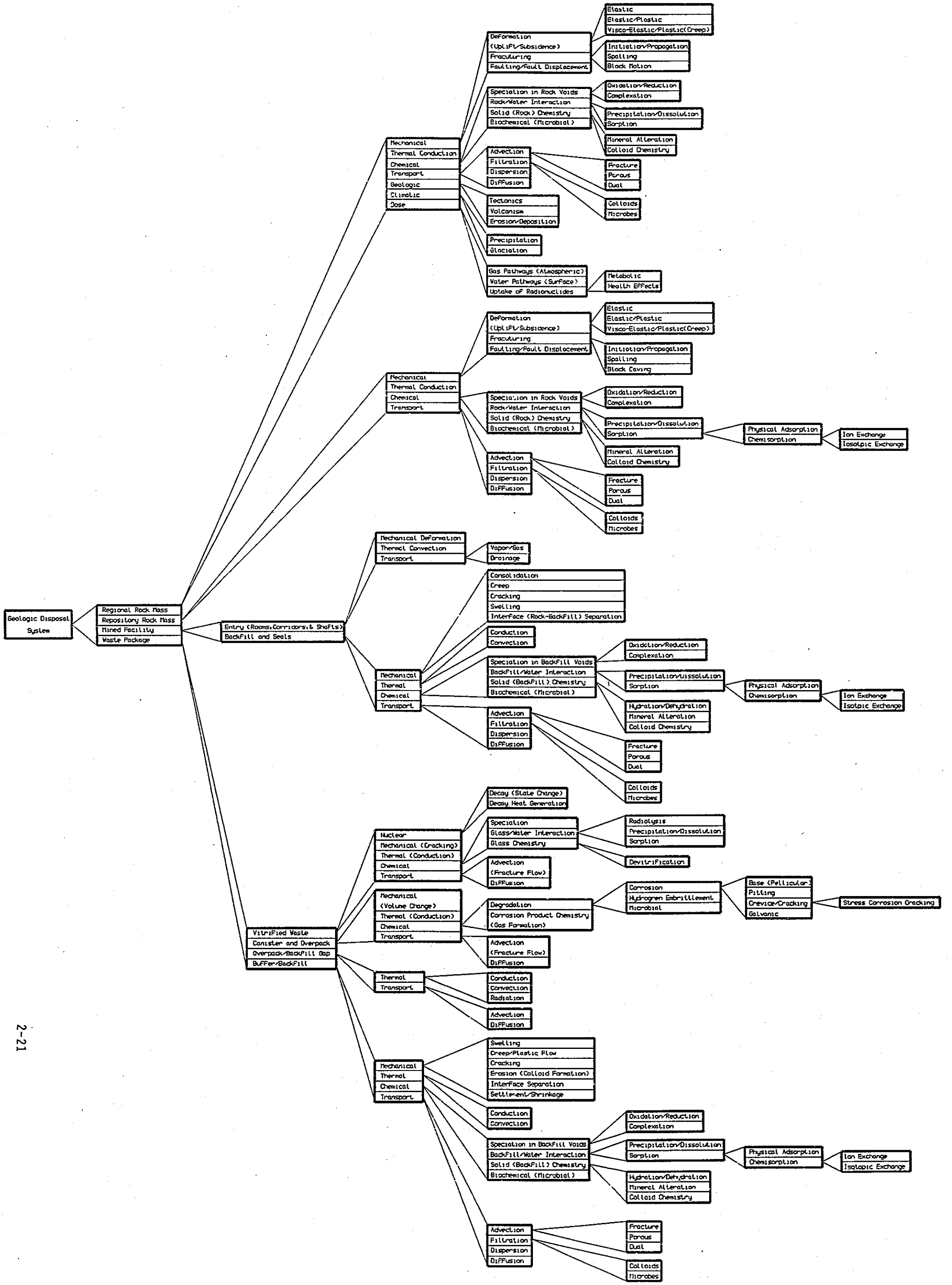


Figure 6 Schematic of the System Integration Model

2.4 STRATEGY FOR DEVELOPMENT OF SYSTEMS INTEGRATION MODEL

2.4.1 Introduction

The System Integration Model schematic, shown in Figure 6, illustrates the hierarchy of processes in each part of the repository system. The implementation of the system integration approach must deal with:

- All the processes as they exist in the schematic hierarchy
- The coupling of these processes
- The use of existing codes (wherever possible) to handle the coupled processes
- Modification and generation of codes or code segments to supplement available techniques
- A means to maintain the quality and integrity of the system models including:

  1. Code configuration control
  2. Preservation and documentation of parametric calculations
  3. Verification and validation

The relationships between these processes and the manner in which they will need to be coupled is also important. Some of the processes and the coupling between them are handled by existing computer codes. Section 3 discusses candidate codes in terms of processes and the coupling which they handle.

The final step in the system integration model will consist of the ASIM ("Advanced System Integration Model"). The ASIM will be a fast-running and simplified total system performance model which provides faithful representation of the system response. Prior to the development of the ASIM, the systems model will not be one model but a computational integration of many models (codes). In this form, the model will represent engineering development activities using many different tools in a controlled and integrated way.

2.4.2 Developmental Phases

The methodology for implementation of an integrated systems approach will be described below in terms of three phases: Simplified Modeling, Complex Modeling, and ASIM. These are pictorially represented by the "kite" diagram (Figure 7), where the width of the kite represents the complexity of models and the vertical axis represents the evolution of the models with time.

Phase 1, Simplified Modeling

The primary focus of this phase will be the development of conceptual models. The effort will focus on learning the relative importance of the principal processes and comparing different means of representing and coupling them. The verification and validation efforts will begin to build up a background of confidence with these simpler combinations of models. Use of such simpler models

will help develop a better understanding of the general behavior of generic sites under a variety of scenarios. Initial calculations will be for the undisturbed "base case" which considers normal processes.

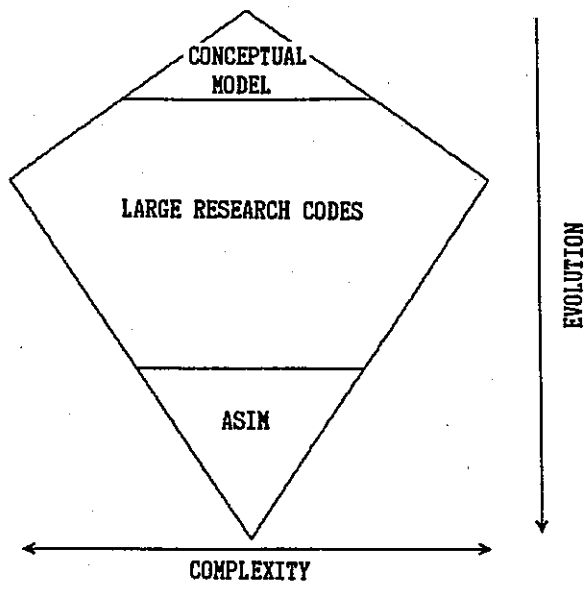


Figure 7. Development Process of the System Integration Model

Figure 8 shows the suggested processes and coupling that should be considered during Phase 1 modeling. The more prominent coupled processes are modeled in many existing codes. For example, thermal-mechanical rock response, flow and equilibrium physical adsorption, and thermal-chemical interaction for elementary relationships such as solubility of single species are simulated by several state-of-the-art computer codes. Coupling within a particular scale (such as the waste package) is done in existing codes such as AREST-PNC and WAPPA. Coupling between scales or between more complex processes (such as thermal and multi-species solubility) will require multiple codes. In such cases the coupling will generally be unidirectional. That is, one process affects the other but not significantly vice versa. For example the temperature has a strong effect on the species solubility but where concentrations or heats of solution are small the dissolution/precipitation does not use or contribute significant amounts of heat or affect overall heat transfer properties. Thus the temperature affects chemistry but the chemistry does not significantly affect temperature. In this case the output of one code (thermal calculations) can become input to another.

The system integration then consists of appropriate parameter tracking and preprocessor software to pass data from one code to the other. Where there is significant coupling in both directions (such as with thermal and mechanical) then coupling must be integrated within the same computational model to allow iterative or analytical solution of the coupled system. This may require some code modification or even new code development. Some areas where this might be need during Phase 1 are:

- Thermal and mechanical coupling in the rock mass or backfills
- Mechanical and chemical coupling in the buffer or backfill
- Mechanical in backfills and mechanical in surrounding rock

Phase 2, Complex Calculations

As more is learned about generic and (possibly) specific sites and more experience is gained with the simpler calculations, then more second order types of processes and process couplings will be studied in order to provide a complete understanding of the role of all possible processes in the total

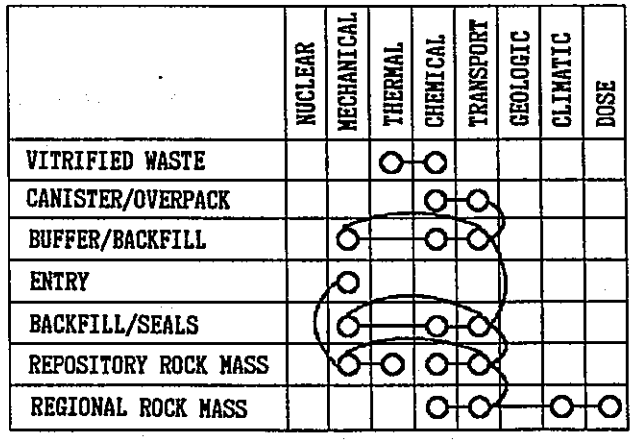


Figure 8. Principal Process Coupling

system performance. All of the processes shown in Figure 6 along with the couplings discussed under Sec.3 will need to be considered during this phase.

The main objective of this phase will be to gain sufficient understanding and data to be able to reduce the total system response to a more simplified model which reflects the important processes and their function (the "kite" begins to narrow). This provides the basis for ASIM development.

Phase 3, Development of ASIM

The final stage of development of the System Integration Model is the Advanced System Integration Model (ASIM). As the "kite" diagram in Figure 7 shows, the degree of complexity of this model becomes very small compared to the large engineering codes. This does not mean that the code is simple in the sense that it does not simulate all the necessary processes and couplings. Rather the code is less complex because it only simulates what is essential for a full representation of the system. This simplification results from what has been learned during the studies with the large research codes.

There are several approaches that might be used to develop the final ASIM. These include:

- Simplification of models through sensitivity analysis
- Development of response surfaces (data correlation)
- Use of simplifying assumptions ("conservative")
- Simplification of models through uncertainty analysis

It is likely that more than one of these methods will be used in combination. During the large scale studies (wide portion of the "kite") sensitivity and uncertainty analyses will be carried out. At the same time a large data base of analytical results will be built up. The experience of all these studies will help to guide which of these techniques will be used to develop the final ASIM.

Sensitivity Analysis

This technique involves the use of parametric studies with large codes to identify parameters which have an insignificant impact on repository performance for all scenarios of interest. Such analyses can include multiple code runs using sampling techniques, and development of adjoint solutions which allow estimation of derivatives (for example the GRESS system). When insensitive parameters are identified, portions of the model using these parameters can be simplified.

Response Surfaces

The large amount of data that are generated by detailed parametric analysis can be assembled into tables and possibly curve fit with correlating equations. These tables or equations can then be used as response functions. That is, an output result can be directly estimated as a "looked up" value given a certain input parameter. The complex codes are then replaced by a series of response surfaces. Of course, a very large data base is needed for such an approach.

Simplifying Assumptions

This is very similar to sensitivity analysis. It is different in that the simplifications are usually imposed as a result of assumptions about the physics of the system rather than as a conclusion from formal parametric sensitivity (mathematical) tests. Confidence that the assumption is valid can come form both calculations and results of physical testing. The assumptions are justified by the extensive experience after the large code (and associated testing) studies. One common simplifying assumption is the "conservative" approach where a mitigating process is ignored and the system still performs satisfactorily. Conservation assumptions have often been employed early in performance assessment (conceptual modeling stage) but the confidence in these results must be low since the interaction of

many processes is not easily estimated before extensive study. In fact, the interaction of two conservative assumptions can occasionally produce a non-conservative answer.

Uncertainty Analysis

The application of this technique is similar to sensitivity analysis. However, in sensitivity analysis parameters which have minimal effect over their applicable range are identified while in uncertainty analysis the effect of uncertainty of values of parameters is estimated. In the case of uncertainty analysis we may identify that large uncertainty in some parameters has little effect on the confidence in the final performance. Modeling of such parameters' effects then can be simplified.

2.4.3 Code Configuration and Integrity Control

Confidence in the performance assessment of the repository system is totally reliant on the confidence in the calculational tools. Because of the time and space scale of the system it is not possible to perform real-time and real-scale proof tests. The confidence in the calculations is then completely dependent on the demonstrated integrity and control of the calculational methods. The System Integration model (a calculational system) must be developed with such integrity and control.

Code Configuration

In a typical code development and application environment it is very difficult to control and track all modifications made to a computer code. Code developers are constantly testing and improving the features and capabilities of a computer code. Staff engineers are using one or more versions of a computer code to perform engineering analyses. These engineering analyses typically require special constitutive models or boundary conditions which must be added to the computer code to perform the analysis. All of these developmental and application specific computer code modifications typically result in a new and unique version of the computer code. Even a small engineering staff (less than six people) performing 20 analysis studies a year can easily generate 100 unique versions of a computer code.

ATLAS is a software tool which provides modification control and Quality Assurance (QA) tracking of computer codes. Once a computer code is placed under ATLAS configuration control, ATLAS:

- Archives the current and all subsequent versions of a computer code
- Controls all modifications made to a computer code
- Documents all modifications made to a computer code

ATLAS archives and tracks all previous versions of a computer code. This feature protects against the accidental erasure or loss of older versions of a computer code. All previous versions of a computer code are also accessible at any time for review, modification, and Verification and Validation. ATLAS controls all modifications made to a computer code. Code users use ATLAS to make all developmental, error correction, and application specific modifications to a computer code. Finally, ATLAS documents all developmental, error correction, and application specific modifications made to a computer code. This documentation provides a complete QA record of all changes made to any version of a computer code.

Control of Parametric Cases

Parametric data used for engineering and research codes are typically drawn from a number of different sources. These sources include laboratory and in situ test data, site and design databases, published results from previous modeling studies, and data generated by other research and engineering codes (temperatures and stresses for example). The origin and integrity of these data are difficult to trace without some form of data management and control. PARATRAC is an information

management and integration system developed for use on large environmental and geotechnical site investigation programs. PARATRAC functions through a combination of relational database management systems (RDBMS), geographic information systems (GIS), analytic/numerical models, and computer graphics. PARATRAC provides a framework which links and relates the data needs of engineering and research codes to the currently available data for one or more sites. These data can be extracted from databases which contain generic, laboratory, and available in situ test data, as well as the computed results from other engineering and research codes.

Code Integrity

Public confidence in the results of integrated system calculations is very dependent on the ability to demonstrate that the codes have been sufficiently verified and validated. As used in this report, verification is the process of demonstrating that a computer program accurately solves the equations it was designed tosolve. Validation is the process of demonstrating that a computer program can accurately simulate the response of the natural environment. Both verification and validation (V&V) are designed to build confidence in the results from performance assessment predictions. Verification is usually a straightforward process, while validation is very difficult because of the long time scales for nuclear waste migration and because of the complexity of the geologic environment.

Each of the large codes used during the research period (wide portion of the "kite') will need to be independently verified through the use of expert review, comparison to analytical solutions and code to code comparison (benchmarking). In addition, the research codes must be validated (i.e. compared to measurements in the laboratory, large scale tests or in situ tests). Many codes currently in use have some degree of verification and a few have been partially validated. (See code reviews in Section 3.) This is useful but it must be recognized that modifications to such codes (as is often needed) require a certain degree of revalidation and reverification. It is also true that the current state of V&V of existing codes is usually not complete enough for full confidence in performance assessment calculations. Experience in many countries is such that while there may be a considerable amount of verification, validation is usually not complete or totally missing.

As the ASIM is developed, the V&V problem is somewhat simplified and changed. If the ASIM consists mainly of response surfaces then the main task will be verification. This approach is valid because if the response surfaces are constructed from data generated by validated research codes, it can then be assumed that the response surfaces will be validated if it can be shown that they are faithful representations of the results from the research codes and that any other codes used to fit or manipulate the data are correct. Therefore, what is mainly needed here is data base and code verification to produce an ASIM with full V&V. (In fact, additional work may be required if the interaction of multiple response surfaces produces unusual or non-conservative interactions.)

Also important is the V&V of all the integration tools such as data bases, pre-processors, post-processors, and management software (such as ATLAS and PARATRAC). The V&V of management software is often obtained by the experience of many users.

In each step of the development of a system integration model (as we proceed down the "kite" in Figure 7) it will be necessary to carry out a comprehensive independent verification and validation (IV&V) of all the elements of the integrated calculational system. This will involve independent review, calculational comparisons and comparisons with test data. The result is a system model that can be used with confidence in demonstrating the performance of the geologic disposal system.

3. REVIEW OF CANDIDATE COMPONENT PROCESS MODELS

3.1 CODE SURVEY

The review of candidate component process models involved a preliminary survey of 39 existing computer codes. The component processes have been categorized into eight process types: nuclear, mechanical, thermal, chemical, transport, geologic, climatic, and dose. The detailed description of the component processes is described in the discussion of Sec.4. The process type breakdown for the 39 codes is as follows:

Process Type	Number of Codes Surveyed
Nuclear	0
Mechanical	6
Thermal	5
Chemical	8
Transport	11
Geologic	0
Climatic	0
Dose	9

At this time, no codes for modeling nuclear, geologic, and climatic processes were surveyed because they involve second order impact on performance assessment or involve disruptive scenarios that have not been considered here.

Most of the information for the review was obtained from the code documentation. Information were also obtained from related code benchmark, survey, and compendium reports. These reports are identified in the bibliography.

The results of the code survey are conveyed in the form of charts. Codes for mechanical and thermal, chemical, transport, and dose process types are presented in Table 2, Table 3, Table 4, and Table 5, respectively.

3.2 TABLE DESCRIPTION

This section describes the information presented in Table 2 through Table 5.

Code Name - Name of the code as specified in the code documentation.

Authors and Affiliation - Names and affiliation of the authors of the version of the code that was surveyed. Some listed authors are the original creators of the code. Other listed authors made revisions to the code to create the more recent version that was surveyed in this review.

Processes Simulated - This entry lists the processes the code simulates. Under each process type, the applicable processes simulated are noted (see the discussion in Section 4). Some codes can simulate processes in two different process types. For example, HEFF can simulate mechanical elastic deformation and thermal conduction processes.

Description and Capabilities - This entry discusses the code's modeling and solution techniques, code features, and capabilities.

Status of Verification and Validation - This entry discusses any known work on the verification and validation of the code. Additionally, some benchmark studies may also be noted.

Documentation - Reference documentation for the version of the code surveyed. The report number(s), originating and issuing organizations, and publish date are given. This entry also discusses the contents of the documentation. Compliance with NUREG-0856 requirements and guidelines is noted when applicable.

Similar Codes - Other codes with similar features, capabilities, or solution techniques. Codes listed in this entry may or may not be surveyed in this review. Some codes may not have any entry.

Other Notes - Other pertinent facts related to the code are specified in this entry. Examples of such facts include relationship with older or other codes, code size, computer system types, and pre- and post-processors.

BIBLIOGRAPHY

Bauer, Stephen J. and Laurence S. Costin, "Thermal and Mechanical Codes First Benchmark Exercise Part II: Elastic Analysis," SAND89-0757, Sandia National Laboratories, Albuquerque, NM, 1990.

Broyd, T. W. et al., "A Directory of Computer Programs for Assessment of Radioactive Waste Disposal in Geological Formations," Atkins Research and Development, Epsom, Surrey, UK, 1983, updated 1985. Work performed under the European Community's Research Programme (1980-1984).

Costin, Laurence S. and Stephen J. Bauer, "Thermal and Mechanical Codes First Benchmark Exercise Part I: Thermal Analysis," SAND88-1221, Sandia National Laboratories, Albuquerque, NM, 1990.

Fluor Technology, Inc., "Rock Mechanics Models Evaluation Report," DOE/CH/46656-09, 1987. Prepared for the U.S. Department of Energy.

McBride, A. F. et al., "Compendium of Technical Computer Codes Used in Support of the DOE Office of Civilian Radioactive Waste Management", ORNL/TM-10919, Oak Ridge National Laboratory, 1989. Prepared for the U.S. Department of Energy.

Mills, M. and D. Vogt, "A Summary of Computer Codes for Radiological Assessment," NUREG/CR-3209, U.S. Nuclear Regulatory Commission, 1983.

Morgan, Harold S., Raymond D. Krieg, and Rudolph V. Matalucci, "Comparative Analysis of Nine Structural Codes Used in the Second WIPP Benchmark Problem," SAND81-1389, Sandia National Laboratories, Albuquerque, NM, 1981.

Williams, P. T. et al., "Assessment of Thermal Analysis Software for the DOE Office of Civilian Radioactive Waste Management," SAIC-87/1943, Science Applications International Corporation, 1988. Prepared for the Oak Ridge National Laboratory, Oak Ridge, TN.

この頁はPDF化されていません。

内容の閲覧が必要な場合は、技術資料管理担当箇所で原本冊子を参照して下さい。

（3－3頁）～（3－11頁）

4. STRATEGY FOR COUPLING

4.1 REVIEW OF COUPLING STUDIES

The principal couplings between the major process types is summarized in Figure 8 and briefly discussed in Section 2.4.2. This section provides a more detailed discussion of the coupling between size scales, followed by discussion of the individual process couplings that are known to be important at this time.

4.1.1 Transport Coupling at Size Scale Boundaries

Transport coupling at scale or boundaries is necessary to provide continuity of specie and concentrations from one size scale to the next. In modeling terms, the transport coupling at scale or subsystem boudaries represents the source terms for radionuclide migration within the model. For example, waste package analyses will determine the specie and concentration of radionuclides that are released into the near-field environment of the mined facility and repository. These data for specie and concentration, as a function of time, must be used as boundary conditions for near-field models.

4.1.2 Mechanical Coupling at Size Scale Boundaries

Mechanical coupling at scale boundaries involves the transfer of stress from one size scale or subsystem to another. In modeling terms, the mechanical coupling at scale or subsystem boundaries can be considered as stress boundary conditions for a model. For example, waste package analyses typically require rock stresses to determine the impact of rock mass movement on waste package performance. Mined facility and repository rock mass models use regional in situ stress conditions to develop initial and boundary conditions.

4.1.3 Thermal Coupling at Size Scale Boundaries

Thermal coupling at scale boundaries is necessary to provide thermal continuity from one size scale or subsystem to the next. In modeling terms, the waste packages represent source terms and thermal coupling at scale or subsystem boundaries will be represented as a temperature or heat flux boundary conditions for a model. The heat generated in the vitrified waste is then transported through the waste package subsystem out into the mined facility and repository rock mass subsystems. Ultimately, the heat generated by the vitrified waste is dissipated into the regional rock mass.

4.1.4 Thermal and Chemical Coupling

Issue

Chemical reactions are temperature dependent.

What is Being Coupled

Heat is generated by the emplaced high-level nuclear waste. This heat raises the local temperature of the repository rock mass above what it would be due to the preexisting geothermal gradient. This heat pulse, and the associated change in temperature, increases in magnitude as fission products in the waste decay and a thermal gradient is established; it then decreases over a long time until the original thermal conditions are restored.

The equilibrium constant of chemical reactions is temperature dependent. Thus the relative stability of aqueous species, solids (affected by precipitation or dissolution), and surface phases bound by

various sorption processes depends on temperature and varies appreciably over the range of temperature fluctuation expected from repository heating.

Chemical models generally use 25 degrees C as a reference temperature; however, these models must be able to operate throughout the temperature range of concern. Further, they must be coupled to a thermal model which provides the appropriate temperature for the time and location of the chemical calculation. Sensitivity analyses of geochemical models have shown that changes of a few degrees C can result in more than an order of magnitude in key chemical model results, such as the solubility limits of actinides (e.g., Uranium solubility, Muller and Duda, 1983).

Treatment of Interaction

The chemical equilibrium constant of any reaction is a function of the chemical potential of the products and reactants of the reaction. For fundamental thermodynamic reasons, these chemical potentials are dependent on temperature and pressure. Pressure variations in near-earth-surface chemical reactions (as opposed to reaction in the earth's core or in high-pressure reactors) are not sufficient to appreciably affect chemical potentials, but geothermal and repository-induced thermal variations are definitely significant.

Although temperature's effect on chemical reactions is well known near 25 degrees C, methods of accounting for the interactions between temperature and chemistry require more and more data and become correspondingly less and less reliable as temperature varies from this reference temperature. Reactions of concern in nuclear waste disposal can be modeled reliably in the range of 4 to about 50 degrees C using adjustments to equilibrium constants based on enthalpy of formation. Above 50 degrees C, data from empirical observations in more sophisticated temperature-effect models is needed.

Since geochemical codes generally account for variations in temperature, accounting for the interaction between temperature and chemistry is as simple as providing these codes with the appropriate thermal (boundary) conditions. Since both temperature and chemistry (composition and speciation) will vary with location and time, particularly in the waste package and backfill, providing thermal input to geothermal calculations may involve successive solutions of thermal and dependant chemical calculations for the same time-step. Passing of thermal information to the geochemical calculations can be optimized by spatially gridding the thermal and chemical calculational network in a mutually congruent way, or by only passing new thermal data at a point when temperature changes by more than a pre-determined amount per time-step (or set of time-steps).

Best Treatment

Most geochemical codes used in nuclear waste management have the capability of treating the temperature dependence of chemical reactions. Therefore, codes need not be selected based heavily on this feature. Codes, such as EQ3/6 (Wolery, 1979) and PHREEQE (Parkhurst, et al., 1980), are appropriate. Their ability to accurately simulate the coupled effect depends on the availability of suitable data.

Coupling thermal data to the geochemical codes is best done via a data controller, which stores results from the calculations of thermal codes and provides them to the selected geochemical code.

4.1.5 Thermal and Mechanical Coupling

Issue

Changes in temperature result in changes in the mechanical stress state (pressure) of a geologic or engineered material.

What is Being Coupled

The coupling mechanism between thermal and mechanical processes is generally described by the temperature change effect on mechanical pressures. Most analytical solutions in thermoelasticity (Nowacki, 1962), numerical solutions in thermo-plasticity (Bland, 1956), and numerical models for non-linear geologic materials (Hart and St. John, 1986) are based on this one-way coupling assumption. Mechanical work and/or strain energy can increase or decrease the total energy in a system and therefore result in temperature changes. For most problems in elasticity, this effect is small and usually ignored. Massive material failure accompanied by large dilitation and volumetric strain changes could have a significant non-linear effect on thermal properties such as conductivity. This type of mechanical-thermal coupling is only expected to be important for the treatment of disruptive scenarios involving the catastrophic failure of entries.

Treatment of Interaction

Thermal-mechanical coupling is typically introduced as an additional pressure term in the stress-strain formulation. The incremental pressure (dp) due to thermal expansion is given by:

$$dp = KadT$$

where K = bulk modulus, a = volumetric thermal expansion coefficient, and dT = incremental temperature change. For porous materials Garg (1977) developed a relationship between porosity and temperature:

$$dn/n = (af - a)\, dT$$

where af = volumetric thermal expansion coefficient of the fluid.

Best Treatment

Most stress analysis codes have the capability to compute stress changes due to changes in temperature. Fully coupled codes such as STEALTH compute the temperature and thermal-stress field simultaneously. Stress analysis codes such as SPECTROM and ADINA require temperature inputs from a suitable thermal analysis code.

4.1.6 Chemical and Mechanical Coupling

Issue

The swelling of clays due to chemical hydration can exert mechanical forces on its surroundings.

What Is Being Coupled

Clay minerals, such as bentonite, used as buffer and backfill in the waste package (surrounding the waste canister in the emplacement hole) or in the mined facility will be emplaced at water contents well below saturation (probably on the order of 10 to 20% saturation). After repository closure, repositories below the water table will resaturate. This will provide water to the hydration reactions of clay minerals. Increasing saturation through these hydration reactions is generally accompanied by changes in mineral structure and increases in volume.

Volume increases due to the hydration of clays in a confined space result in mechanical swelling pressures. These pressures can be on the order of the lithostatic pressures in a deep geologic repository (Pusch, 1980). Thus, the resulting pressures can be sufficient to restore, or perhaps exceed, the original (pre-excavated) stress states in the host rock.

Pressure from the hydration of backfill must therefore be considered in the mechanical design of the repository. This is accomplished by coupling the extent of mineral hydration and volume change (which is itself dependent on the transport and availability of water into the backfill) to the development of swelling pressure.

Treatment of Interaction

Chemical models which simulate reaction path as well as speciation can calculate the mass balances associated with the formation of hydrated minerals from less hydrated ones. This calculation results in the amount (generally, the number of moles) of minerals "created and destroyed" in the processes. Given the density of these minerals, the net increase/decrease of volume may be calculated.

Changes in volume due to the hydration of clays result in changes in the mechanical state of the clay material. The compressibilities of the solid grains, the bulk material, and the pore fluid interact to determine the final stress and pore volume state of the hydrated clay material.

Best Treatment

The net volume change in the total mineral phase can be calculated by a post-processor to the geochemical code of choice, probably linked through a data controller. The volume results can be provided to the mechanical code in the same way.

4.1.7 Chemical and Transport Coupling

Issue

The concentration and speciation of radioelements released from nuclear waste influences how rapidly these radioelement are transported through groundwater.

What Is Being Coupled

"Transport" denotes the movement of water and associated solutes, generally in saturated media like backfill or a rock mass. This is a result of the advection of solution through the medium, but the water solvent and the natural or repository-related solute do not undergo the same advective processes. Sources and sinks for solute species are more numerous and diverse than for water.

The movement of water depends only on hydraulic gradient, hydrodynamic dispersion, (second order diffusion of water) and the hydraulic properties of the medium.

Movement of solute within the water depends also on solid, aqueous and pore diffusion; sorption; and precipitation/dissolution (Langmuir, Muller and Duda, 1983). These processes depend on the speciation and concentration of the solutes, which is calculated by chemical models.

Thus, the chemical and hydraulic properties and processes occurring in the repository system must be coupled to fully account for the transport of solutes.

Treatment of Interaction

There are three independent ways of treating the interaction between chemistry and transport:

1. Adjusting water velocities with distribution coefficients to calculate solute velocities (and resulting concentrations)

2. Writing the advection-dispersion equation to account for all sources and sinks of solute as well as water

3. Using hydrology codes to model water movement, geochemistry codes to model species concentrations in the water, and coupling the results via a mixing-cell model

Each of these treatments are discussed below, with examples of codes which employ the approach.

Distribution coefficients - Transport modeling which couples hydrologic and chemical modeling via distribution coefficients relies on the retardation equation, defining retardation factor (R) as a function of the aquifer matrix density, the effective porosity and the distribution coefficient of the solute being transported. Water velocity, calculated with Darcy's law models, is multiplied by R (which is less than 1) to model solute velocity.

This approach can be valid for single species in homogeneous and well-characterized media, such as ion-exchange columns for which the relationship was originally defined, but does not apply to natural systems. The derivation of the retardation equation (Muller, 1983) involves assumptions such as:

- Elements having only one species in solution (single oxidation state, single ionic form)
- Well defined flow path and travel times (step function breakthrough curves)
- Residence time in a flow control volume equals transit time of species
- All fluid volume in a control volume is available to advective transport (no dead-end pores, such as those occurring in crystalline rocks)
- The density of the matrix (aquifer material) is homogeneous and constant
- All void-space is saturated with water
- The effective porosity of the matrix (aquifer material) is homogeneous and constant
- Voids not interconnected with the interconnected void space are accounted for in the density value
- No significant kinetic or diffusion effects occur
- Measured distribution coefficients are representative of real-world conditions

Historically, most transport models used this treatment (e.g., FEMWASTE; Yeh, 1989), but the approach now has been generally discredited for inorganic species (e.g., Reardon, 1981). Nevertheless, in the absence of data about aquifer properties, environmental conditions, and contaminant properties, the treatment may give some bounds on the potential mobility of contaminants (Serne and Muller, 1987).

Advective-dispersion Equation - Transport models can be written which fully account for all sources and sinks of contaminant species just as they do of the water which is transporting them. This effectively results in an expression of the advective-dispersion equation of each contaminant considered containing terms for:

aqueous diffusion
matrix diffusion (both solid and dead-end pore)
hydrodynamic dispersion
precipitation/dissolution
chemical substitution reactions
isotopic exchange
ion exchange
direct adsorption

Not all of these mechanisms are important for all species under all conditions, so models have been constructed which systematically account for relevant mechanisms (e.g., CHMTRN; Miller and Benson, 1983). These models tend to be either extremely complete and cumbersome or, by computational necessity, over-simplified.

One method to reduce the complexity of this treatment is to write the advective-dispersion equation for only one (master) species for each element considered by the model. Once the total elemental concentration in solution is thus determined, speciation among other solute phases can be calculated separately and independently by the code (e.g., HYDROGEOCHEM; Yeah and Tripathi, 1990).

The benefit of this treatment is it's flexibility. The models of each chemical source/sink term may be as simple or as sophisticated as the problem warrants. For example, sorption may be modeled as a simple equilibrium distribution (as discussed above), as an adsorption isotherm, as mass-actions, or as surface complexation, as appropriate (Serne and Muller, 1987).

Mixing cells - Transport models taking maximum advantage of previous hydrologic model and geochemical model development can combine their results using a mixing cell approach. This involves gridding the region of interest into a three dimensional system of volumes. Reductions in dimensionality for symmetry are allowed. Hydrologic models (based on Darcy's law) are used to calculate the fluxes of water among adjacent cell volumes at each time-step. Then a geochemical model is used to calculate distribution and mass sources/sinks of solutes within each cell in the same time-step.

This assumes that concentrations are homogeneous within the cell (mixing). The resulting transport/mass-balance/source-sink calculational cycle takes full advantage of the capabilities of sophisticated hydrology codes for water movement and sophisticated geochemical codes for the chemical processes enumerated in above (e.g., Langmuir, Muller and Duda, 1983). The interface between two codes can be achieved using a data controller which manages the data grid and calculation timing.

An important consideration in this treatment of the interaction of geochemistry and transport is in avoiding artificial (calculational) dispersion in the model results. This can occur when the system being modeled is inappropriately gridded. Sensitivity to alternative grids and sufficiently small grids in areas of rapid flow or geochemical evolution are important.

Best Treatment

The distribution coefficient approach is least reliable. The preferred approach between the remaining two depends on the modeling application (i.e., what is the object of the modeling exercise). The complete advection-dispersion approach is more comprehensive when fully implemented, but may be cumbersome to implement and use. The mixing cell approach takes maximum advantage of the state of the art codes in hydrology and geochemistry, but can be difficult to manage computational. These two treatments are conceptually identical and will ideally produce the same results.

4.1.8 Mechanical and Transport Coupling

Issue

The mechanical deformation of porous and/or fractured media directly influences the transport of fluids through the repository rock mass and engineered backfill materials.

What is Being Coupled

The theoretical analyses of mechanical-transport coupled flow problems typically assume a two-way interaction. The mechanical volumetric strain of the saturated porous or fracture matrix influences fluid density and generates changes in fluid (pore) pressure. Changes in fluid pressure affect the compressibility and effective stress state of the rock or backfill material. Another aspect of mechanical-transport coupling is the numerical treatment of a fractured, porous media. The mechanical-transport coupling can be treated as either a porous, fractured, or dual (porous and fracture) medium.

Treatment of Interaction

Buffer and backfill materials such as bentonite will probably be treated as porous material from the standpoint of mechanical-transport coupling. The strongest coupling mechanism will be the influence of the stress carried by the pore fluid on the mechanical behavior of the material. Since Terzaghi (1923) first described his classical "effective stress" concept, the effect of fluid pore pressure on the deformation and strength of saturated porous media has been widely studied. The deformation of the porous media is then related back to changes in porosity which directly impacts the flow field.

A fractured, porous rock mass can be treated as either a discrete system of fractures, taking into account the detailed fracture distributions, or as a continuum representing the spatial average of the fractures. If the flow through the porous rock matrix is not negligible, the fractured rock mass can be treated as two overlapping regions with two porosities, one representing the fractures and another the porous rock mass. The choice between the discrete, dual-porosity, and porous media models depends on the characteristics of the fracture network, the size of the region, and the physical processes of interest. For near-field (waste package scale), it may be necessary to model the detailed fluid movement in order to understand the radionuclide transport and rock displacement in the fracture network. For regional analyses, it may be sufficient to model the average behavior of fluid flow in the rock mass.

Best Treatment

Over the past few decades several numerical codes have been developed to model various aspects of the coupled mechanical-transport processes. Use has been made of different forms and combinations of finite difference (Hart and St. John, 1986), finite element (Noorishad et al., 1982), and discrete element (Cundall, 1985) techniques to model coupled mechanical-transport (and thermal) fluid flow and transport. The choice of a code or codes depends on the details of the flow system being modeled and the physical processes of interest.

4.1.9 Geothermal and Hydrological Coupling

Issue

The evolution of geothermal heat can affect the hydrological behavior of the rock mass.

What Is Being Coupled

A waste repository in a geologic medium can be affected by heat that arises from the stored waste or from some geothermal activity in the vicinity. If the rock surrounding the repository is unsaturated (dry), the movement of heat will be purely conductive but, under saturated conditions, heat will be moved away from the repository by conduction and convection. The coupled effects of heat and ground water flow can result in complex flow fields.

Treatment of Interaction

If it is assumed that the heat distribution does not affect ground water flow, the flow equation is solved first and then the results are introduced into the thermal energy equation thus predicting the energy distribution. Because forced convection is the dominant heat transport process, the coupling is bi-directional or two-way. The resulting temperature distribution affects the flow caused by buoyancy and the flow field affects the selection of the energy equation through convection. Heat released from the repository may alter the flow field which may impact the transport of radionuclides to the accessible environment. This problem can be solved using several existing codes, including SWIFT II, which can solve the coupled equations governing ground water flow and heat transport.

4.1.10 Geomechanical Hydrological coupling

Issue

Mechanical stresses in the rock can alter its flow properties.

What Is Being Coupled

Mechanical alteration of the rock mass surrounding a repository can be accomplished by changes in rock stresses. The changes may be due to loading or unloading of an overburden glacier, erosion, and deposition, folding and faulting. The stress redistribution will result in changes of permeability by opening or closing fractures and by causing settling and compaction of unconsolidated sediments. There will also be changes in fluid pressure.

Treatment of Interaction

Changes in stress and strain, no matter what the cause, can be assessed by modeling stress-strain response and analyzing any subsequent changes in hydrologic parameters. These parameters can then be passed to a hydrological or transport code through a data controller.

4.1.11 Flow-Transport-Climate Coupling

Issue

The climate affects the local hydrological and geohydrological properties.

What Is Being Coupled

Water infiltration and water table alteration are coupled with the regional hydrologic behavior.

Treatment of Interaction

Hydrological-climate coupling is accomplished by assessing the effects of changes on rates of infiltration into an aquifer. Changes in rates of infiltration can be the result of many events such as changes in rates of precipitation, changes in base level, and changes in overburden thickness. The

changes in infiltration are handled with a source term in the flow equation. The transport equations are handled by combining the appropriate continuity and constitutive relations.

4.1.12 Modification of Flow Field and Transport Processes in Rock Mass

This section discusses the general interactions of the geological system with the flow and transport behavior of the rock mass.

Sources of thermal effects include:

- Waste heat generation
- Volcanism
- Geothermal heat sources

The results of thermal effects include:

- Phase change (in unsaturated rock)
- Buoyancy changes
- Water density changes

The sources of mechanical effects include:

- Tectonic activity
- Mass of overburden changes (erosion/deposition, glaciers)

The results of mechanical effects include:

- Formation of an alteration of preferential flow paths
- Stress redistribution within the rock mass
- Fluid pressure changes cause hydraulic fracturing

The sources of climate effects include:

- Precipitation rate changes
- Immobilizing water (such as glaciers)

The results of climate effects include:

- Infiltration rate changes
- Base level changes thus changing gradients

The transport processes themselves can cause solution and precipitation of minerals. This can change permeability by clogging pores. This may cause matrix diffusion of radionuclides and can cause fractures and formation of colloids

Thermal effects can modify geochemistry.

4.2 IMPLEMENTATION OF COUPLING

The first step in the implementation of coupling is to identify how the processes may be coupled together in the physical system. As can be seen from Figure 6 there are many processes at many levels within the repository system. As our initial effort in developing a coupling strategy we have developed a listing and explanation of all the process couplings that need to be considered in the Geologic Disposal System. These couplings are presented below in several charts. Each chart is

marked with arrows that show the direction of influence of the coupling (one-way or both ways). The arrows are numbered with explanatory notes which are listed in the section for that chart. We have also identified which couplings are secondary (i.e., not dominant or of greatest importance). Figure 9 shows the relationships between Figure 10 through Figure 17.

Of most concern would be two-way, primary couplings. These are hardest to deal with since they are implicit and iterative by nature. One way coupling can be handled by calculating the influencing phenomenon and feeding the results into the calculation of the phenomenon it influences. Fortunately, there are relatively few two-way couplings.

4.2.1 Waste Package

The waste package is, in itself, a highly complex and coupled system. Most waste package codes (such as WAPPA) are small system level models. There are many sub-components and many processes to be considered. The coupling chart for the waste package is necessarily very large with many identified couplings. The waste package chart is presented in Figure 10. The explanatory notes for the arrows shown on the chart are as follows:

(1) Nuclear decay is source of internal heat generation.
(2) Heat source.
(3) Thermal expansion.
(4) Devitrification increases the potential for cracking.
(5) Canister/overpack stresses can initiate Mode I (tensile) and/or Mode II (shear) fracturing.
(6) Radiation can weaken and/or damage materials.
(7) Leaching weakens glass.
(8) Cracking increases sorptive area.
(9) Cracking increases porosity for advective transport.
(10) Cracking increases pathways for diffusion.
(11) Aqueous chemical processes are temperature dependent.
(12) Temperature is the primary driver for devitrification.
(13) Diffusion is temperature dependent.
(14) Waste form is heat source.
(15) Source of available corrosive species (secondary effect).
(16) Source of hydrogen for embrittlement.
(17) Contributes electrolytes for galvanic corrosion (secondary effect).
(18) Source of solutes for corrosion product production.
(19) Vitirfied waste is the source of outwardly transported species.
(20) Dissolution releases nuclides.
(21) Hydraulic continuity (bi-directional).
(22) Corrosion product chemistry contributes to material swelling.
(23) Base corrosion is the principal source of corrosion products.
(24) Source of corrosion products.
(25) Thermal expansion.
(26) Hydrogen embrittlement increases the potential for stress corrosion cracking.
(27) Chemical degradation processes are temperature dependent.
(28) Microbial processes are temperature dependent.
(29) Advective transport provides water and nutrients for microbial growth.
(30) Corrosion products sorb nuclides and environmental species.
(31) Corrosion products are source of colloids in backfill.
(32) Corrosion products provide solutes for transport.
(33) Thermal continuity (bi-directional).
(34) Formation of corrosion products decrease permeability of gap.
(35) Water impacts swelling.

(36) Hydration is temperature dependent, particularly after emplacement.
(37) Mineral alteration can cause swelling.
(38) Mineral alteration and dehydration can cause cracking.
(39) Material creep is temperature dependent.
(40) Degree of hydration influences material creep rate.
(41) Changes in buffer/backfill porosity affect transport.
(42) Buffer/backfill erosion is a source of colloids.
(43) Unfiltered colloids may migrate.
(44) Settlement and shrinkage contributes to volume change and cracking in buffer/backfill material.
(45) Volume reduction in buffer/backfill leads to voids at the buffer/backfill-rock interface.
(46) Moisture content of buffer/backfill materials impacts settlement and shrinkage rates.
(47) Chemical processes are temperature dependent.
(48) Diffusion is temperature dependent.
(49) Solution concentration drives precipitation/dissolution.
(50) Solution concentration determines availability of species to be sorbed.
(51) Solution concentration determines availability of species for mineral alteration.
(52) Solution concentration determines availability of species for colloid formation.
(53) Solution concentration determines nutrient availability.
(54) Advection provides major source term for chemical species in solution.
(55) Hydrodymanic dispersion has a secondary influence on chemical processes.
(56) Diffusion is a source/sink for chemical processes.
(57) Physical adsorption is a principal colloid filtration process.
(58) Physical adsorption is a microbial filtration process.
(59) Ion exchange is the principal process whereby colloids absorb nuclides.
(60) Pseudo colloids (microbe precipitates) are solubility controlled.
(61) Changes in mineral distribution affect surface characteristics for sorption.
(62) Water availability through advection and diffusion influences microbial growth.
(63) Water availability through advection and diffusion drives hydration/dehydration.
(64) Formation of colloids is source term for filtration.
(65) Microbial growth is source term for microbial filtration.
(66) Advection is driving process for filtration.
(67) hydrodynamic dispersion is water velocity dependent.
(68) Advection affects concentration gradients which drives diffusion.
(69) Mineral alteration contributes to interface separation.

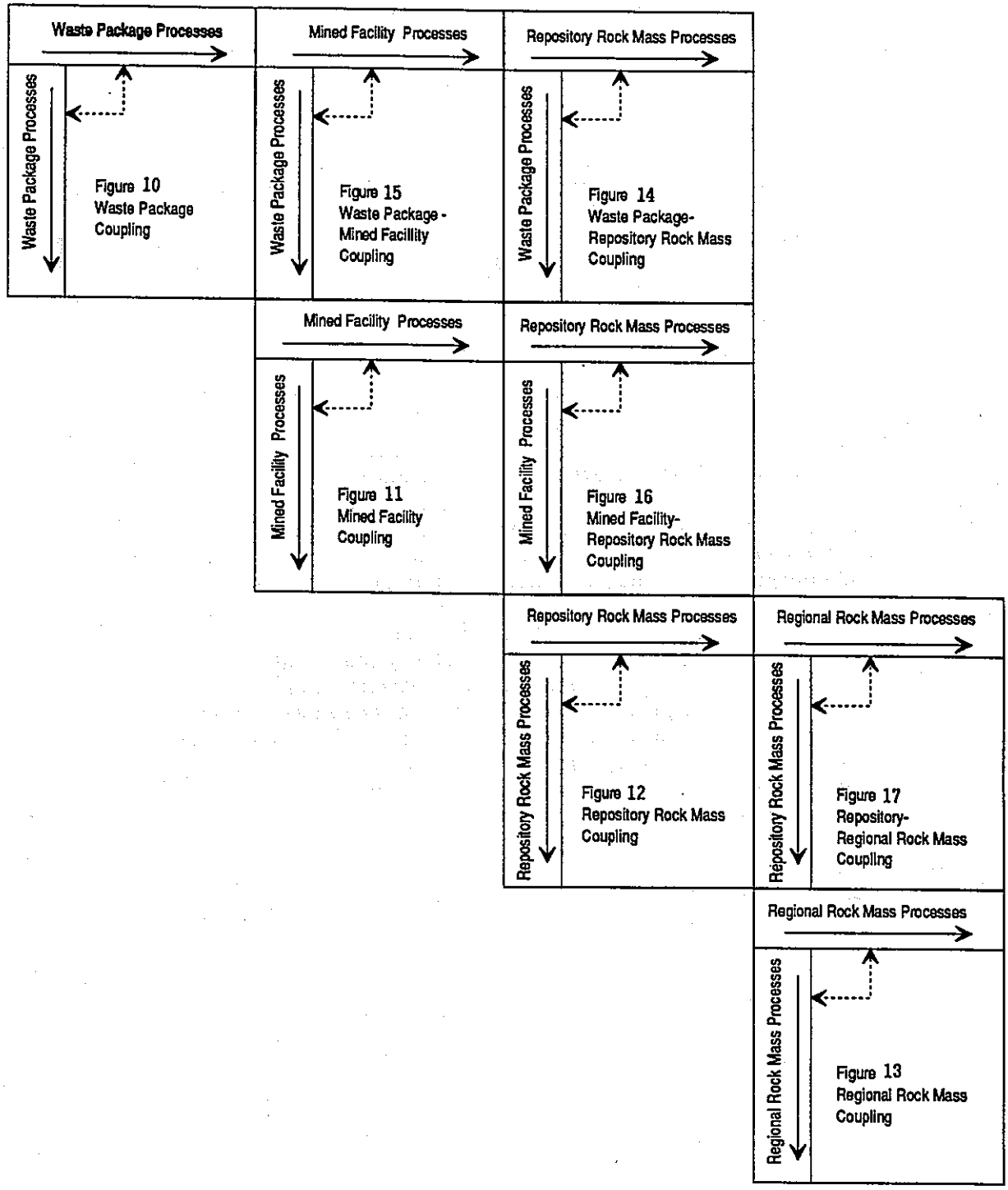


Figure 9. Schematic of the Coupling Diagrams for the Entire System

この頁はPDF化されていません。

内容の閲覧が必要な場合は、技術資料管理担当箇所で原本冊子を参照して下さい。

（4－13頁）～（4－17頁）

4.2.2 Mined Facility

The mined facility consists of relatively few components: rooms, shafts, and the backfill they may contain. Since the backfill serves a complex function as a water barrier and as a sorption medium, there are several processes to be considered and hence a considerable number of process couplings. The mined facility chart is presented in Figure 11. The explanatory notes for the arrows shown on the chart are as follows:

(1) Volume increase due to mineral hydration.
(2) Volume reduction leads to voids contributes to rock-backfill interface separation.
(3) Mineral changes contribute to volume change and cracking.
(4) Consolidation contributes to volume change and cracking.
(5) The degree of hydration influences the creep rate.
(6) Formation on colloids provides source term for filtration.
(7) Water flow into mined facility contributes to the amount of water available for drainage in open entries.
(8) Chemical processes are temperature dependent.
(9) Diffusion is temperature dependent.
(10) Dispersion is temperature dependent.
(11) Thermal conduction through seal bulkheads can induce thermal convection in open entries.
(12) Creep rate is temperature dependent.
(13) Thermal expansion contributes to cracking and interface separation.
(14) Swelling of backfill provides back pressure which reduces entry deformation.
(15) Deformation of entries influences vapor/gas transport by altering entry geometry.
(16) Rock-backfill separation reduces roof support which leads to increased entry deformation.
(17) Changes in porosity in entry backfill and seals influences vapor/gas transport.
(18) Gas solubility of backfill and seal materials impacts vapor/gas transport.
(19) Water transport of dissolved gasses.
(20) Gaseous diffusion.
(21) Changes in backfill and seal porosity impacts he effectiveness of engineered barriers and hence the amount of water leaking into open entries.
(22) Deformation of entries contributes to the consolidation of backfill.
(23) Degree of backfill saturation affects consolidation.
(24) Advection provides a major source term for chemical species in solution.
(25) Diffusion is a secondary source/sink to chemical processes.
(26) Advection changes concentration gradients which drive diffusion.
(27) Hydrodynamic dispersion has a secondary impact on chemical processes by changing concentration.
(28) Pseudo-colloids (i.e., micro precipitates) are solubility controlled.
(29) Solution concentration drives precipitation/dissolution.
(30) Solution concentration drives availability of species to be sorbed.
(31) Availability of water (advective or diffusive) influences hydration/dehydration.
(32) Solution concentration determines the availability of species for mineral alteration.
(33) Solution concentration determines the availability of species for colloid formation.
(34) Temperature influences microbial activity.
(35) Concentration of chemical species determines nutrient availability.
(36) Physical adsorption is a colloidal filtration process.
(37) Water availability through advection and diffusion influences microbial growth.
(38) Microbial growth is a source term for microbial filtration.
(39) Physical adsorption is a microbial filtration process.
(40) Changes in backfill and seal porosity affects transport.
(41) Changes in backfill and seal porosity affects available diffusion cross sections and pathways for hydrodynamic dispersion.

(42) Advection is principal transport process for filtration
(43) Changes in mineral distribution affects surface characteristics for sorption (sorptive area).
(44) Hydrodynamic dispersion is water velocity dependent.
(45) Ion exchange is the principal process by which colloids sorb radionuclides.
(46) Mineral alteration contributes to interface separation.

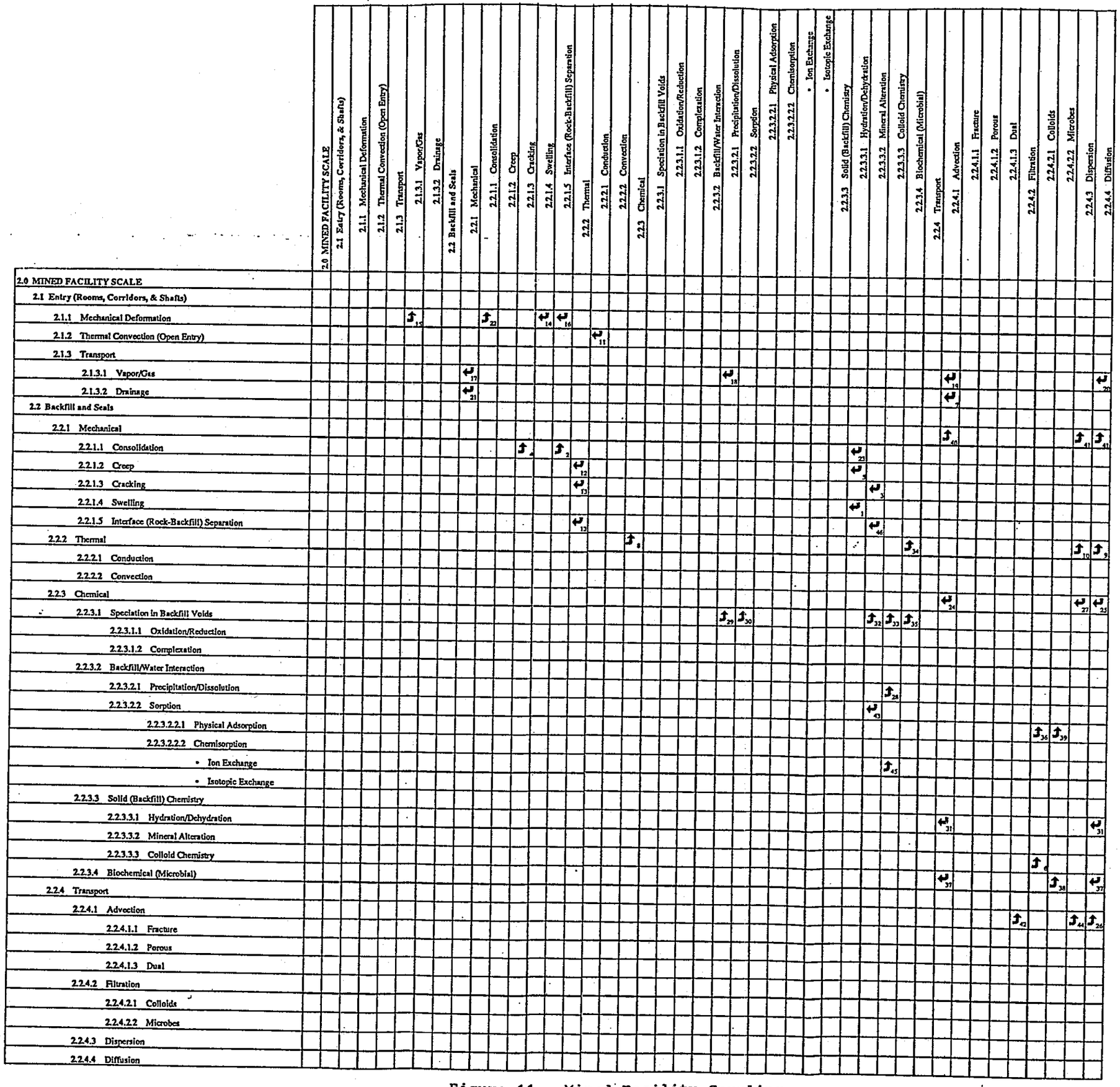


Figure 11 Mined Facility Coupling

4.2.3 Repository Rock Mass

The mined facility consists of essentially one component: the rock mass that surrounds the mined facility. There are several processes to be considered and hence several process couplings. The repository rock mass chart is presented in Figure 12. The explanatory notes for the arrows shown on the chart are as follows:

(1) Thermal expansion.
(2) Fracturing directly affects stress and deformation fields.
(3) Fractures provide pathways (Dead end pores).
(4) Rock deformation modifies matrix porosity.
(5) Precipitation impacts matrix porosity.
(6) Precipitation alters fracture aperture geometry.
(7) Rock deformation drives spalling and block caving.
(8) Fracturing can act as ultra filter.
(9) Hydrodynamic dispersion is dependent on flow velocity.
(10) Rock deformation drives faulting.
(11) Faults provide water pathways.
(12) Chemical processes are temperature dependent.
(13) Solution concentration drives precipitation/dissolution.
(14) Solution concentration drives availability of species to be sorbed.
(15) Solution concentration determines availability of species for mineral alteration.
(16) Solution concentration determines availability of species for colloid formation.
(17) Solution concentration determines availability of nutrients for microbial growth.
(18) Advection provides major source term for chemical species in solution.
(19) Hydrodynamic dispersion has a secondary effect on chemical processes by changing solution concentrations.
(20) Diffusion has a secondary effect on chemical processes by changing solution concentrations.
(21) Changes in mineral distribution affect surface characteristics for sorption.
(22) Ion exchange is the principal process by which colloids sorb aqueous species.
(23) Physical adsorption is a filtration process.
(24) Water availability through advection influences microbial growth.
(25) Microbial growth is source term for microbial filtration.
(26) Colloid formation is source term for colloid filtration.
(27) Advection is driving process for filtration.
(28) Advection affects concentration gradient.

	3.0 REPOSITORY ROCK MASS	3.1 Mechanical	3.1.1 Deformation (Uplift/Subsidence)	3.1.1.1 Elastic	3.1.1.2 Elastic-Plastic	3.1.1.3 Visco-Elastic/Plastic (Creep)	3.1.2 Fracturing	3.1.2.1 Initiation/Propagation	3.1.2.2 Spalling	3.1.2.3 Block Caving	3.1.3 Faulting/Fault Displacement	3.2 Thermal Conduction	3.3 Chemical	3.3.1 Speciation in Rock Voids	3.3.1.1 Oxidation/Reduction	3.3.1.2 Complexation	3.3.2 Rock/Water Interaction	3.3.2.1 Precipitation/Dissolution	3.3.2.2 Sorption	3.3.2.2.1 Physical Adsorption	3.3.2.2.2 Chemisorption	• Ion Exchange	• Isotopic Exchange	3.3.3 Solid (Rock) Chemistry	3.3.3.1 Mineral Alteration	3.3.3.2 Colloid Chemistry	3.3.4 Biochemical (Microbial)	3.4 Transport	3.4.1 Advection	3.4.1.1 Fracture	3.4.1.2 Porous	3.4.1.3 Dual	3.4.2 Filtration	3.4.2.1 Colloids	3.4.2.2 Microbes	3.4.3 Dispersion	3.4.4 Diffusion
3.0 REPOSITORY ROCK MASS																																						
3.1 Mechanical																																						
3.1.1 Deformation (Uplift/Subsidence)							↑2		↑7	↑7	↑10	↵1																	↑4	↑4							
3.1.1.1 Elastic																																						
3.1.1.2 Elastic-Plastic																																						
3.1.1.3 Visco-Elastic/Plastic (Creep)																																						
3.1.2 Fracturing																		↵6											↑3		↑3	↑8					↑3
3.1.2.1 Initiation/Propagation																																						
3.1.2.2 Spalling																																						
3.1.2.3 Block Caving																																						
3.1.3 Faulting/Fault Displacement																													↑11									
3.2 Thermal Conduction													↑12																									
3.3 Chemical																																						
3.3.1 Speciation in Rock Voids																		↑13	↑14							↑15	↑16	↑17	↑18						↑19	↑20
3.3.1.1 Oxidation/Reduction																																						
3.3.1.2 Complexation																																						
3.3.2 Rock/Water Interaction																													↑18							↑19	↑20
3.3.2.1 Precipitation/Dissolution																													↑5								
3.3.2.2 Sorption																										↵21						↑23					
3.3.2.2.1 Physical Adsorption																																						
3.3.2.2.2 Chemisorption																																						
• Ion Exchange																																						
• Isotopic Exchange																											↑22										
3.3.3 Solid (Rock) Chemistry																																						
3.3.3.1 Mineral Alteration																																						
3.3.3.2 Colloid Chemistry																																↑26						
3.3.4 Biochemical (Microbial)																													↵24				↑25					
3.4 Transport																																						
3.4.1 Advection																																↑27				↑9	↑28
3.4.1.1 Fracture																																						
3.4.1.2 Porous																																						
3.4.1.3 Dual																																						
3.4.2 Filtration																																						
3.4.2.1 Colloids																																						
3.4.2.2 Microbes																																						
3.4.3 Dispersion																																						
3.4.4 Diffusion																																						

Figure 12 Repository Rock Mass Coupling

4.2.4 Regional Rock Mass

The regional rock mass consists of essentially one component: the rock mass that surrounds the repository rock mass. There are relatively few processes to be considered and therefore relatively few process couplings. The regional rock mass chart is presented in Figure 13. The explanatory notes for the arrows shown on the chart are as follows:

(1) Faulting/Fault displacement induces rock deformation.
(2) Tectonics drives rock deformation.
(3) Glaciation induces rock deformation.
(4) Tectonics is the principal process driving faulting.
(5) Faults provide pathways for transport.
(6) Geothermally driven thermal expansion.
(7) Chemical processes are temperature dependent.
(8) Volcanism impacts geothermal conditions.
(9) Advection provides major source term for chemical species in solution.
(10) Rock-water interaction contributes to retardation.
(11) Diagenesis and other changes in rock chemistry influence rock-water interaction.
(12) Rock chemistry is temperature dependent.
(13) Solution concentration drives precipitation, dissolution, and sorption.
(14) Base level changes.
(15) Transport-to-dose interface.
(16) Tectonics induce volcanism.
(17) Climate influences gaseous and water pathways.
(18) Major glaciation influences climate.
(19) Metabolism determines uptake of radionuclides.

	4.0 REGIONAL ROCKMASS	4.1 Mechanical	4.1.1 Deformation (Uplift/Subsidence)	4.1.2 Faulting/Fault Displacement	4.2 Thermal Conduction	4.3 Chemical	4.3.1 Speciation in Rock Voids	4.3.1.1 Oxidation/Reduction	4.3.1.2 Complexation	4.3.2 Rock/Water Interaction	4.3.2.1 Precipitation/Dissolution	4.3.2.2 Sorption	4.3.3 Rock Chemistry	4.4 Transport	4.4.1 Advection (Porous)	4.4.2 Dispersion	4.5 Geologic	4.5.1 Tectonics	4.5.2 Volcanism	4.5.3 Erosion/Deposition	4.6 Climatic	4.6.1 Precipitation	4.6.2 Glaciation	4.7 Dose	4.7.1 Gas Pathways (Atmospheric)	4.7.2 Water Pathways (Surface)	4.7.3 Uptake of Radionuclides	4.7.3.1 Metabolic Process	4.7.3.2 Health Effects
4.0 REGIONAL ROCKMASS																													
4.1 Mechanical																													
4.1.1 Deformation (Uplift/Subsidence)																													
4.1.2 Faulting/Fault Displacement																													
4.2 Thermal Conduction																													
4.3 Chemical																													
4.3.1 Speciation in Rock Voids																													
4.3.1.1 Oxidation/Reduction																													
4.3.1.2 Complexation																													
4.3.2 Rock/Water Interaction																													
4.3.2.1 Precipitation/Dissolution																													
4.3.2.2 Sorption																													
4.3.3 Rock Chemistry																													
4.4 Transport																													
4.4.1 Advection (Porous)																													
4.4.2 Dispersion																													
4.5 Geologic																													
4.5.1 Tectonics																													
4.5.2 Volcanism																													
4.5.3 Erosion/Deposition																													
4.6 Climatic																													
4.6.1 Precipitation																													
4.6.2 Glaciation																													
4.7 Dose																													
4.7.1 Gas Pathways (Atmospheric)																													
4.7.2 Water Pathways (Surface)																													
4.7.3 Uptake of Radionuclides																													
4.7.3.1 Metabolic Process																													
4.7.3.2 Health Effects																													

Figure 13 Regional Rock Mass Coupling

4.2.5 Waste Package - Repository Rock Mass

The waste package interacts through some processes with the repository rock mass. There are a few important processes and associated couplings. The couplings are depicted in Figure 14 and the notations for this chart are as follows:

(1) Stress continuity.
(2) Thermal continuity.
(3) Hydraulic continuity (including colloid pathways).
(5) Backfill swelling seals rock fractures.
(6) Mineral alteration contributes to interface separation.

	3.0 REPOSITORY ROCK MASS	3.1 Mechanical	3.1.1 Deformation (Uplift/Subsidence)	3.1.1.1 Elastic	3.1.1.2 Elastic-Plastic	3.1.1.3 Visco-Elastic/Plastic (Creep)	3.1.2 Fracturing	3.1.2.1 Initiation/Propagation	3.1.2.2 Spalling	3.1.2.3 Block Caving	3.1.3 Faulting/Fault Displacement	3.2 Thermal Conduction	3.3 Chemical	3.3.1 Speciation in Rock Voids	3.3.1.1 Oxidation/Reduction	3.3.1.2 Complexation	3.3.2 Rock/Water Interaction	3.3.2.1 Precipitation/Dissolution	3.3.2.2 Sorption	3.3.2.2.1 Physical Adsorption	3.3.2.2.2 Chemisorption	• Ion Exchange	• Isotopic Exchange	3.3.3 Solid (Rock) Chemistry	3.3.3.1 Mineral Alteration	3.3.3.2 Colloid Chemistry	3.3.4 Biochemical (Microbial)	3.4 Transport	3.4.1 Advection	3.4.1.1 Fracture	3.4.1.2 Porous	3.4.1.3 Dual	3.4.2 Filtration	3.4.2.1 Colloids	3.4.2.2 Microbes	3.4.3 Dispersion	3.4.4 Diffusion
1.0 WASTE PACKAGE SCALE																																					
1.4 Buffer/Backfill																																					
1.4.1 Mechanical		1																																			
1.4.1.1 Swelling																													5								
1.4.1.2 Creep/Plastic Flow																																					
1.4.1.3 Cracking																																					
1.4.1.4 Erosion (Colloid Formation)																																					
1.4.1.5 Interface Separation																									6												
1.4.1.6 Settlement/Shrinkage												2																									
1.4.2 Thermal																																					
1.4.2.1 Conduction																																					
1.4.2.2 Convection																																					
1.4.3 Chemical																																					
1.4.3.1 Speciation in Backfill Voids																																					
1.4.3.1.1 Oxidation/Reduction																																					
1.4.3.1.2 Complexation																																					
1.4.3.2 Backfill/Water Interaction																																					
1.4.3.2.1 Precipitation/Dissolution																																					
1.4.3.2.2 Sorption																																					
1.4.3.2.2.1 Physical Adsorption																																					
1.4.3.2.2.2 Chemisorption																																					
• Ion Exchange																																					
• Isotopic Exchange																																					
1.4.3.3 Solid (Backfill) Chemistry																																					
1.4.3.3.1 Hydration/Dehydration																																					
1.4.3.3.2 Mineral Alteration																																					
1.4.3.3.3 Colloid Chemistry																																					
1.4.3.4 Biochemical (Microbial)																																					
1.4.4 Transport																																					
1.4.4.1 Advection																													3								
1.4.4.1.1 Fracture																																					
1.4.4.1.2 Porous																																					
1.4.4.1.3 Dual																																					
1.4.4.2 Filtration																																					
1.4.4.2.1 Colloids																																					
1.4.4.2.2 Microbes																																					
1.4.4.3 Dispersion																																				3	
1.4.4.4 Diffusion																																					3

Figure 14 Waste Package - Repository Coupling

4.2.6 Waste Package - Mined Facility

The only coupling of concern between the mined facility and the waste package are boundary condition continuities. These are identified in Figure 15 with the following notes:

(1) Stress continuity.
(2) Thermal continuity.
(3) Hydraulic continuity.

	2.0 MINED FACILITY SCALE	2.1 Entry (Rooms, Corridors, & Shafts)	2.1.1 Mechanical Deformation	2.1.2 Thermal Convection (Open Entry)	2.1.3 Transport	2.1.3.1 Vapor/Gas	2.1.3.2 Drainage	2.2 Backfill and Seals	2.2.1 Mechanical	2.2.1.1 Consolidation	2.2.1.2 Creep	2.2.1.3 Cracking	2.2.1.4 Swelling	2.2.1.5 Interface (Rock-Backfill) Separation	2.2.2 Thermal	2.2.2.1 Conduction	2.2.2.2 Convection	2.2.3 Chemical	2.2.3.1 Speciation in Backfill Voids	2.2.3.1.1 Oxidation/Reduction	2.2.3.1.2 Complexation	2.2.3.2 Backfill/Water Interaction	2.2.3.2.1 Precipitation/Dissolution	2.2.3.2.2 Sorption	2.2.3.2.2.1 Physical Adsorption	2.2.3.2.2.2 Chemisorption	• Ion Exchange	• Isotopic Exchange	2.2.3.3 Solid (Backfill) Chemistry	2.2.3.3.1 Hydration/Dehydration	2.2.3.3.2 Mineral Alteration	2.2.3.3.3 Colloid Chemistry	2.2.3.4 Biochemical (Microbial)	2.2.4 Transport	2.2.4.1 Advection	2.2.4.1.1 Fracture	2.2.4.1.2 Porous	2.2.4.1.3 Dual	2.2.4.2 Filtration	2.2.4.2.1 Colloids	2.2.4.2.2 Microbes	2.2.4.3 Dispersion	2.2.4.4 Diffusion
1.0 WASTE PACKAGE SCALE																																										
1.4 Buffer/Backfill																																											
1.4.1 Mechanical									↔1																																		
1.4.1.1 Swelling																																											
1.4.1.2 Creep/Plastic Flow																																											
1.4.1.3 Cracking																																											
1.4.1.4 Erosion (Colloid Formation)																																											
1.4.1.5 Interface Separation																																											
1.4.1.6 Settlement/Shrinkage																																											
1.4.2 Thermal															↔2																												
1.4.2.1 Conduction																																											
1.4.2.2 Convection																																											
1.4.3 Chemical																																											
1.4.3.1 Speciation in Backfill Voids																																												
1.4.3.1.1 Oxidation/Reduction																																											
1.4.3.1.2 Complexation																																											
1.4.3.2 Backfill/Water Interaction																																											
1.4.3.2.1 Precipitation/Dissolution																																											
1.4.3.2.2 Sorption																																											
1.4.3.2.2.1 Physical Adsorption																																											
1.4.3.2.2.2 Chemisorption																																											
• Ion Exchange																																											
• Isotopic Exchange																																											
1.4.3.3 Solid (Backfill) Chemistry																																											
1.4.3.3.1 Hydration/Dehydration																																											
1.4.3.3.2 Mineral Alteration																																											
1.4.3.3.3 Colloid Chemistry																																											
1.4.3.4 Biochemical (Microbial)																																											
1.4.4 Transport																																											
1.4.4.1 Advection																																											
1.4.4.1.1 Fracture																																											
1.4.4.1.2 Porous																																											
1.4.4.1.3 Dual																																											
1.4.4.2 Filtration																																											
1.4.4.2.1 Colloids																																											
1.4.4.2.2 Microbes																																											
1.4.4.3 Dispersion																																											
1.4.4.4 Diffusion																																											

Figure 15 Waste Package - Mined Facility Coupling

4.2.7 Mined Facility - Repository Rock Mass

In addition to continuity couplings, the mined facility and repository rock mass interact mechanically through some important couplings. These are identified in Figure 16. The following notes apply to this chart:

(1) Stress continuity.
(2) Thermal continuity.
(3) Hydraulic continuity (including colloid pathways).
(4) Changes in entry geometry.
(5) Backfill swelling seals rock fractures.
(6) Mineral alteration contributes to interface separation.

	3.0 REPOSITORY ROCK MASS	3.1 Mechanical	3.1.1 Deformation (Uplift/Subsidence)	3.1.1.1 Elastic	3.1.1.2 Elastic-Plastic	3.1.1.3 Visco-Elastic/Plastic (Creep)	3.1.2 Fracturing	3.1.2.1 Initiation/Propagation	3.1.2.2 Spalling	3.1.2.3 Block Caving	3.1.3 Faulting/Fault Displacement	3.2 Thermal Conduction	3.3 Chemical	3.3.1 Speciation in Rock Voids	3.3.1.1 Oxidation/Reduction	3.3.1.2 Complexation	3.3.2 Rock/Water Interaction	3.3.2.1 Precipitation/Dissolution	3.3.2.2 Sorption	3.3.2.2.1 Physical Adsorption	3.3.2.2.2 Chemisorption	• Ion Exchange	• Isotopic Exchange	3.3.3 Solid (Rock) Chemistry	3.3.3.1 Mineral Alteration	3.3.3.2 Colloid Chemistry	3.3.4 Biochemical (Microbial)	3.4 Transport	3.4.1 Advection	3.4.1.1 Fracture	3.4.1.2 Porous	3.4.1.3 Dual	3.4.2 Filtration	3.4.2.1 Colloids	3.4.2.2 Microbes	3.4.3 Dispersion	3.4.4 Diffusion
2.0 MINED FACILITY SCALE																																					
2.1 Entry (Rooms, Corridors, & Shafts)																																					
2.1.1 Mechanical Deformation			1						4	4																											
2.1.2 Thermal Convection (Open Entry)												2																									
2.1.3 Transport																													3								
2.1.3.1 Vapor/Gas																																					
2.1.3.2 Drainage																																					
2.2 Backfill and Seals																																					
2.2.1 Mechanical			1						4	4																											
2.2.1.1 Consolidation																																					
2.2.1.2 Creep																																					
2.2.1.3 Cracking																																					
2.2.1.4 Swelling																															5						
2.2.1.5 Interface (Rock-Backfill) Separation																									6												
2.2.2 Thermal												2																									
2.2.2.1 Conduction																																					
2.2.2.2 Convection																																					
2.2.3 Chemical																																					
2.2.3.1 Speciation in Backfill Voids																																					
2.2.3.1.1 Oxidation/Reduction																																					
2.2.3.1.2 Complexation																																					
2.2.3.2 Backfill/Water Interaction																																					
2.2.3.2.1 Precipitation/Dissolution																																					
2.2.3.2.2 Sorption																																					
2.2.3.2.2.1 Physical Adsorption																																					
2.2.3.2.2.2 Chemisorption																																					
• Ion Exchange																																					
• Isotopic Exchange																																					
2.2.3.3 Solid (Backfill) Chemistry																																					
2.2.3.3.1 Hydration/Dehydration																																					
2.2.3.3.2 Mineral Alteration																																					
2.2.3.3.3 Colloid Chemistry																																					
2.2.3.4 Biochemical (Microbial)																																					
2.2.4 Transport																																					
2.2.4.1 Advection																													3								
2.2.4.1.1 Fracture																																					
2.2.4.1.2 Porous																																					
2.2.4.1.3 Dual																																					
2.2.4.2 Filtration																																					
2.2.4.2.1 Colloids																																					
2.2.4.2.2 Microbes																																					
2.2.4.3 Dispersion																																					
2.2.4.4 Diffusion																																					

Figure 16 Mined Facility - Repository Coupling

4.2.8 Repository Rock Mass - Regional Rock Mass

The interaction of these two rock masses is strictly through boundary continuity. The two rock masses are separated as a calculational convenience since the calculations are performed on much different spatial and time scales. Figure 17 is the chart for this coupling and the following notes apply:

(1) Stress continuity.
(2) Thermal continuity.
(3) Hydraulic continuity.

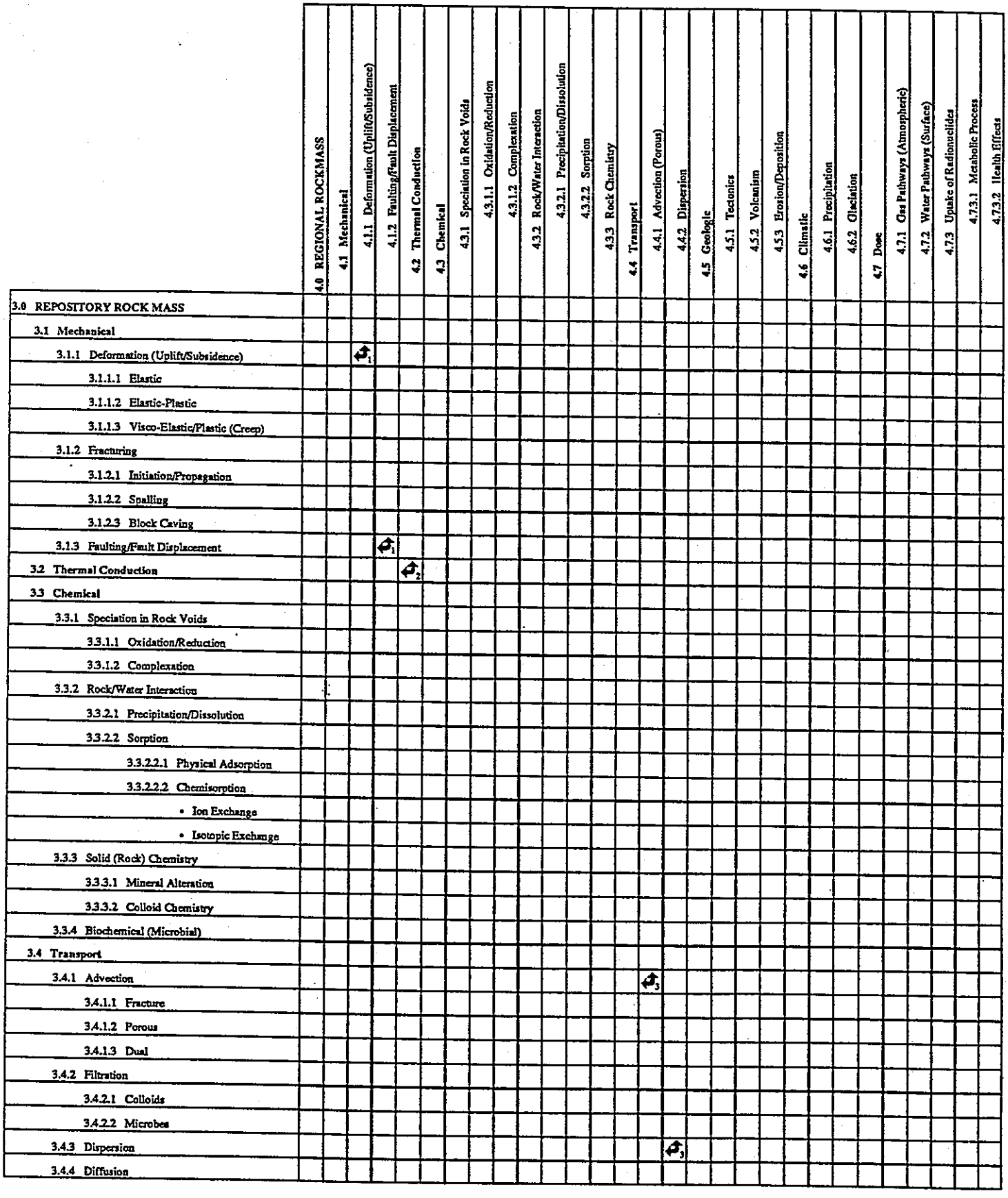


Figure 17 Repository Rock Mass - Regional Rock Mass Coupling

BIBLIOGRAPHY

Bland, D. R., 1956. "Elastoplastic Thick-Walled Tubes of Work-Hardening Material Subjected to Internal and External Pressures and to Temperature Gradients", Journal of Applied Physics, 12, 209-229.

Cundall, P.A., 1985. "Distinct Element Models of Rock and Soil Structure," E.T. Brow (ed.), Analytical and Computational Methods and Engineering Rock Mechanics.

Garg S. K., J. W. Pritchett, M. H. Rice, and T. D. Riney, 1977. U.S. Gulf Coast Prepressured Geothermal Reservoir Simulation.

Hart, R. D. and C. M. St. John, 1986. "Formulation of a Fully-coupled Thermal- Mechanical-Fluid Flow Model for Non-linear Geologic Systems", Int. J. Rock Mech. Min. Sci. and Geomech. Abstr., 23:213-224.

Miller, C.W. and L.V. Benson, Simulation of solute transport in a chemically reactive heterogeneous system: Model development and application, Water Resources Research 19 (1983) 381-391.

Muller, A.B., Sorption: Modeling and measurement for nuclear waste disposal studies, ACCEDE Nuclear Energy Agency Report RWM-4 (1983) 85p.

Muller, A.G., and L.E. Duda, The Uranium-Water system: Behavior of dominant aqueous and solid components, Sandia National Laboratories Report 83-0105 (1983) 160p.

Muller, A.G., D. Langmuir and L. Duda, The formulation of an integrated physicochemical-hydrologic model for predicting waste nuclide migration in geologic media, Materials Research Society Symposium Proc. 15 (1983) 547-564.

Noorishad, J., M.S. Ayatollahi, and P.A. Witherspoon, 1982. "A Finite Element Method for Coupled Stress and Fluid Flow Analysis in Fractured Rock Masses," Int. J. Rock Mech. Min. Sci. and Geomech. Abstr., 26:341-349.

Nowacki, W., 1962. "Thermoelasticity", International Series of Monographs on Aeronautics and Astronautics Div. I: Solid and Structural Mechanics, Vol. 3., Addison-Wesley, New York.

Pusch, R., Swelling pressure of highly compacted Bentonite, Univ. of Lulea, KBS Report TR 80-13 (1980).

Parkhurst, D.L., D. C. Thorstenson and L.N. Plummer, PHREEQE: A computer program for geochemical calculations, U.S. Geologic Survey Report WRI 80-96 (1982) 210p.

Reardon, E.J., Kd's: Can they be used to describe reversible ion sorption reaction in contaminant migration?, Ground Water 19 (1981) 279-286.

Serne, R.L. and A.B. Muller, A perspective on adsorption of radionuclides onto geologic media, in The Geologic Disposal of High Level Radioactive Wastes (D.G. Brookins, ed.), Theophrastus Pubs: Athens (1987) 407-443.

Wolery, T.J., Calculation of chemical equilibrium between aqueous solutions and minerals: The EQ3/6 software package, Lawrence Livermore Laboratory Report UCRL-52658 (1979).

Yeh, G.T., FEMWASTE: A finite element model of waste transport through saturated-unsaturated porous media: First revision, Oak Ridge National Laboratory Report ORNL-5601/R1 (1989).

Yeh, G.T. and V.S. Tripathi, HYDROGEOCHEM: A coupled model of HYDROlogic Transport and GEOCHEMical Equilibria in Reactive Multicomponent Systems, Oak Ridge National Laboratory Report ORNL-6371 (1990) 318p.

5. SUMMARY OF MODEL INTEGRATION STUDY

Over the next 20 years, Japanese scientists and engineers will be developing a mined geologic disposal system as a repository for reprocessed high-level nuclear waste. Analysis of the response of a geologic disposal system, usually called performance assessment, is a critical activity for the development of a practical repository. Performance assessment predictions are important to demonstrate that the repository system will perform within acceptable limits, thereby building public confidence and ensuring the protection of the public's health and safety. In addition, the same performance assessment predictions will be a key input to any licensing or regulatory actions for the repository.

The development of efficient, integrated computer programs for performance assessment of a Japanese repository will be a difficult and challenging activity for the Power Reactor and Nuclear Fuel Development Corporation (PNC). The development of integrated computer programs is difficult because of the large number of complex physical processes that may be important in a geologic disposal system. In addition, accurate prediction of repository response over very long periods of time (1,000 to 10,000 years) and in the inhomogeneous geologic environment is a very challenging task, requiring extensive verification and validation of the computer programs.

This study is an initial step in developing an efficient, integrated computational system for repository performance assessment. The study had three main tasks, which are documented in this report:

- Develop preliminary system integration concept. This task included the definition of a preliminary conceptual site, definition of the base case scenario, the development of an integrated computational approach to repository performance assessment, and the definition of a complete set of processes for the geologic disposal system. This set of processes only applies to the base case scenario. Additional processes need to be identified for disruptive scenarios.

- Review candidate models. Based on the processes identified in the first task, a review was performed of major computer programs for completeness of documentation and for the status of verification and validation activities.

- Review methodology for models of coupled processes. This task included the identification of coupled processes and a review of the status of models for the most important coupled processes.

The integrated computational approach is largely conceptual at this point in time. Key issues for the development of detailed implementation plans and work activities include: (1) selection of a complete set of models and computer programs, (2) completion of a scenario library and conceptual site data base, (3) implementation of a verification and validation program for near-field computer programs, and (4) design of an integrated software/hardware system with user-friendly input and output capabilities. These activities are recommended efforts for the coming year.

Based on these issues, we recommend consideration of potential tasks

Task 1: System Integration Planning

Task 2: Data Management System

Task 3: Verification and Validation and Code Management

Task 4: Pre- and Post-Processors

In developing this plan for Heisei.3, we have also focussed on two facts: (1) the waste package is the most important barrier in the Japanese repository, and (2) candidate repository sites have not been selected by the Japanese Government. Our tasks are therefore designed to help focus on the waste-package and near-field analyses that will be required for the Heisei.8 report, as well as develop generic site models that can be used to develop and test performance assessment tools. Each task is discussed in turn below.

TASK 1: SYSTEM INTEGRATION PLANNING

Task 1 is a continuation of the three tasks that were begun during Heisei.2. In addition, we strongly recommend further definition and review of "disruptive" or off-normal scenarios and the development of a scenario library. The specific activities and the rationale for them follows.

System Integration Model. Continued definition of the system integration model will require the following subtasks: identify data needs for the relevant processes, identify data needs for the generic site models, and develop specifications for the data controller and computational platform. The identification of data needs for the relevant processes is a direct extension of the list and hierarchy of processes (Figure 6) developed during this initial study. Definition of these data needs is useful for designing the generic site model and data base and for recommending new experiments for the ENTRY Project or for in situ testing. The identification of data needs for the generic site model is the initial step in building conceptual site models that will form the basis for all calculations, including the calculations for the Heisei.8 report. Once the parameters in the conceptual site data base are defined, PNC can maintain a degree of uniformity and consistency that will assist in benchmarking and verification of computer codes. Finally, the development of specifications for the data controller and computational platform will define the hardware and software needs for an integrated computational system (or platform) that can ultimately perform the sequence of calculations illustrated in Figure 2 of this report.

Complete Code Survey. Our initial code survey has included 39 codes. Additional codes have been identified during this process, and codes for other process types, such as nuclear, must be added to the list. This activity will complete the initial code survey, identify any developmental needs for new processes, and recommend a final suite of codes for both the basic calculations and for verification and validation. Note that the choice of computer codes will have some impact on the development of specifications for the computational platform in the system integration activity.

Complete Coupling Study. Our list and hierarchy of processes have identified over 160 potential couplings between processes in the four size scales. We have also identified and discussed the principal coupled processes. This activity will complete the coupling study and develop a strategy and plan for implementing coupled calculations on the PNC computational platform and data controller.

In addition to these three tasks, the development of a scenario library appears to be a high priority task. The definition of disruptive scenarios is important because these scenarios define the full range of processes that must be considered by performance assessment. In addition, an initial risk assessment on the scenarios will indicate which processes are most important in terms of consequences for the public and biosphere. And finally, the scenario library is part of the basis for the Heisei.8 report on near-field response. SAIC recommends the development of a scenario library and an assessment of risk in the near future.

TASK 2: DATA MANAGEMENT SYSTEM

This task will develop data system specifications for the computational platform and to prepare a plan for implementation of PARATRAC into PNC's facility. The data system will include generic site data, computational data (mesh, stratigraphic model, and material properties), coupling data (primarily boundary conditions). This computational data system is therefore one part of a total engineering data base that PNC will eventually require for the nuclear waste program. This larger engineering data base would encompass data from in situ experiments, data from ENTRY Project experiments, and data from other laboratory experiments, as well a computational data. In addition to the computational data specifications, we will prepare a plan for introduction of PARATRAC into PNC's facilities. PARATRAC is a user-friendly application and interface that was developed to control data from site characterization studies and from laboratory experiments. PARATRAC will provide a user-friendly window into the large engineering database discussed in this paragraph.

TASK 3: VERIFICATION, VALIDATION, AND CODE MANAGEMENT

Verification, validation, and code management are central to building confidence in the accuracy of any performance assessment system; these activities therefore deserve the highest priority in PNC's program. SAIC will develop and implement a code configuration control and management program for PNC during Heisei.3. This activity will include developing a code configuration control program and procedures, and install and provide training with the ATLAS program.

SAIC also recommends that PNC develop verification and validation plans for the major near-field and waste package codes. Candidates include AREST-PNC, RELEASE, TAGSEÇ, and FEMWATER. Verification activities and calculations should begin as soon as possible, if they have not already been started.

TASK 4: PRE- AND POST-PROCESSORS

Any data controller and computational platform requires user friendly pre- and post-processors for several reasons. First, these software tools help to eliminate errors when analysts are preparing input data for or reviewing the output data from calculations. Second, these software tools improve efficiency which will be important when many calculations are performed for the Heisei.8 and Heisei.13 reports. And lastly, these tools decrease the learning time for new analysts.

SAIC recommends that existing pre- and post-processors be reviewed to ensure that they are highly accessible and usable by the Japanese scientist or engineer, and that a common interface be developed (to the maximum extent possible) to ensure that the an analyst just has to learn one interface, rather than learning separate input requirements for multiple computer codes.

6．プロセスモデルの確証

6.1 INTRAVALフェーズ２のテストケース

INTRAVALは、地層処分を実施した場合の処分場から地表への核種移行に関する知見を増進し、核種移行の評価モデルの確証と確証プロセスを検討するために国際協力で実施されているプロジェクトであり、フィールド試験を中心に室内試験およびナチュラルアナログの検討が行なわれている。INTRAVALは1987年から始まり、1990年度にフェーズ１を終了し、1991～1993年度はフェーズ２作業となる。フェーズ１では室内試験，フィールド試験，ナチュラルアナログの17のテストケース（表－6参照）について検討が行なわれ、主に、含まれるプロセスの把握に検討の中心が置かれた（テストケースの幾つかは、フェーズ２作業に引き継がれる）。

フェーズ２では表－7に示すように10のテストケースが考えられており、フィールド試験やナチュラルアナログを基にした評価モデルの確証作業が行なわれる予定である。これらのテストケースは表－8に示すように、主に①結晶性岩中の流れと移行，②不飽和帯中の流れと移行，③粘土中の流れと移行，④ナチュラルアナログから成っている。

INTRAVALのフェーズ２のテストケースは、フィールド試験やナチュラルアナログから構成されており、プロセスモデルの確証に非常に有益であると考えられる。

6.2 テストケースの取り組み方針

6.2.1 確証について

(1) 地層中の核種移行モデル

地層中の核種移行は概念的には表－9に示すモデルで表せる。しかしながら実際の地層処分の体系を考えた場合、第２章や第４章で述べたように地層の状態や核種の物理化学的性質に影響され、非常に複雑な系となっている。

(2) 確証について

確証とは現実に起こる定量的挙動に対する理論予測の信頼性を評価することと考えられるが、地層処分の体系においては、対象とする現象が多様で複合的なことおよび場所，条件等の状況が多様で自然物を含むことより一般性のある状況設定が難しく、特定の現象，特定の状況に応じた個別的な実証が選定される。

確証の方法としては、①室内試験，②フィールド試験，③ナチュラルアナログが利用される。室内試験は、基礎モデルの立証やパラメータの定量化には有効だが時間と空間のスケールの制約がある。ナチュラルアナログは時間的空間的スケールにおいて非常に有効な方法ではあるが、現時点では十分な定量的評価までには至っていない。フィールド試験は実際の地層中での試験データであり、室内試験よりも地層処分の状況に近く、地層中の放射性核種移行に影響するプロセスを把握するうえで重要である。フィールド試験に基づく確証は、空間的および時間的なスケールが大きく、地層の非均質性を含み、実際にどのプロセスが重要なのかを把握するうえで有益である。また、評価コードの環境条件の取り扱いに関する知見も得られる。

なお、確証が上述したように個別的なケースに対して行なわれるため、幅広いケースに対する確証作業が必要になってくると考えられる。

(3) 確証における較正と予測について

通常は次の較正と予測の手順で確証作業が行なわれる。

① 較正（calibrationまたはhistory matching）による検討

試験結果を再現するためにはどのようなモデルとパラメータが必要かの検討であり、現象把握に有益である。準備した評価モデルの適合性や試験結果を再現するパラメータ値が把握できる。

② 予測（predictionまたはblind prediction）による検討

準備した評価モデル・評価コードによる予測と試験の観測値との比較により予測の信頼性を評価する方法である。確証には予測による評価が必要である。なお、予測において必要なデータもしくはパラメータをどのような手順で設定するか体系化しておくことが重要と考えられる。

6.2.2 Finnsjönに対する取組み方針

(1) 試験概要と試験データ

スエーデンのFinnsjönにおいて、割れ目帯でのトレーサ試験が行われた[5,10]。試験場所はゾーン2（表－8（7/14）中の図－B）と呼ばれる地表にほぼ水平な割れ目帯が選ばれた。トレーサ試験は、ⓐ揚水試験，ⓑ ダイポール試験の2種類である。以下にこれらの試験の概要を説明する。

（i） 試験場所

ゾーン2は、主に花崗閃緑岩で地表にほぼ平行に存在しており、ゾーン2の上表面は地下100～240mに位置している。ゾーン2の巾は約100mであり、この中に3つの透水性の良い層があり、それらの層の透水係数が上から順に$2X10^{-4}$，$1X10^{-4}$，$1X10^{-5}$m/sと他の領域よりも透水係数が高いと考えられている。ゾーン2の平均の透水係数は$5X10^{-6}$m/sである。

ゾーン2では、自然の地下水の水頭勾配は1m/350m～1m/150mである。

（ii） 揚水試験（radially converging experiment）

BFI02から水を汲み上げ、BFI01，KFI06，KFI11にトレーサを注入した（表－8（7/14）中の図－B参照）。BFI02とBFI01，KFI06，KFI11の距離はそれぞれ168，189，155mである。トレーサの注入位置は表－10に示すようにゾーン2中の透水係数の大きい上部，中部，下部の合計9ヶ所であり、トレーサの種類は全部で11種類で、このうち、8種類は5～7週間連続的に注入し、3種類はパルス状に注入した。

使用したトレーサは、DTPAおよびEDTAと希土類金属との錯合体，蛍光染料（ウラニン，アミノG酸），陰イオン（I^-，ReO_4^-）であり、これらは安定で非吸着性のトレーサである。

トレーサの連続注入はトレーサ注入部分と接続した循環ラインに一定流量でトレーサを注入する方法で行った。注入方法の概略を図－18，19に示す。濃度Cooのトレーサを流量qで注入し、系内の圧力上昇を防ぐため、同時に流量qで水を排出した。注入流量qは、2mℓ/minである。パルス注入した3種類のトレーサのうち、I^-を使用したケースは、連続注入する予定であったが、注入初期に装置の故障により注入が停止したため、パルス注入として試験が終わったものである。他の2種類のトレーサのパルス注入は、トレーサ注入部

分をトレーサ溶液で置換して行った。この後、図－18に示すラインを循環させ、系内のトレーサ濃度を均一にした。トレーサ濃度の減少は、逐次ラインの水を採取することで監視した。

注入したトレーサはBFI02より回収した。BFI02における水の汲出し方法を表－11に示す。水の汲出しは、地下水流の定常状態を維持するために、トレーサ注入の約6週間前に開始した。水の汲出し流量は2ℓ/secである。BFI02から汲出した水をオートサンプラで採取し、水中のトレーサの分析を行った（図－20参照）。

トレーサ注入開始から52日後（トレーサの注入完了済）、ゾーン2の透水係数の低い層を通って別の透水係数の高い層へ移行するトレーサを調べるために、詳細サンプリングを実施した。すなわち、BFI02のゾーン2中から厚さ2mの7つの部分を選択し、それぞれの部分から水を汲出して（揚水流量2ℓ/min）水中のトレーサを分析した。詳細サンプリングは4日間行い、この後、ゾーン2の全体の層からの揚水を再び継続した。

(iii) ダイポール試験

本試験は、BFI01にトレーサを注入し、BFI02から水を汲出し、この水を再びBFI01に戻し、循環させるものである（表－8（8/14）の図－C参照）。トレーサの注入位置は揚水試験でも用いたゾーン2中の上部の最も透水性の高い部分である。揚水量は2ℓ/sに設定され、流れが定常状態になるようにトレーサ注入の少なくとも2週間前からポンプを起動した。

トレーサの注入（BFI01とKFI11を使用）は、7週間に合計15回行った。使用したトレーサは、ⓐ放射性のトレーサ（吸着性，非吸着性），ⓑ非放射性のトレーサである。使用したトレーサと注入状況を表－12に示す。BFI01への13回のトレーサの注入時間は各ケース約4分である。また、2回のKFI11へのトレーサ注入時間は各ケース約60分である。

トレーサは、揚水試験の場合と同じ方法で、BFI02（汲出し側）とKFI11（注入側）におけるゾーン2の上部の透水性の高い層で採取した。

また、KFI11のゾーン2の下部とKFI06においてもサンプリングを行った。

（iv） 実験データ

揚水試験により得られたデータは以下の通りである。

a. BFI02におけるトレーサの破過曲線

b. BFI02のポンプ容量，汲み上げた水の温度と電気伝導度

c. 井戸（BFI01，BFI02，KFI06，KFI11，HFI01）における地下水レベル

d. BFI02とトレーサ注入部とのヘッド差

e. トレーサの初期濃度と注入部におけるトレーサ濃度

f. トレーサ貯蔵タンクの体積

g. トレーサ注入部における地下水流量

h. 詳細サンプリング時のトレーサ濃度

これらのデータを表－13，14に示す。

Dipole試験で得られたデータは以下の通りである。

a. 井戸（BFI02，KFI11，KFI06）におけるトレーサの破過曲線

b. 井戸の地下水レベル

c. ゾーン2の上部，中部，下部のヘッド

d. BFI02とのヘッド差

e. 注入／揚水率

f. BFI02における水の電導度と温度

g. BFI01における酸化還元電位

これらのデータを表－15～22に示す。

⑵ 揚水試験に関する取組み方針（案）

揚水試験は透水性の良いほぼ水平な亀裂媒体でのトレーサ（非吸着性，安定核種）の移行試験であり、水頭勾配は揚水（BFI02）により形成される（図－21参照）ので、評価モデル・評価コードの確証の点からは次のように取組めば良いのではないかと考えられる。

（i） 目 標

① 亀裂媒体での核種移行に対する多孔質媒体移流分散モデルの適用性の確認。（FEMWATER＋FEMWASTEコードでの評価の適用性確認）

② マトリックス拡散の寄与に関するモデル化の方法の把握。

③ 亀裂媒体での核種移行における流路のモデル化の方法把握。（チャンネルモデル等の他のモデルとの比較検討による評価）

（ii） 評価モデル・評価コード

① 多孔質媒体移流分散モデルでの検討を行なう。体系は２次元とする。

・FEMWATERによる揚水孔への水の速度算出

・FEMWASTEによるサンプリング点の濃度変化算出

② 多孔質媒体移流分散モデルによる計算結果と試験結果の比較評価により摘出した評価モデル・評価コードの改良点を基に、代替モデルの候補の検討を行なう。

③ 試験結果に対し適合性の良いと考えられる代替モデルに基づくコードにより、試験結果の検討を行なう。

（iii） 検討に際しての課題

① 代替モデルに基づくコードの準備

（iv） 検討方針（案）

揚水試験に関する検討方針（案）を表－23に示す。多孔質媒体移流分散モデルに代わる代替モデルのコードによる検討には、かなりの準備を要するものと考えられる。

(3) ダイポール試験に関する取組み方針（案）

ダイポール試験は透水性の良いほぼ水平な亀裂媒体でのトレーサ（非吸着性と吸着性および安定核種と放射性）を用いた移行試験であり、水頭勾配は揚水（BFI02）と注水（BFI01）により形成される（図－21）。評価モデル・評価コードの確証の点からは、以下に述べる揚水試験との違いを考慮すれば、取組み方針の考え方としては表－23に示した揚水試験の場合と同じで良いと考えられる。

① トレーサとして吸着性と非吸着性を使用しているので、吸着の効果に対するモデル検討ができる。

② トレーサとして放射性核種と安定核種を使用しているので、放射能の減衰を利用した核種移行の時間依存性や遅延効果の時間依存性の観点からモデル検討ができる。

③ 多孔質媒体移流分散モデルにおいて、図－21に示すような体系であるため、FEMWATER＋FEMWASTEに代わるコード（例えば、ＰＮＣ殿で開発したDIPOLEコード）が必要となる。

(4) 揚水試験に関するFEMWATER, FEMWASTEによる検討例

揚水試験に関し、FEMWATER, FEMWASTEを使用して、検討に着手した。検討はパラメータのフィッティングによる最適値を算出するまでには至っていない。

（ｉ） 検討例

① 検 討 ケ ー ス：KFI06による上部の透水性の良い層におけるI^-の移行試験（表－14参照）

② トレーサの注入：117時間I^-を注入

③ 検 討 手 順：ⓐ 移流分散の１次元モデルで主要パラメータ設定（ペクレ数，ポア速度等）

ⓑ FEMWATERでBFI02に向う流速分布計算（KFI06とBFI02の水頭差0.6m）

ⓒ FEMWASTEでトレーサの移行計算（マトリックス拡散，吸着はなしとして計算）

④ 検討結果

トレーサの移行の状態を図－22に示す。出口（BFI02）における濃度の計算結果と試験結果の比較を図－23に示す。図－23を見ると、測定濃度がピークに至る以前は計算値と測定値の一致は比較的良いが、濃度の減衰傾向が異なっており、計算結果では濃度の減衰が速い。実際の体系では、何らかのトレーサの滞留の寄与（例えば、マトリックス拡散等）があるものと考えられる。

（ii） 今後の検討のために

Finnsjönテストケースは透水性の良い亀裂媒体中の核種の移行試験であり、多くのトレーサによる試験データが得られているため、上述したようにFinnsjönテストケースの確証作業により、以下の点に関して有益な知見が得られるものと考えられる。

① 亀裂媒体に対する流路のモデル化

② マトリックス拡散の効果

③ 吸着効果（ダイポール試験）

④ 放射能の半減期を利用した遅延効果等の時間依存性（ダイポール試験）

6.2.3 Molに対する取組み方針

(1) 試験概要と試験データ

ベルギーのMolの地下試験場において、実施しているトリチウムの移行試験について概要を述べる。

（ｉ） 試験場および試験装置

1982年にSCK/CENによってMolの粘土層中の地下220mに地下試験場（URL）が建設された（表－8（11/14）の図－A）。1985年にURLの右端に一連のピエゾメータを設置した（表－8（11/14）の図－BのCP1の部分）。これらはステンレス製で9つのピエゾメータが0.9m間隔に置かれている。各ピエゾメータは２重管でできており（表－8（11/14）の図－C）、外側の管はフィルタになっている。２重管の中央部分には、内径2mmのパイプがURLの部分と連結されている。パイプの内容積は3.14mℓ/mである。２重管の中央部分の内容積は75.4mℓでフィルタの空隙部分の容積は13.0mℓである。パイプの全内容積は表－24に示すとおりである。

（ii） 圧力分布測定

URLの端の垂直な縦坑内が大気圧のためにピエゾメータの近くに水力学的な圧力勾配を生ずる。ピエゾメータ内に水の圧力をマノメータによって測定した。

（iii） トレーサの注入

一連のピエゾメータCP1を設置して約2.5年後にトレーサ（HTO）を注入した。トレーサの注入方法は、次の方法で行った。

925MBqのHTOの入った容器をフィルタNo.2とNo.5の間に接続した。これらのフィルタの間には、0.39MPaの差圧がある（図－24参照）ため、フィルタNo.5に5.61mℓ/dayの流量でHTOが注入された。No.5への全注入量は280.5mℓであった。トレーサ注入後、容器を分離し、系内を隔離した。

（iv） 試料の採取および濃度測定

フィルタNo.4とNo.6より試料を採取した。採取量は粘土中のトリチウム濃度分布を乱さないようにするためにできる限り少量とした。試料の採取はトレーサを注入してから3ヶ月後，2ヶ月間隔で行った。採取量は少なくともピエゾメータ内の水の滞留部分の容積とし、測定に十分な放射能を得るために、

8個のサンプルを1つに集めて濃度を測定した。トリチウムの測定には、液体シンチレーションカウンタを用いた。

測定されたトリチウム濃度Csからフィルタ中のトリチウム濃度Cjを求めるために、ⓐ水の滞留部分の（Vsp）のトリチウム濃度は、前回採取した試料のトリチウム濃度Ciに等しい，ⓑフィルタ内側およびフィルタの空隙部（Vs－Vsp）のトリチウム濃度はその場所の粘土中のトリチウム濃度とあまり差がないと仮定することにより、下式よりフィルタ中のトリチウム濃度を推定した。

$$Cj=\frac{(Vs\cdot Cs-Vsp\cdot Ci)}{(Vs-Vsp)}$$

ここで、Vs ：サンプリング系の全内容積

Cs ：試料中のトリチウム濃度

Vsp：水の滞留部分の容積

Ci ：前回のトリチウム濃度

（v） 試験データ[9)]

粘土中の深さ方向の圧力分布を図－24に示す。フィルタNo.4の9回目のサンプリングの資料を8回に分けて測定したトリチウム濃度を図－25に示す。図－25はサンプリングにより採取したトリチウム量を試料量の関数としてプロットしたものであり、この図中の直線は上記のトリチウム濃度の計算式の妥当性を示している。

フィルタNo.4とNo.6のトリチウム濃度を図－26に示す。横軸はトリチウムを注入操作開始してからの経過時間である。図中の計算値はMICOFプログラムにより、下記のパラメータを用いて計算した値である。これらのパラメータ室内での実験に基づいたものとのことである。

(2) 取組み方針（案）

Molテストケースは、粘土層でのHTOの移行に関するフィールド試験[9)]であるので、評価モデル・評価コードの確証の点から次のように取組めば良いのではないかと考えられる（表－25参照）。ただし、以下の取組み方針（案）は、試験データの詳細が入手できた時点で見直すものとする。

（ｉ） 目　標

① 評価モデルは多孔質媒体の移流分散モデルで核種移行が表される。

② 室内試験データにより予測可能である。

③ 用意した３次元コードで予測できる（コードでの確証作業を行う）。

（ii） 評価モデル・評価コード（体系は図－27参照）

① 地下水の流れは３次元でダルシー則（定常状態）より算出する。ピエゾメータ部での水頭勾配の形成原因により、計算体系は設定する必要がある（形状によっては２次元円筒座標（角度方向に対称）でも評価可能）。透水係数に異方性があれば、３次元での評価が必要となる。

② トリチウムの移行は３次元の多孔質媒体での移流分散モデル（吸着なし，放射能の崩壊による減衰考慮）とする。図－26に見られるように、フィルタNo.4とNo.6の濃度に殆ど違いがないことから、核種移行におけるダルシー流速の影響は非常に小さい可能性がある。

（iii） 検討に際しての課題

① ３次元の水の流れおよび核種移行コードの準備。

（iv） 検討方針（案）

Molテストケースに関する検討方針（案）は表－25に示す。

6.3 引用文献

1. T.C Yeh et al., Simulation of Liquid and Vapor Movement in Unsaturated Fractured Rock at the Apache Leap Tuff Site, NUREG/CR-5097, (1988)
2. INTRAVAL Phase II Test Case: Las Cruces Trench Site, INTRAVAL KU(91)12, (1990)
3. K.Schelkes et al., INTRAVAL Phase II Test Case: Saline Groundwater Movement in an Erosional Channel Crossing a Salt Dome, BGR, (1990)
4. Poroposal for the Isolation Pilot Plant Test Case on Flow and Transport in Heterogeneous Fractured Media (INTRAVAL Phase II), INTRAVAL KU(90)73, (1990)
5. E.Grustafsson et al., Radially Converging Trancer Experiment in a Low-Angle Fracture Zone at the Finnsjon Site, Central Sweden, IRAP 88313 (1989)
6. H.Abelin et al., 3-D Migration Experiment-Report1, TR 87-19(SKB) (1987)
7. H.Abelin et al., 3-D Migration Experiment-Report2, TR 87-20(SKB) (1987)
8. H.Abelin et al., 3-D Migration Experiment-Report3, TR 87-21(SKB) (1987)
9. Three Dimensional In-Situ Migration Experiment in the Boom Clay Formation at the MOL Site in Belgium, INTRAVAL KU(91)13, (1991)
10. C.F.Tsang and S.Neuman, Studies of Tracer Experiments in a Fracture Zone at the Finnsjon Research Area, INTRAVAL Phase I ﾚﾎﾟｰﾄ ﾄﾞﾗﾌﾄ, (1991)

表－６　　ＩＮＴＲＡＶＡＬプロジェクトでの試験ケース

No.	フェーズ１ ケースNo*1	フェーズ２ ケース*2	試験実施機関または場所	*3 種類	試　　験　　内　　容
1	ケース１ａ		英国　Harwell	L	湿った粘土中の放射性核種の室内移行試験。
2	ケース１ｂ		スイス　PSI	L	結晶性の掘りだした岩による室内でのウランの移行試験。
3	ケース２		スウェーデン　KTH	L	花崗岩の単一の自然にできた裂目における室内での放射性核種の移行試験。
4	ケース３		米国　Hanford	F	地下約1000mの深い玄武岩中でのトレーサによるフィールド試験。
5	ケース４	○	スウェーデン，国際協力のStripaプロジェクトによる	F	結晶性の岩での水の流れとトレーサの移行のフィールド試験。大きなブロックの岩の領域での水の流路の空間分布を試験の目的としている。
6	ケース５	○	スウェーデン　Finnsjön地区	F	割れ目帯でのトレーサによるフィールド試験。透水性の大きな岩の割れ目帯での輸送特性の把握を試験の目的としている。
7	ケース６		スイス　Grimsel Rock Lab.	F	大きな割れ目帯における透水性とトレーサ移行のフィールド試験。地質的水力的な境界条件(大きなスケール，中間的なスケール，小スケール)が求められている。
8	ケース７ａ		ブラジル　Minas GeraisのPocos de Caldas	N	オープンピットのウラン鉱山における酸化還元反応のフロントと放射性核種の移行に関する測定。
9	ケース７ｂ		ブラジル　Minas Gerais	N	Morro de Fernoのコロイド（Ｔｈと希金属）の移行に関する測定。
１０	ケース８	○	オーストラリア Alligatorリバー地区のKoongarraサイト	N	天然鉱脈でのウランおよび他の核種の溶出と移行に関する測定。
１１	ケース９		カナダ　AECL	L	単一の自然の割れ目を持つ結晶性の岩（花崗岩）での放射性核種の移行の室内試験。
１２	ケース１０	○	米，NRC，Las Cruces	(F)	表層の砂漠の土による湿ったフロントの移行を用いた多孔質体中の不飽和流と移行に関するトレンチ試験。
１３	ケース１１	○	米，NRC，Apache Leap Tuffサイト	F，L	不飽和な割れ目を持つ岩での流れと移行の室内試験とフィールド試験。
１４	ケース１２		米，DOE，Nevada Testサイト	F	部分的に飽和した凝炭岩状の岩での水文的な条件を変えたフィールド試験。
１５	ケース１３		オランダ，RIVM	L	ガラスベッドの多孔質中の濃度の高い条件での塩の移行の室内試験。
１６	ケース14a	○	独，Gorleben Salt Dome	F	高い塩分を含んだ地下水の汲み上げのフィールド試験であり、岩塩層上部の滞留水の性質を調べる。
１７	ケース14b	○	独，Gorleben Salt Dome	F	岩塩ドームを横切る浸食性のチャンネル中の地下水の動きに関するフィールド試験。
１８	－	○	米，WIPP(1)	F	蒸発沈積層での塩水の流れ（不飽和）のフィールド試験。
１９	－	○	米，WIPP(2)	F	非均質な割れ目のある媒体での不飽和な水の流れと移行に関するフィールド試験。
２０	－	○	ベルギー，Mol	F	粘土中のトリチウムの移行に関するフィールド試験。
２１	－	○	カナダ，Twin Lake	F	滞水した砂および砂利でのトレーサ移行のフィールド試験。

注　＊１）ケースNo.がない表中で「－」の欄はフェーズ１には含まれず、フェーズ２で計画されているケースである。
　　＊２）○印のケースが現時点でフェーズ２作業において取り上げられる予定のケースである。
　　＊３）種類の欄のＬ，Ｆ，Ｎは次のことを意味する。
　　Ｌ：室内試験，　Ｆ：フィールド試験，　Ｎ：ナチュラルアナログ

表－7　　INTRAVAL　フェーズ2のテストケース

No.	タイトル	種類*1	試験の内容	試験実施機関	試験期間	データの状況	評価状況（１９９１年5月時点）
1	Appache Leap Tuff	F，L	亀裂を持つ岩の不飽和帯における流れと移行	米国　NRC	試験完了 （新たな試験を計画中）	室内試験（コア試験，ブロック試験）とフィールド試験のデータが得られている。	多相流のモデルにより、水分の分布，温度分布，トレーサ含有量が計算された。測定値と計算値の差は、媒体の不均一性，物質データの不足，測定誤差によると考えられる。
2	Las Cruces	（F）	多孔質媒体中の不飽和水流と移行	米国　NRC	Plot1,Plot2a：完了 Plot2b　　：継続中	Plot1とPlot2aのデータはデータベース化されている。	１次元移流－分散モデル，有限要素法によるコード（VAM2D，TRUST，TRUMP等）を用いたモデル，PORFLOコードを用いたモンテカルロシミュレーション，BIGFLOコードを用いた統計的モデルシミュレーションにより、水の流れやトレーサ移行を解析している。
3	Gorleben	F	岩塩近くの地下水流と塩分の移行	ドイツ　BGR	揚水試験：1984年完了 塩水の移行試験：継続中	揚水試験のデータがフロッピィディスクに保管されている。	データの公開が遅れたため（1991年公開）、モデル評価を行ったチームはない。
4	WIPP 1	F	エバポライト層中の塩水の流れ	米国　DOE	継続中	データ採取中	採取されたデータのモデルのモデル評価は行われていない。
5	WIPP 2	F	WIPPサイトの地下水流	米国　DOE	1975～1992	全ての井戸で採取したデータが得られている。	フラクタルを扱ったモデルによる透水性の評価，地下水流計算コード（SWIFT2）を用いた評価，チャンネルモデルによる予備検討等が行われている。水力学的なモデル計算は1979年から数多く行われている。
6	Finnsjon	F	亀裂媒体中のトレーサ移行試験	スウェーデン SKB	試験完了（1989） （トレーサ試験1984～1989）	試験データはフロッピィディスクに保管されている。	揚水試験に関して、チャンネルモデル，２次元の移流分布モデル，マトリックス拡散を考慮したモデル，ネットワークモデル等種々なモデルにより、評価が行われた。 Dipole試験についても同様なモデルにより評価が行われているが、揚水試験に比べて評価例は少ない。
7	Stripa	F	亀裂を持つ岩中の地下水流とトレーサ移行試験	OECD/NEA International Stripa Project	試験完了（1986）	試験データはフロッピィディスクに保管されている。	移流，分散，マトリックス拡散を考慮したモデル，チャンネルモデル，DISCFRACコードを用いたネットワークモデル，フラクタルな構造を扱ったモデルを用いて、データ解析が行われ、モデルパラメータが求められている。
8	Mol	F	粘土中のトリチウムの移行試験	ベルギー SCK／CEN	1982～継続中	データ採取中	３次元の移流分散モデルによりデータ解析が行われたが、データ公開が最近のため、評価例は少ない。
9	Twin Lake	F	帯水層中のトレーサ移行試験	カナダ	1982～1988 1990～計画中	1982～1983の試験データが得られている。	予備解析が行われているが、評価例は殆どない。
１０	Alligator Rivers	N	放射性核種移行のナチュラルアナログ研究	Alligator Rivers Analogue Project	1981～継続中	データ採取中	３次元の地下水流モデル，１次元の核種移行モデル，媒体の不均一性と水力学的特性の時間変化を考慮したモデルにより評価されている。

＊１）種類の欄のL，F，Nは次のことを意味する。
　　L：室内試験，　　F：フィールド試験，　　N：ナチュラルアナログ

表－８　　ＩＮＴＲＡＶＡＬ　フェーズ２　テストケースの試験内容（１／１４）

ケース：ﾌｪｰｽﾞ1の11	Apache Leap Tuff（亀裂を含む岩中の不飽和流と核種移行）
資料名：①　INTRAVAL Progress Report No.5, ②　NUREG/CR-5097[1]	

1．試験場所

米国のアリゾナ州Superior近くのU.S.NRC Apache Leap Tuffサイト

2．試験方法

2.1 試験の種類

フィールド試験と室内試験（ブロック試験とコア試験）

2.2 試験方法

(1)　フィールド試験

30X30X30mのオーダの試験場に９つの試験孔を３列に掘った（図－Ａ）。地表をプラスチックシートで覆い、水の侵入と蒸発を防いだ。試験の測定項目は水力学的分散，含水率，透水係数，空隙率，温度，試験孔での空気流量等である。

現在、１つの穴の近くの岩を水で飽和させ、他の穴における水分量を測定する実験を行ったが水分は検出されなかった。

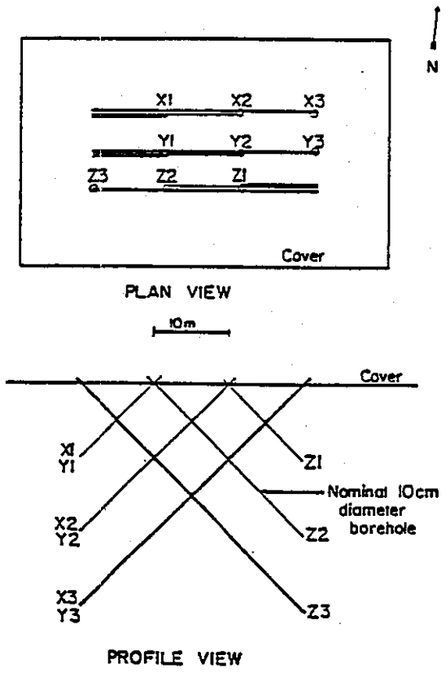
(2)　ブロック試験

試料はサイトから取出した中央に亀裂を持ったブロックである（図－Ｂ）。

20cmX20cmX49.5cmのブロックを用いて、飽和定常流れの予備試験を実施し、装置のキャリブレーションを行った。

21cmX20cmX66cmのブロックを用いてブロック上部に水を吸収させ、下部を大気開放し、ぬれ面の移動を観測した。

また、同じブロックを用いて割れ目中に定常流れを生じさせて、非吸、着性のトレーサをパルス状に与えて割れ目中および出口のトレーサ濃度を監視した。



図－Ａ　　試験孔の配置

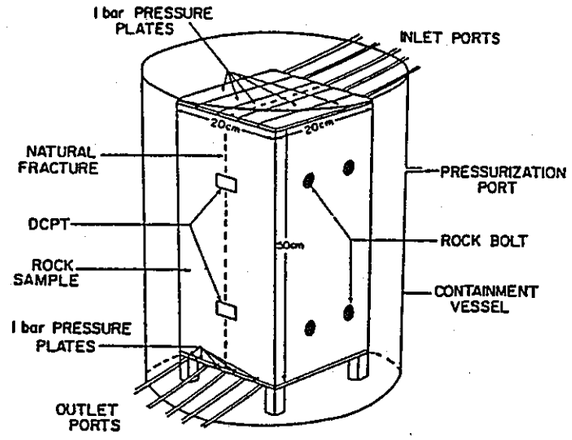
(3)　コア試験

長さ12.72cm，直径6.4cmの試料を乾燥させ、ヨウ化カリウムの溶液に部分的に侵した。

試料から水分，空気が放出しないように表面をシールした後、試料両端を一定温度（5℃と70℃）に32日間維持した（図－Ｃ）。

試験中、低温側から１cm間隔で温度と飽和度を測定した。

また、最後に試料を8つに分割することにより、試料中の濃度分布を測定した。



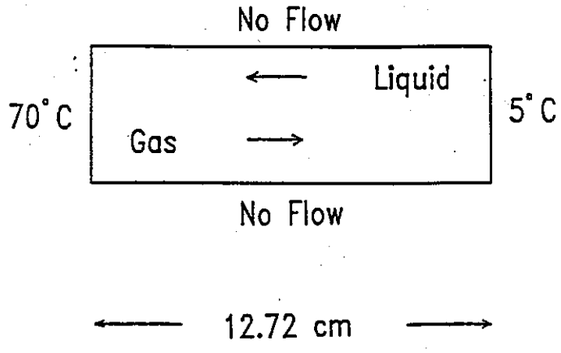
図－Ｂ　　ブロック試験の試験装置

3．試験結果

データ未入手

4．その他

なし



図－Ｃ　　コア試験の概略図

表－８　　ＩＮＴＲＡＶＡＬ　フェーズ２　テストケースの試験内容（２／１４）

ケース：ﾌｪｰｽﾞ1の10	Las Cruces（土壌中の不飽和流とトレーサ移行）
資料名：①　INTRAVAL Progress Report No.5, ②　INTRAVAL KU(91)12[2)]	

1．試験場所

米国のニューメキシコ州のLas Crncesの北東40kmにあるニューメキシコ州立大学の農場

2．試験方法

2.1 試験の種類

土壌表面からの水とトレーサの移行試験

2.2 試験方法

(1)　室内試験

土壌サンプルを採取し、室内で土壌／水の残留率，飽和透水係数を測定した。

(2)　水とトレーサの移行試験

土壌に長さ16.5m，巾48m，深さ6.0mの溝を掘った。溝に接して２つの水を注入する領域（4X9mと1X12m）を設けた。

①　Plot 1試験

トリチウム水を土壌表面（溝の南側の領域）に1.76cm/dayの割合で添加した。

トリチウムおよび水の移動，水の含有量を測定した。

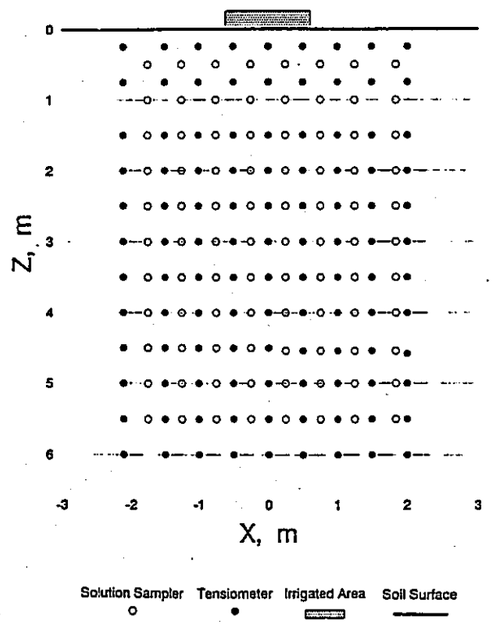
②　Plot 2a試験

水を土壌表面(溝の北側の領域)に0.43cm/dayの割合で75.5日間添加した。最初の11.5日間は、トリチウム*1と臭化物*2を添加した。

トリチウムと臭化物の移動を溝の壁に挿入した約50個のサンプラーで監視した（図－Ａ）。

＊１：トリチウム濃度＝0.1mCi/ℓ

＊２：臭化物濃度＝0.8g/ℓ



図－Ａ　　サンプラー挿入位置

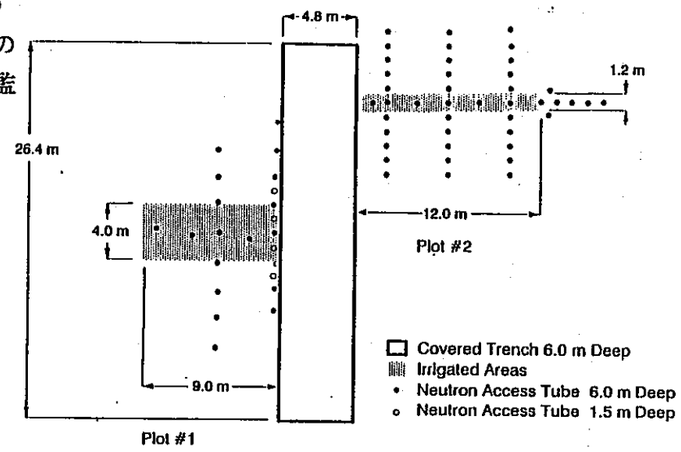
また、水の移動を約50個のテンシオメータ（図－Ａ）および4つの異なる面に配置した約1000個の中性子検知管（図－Ｂ）により監視した。

③　Plot 2b試験

Plot 2aと同様の試験であるが、トレーサとして、

・トリチウム
・臭化物
・ボロン
・クロム
・有機化合物
（PFBA, DFBA）

を用い、水の添加割合をPlot 2aの4倍にして試験を行うことを計画している。



図－Ｂ　　水の移動の観測位置

3．試験結果

Plot 1とPlot 2aの試験結果は、Las Crncesのデータベースにある。Plot 2bの試験結果も同様のフォーマットで入力される予定である。

データ未入手。

4．その他

なし

表－８　　ＩＮＴＲＡＶＡＬ　フェーズ２　テストケースの試験内容（３／１４）

ケース：ﾌｪｰｽﾞ1の14	Gorleben（岩塩近傍における地下水流れ）
資料名：①　INTRAVAL Progress Report No.5, ②　BGRレポート[3)]	

１．試験場所

ドイツのLower Saxonyの北東に位置するGorleben岩塩

２．試験方法

2.1 試験の種類

揚水試験と塩水の移行試験

2.2 試験方法

(1)　揚水試験

岩塩水の深い帯水層の地下水を３週間汲み上げる（図－Ａ）。揚水量は30m^3/hrである。

約20ヶ所の観測井戸で１日１回以上の頻度で５週間にわたり、監視した。監視項目は地下水レベル，電気伝導度である。

また、岩塩近くの空隙率，透水性，化学組成等も調べた。

(2)　塩水の移行試験

本試験は、上記試験の拡張試験であり、Gorleben地域の複雑な地下水流れを記述するためのものである。

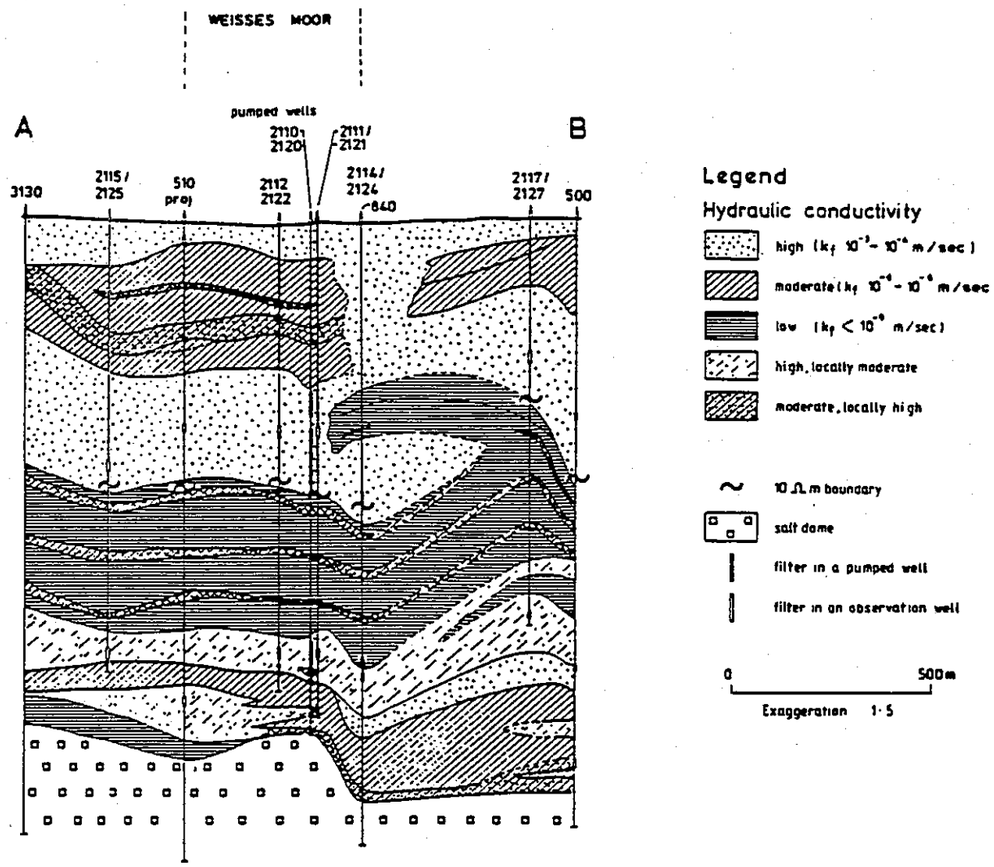
すなわち、岩塩近くの現在の地下水の流れの状況と今後1000年にわたる塩／水系の流れの予測やトレーサ（^{14}C）を用いて、ソースタームの移行特性を行うための試験が予定されている。

３．試験結果

データ未入手

４．その他

なし



図－Ａ　　試験場所の断面図

表－8　　INTRAVAL　フェーズ2　テストケースの試験内容（4／14）

ケース：No.未定	WIPP-I（エバポライト層中の塩水の流れ）
資料名：INTRAVAL Progress Report No.6	

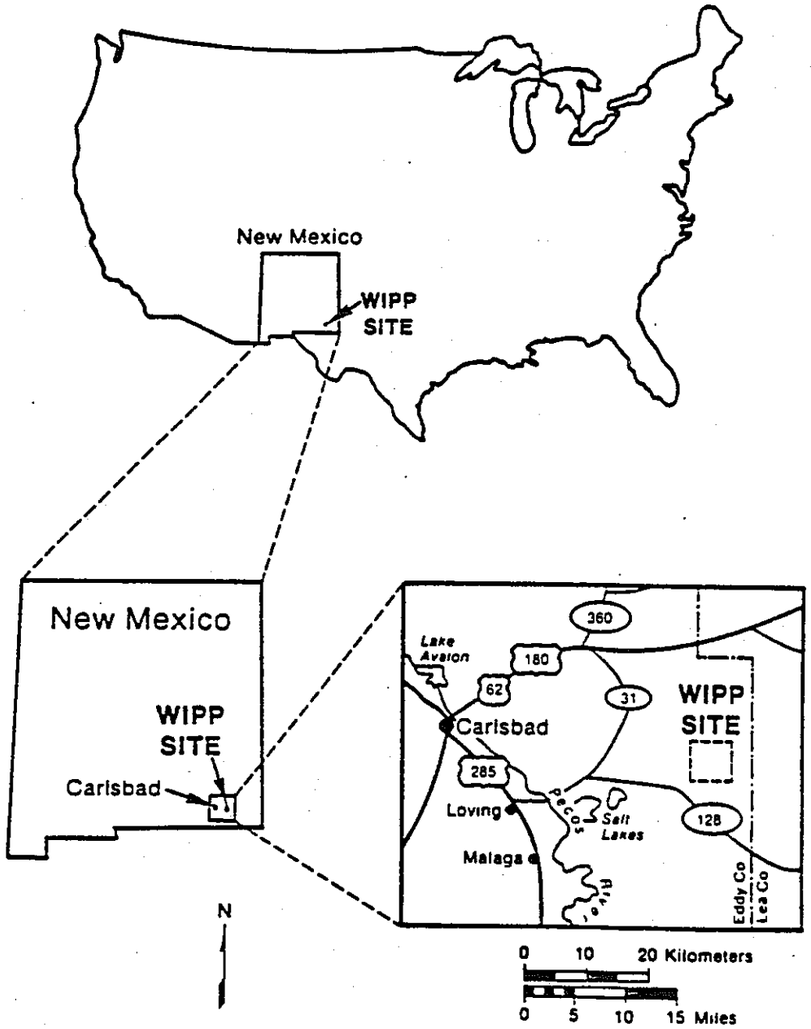
1．試験場所
　米国ニューメキシコ州WIPPサイト（図－A）の地下655mにある地下処分場

2．試験方法
　2.1 試験の種類
　　エバポライト層中の塩水の自然な流れを決定するための試験

　2.2 試験方法
　　WIPPサイトの地下655mにある処分場は主に岩塩からなるエバポライト層の中にある。
　　WIPP-1の試験は、この層中における塩水の自然な流れを決定することにある。試験は塩水の流れがダルシーの法則によって正確に表せるか否かを評価するためのデータを得るために計画された。
　　主な測定項目は、塩水の流量，気孔部の圧力，浸透性である。試験のスケールは4.5cm～3mの範囲である。

3．試験結果
　データ未入手

4．その他
　なし



図－A　　ＷＩＰＰサイトの位置

表－８　　ＩＮＴＲＡＶＡＬ　フェーズ２　テストケースの試験内容（５／１４）

ケース：No.未定	WIPP-Ⅱ（亀裂媒体中の地下水流れ）

資料名：①INTRAVAL Progress Report No.5, ②INTRAVAL KU(90)73[4)]

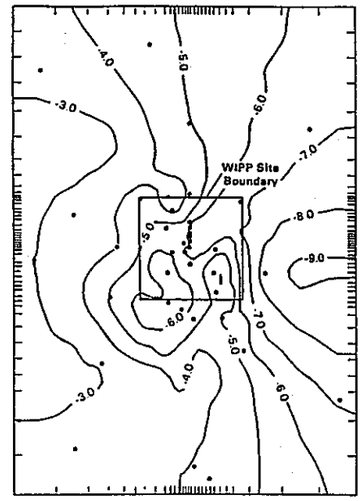
１．試験場所
米国のニューメキシコ州のWIPPサイト（地下655mの廃棄物処分場）

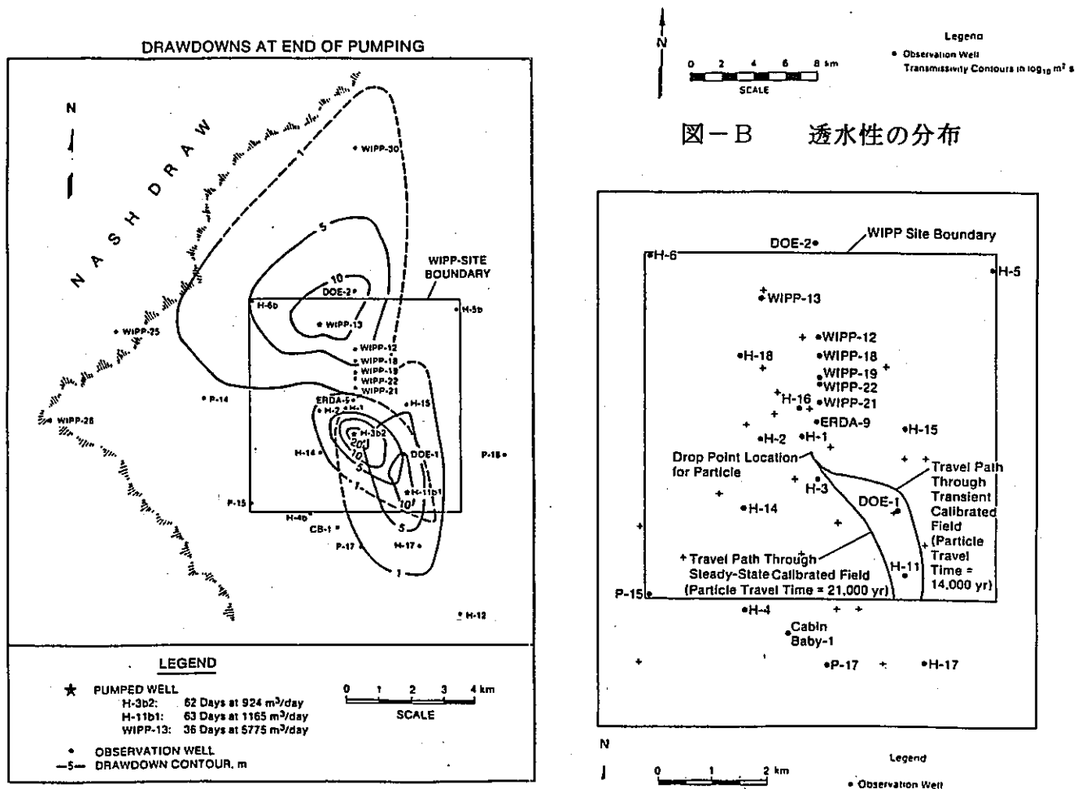
２．試験方法
2.1 試験の種類
WIPPサイトにおける地下水流の測定試験

2.2 試験方法
(1) 地質調査
1975年からWIPPサイトの地表の調査を行った。
(2) 水理学的調査
WIPPサイトに60個の井戸を掘り、水理学的情報を得た。

３．試験結果
(1) 透水性
・60個の井戸で透水性に関するデータを得た（図－Ａ）。この結果より、東から西にWIPPサイトを横切って6オーダにわたって透水性が増加している。
透水性の変化は亀裂と関係している。
・サイトの南東方向の3つの井戸（DOE-1, H-3, H-11）のデータよ、低い透水性の領域の中に比較的透水性の高い部分が存在している。
この透水性の高い領域は、WIPPサイトの中央から南方に広がっている（図－Ｂ）。
(2) 地下水レベル
・揚水井戸のまわり6kmの範囲で井戸の地下水レベルを観測した（図－Ｃ）。このデータはこの地下水流れのモデル計算に用いられる。
・地下水名が利の モデルのより、計算された地下水の流れを用いて溶質の移行モデル計算を行い、透水性の高い領域が溶質のソース点からWIPPサイトの境界領域への移行に関して影響を与えることがわかった（図－Ｄ）。
(3) 化学分析
地下水流れに関する情報を得るために、分析データ（地下水中のNa濃度，C濃度，T濃度，岩塩分布，$^{234}U/^{238}U$）が得られている。

４．その他
なし

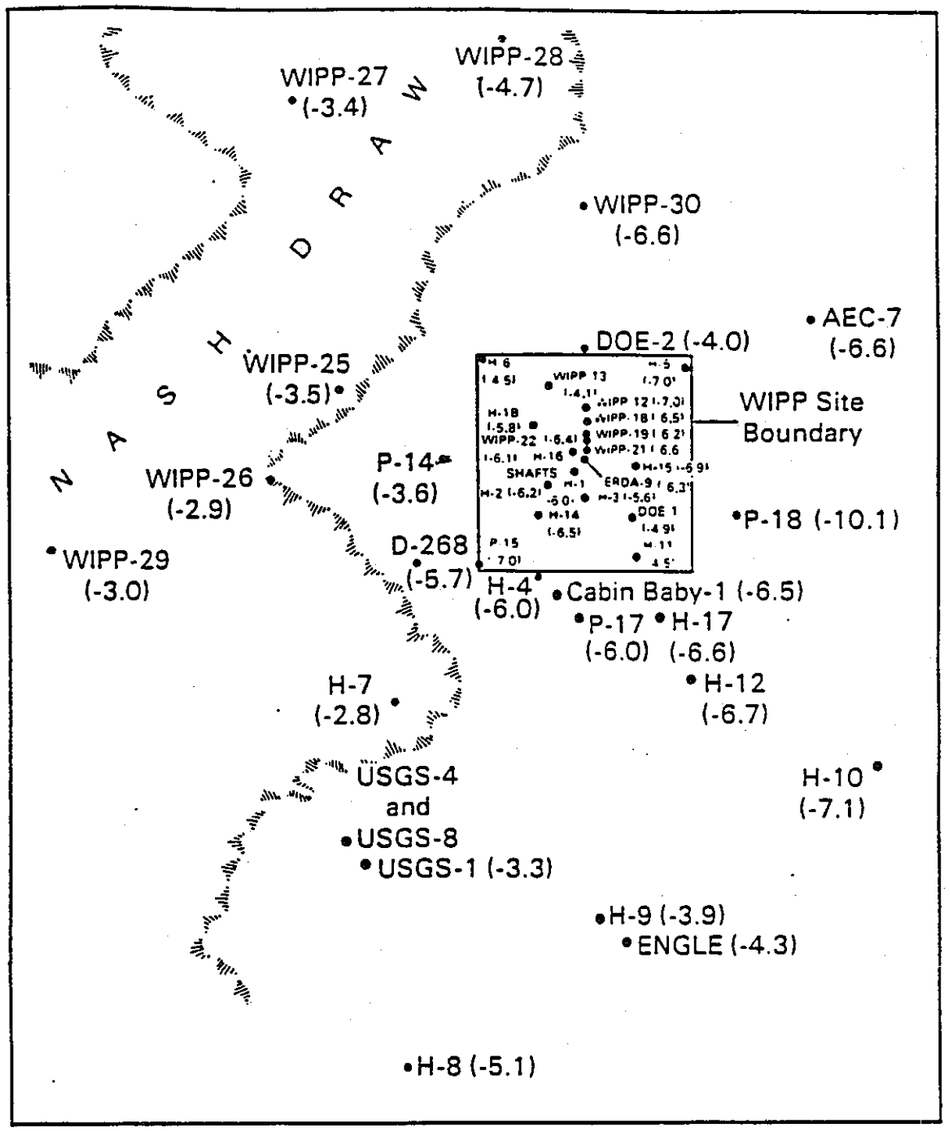




図－Ｃ　　揚水試験結果

図－Ｂ　　透水性の分布

図－Ｄ　　地下水流路と移動時間



図－A　　井戸の位置とその位置における透水量係数

表－８　　ＩＮＴＲＡＶＡＬ　フェーズ２　テストケースの試験内容（７／１４）

ケース：ﾌｪｰｽﾞ1の5	Finnsjön（亀裂中のトレーサ試験）

資料名：①　INTRAVAL Progress Report No.5, ②　IRAP-88313[5)]

１．試験場所

スェーデンのFinnsjön試験場

２．試験方法

2.1 試験の種類

揚水試験とダイポール試験

2.2 試験方法

(1) 3つの井戸（BFI01, KFI06, KFI11）にトレーサを注入し、水を汲み上げた（図－Ａ）。

トレーサの注入部分は、Zone-2と呼ばれる割れ目帯のうち、透水性の高い部分である（図－Ｂ）。

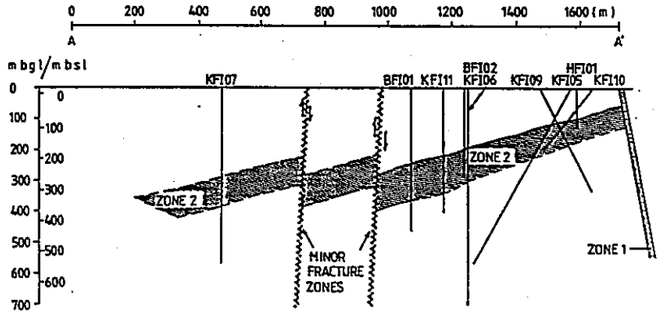
使用したトレーサは11種類（DTPAおよびEDTAと希土類金属との錯合体，蛍光染料（ウランとアミノG酸），陰イオン（I^-とReO_4^-））である。

11種類のトレーサのうち、8つは連続5～7週間、3つはパルス状に注入し、出口（BFI02）におけるトレーサ濃度を測定した。

(2) ダイポール試験

BFI01にトレーサを注入し、BFI02から水を汲み出し、この間で水を循環させた（図－Ｃ）。注入部分はZone2の中の上部である。

20種類のトレーサを用いて、約4分間パルス状に与え、出口（BFI02）のトレーサ濃度を測定した。



図－Ｂ　　ゾーン２の位置

３．試験結果

(1) 揚水試験

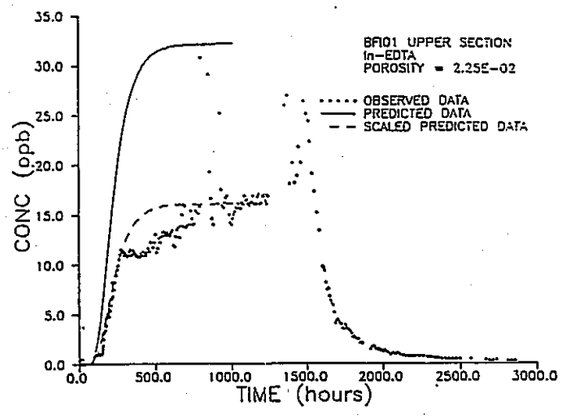
・トレーサの破過曲線（例：図－Ｄ）
・揚水と水頭のデータ
・入口のトレーサ濃度
・詳細サンプリング時のトレーサ濃度
・水質データ

(2) ダイポール試験

・トレーサの破過曲線
・水頭のデータ
・水の注入／揚水流量
・水質データ
・トレーサ初期濃度（データ未入手）

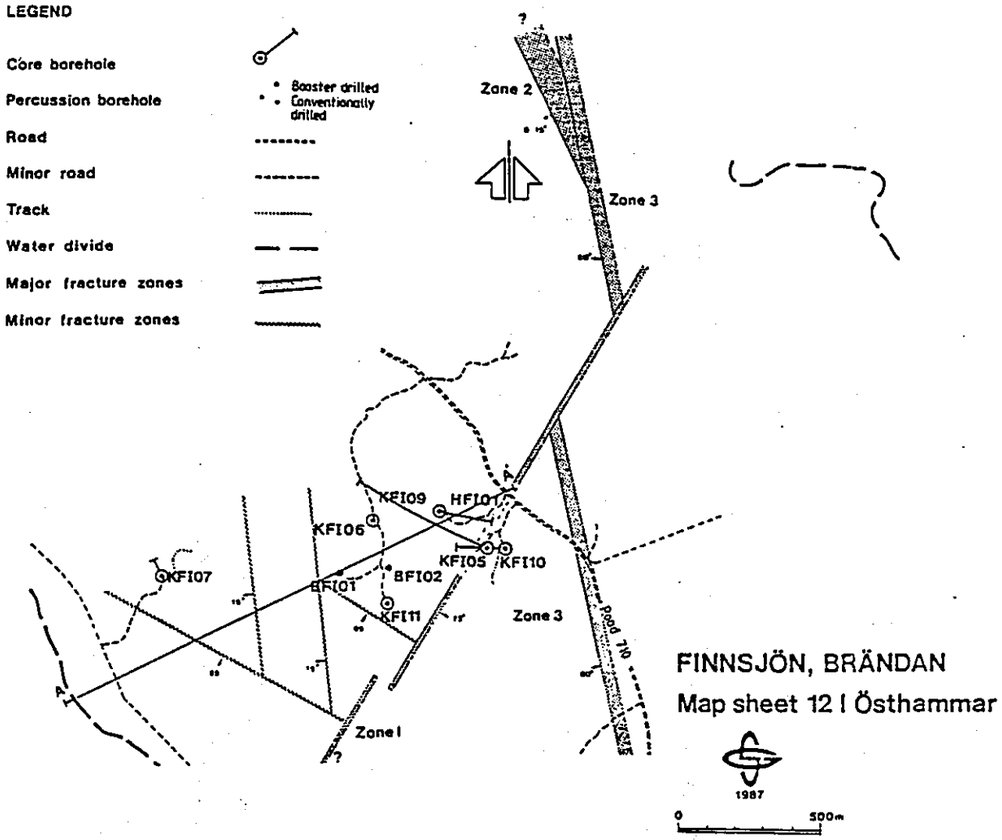
４．その他

1989年末に試験は終了している。

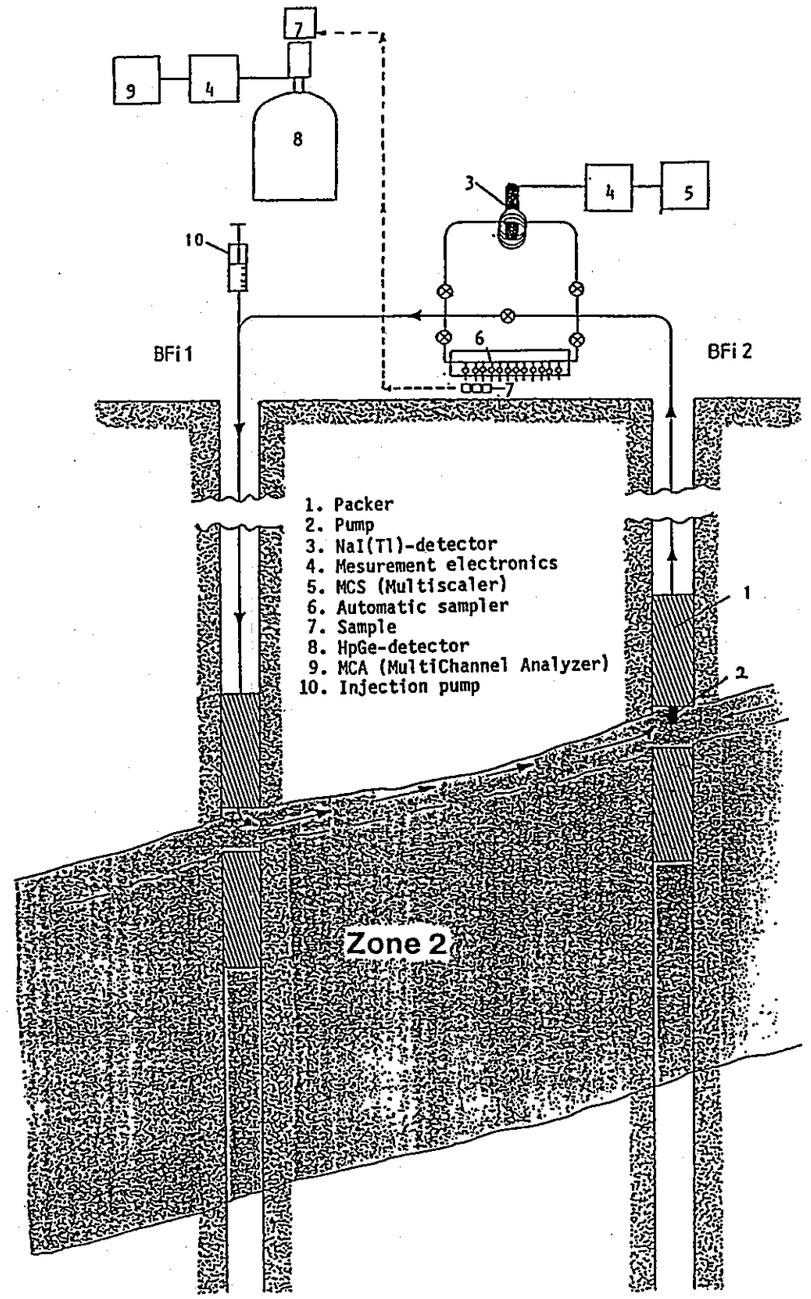


図－Ｄ　　破過曲線の例

表－８　　ＩＮＴＲＡＶＡＬ　フェーズ２　テストケースの試験内容（８／１４）



図－Ａ　　Ｆｉｎｎｓｊöｎサイト



図－Ｃ　　ダイポール試験装置

表－8　　INTRAVAL　フェーズ2　テストケースの試験内容（9／14）

ケース：ﾌｪｰｽﾞ1の4	Stripa（亀裂媒体中の地下水流れとトレーサ移行）
資料名：①INTRAVAL Progress Report No.5, ②Stripa Project 87-19[6], 87-20[7], 87-21[8]	

1．試験場所

スェーデンのStripa鉱山

2．試験方法

2.1 試験の種類

花崗岩中のトレーサ移行試験

2.2 試験方法

Stripa鉱山の地下360mに長さ75m，腕の長さ25mの抗道を掘った（図－A）。

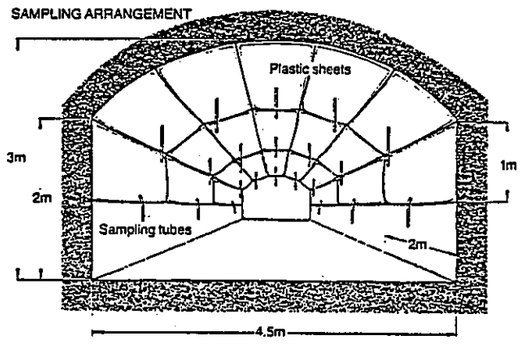
抗道の天井と壁の上部に、地下水を採取するためのプラスチックシート（1枚の面積＝2m²合計375枚）を設けた（図－B）。

トレーサ注入孔を掘る前に、地下水の流量を測定した。

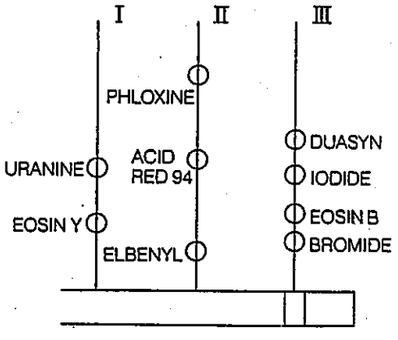
天井から上部へ長さ70m，直径76mmのトレーサ注入孔を3ヶ所掘った。

トレーサ注入孔のうち、透水性の高い9ヶ所にトレーサを連続的に一定圧力で注入した（図－C）。トレーサの注入領域の長さは2.5m，注入期間は20ヶ月である。

トレーサ注入後プラスチックシートで採取した地下水中のトレーサ濃度を測定した。水の採取は10時間毎に行い、トレーサ注入完了後6ヶ月まで行った。



図－B　　プラスチックシートの位置



図－C　　トレーサ注入位置とトレーサの種類

3．試験結果

(1) 地下水の流量

試験場への地下水の流れは不均一であることがわかった（図－D）。

145枚のプラトチックシートで水が検出され、プラスチックシートで覆われた部分の3%で全地下水量の50%を占めている。

(2) 地　質

トレーサ注入孔での割れ目の測定の結果試験場には、4つの割れ目帯があることが推定された（図－5）。

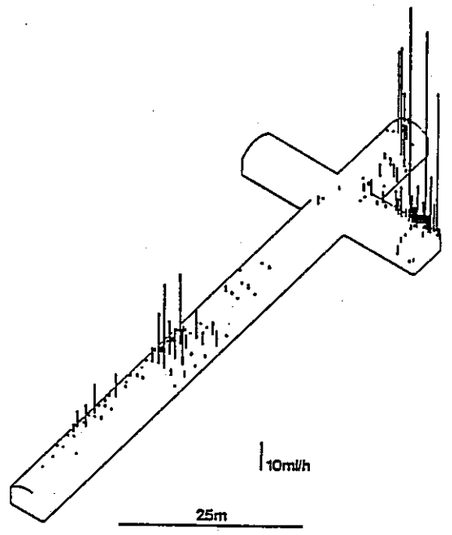
また、100以上の細かい割れ目が記録された。

(3) トレーサ濃度

9つのトレーサのうち、6つのトレーサが検出された。抗道の右の腕の部分にはどのトレーサも検出されなかった。

地下水流量の高い部分でのトレーサの侵入部分は図－Fとなった。

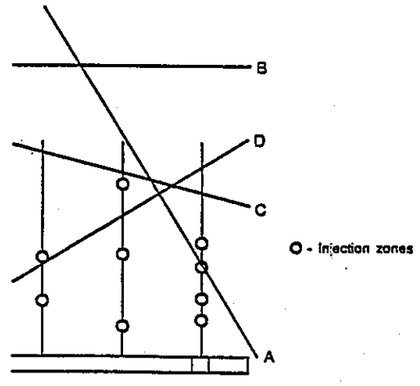
一方、トレーサの破過曲線（例）は図－Gとなった。



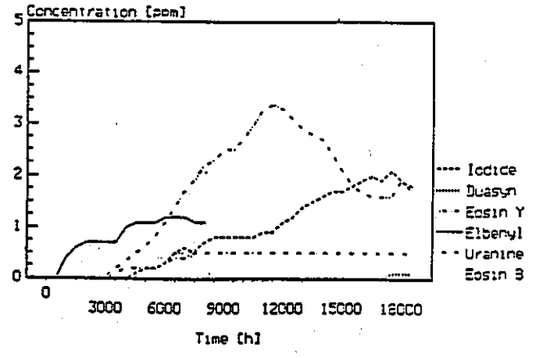
図－D　　地下水の流量

4．その他

試験は完了している。

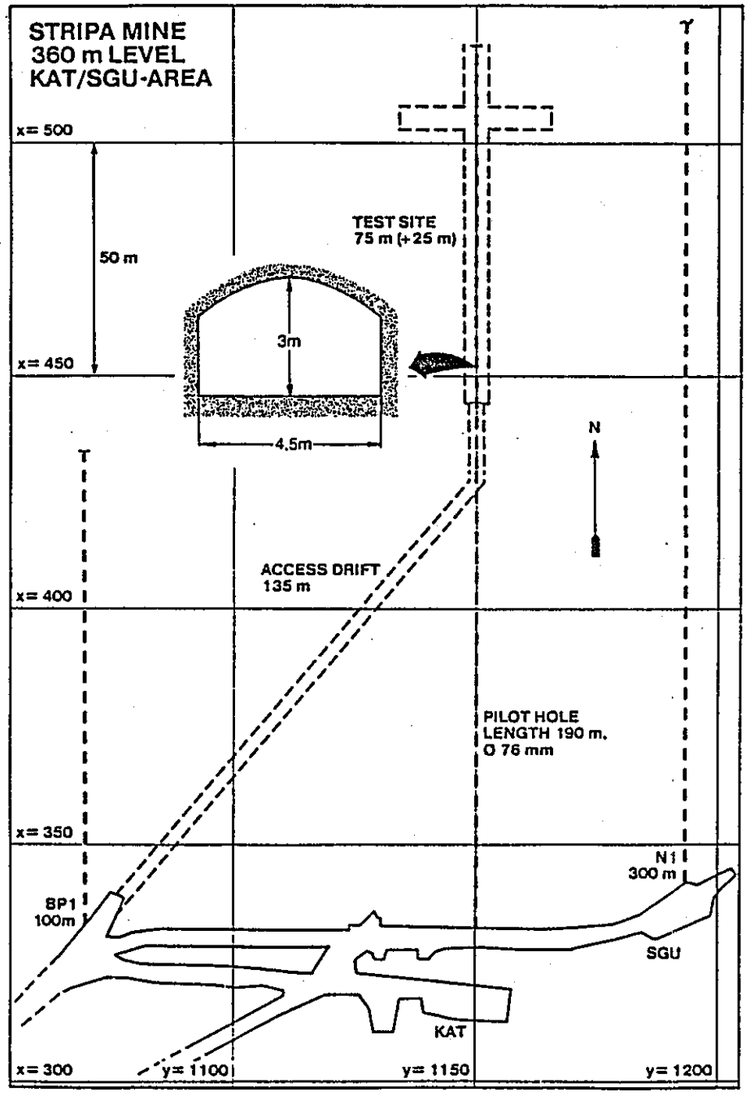


図－E　　トレーサの注入位置と割れ目帯の位置

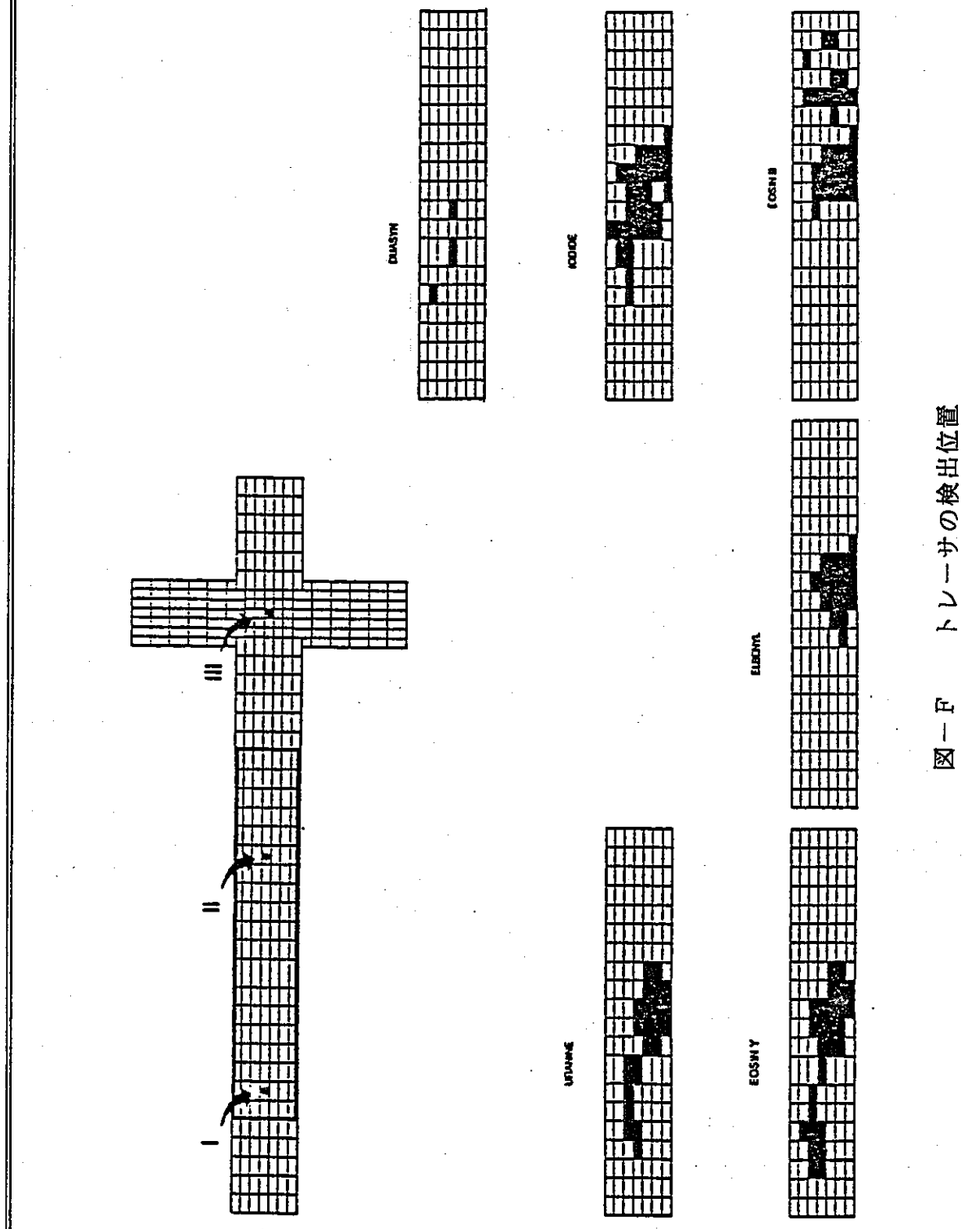


図－G　　トレーサの破過曲線

表－８　　ＩＮＴＲＡＶＡＬ　フェーズ2　テストケースの試験内容（１０／１４）



図－Ａ　　試験場の位置



図－Ｆ　　トレーサの検出位置

表－8　　INTRAVAL　フェーズ2　テストケースの試験内容（１１／１４）

ケース：No.未定	Mol（粘土中のトリチウムの移行試験）

資料名：Three Dimensional In-Situ Migration Experiment in the Boom Clay Formation at the MOL Sitein Belgium. (February 12, 1991)[9]

1．試験場所

ベルギーのMolの地下200mに建設された地下試験施設のCP1（図－Ａ）。

2．試験方法

2.1 試験の種類

粘土中のトリチウムの移行試験

2.2 試験方法

① 図－AのCP1の場所にピエゾメータを0.9m間隔で設置する（図－Ｂ）。
ピエゾメータは、2重管になっており、外管は焼結ステンレス鋼のフィルタである。また、2つの管の隙間は、直径2mmの管で抗道とつながっており、トレーサが注入できるようになっている（図－Ｃ）。

② 円管の隙間の水圧をマノメータで測定する。

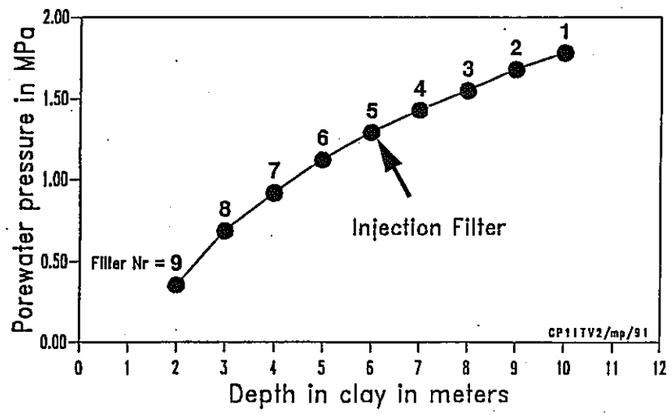
③ 実験装置を設置して2.5年後、トレーサ（トリチウム）をNo.5のフィルタに注入する。
注入方法はトリチウム水の入った容器をフィルタNo.2とNo.5の間に連結させ、差圧によりNo.5にトリチウム水を注入する方法で行った。
No.5の内容積の2.4倍のトリチウムを注入後、容器を切り離した。

④ トレーサを注入して3ヶ月後に2ヶ月間隔でフィルタNo.4とNo.6中のトリチウム濃度を測定する。

3．測定結果

3.1 圧力測定結果

抗道の端近くの垂直のシャフトは大気圧のため、試験場所近傍に圧力勾配を生じている（図－Ｄ）。



図－Ｄ　　ＤＰ１中の圧力分布

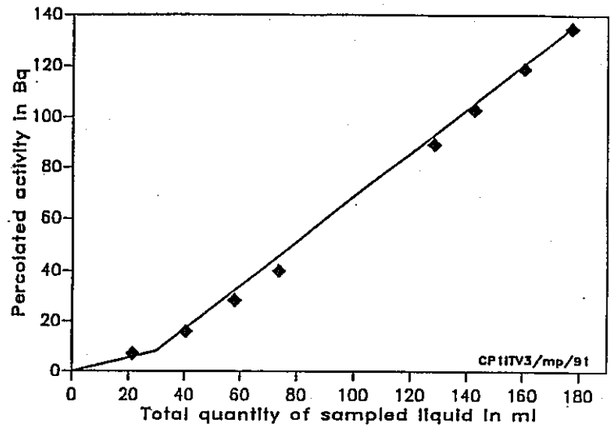
3.2 試料採取量とトリチウム濃度の測定結果

測定したトリチウム濃度Csから、フィルタ近傍の濃度Cjを次式を用いて計算した。

$$Cj=\frac{Vs\cdot Cs-Vsp\cdot Ci}{Vs-Vsp}$$

ここで、Vs ：全内容積
Vsp：トレーサ注入パイプの内容積
Ci ：前回のトリチウム測定濃度

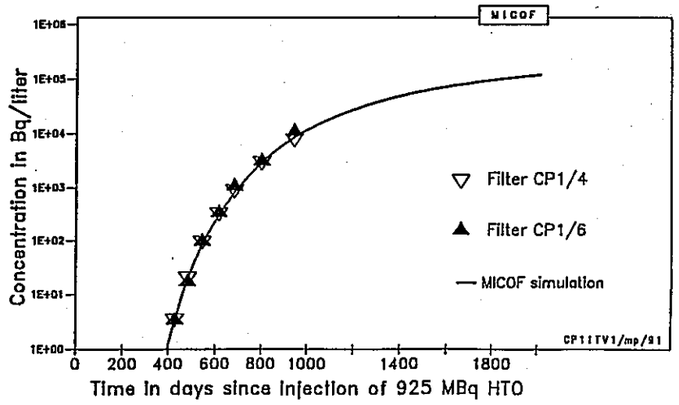
試料No.9を8回に分けて測定したトリチウム濃度は上記の補正式の関係を示している（図－Ｅ）。



図－Ｅ　　試料No.9の試料量とトリチウム濃度の関係

3.3 トリチウム濃度分布の測定結果

トレーサ注入後の経過時間とフィルタNo.4およびNo.6のトリチウム濃度の計算結果は図－Ｆとなる。



図－Ｆ　　フィルタNo.4とNo.6におけるトリチウム濃度

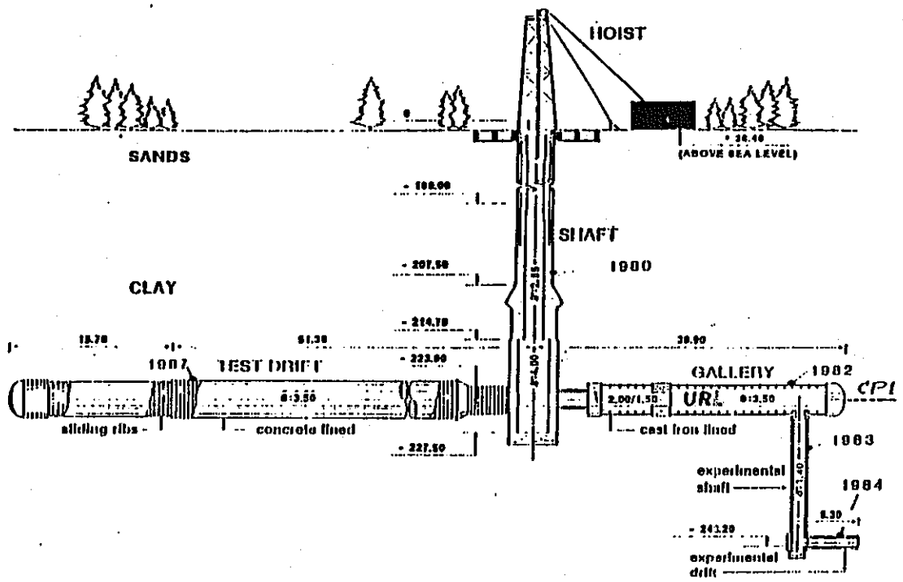
4．その他

4.1 シミュレーション結果

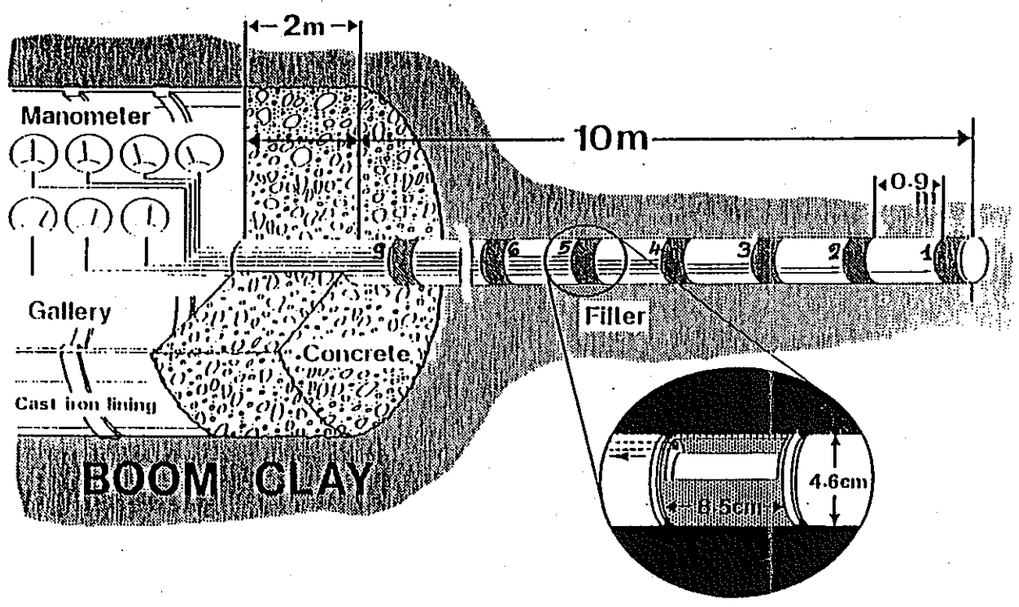
室内試験の測定結果に基づく下記のパラメータを用いて、MICOFプログラムにより、図－Ｆのトリチウム濃度分布をシミュレーションした結果を、同図中の曲線で示す。

- hydraulic conductivity	K	= 3.2E-12	m/s
- hydraulic gradient	dh/dx	= -18.9	m/m
- diffusion access. porosity	n	= 0.35	-
- dispersion length	a	= 0.002	m
- retardation factor	R	= 1	-
- half live HTO	T	= 12.28	year
- Darcy velocity (x direction)	Vd	= 6.0E-11	m/s
- dispersion constant (x)	Dx	= 4.1E-10	m2/s
- dispersion constant (y)	Dy	= 4.1E-10	m2/s
- dispersion constant (z)	Dz	= 2.0E-10	m2/s

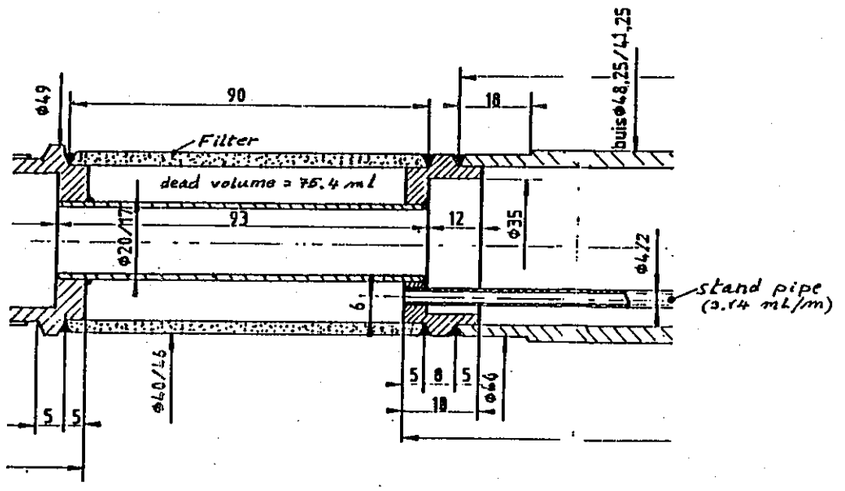
表－8　　INTRAVAL　フェーズ2　テストケースの試験内容（１２／１４）



図－A　　地下試験施設



図－B　　ピエゾメータの外観図



図－C　　フィルタの概略図

表－８　　ＩＮＴＲＡＶＡＬ　フェーズ２　テストケースの試験内容（１３／１４）

ケース：No.未定	Twin Lake（砂地中のトレーサ移行試験）
資料名：INTRAVAL Progress Report No.5	

１．試験場所
　カナダのTwin Lakeサイト

２．試験方法
　2.1 試験の種類
　　砂れき層中のトレーサ移行試験

　2.2 試験方法
　　Twin Lakeサイトの砂れき層中で自然な地下水流れの下での放射性トレーサの移行試験を行った。
　トレーサの測定点は流れの方向に5m，流れに垂直方向に0.5～1mの間隔で設置されている。
　1982～1983年の試験でよう素の広がりに関するデータを約500点得た。また、水理学的データ，地質学的データも採取した。
　　新たな試験を1990年秋より予定している。

３．試験結果
　データ未入

４．その他
　なし

表－８　　ＩＮＴＲＡＶＡＬ　フェーズ２　テストケースの試験内容（１４／１４）

ケース：ﾌｪｰｽﾞ1の8	Alligator Rivers（ナチュラルアナログ）

資料名：INTRAVAL Progress Report No.5

１．試験場所

オーストラリアのAlligatro River地域のKoongarraサイト

２．試験方法

2.1 試験の種類

ウラン鉱床中の放射性核種の移行

2.2 試験方法

140個のウラン鉱石の成分分析結果，ウラン鉱石近くで採取した107個の岩，地表の地質分布等により地質学的データを採取した。

24回の揚水／回復試験と50回の水の圧力試験により地層中の水力学的データを採取した。

ウラン鉱床中の放射性核種（^{238}U, ^{234}U, ^{226}Ra, ^{222}Rn, ^{232}Th, ^{230}Th, ^{129}I, ^{99}Tc, ^{36}Cl, ^{14}C, ^{3}H）を分析した。また、安定核種についてもデータを採取した。

３．試験結果

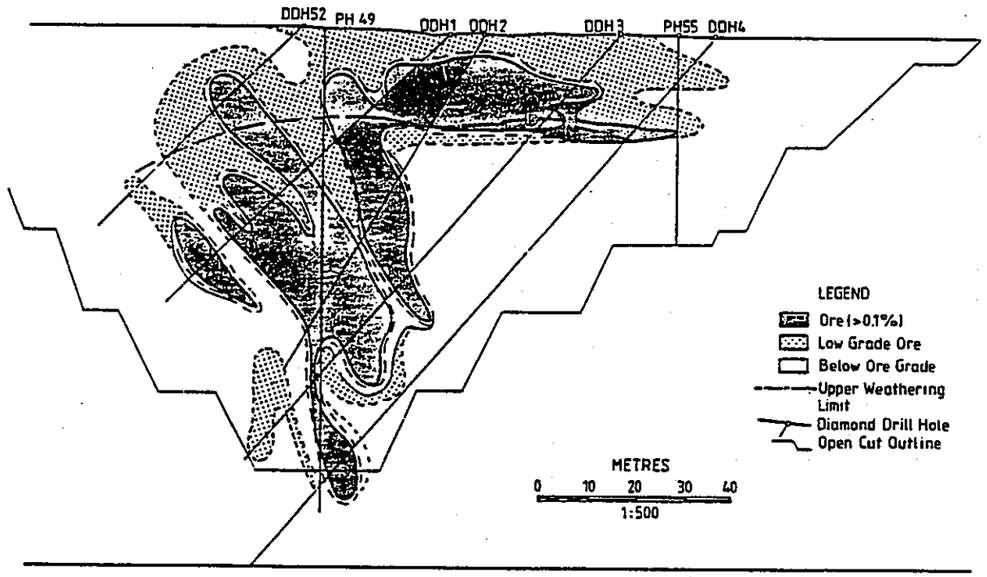
データ未入手

４．その他

Koongarraウラン鉱床の主な特徴は以下のようである。

ウラン鉱床は、2つの鉱石体に分かれている。本研究対象であるNo.1の鉱石体には、地表から深さ20～25mの固化帯に二次的な鉱物が存在し、約80mにわたって広がっている（図－Ａ）。

No.2の鉱石体には、二次的な鉱物は見られない。



図－Ａ　　試験場の断面図

表－9　　放射性核種の移行のプロセスモデル例

$$\frac{\partial C_i}{\partial t} = -V\frac{\partial C_i}{\partial x} + D_L\frac{\partial^2 C_i}{\partial x^2} - \lambda_i C_i + \lambda_{i-1} C_{i-1} + D_e \alpha \left.\frac{\partial C_i}{\partial z}\right|_{z=0} - \frac{\partial S_i}{\partial t}$$

a　　b　　c　　d1　　d2　　e　　f

a）移行プロセスに依存した放射性核種の濃度の時間変化

b）移流：地下水のポア流速Vに支配される。ここで、$V = V_d / \phi$，V_dはダルシー流速，ϕは空隙率である。

c）分散：分散係数D_Lに支配される。D_Lは地下水の流速に依存し、流れがないときは$D_L = D_m$（D_mは分子拡散係数）である。

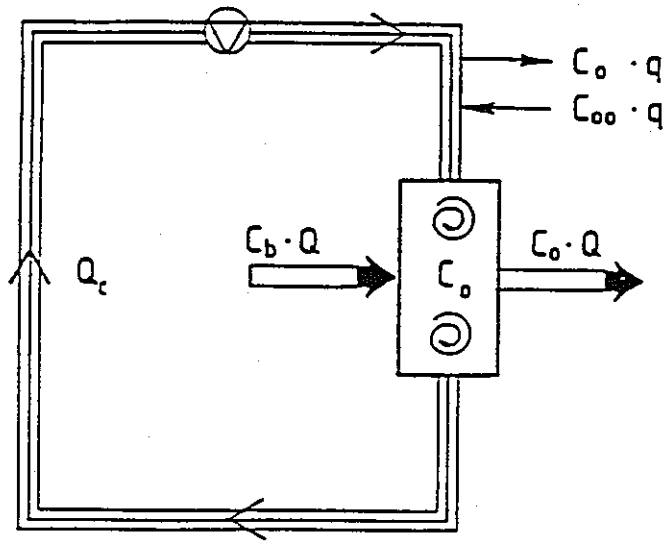
d1,d2）放射能の崩壊：親核種ｉ－１は崩壊により、娘核種ｉを生ずる。λ_i，λ_{i-1}はそれぞれ核種ｉ，ｉ－１の崩壊定数である。

e）マトリックス拡散：亀裂中のよどんだ水や母岩中の空隙部における有効拡散係数D_eに支配される。αは単位体積の地下水と接する母岩の表面積，ｚは母岩表面からの距離である。

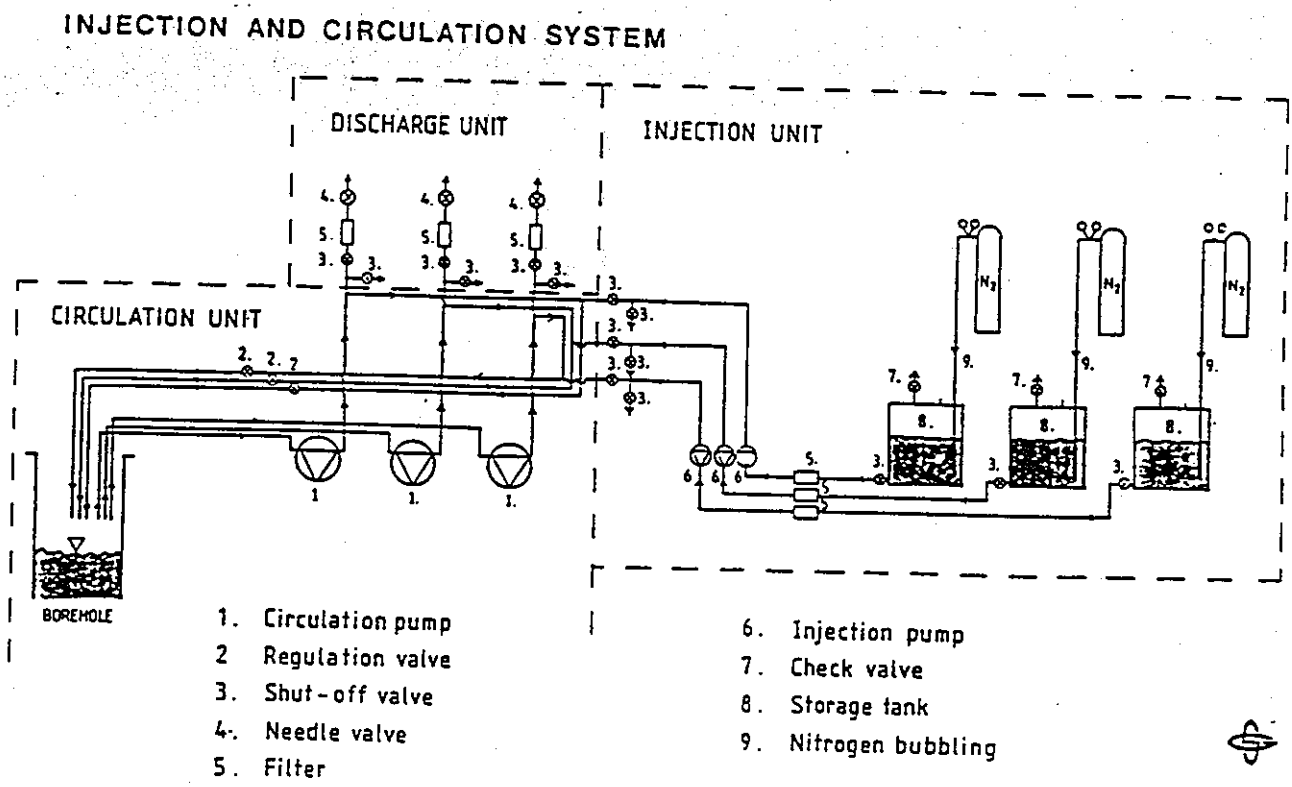
f）固相との相互作用：岩の表面における吸着，脱離を表す。S_iは岩の表面における核種ｉの濃度である。

表－１０　　トレーサの注入位置と使用したトレーサ

Borehole	Interval (m)	Interval length	Transmissivity T (m^2/s)	Type of injection	Tracer
BFI01	Upper; 241.5 - 246.5	5.0	1.29E-3	cont.	Im-EDTA
	Middle; 263.5 - 266.5	3.0	2.47E-6	cont.	Uranine
	Lower; 351.5 - 356.5	5.0	1.03E-4	cont.	Ho-EDTA
KFI06	Upper; 212.0 - 217.0	5.0	5.60E-4	cont.	Iodine
	Middle; 236.5 - 239.5	3.0	4.24E-6	cont.	Yb-EDTA
	Lower; 252.5 - 271.5	19.0	6.68E-4	cont.	ReO_4
KFI11	Upper; 221.5 - 226.5	5.0	3.71E-4	cont.	Gd-DTPA
				pulse	Amino G Acid
				pulse	Tm-EDTA
	Middle; 287.5 - 294.5	7.0	1.61E-6	cont.	Er-EDTA
	Lower; 329.5 - 338.5	9.0	1.52E-5	cont.	Dy-EDTA



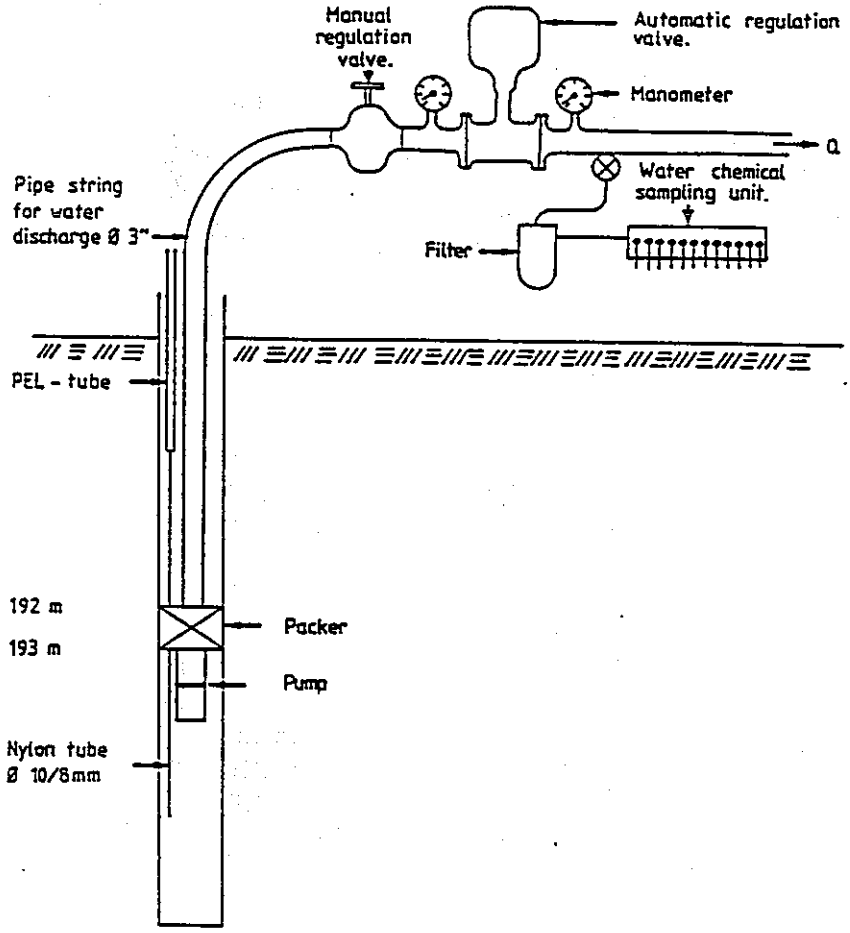
図－１８　　トレーサ注入の概念図



図－１９　　トレーサ注入装置

表－１１　　ＢＦＩ０２における揚水に関するデータ

Pumping interval: 193.0 m - 288.7 m Section length: 95.7 m Transmissivity: 2.58 E-3 m^2/s Pumping rate: 2.0 l/s


Manual regulation valve.
Automatic regulation valve.
Manometer
Q
Water chemical sampling unit.
Filter
Pipe string for water discharge Ø 3"
PEL - tube
192 m
193 m
Packer
Pump
Nylon tube Ø 10/8mm

図－２０　　揚　水　装　置

表－１２　　ダイポール試験におけるトレーサ注入状況

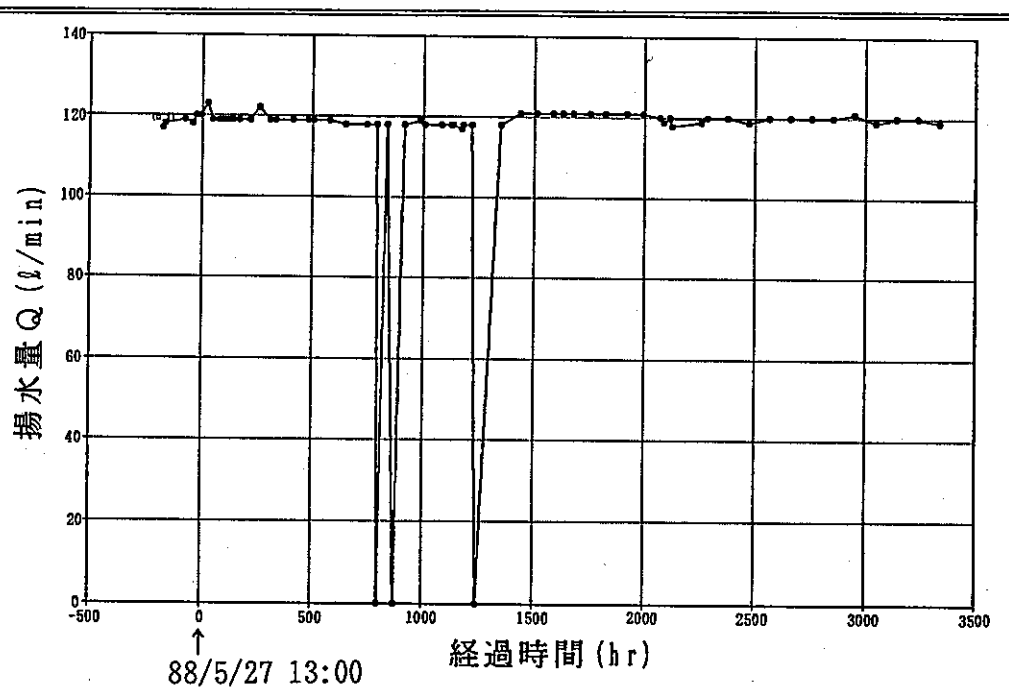
Injection	Day after pump start	Tracer	Half-life
A	14	Rhodamine WT	Dye tracer
1	23	$^{82}Br(I)^-$	1.47 d
2	24	$^{99m}Tc(VII)O_4^-$ $^{186}Re(VII)O_4^-$	6.01 h 3.78 d
3	26	$^{131}I(I)^-$	8.04 d
4	31	$^{99m}Tc(VII)O_4^-$	6.01 h
5	32	$^{58}Co(II)^+$ $^{86}Rb(I)^+$	70.92 d 18.66 d
6	35	$^{24}Na(I)^+$ $^{82}BR(I)^-$ $^{99m}Tc(VII)O_4^-$ $^{131}I(I)^-$ $^{186}Re(VII)O_4^-$ $^{201}Tl(I)^+$	14.66 h 1.47 d 6.01 h 8.04 d 3.78 d 3.05 d
7	39	$^{51}Cr(III)$-EDTA $^{111}In(III)$-EDTA $^{140}La(III)$-DOTA $^{160}Tb(III)$-EDTA $^{169}Yb(III)$-EDTA $^{177}Lu(III)$-EDTA	22.70 d 2.81 d 1.68 d 72.1 d 32.0 d 6.71 d
8	43	$^{58}Co(III)$-EDTA	70.92 d
B	44	Blue Dextran 2000	Macro molecule
9*	46	$^{131}I(I)^-$	8.04 d
10*	47	$^{131}I(I)^-$	8.04 d
C	48	In-EDTA	Metal complex
D	49	Gd-DTPA Tm-EDTA	Metal complex Metal complex
E	54	Rhodamine WT	Dye Tracer

*Injection in hole KFI11, upper section.

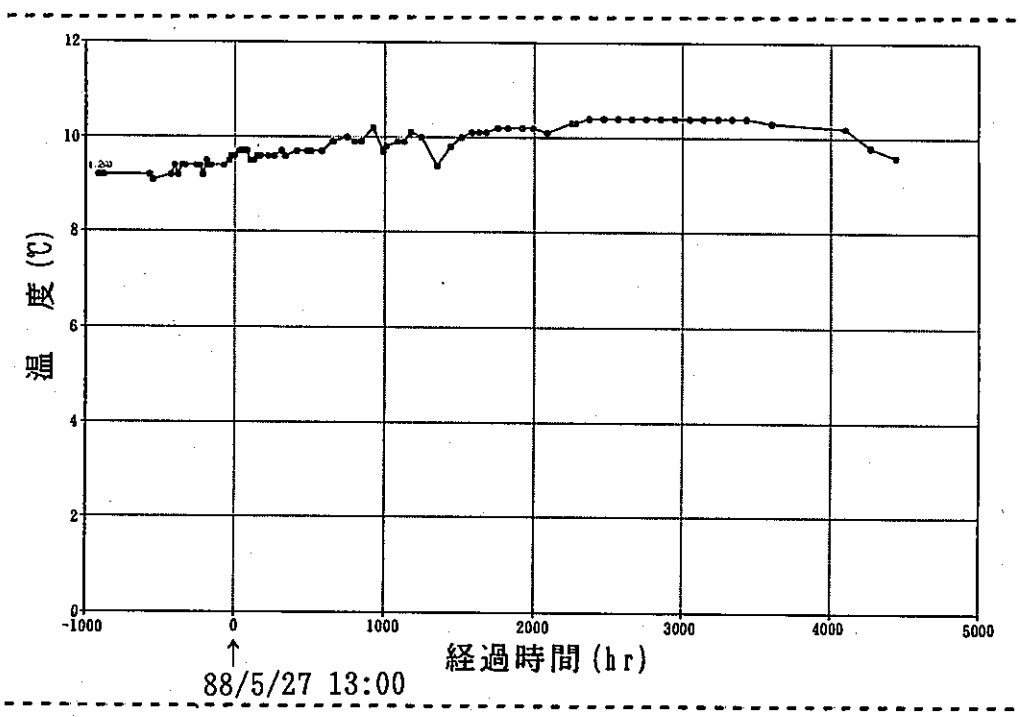
表－１３　　揚水および水頭に関するデータ（１／４）

ＢＦＩ０２に関するデータ

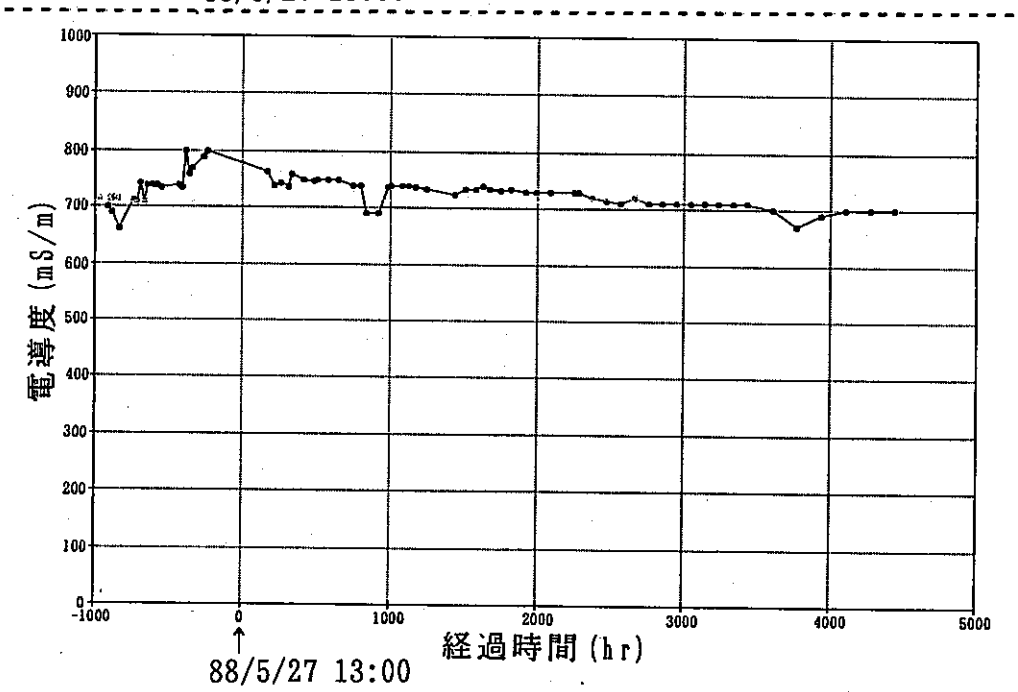
ポンプ容量（ℓ／min）



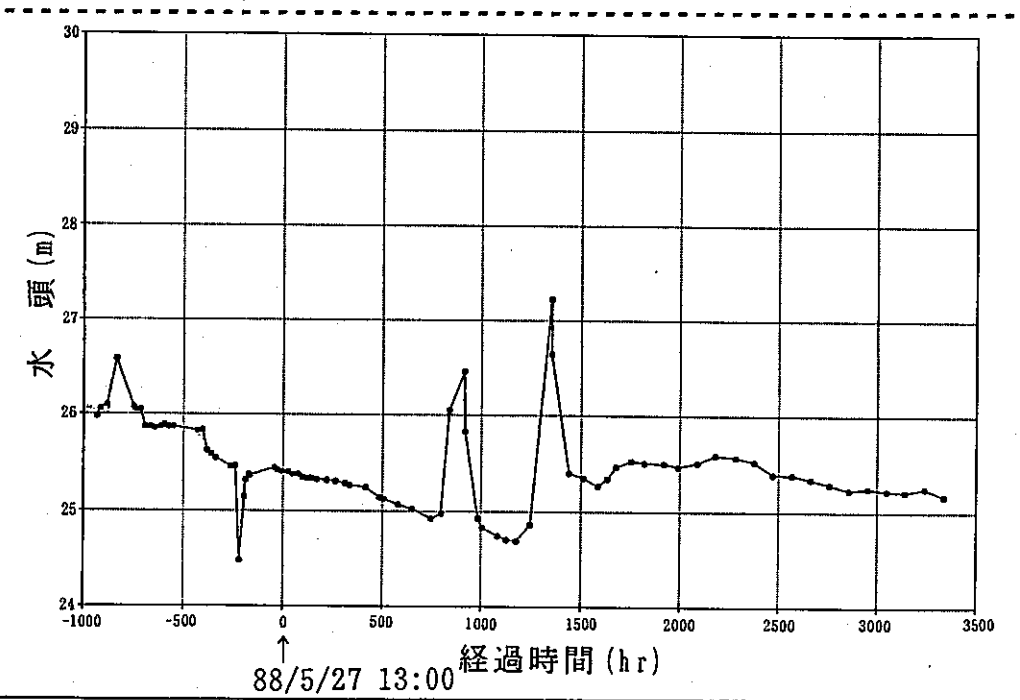
水温（℃）



電導度（mS/m）



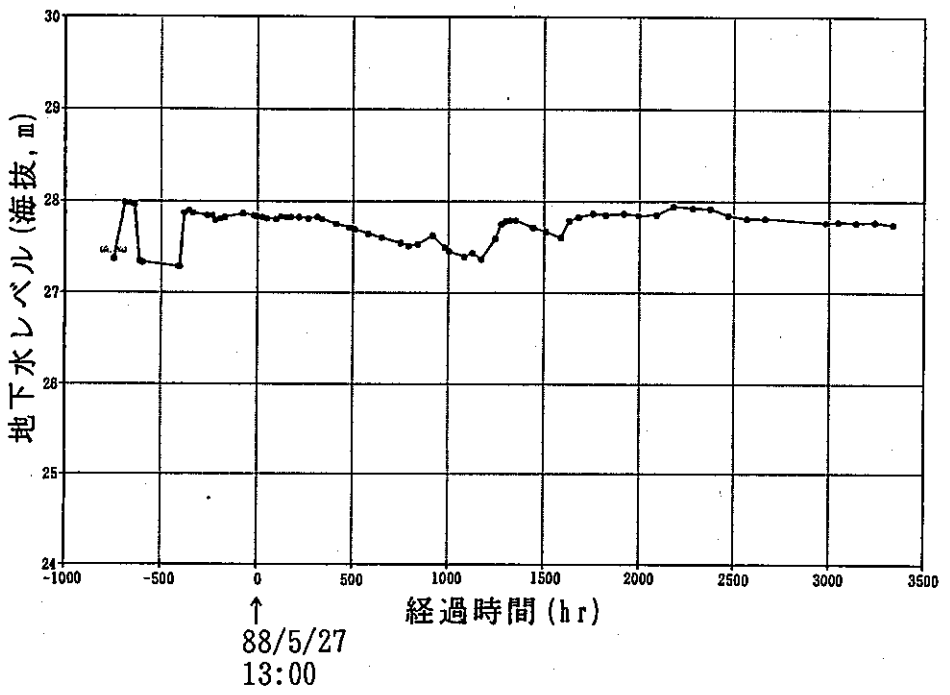
水頭（m）



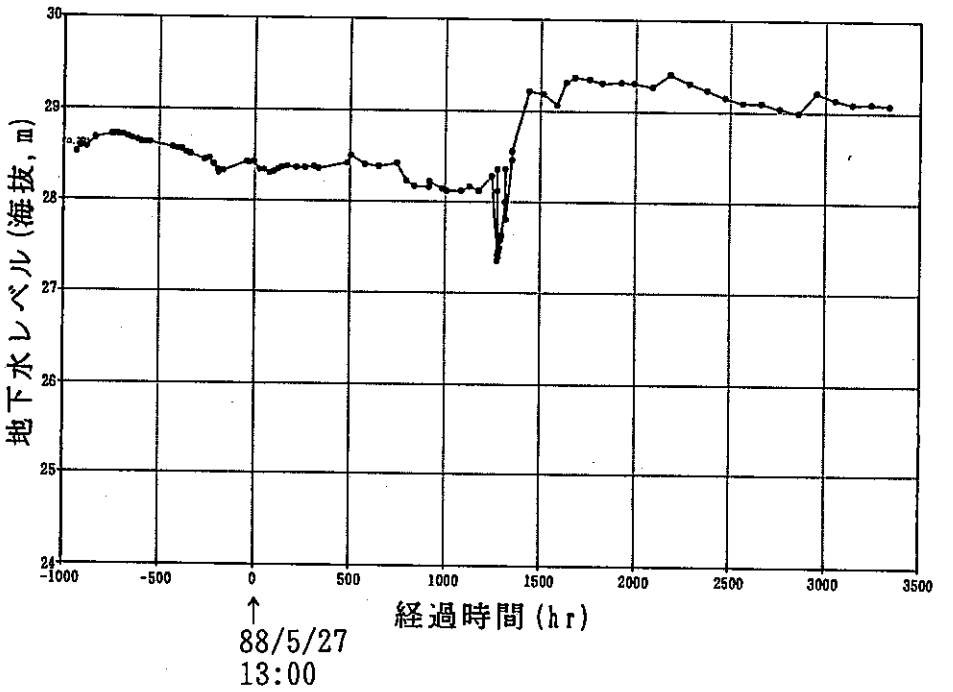
表－１３　　揚水および水頭に関するデータ（２／４）

地下水レベル（海抜，m）

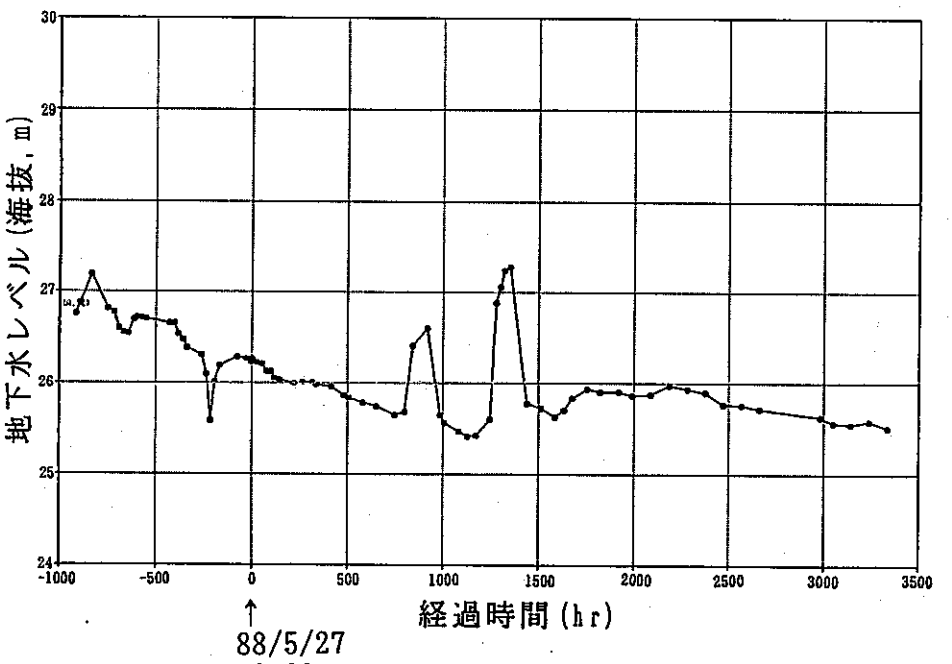
BFI01



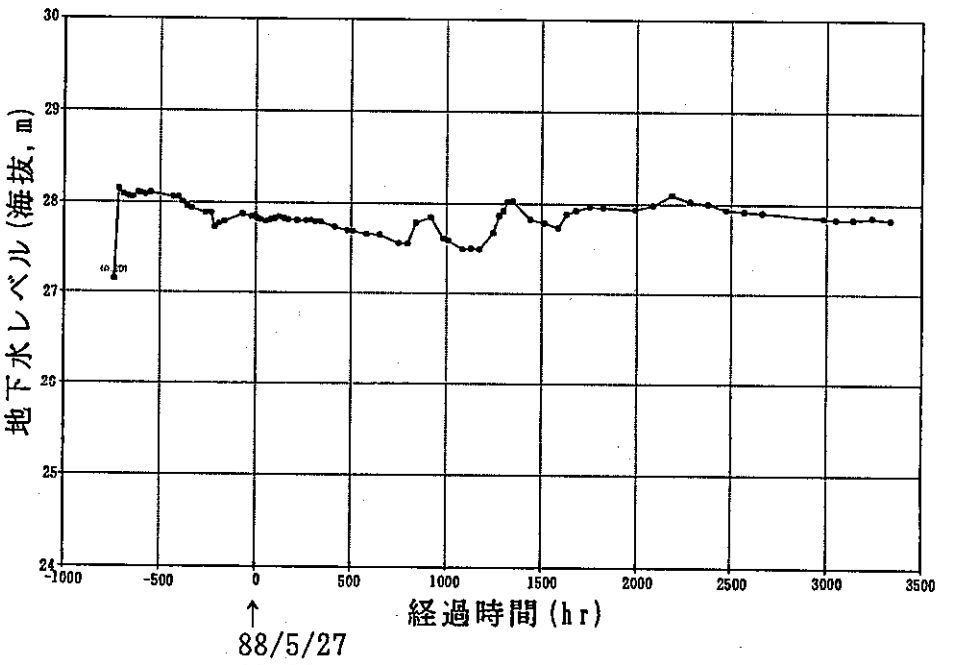
BFI02



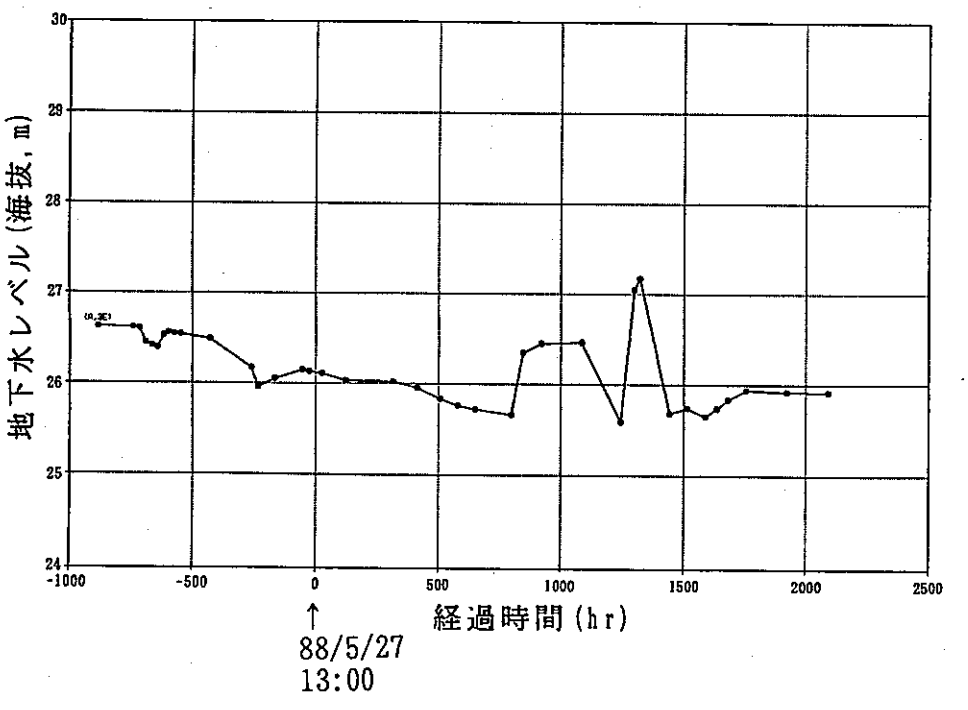
KFI06



KFI11



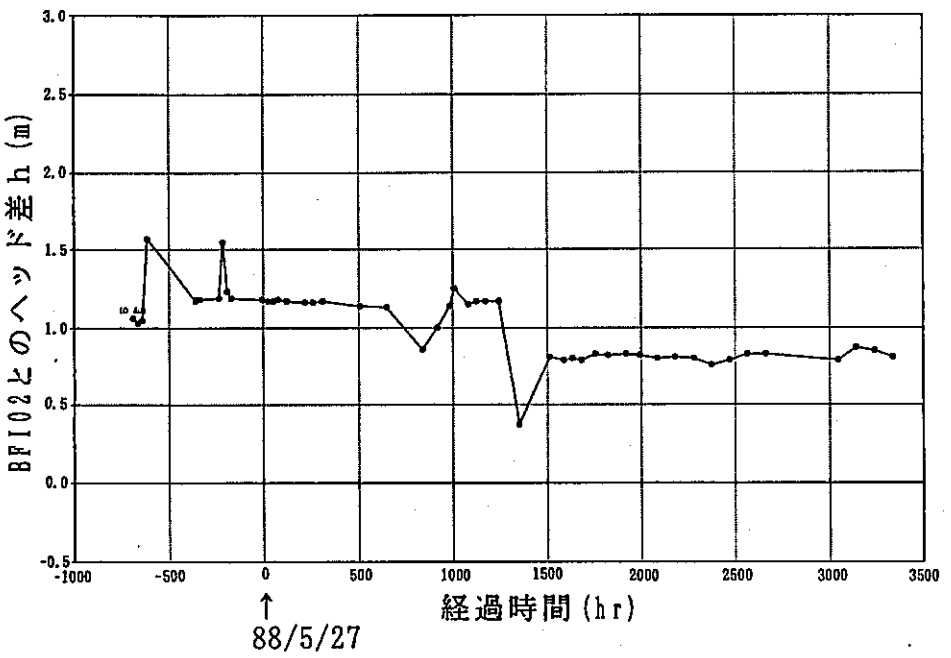
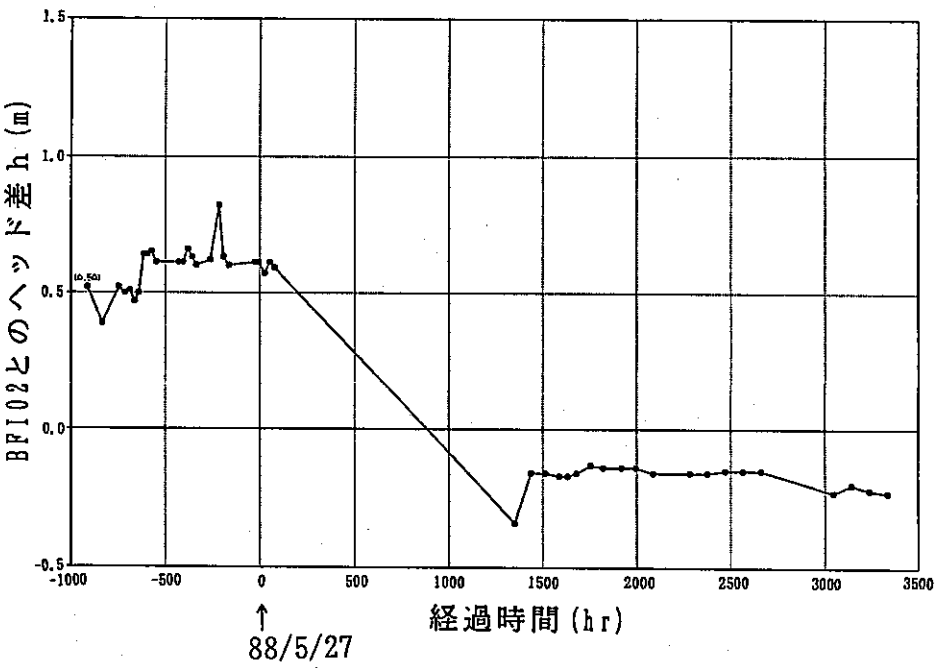
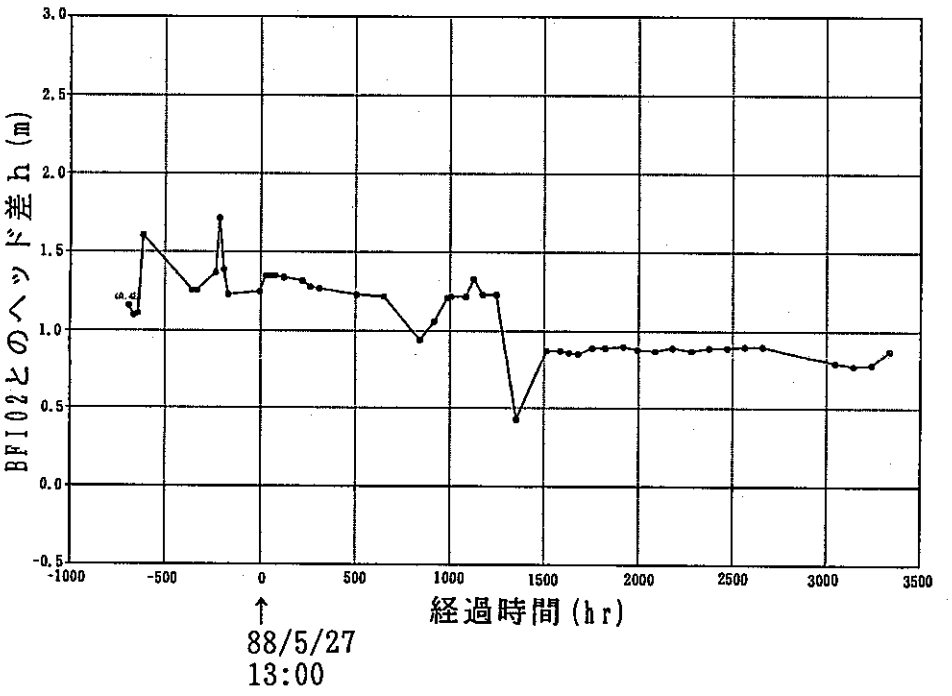
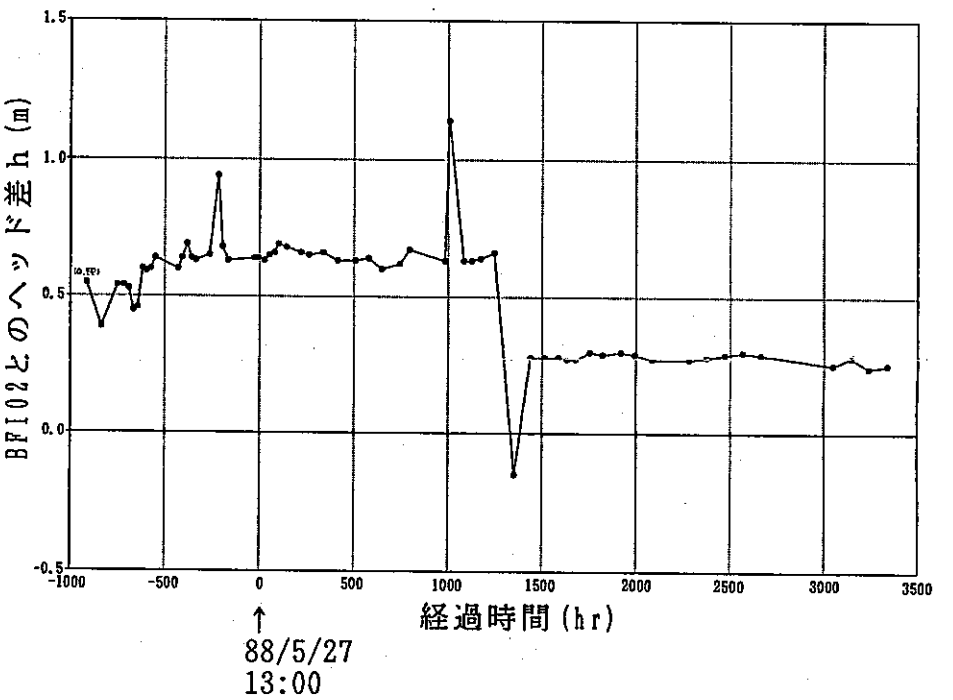
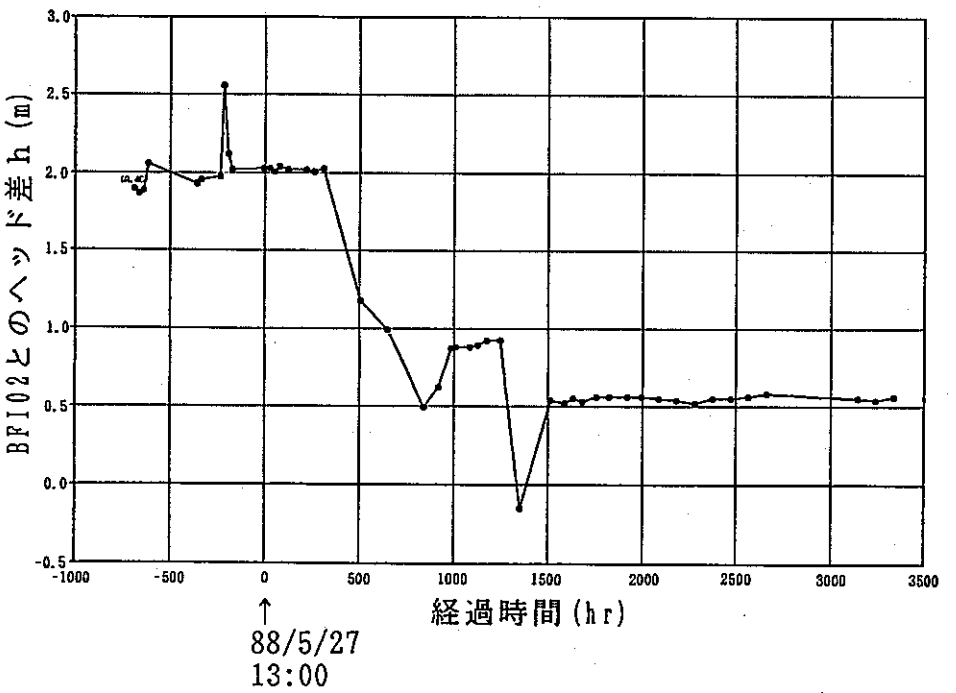
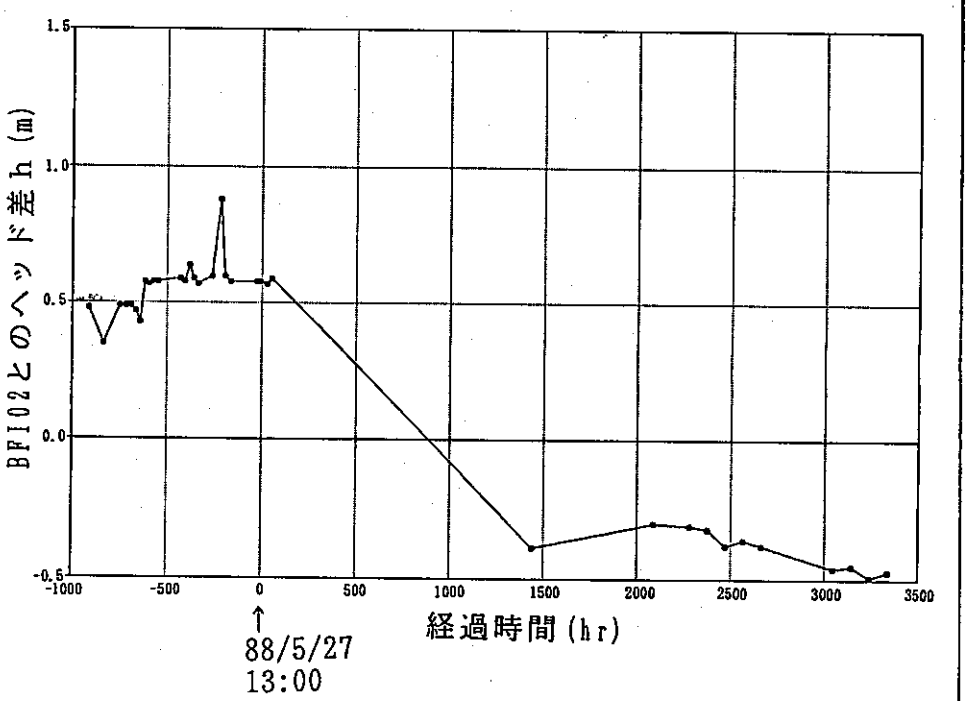
HFI01



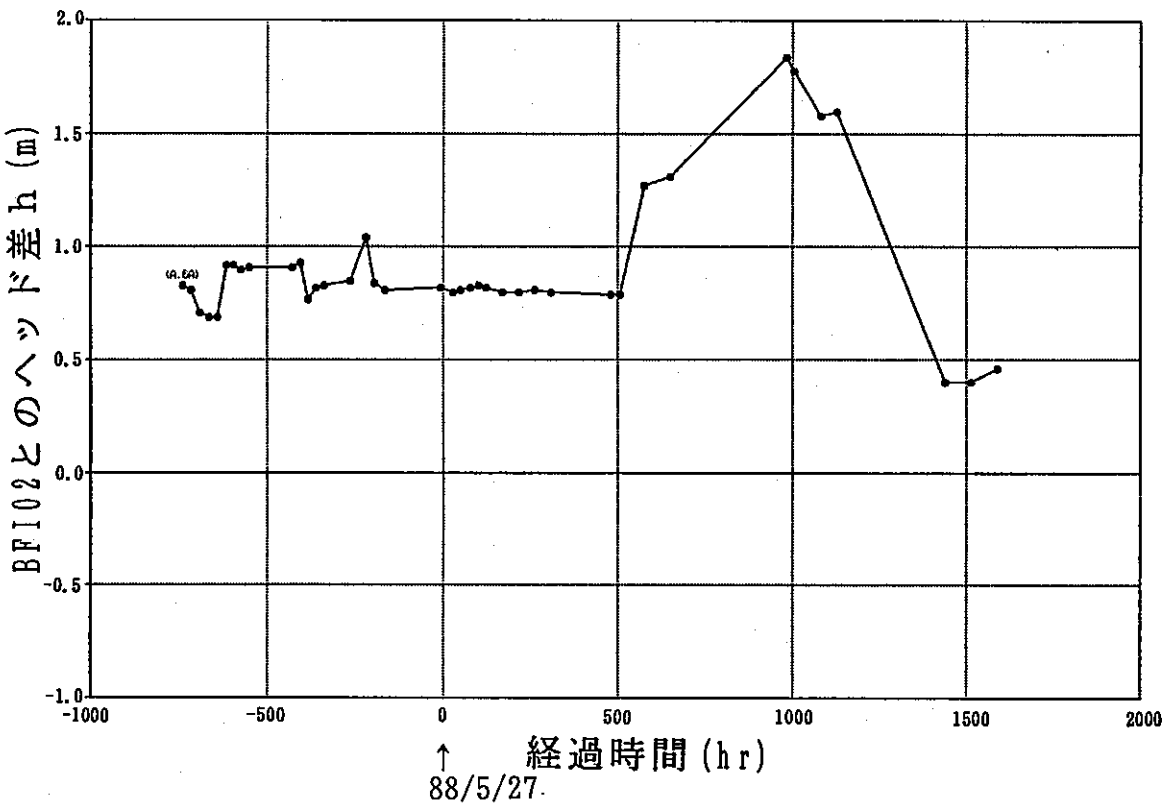
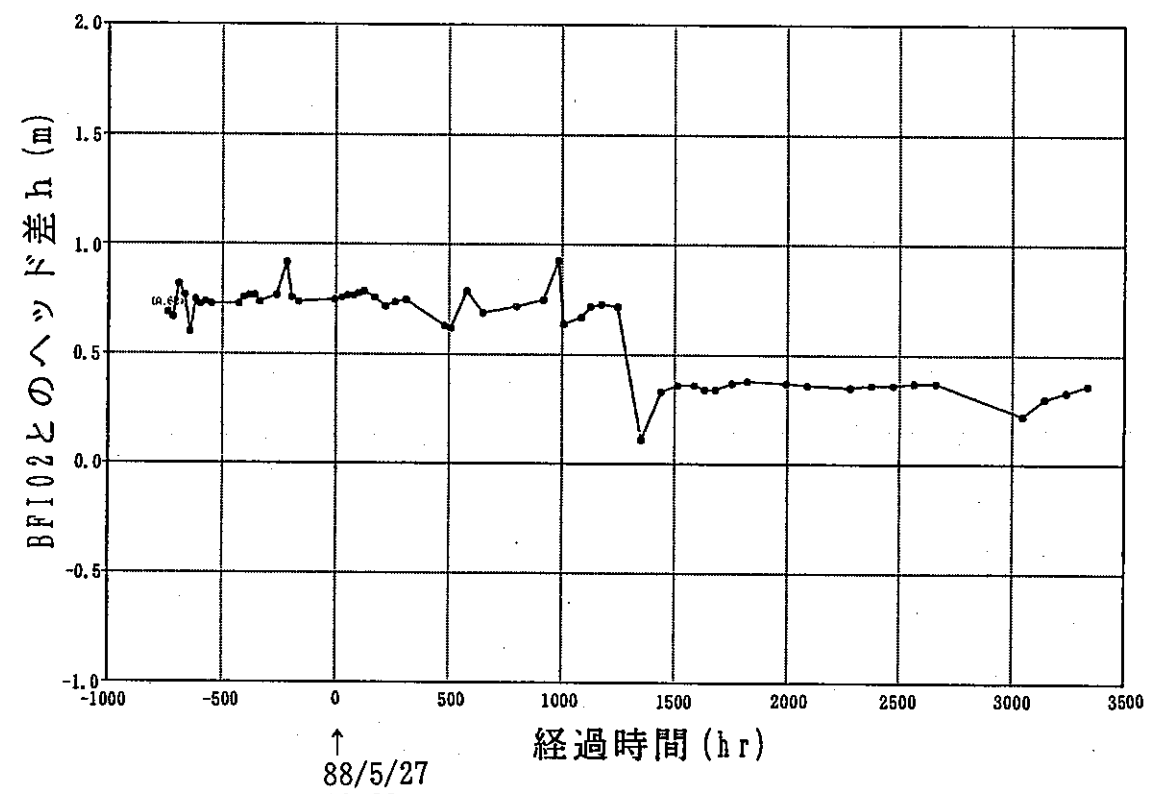
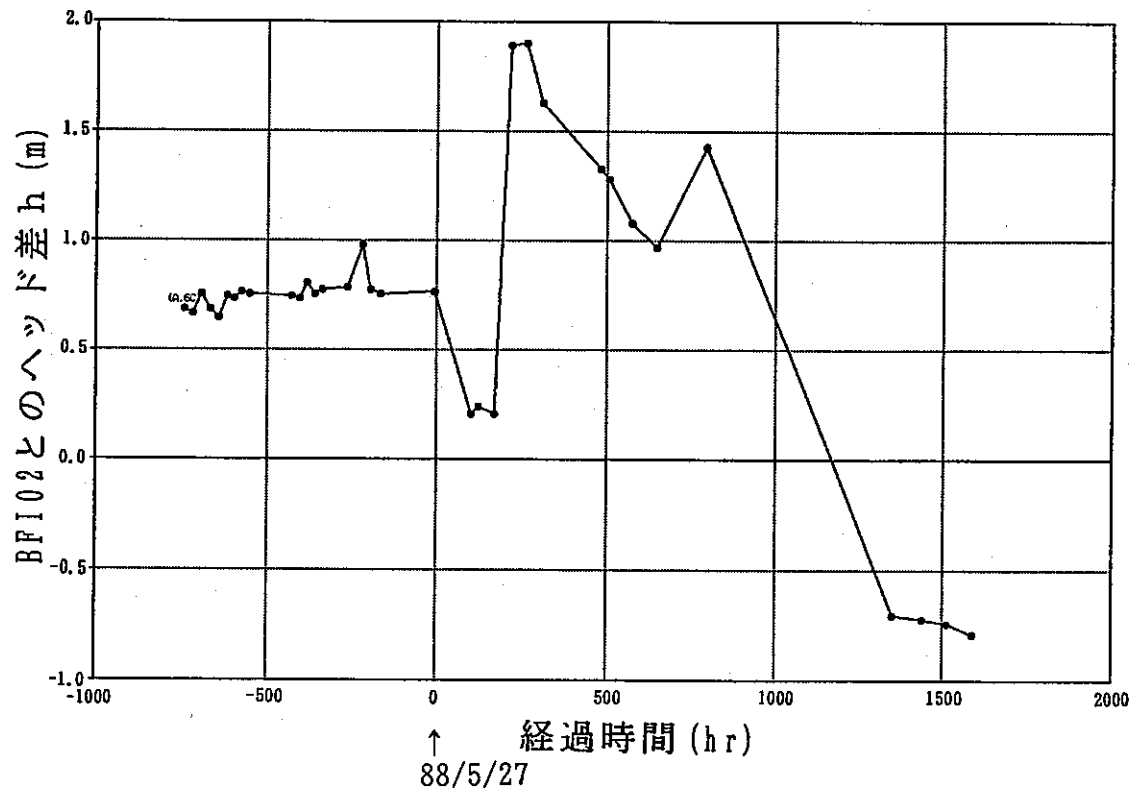
—

—

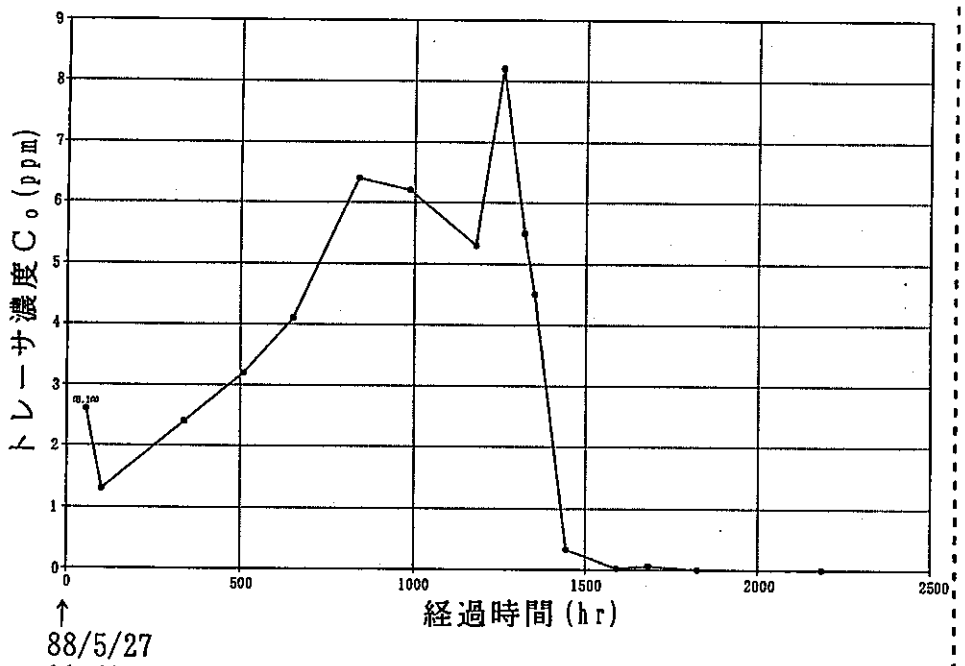
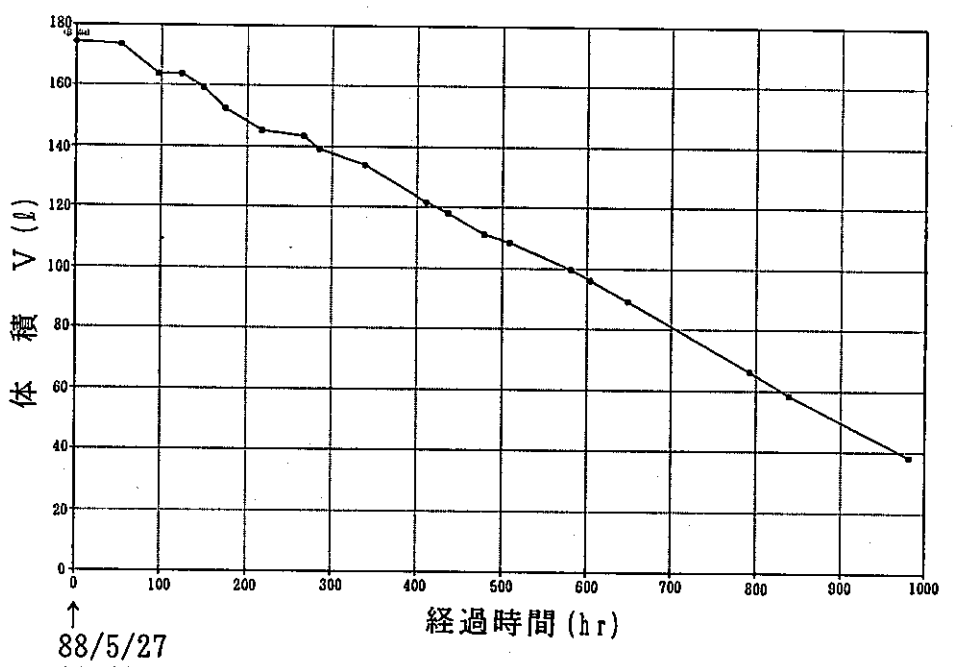
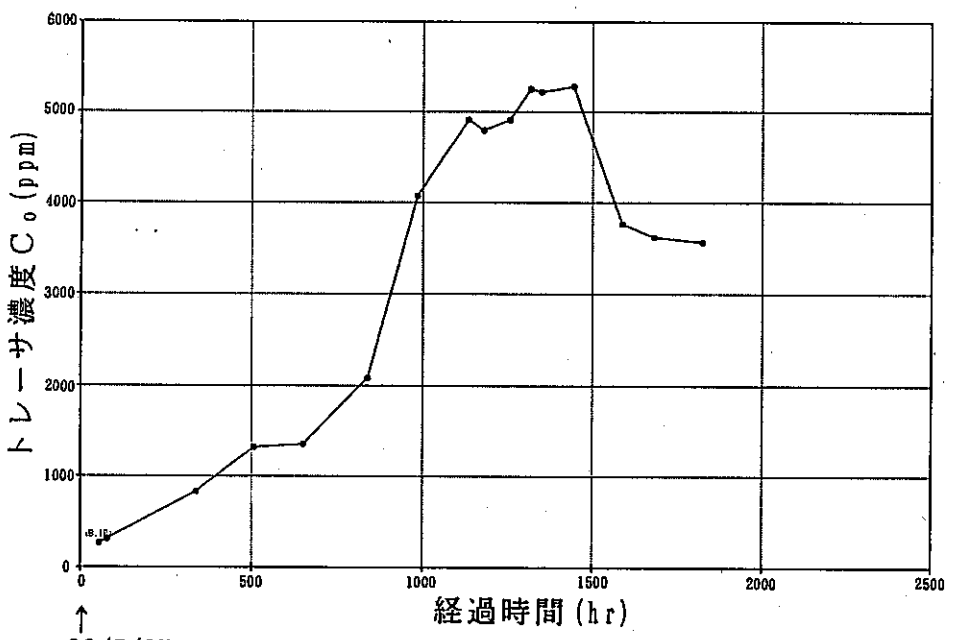
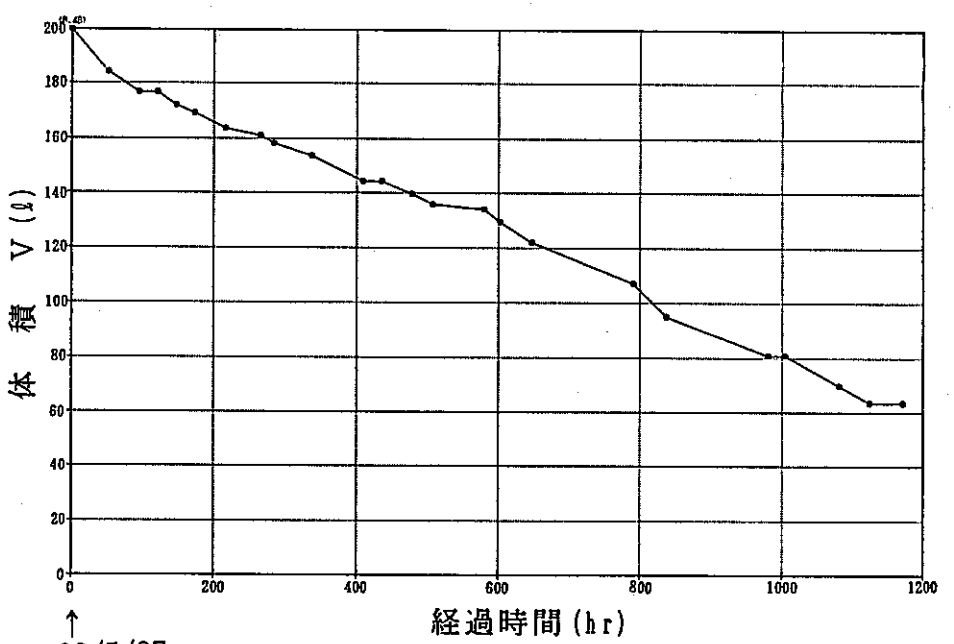
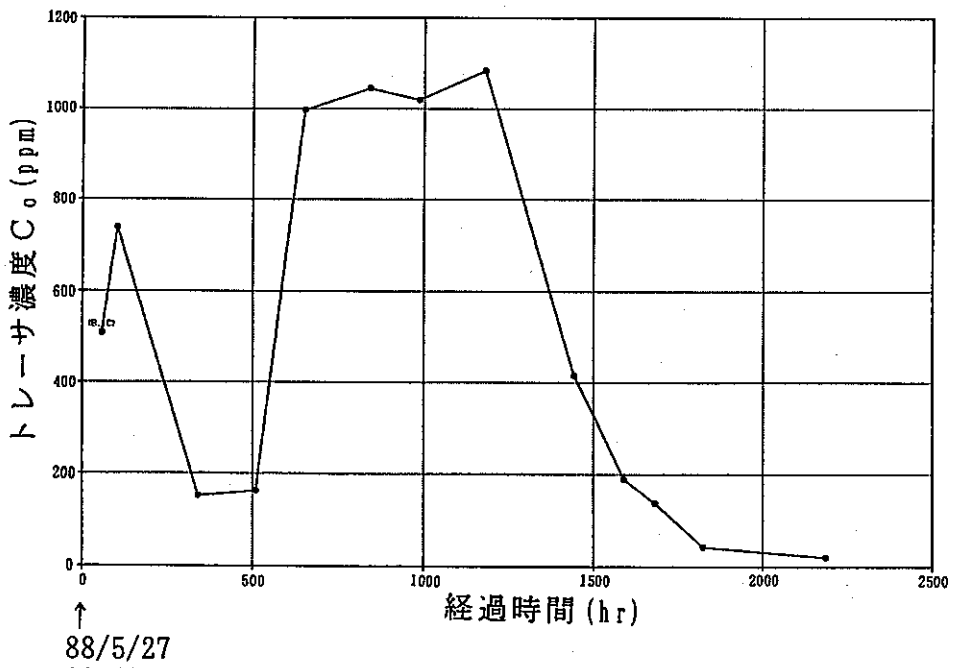
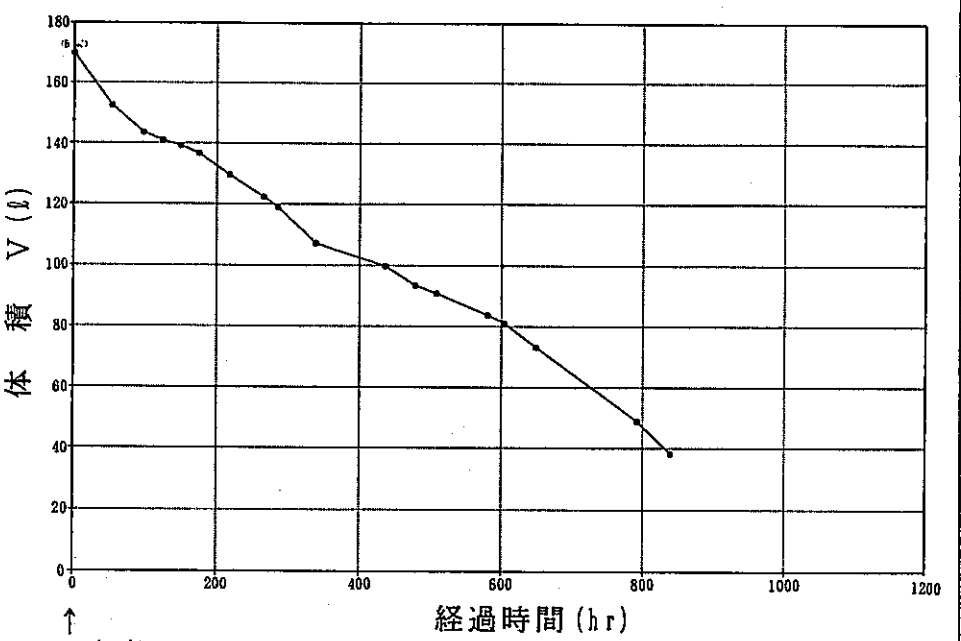
表－１３　　揚水および水頭に関するデータ （３／４）

トレーサ注入部	ＢＦＩ０２とのヘッド差（m）	
	ＢＦＩ０１	ＫＦＩ０６
上　部		
中　部		
下　部		

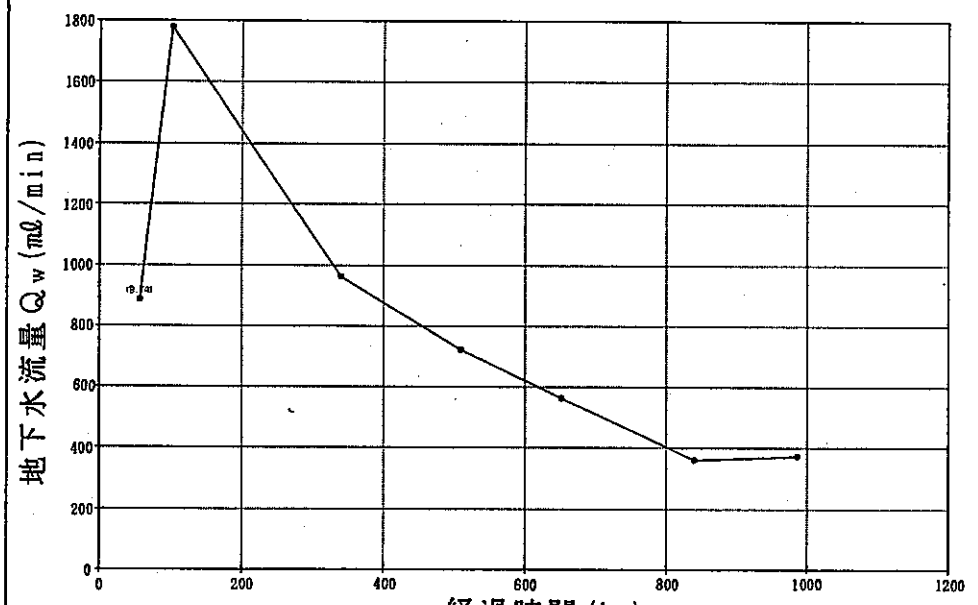
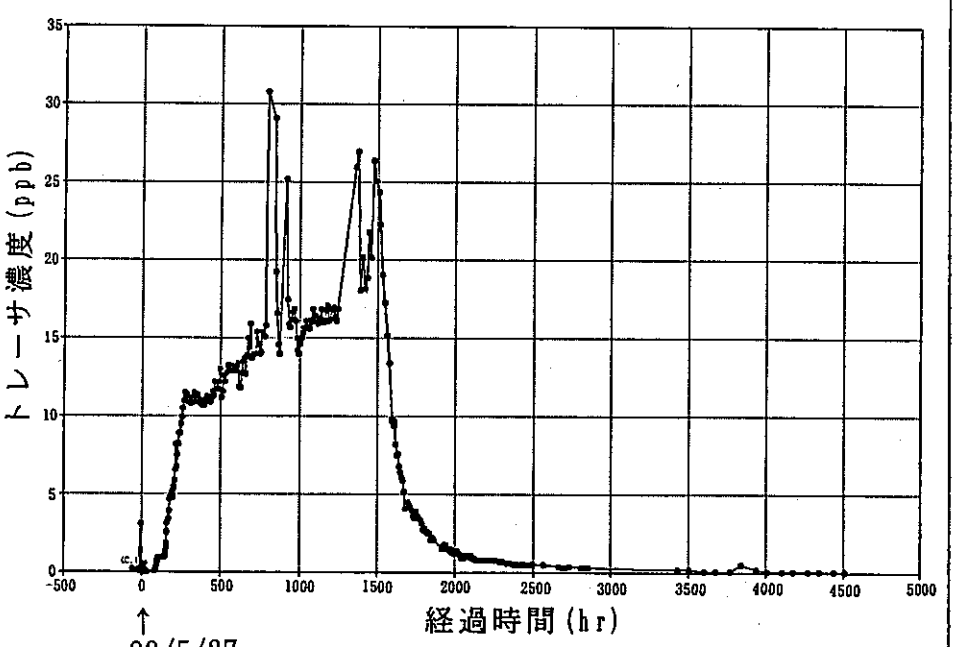
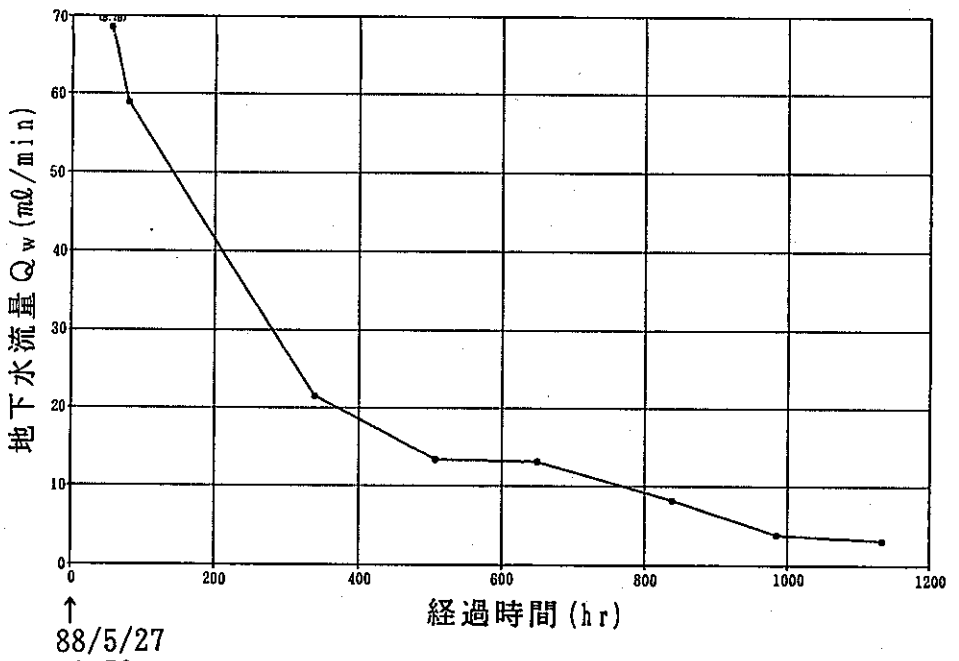
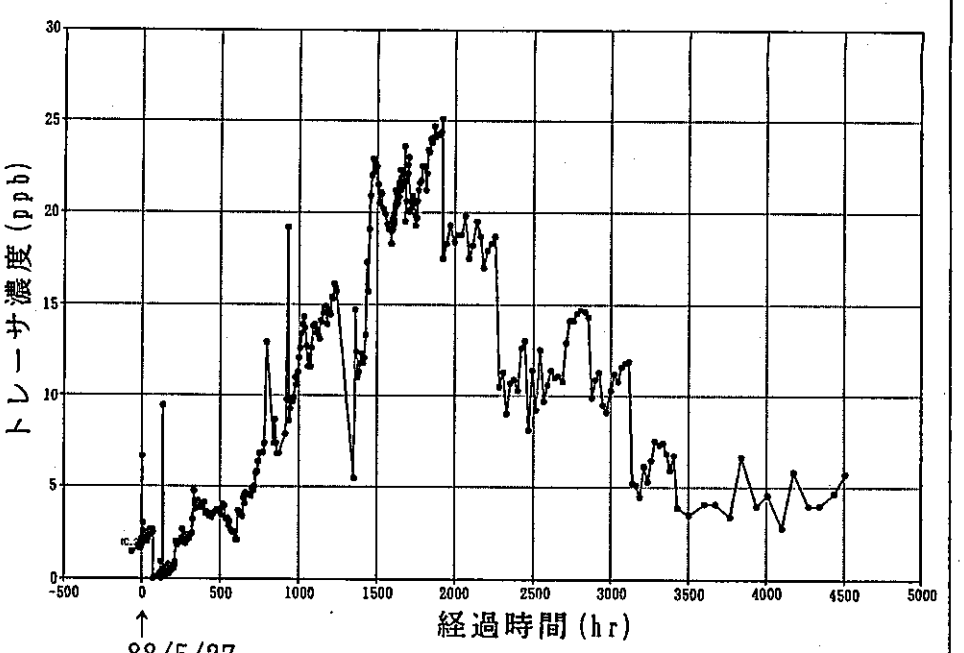
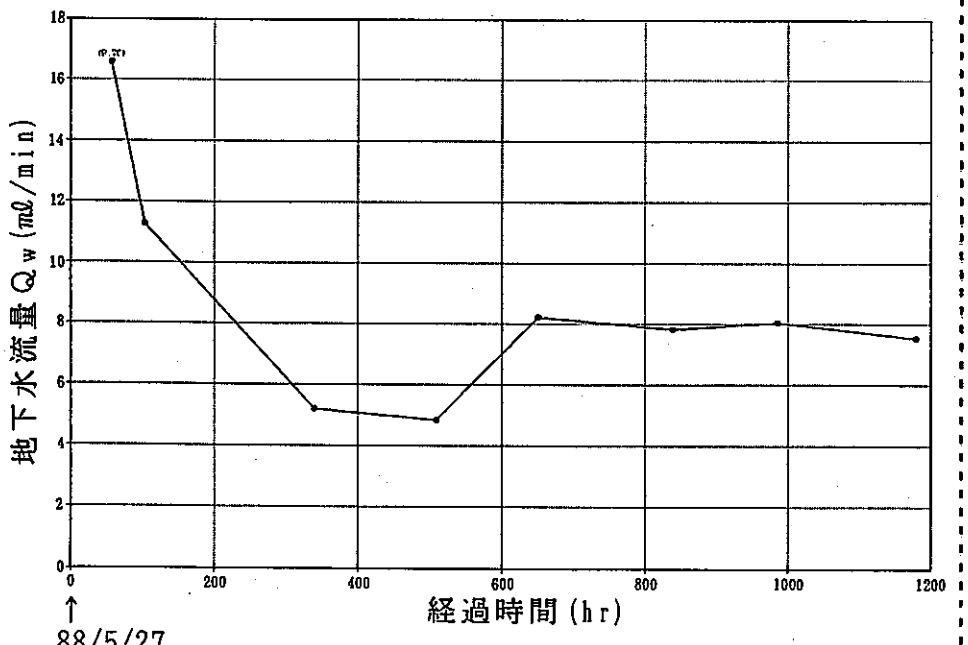
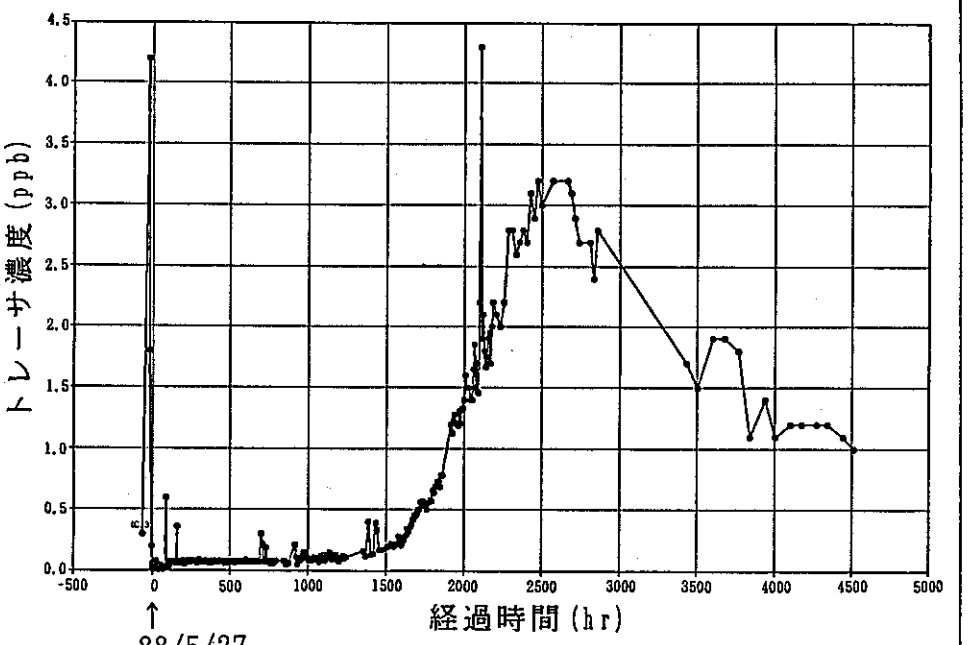
表－１３　　揚水および水頭に関するデータ（４／４）

トレーサ注入部	ＢＦＩ０２とのヘッド差（m）
	ＫＦＩ１１
上　部	
中　部	
下　部	

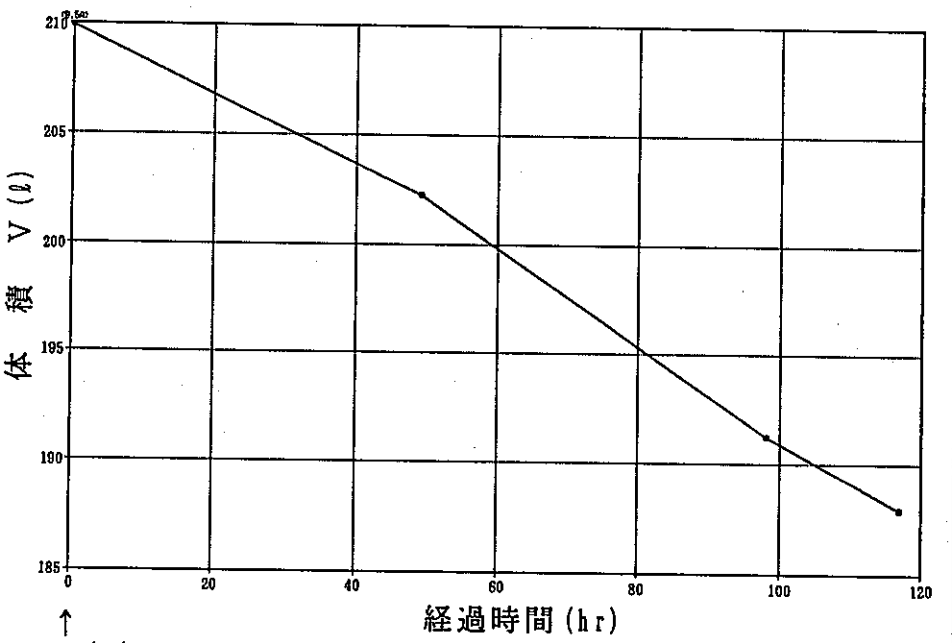
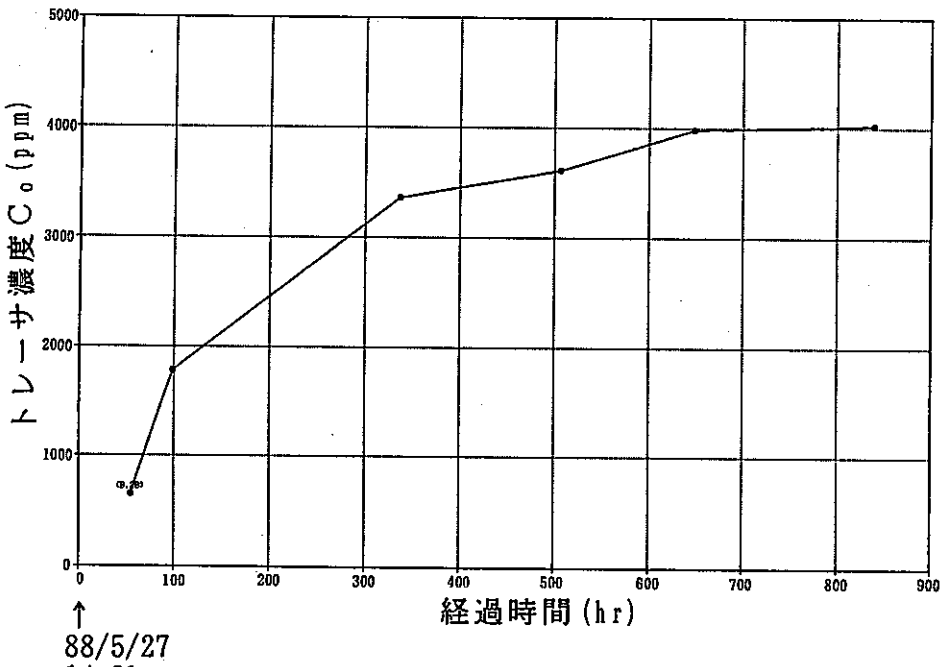
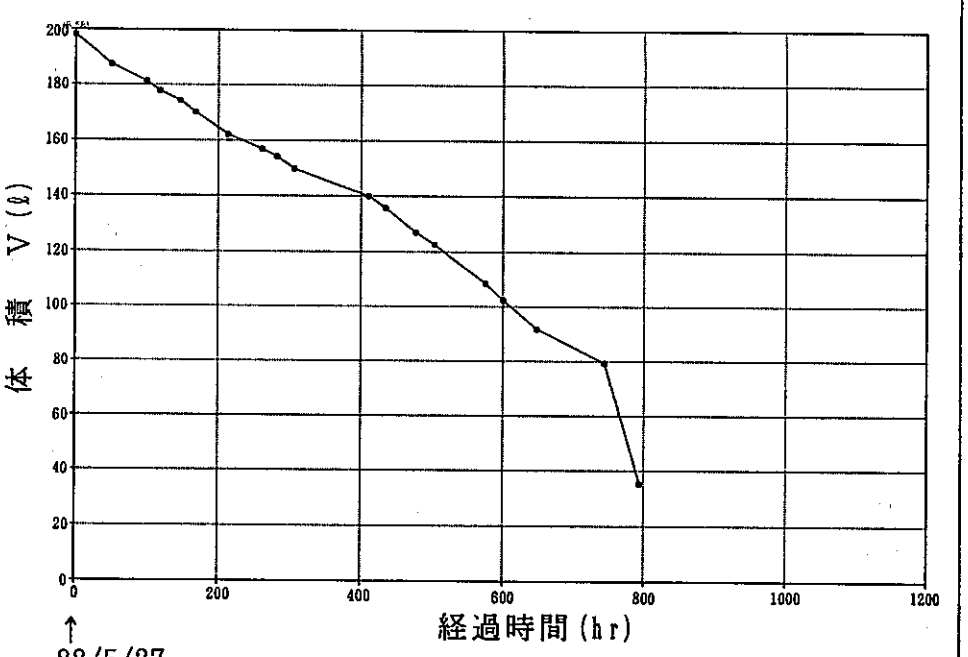
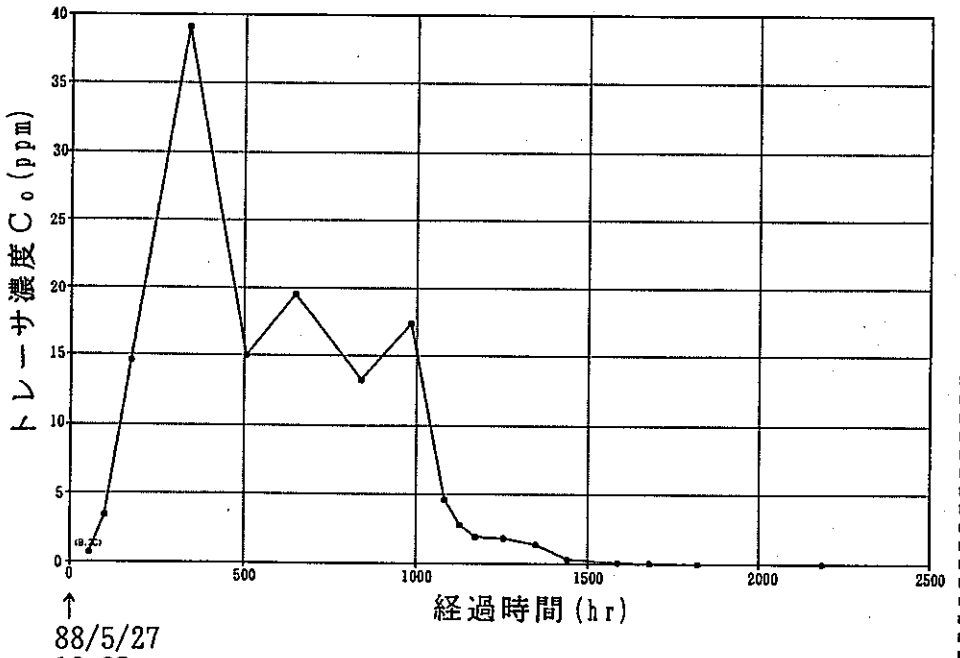
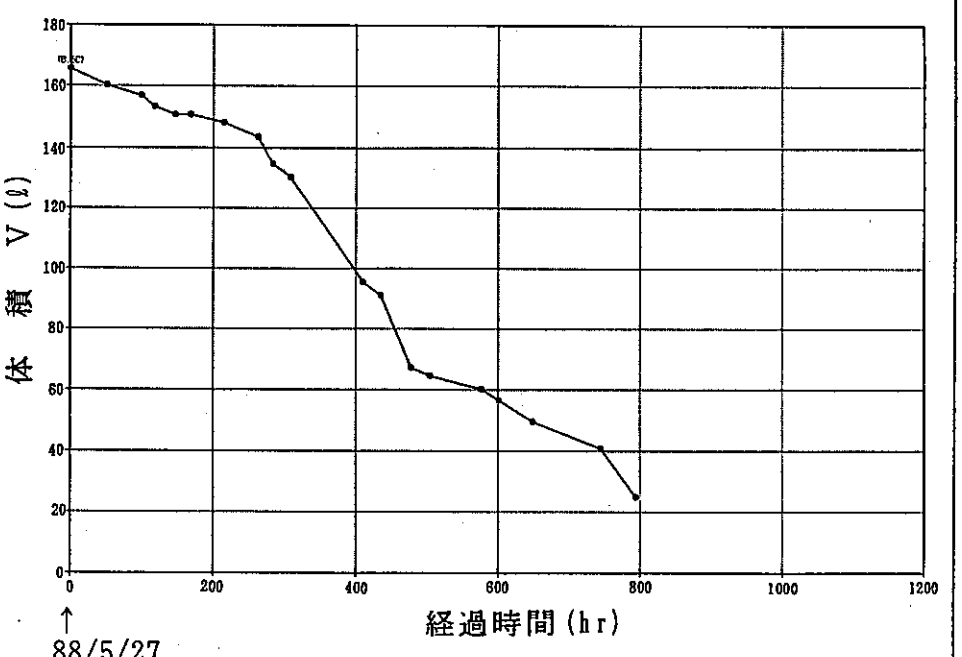
表－１４　　トレーサ注入に関するデータ（１／７）

トレーサ注入部	注入部のトレーサ濃度（ppm）	トレーサ貯蔵タンク内容積（ℓ）
BFI01 上部		
BFI01 中部		
BFI01 下部		

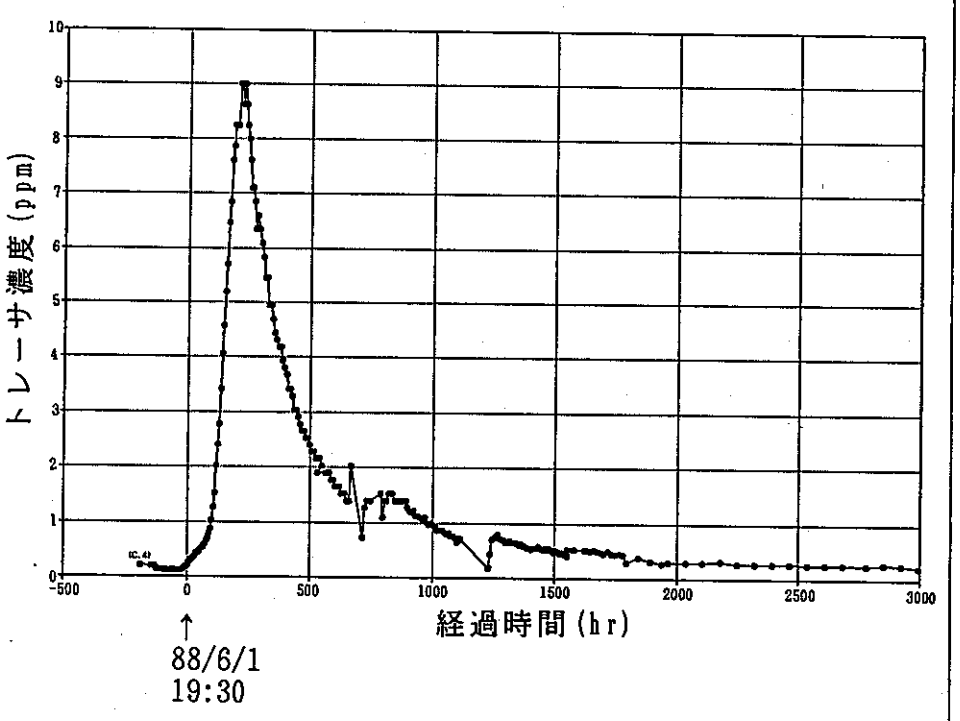
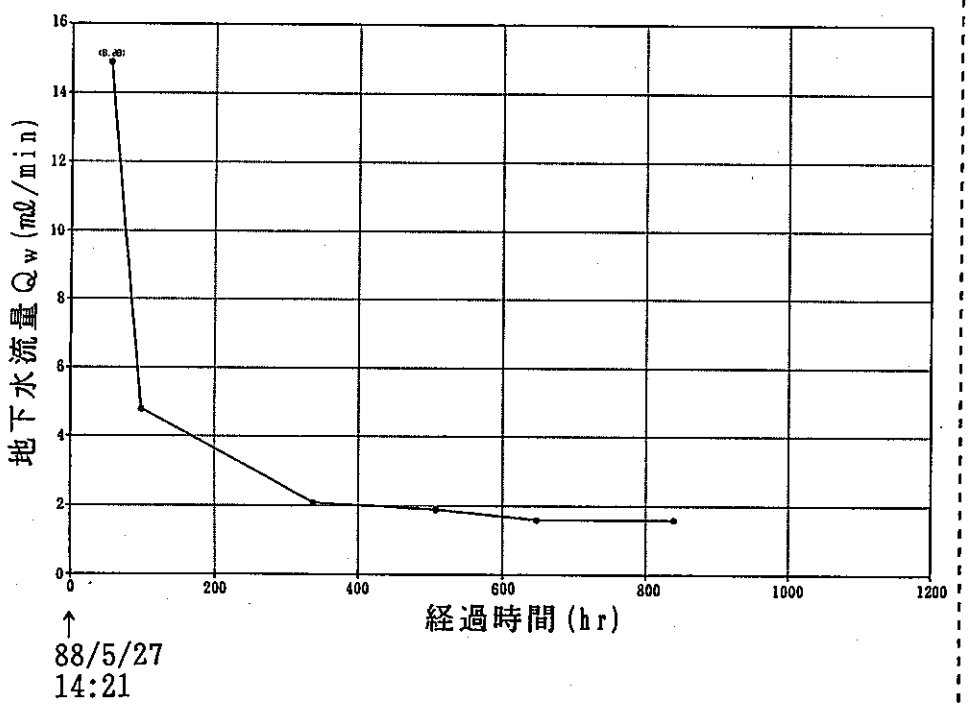
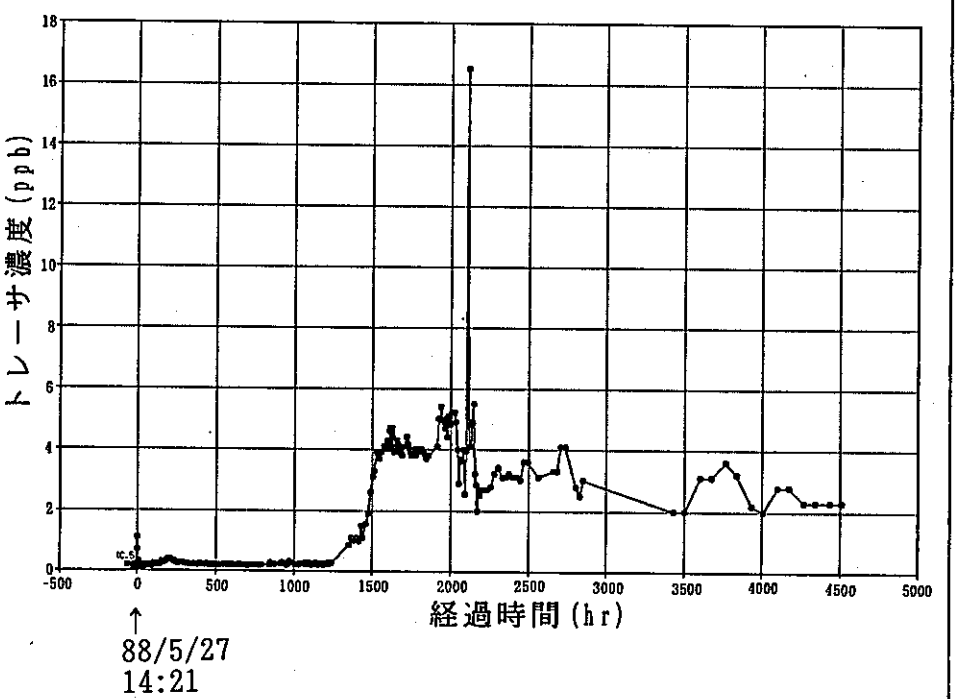
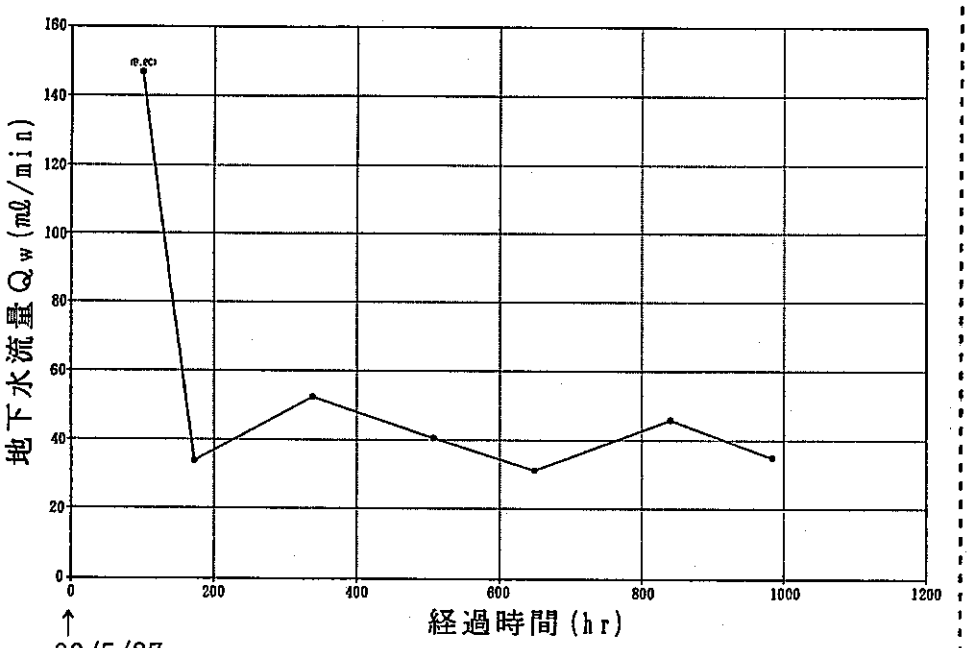
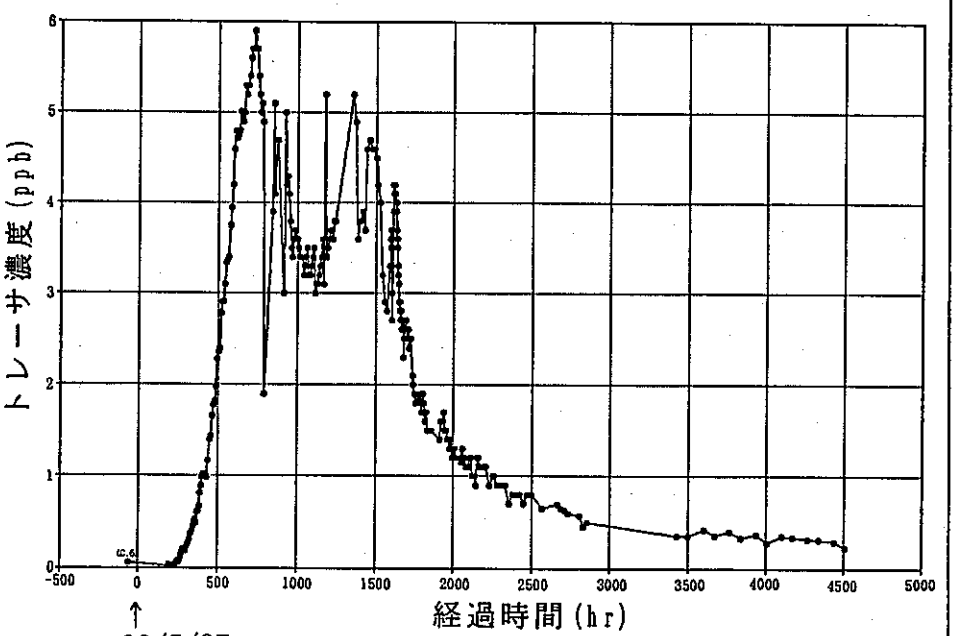
表－１４　トレーサ注入に関するデータ（２／７）

トレーサ注入部	地下水流量（mℓ／min）	トレーサ出口濃度（ppb）
BFI01 上部		
BFI01 中部		
BFI01 下部		

表－１４　　トレーサ注入に関するデータ（３／７）

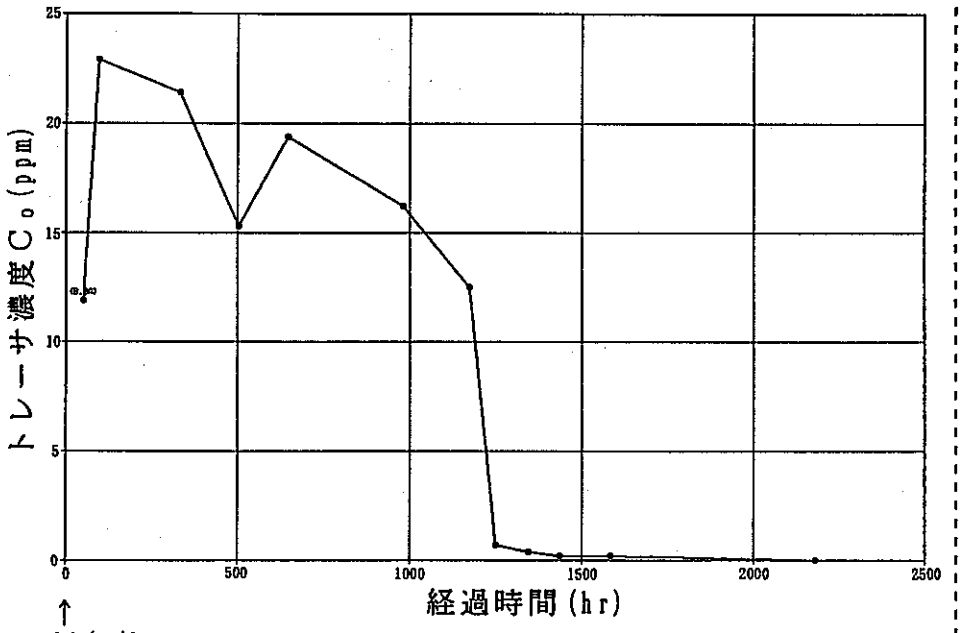
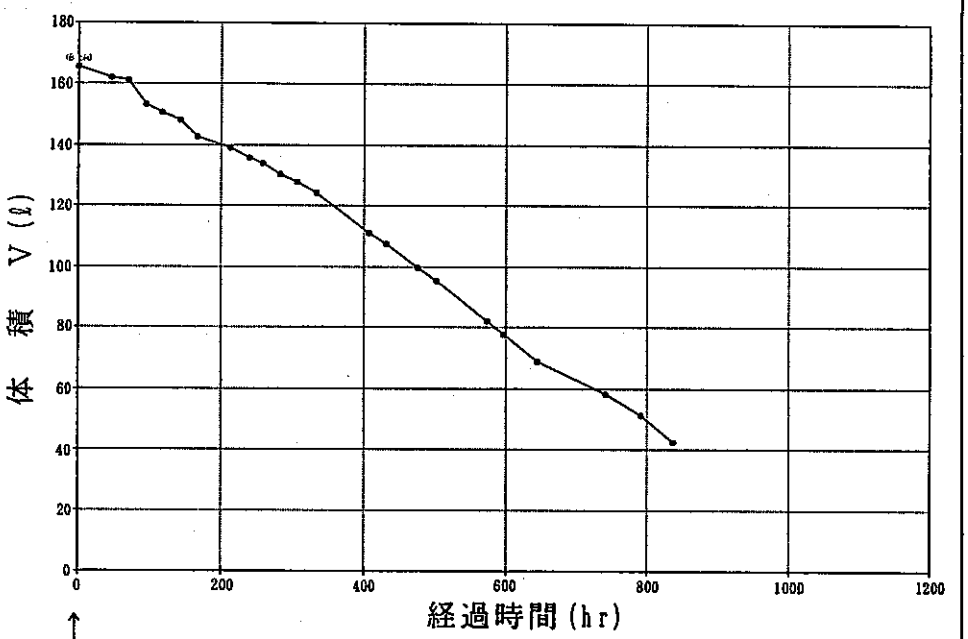
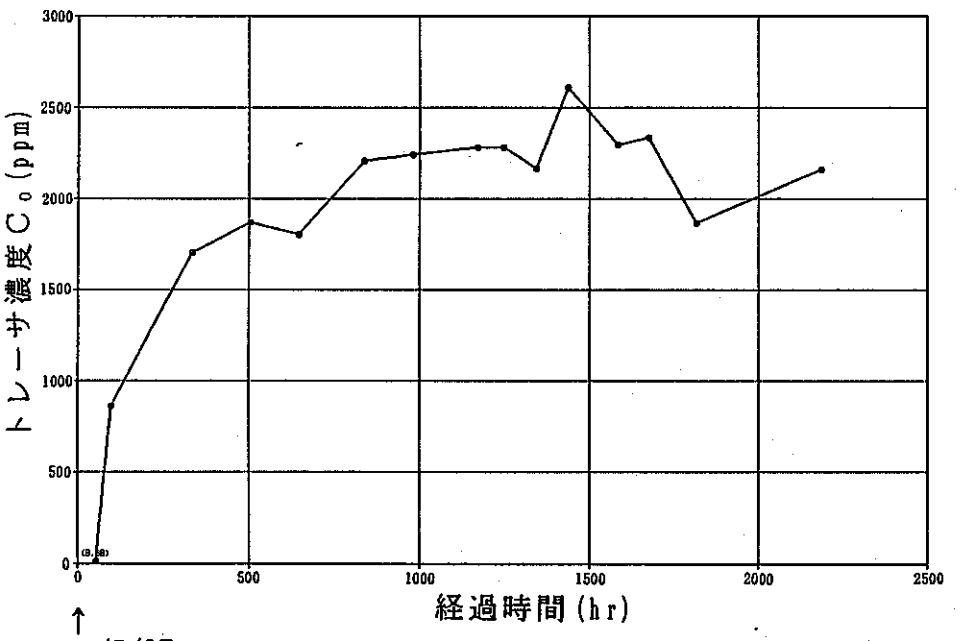
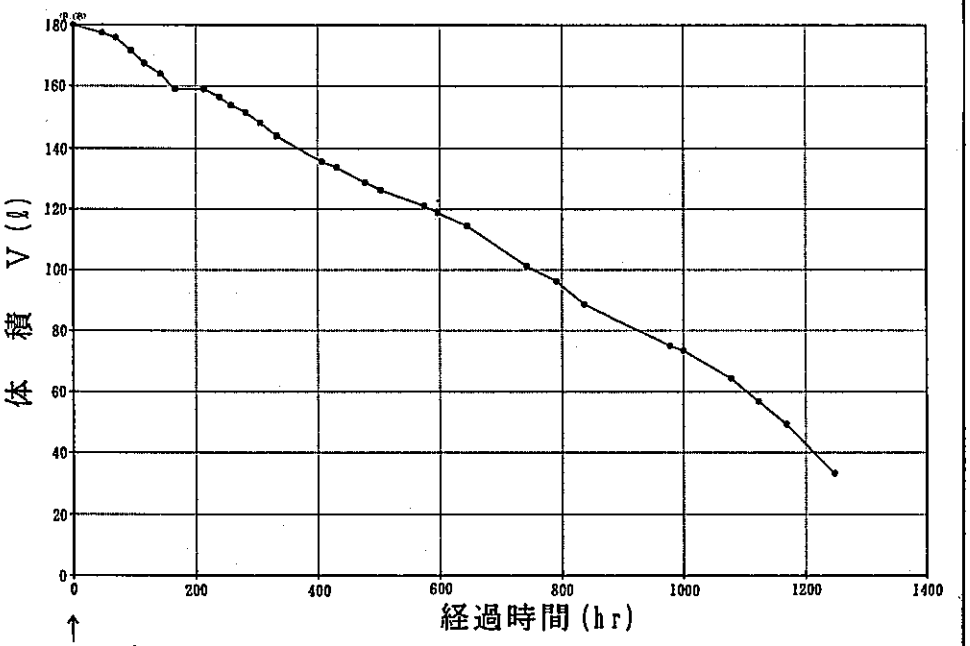
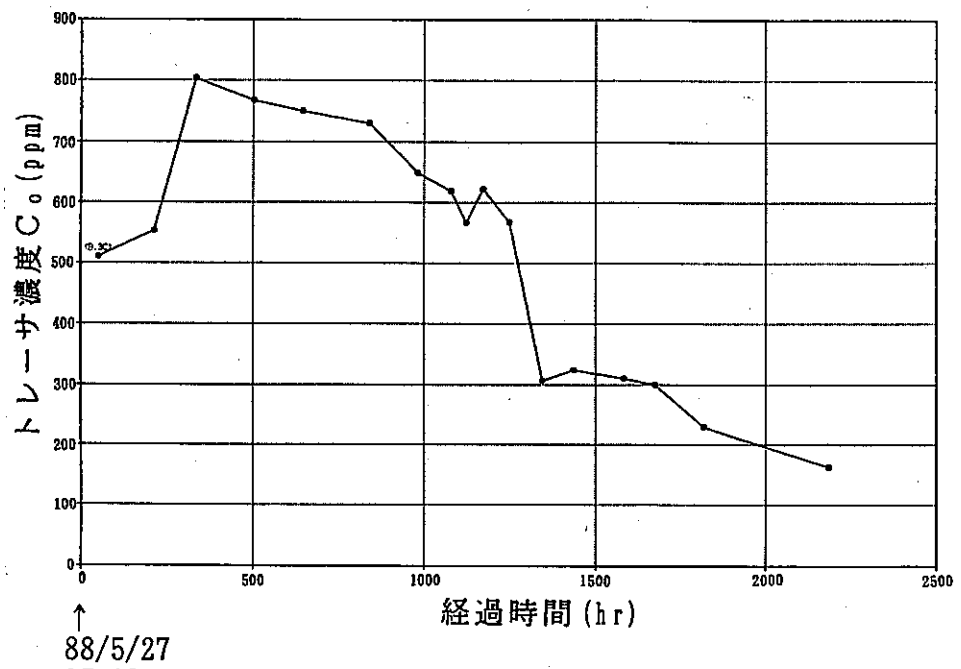
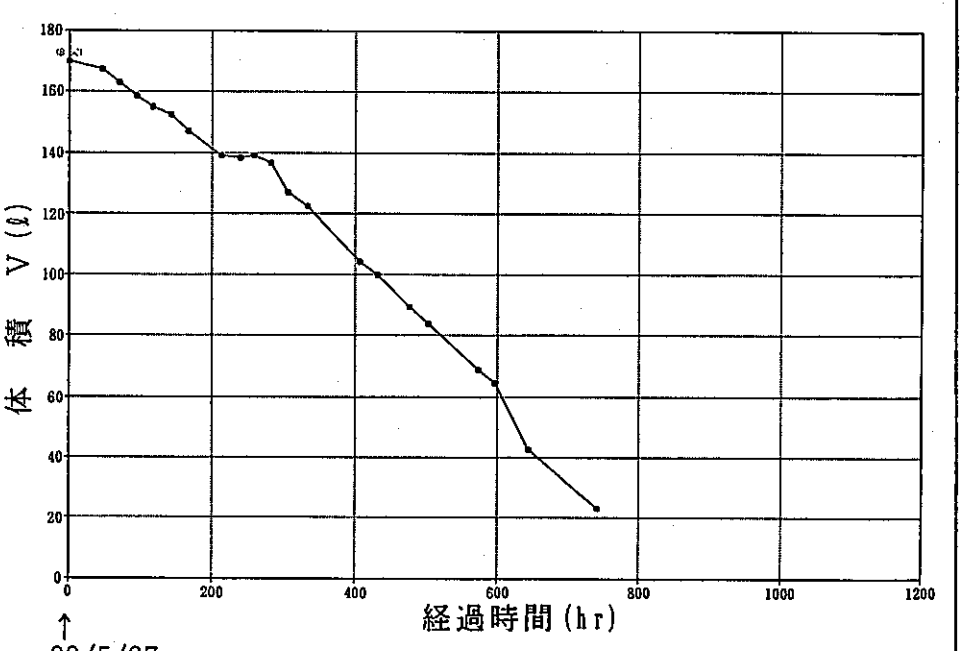
トレーサ注入部	注入部のトレーサ濃度（ppm）	トレーサ貯蔵タンク内容積（ℓ）
KFI06 上部	――	 ↑ 88/5/27 15:24
KFI06 中部	 ↑ 88/5/27 14:21	 ↑ 88/5/27 14:21
KFI06 下部	 ↑ 88/5/27 13:35	 ↑ 88/5/27 13:35

表－１４　　トレーサ注入に関するデータ（４／７）

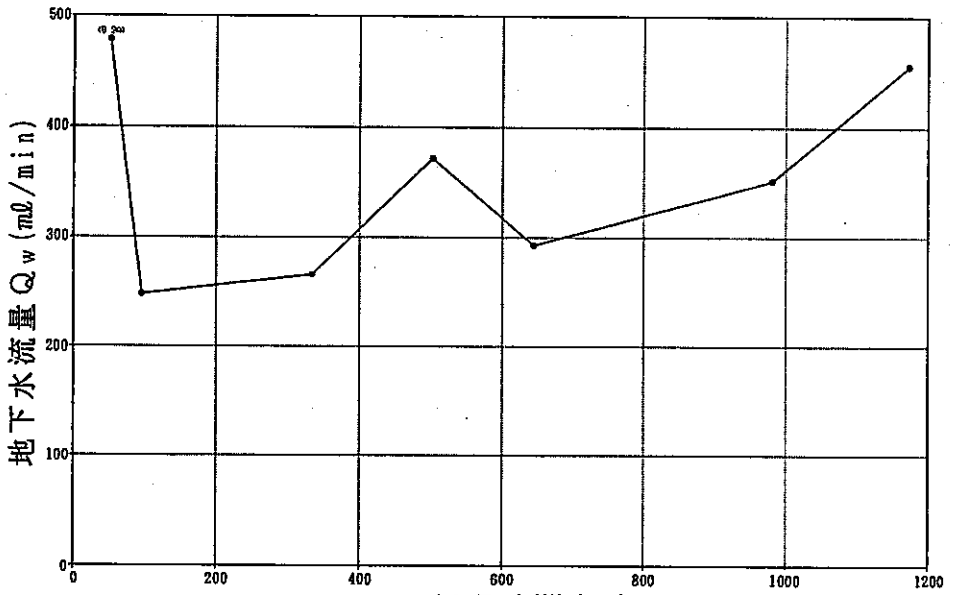
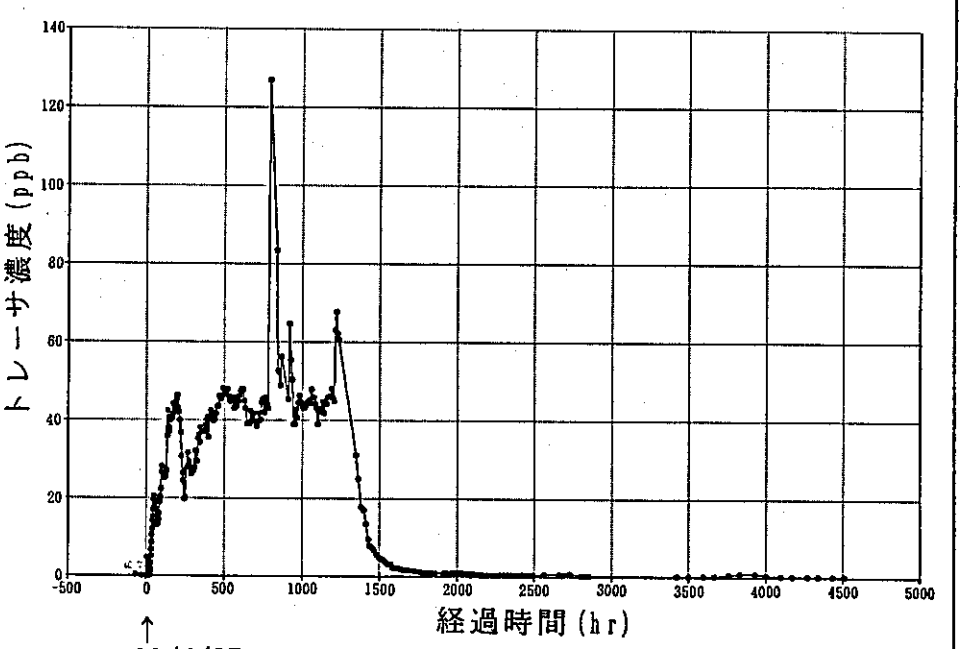
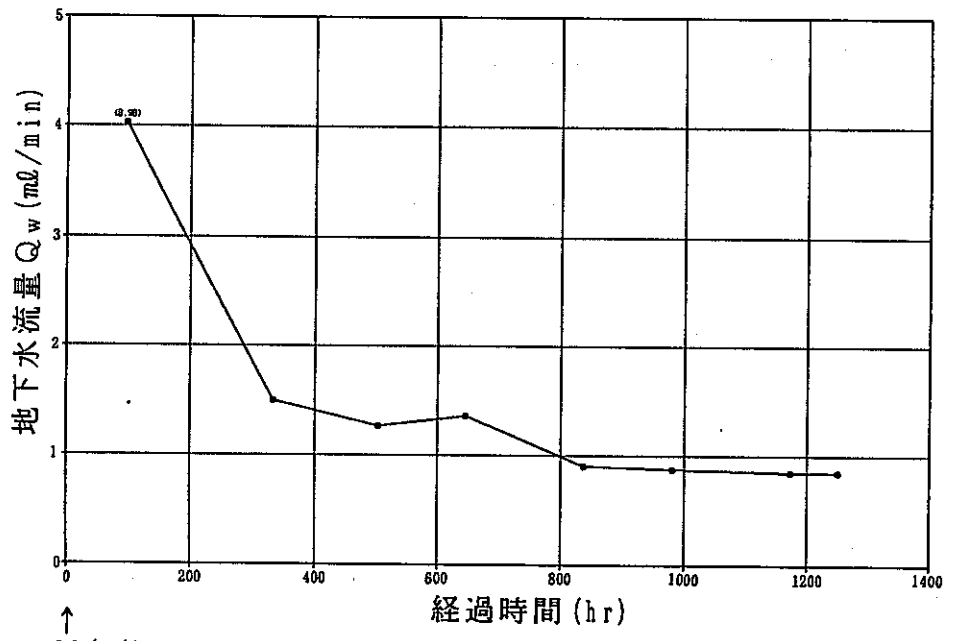
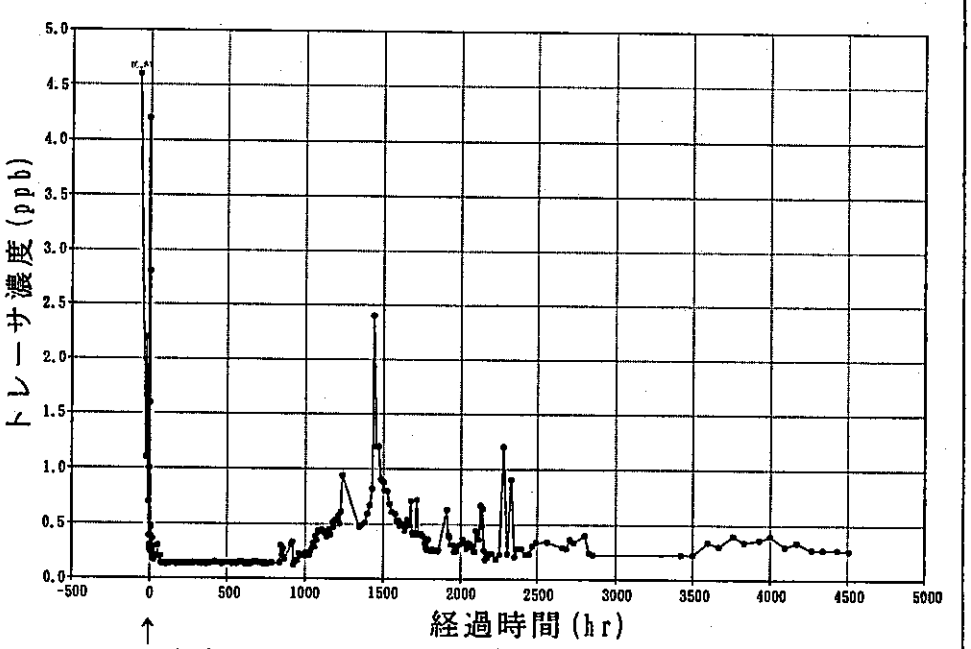
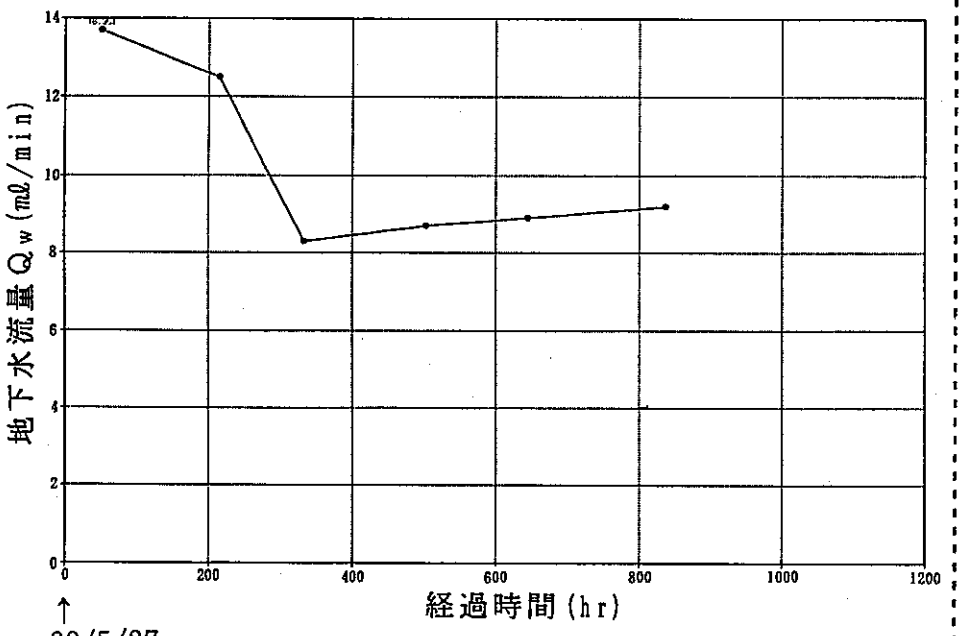
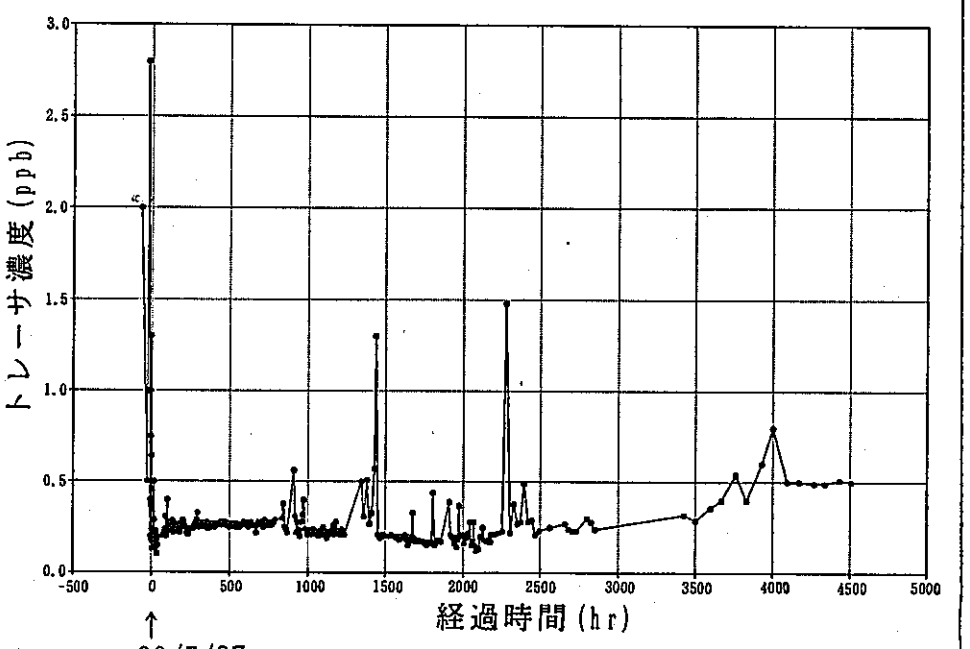
トレーサ注入部	地下水量（mℓ／min）	トレーサ出口濃度*）（ppb）
KFI06 上部	——	
KFI06 中部		
KFI06 下部		

＊）ただし、ＫＦＩ０６上部のトレーサ濃度の単位はppmである。

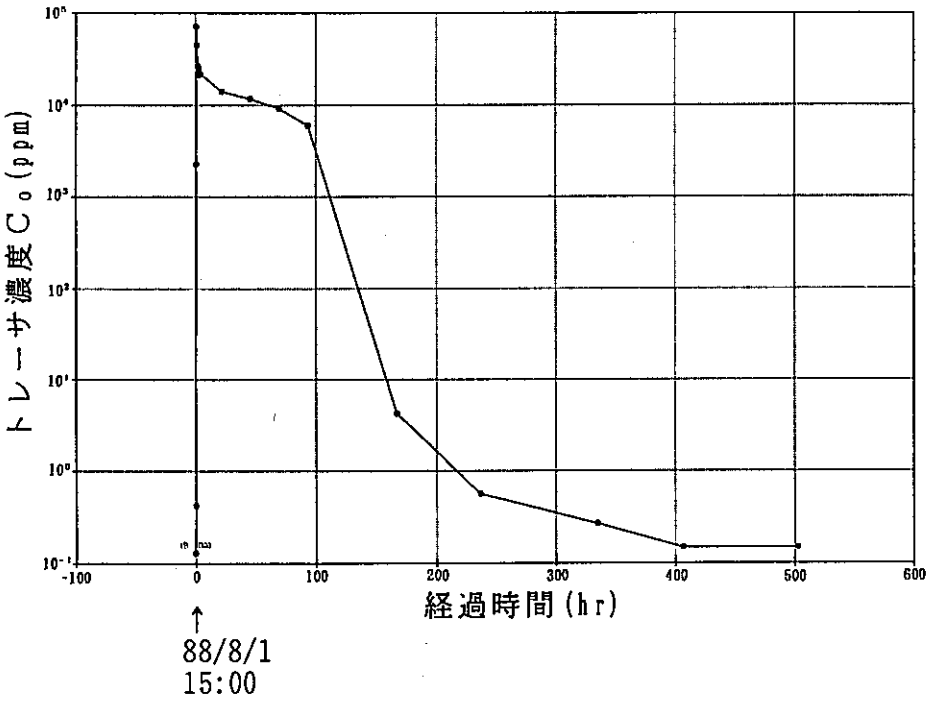
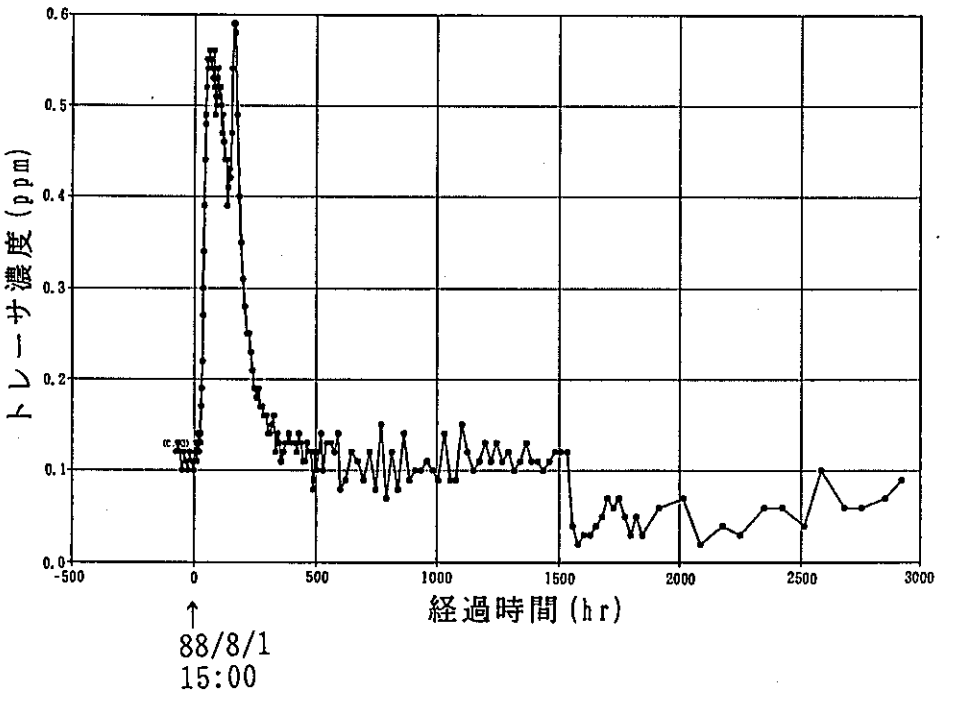
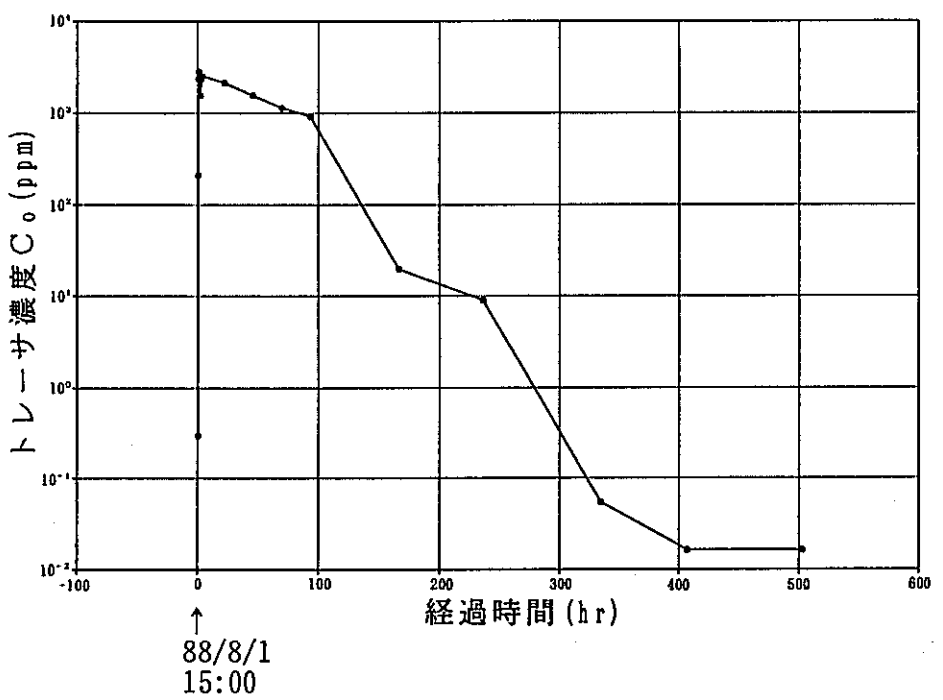
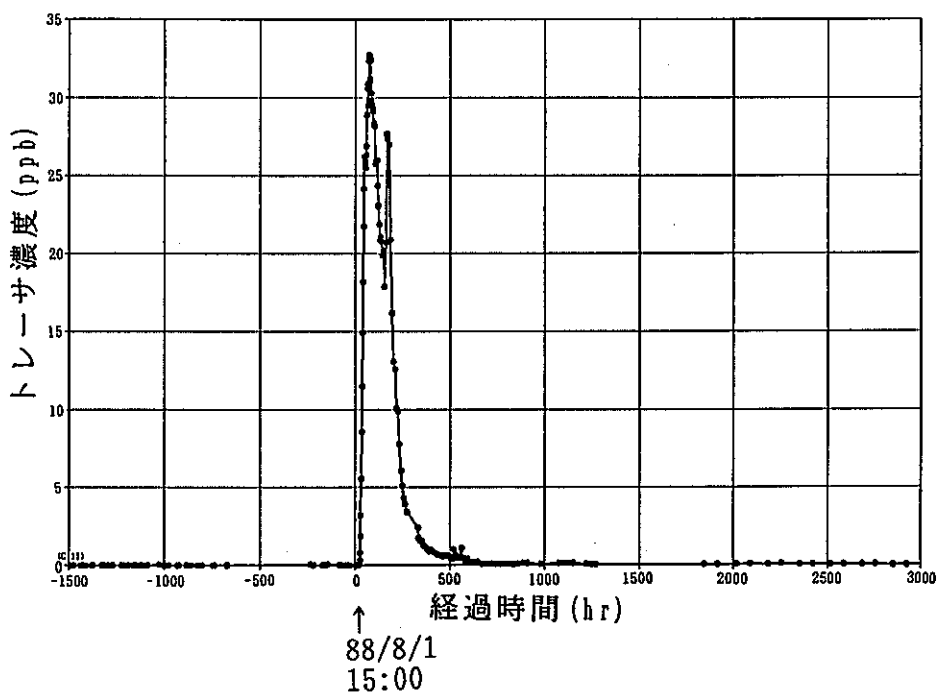
表－１４　　トレーサ注入に関するデータ（５／７）

トレーサ注入部	注入部のトレーサ濃度（ppm）	トレーサ貯蔵タンク内容積（ℓ）
KFI11 上部		
KFI11 中部		
KFI11 下部		

表－１４　トレーサ注入に関するデータ（６／７）

トレーサ注入部	地下水流量（mℓ／min）	トレーサ出口濃度（ppb）
KFI11 上部		
KFI11 中部		
KFI11 下部		

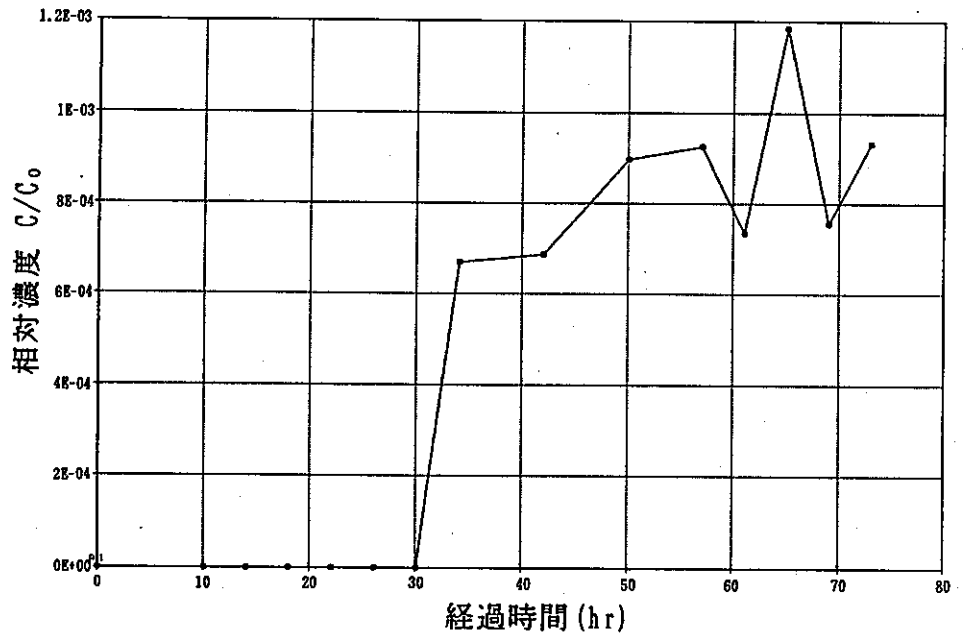
表－１４　　トレーサ注入に関するデータ（７／７）

トレーサ注入部	注入部のトレーサ濃度（ppm）	トレーサ出口濃度（ppb）
BFI11*) 上部		
BFI11 上部		

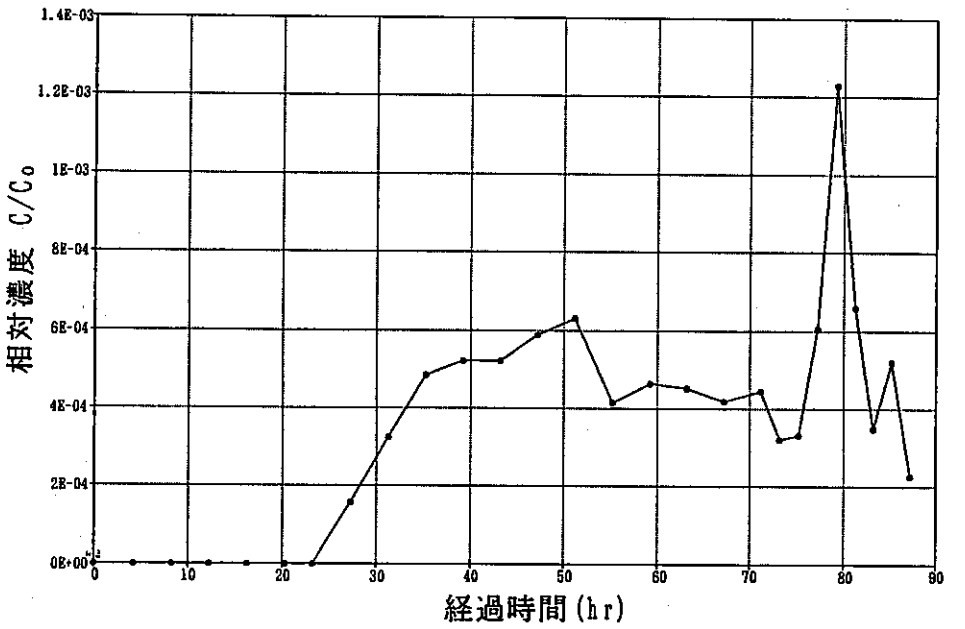
*）ただし、トレーサ濃度出口濃度の単位はppmである。

表－１５　　ＢＦＩ０２におけるトレーサ相対濃度（１／３）

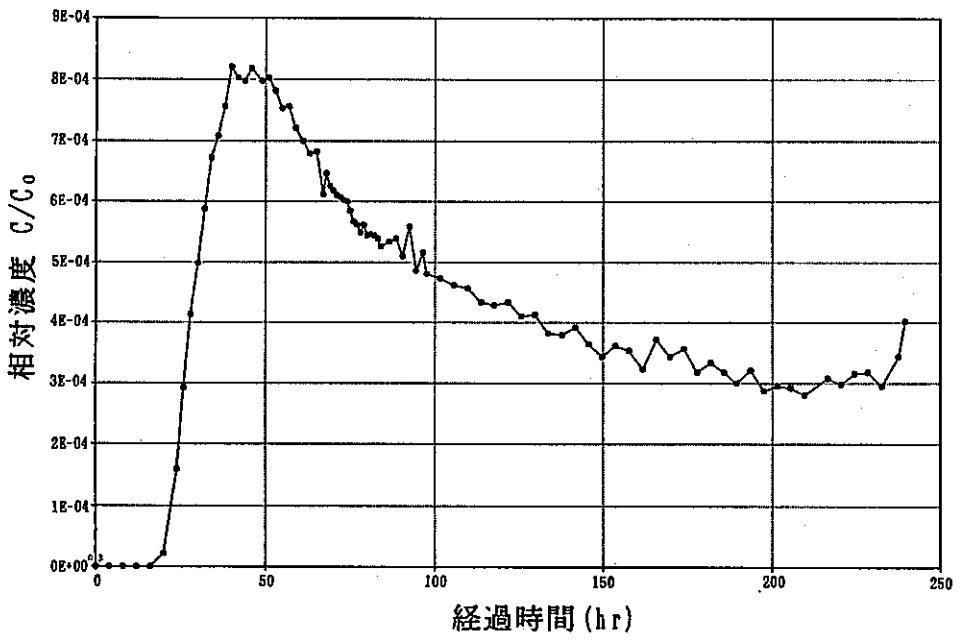
Ｂｒ－８２（注入ケース１）



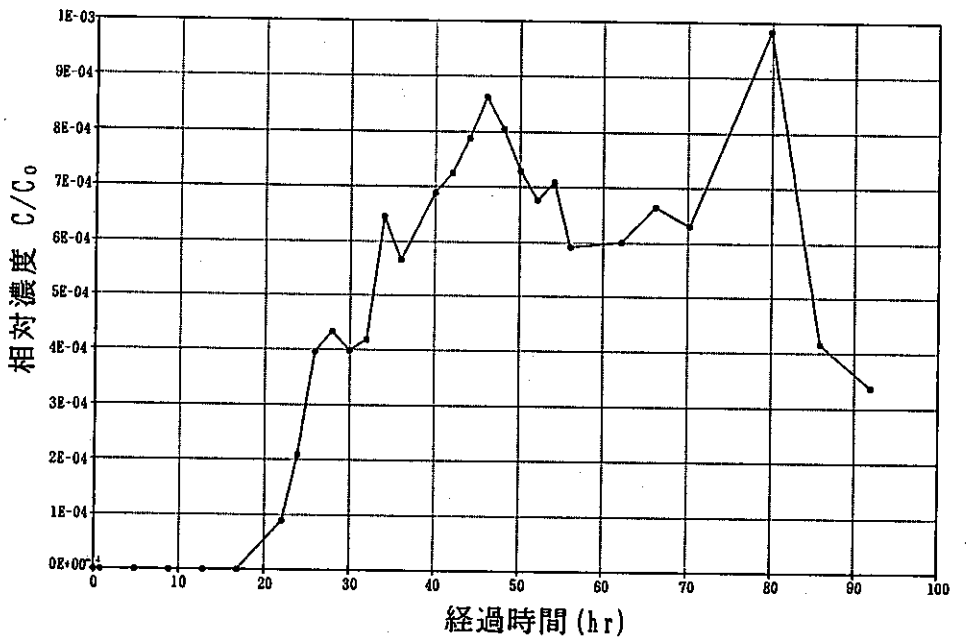
Ｒｅ－１８６（注入ケース２）



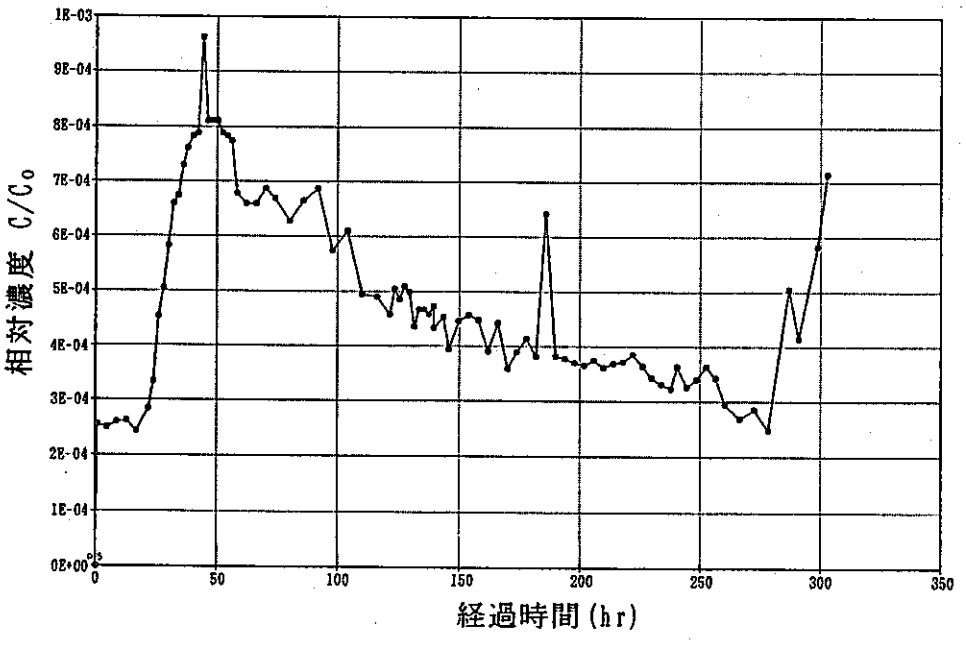
Ｉ－１３１（注入ケース３）



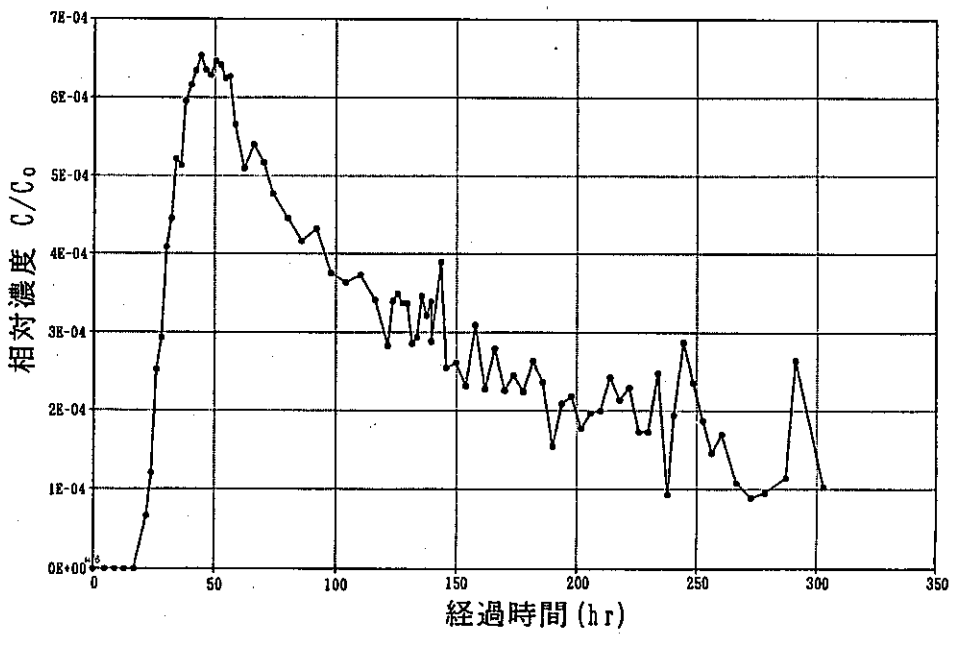
Ｂｒ－８２（注入ケース６）



Ｉ－１３１（注入ケース６）

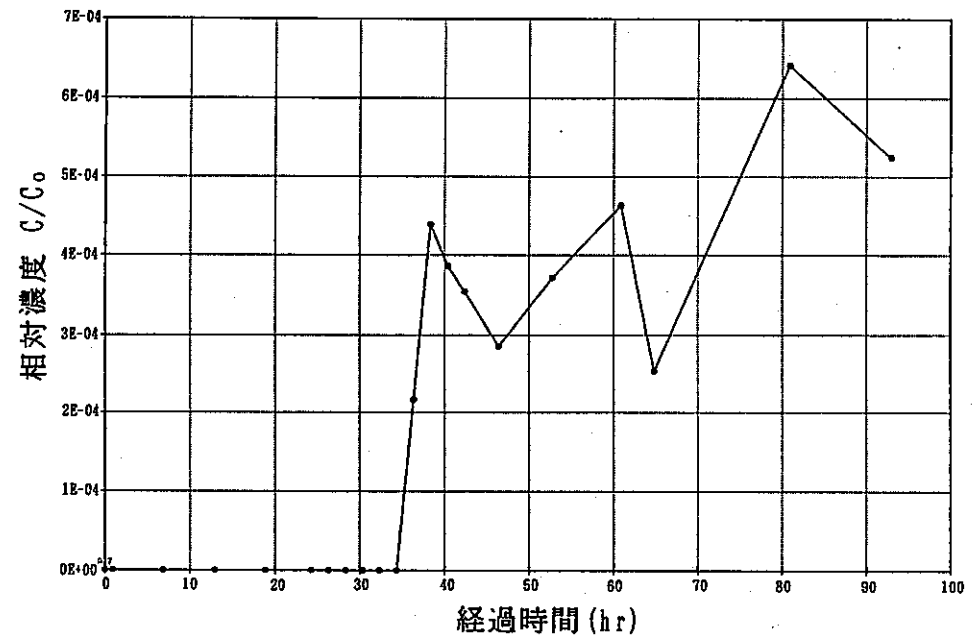


Ｒｅ－１８６（注入ケース６）

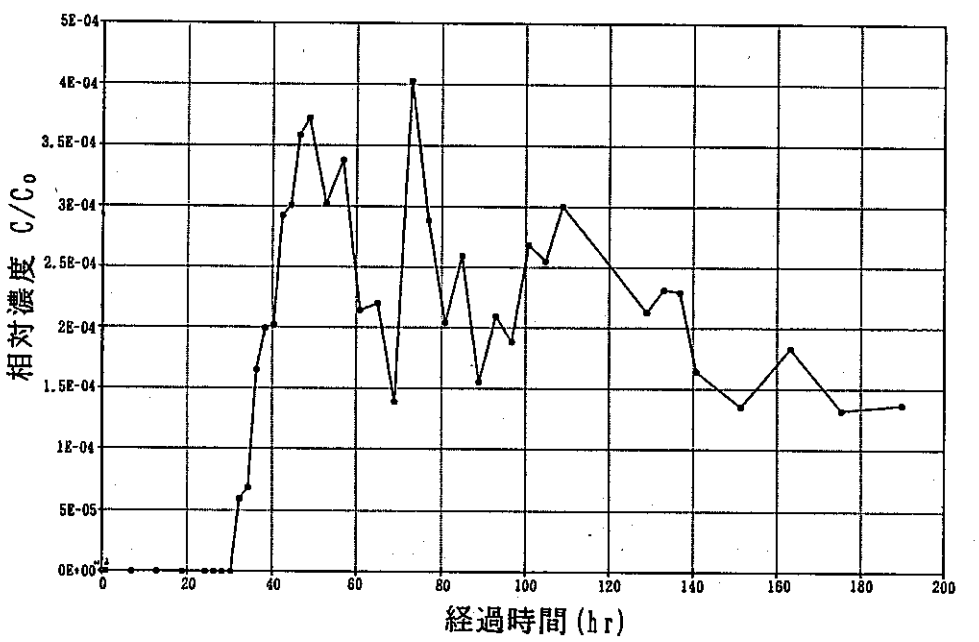


表－１５　ＢＦＩ０２におけるトレーサ相対濃度（２／３）

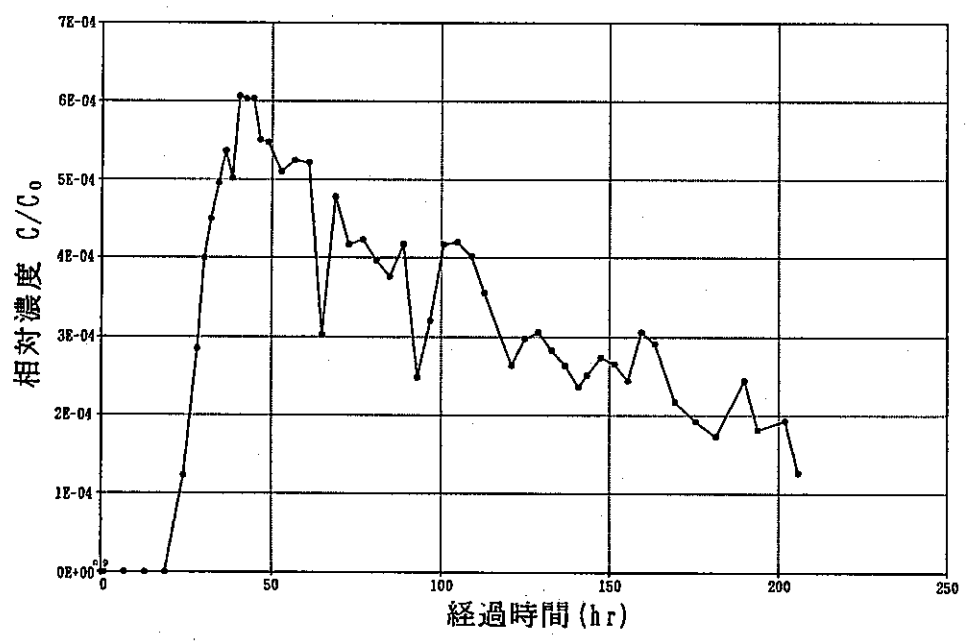
Ｌａ－１４０（注入ケース７）



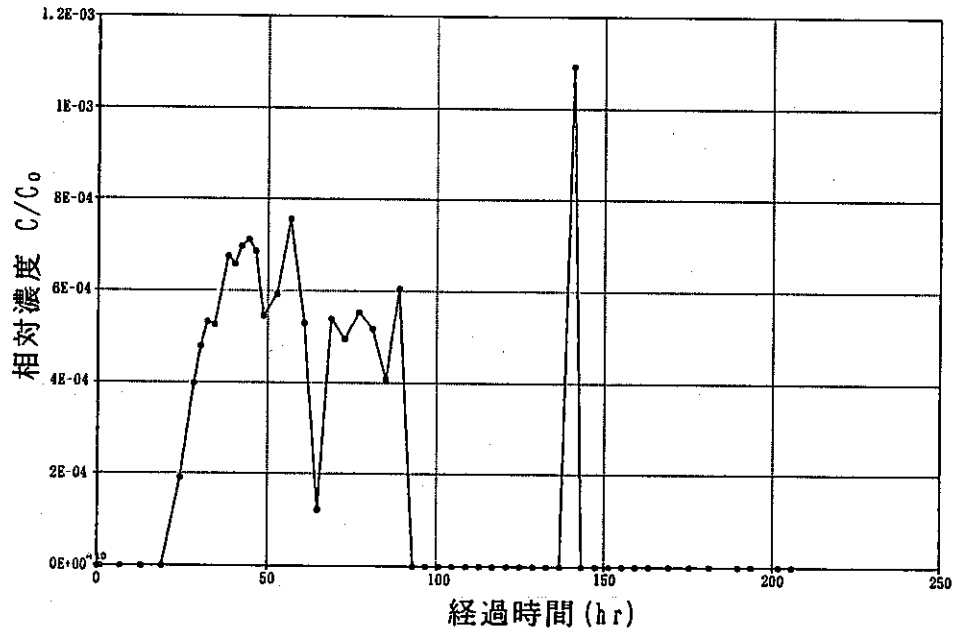
Ｌｕ－１７７（注入ケース７）



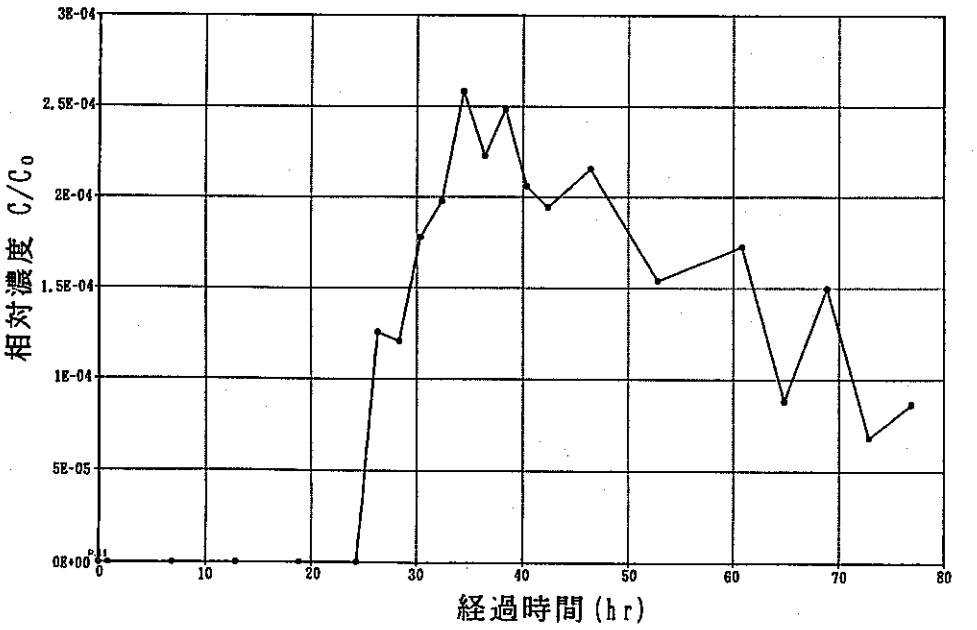
Ｃｒ－５１（注入ケース７）



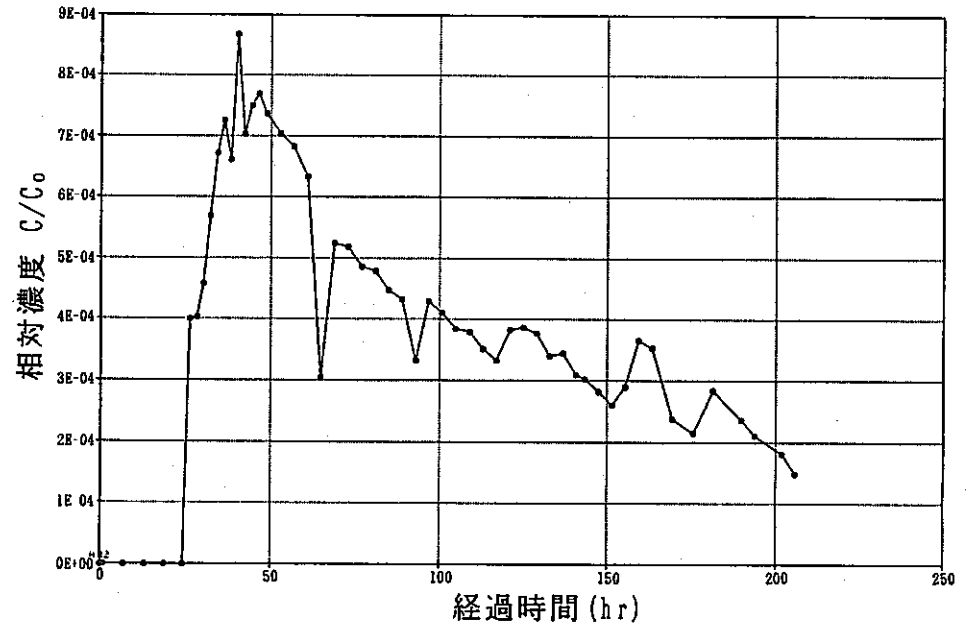
Ｉｎ－１１１（注入ケース７）



Ｔｂ－１６０（注入ケース７）

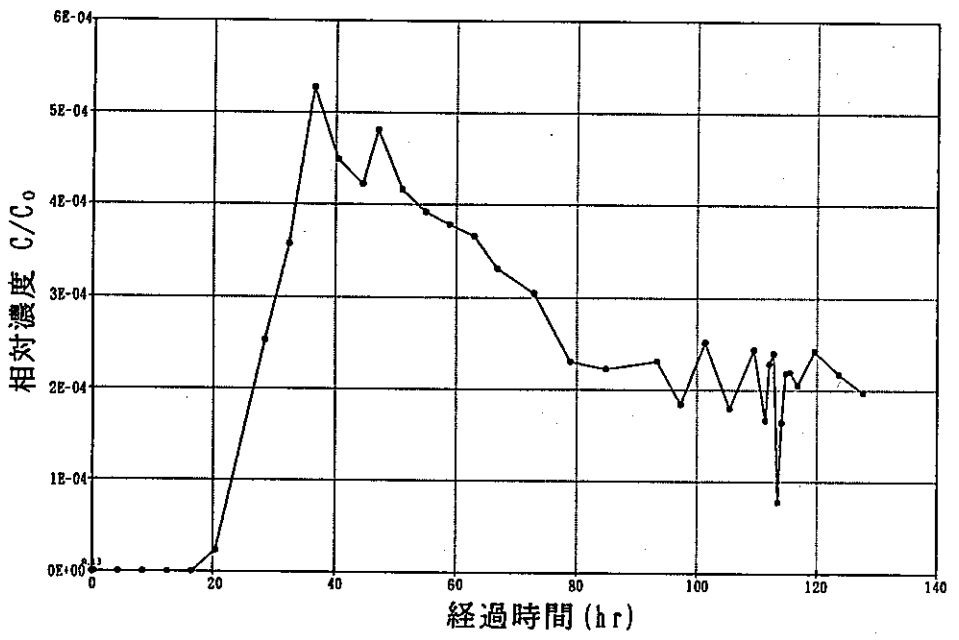


Ｙｂ－１６９（注入ケース７）

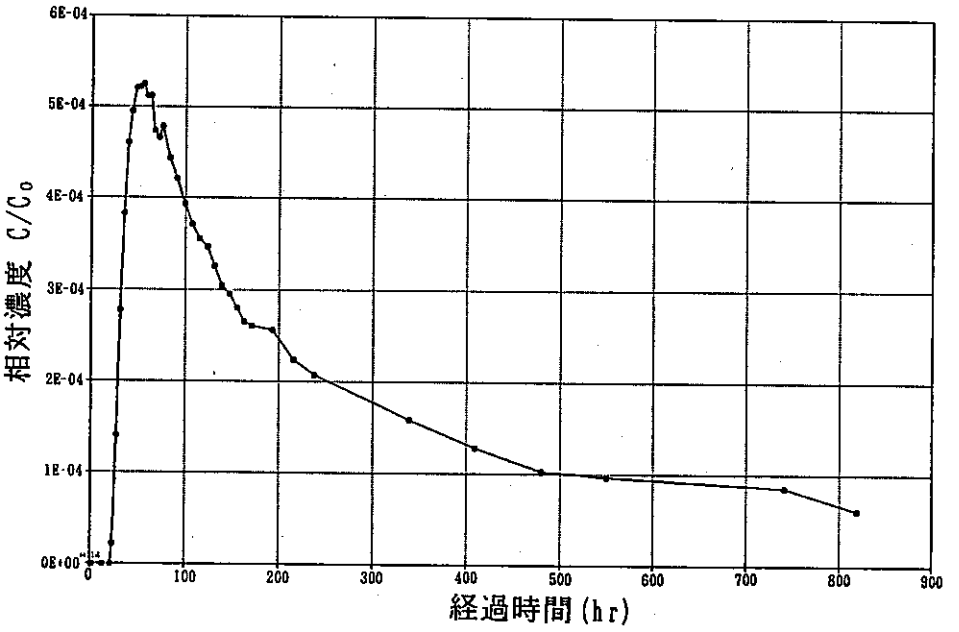


表－１５　　ＢＦＩ０２におけるトレーサ相対濃度（３／３）

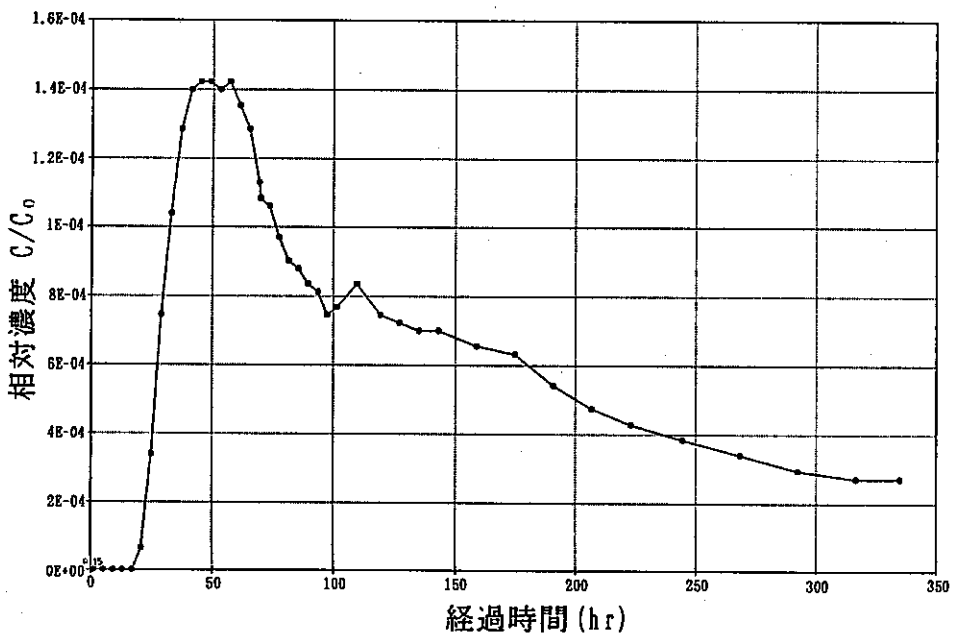
Ｃｏ－５８（注入ケース８）



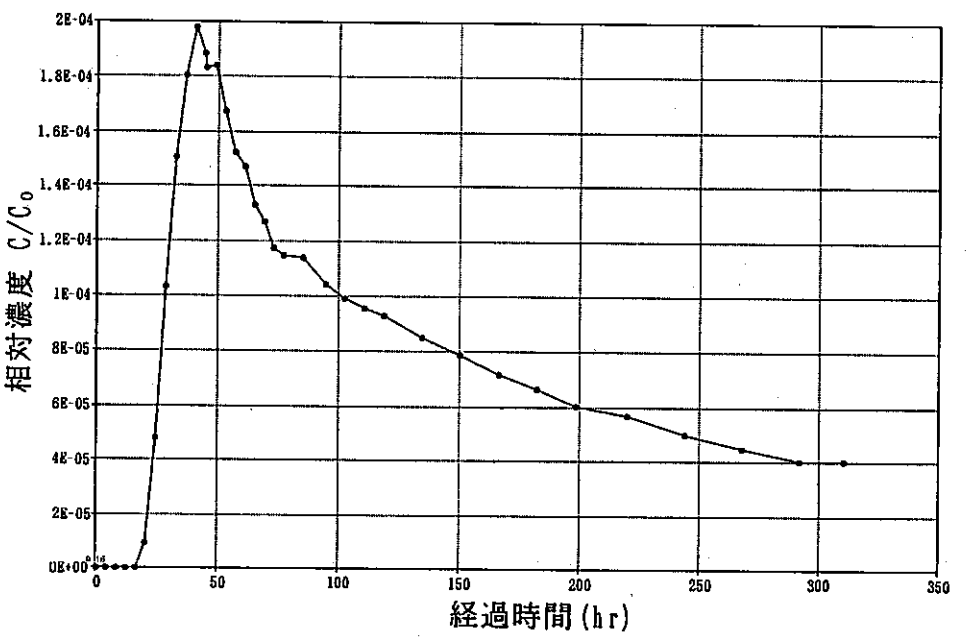
ロダミンＷＴ（注入ケースＡ）



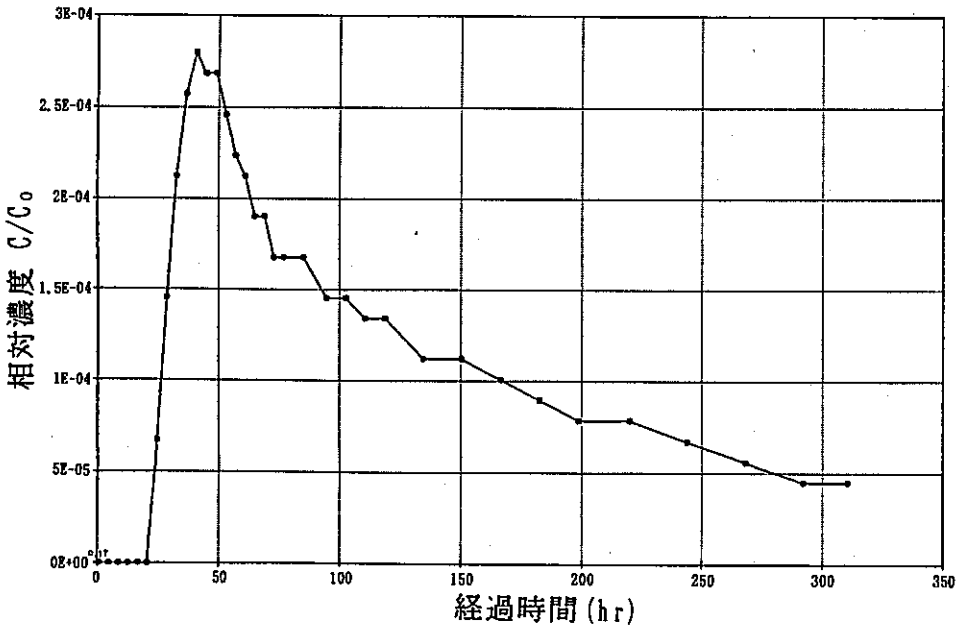
Ｉｎ－ＥＤＴＡ（注入ケースＣ）



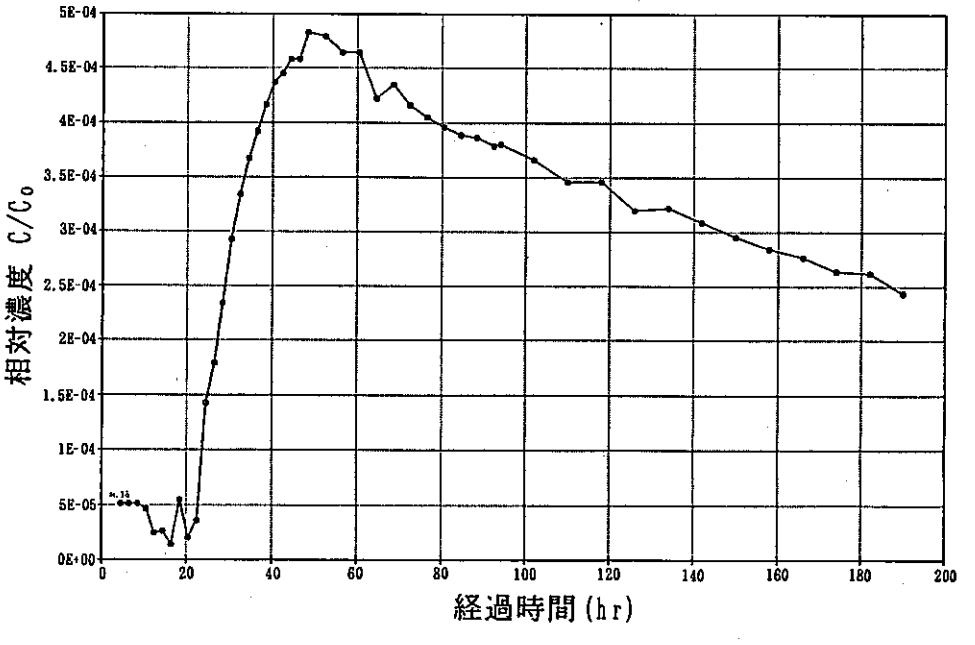
Ｇｄ－ＤＴＰＡ（注入ケースＤ）



Ｔｍ－ＥＤＴＡ（注入ケースＤ）

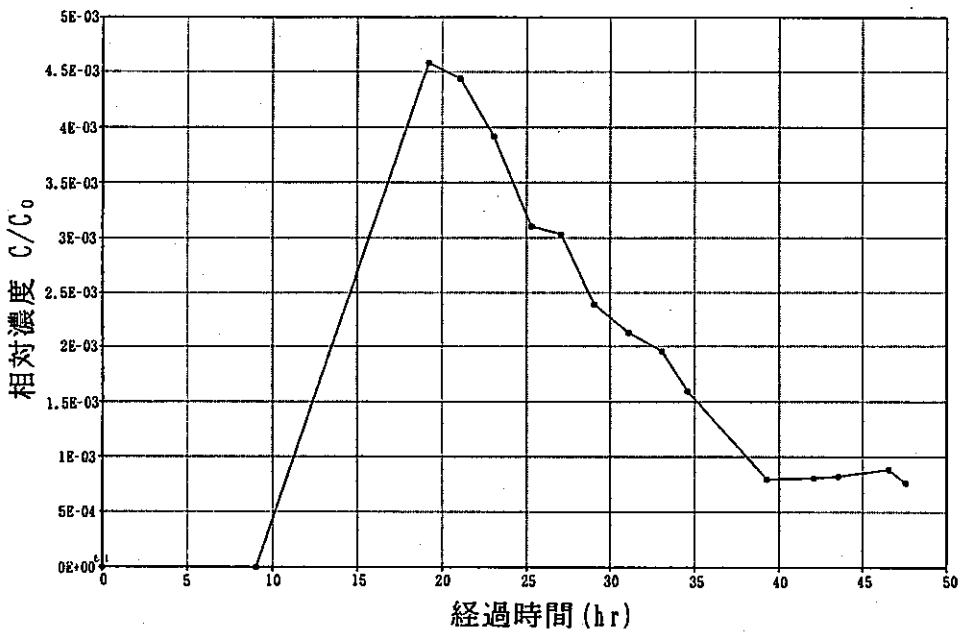


ロダミンＷＴ（注入ケースＥ）

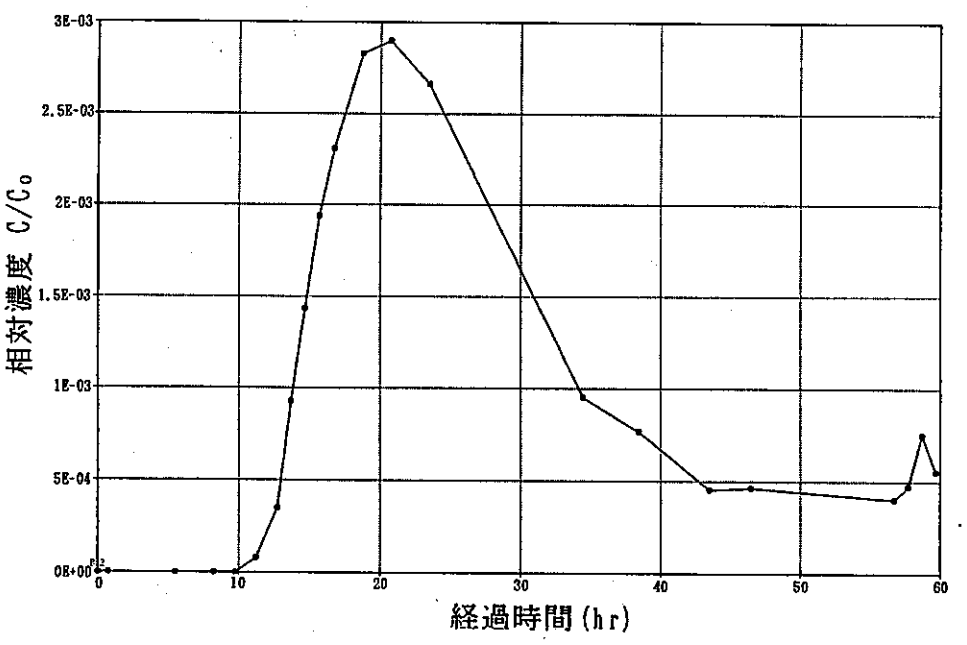


表－１６　　ＫＦＩ１１におけるトレーサ相対濃度（１／４）

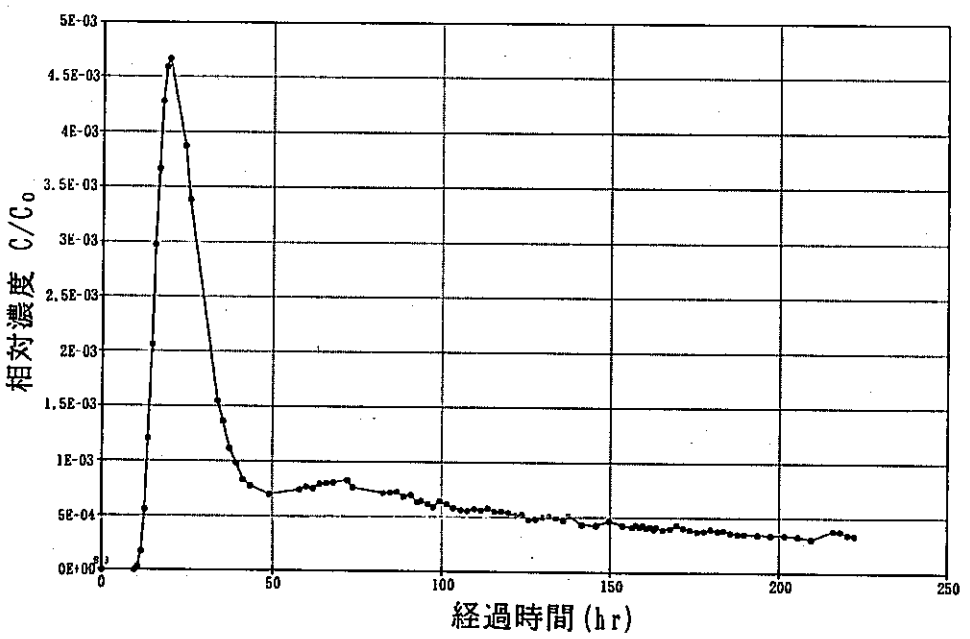
Ｂｒ－８２（注入ケース２）



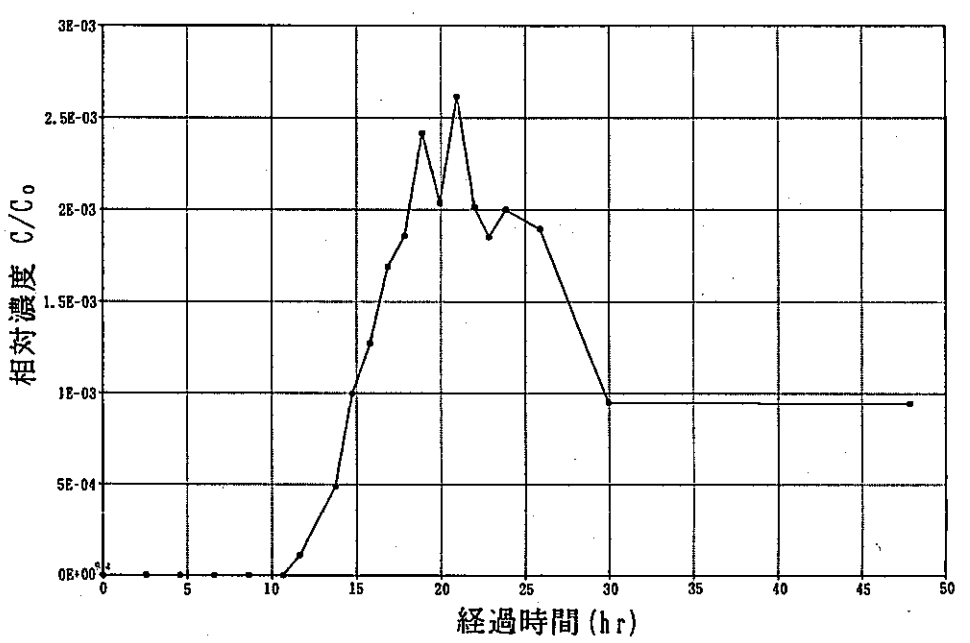
Ｒｅ－１８６（注入ケース２）



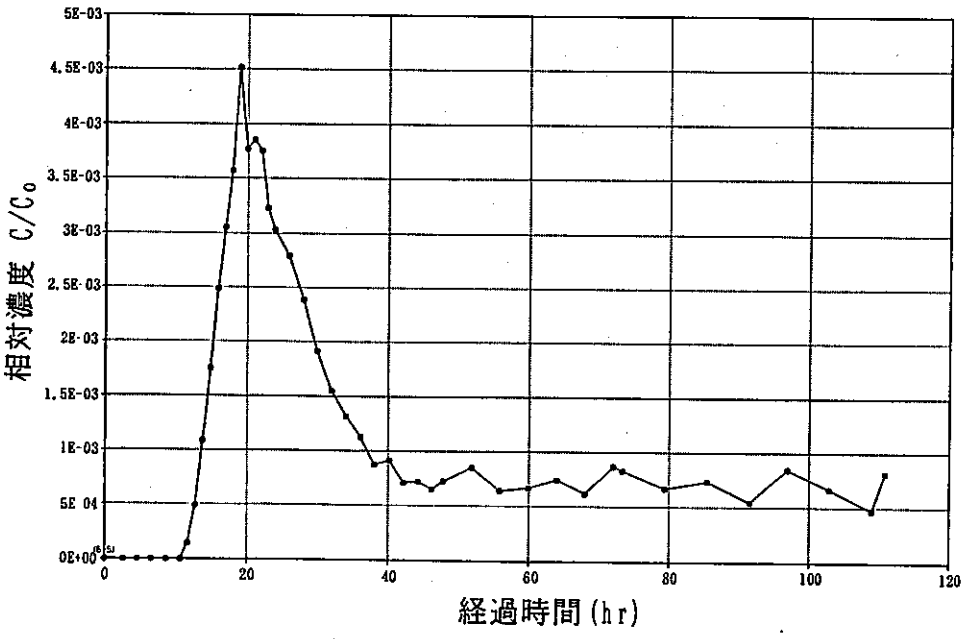
Ｉ－１３１（注入ケース３）



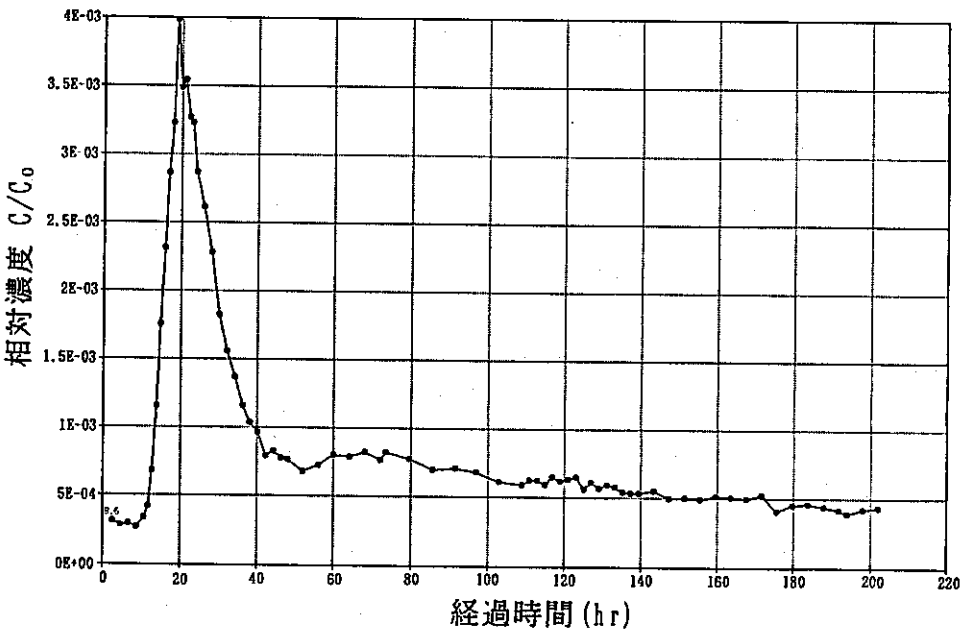
Ｎａ－２４（注入ケース６）



Ｂｒ－８２（注入ケース６）

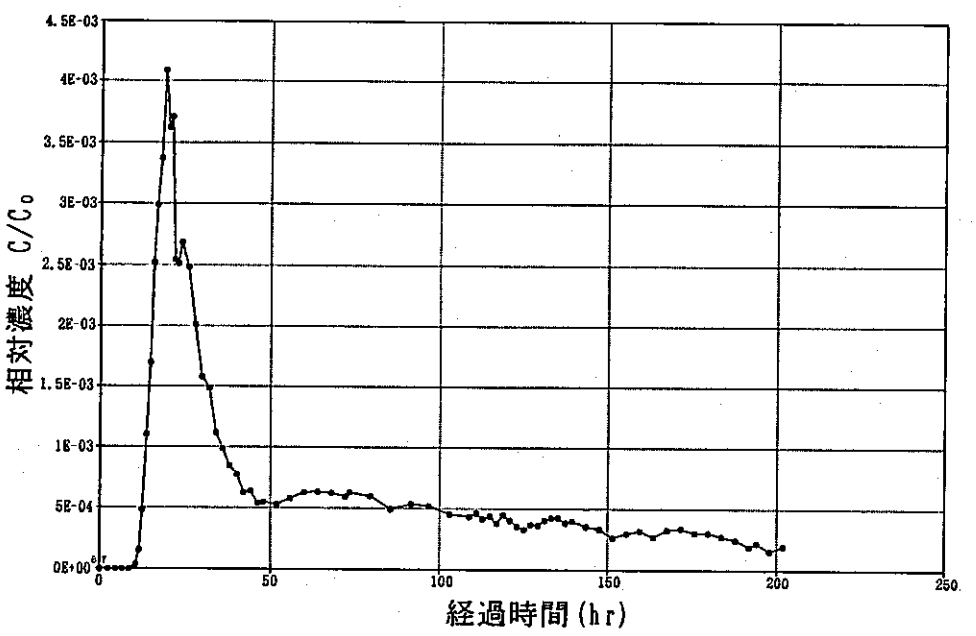


Ｉ－１３１（注入ケース６）

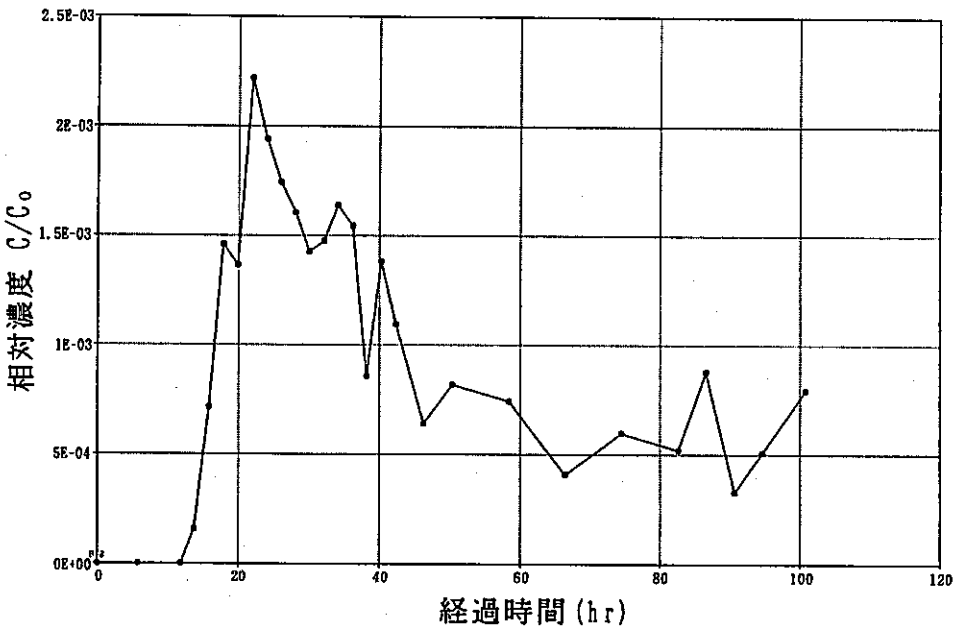


表－１６　　ＫＦＩ１１におけるトレーサ相対濃度（２／４）

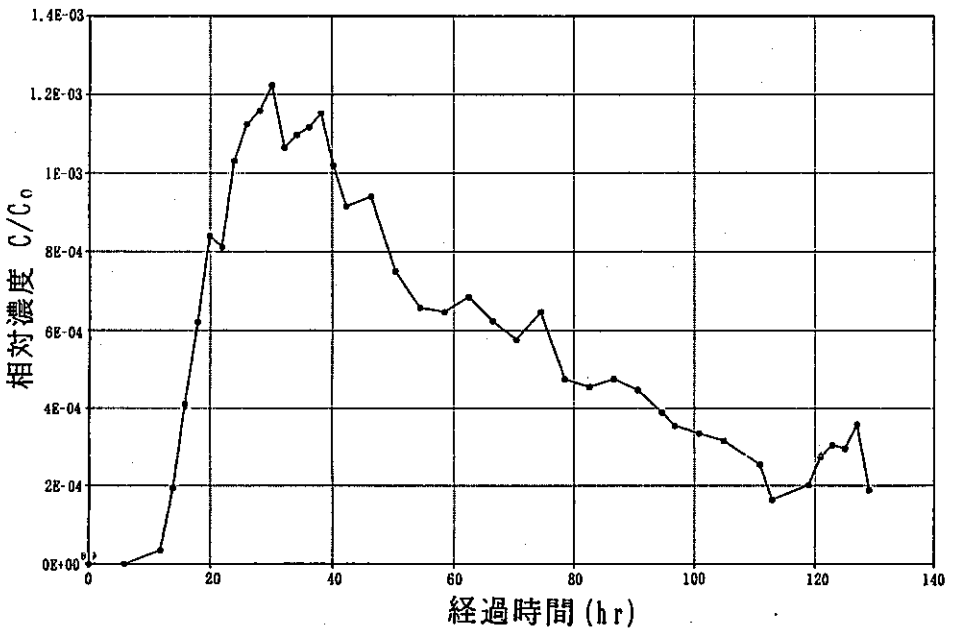
Ｒｅ－１８６（注入ケース６）



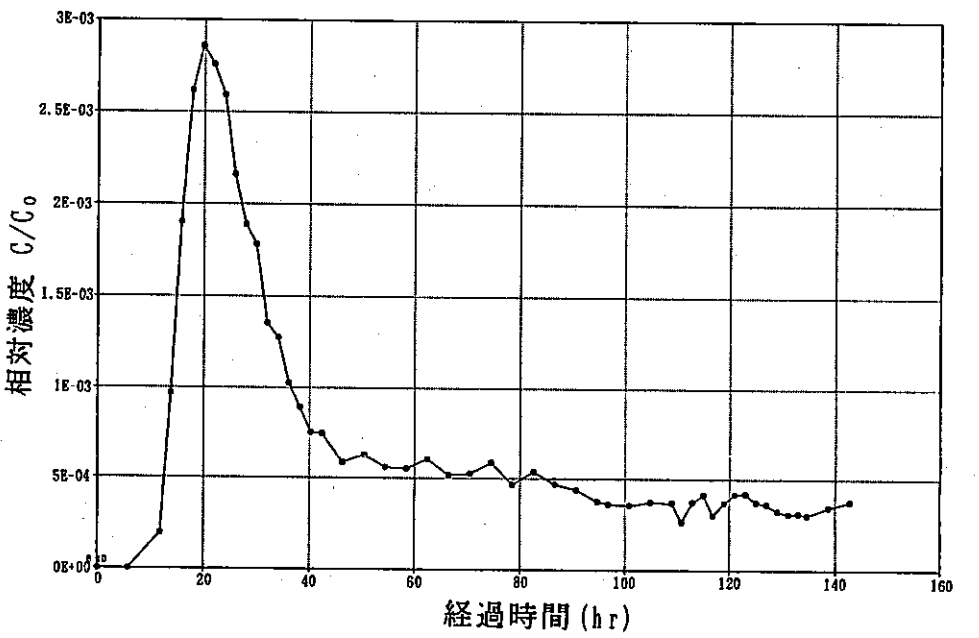
Ｌａ－１４０（注入ケース７）



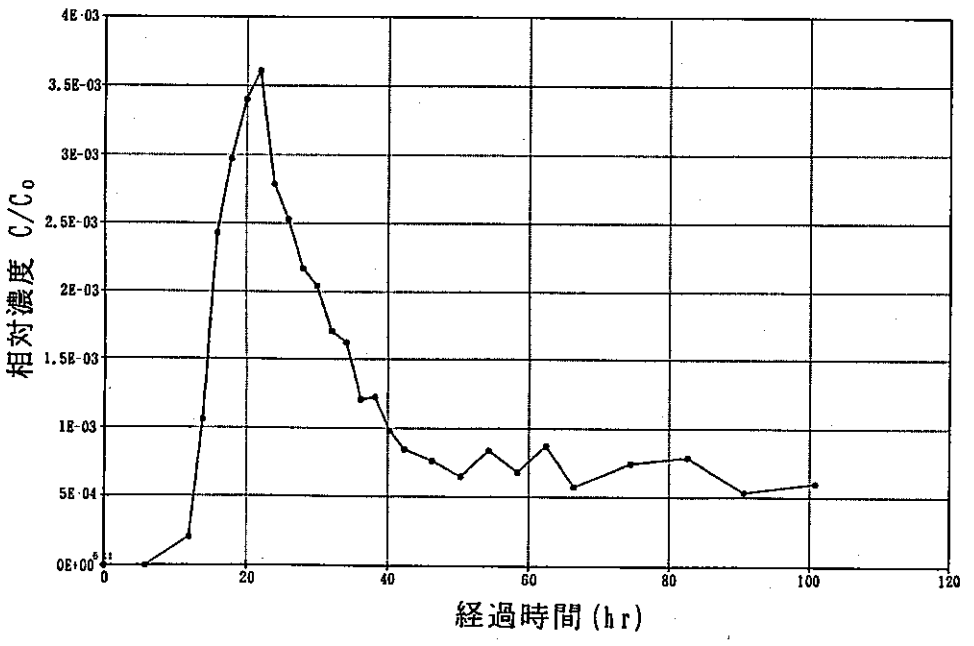
Ｌｕ－１７７（注入ケース７）



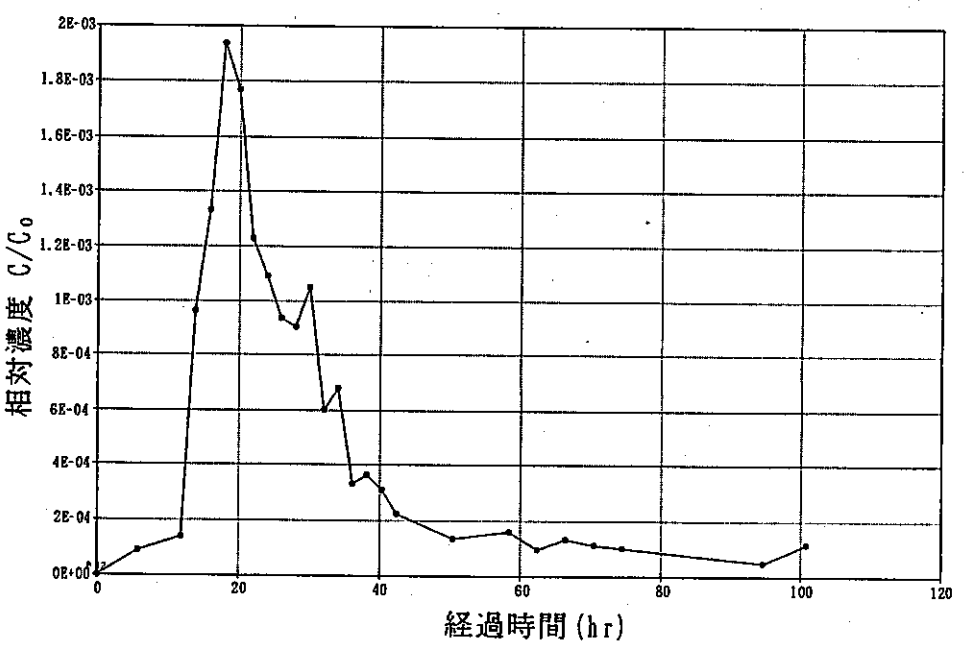
Ｃｒ－５１（注入ケース７）



Ｉｎ－１１１（注入ケース７）

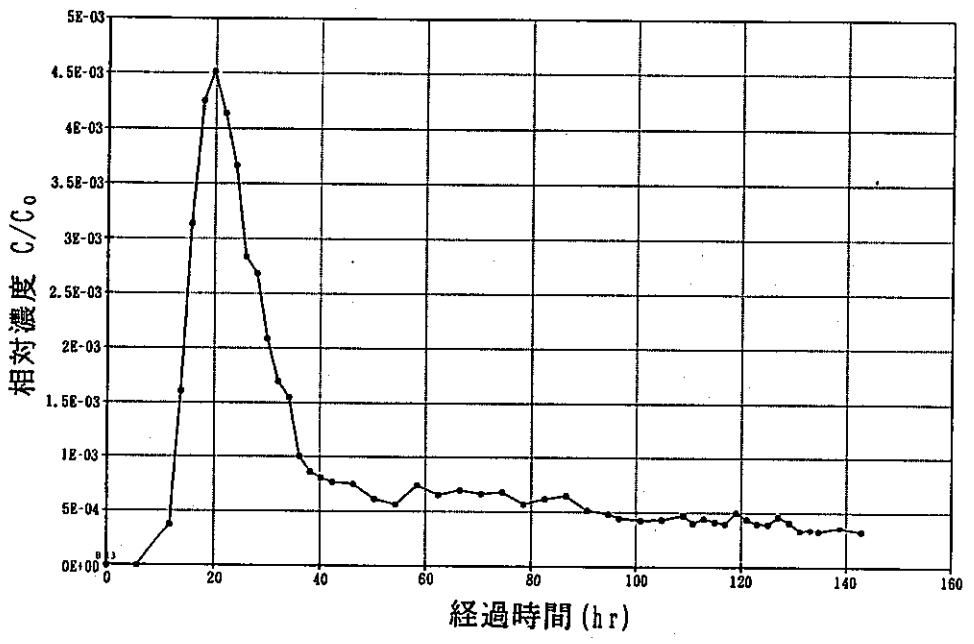


Ｔｂ－１６０（注入ケース７）

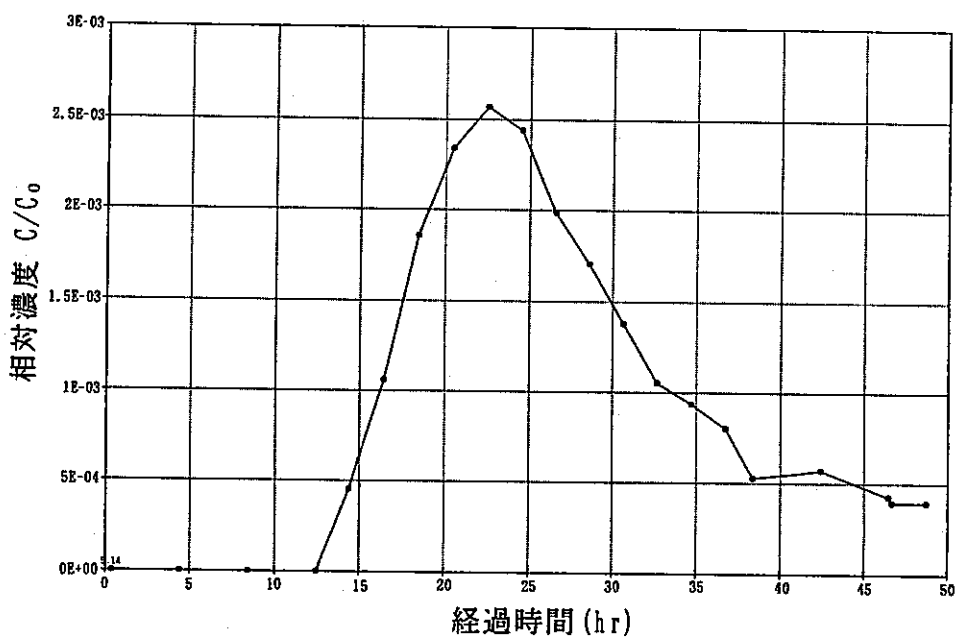


表－１６　　ＫＦＩ１１におけるトレーサ相対濃度　（３／４）

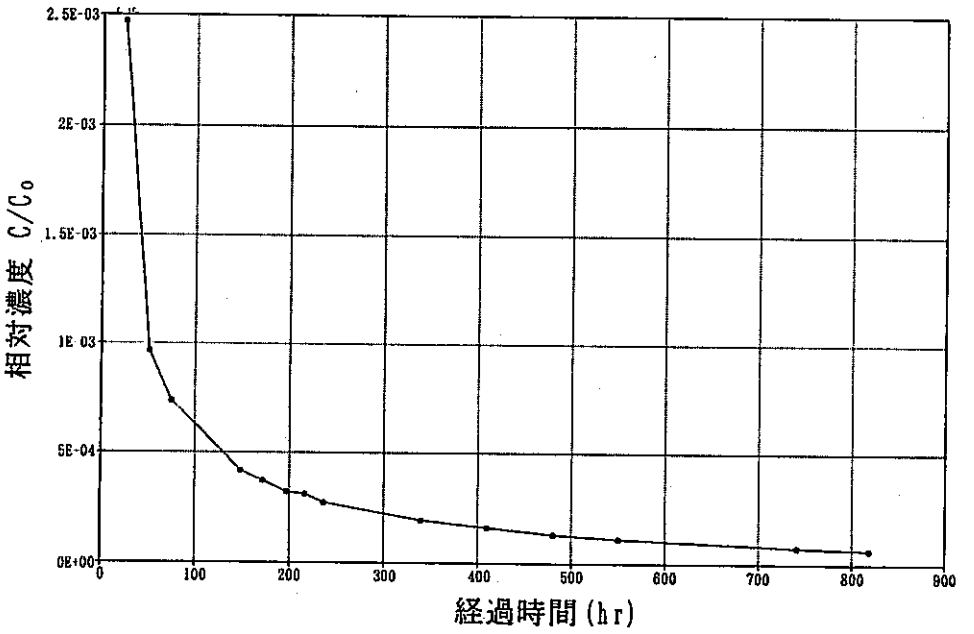
Ｙｂ－１６９（注入ケース７）



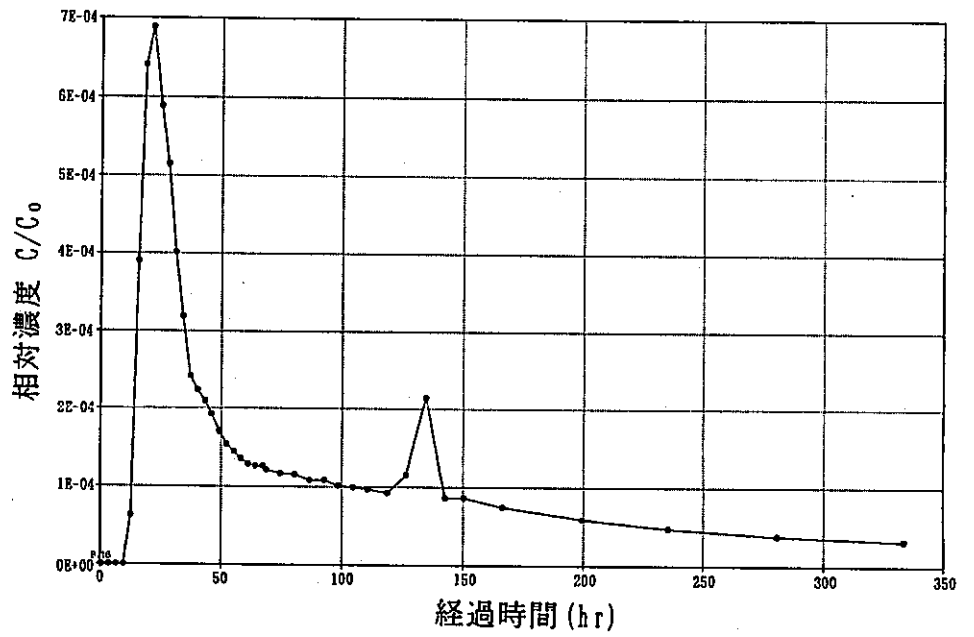
Ｃｏ－５８（注入ケース７）



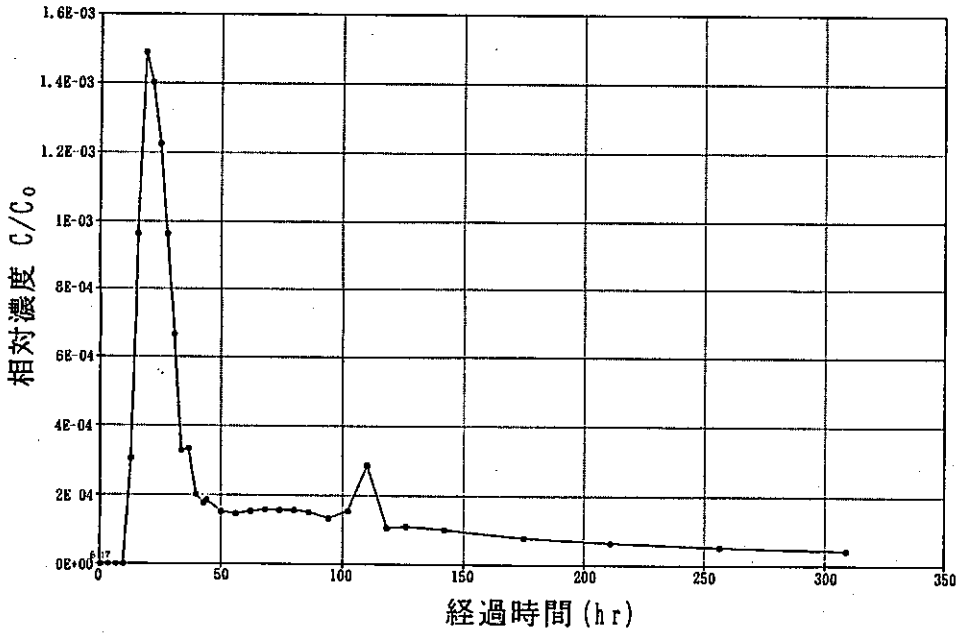
ロダミンＷＴ（注入ケースＡ）



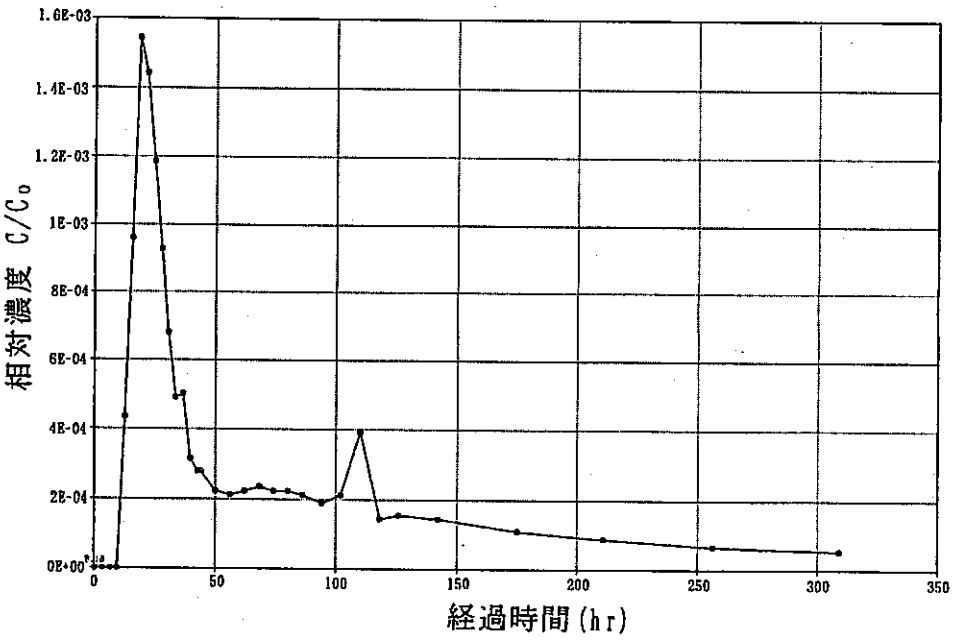
Ｉｎ－ＥＤＴＡ（注入ケースＣ）



Ｇｄ－ＤＴＰＡ（注入ケースＤ）

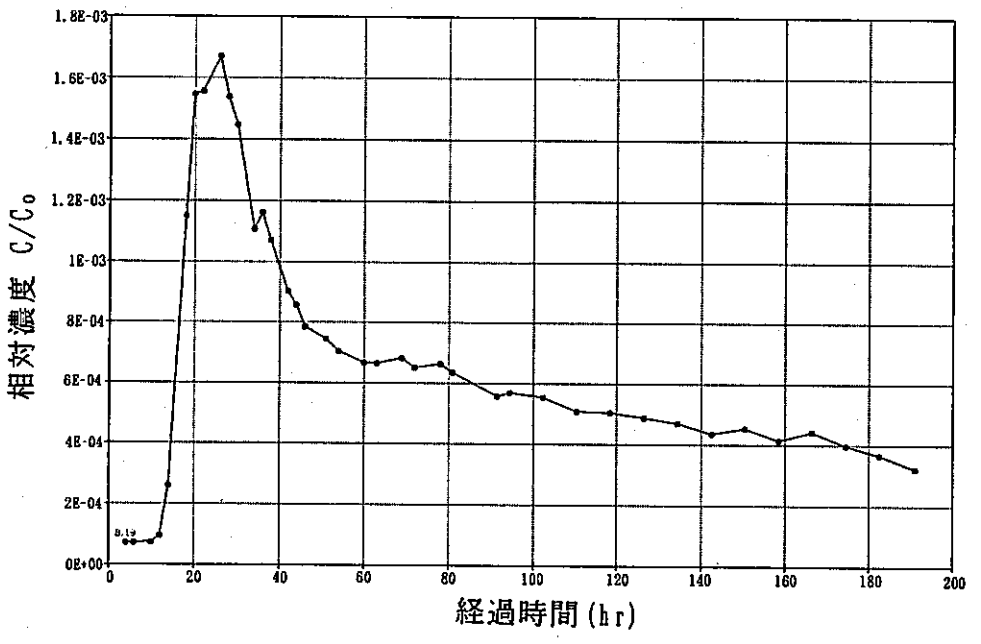


Ｔｍ－ＥＤＴＡ（注入ケースＤ）

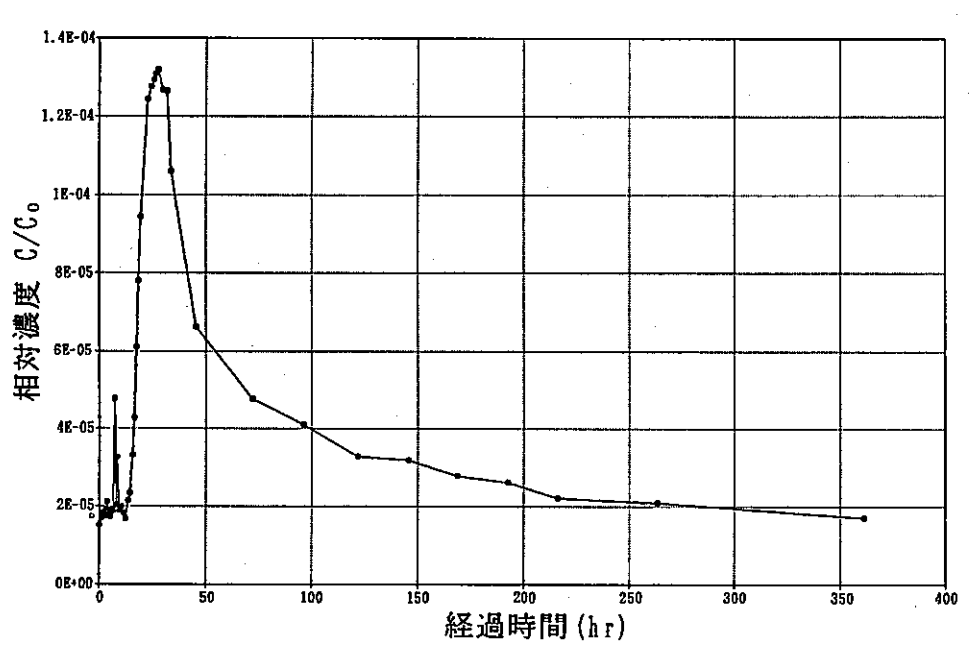
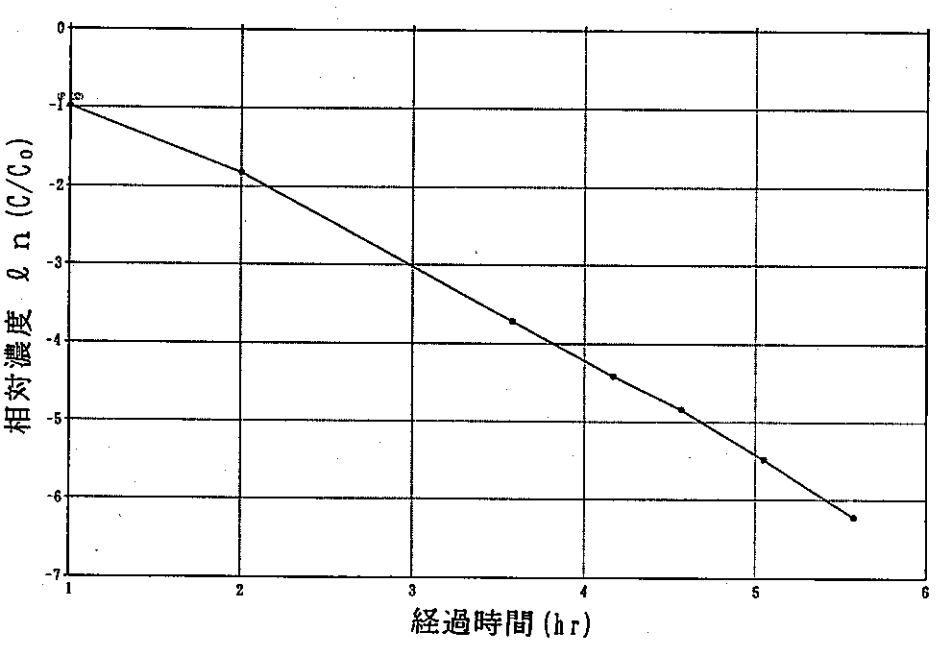


表－１６　　ＫＦＩ１１におけるトレーサ相対濃度　（４／４）

ロダミンＷＴ（注入ケースＥ）



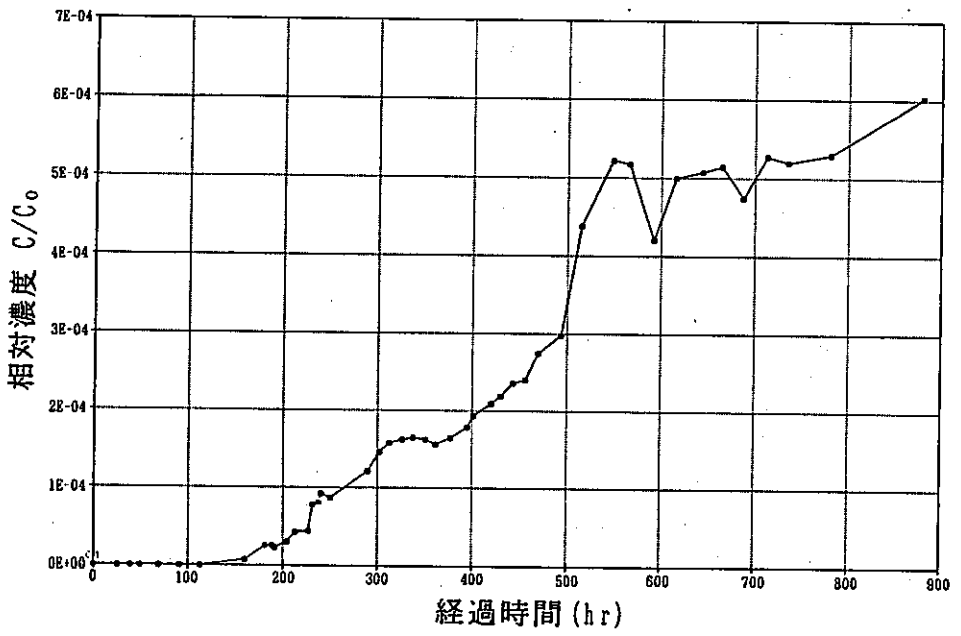
表－１７　　ＢＦＩ０２，ＫＦＩ１１におけるトレーサ濃度*

ＢＦＩ０２におけるＩ－１３１（注入ケース１０）	ＫＦＩ１１におけるＩ－１３１（注入ケース９）
	

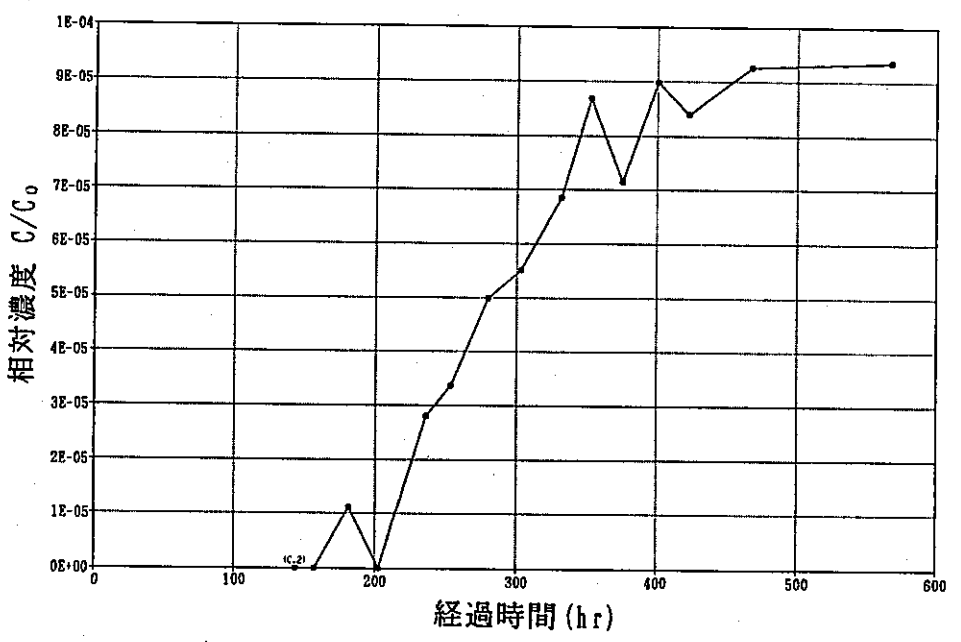
＊：ＫＦＩ１１上部にトレーサを注入したケース

表－１８　　ＫＦＩ０６におけるトレーサ相対濃度

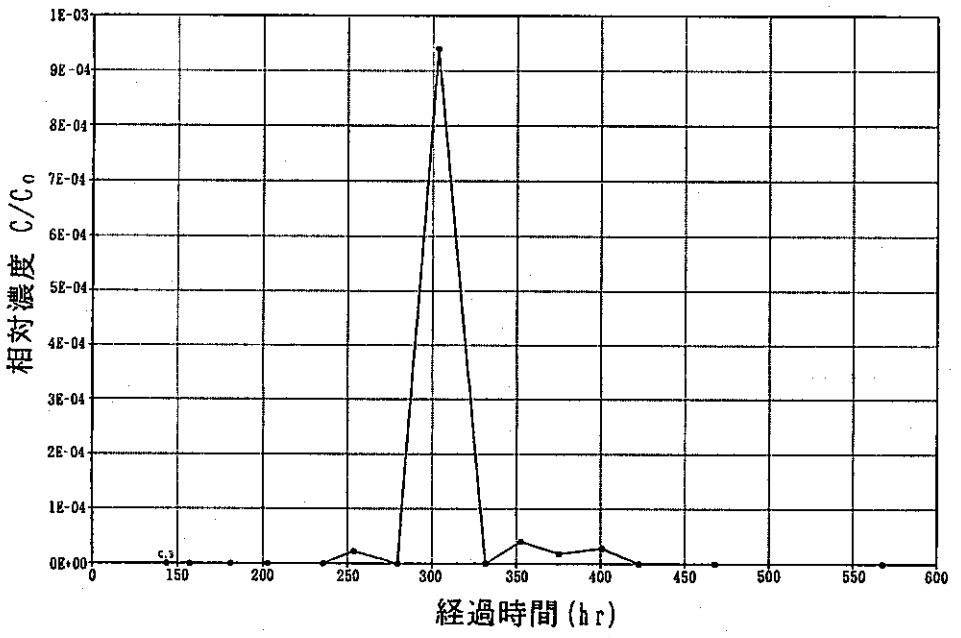
Ｉ－１３１（注入ケース３）



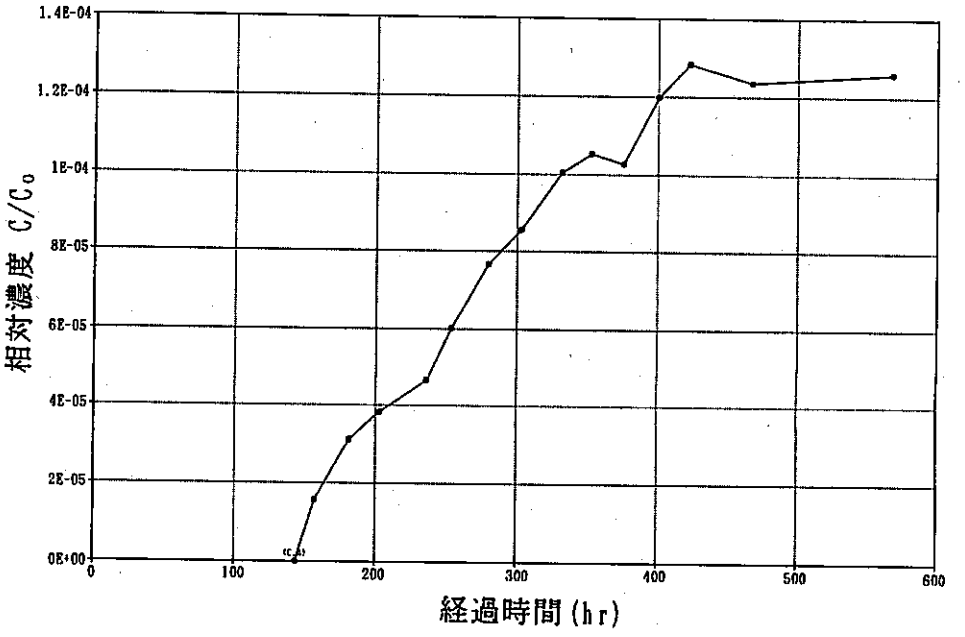
Ｃｒ－５１（注入ケース７）



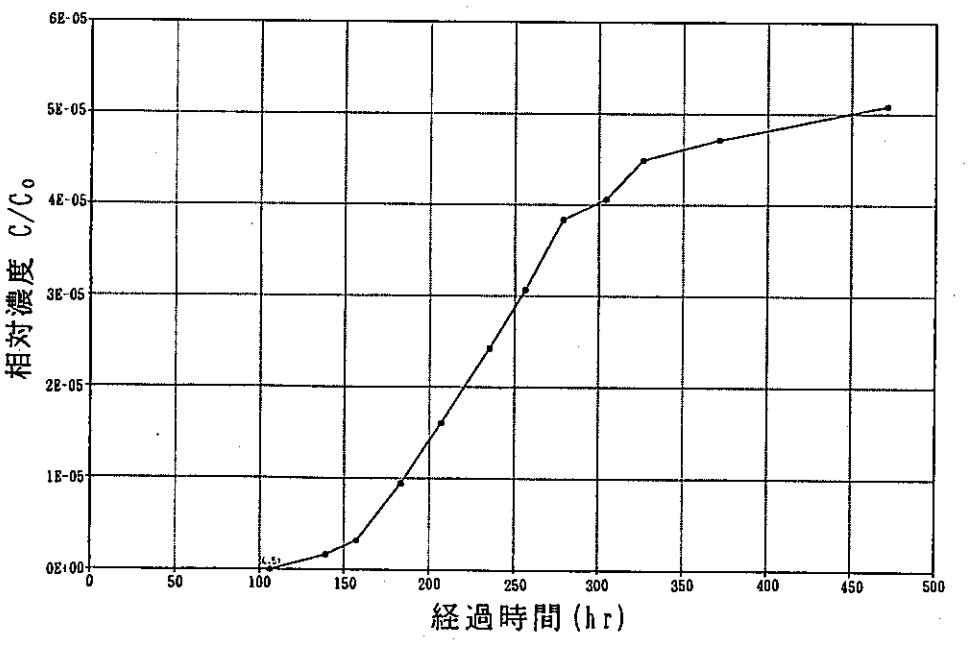
Ｔｂ－１６０（注入ケース７）



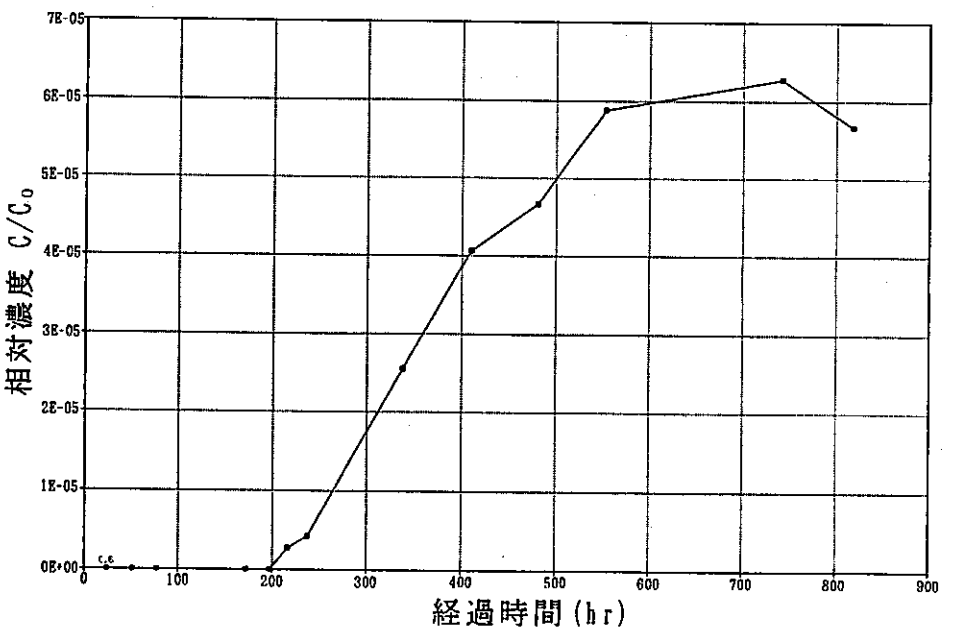
Ｙｂ－１６９（注入ケース７）



Ｃｏ－５８（注入ケース８）

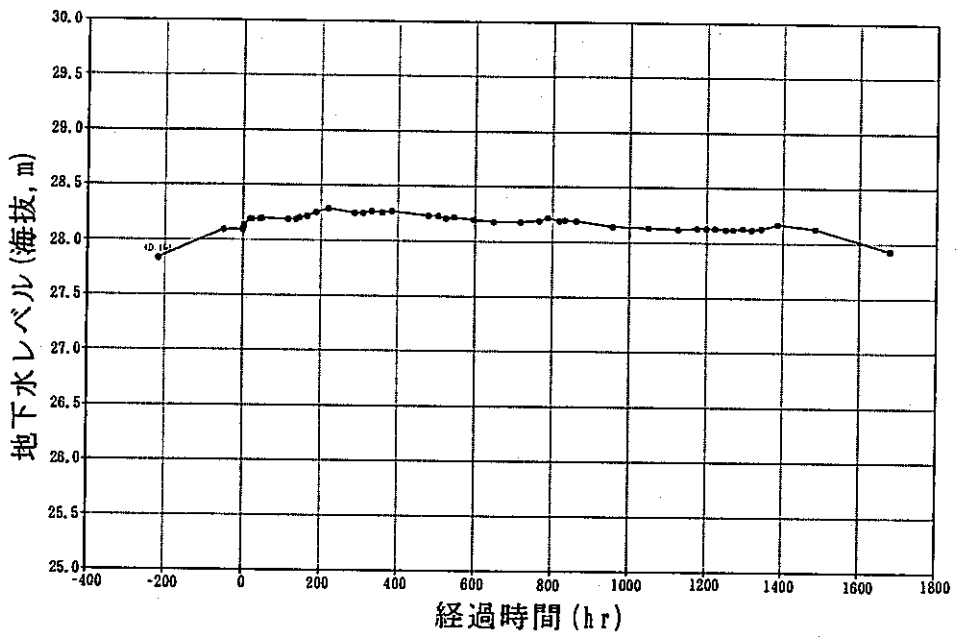


ロダミンＷＴ（注入ケースＡ）

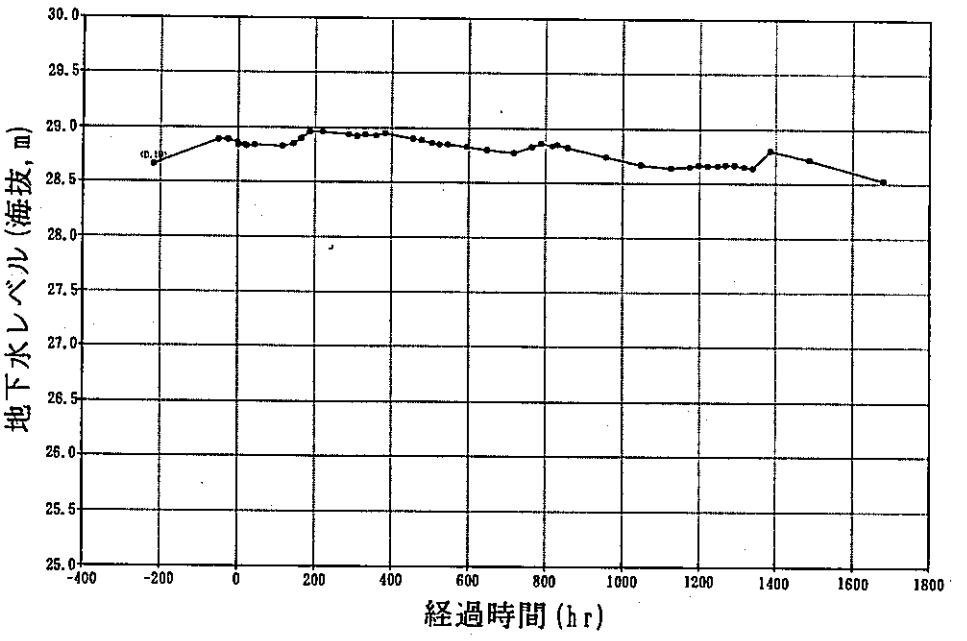


表－１９　井戸中の地下水レベル（１／２）

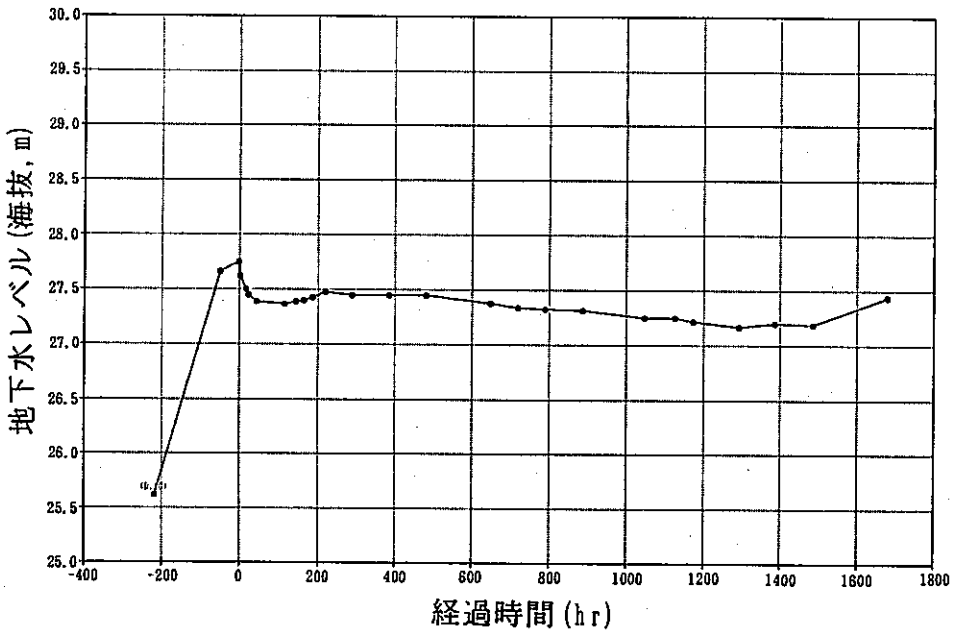
BFI01



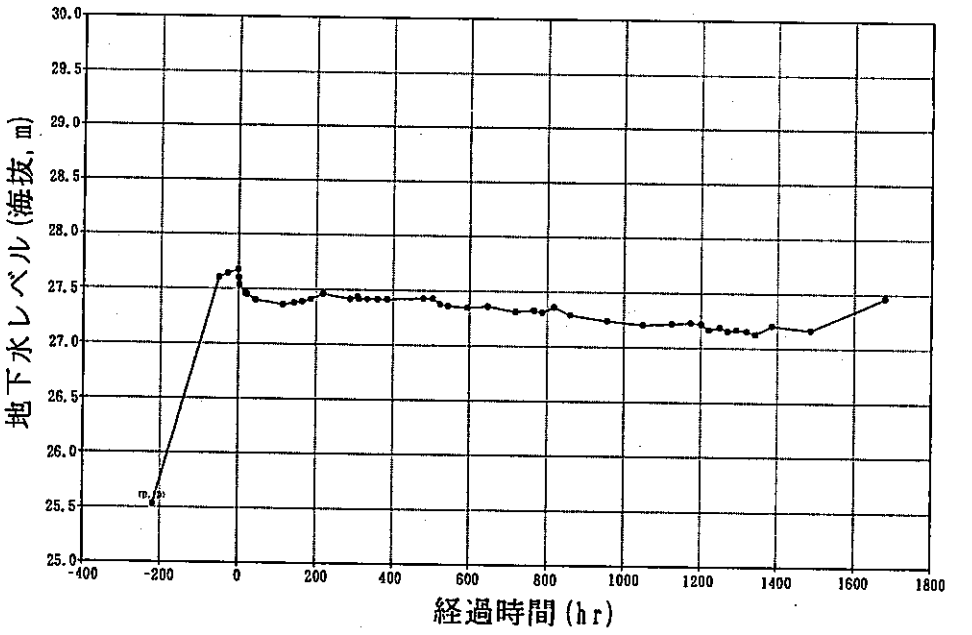
BFI02



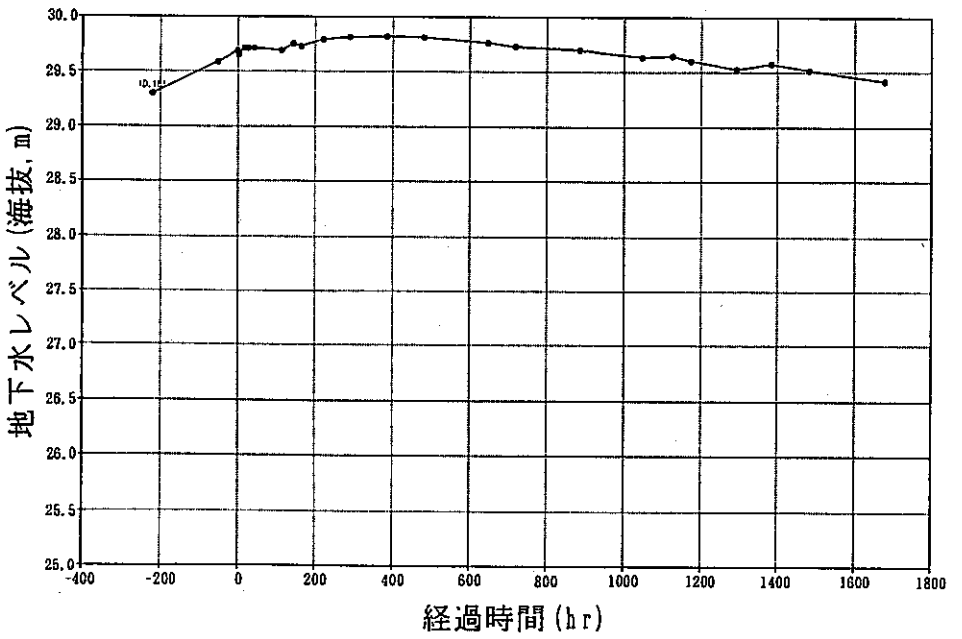
KFI05



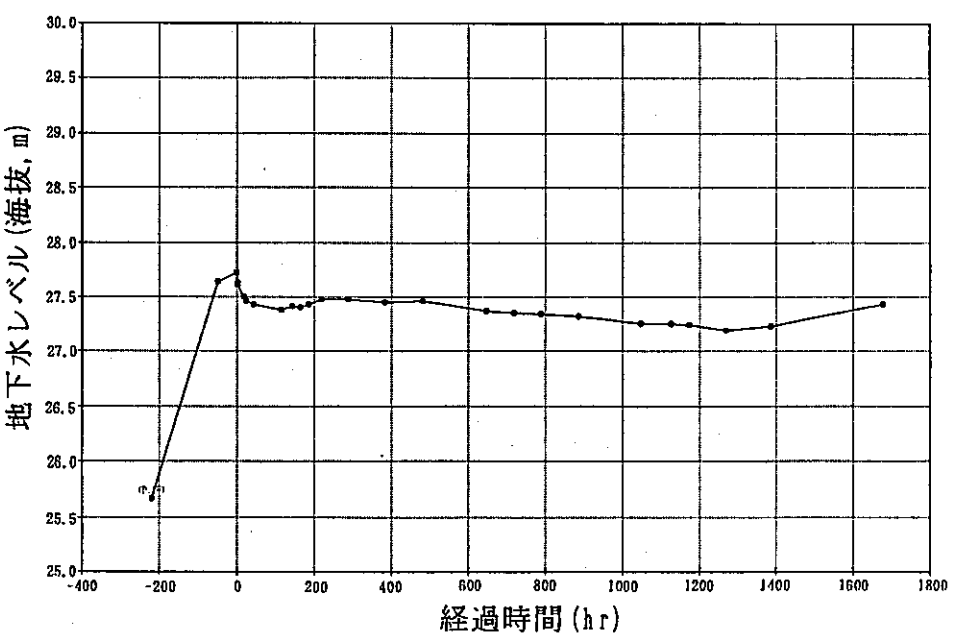
KFI06



KFI07

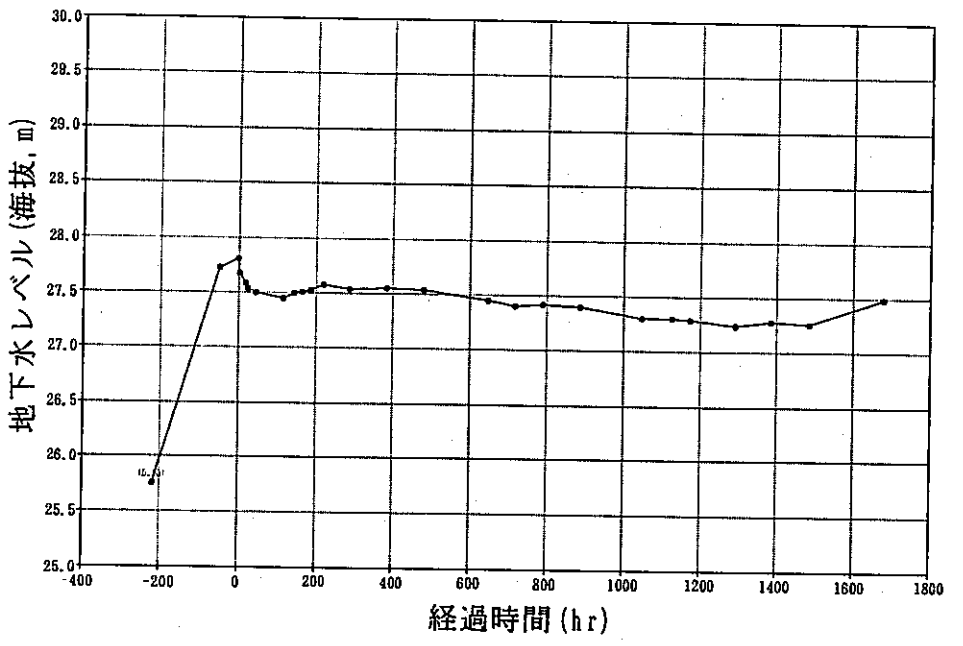


KFI09

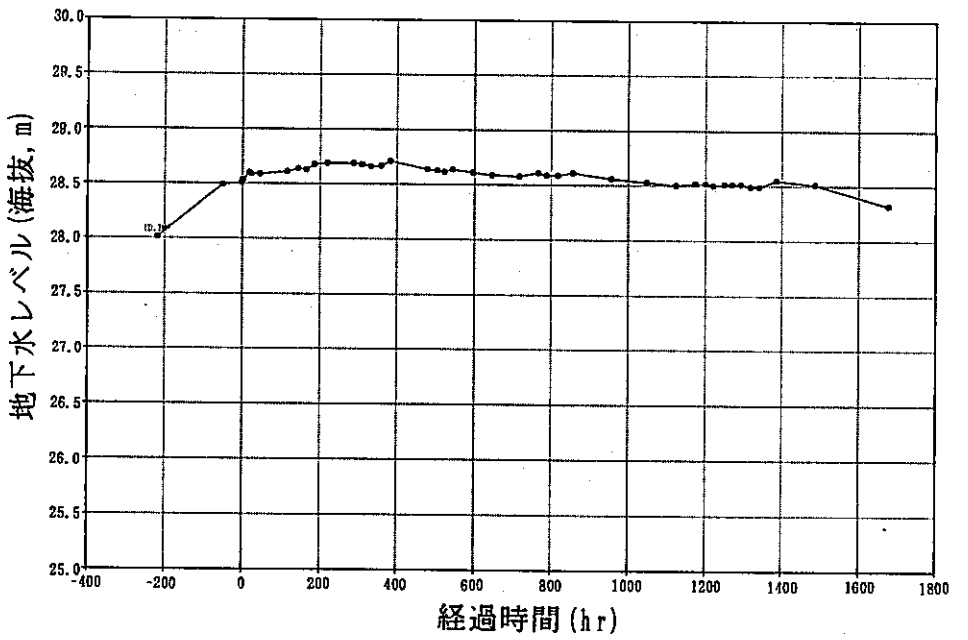


表－１９　　井戸中の地下水レベル（２／２）

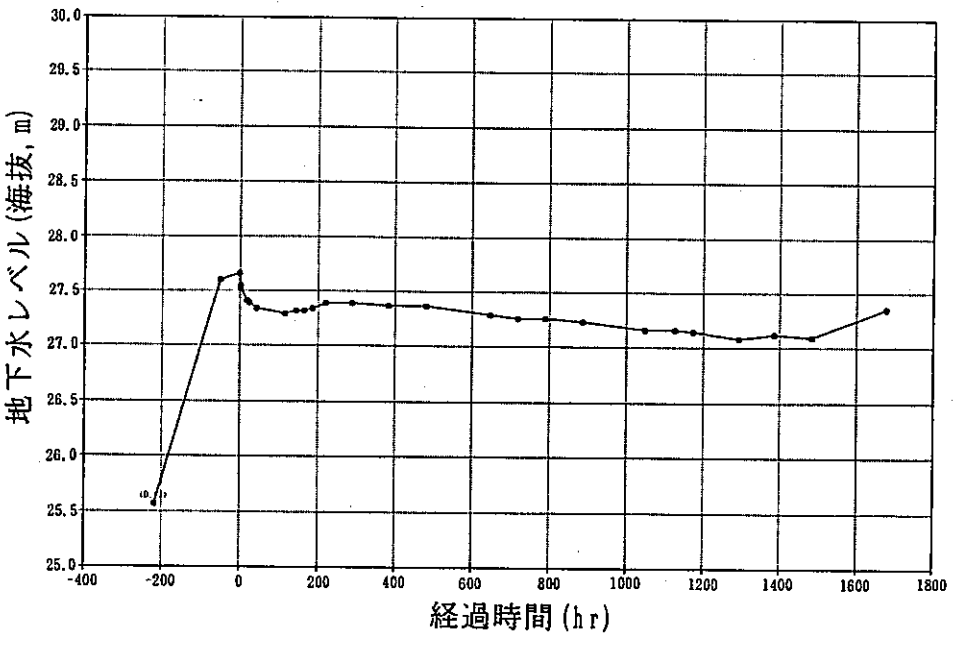
KFI10



KFI11

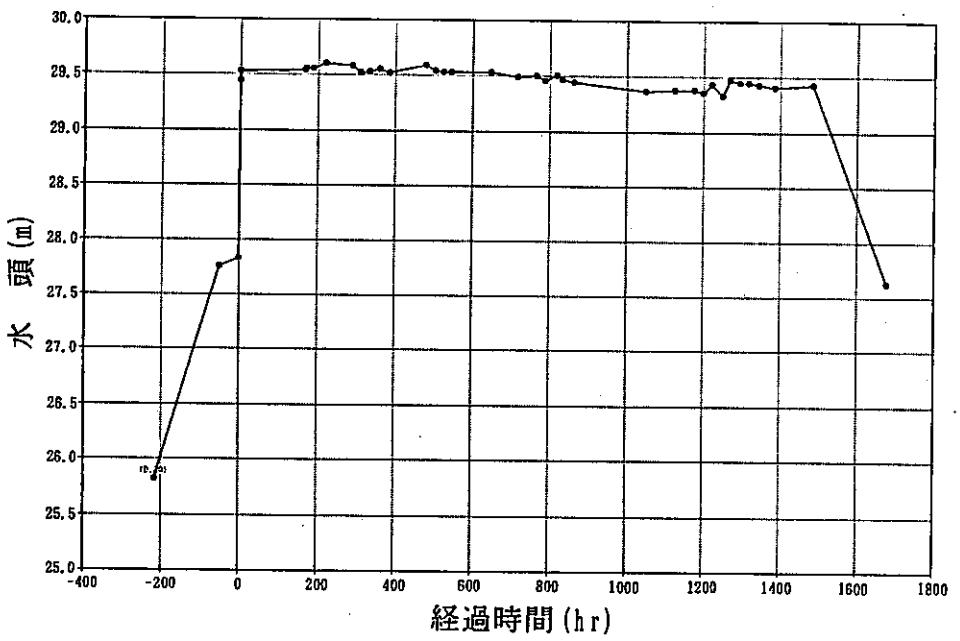


HFI01

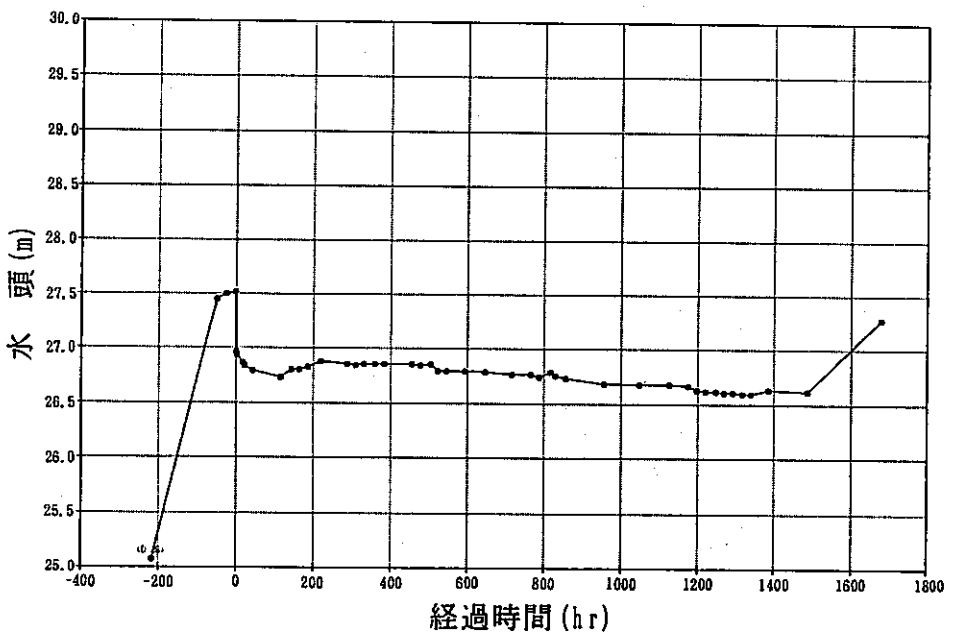


表－２０　　ゾーン２中の水頭（１／２）

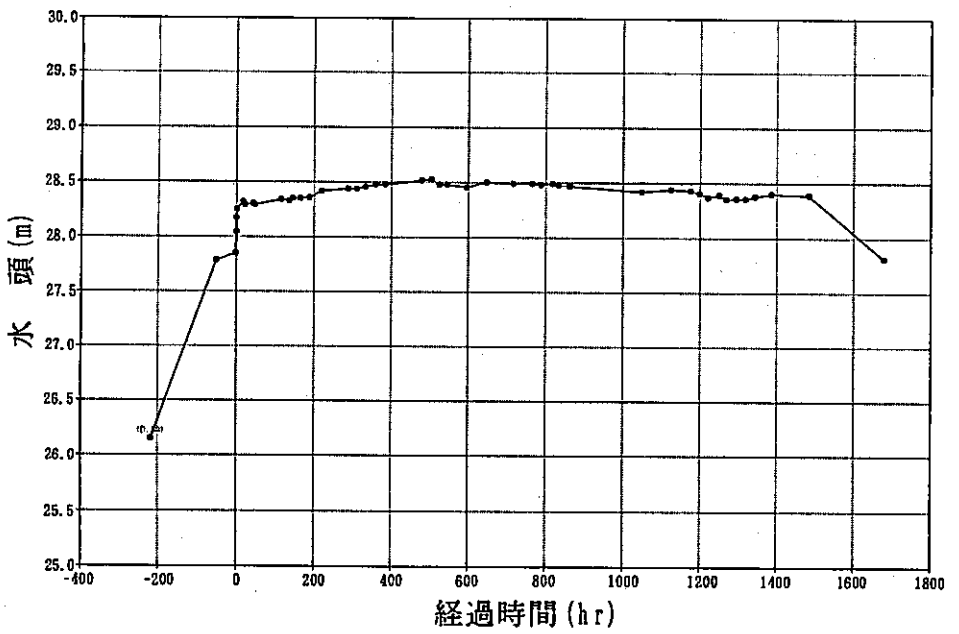
ＢＦＩ０１上部



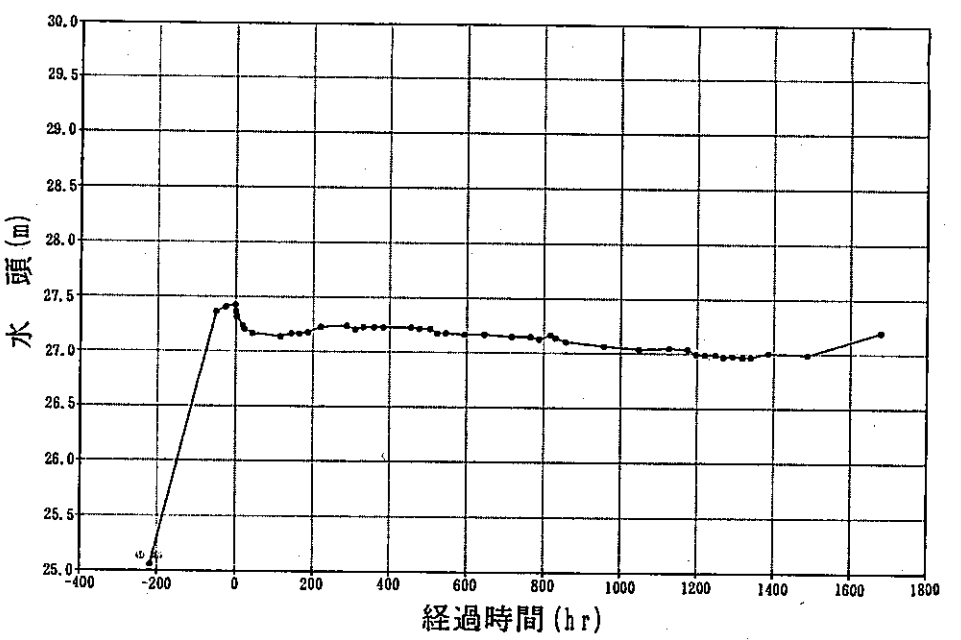
ＢＦＩ０２上部



ＢＦＩ０１下部

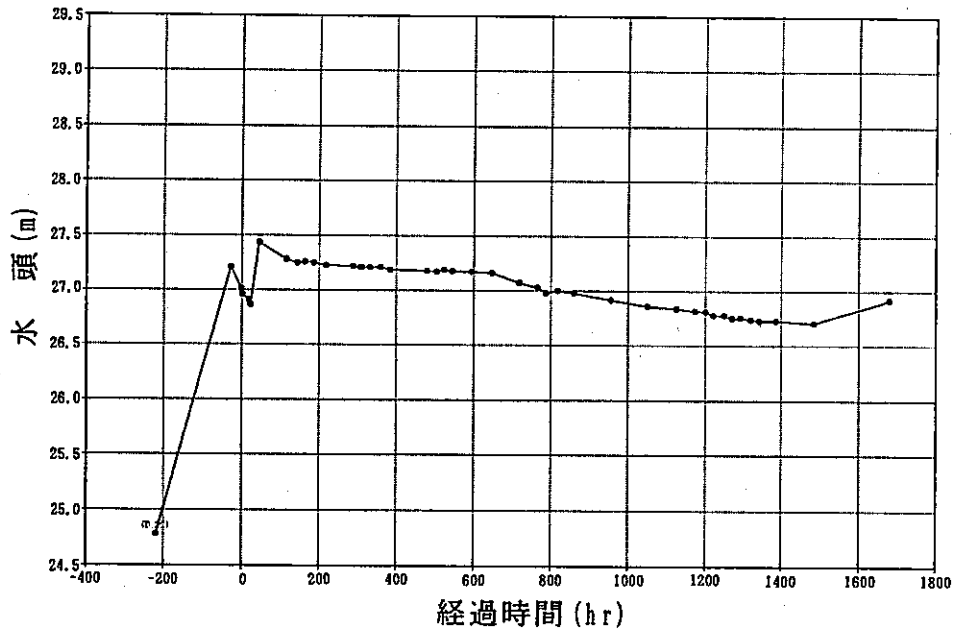


ＢＦＩ０２下部

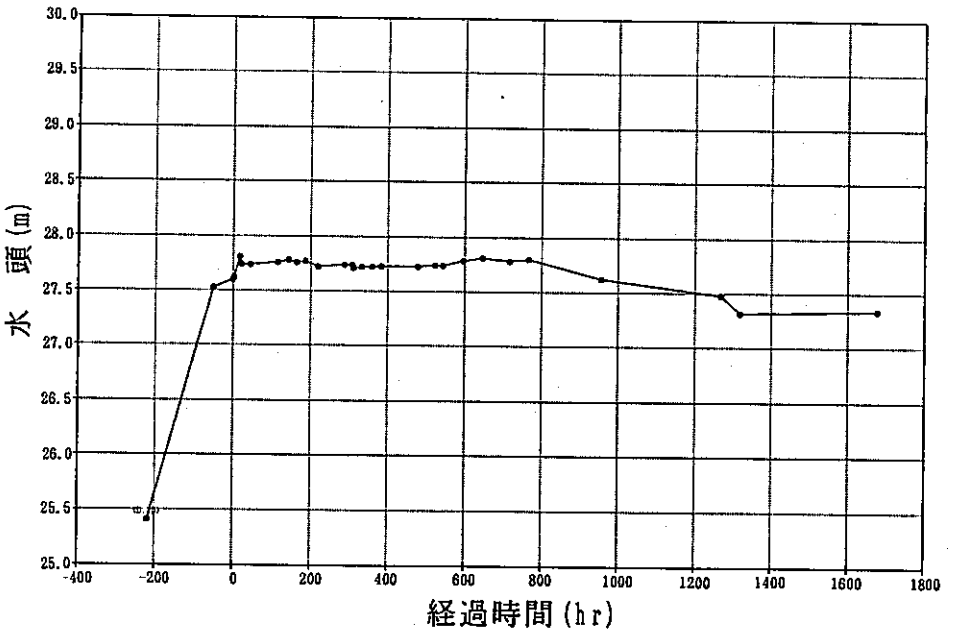


表－２０　　ゾーン２中の水頭（２／２）

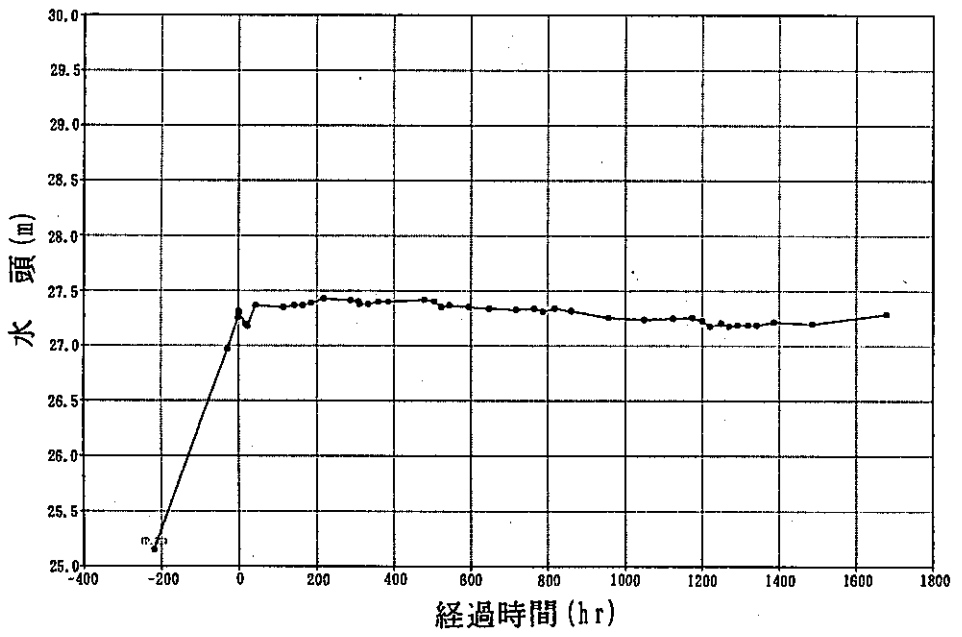
KFI06上部



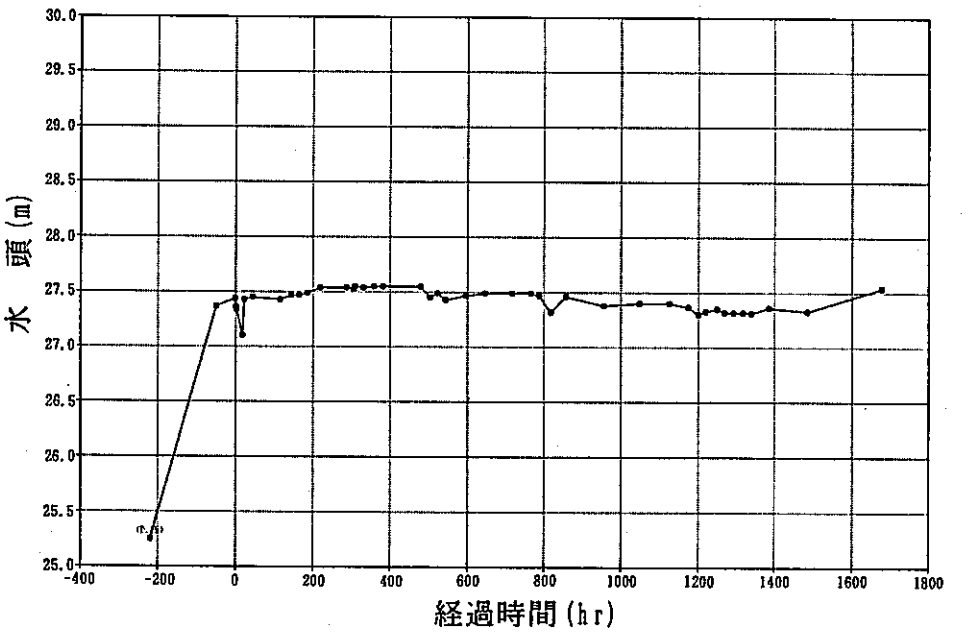
KFI11上部



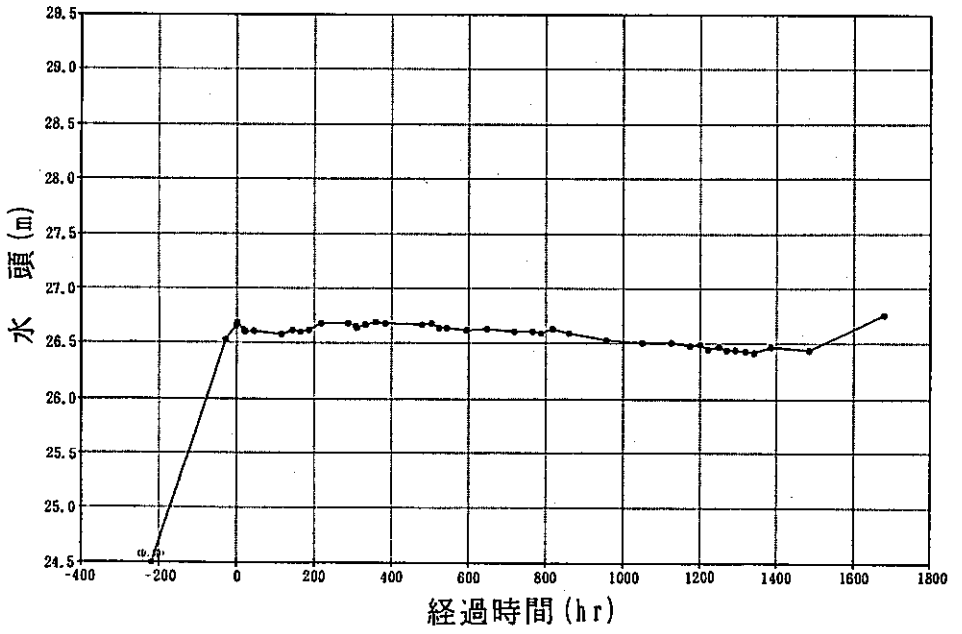
KFI06中部



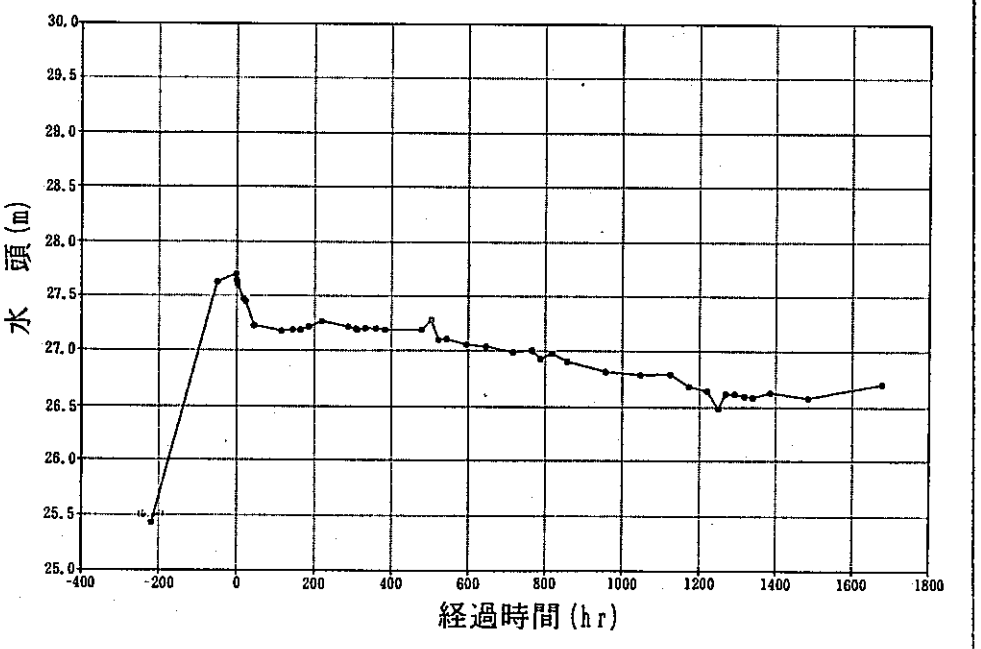
KFI11中部



KFI06下部

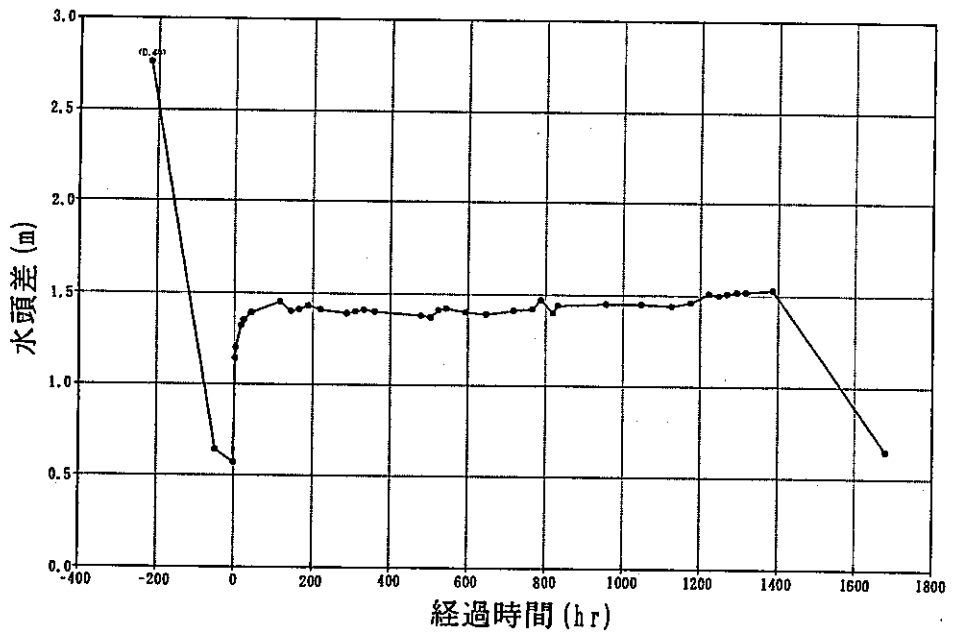


KFI11下部

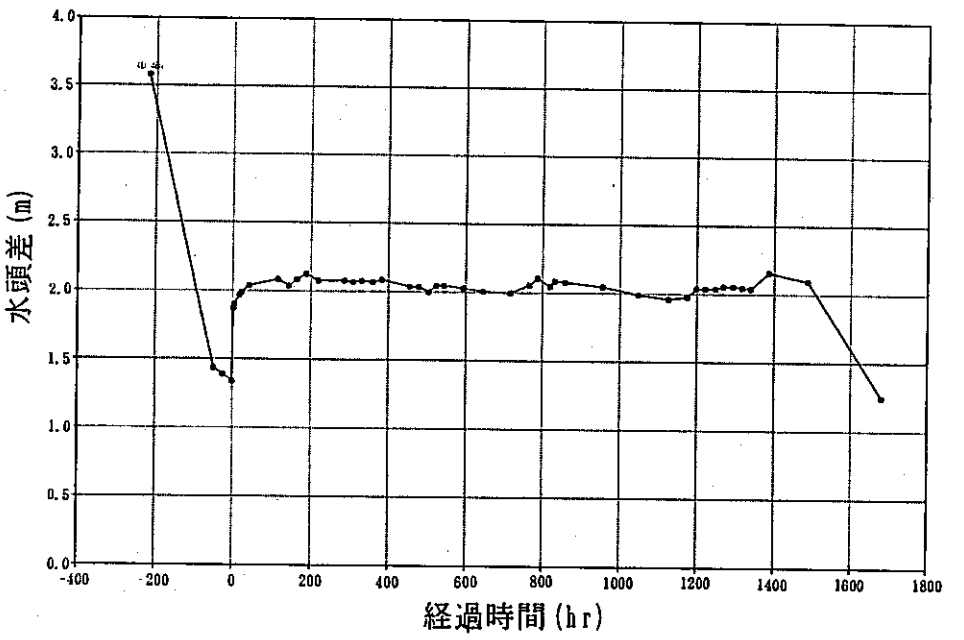


表－２１　　ＢＦＩ０２の揚水部分との水頭差（１／３）

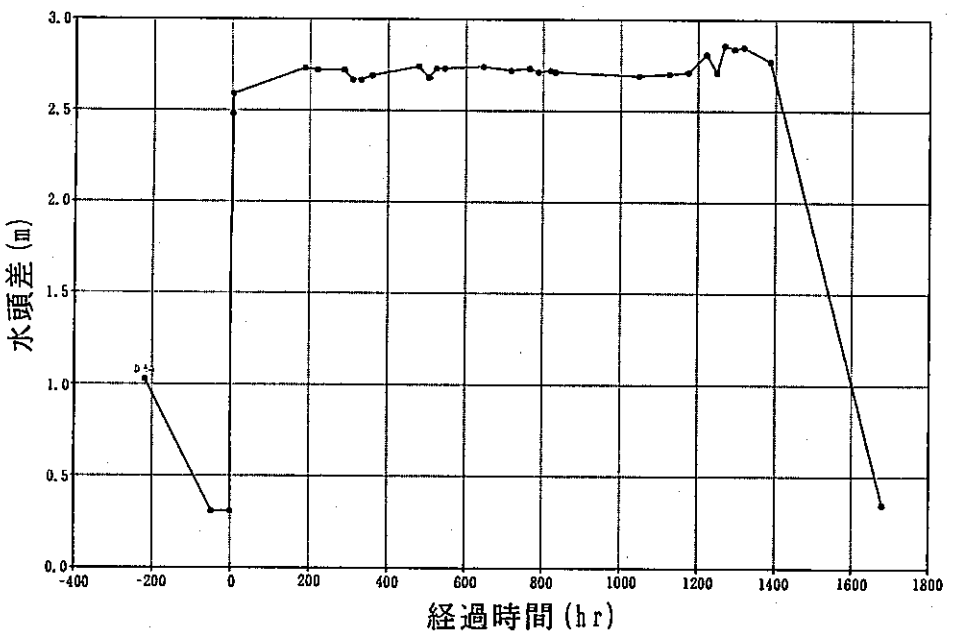
ＢＦＩ０１の地下水面



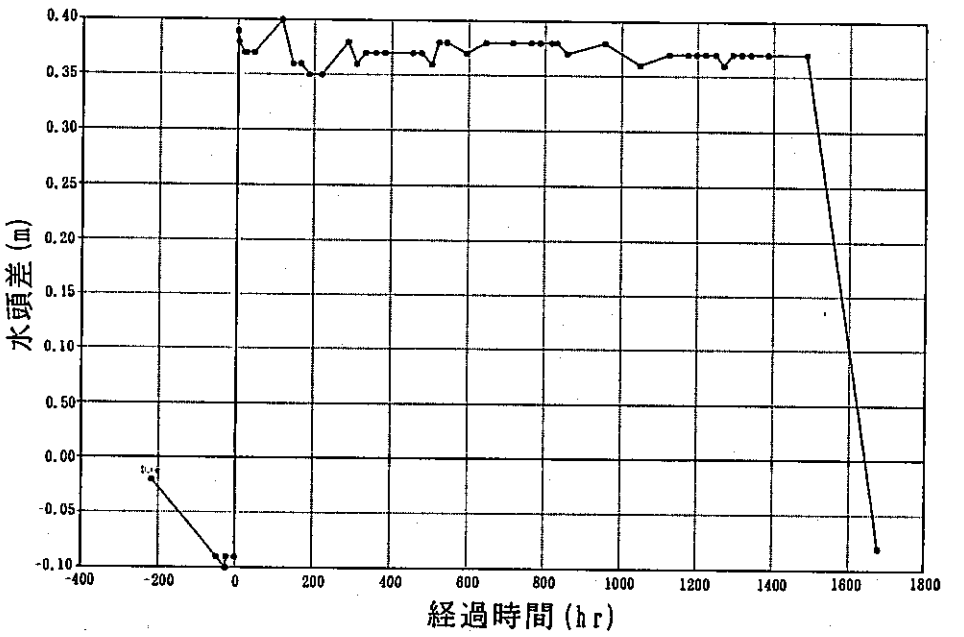
ＢＦＩ０２の地下水面



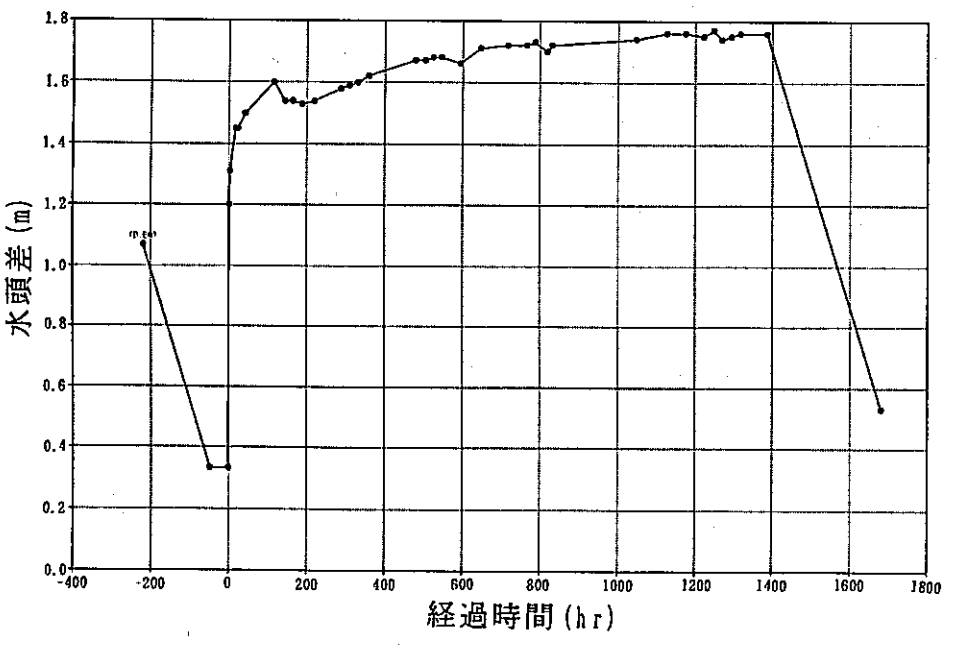
ＢＦＩ０１上部



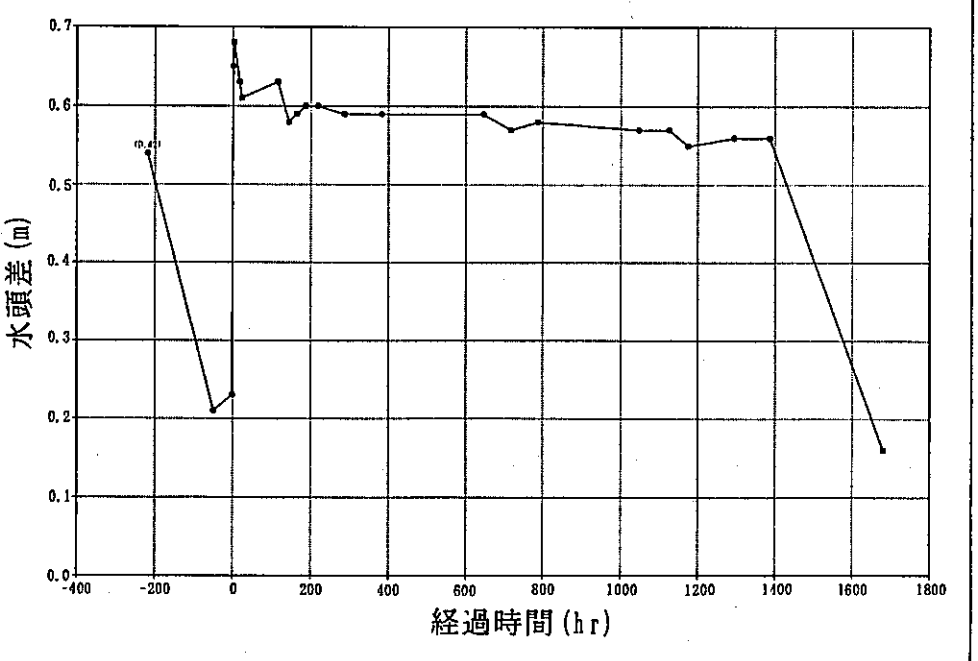
ＢＦＩ０２下部



ＢＦＩ０１下部

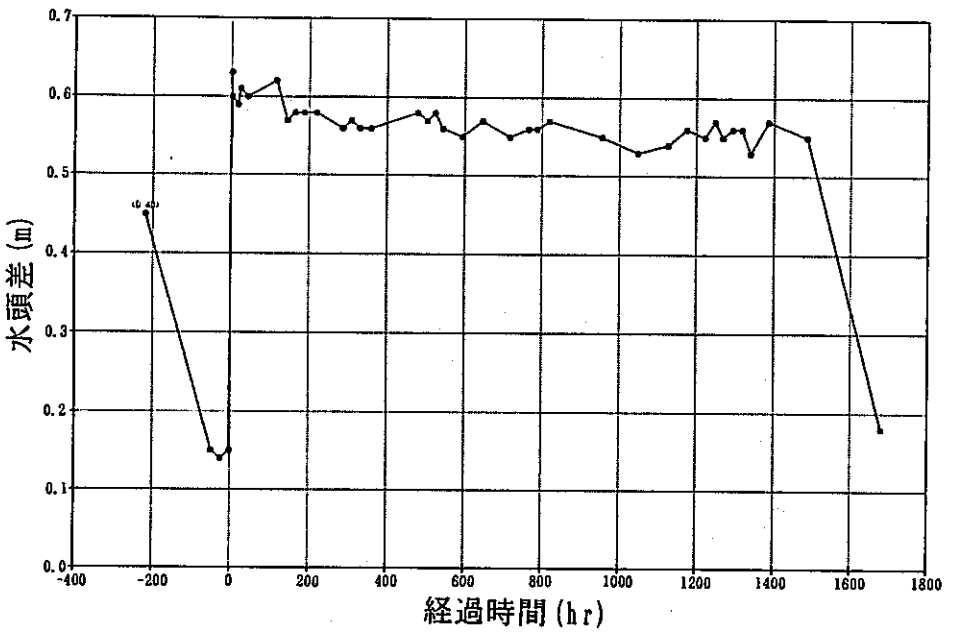


ＫＦＩ０５の地下水面

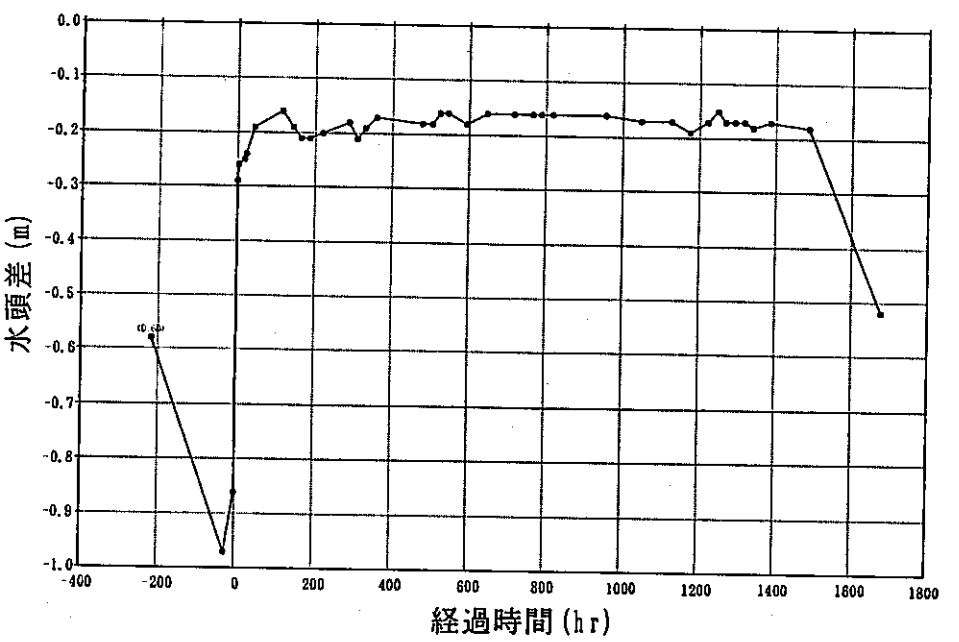


表－２１　　ＢＦＩ０２の揚水部分との水頭差（２／３）

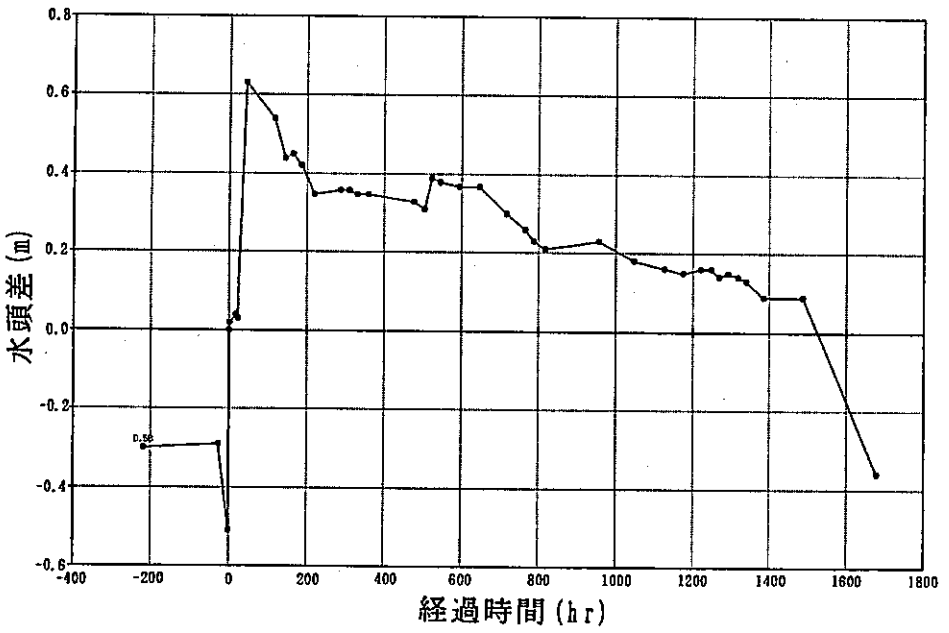
ＫＦＩ０６の地下水面



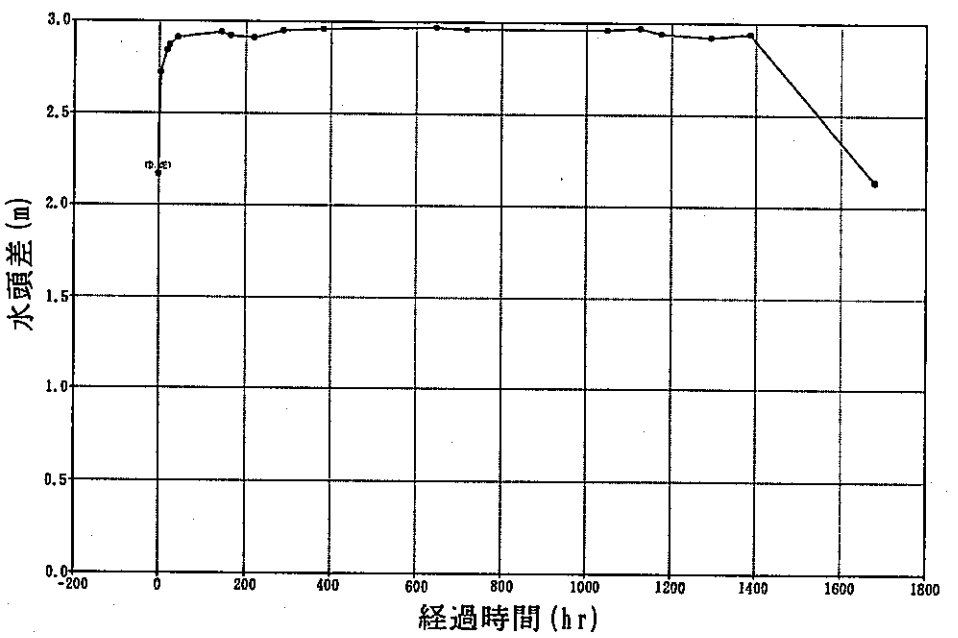
ＫＦＩ０６下部



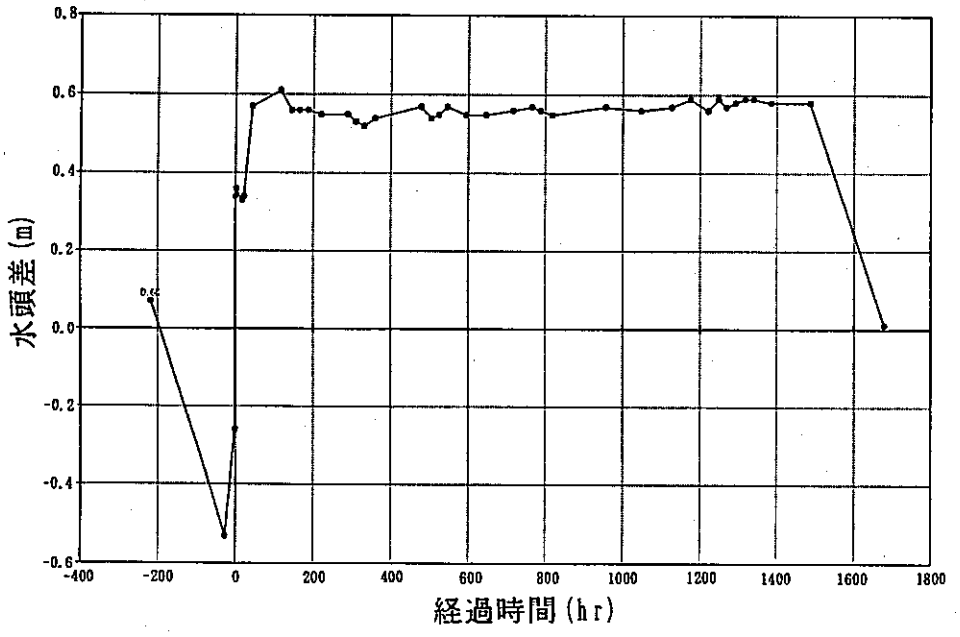
ＫＦＩ０６上部



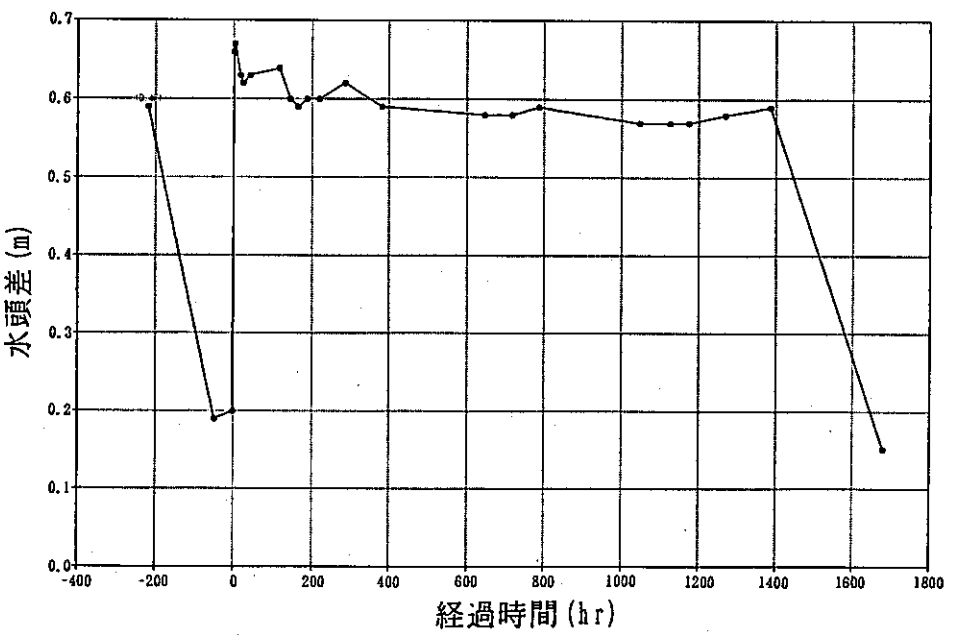
ＫＦＩ０７の地下水面



ＫＦＩ０６中部

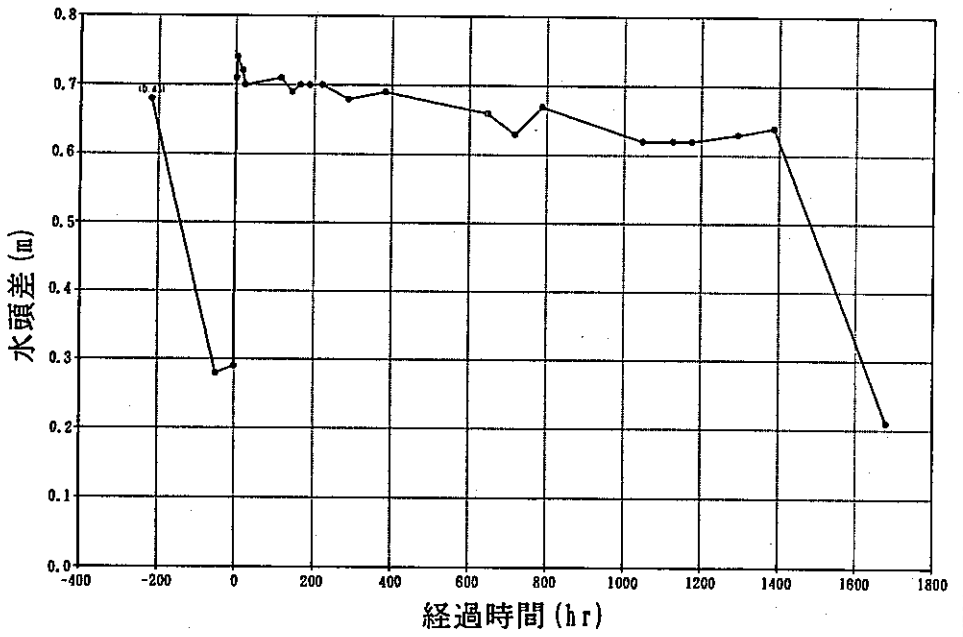


ＫＦＩ０９の地下水面

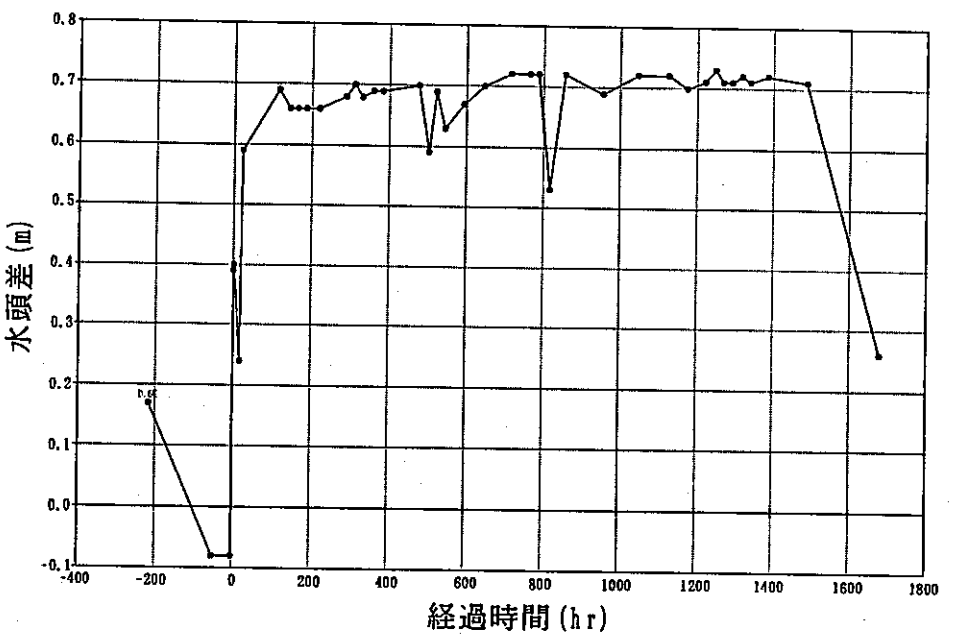


表－２１　　ＢＦＩ０２の揚水部分との水頭差（３／３）

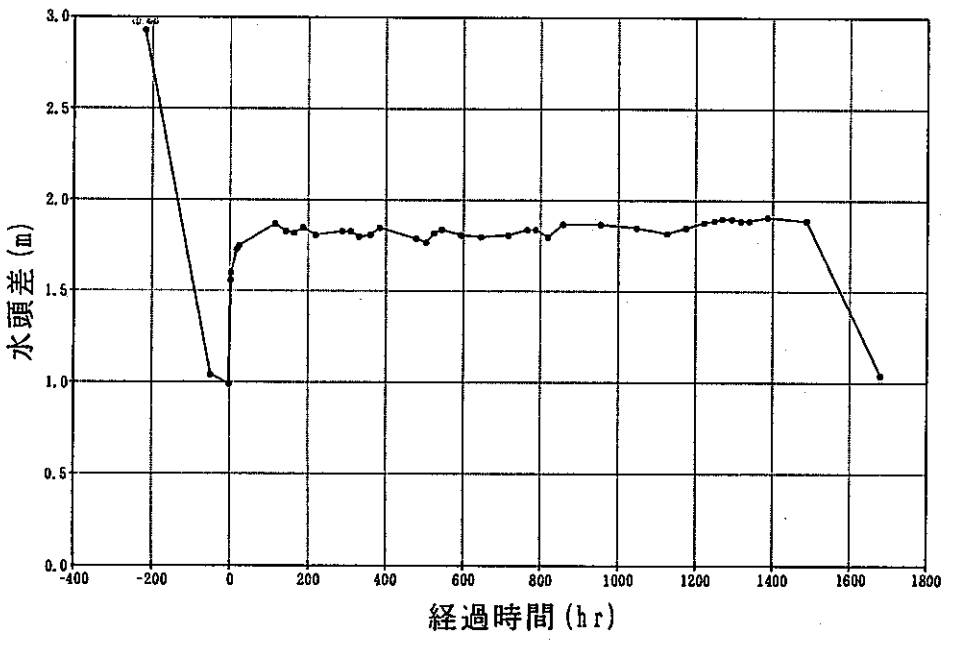
ＫＦＩ１０の地下水面



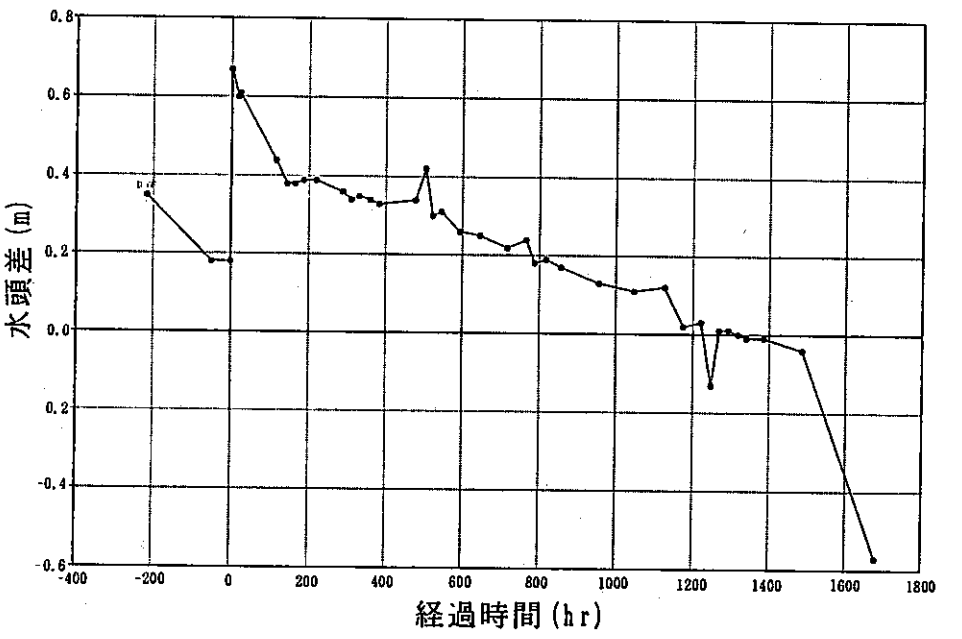
ＫＦＩ１１中部



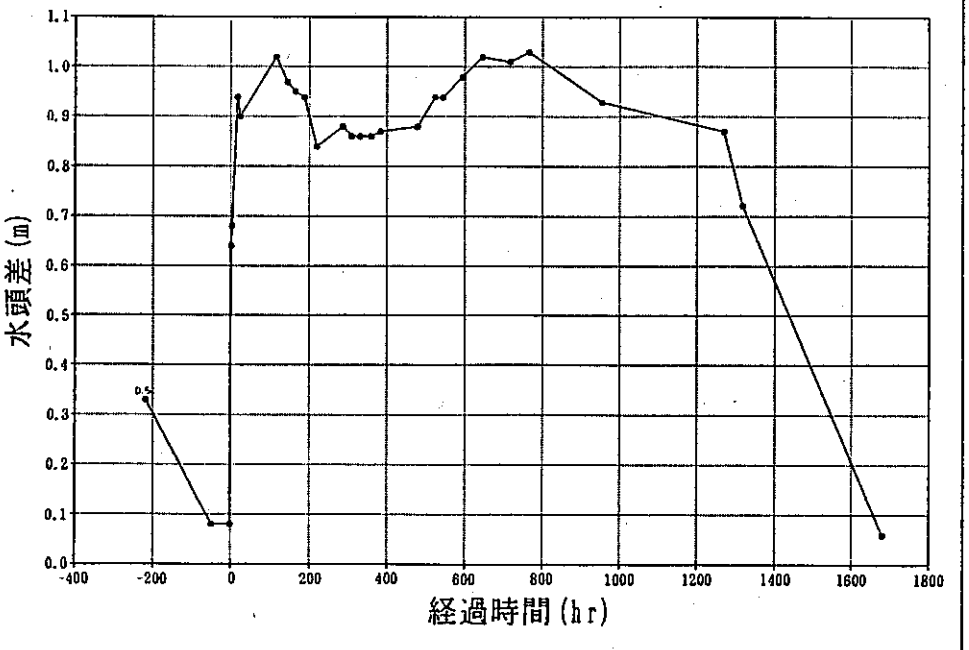
ＫＦＩ１１の地下水面



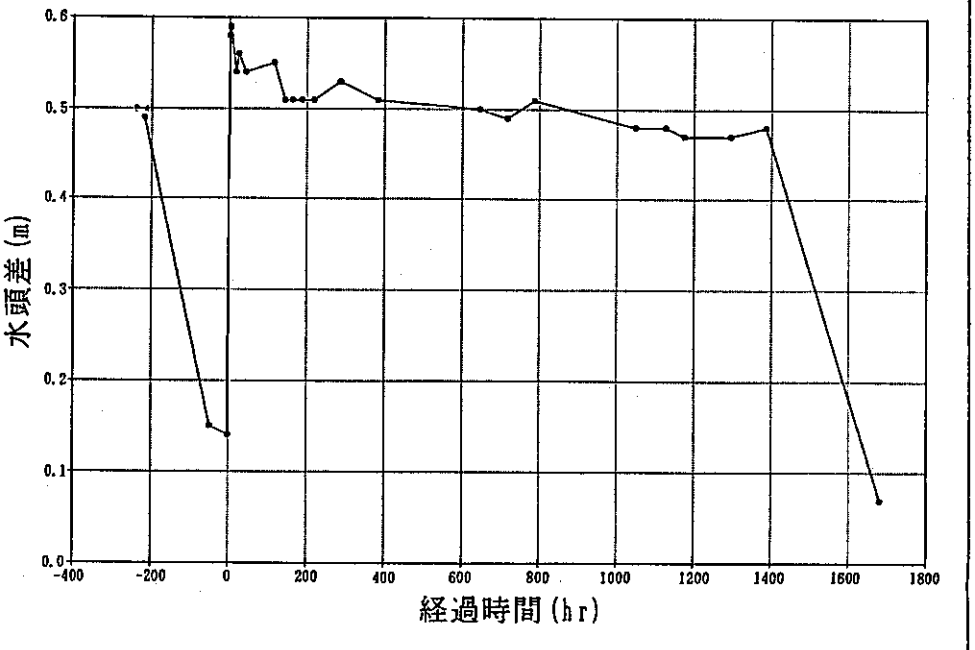
ＫＦＩ１１下部



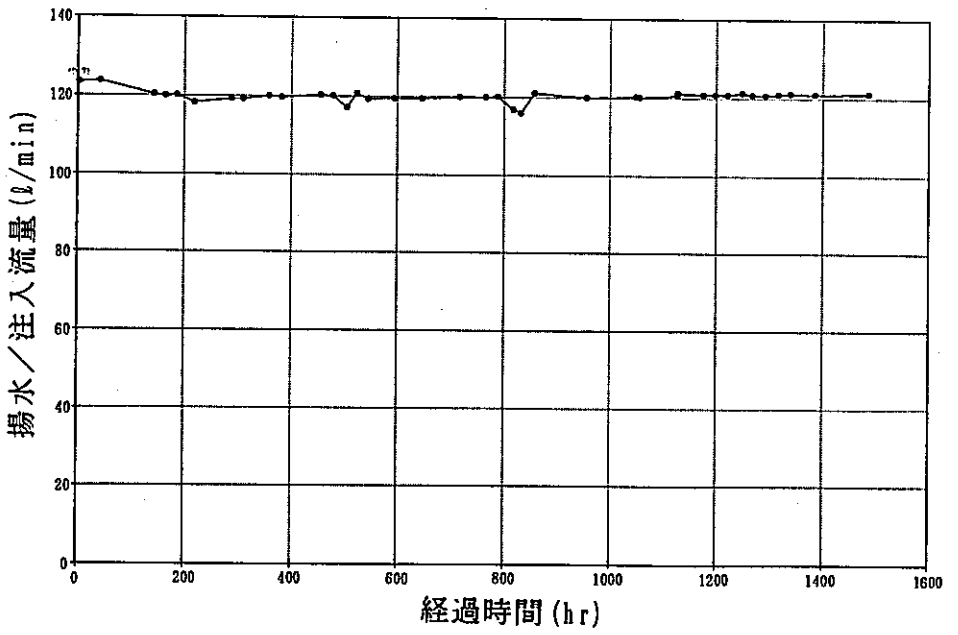
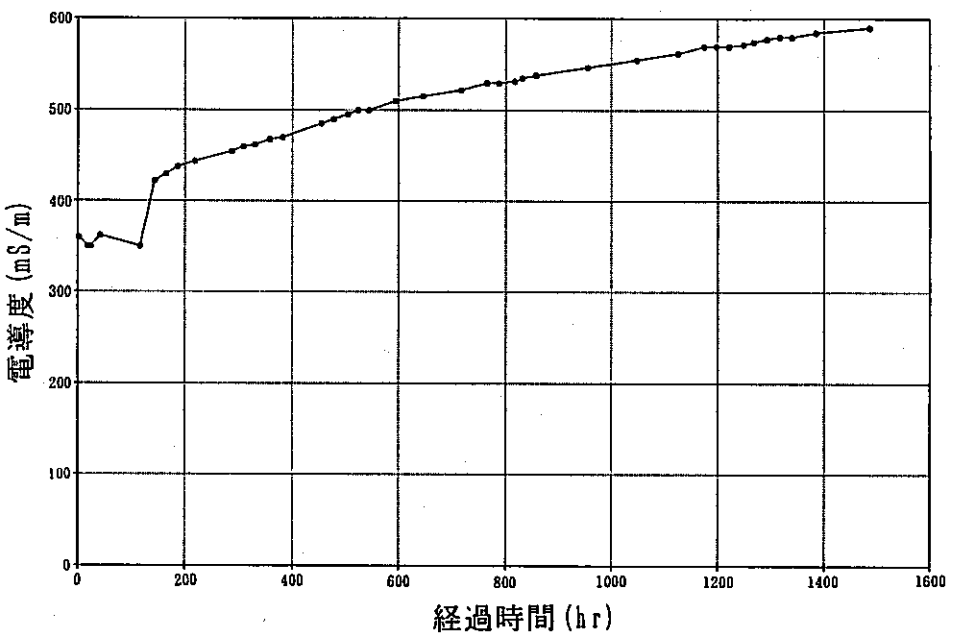
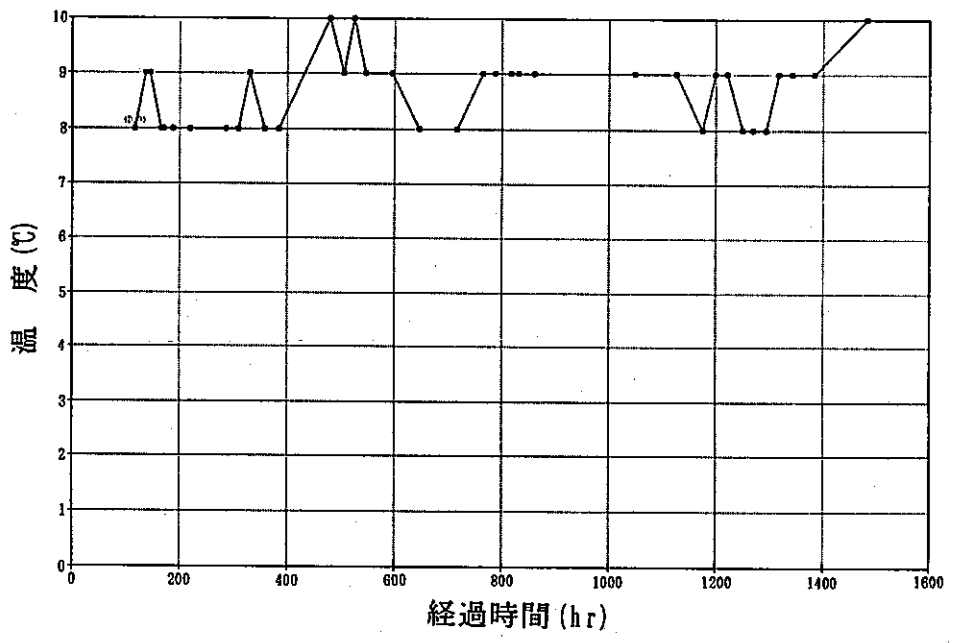
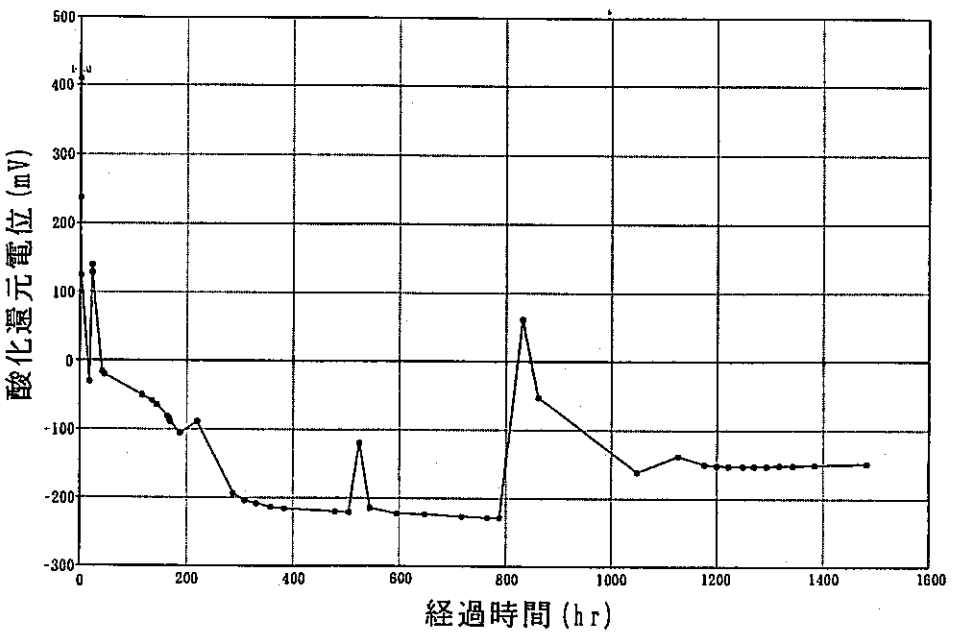
ＫＦＩ１１上部



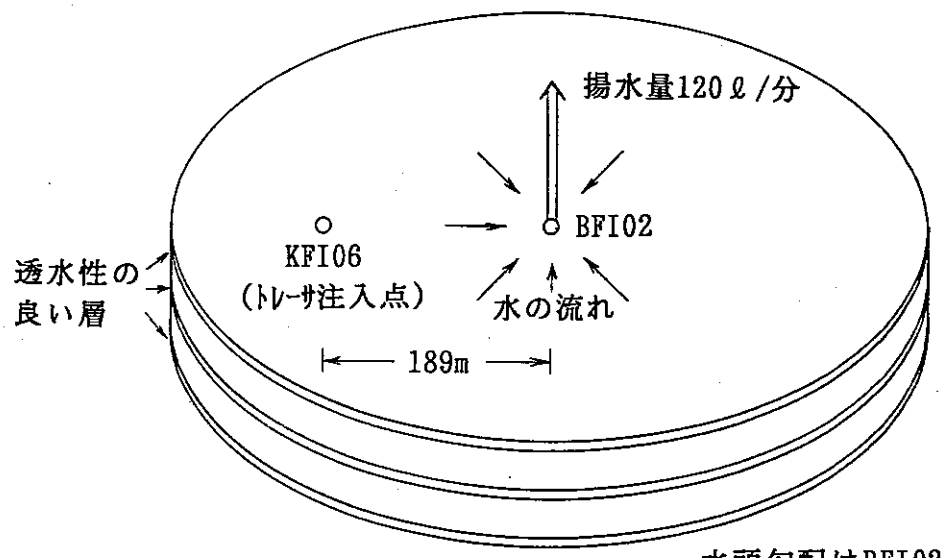
ＨＦＩ０１の地下水面



表－２２　　揚水に関するデータ

揚水／注入流量 （ℓ／min）	
BFI02における 電導度 （mS/m）	
BFI02における 温度 （℃）	
BFI01における 酸化還元電位 （mV）	

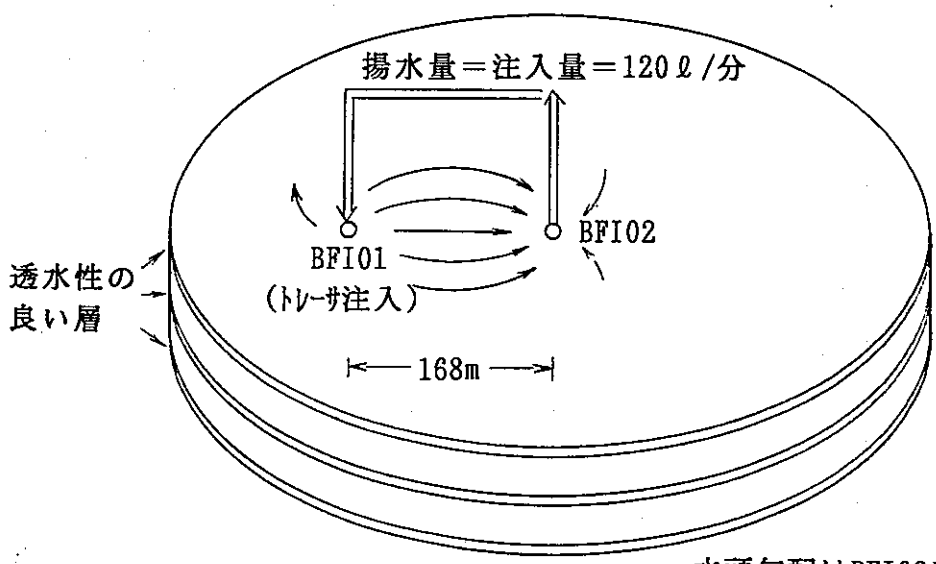
揚　水　試　験



BFI01，KFI11からも
トレーサを注入

水頭勾配はBFI02による揚水により形成される。透水性の良い各層の厚さは薄いので、ほぼ平面上のBFI02に向う２次元的な流れが形成される。

ダイボール試験



水頭勾配はBFI02による揚水とBFI01による注水により形成される。流れは、ほぼ２次元的である。

図－２１　　Ｆｉｎｎｓｊöｎテストケースの体系

表－２３　　Ｆｉｎｎｓｊöｎ揚水試験に関する検討方針

(1)　フィールド試験データ
（関連した室内試験不明で室内試験データ未入手）

(2)　予備検討－１（比較的簡単なモデルによる較正）
- o 目的：比較的簡単な評価モデルでモデルおよび使用パラメータの適合性を概略評価する。
- o 方法：多孔質媒体移流分散モデルによる検討
（マトリックス拡散の効果も含める）
- o 測定データの時間変化との比較によるパラメータ評価
モデルの性質と地下水の流速や分散係数等のフィッテイングによる使用パラメータの概略推定。（モデルの改良点の摘出）

パラメータの概略値

(3)　使用パラメータの設定

(4)　多孔質媒体移流分散モデルによる検討（コードによる検討）
- o 目的：ｉ）FEMWATER＋FEMWASTEの適合性把握
ii）流速，分散係数等のパラメータ値の把握
iii）モデル（およびコード）の改良点の把握
- o 方法：・FEMWATERによる揚水孔への水の速度算出
・FEMWASTEによるサンプリング点の濃度変化算出

パラメータ
変更

(5)　試験結果と計算結果の比較による妥当性検討
試験結果の濃度推移（各種トレーサ）との比較評価に基づく。
- o フィッティングによるパラメータ値の検討
- o 得られたパラメータ値に対する解度解析検討による信頼性検討
- o 評価モデルの改良点の摘出
- o FEMWATER，FEMWASTEの改良点の摘出

パラメータ値
モデルの改良点

モデルの改良点

(6)　代替モデルの検討
①　代替モデルの摘出
（流路の取扱い，マトリックス拡散等）
②　代替モデルによる単純化した体系での計算と、試験結果との比較による代替モデルの適合性検討。
⬇
③　試験結果に対し、適合性の良いモデルの候補選定。

←ダイポール試験結果の検討に基づくモデルの改良点

モデルの改良点

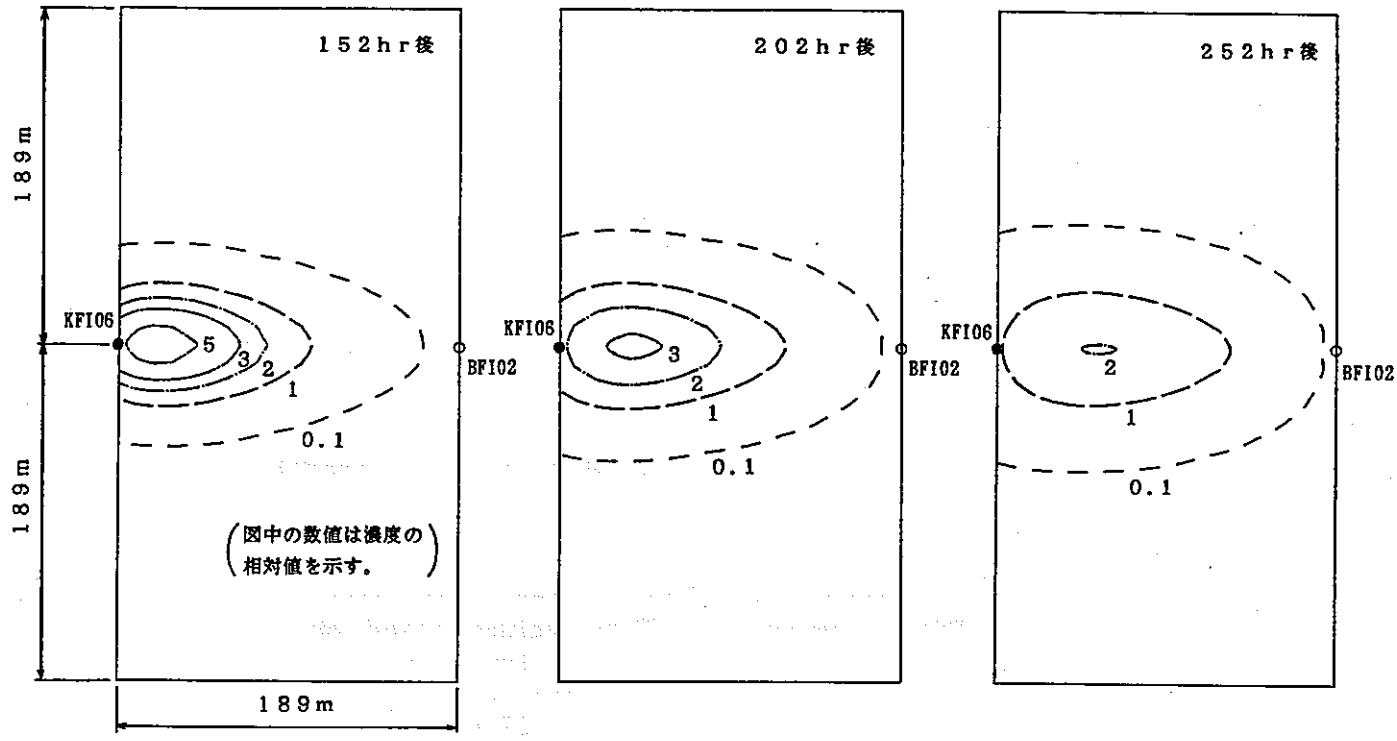
(7)　新モデルによる検討（コードによる検討）
①　コード準備
②　新コードによる計算結果と試験結果の比較検討によるコードの適合性評価

試験結果と整合性が良くない

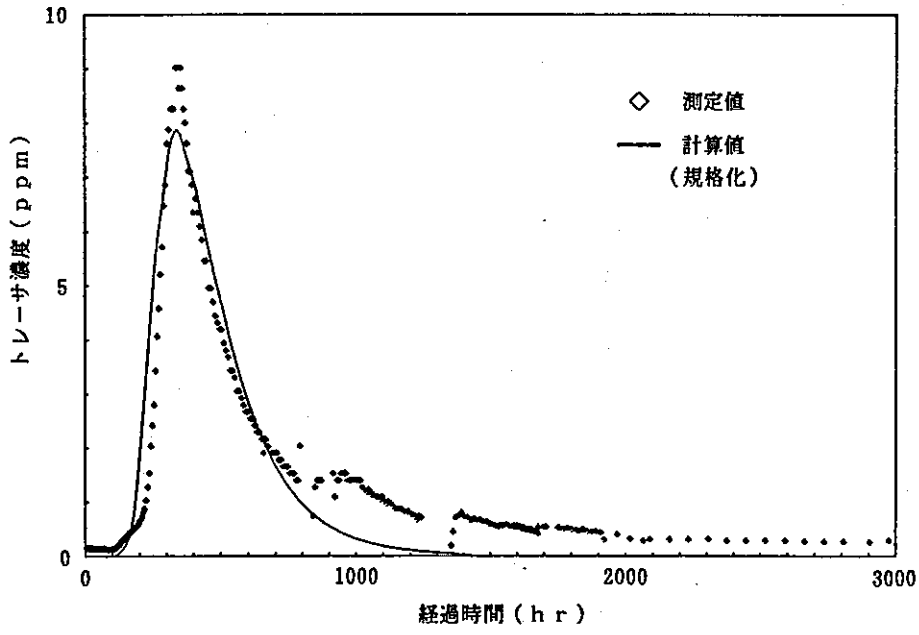
試験結果と計算結果の適合性が良い

(8)　確証された事項および課題評価

確証作業完了



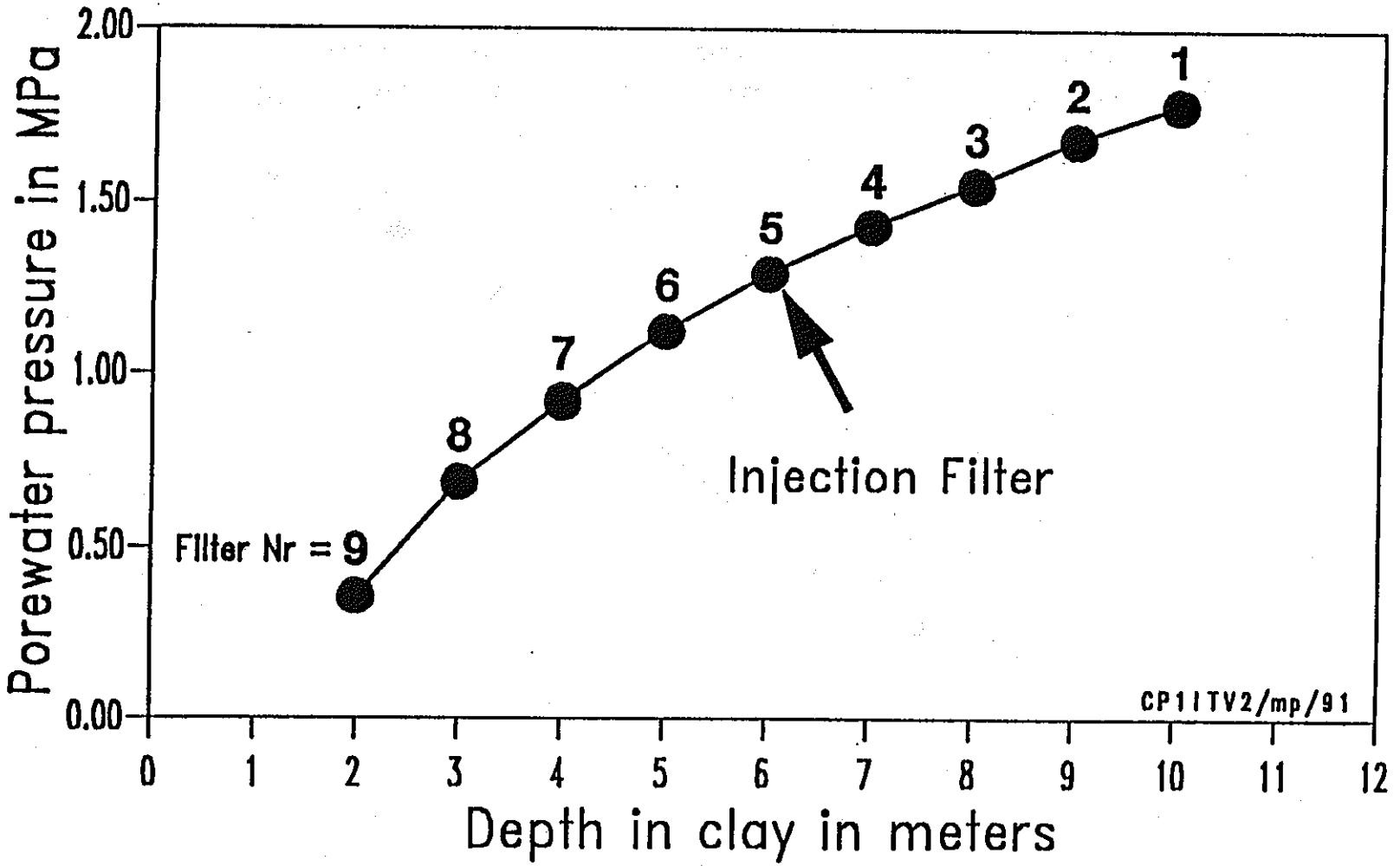
図－２２　トレーサの移行



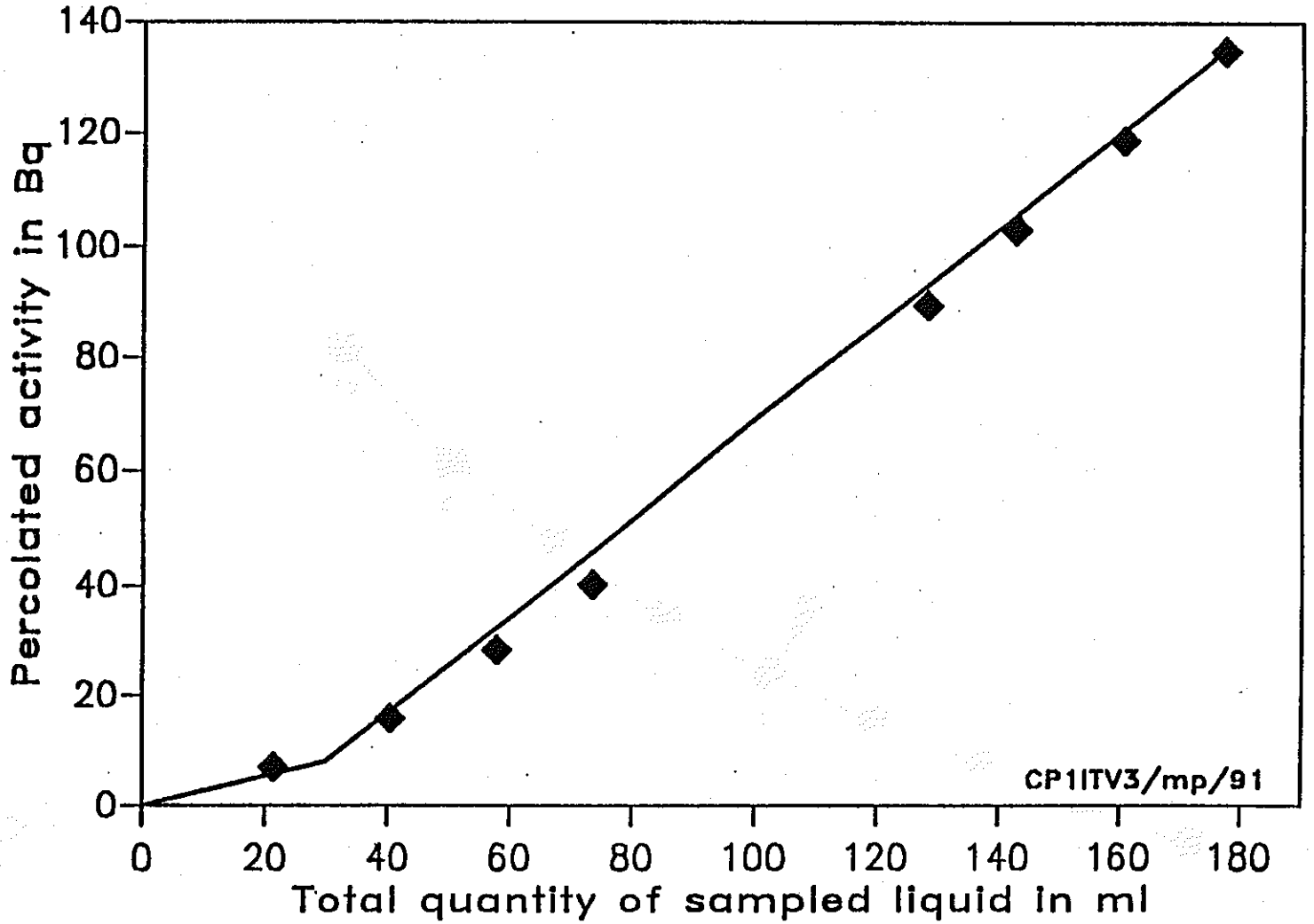
図－２３　出口濃度の測定値と計算値の比較（トレーサI^-）

表－２４　　各フィルタに接続したパイプの内容積

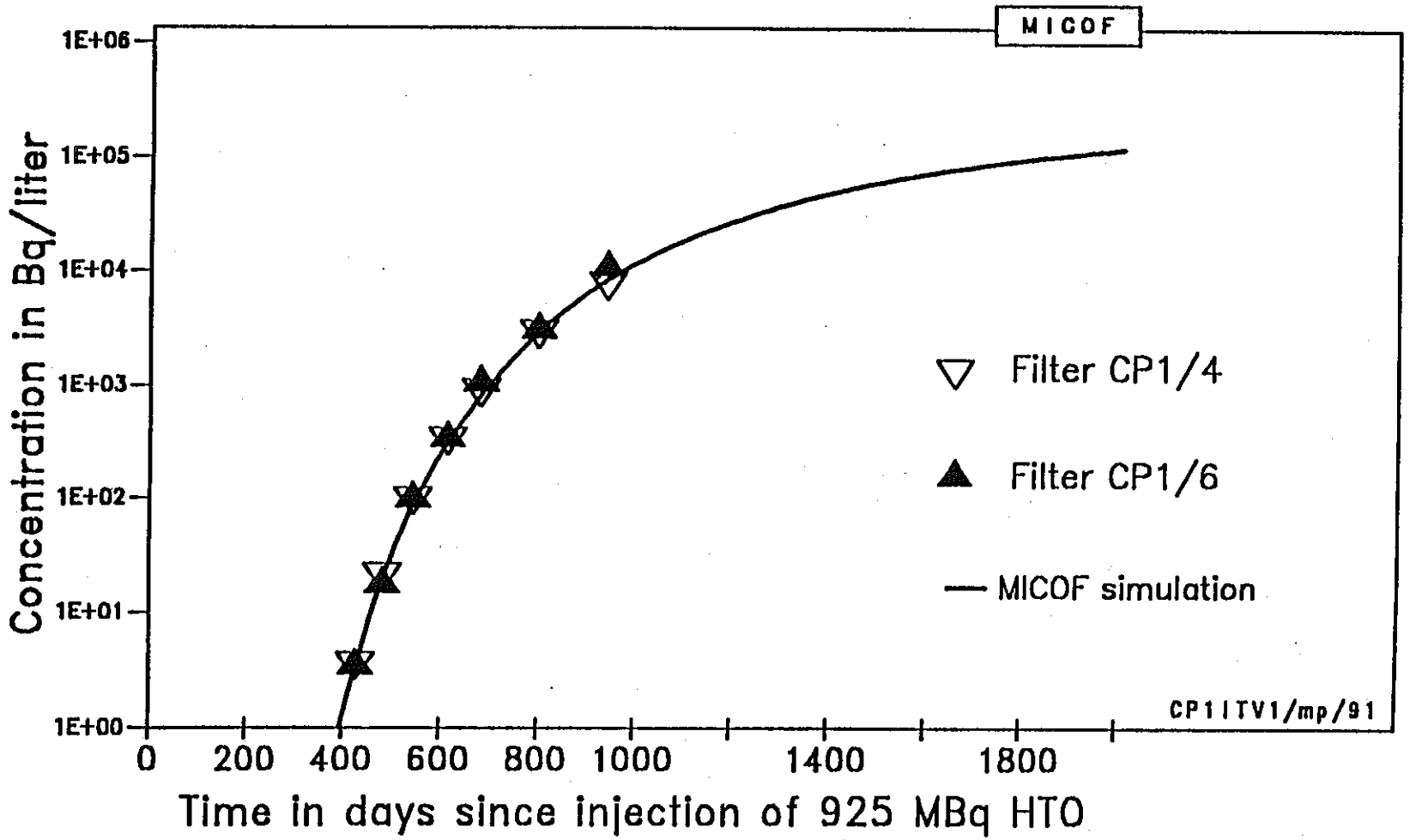
Filter number	Total volume stand pipe (ml)
1	37.68
2	34.54
3	31.40
4	29.83
5	26.69
6	23.56
7	23.55
8	20.41
9	17.27



図－２４　　ＣＰ１における圧力分布



図－２５　　試料No.9の試料量とトリチウム濃度との関係



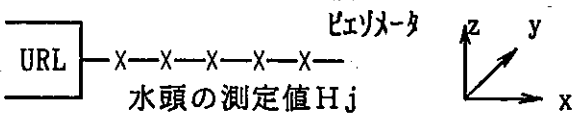
図－２６　　フィルタNo.4とNo.6のトリチウム濃度

表－２５　　Ｍｏｌテストケースに関する検討方針（案）

(1)　サンプリングした粘土の室内試験結果
（詳細データの検討の必要がある）
① K：透水係数（3.2×10^{-12}m/sec）
② φ：ポロシティ（0.35）
③ a：分散長（0.002m）
④ 拡散係数Dm（または、Dm(//),Dm(⊥)）
Dm(//):粘土層に沿った拡散係数（$4.2\times10^{-10}m^2$/sec）
Dm(⊥):粘土層に垂直な拡散係数（$2.0\times10^{-10}m^2$/sec）

（K，a）

(2)　予備検討（単純モデルによる較正）
① 目的：比較的簡単な考察で評価モデル，使用パラメータの適合性および概略を評価する。
② 流れ：x方向にVx（一様）と仮定



$Vx=K\frac{\partial h}{\partial x}$より、Hjを使用してダルシー流速Vxを求める。
③ 核種移行（拡散係数の等方性を仮定）

$$\phi\frac{dC}{dt}=(a|Vx|+\phi Dm)\frac{\partial^2C}{\partial x^2}+\phi Dm\left(\frac{\partial^2C}{\partial y^2}+\frac{\partial^2C}{\partial x^2}\right)-Vx\frac{\partial C}{\partial x}-\lambda\phi C$$

C:トリチウム濃度
λ:崩壊定数
初期条件:No.5フィルタ位置に925MBqのトリチウム，他の場所ではC=0
境界条件:遠方でC=0
④ フィッティングによるパラメータ算出値⇒Dm，$\frac{Vx}{\phi}$
・No.4，No.6の測定値との比較により設定
（No.4とNo.6の測定値に殆ど差がないため(図-24)
Vxは無視できる可能性大。）

（Dm，$\frac{Vx}{\phi}$）

(3)　計算に使用するパラメータ設定
（Dm，φ，K等）

パラメータ見直し

K

(4)　水の流れ評価
① 使用コード：３次元コード必要。
（２次元円筒座標(R，Z，角度方向に対称)でもよいと考えられる。）
② 計算方法（案）
・$V=KVh$より、水のダルシー流速Vを算出
（K:透水係数，h:水頭）
・計算条件：ピエゾメータ部の測定された水頭Hjを再現するよう、h，Vの分布を求める。
・計算体系：水の吸い込み口をシャフトかまたはその他の場所か検討後設定。

計算条件見直し

Dm，φ，a

ダルシー速度分布V

(5)　核種の移行評価（濃度分布算出）
① 使用コード：３次元の移流分散コード必要
水の速度分布に近似を用いると２次元円筒座標でも使用できる可能性がある。
② 計算方法（案）

$$\frac{dC}{dt}=\sum_i\left[\frac{\partial}{\partial x_i}\left(D^*i\frac{\partial C}{\partial x}\right)-Vi\frac{\partial C}{\partial x_i}\right]-\lambda C$$

D*:分散係数，Vi=ポア速度
・初期条件：フィルタNo.5の位置に925MBqのトリチウム、他の地点C=0
（粘土層へのトリチウムの注入を時間の関数で設定する必要があるかどうかは要検討。）
・境界条件：遠方でC=0

計算条件，評価モデル見直し

濃度分布C

(6)　試験結果と計算結果の比較
フィルタNo.4とNo.6の地点で測定濃度との比較検討

不整合

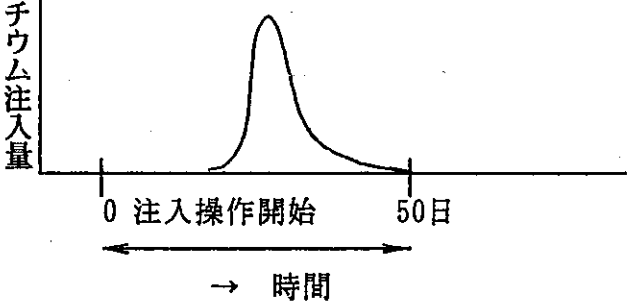
計算結果は試験結果を再現

(7)　設定したパラメータ値の感度解析
測定データのばらつきを考慮して解の信頼性検討

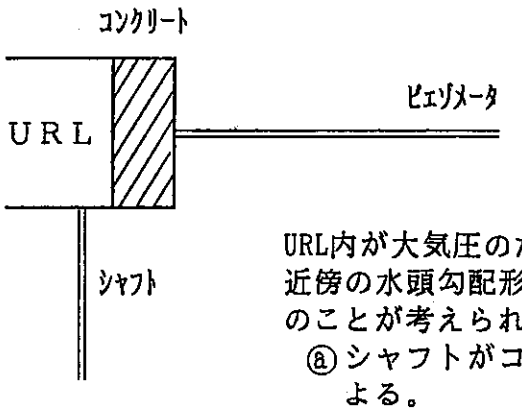
(8)　確証された事項および課題評価

確証作業完了

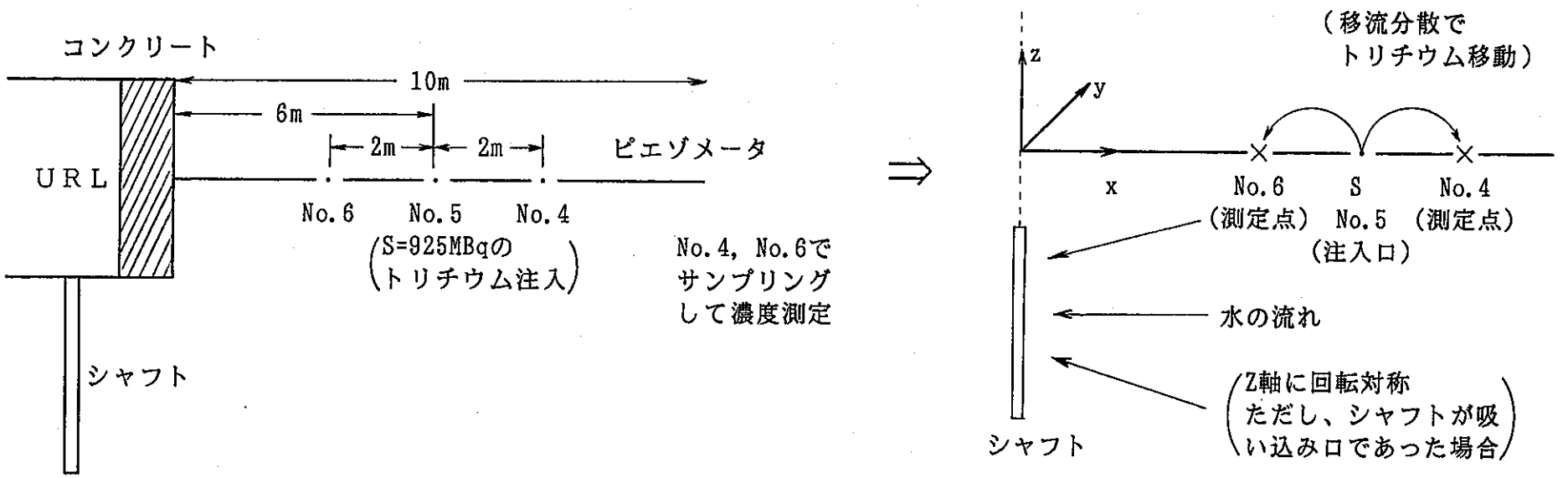
粘土層へのトリチウムの注入
試験体系の詳細データより検討するがパルス状の可能性が大きい。



ピエゾメータ近傍の水頭勾配の形成（図－22参照）



URL内が大気圧のため、ピアゾメータ近傍の水頭勾配形成の原因として以下のことが考えられる。
ⓐシャフトがコンクリートレンガによる。
ⓑURLの端部のコンクリート
原因は詳しい体系データを基に検討。



図－２７　　Ｍｏｌテストケースの評価体系

7．プロセスコードの検証

7.1　検証実施範囲の選定

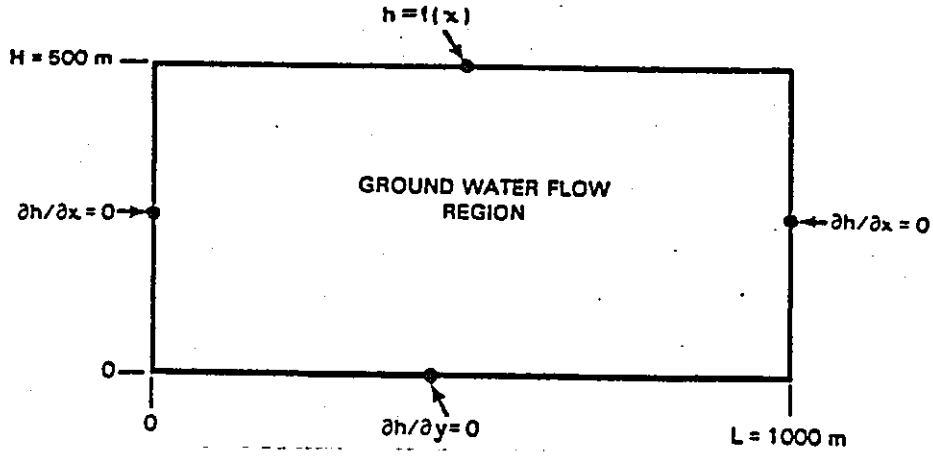
7.1.1　概要

本研究によるコード検証は、ファーフィールドでの性能評価を想定した多孔質媒体中の飽和流と核種移行を対象とし、コードの基本計算能力の確認を基本方針とする。

元年度の委託研究では、計画した検証プランのうち、FEMWASTE-PNCコードを対象に2次元移流－分散問題等の検証計算を実施した。本年度研究では、FEMWATERコードを対象に2次元定常解（飽和定常流）－検証ケース名F1（元年度）－の検証計算を実施する。

7.1.2　問題の内容

一定勾配の地下水面を持ち、不透水境界で囲まれた等方均質な媒体中の2次元定常流れをシミュレーションする。



図－28　解析領域

・基礎式

$$\frac{\partial^2 h}{\partial x^2} + \frac{\partial^2 h}{\partial z^2} = 0$$

・境界条件

底面、側面で

$$\frac{\partial h(0,z)}{\partial x} + \frac{\partial h(L,z)}{\partial x} + \frac{\partial h(x,0)}{\partial z} = 0$$

上部表面で

$$h(x)=H+x\cdot\tan\alpha$$

検証方法はDomenicoの解析解と比較する。

$$h=\left(H+\frac{L\tan\alpha}{2}\right)-\frac{4\tan\alpha}{L}\sum_{m=0}^{\infty}\frac{\cos(\xi_m X)\cosh(\xi_m z)}{\xi_m^2\cosh(\xi_m H)}$$

$$\xi_m=\frac{(2m+1)\pi}{L}$$

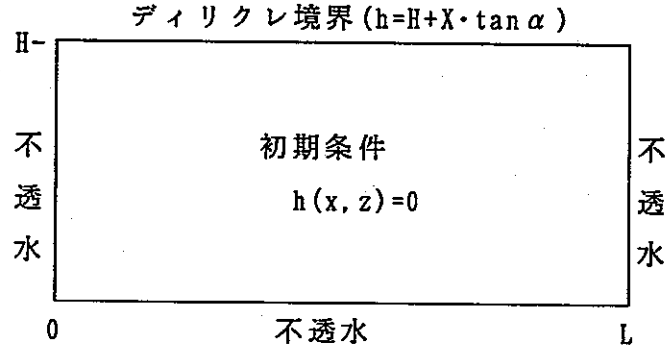
$$U=-\frac{4K\tan\alpha}{L}\sum_{m=0}^{\infty}\frac{\sin(\xi_m X)\cosh(\xi_m Z)}{\xi_m\cosh(\xi_m H)}$$

$$V=\frac{4\tan\alpha}{L}\sum_{m=0}^{\infty}\frac{\cos(\xi_m X)\sinh(\xi_m Z)}{\xi_m\cosh(\xi_m H)}$$

7.2 検証計算と評価

7.2.1 計算パラメータ

計算に使用した初期及び境界条件とパラメータを以下に示す。



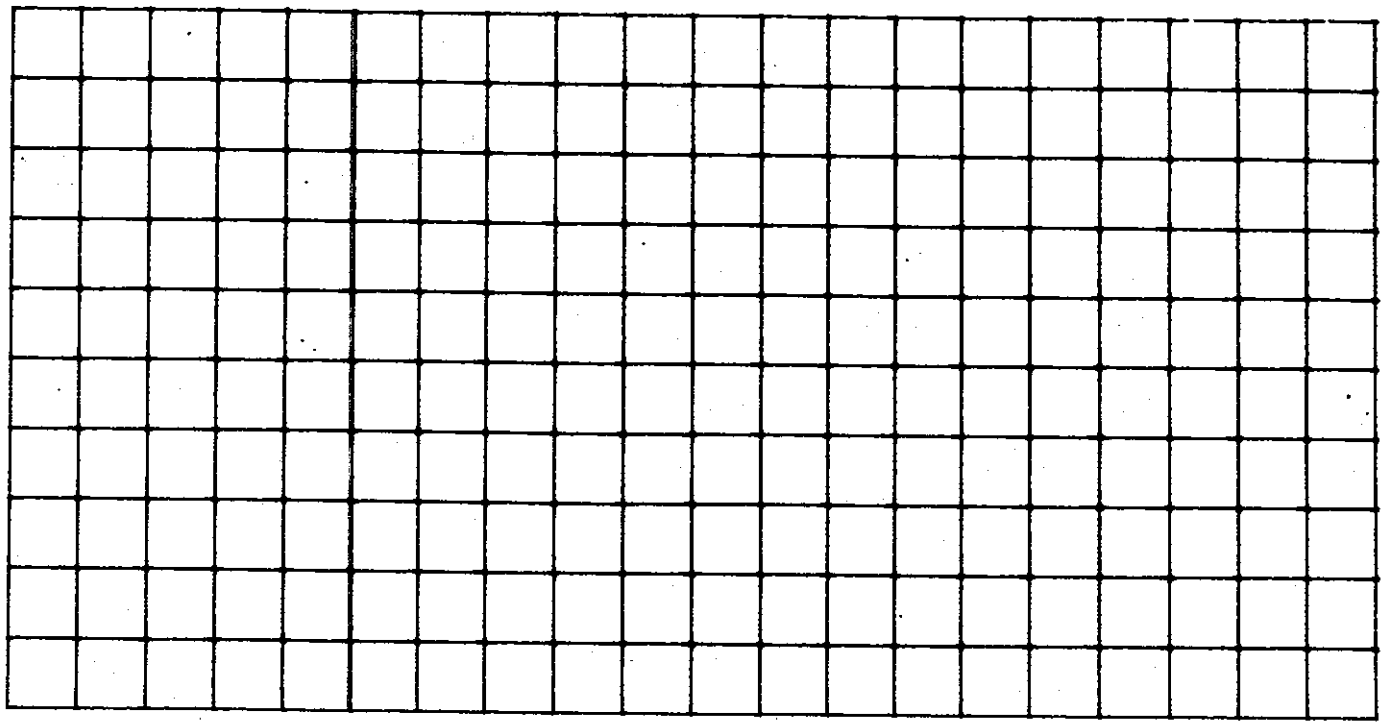
領域幅	L=1000 (m)
領域深さ	H= 500 (m)
透水係数	K=10, 0.1, 0.001 (m/y)
地下水面の勾配	$\tan\alpha$ =0.01, 0.1 (-)
空隙率	ϕ =0.01
水密度	ρ_f=1000(kg/m^3)
圧縮率	$\alpha=\beta=0$
動加速度	g=9.7530×10^{15} (m/y^2)
動粘性係数	η =4.122×10^4 (kg/m/yr)

7.2.2 メッシュ

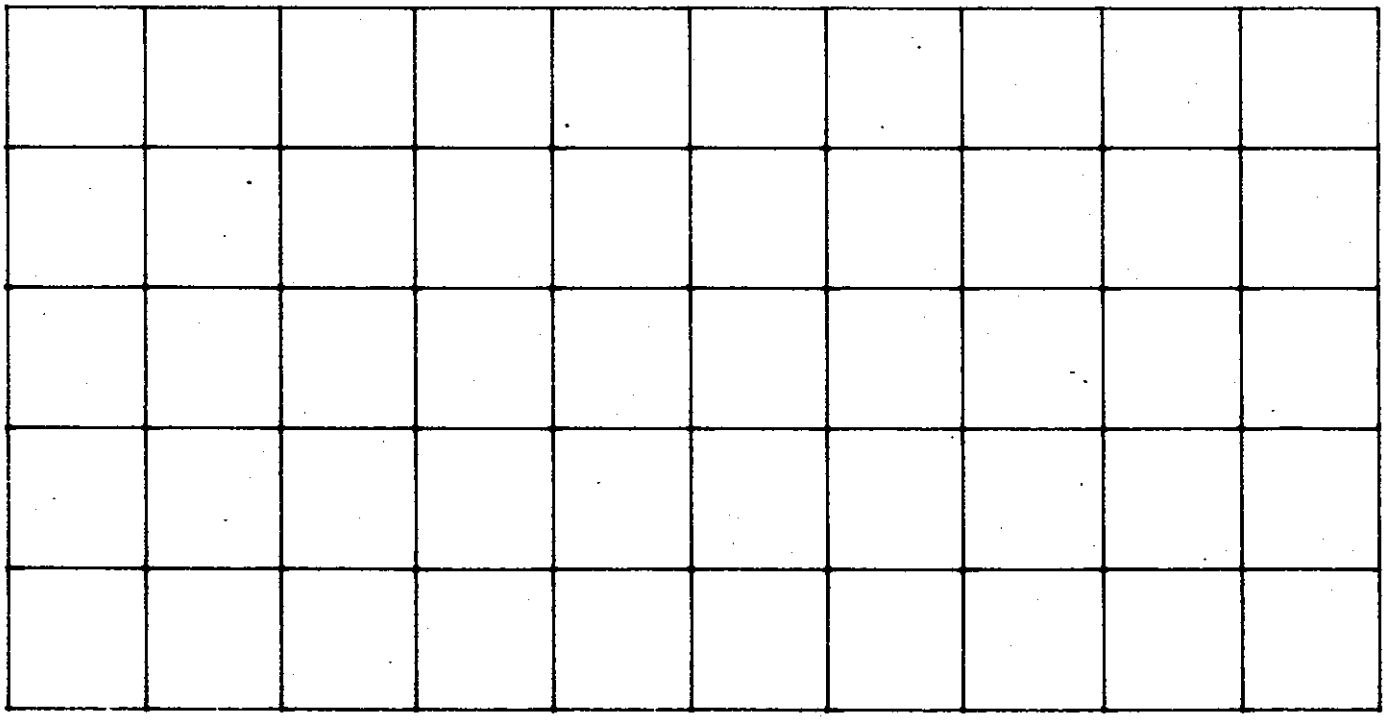
6種類のメッシュを用いて計算を行った。図29～34に各メッシュの分割図を示す。また、各メッシュの要素数、節点数は以下の通り。

表－26　　要素数及び節点数

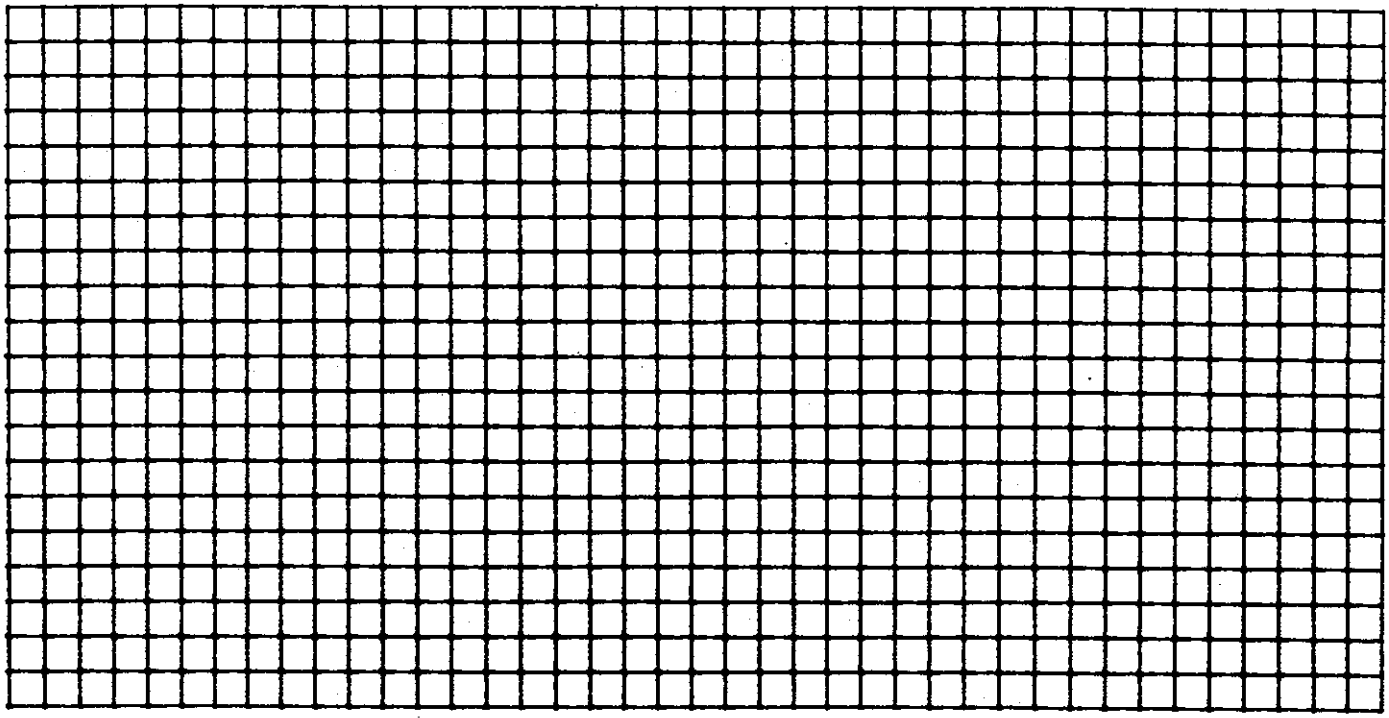
メッシュ	要素数	節点数	
1	200	231	ΔX=ΔZ=50
2	50	66	ΔX=ΔZ=100
3	800	861	ΔX=ΔZ=25
4	242	276	境界近傍細分割
5	242	276	境界近傍細分割
6	288	325	境界近傍細分割



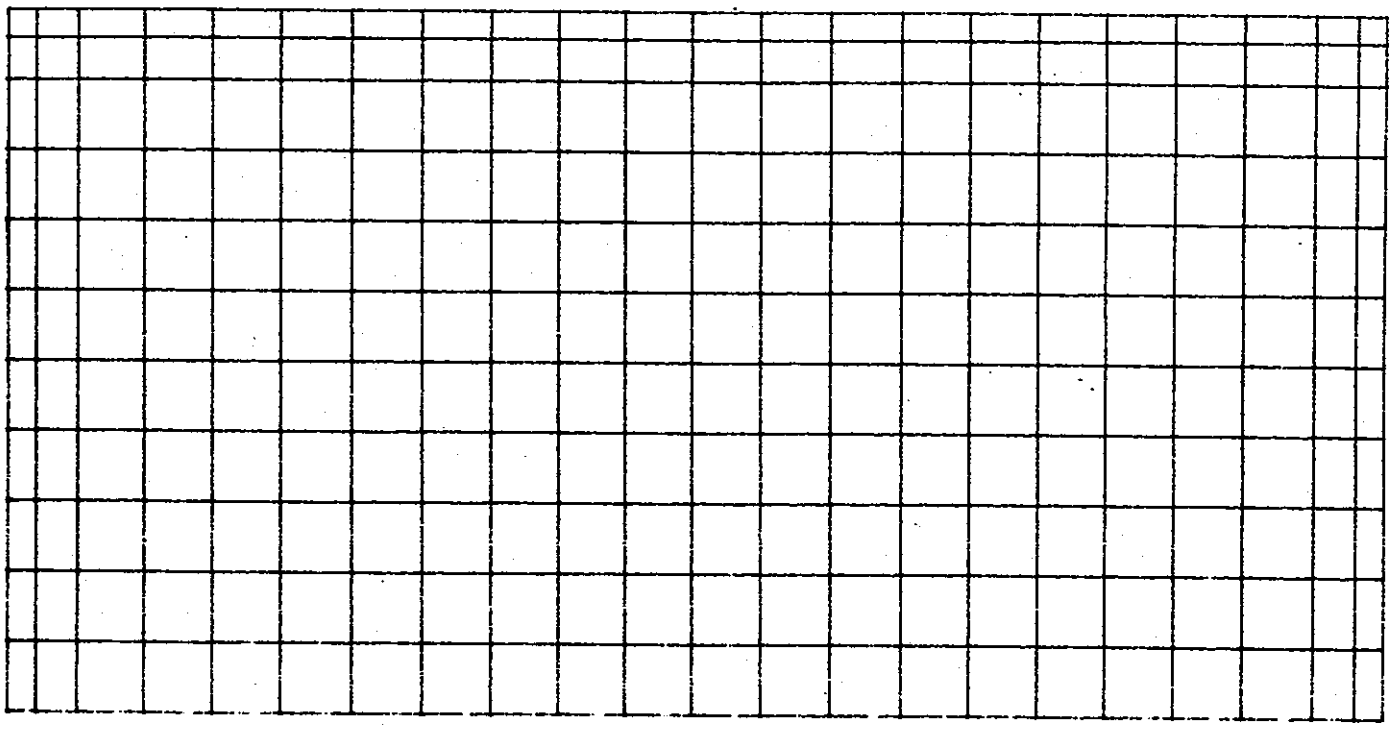
図－29　要素分割図（メッシュ１）



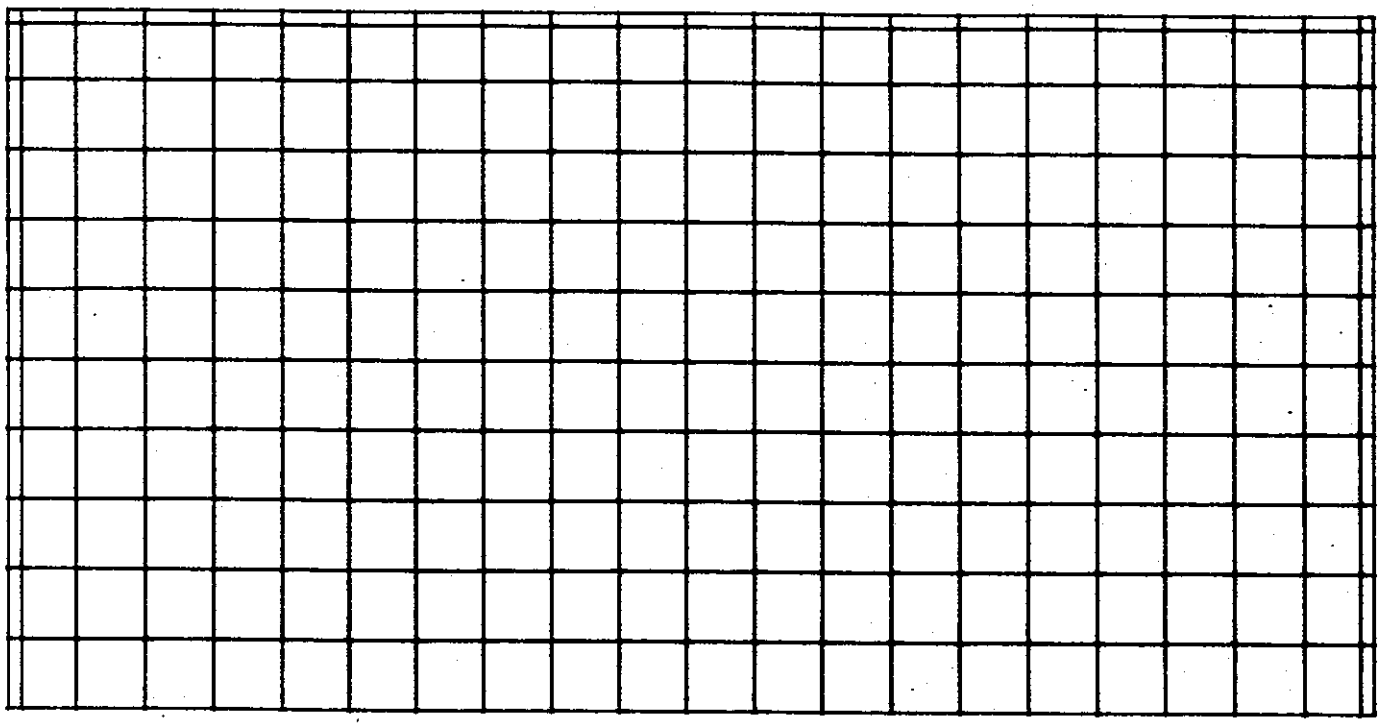
図－30　要素分割図（メッシュ２）



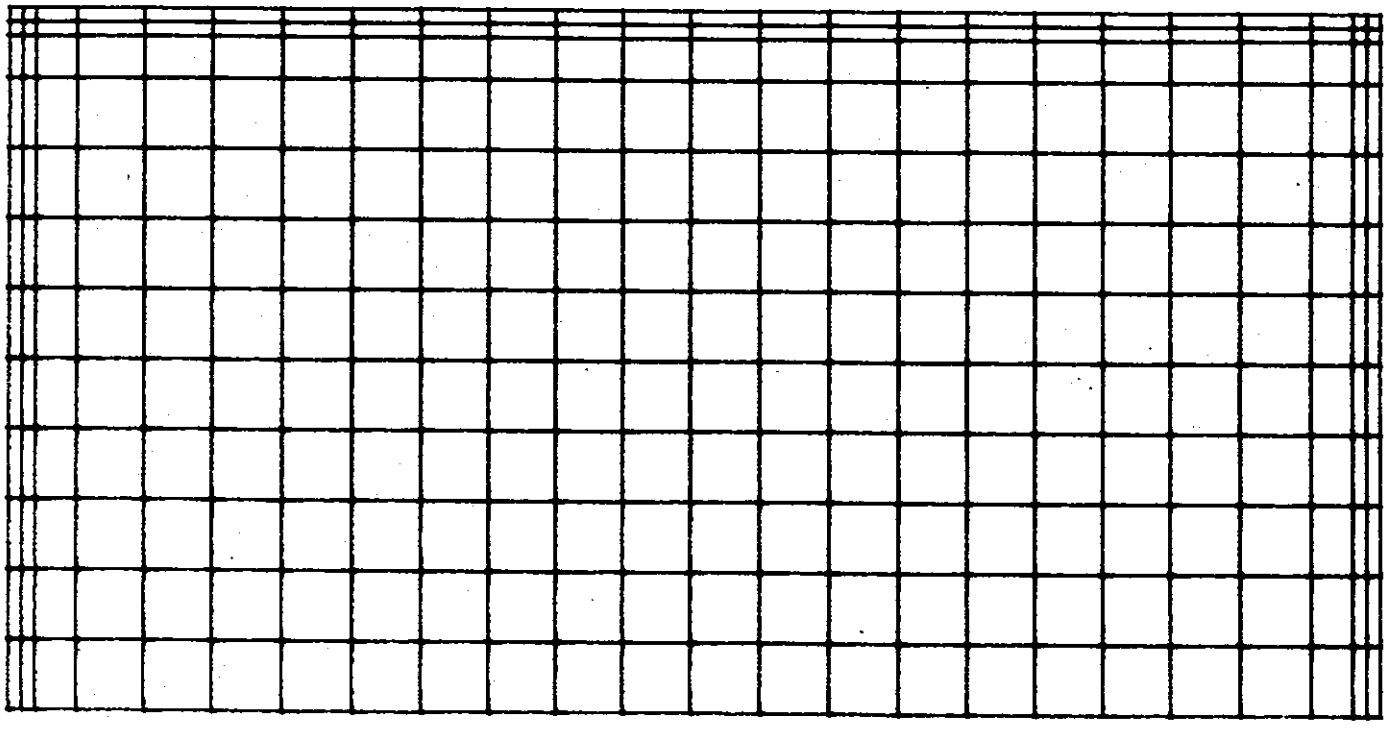
図－31　要素分割図（メッシュ３）



図－32　要素分割図（メッシュ４）



図－33　要素分割図（メッシュ５）



図－34　要素分割図（メッシュ６）

7.2.3 計算ケース

透水係数、地下水面の勾配及びメッシュの違いなどから15の計算ケースを考えた。表－27に設定した計算ケースの一覧を示す。

表－27　計算ケース

ケース	透水係数			勾配 (tan α)		メッシュ	備考
	0.1	0.001	10.0	0.01	0.1		
1	○			○		1	・透水係数の影響評価
2		○		○		1	
3			○	○		1	
4	○			○		2	・透水係数の影響評価
5		○		○		2	・要素分割の比較(↔ケース1,2,3)
6			○	○		2	
7	○				○	1	・地下水勾配の比較(↔ケース1,2,3)
8		○			○	1	
9			○		○	1	
10	○				○	2	・要素分割の比較(↔ケース7)
11	○			○		3	・要素分割の比較(↔ケース1,4)
12	○			○		4	
13	○			○		5	
14	○			○		6	
15	○			○		1	・空隙率(ϕ=0.1)の影響(↔ケース1)

7.2.4 計算結果

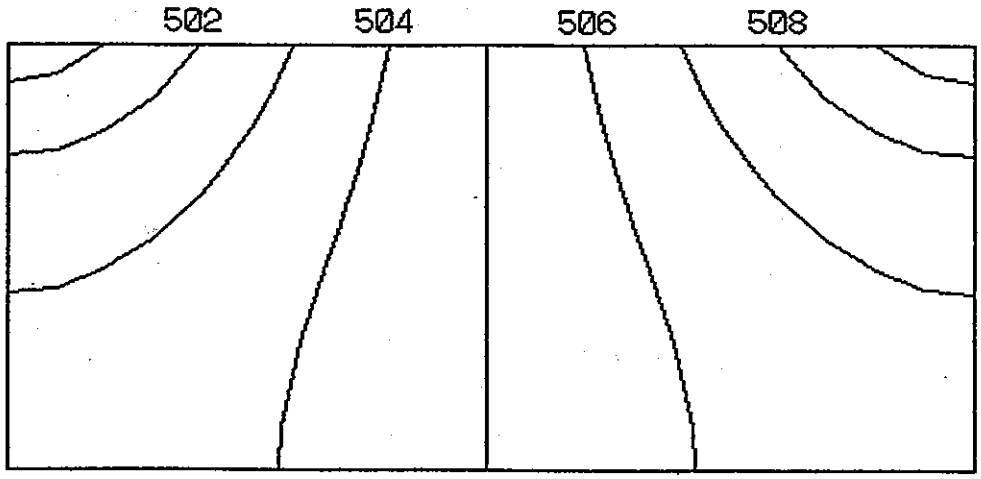
(1) 水頭分布

得られた水頭（全水頭）結果の中から、ケース1，4，7，11，12，13の等水頭線図を図-35～40に示す。問題の諸条件及び境界条件から、得られた水頭分布は物理的に妥当な結果である。

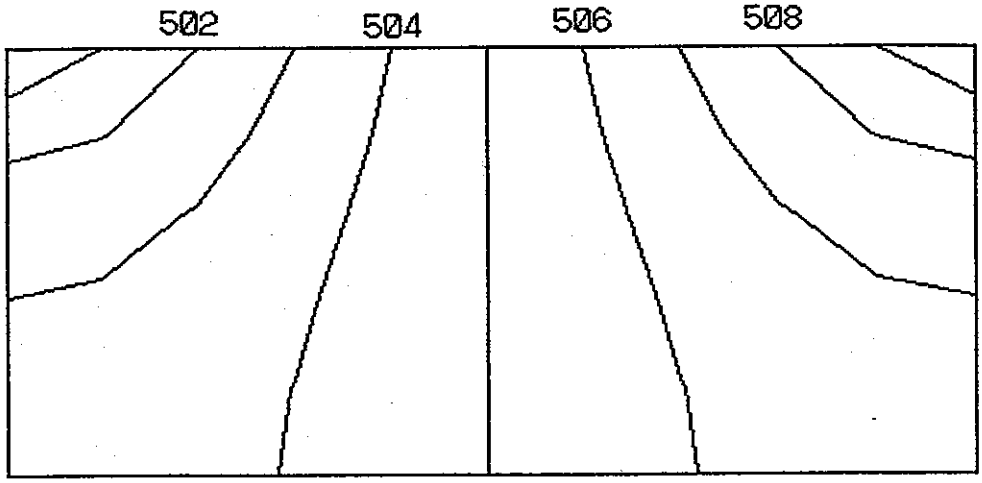
ケース1，2，4，7，10，11，12，13，14の各ケースについて、水頭の水平分布及び垂直分布を図－41～49に示す。各分布とも非常に良く解析解と一致している。透水係数を変えたケース(1↔2)を比べると、全く同一の水頭分布が得られている。また、地下水面の勾配を変えたケース(7，10)でも正確な解を求めている。

表-28に各ケースの最大相対誤差を示す。表より、各ケースの最大相対誤差は 0.07 % 以下であり、非常に良好な結果が得られた。ケース7～10は地下水面の勾配が 0.1 の場合で他のケースより10倍大きなケースであるが、相対誤差も1桁程大きな値となっている。また、ケース1，4，11（メッシュ幅が50，100，25）を比較すると、メッシュ幅が倍になると、相対誤差も倍になっている。境界近傍で細かくメッシュを切ったケース(12～14)では、小さな誤差となっている。

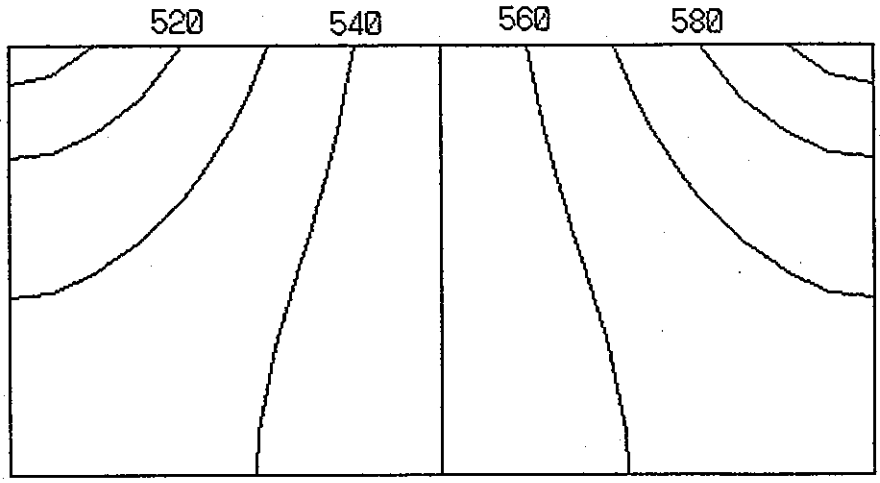
また、透水係数を変えたケース（1～3、4～6、7～9)及び空隙率を変えたケース（1↔15)を比べると、全く同じ水頭分布が得られた。基礎式から明かな様に、水頭はこれらのパラメータには依存せず、コードの妥当性が分かった。



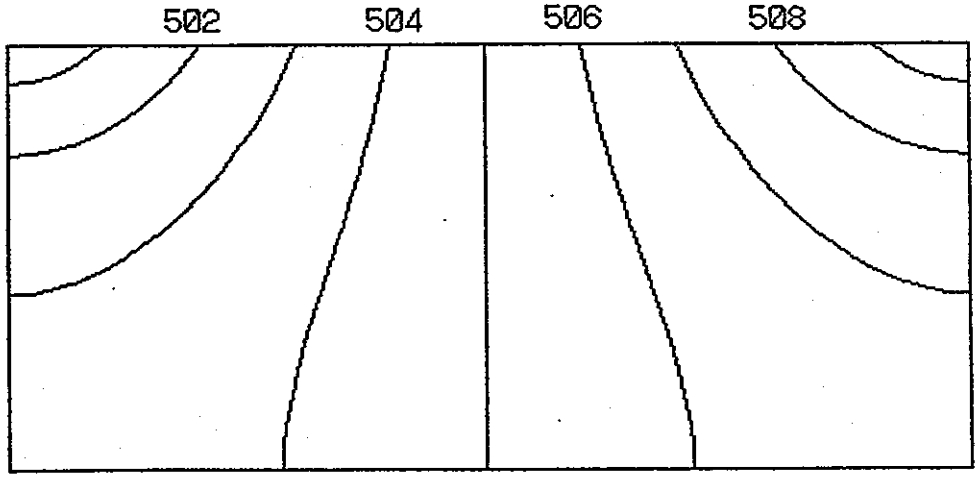
図－35　等水頭線図（ケース１）



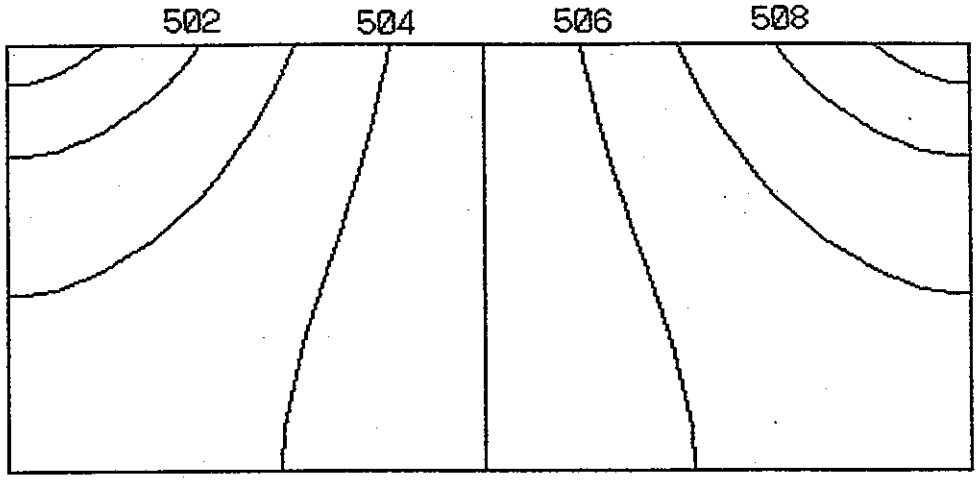
図－36　等水頭線図（ケース４）



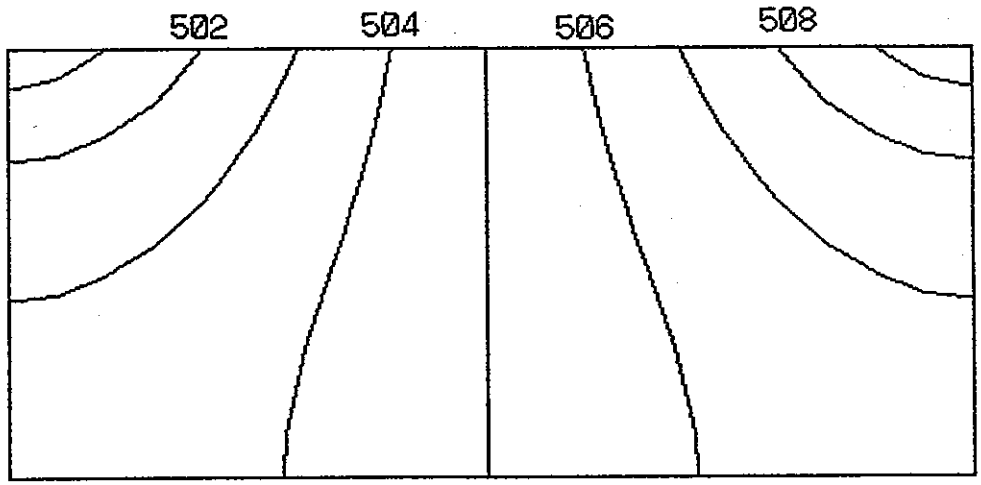
図－37　等水頭線図（ケース７）



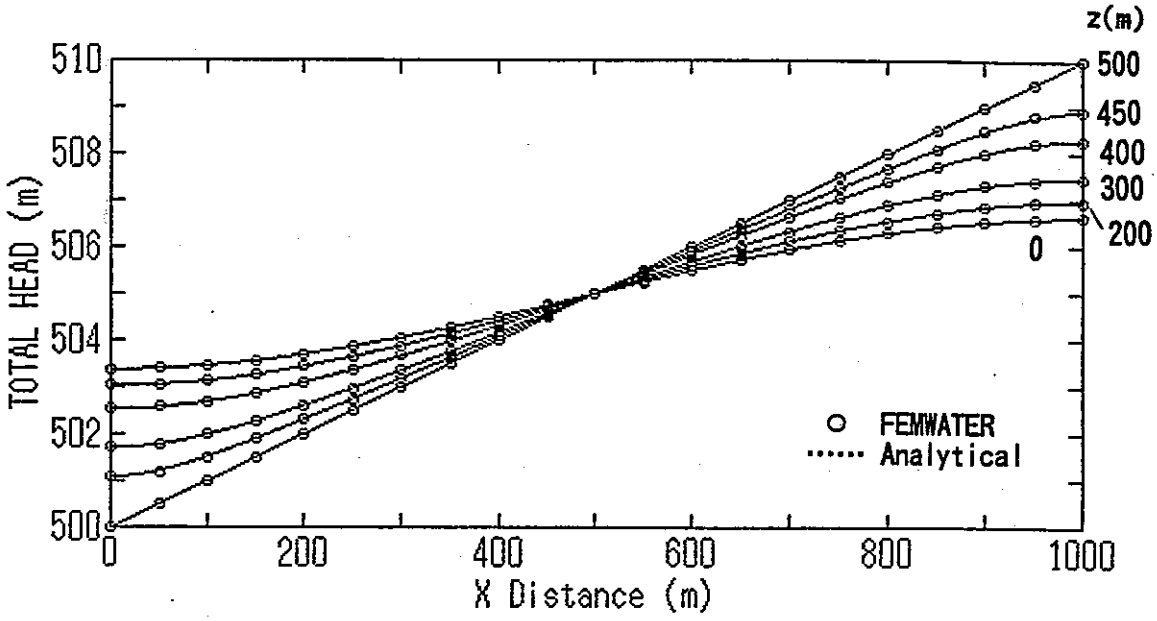
図－38　等水頭線図（ケース11）



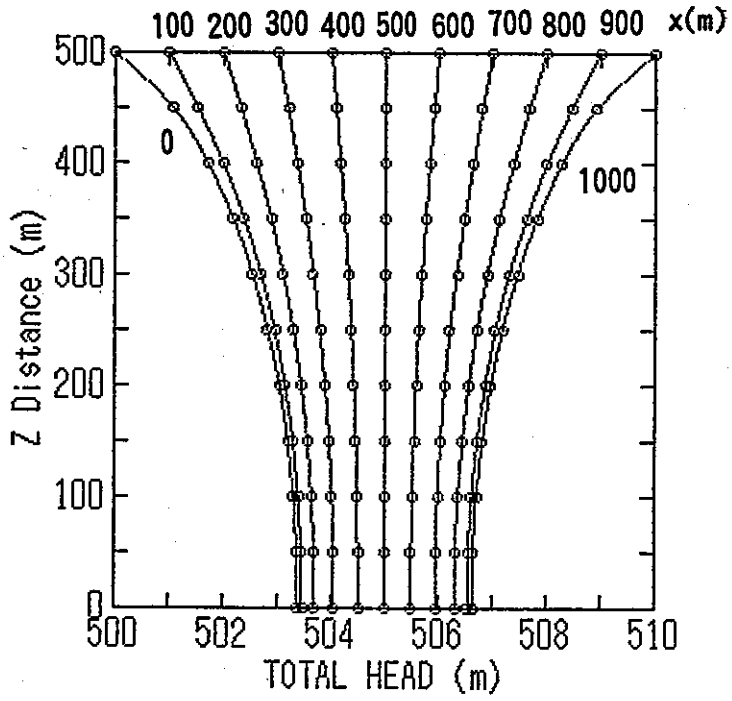
図－39　等水頭線図（ケース12）



図－40　等水頭線図（ケース13）

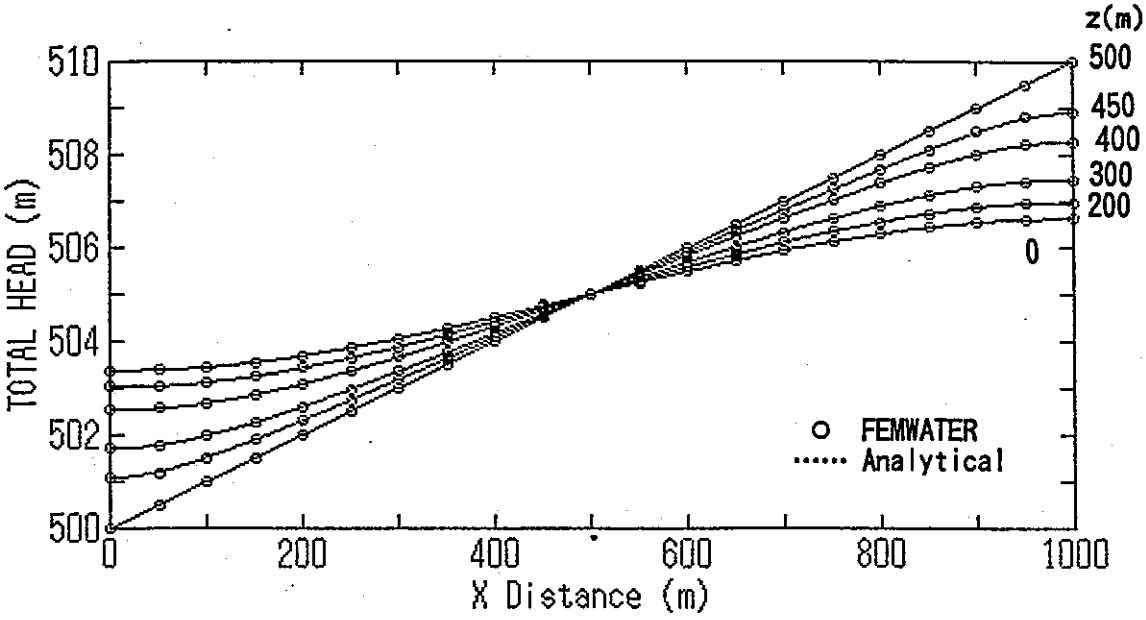


(a)水平分布

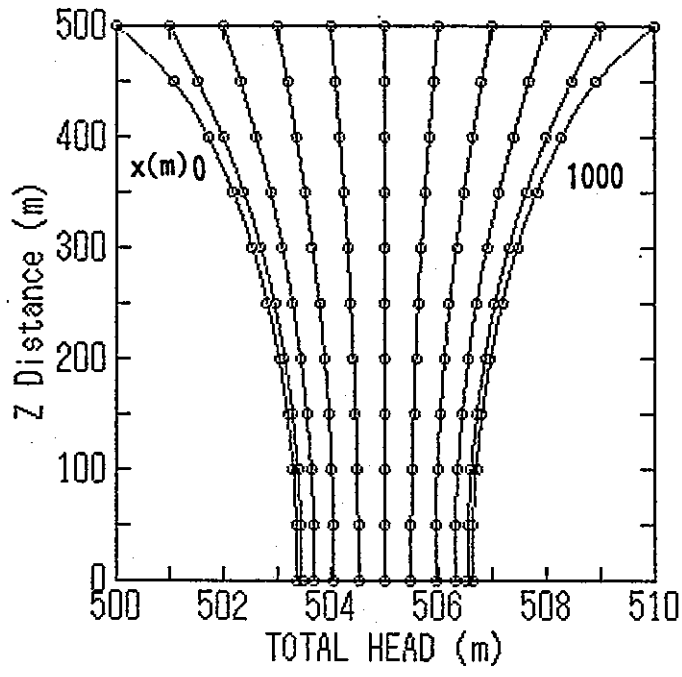


(b)垂直分布

図－41　水頭分布（ケース１）

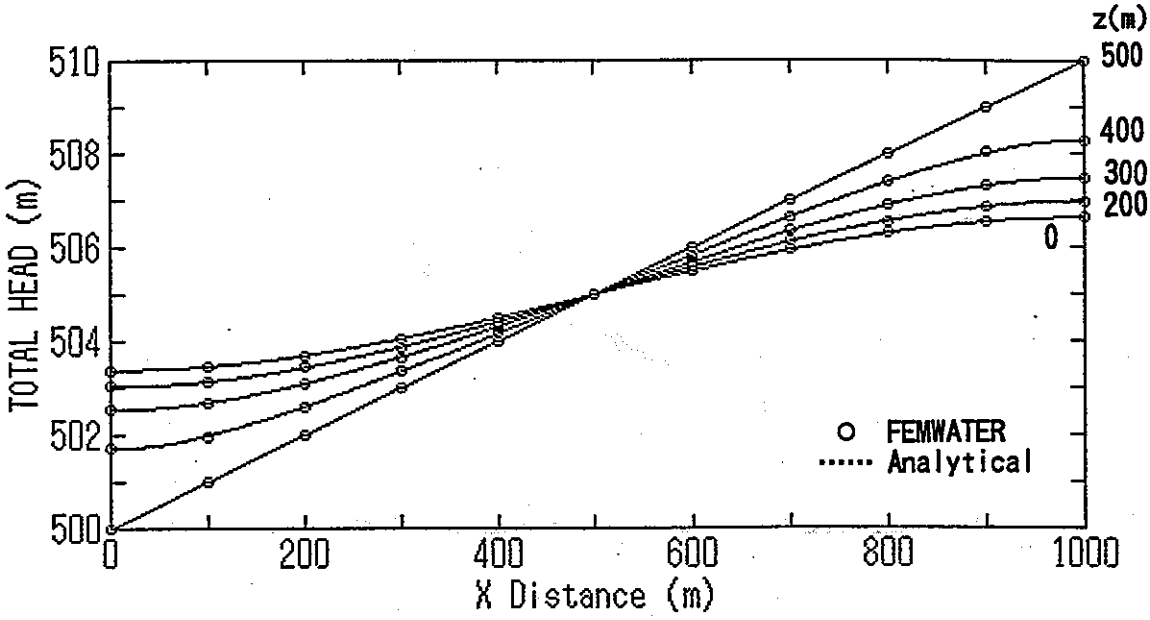


(a)水平分布

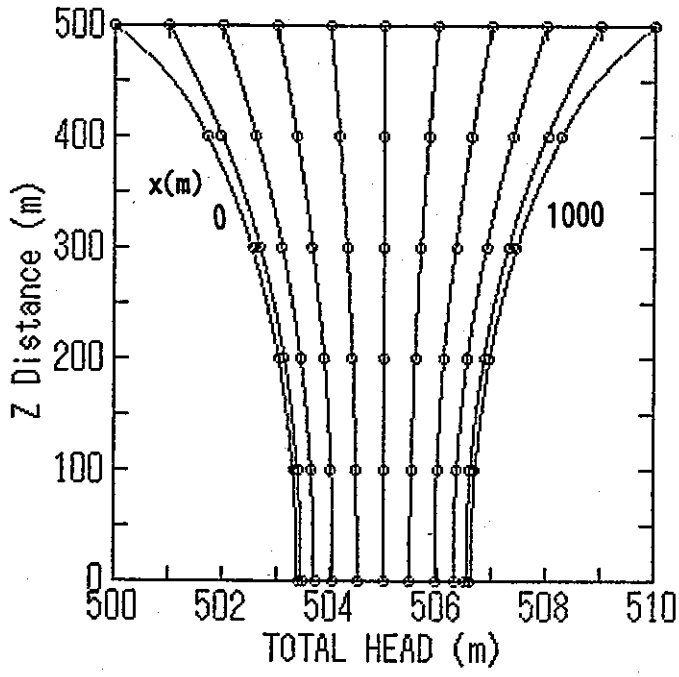


(b)垂直分布

図－42　水頭分布（ケース２）

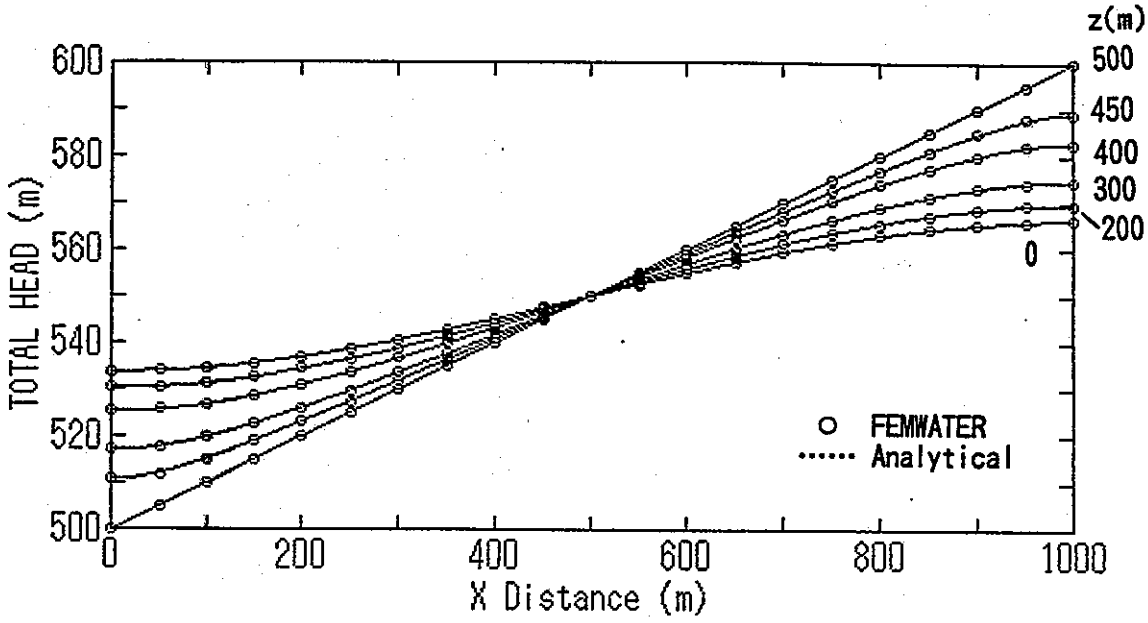


(a)水平分布

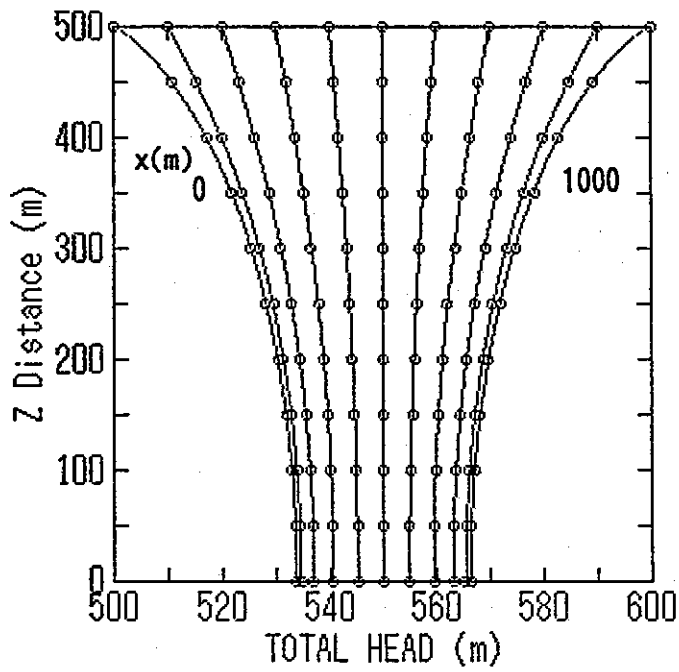


(b)垂直分布

図－43　水頭分布（ケース４）

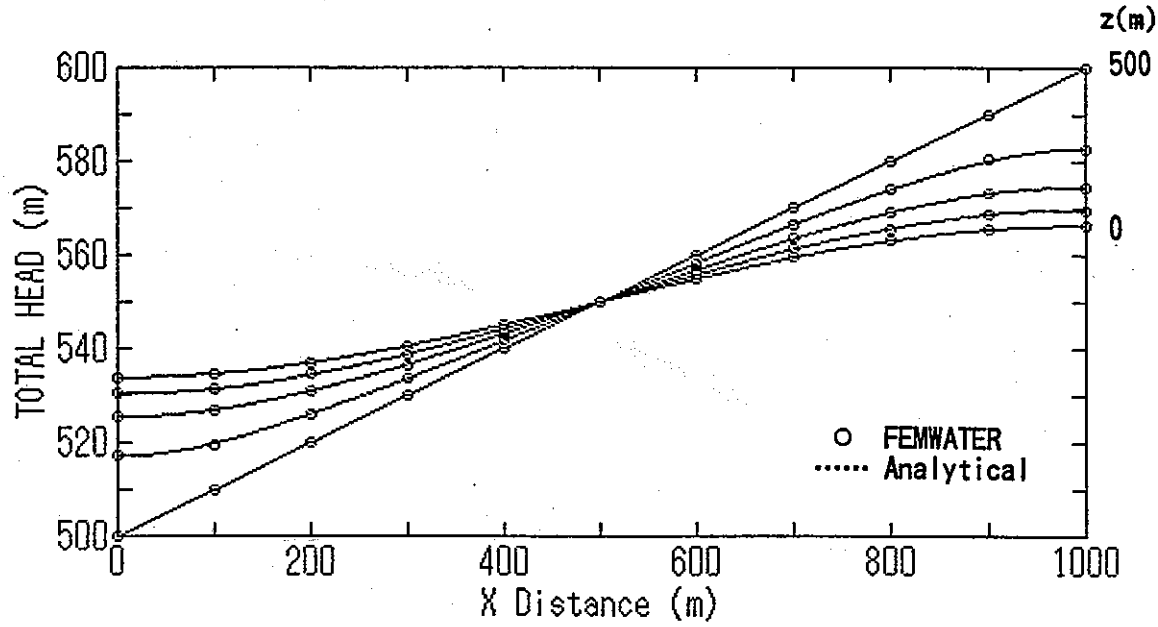


(a)水平分布

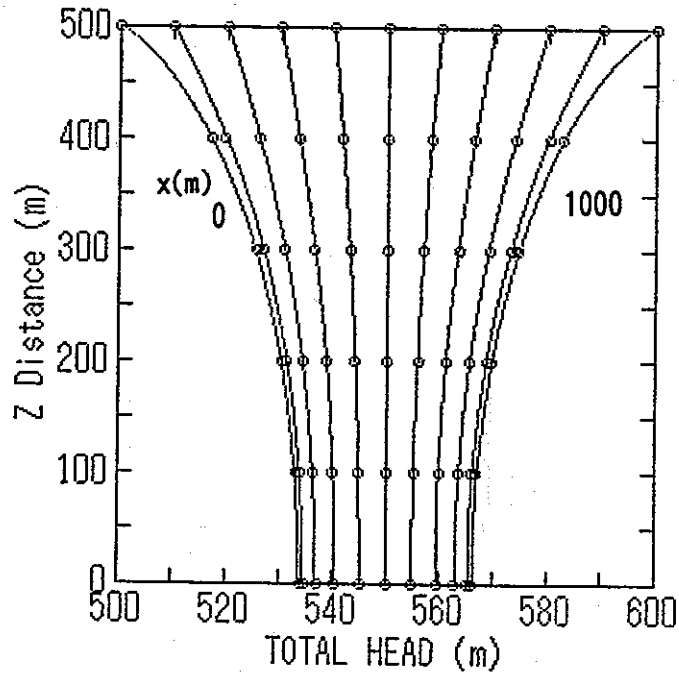


(b)垂直分布

図－44　水頭分布（ケース７）

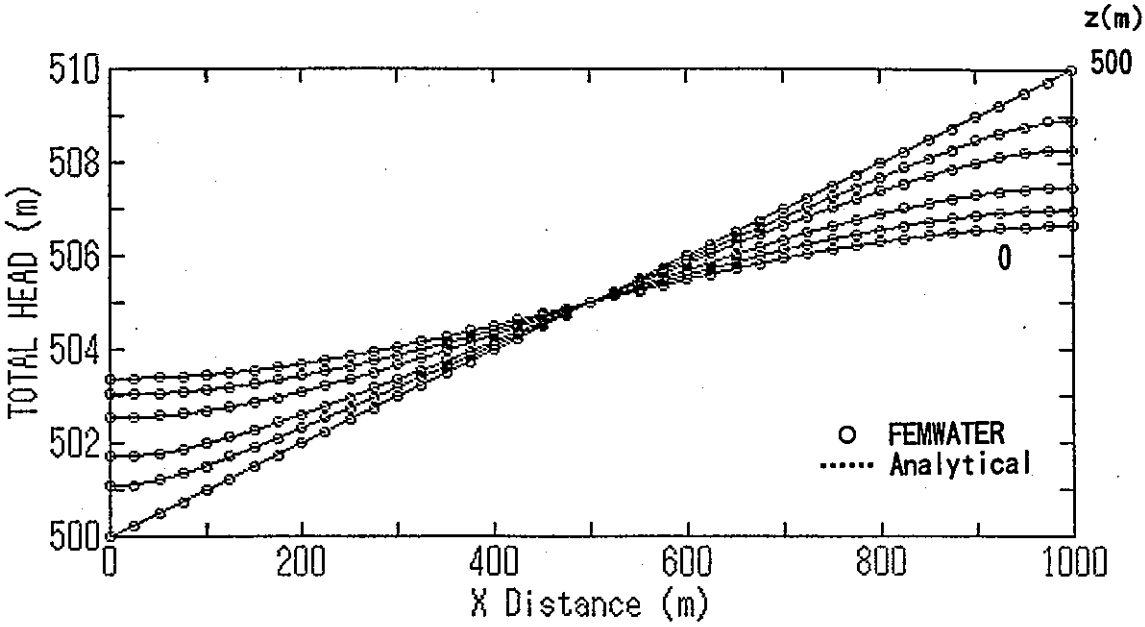


(a)水平分布

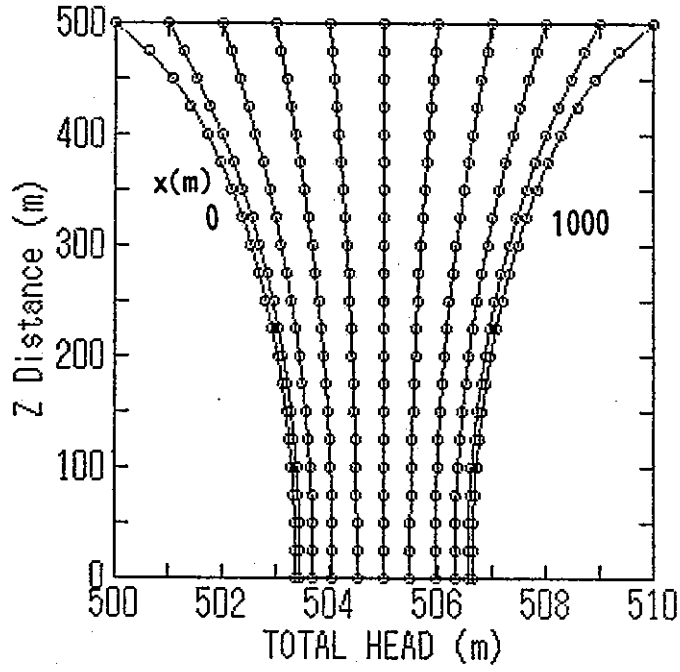


(b)垂直分布

図－45　水頭分布（ケース10）

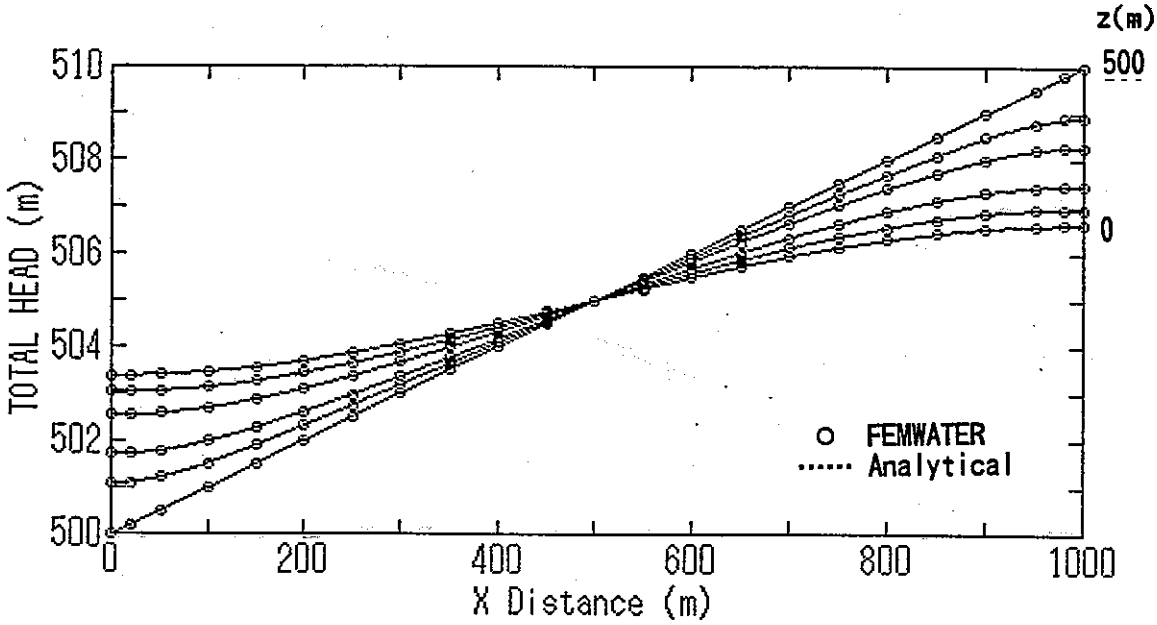


(a)水平分布

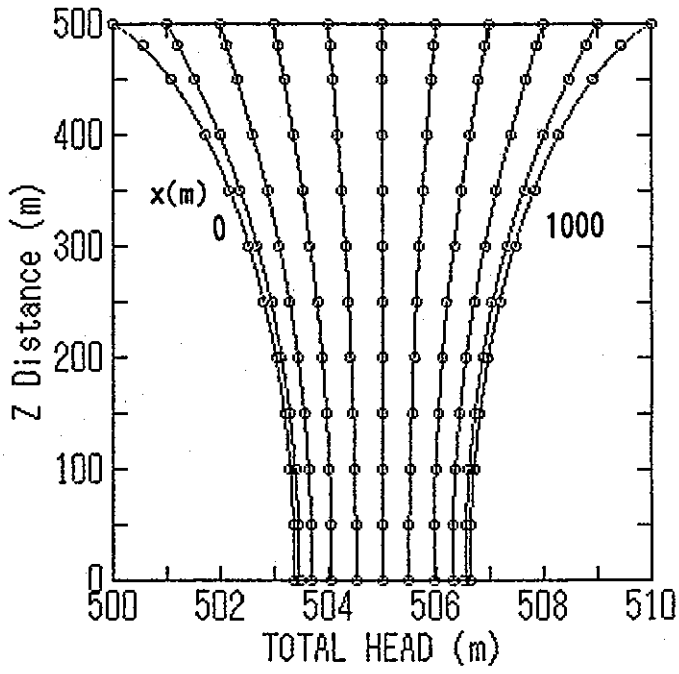


(b)垂直分布

図－46　水頭分布（ケース11）

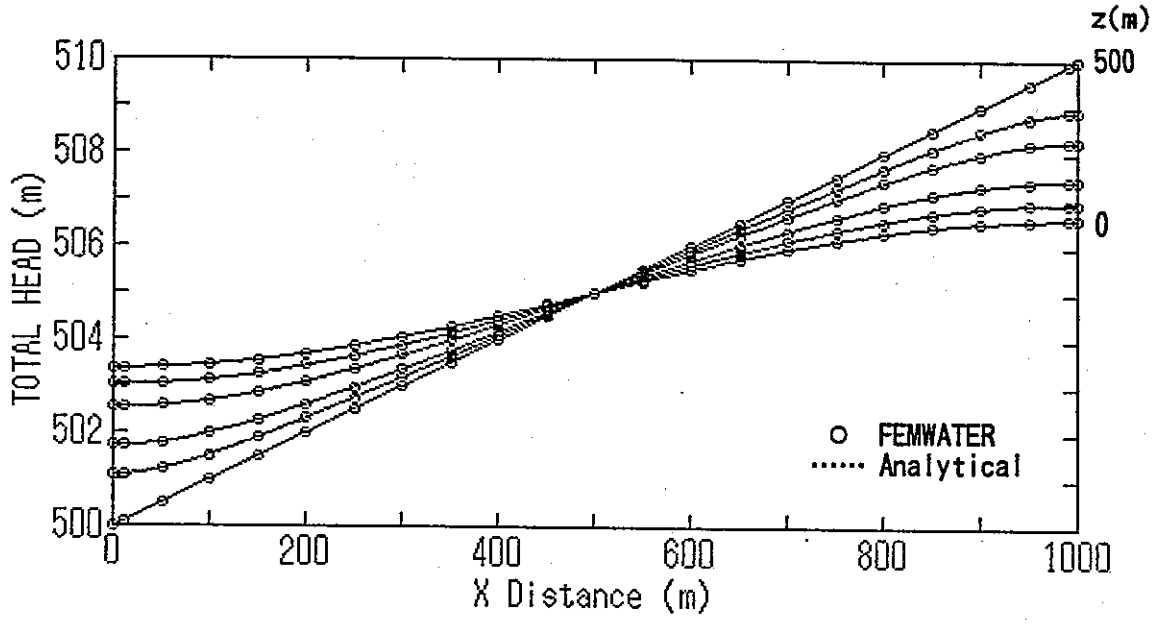


(a)水平分布

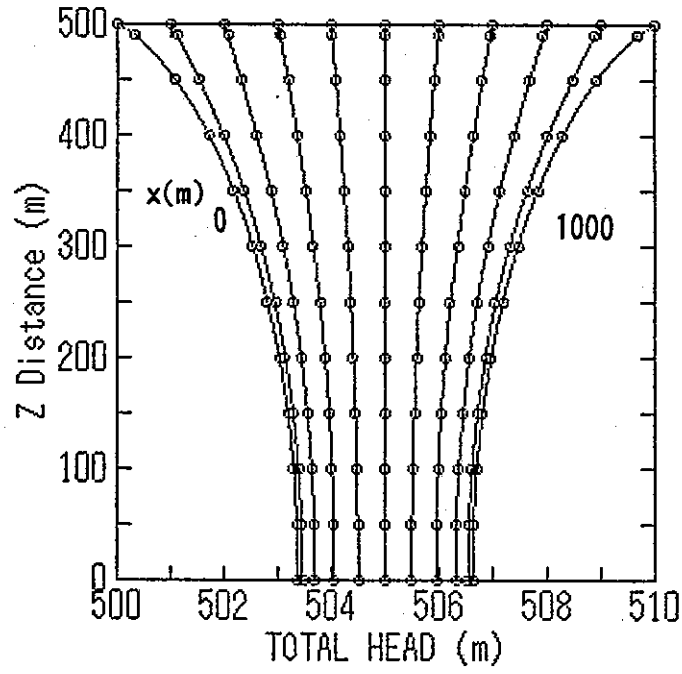


(b)垂直分布

図－47　水頭分布（ケース12）

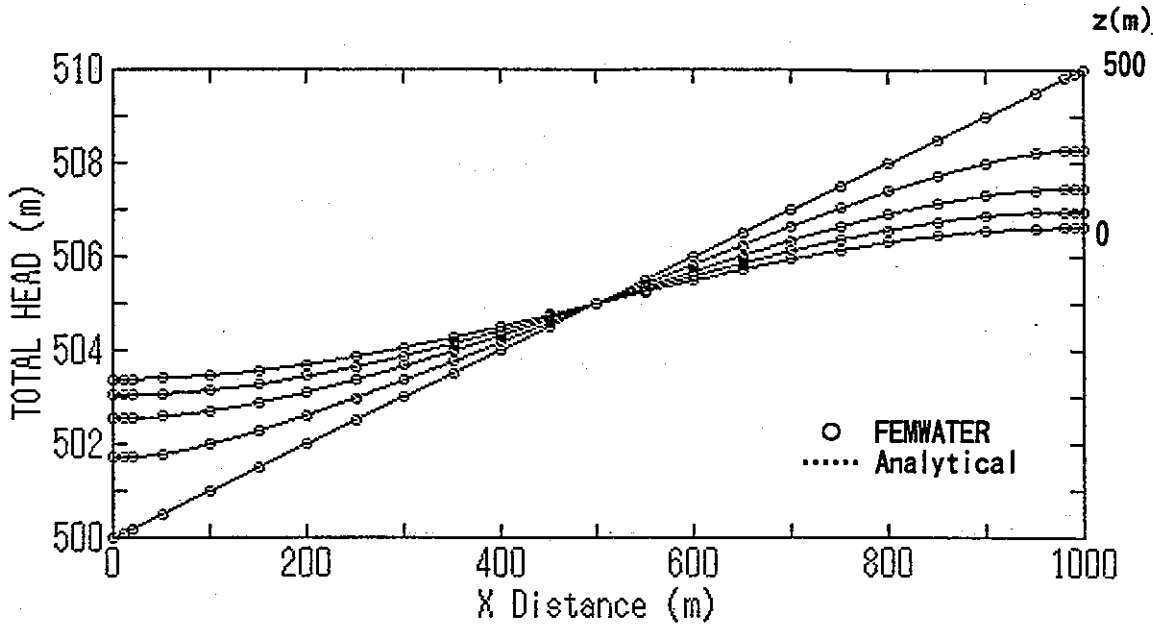


(a)水平分布

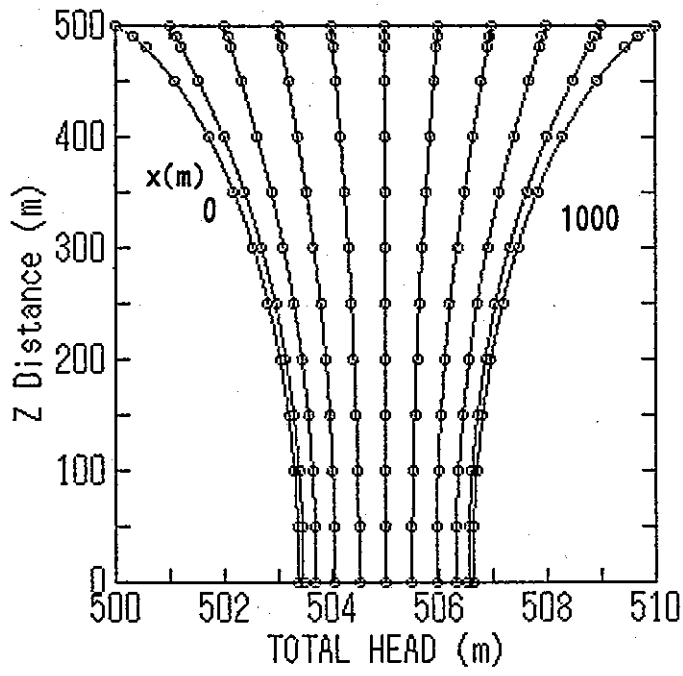


(b)垂直分布

図－48　水頭分布（ケース13）



(a)水平分布



(b)垂直分布

図－49　水頭分布（ケース14）

表－28　　水頭最大誤差

ケース	全水頭の最大誤差＊ (%)	位　　置
1	3.617×10^{-3}	x=50 , z=450
2	3.617×10^{-3}	x=50 , z=450
3	3.617×10^{-3}	x=50 , z=450
4	6.833×10^{-3}	x=100, z=400
5	6.833×10^{-3}	x=100, z=400
6	6.833×10^{-3}	x=100, z=400
7	6.539×10^{-2}	x=50 , z=450
8	6.539×10^{-2}	x=50 , z=450
9	6.539×10^{-2}	x=50 , z=450
10	6.598×10^{-2}	x=100, z=400
11	1.835×10^{-3}	x=25 , z=475
12	1.530×10^{-3}	x=20 , z=480
13	1.676×10^{-3}	x=50 , z=450
14	1.009×10^{-3}	x=100, z=450
15	3.617×10^{-3}	x=50 , z=450

＊ 誤差＝ＡＢＳ $\left[\dfrac{\text{コード計算値}-\text{解析解}}{\text{解析解}}\right]\times100$ (%)

(2) ダルシー流速分布

得られたダルシー流速分布の中から、解析解及びケース1, 4, 11, 12, 13, 14について、流速ベクトル図を図50～56に示す。各ベクトルの大きさは、解析解で得られた最大値($Vmax=7.707\times10^{-3}$)を用いて規格化した。問題の物理的条件及び境界条件から、得られた流速分布は物理的に妥当なものと考えられる。

しかし、境界近傍で比較すると、解析解では、側面境界(x=0, 1000 m)で水平成分 Vx=0 であるが、コード計算結果では、Vx≠0となっているため、ベクトルが傾きを持っている。特に、流入・流出節点すなわち(0,500)及び(1000,500)の節点では、$Vx=-1\times10^{-3}$の値を持つため、ベクトルの傾きが大きくなっている。これは上部境界として、ディリクレ境界条件を適用し、Z=500の各節点で水頭を規定しており($X\cdot\tan\alpha=X\cdot0.01$)、x=0, 1000の節点においても、規定水頭を与えているためである。そのため、上部境界節点(z=500の各節点)では$Vx=-1\times10^{-3}$(m/y)、すなわち、$-K\cdot\tan\alpha=-1\times10^{-3}$の速度成分を持っている。

一方、解析解の上部境界は $h=H+x\cdot\tan\alpha$ ($0<x<1000$) で与えられており、x=0, 1000では側面の境界条件 $\frac{\partial h}{\partial x}=0$で与えられる。そのため、数学的な特異点となり、コードでは完全には模擬できないためと考えられる。

要素分割の影響を比較するため、ケース1, 4, 11, 12, 13, 14について、Vx, Vzの各水平分布と垂直分布を図-57～68に示す。Vx, Vz共に、x=500を中心に対象な分布をしており、境界(x=0, 1000及びZ=500)に近づくにつれて、Vx、Vz共に誤差が大きくなっている。境界近傍($0\leq x\leq50$ m)における各ケースのVx, Vzの垂直分布を距離毎にまとめて図-69～73に示す。但し、Vxは負値のため絶対値を表示した。

x=0 m におけるVxの分布では、解析解が Vx=0 （図中では5×10^{-5}に便宜的に示してある）に対し、コード計算結果は、10^{-5}以上の値を持っている。要素を細かく分割すると(ケース4=100、ケース1=50、ケース11=25)、値も小さくなり、さらに境界近傍を細分したケース(12, 13, 14)では、より小さな値となる。但し、z=500の節点では、先に述べた通り水頭を規定しているため、$-K\cdot\tan\alpha=-10^{-3}$の値を持ってしまう。

x=0 m におけるVzの分布では、z=0, 500 m を除いて、ほぼ良好な結果が得られた。z=0 m では、解析解がVz=0であるのに対し、各ケースとも10^{-5}オーダーの値を持つ。また、z=500 m でのVzを表-29に示す。境界近傍を細

かく分割した方が、Vzが大きくなるものの、解析解に対して約1/2程度の値しか持たない。

x=10 m におけるVxの分布では、Δx=10を2本入れたケース14がほぼ解析解に一致しているのに対し、1本だけのケース13では誤差が大きい。Vzの分布では、両ケースともよく一致している。

x=20 m におけるVxの分布では、Δx=10を2本入れたケース14の方が、Δx=20を1本入れたケース12よりも精度が悪い。x=10 m でケース14がよく一致していた事を考えると興味深い結果である。Vzの分布ではどちらのケースもほぼ一致した。

x=25 m における分布ではVx, Vzとも比較的よく一致している。

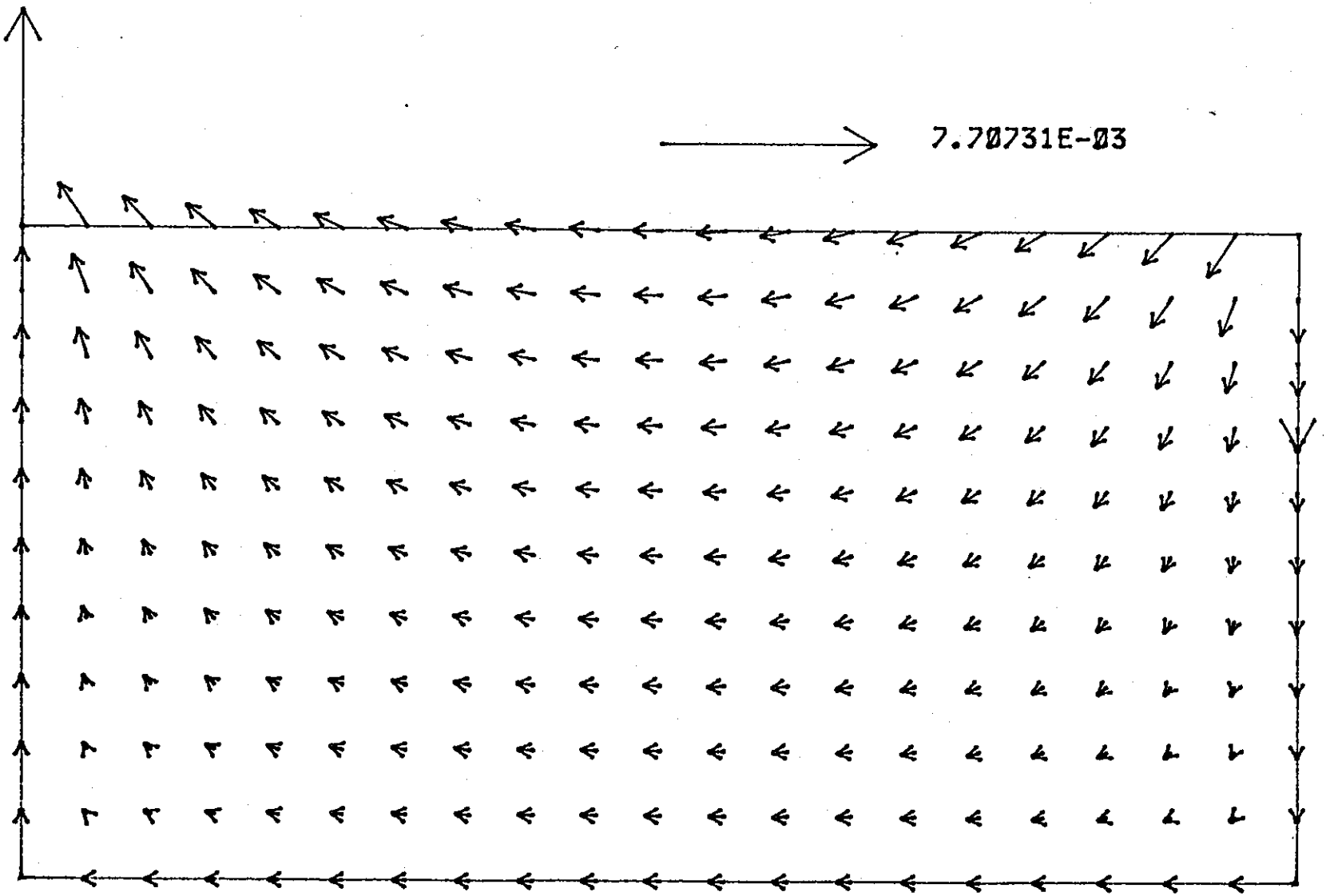
x=50 m におけるVxの分布では、ケース1, 11に比べ、境界近傍を細かくしたケース12, 13, 14の方が精度が悪い。これは、ケース1及び11が正方形要素であるのに対し、ケース12, 13, 14が長方形要素である事に起因するものと考えられる。Vzの分布では、いずれのケースもほぼ一致している。

透水係数及び地下水面の勾配の影響については、解析解からも明らかなように、各ダルシー速度は$K\cdot\tan\alpha$に比例することがわかる。ケース1, 2, 3, 8, 9, 10のVx, Vzの各水平分布及び垂直分布を図-74, 75に示す。Vx, Vzは絶対値で図示した。各ケースの$K\cdot\tan\alpha$は

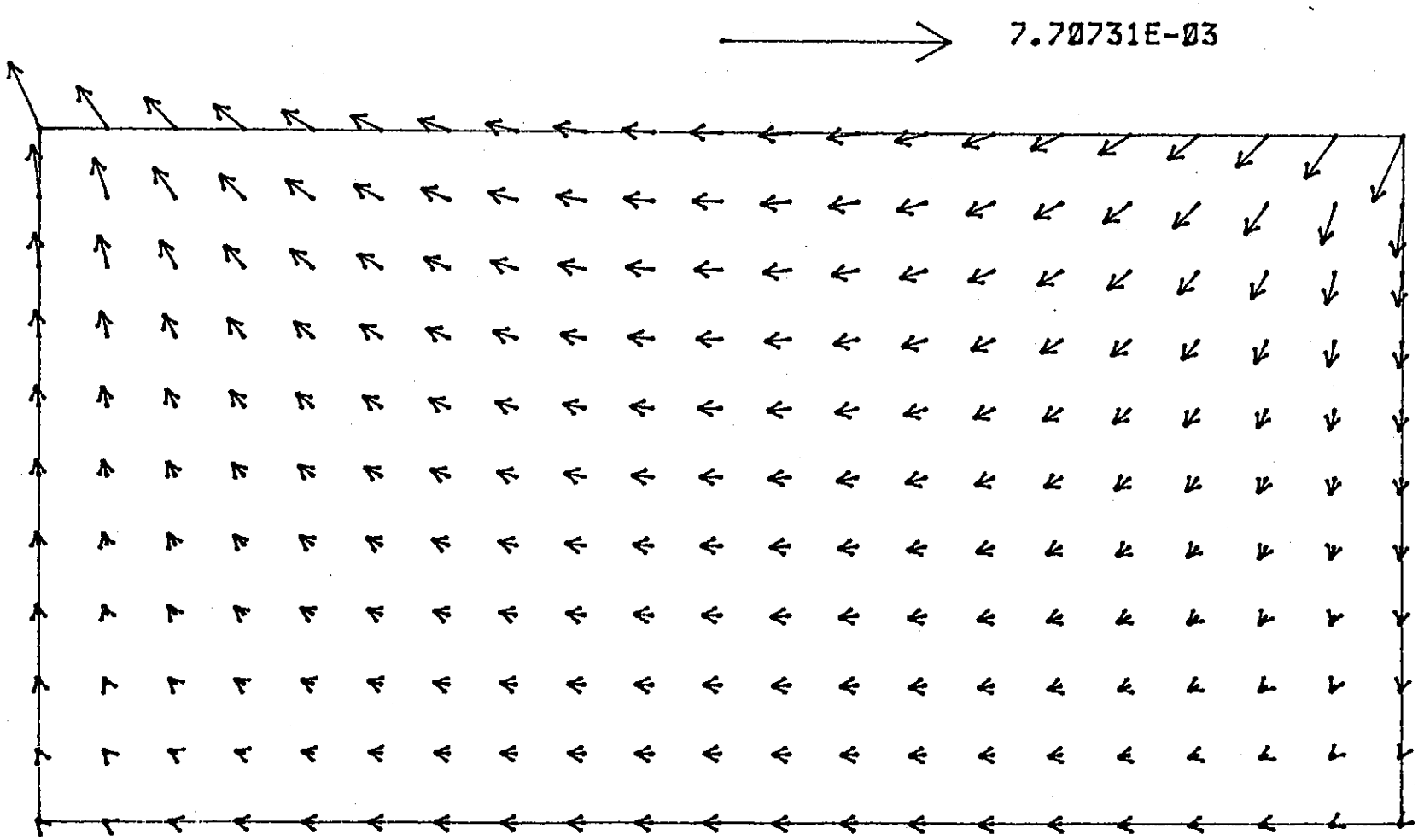
ケース1	$K\cdot\tan\alpha = 1\times10^{-3}$
ケース2	$K\cdot\tan\alpha = 1\times10^{-5}$
ケース3	$K\cdot\tan\alpha = 1\times10^{-1}$
ケース8	$K\cdot\tan\alpha = 1\times10^{-2}$
ケース9	$K\cdot\tan\alpha = 1\times10^{-4}$
ケース10	$K\cdot\tan\alpha = 1$

となっており、各ケースの$K\cdot\tan\alpha$値に応じて得られた結果も各々1桁ずつ異なっており、正確に計算していることがわかった。

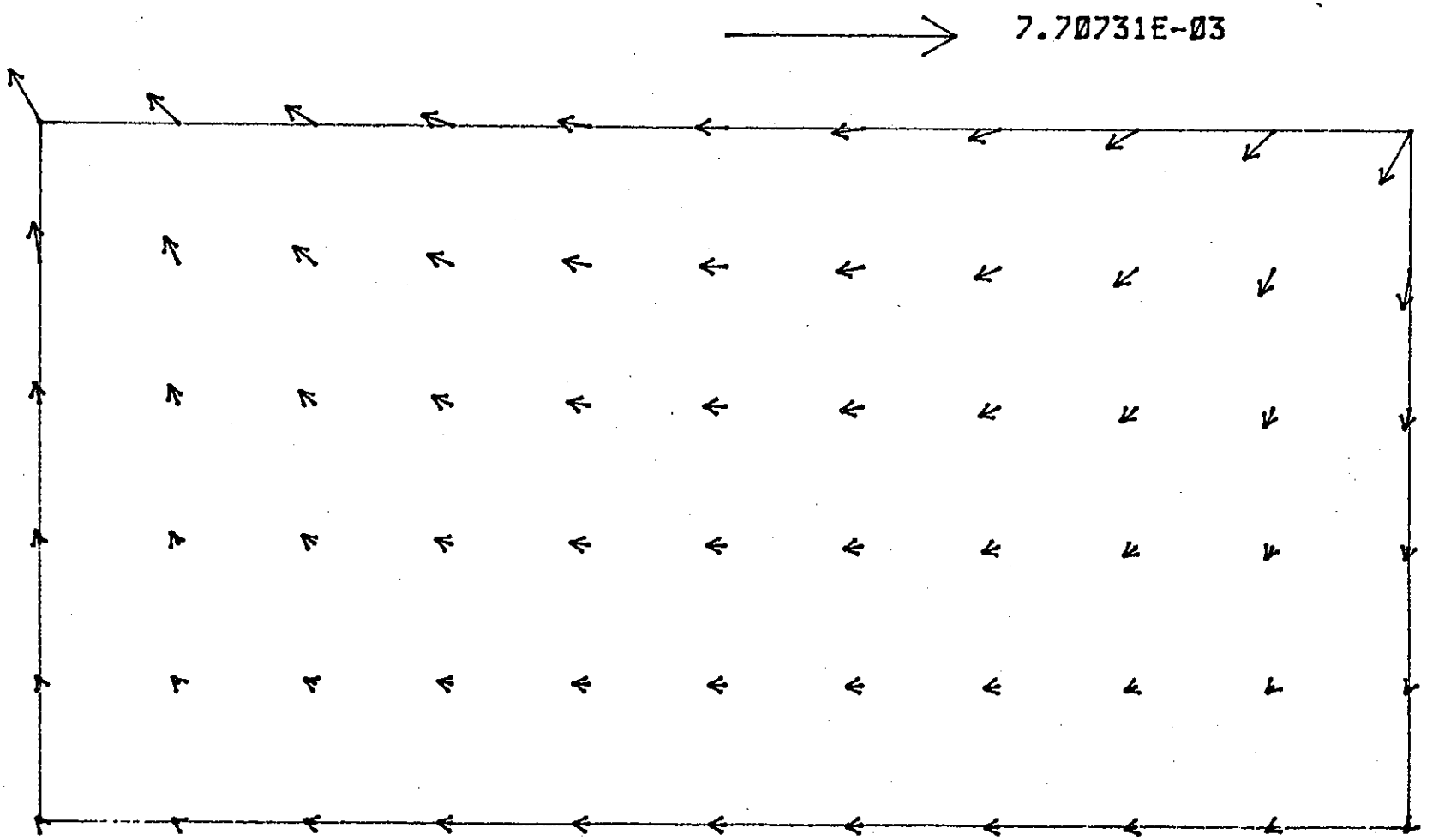
空隙率の影響については、解析解からも明確なとおり、本計算では全く依存しない。ケース1及び15で得られた結果は、完全に同一となり、正確に計算している。



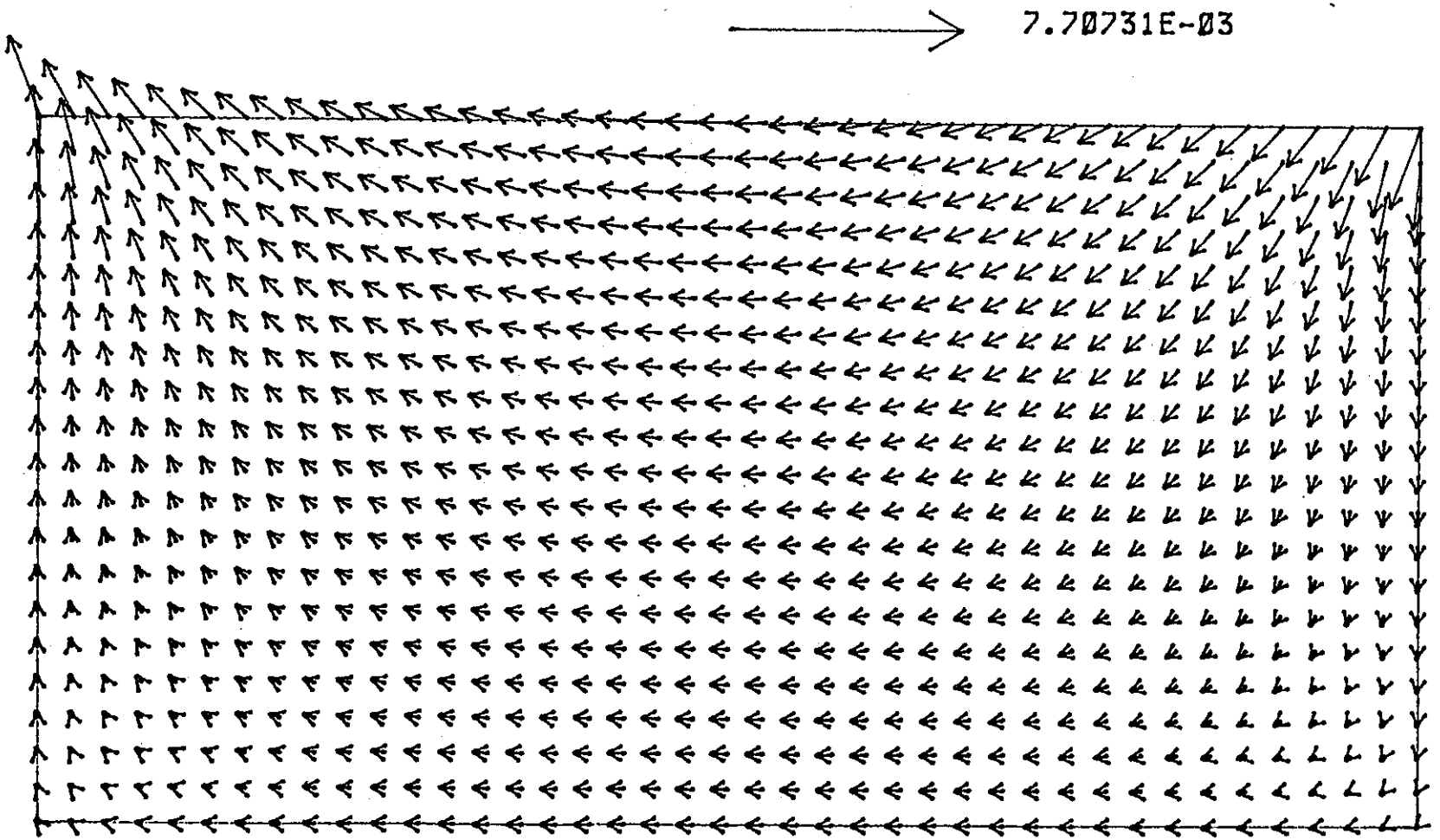
図－50　流速ベクトル図（解析解）



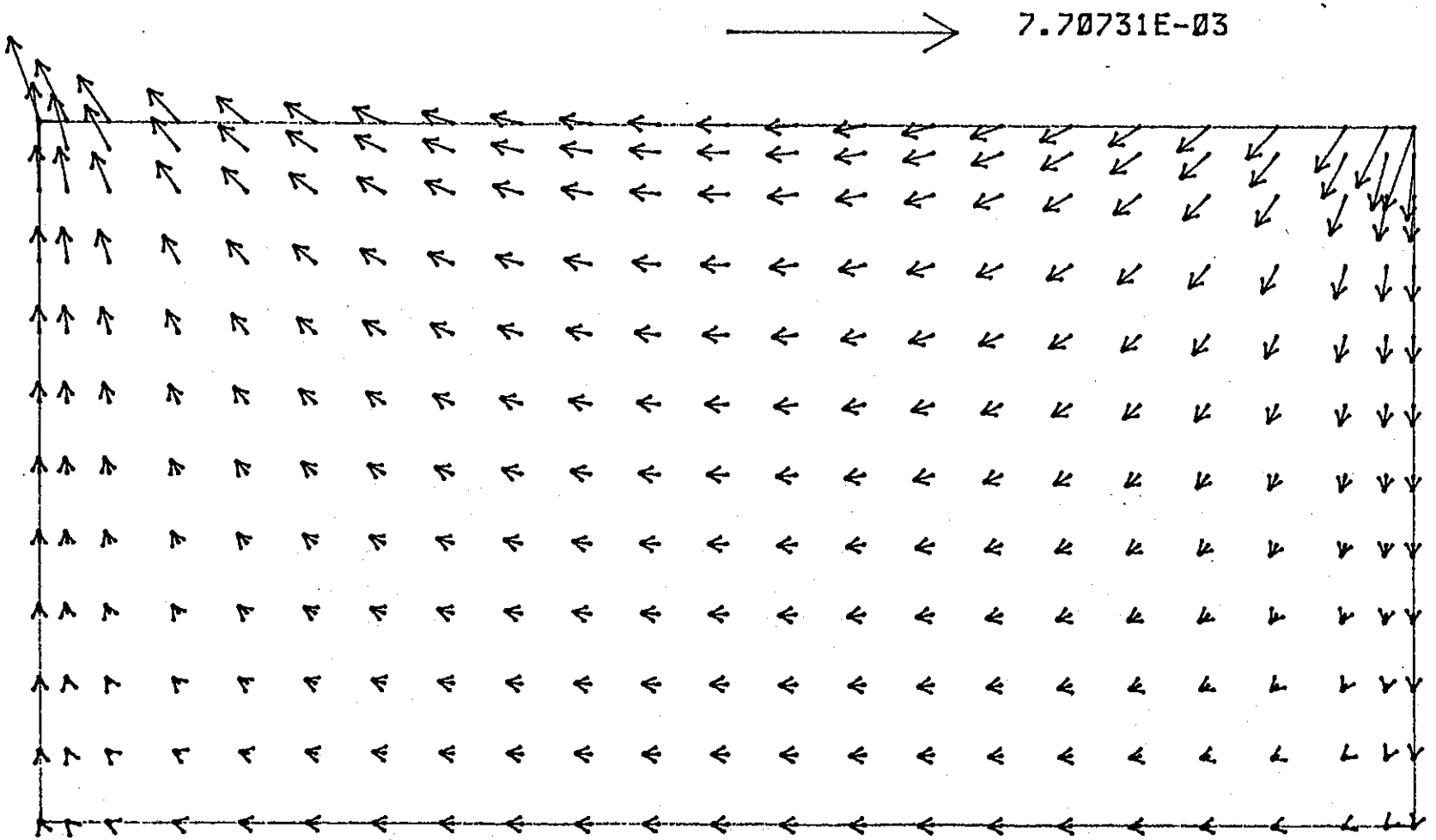
図－51　流速ベクトル図（ケース１）



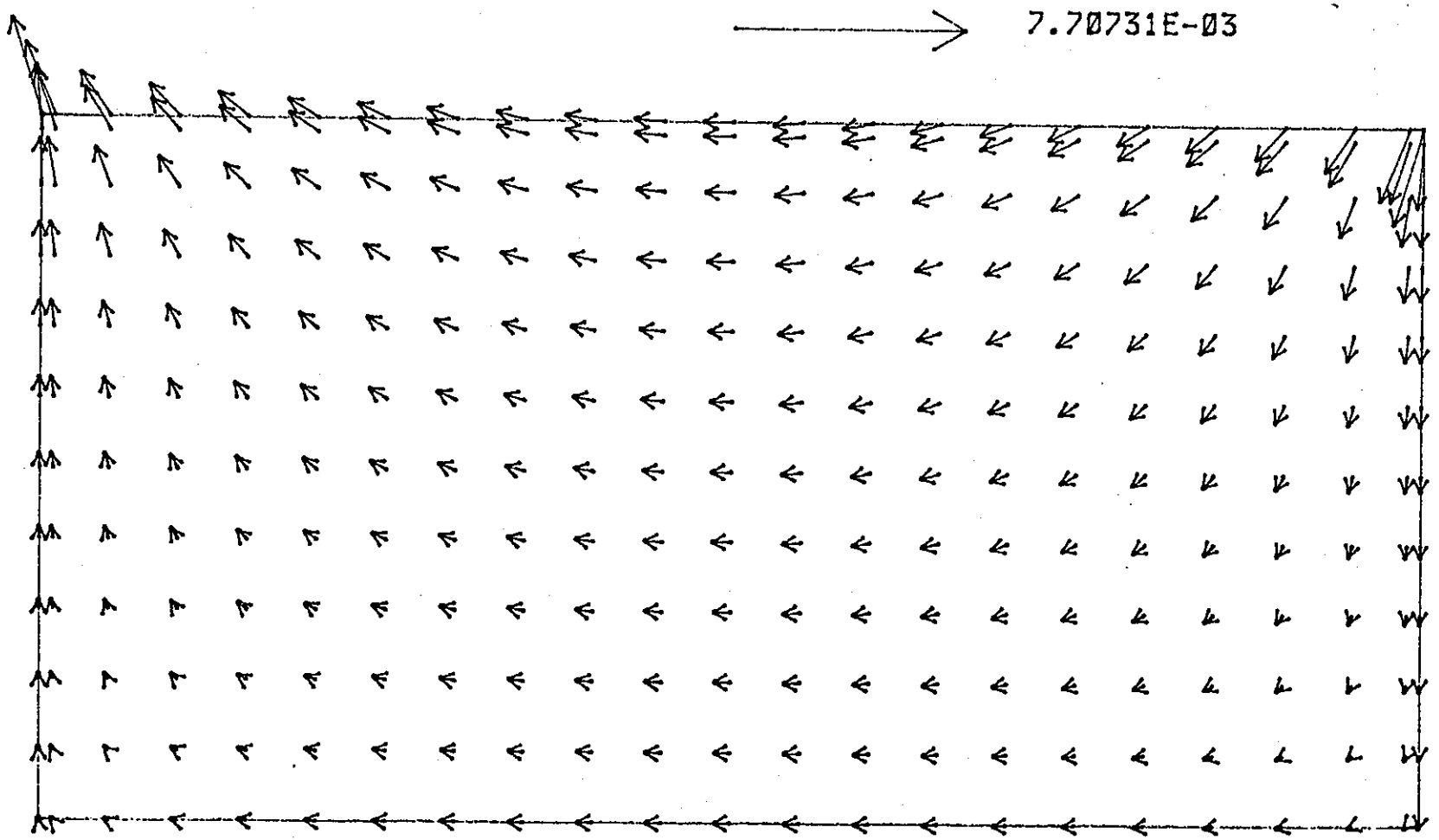
図－52　流速ベクトル図（ケース４）



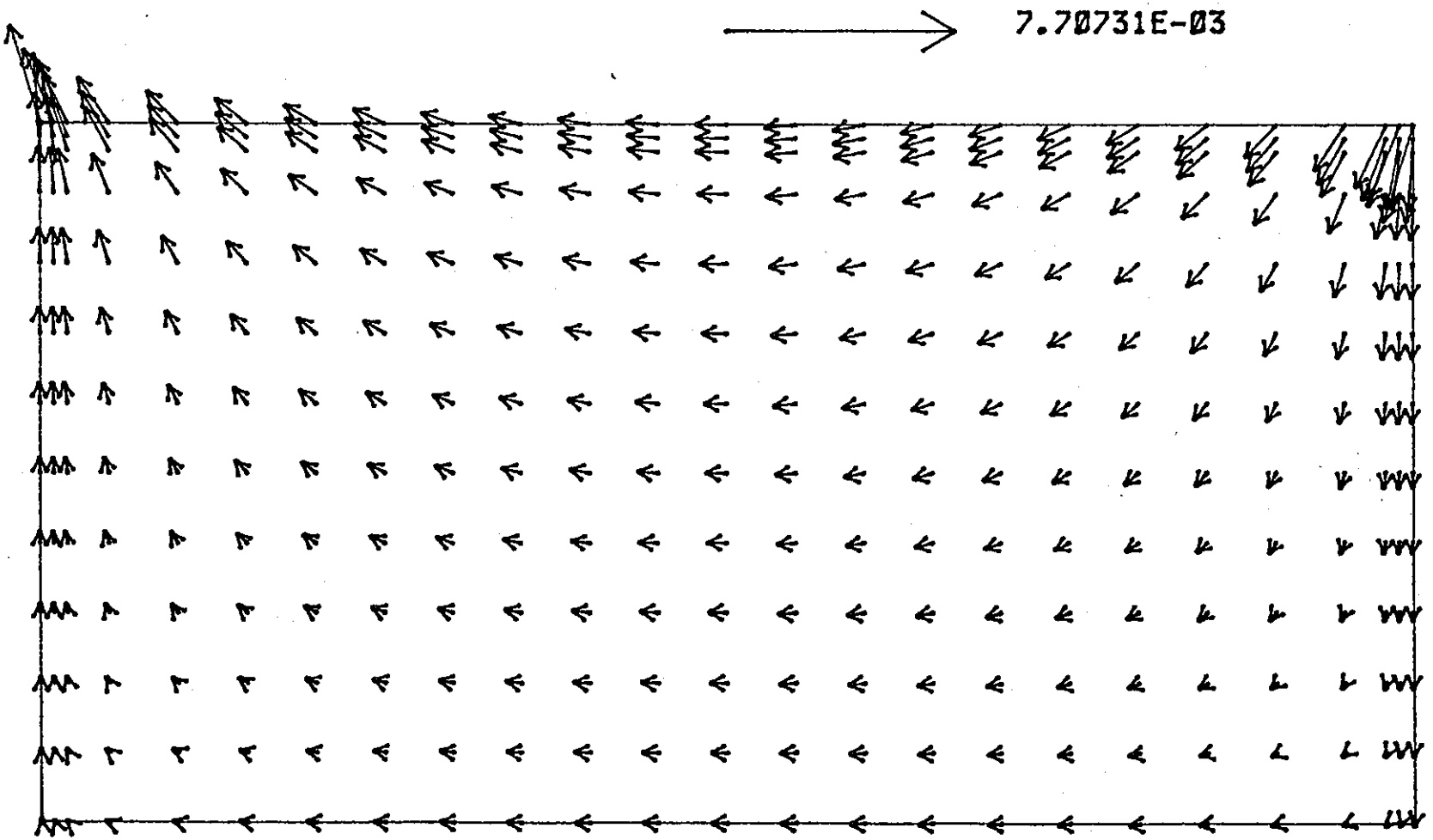
図－53　流速ベクトル図（ケース11）



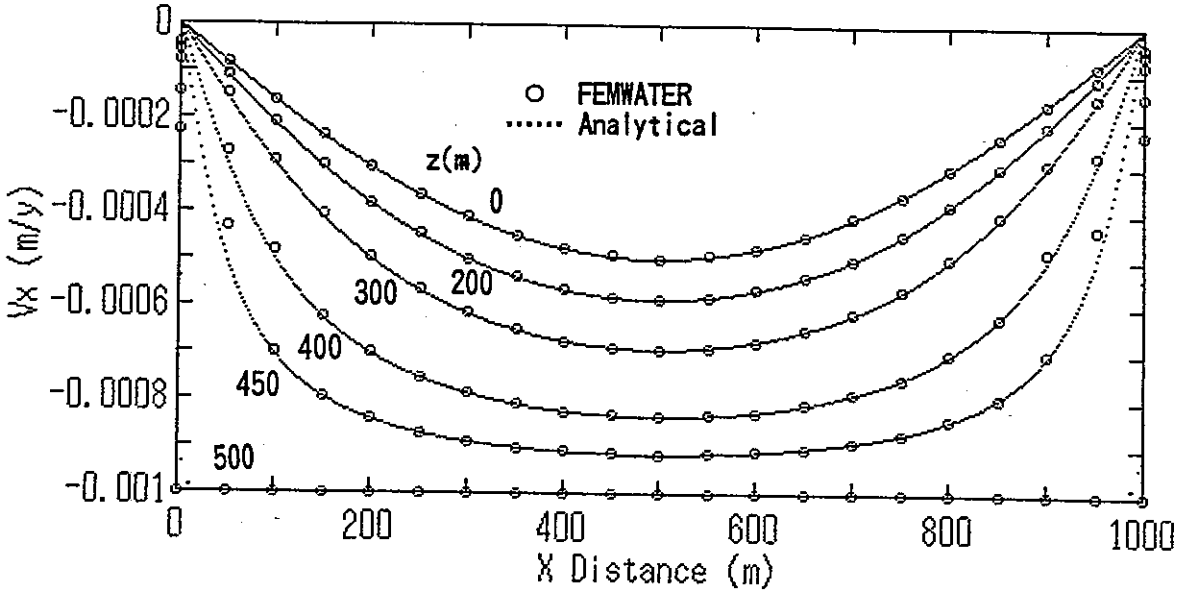
図－54　流速ベクトル図（ケース12）



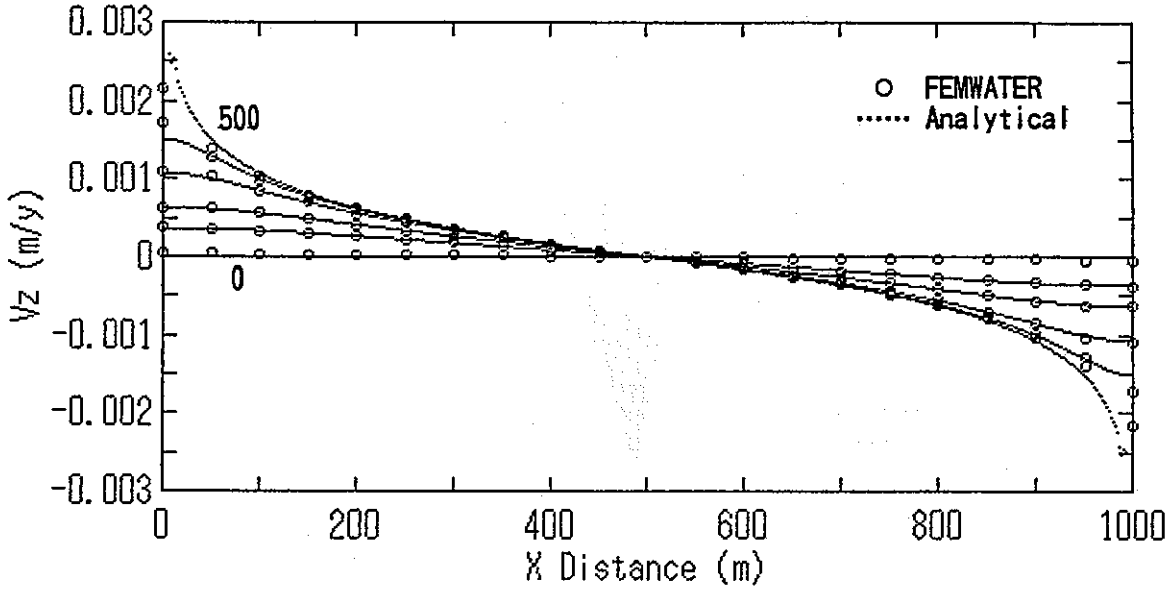
図－55　流速ベクトル図（ケース13）



図－56　流速ベクトル図（ケース14）

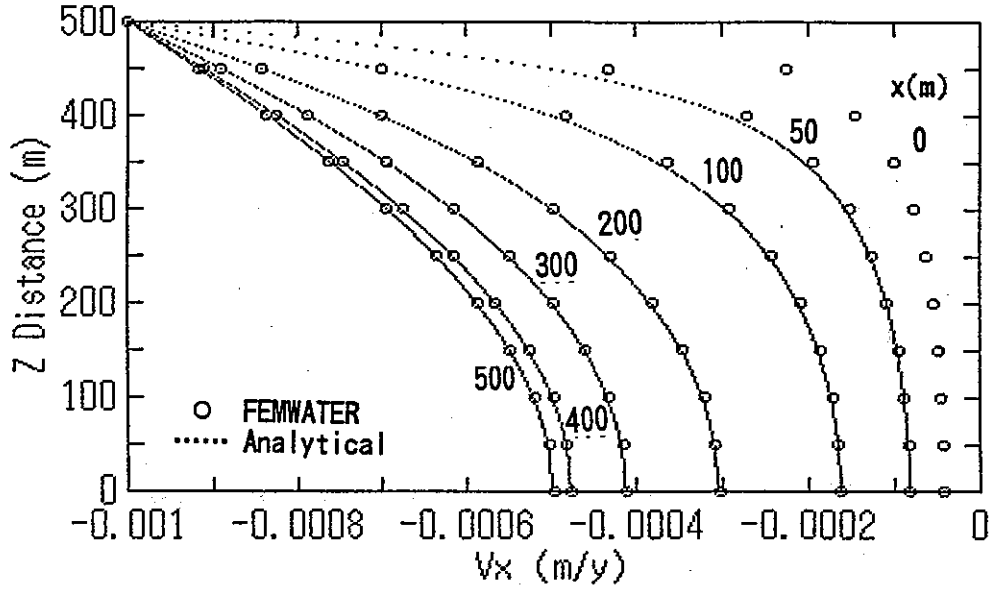


(a) Ｖｘ

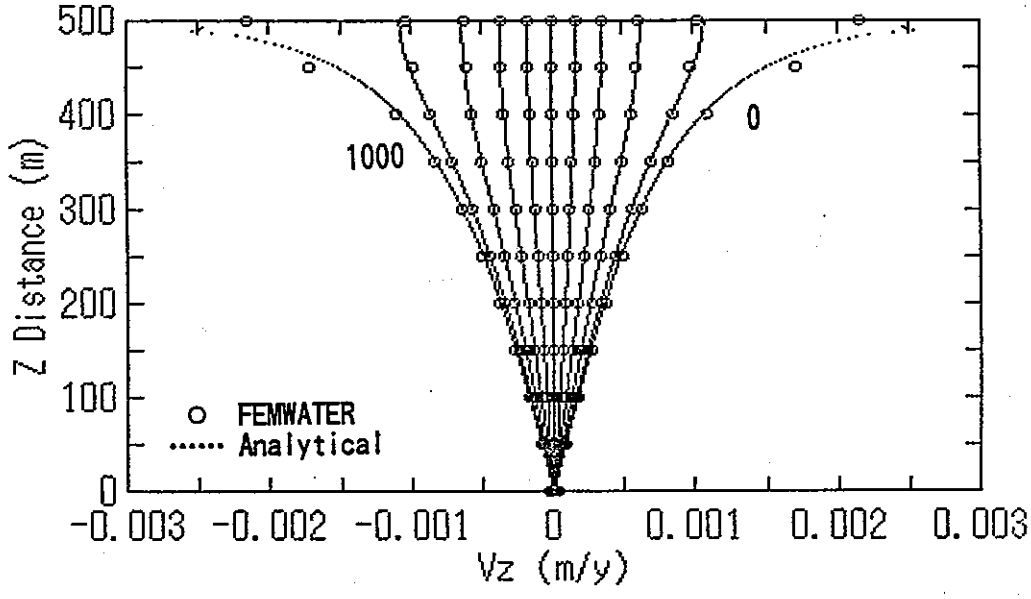


(b) Ｖｚ

図－57　流速の水平分布（ケース１）

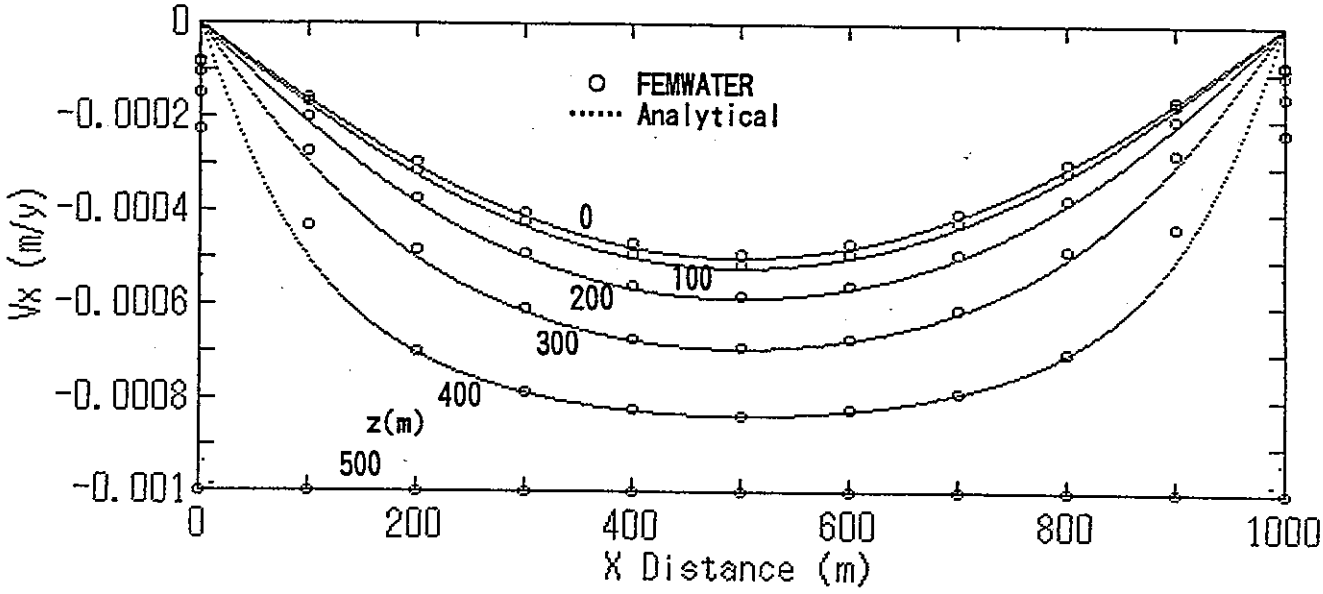


(a) Ｖｘ

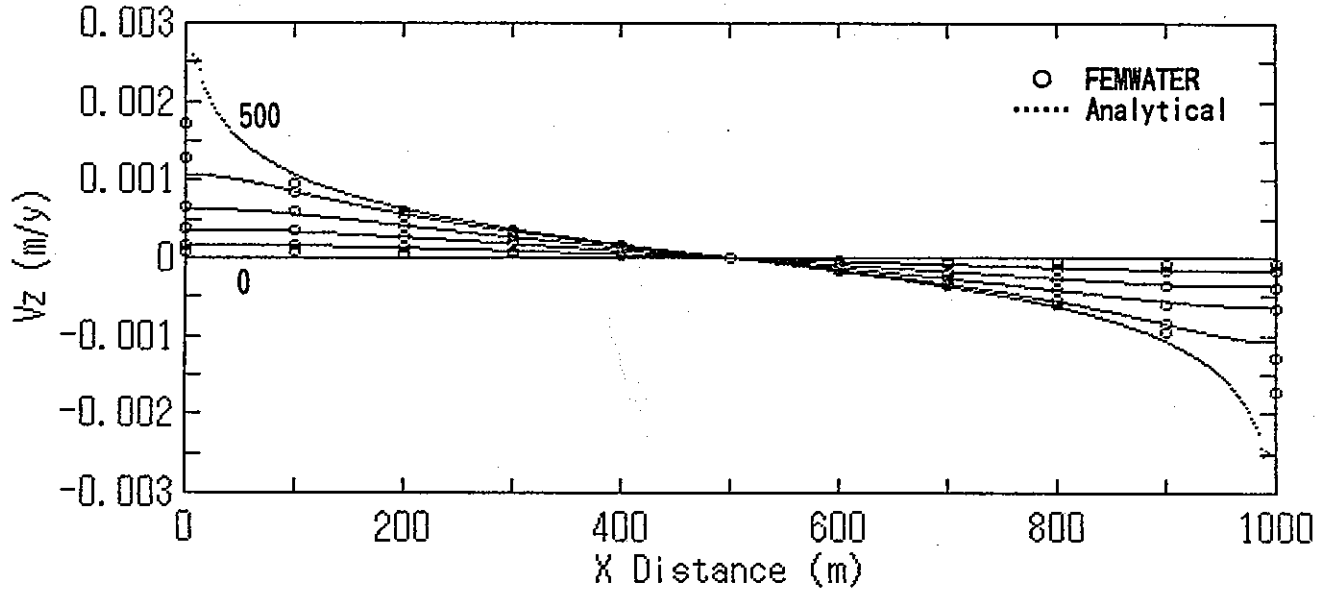


(b) Ｖｚ

図－58　流速の垂直分布（ケース１）

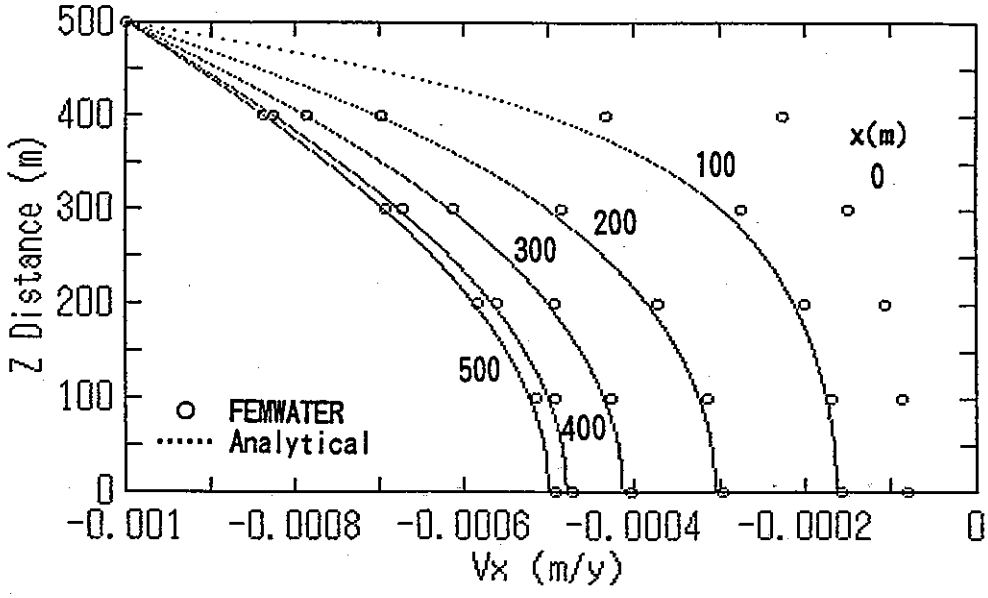


(a) Ｖｘ

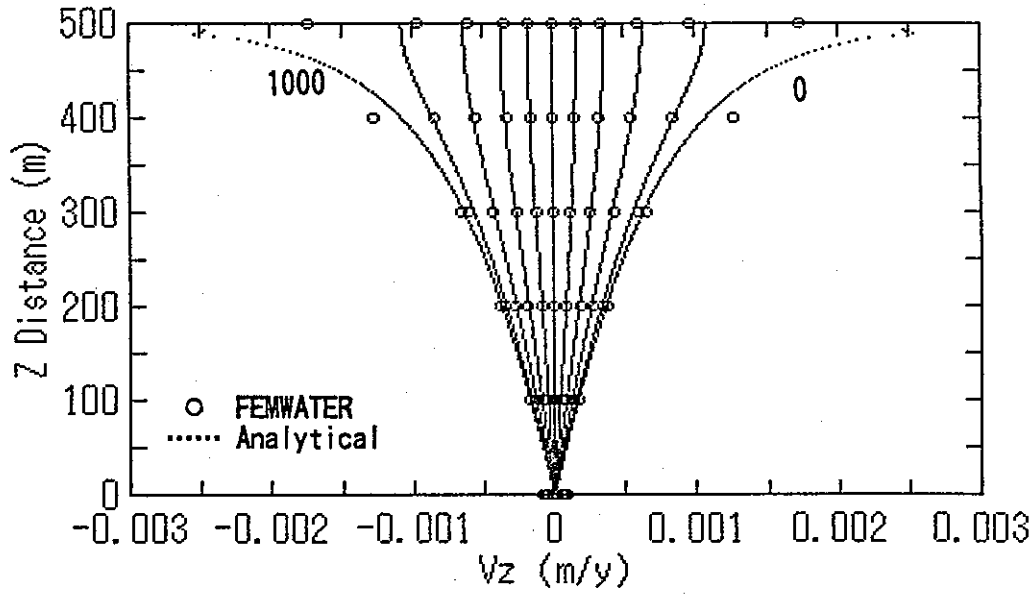


(b) Ｖｚ

図－59　流速の水平分布（ケース４）

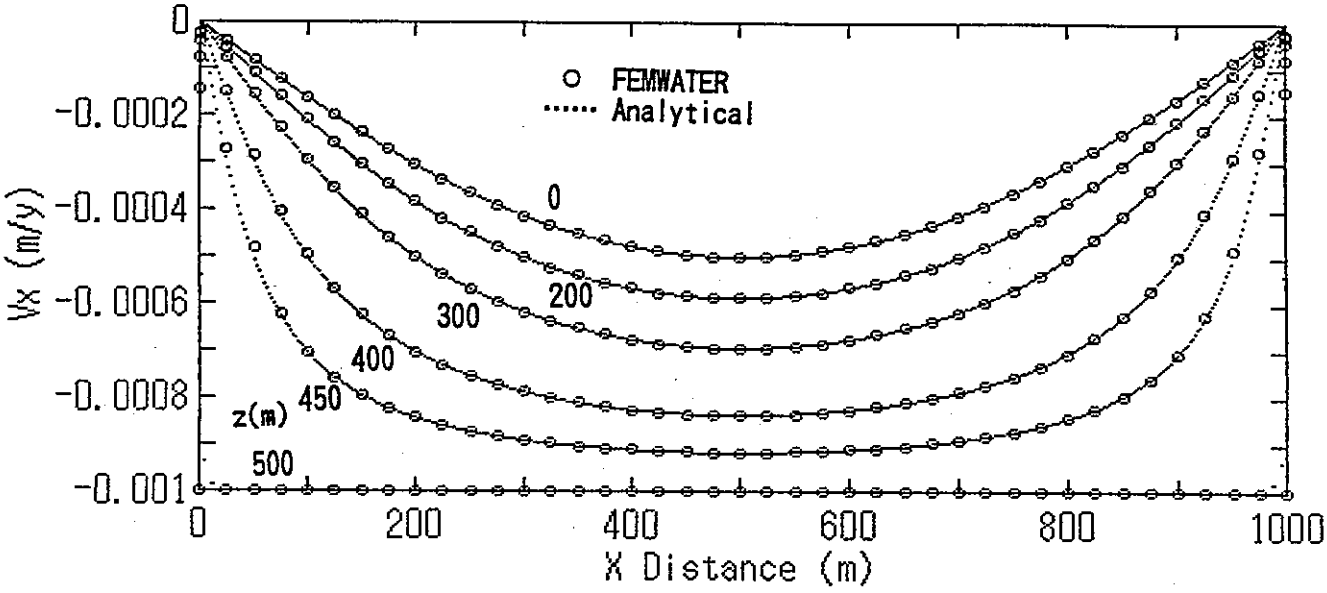


(a) Ｖｘ

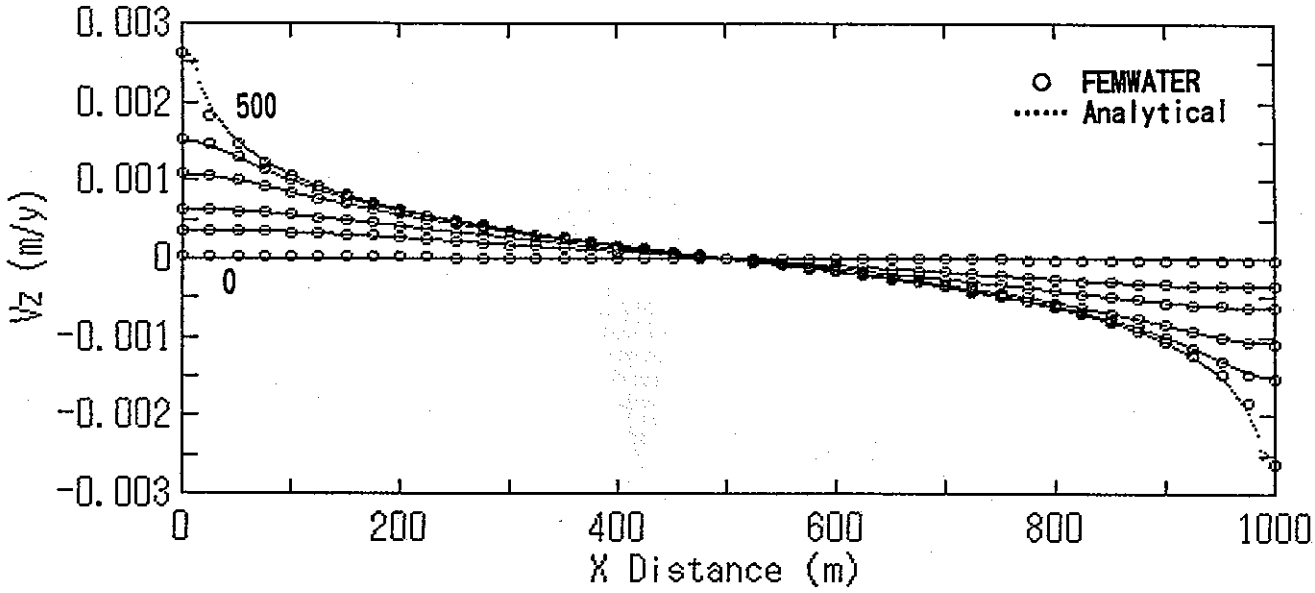


(b) Ｖｚ

図－60　流速の垂直分布（ケース４）

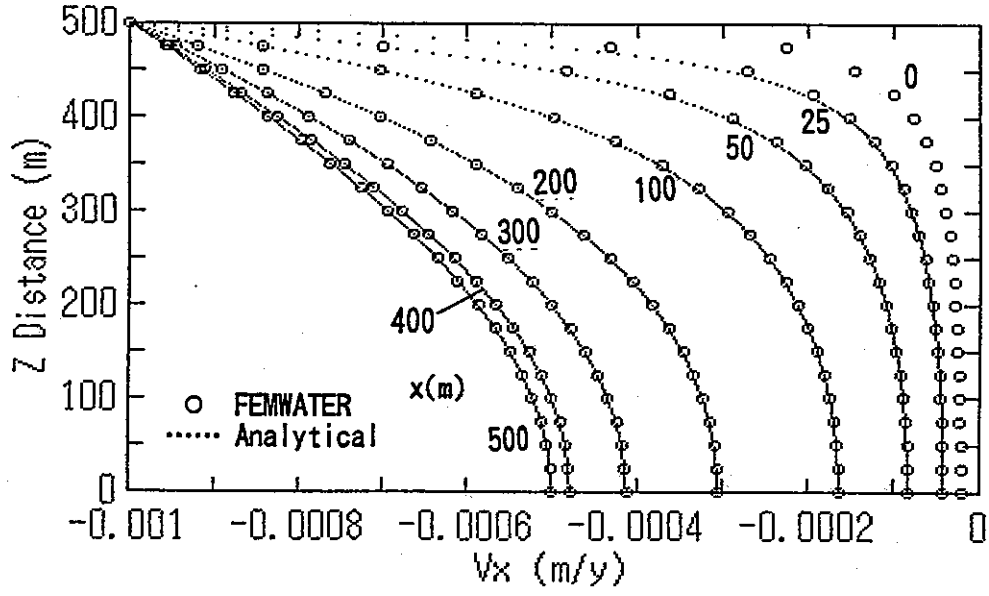


(a) Ｖｘ

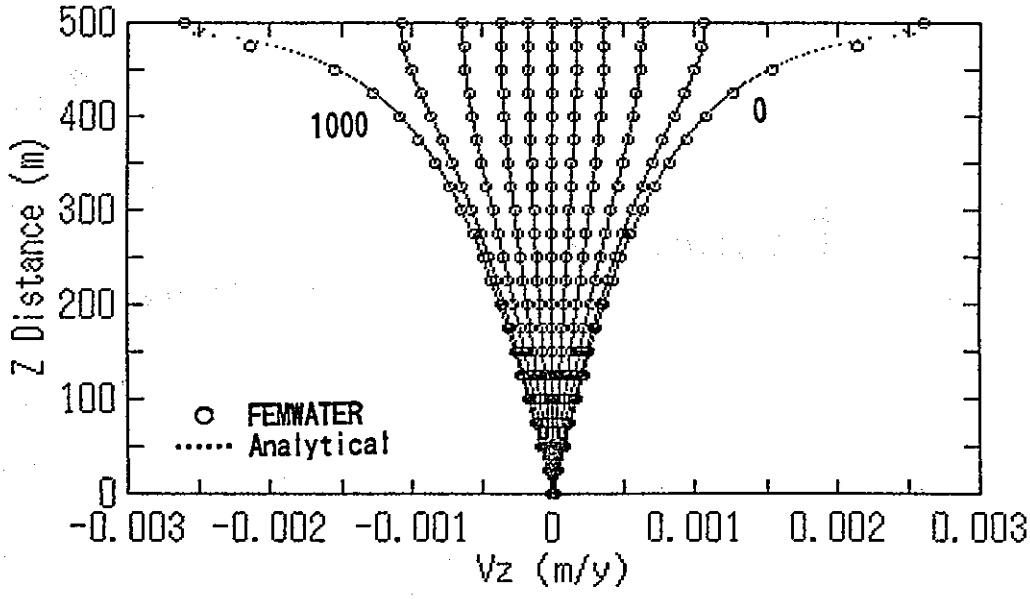


(b) Ｖｚ

図－61　流速の水平分布（ケース11）

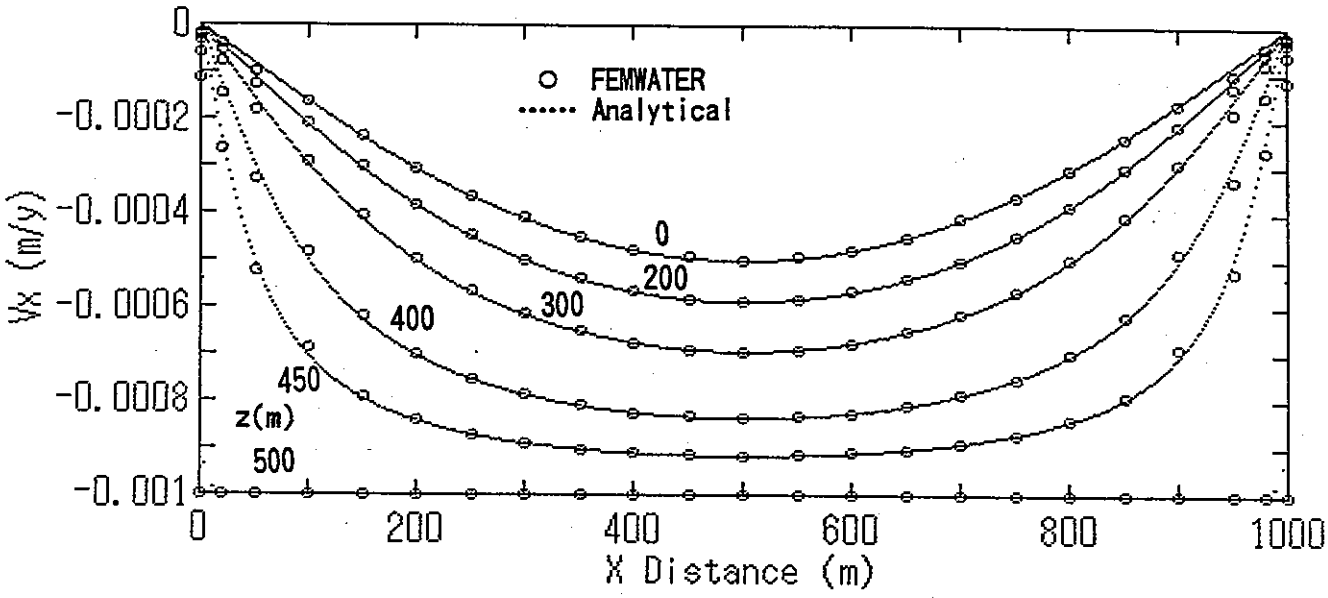


(a) Ｖｘ

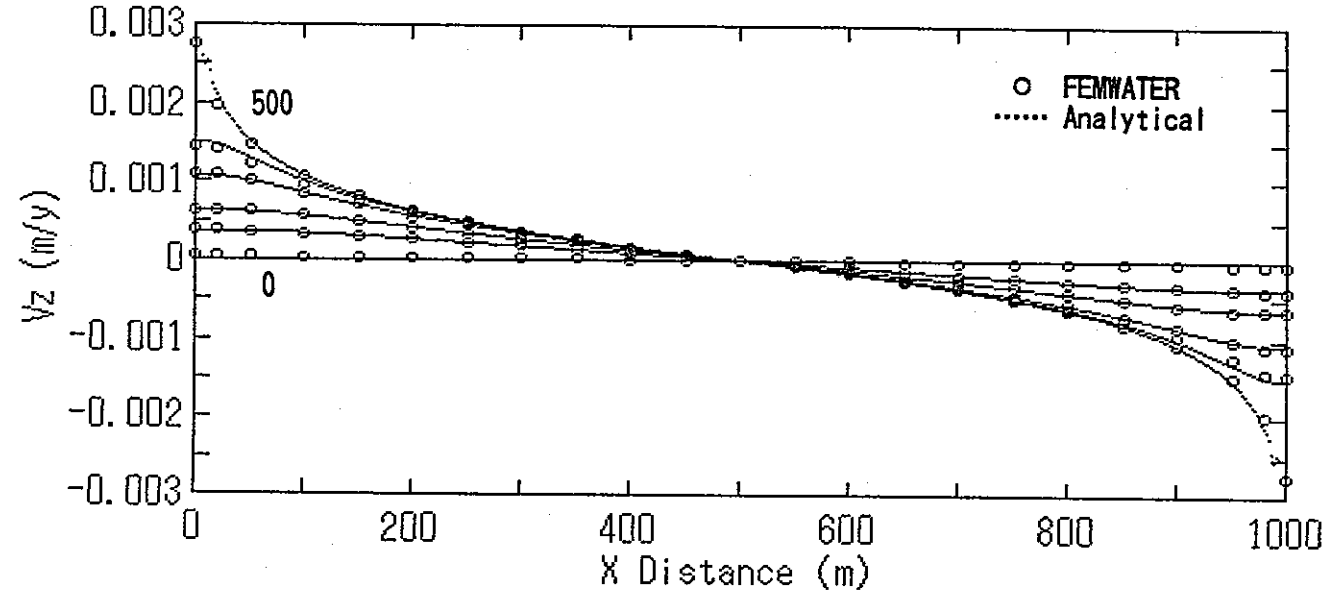


(b) Ｖｚ

図－62　流速の垂直分布（ケース11）

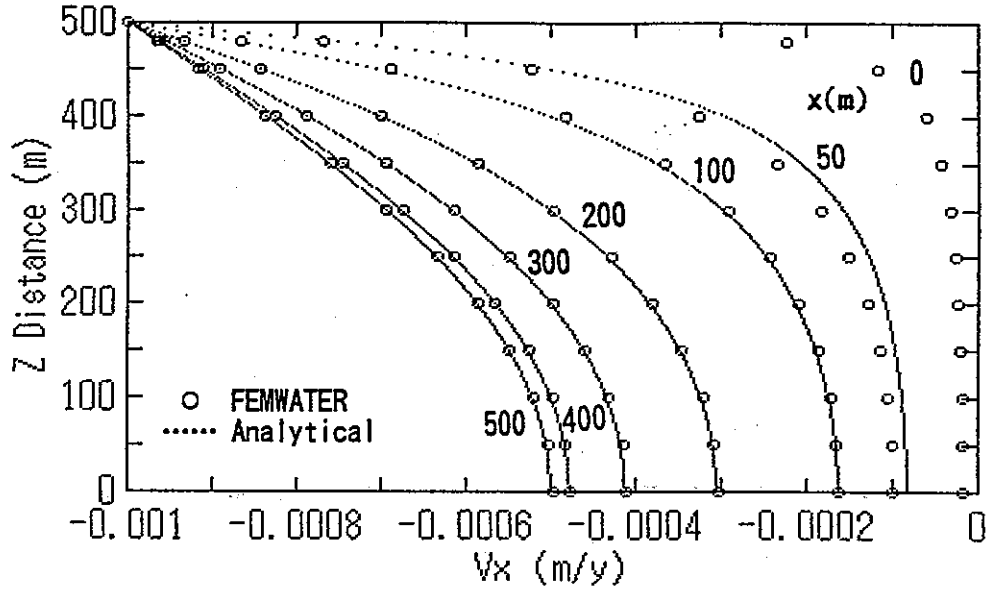


(a) Ｖｘ

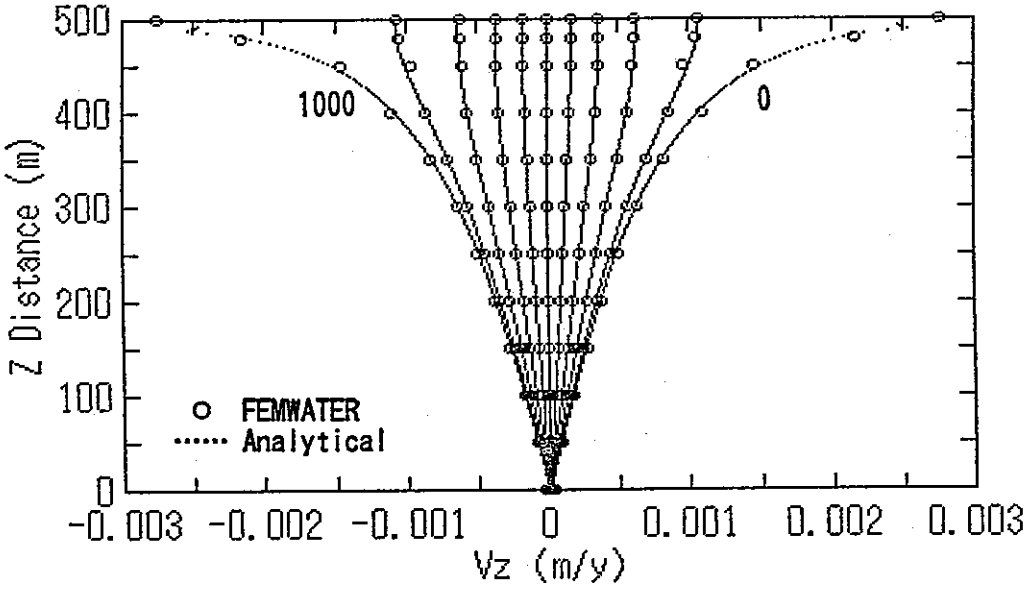


(b) Ｖｚ

図－63　流速の水平分布（ケース12）

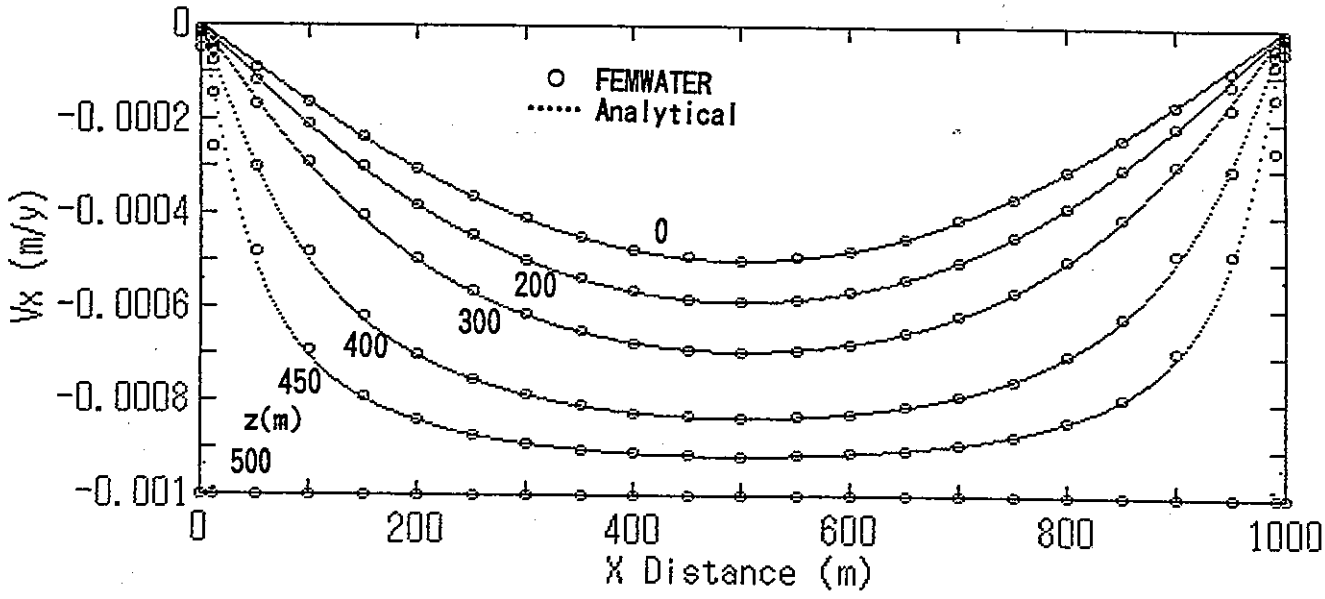


(a) Ｖｘ

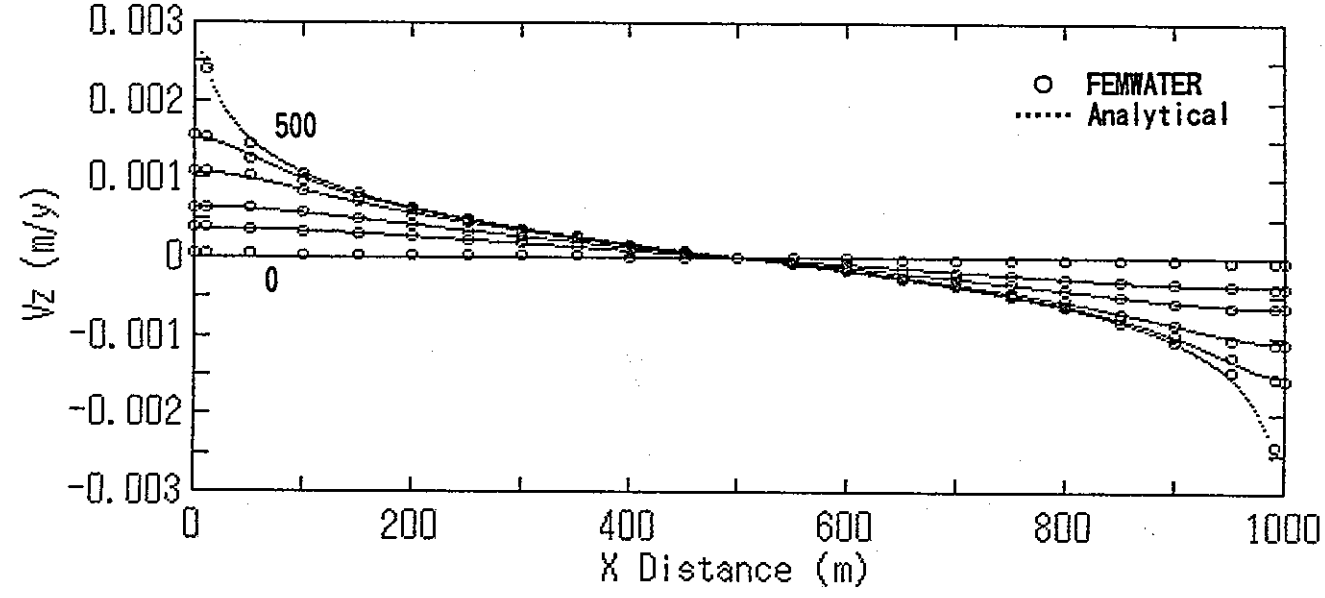


(b) Ｖｚ

図－64　流速の垂直分布（ケース12）

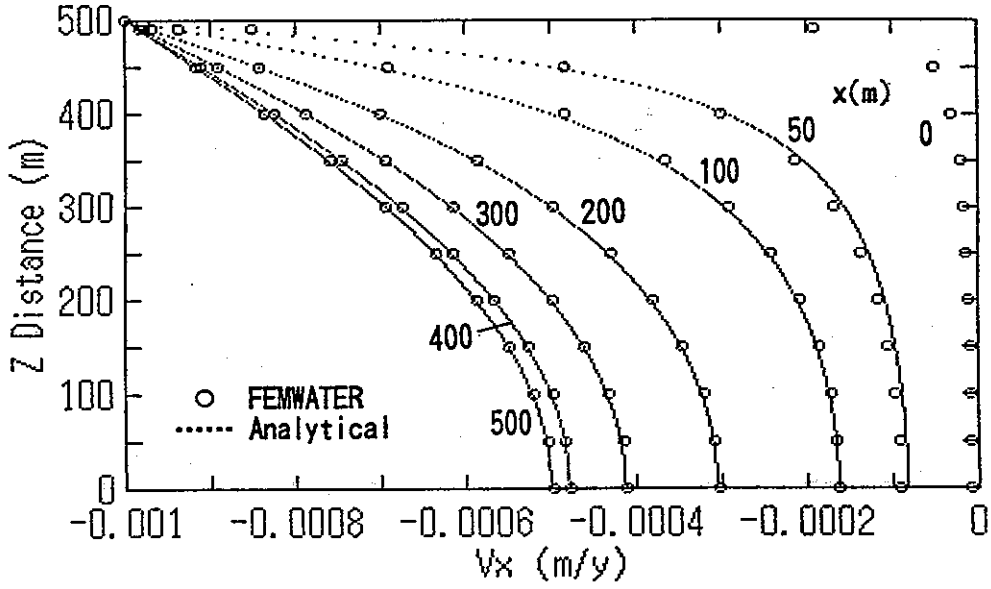


(a) Ｖｘ

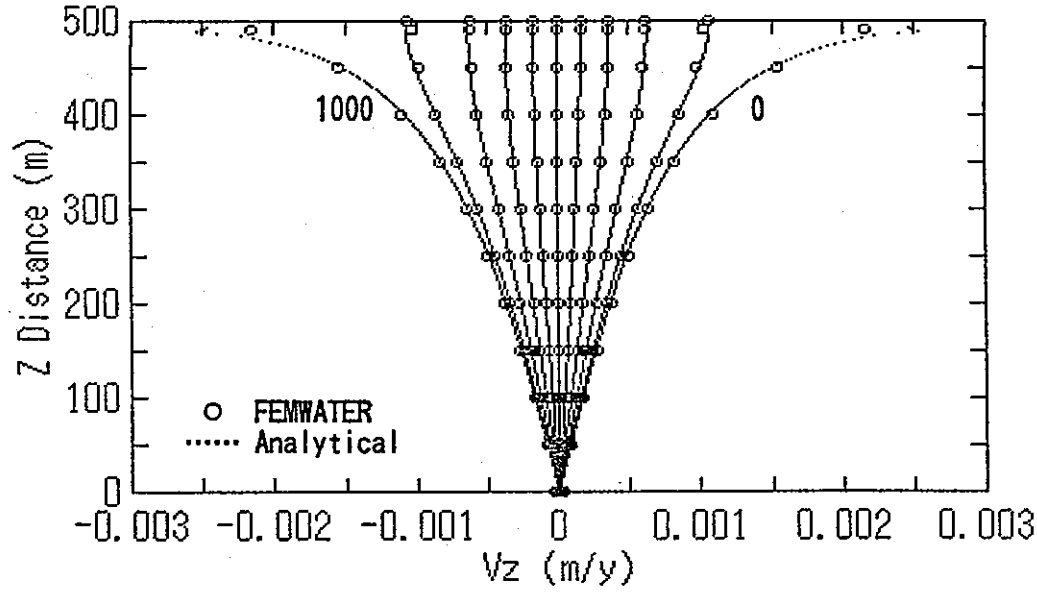


(b) Ｖｚ

図－65　流速の水平分布（ケース13）

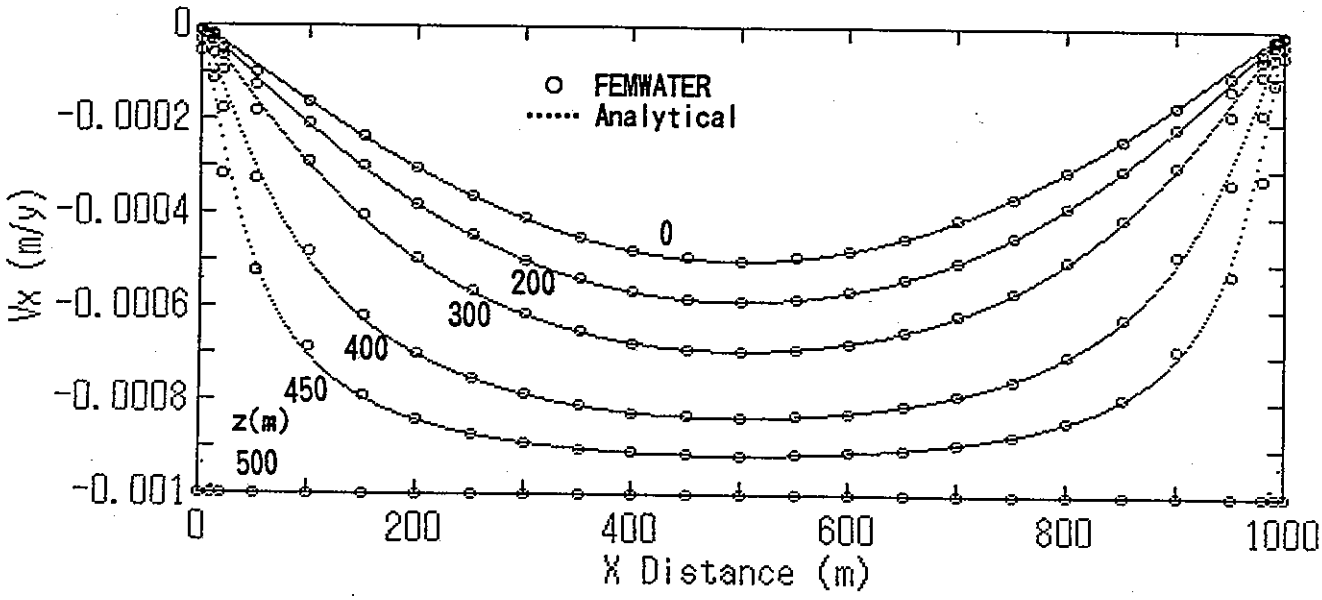


(a) Ｖｘ

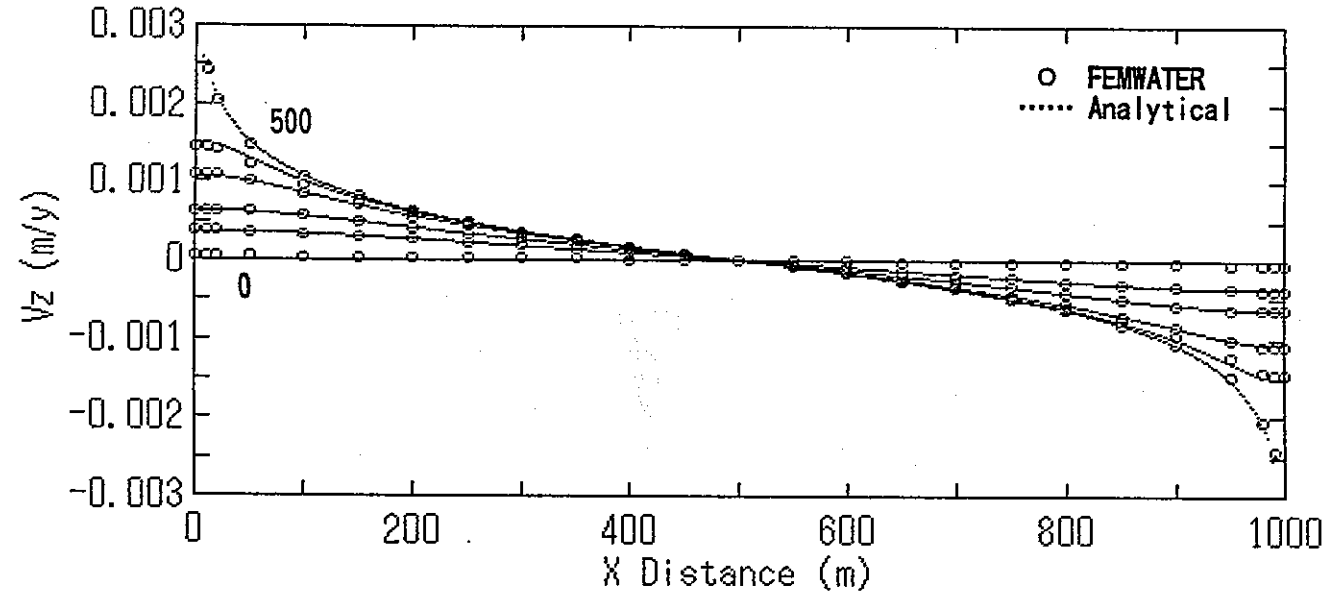


(b) Ｖｚ

図－66　流速の垂直分布（ケース13）

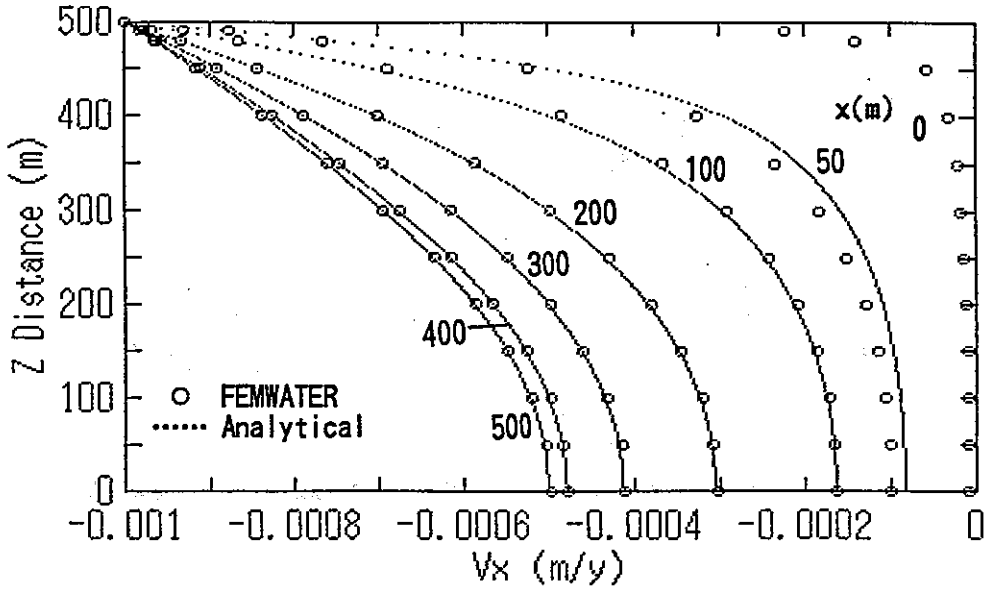


(a) Vx

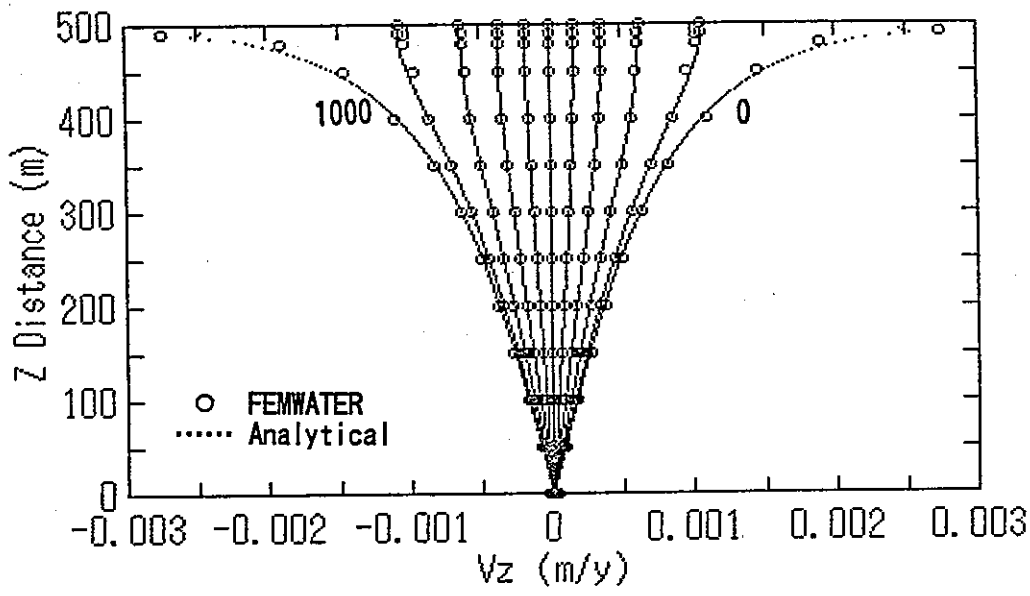


(b) Vz

図－67　流速の水平分布（ケース14）

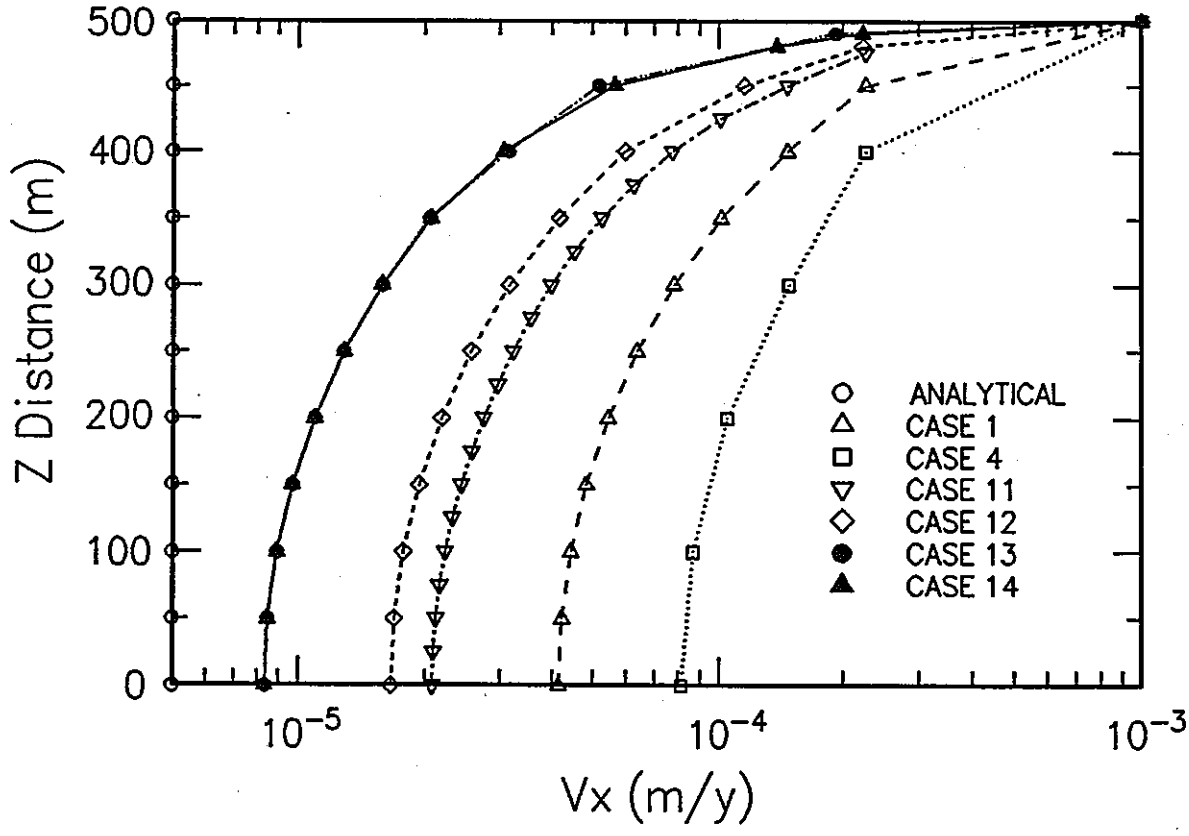


(a) Ｖｘ

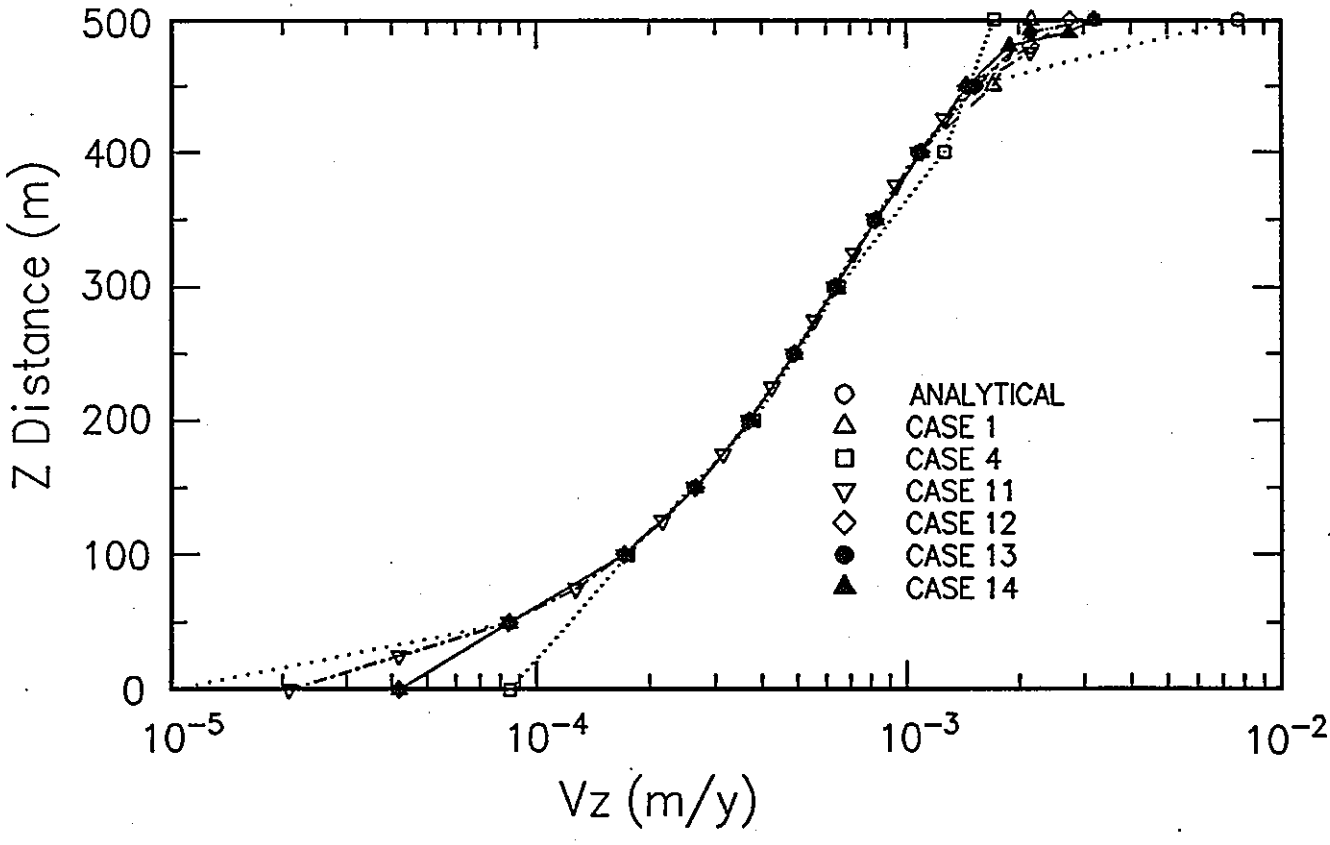


(b) Ｖｚ

図－68　流速の垂直分布（ケース14）

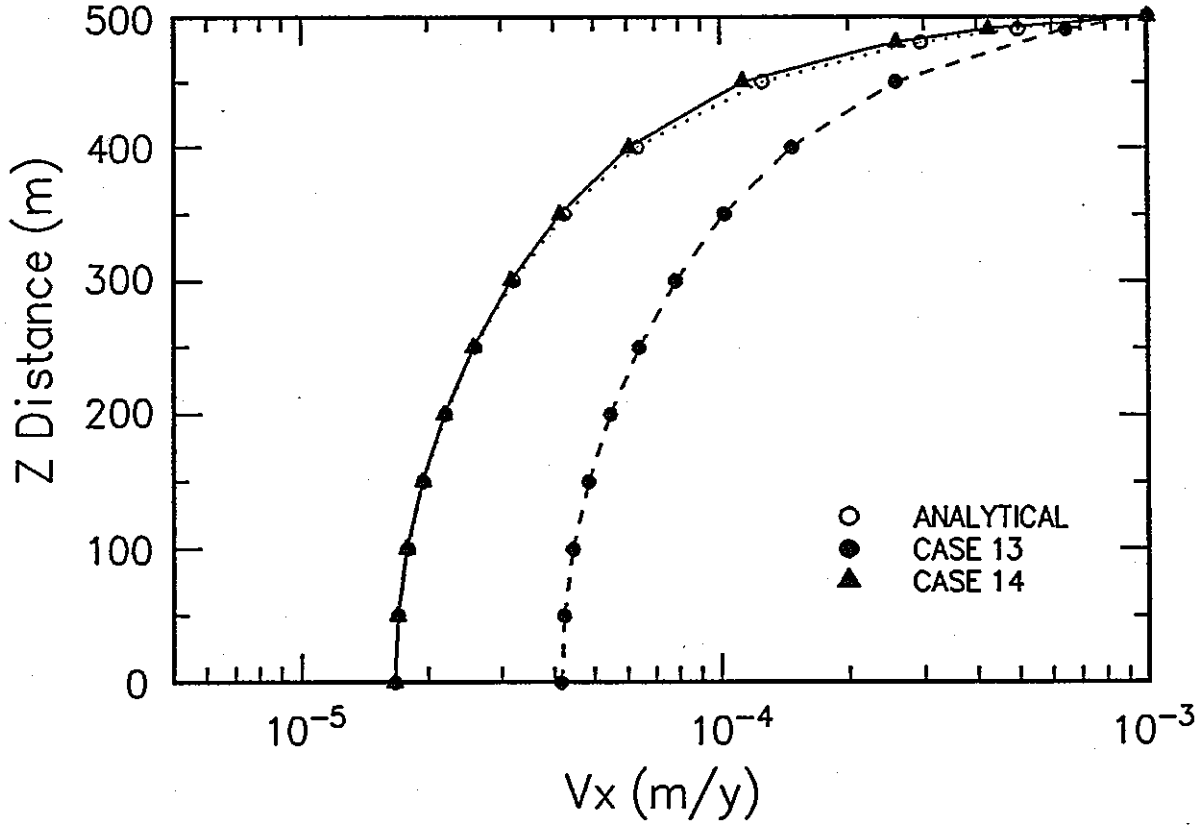


(a) V x

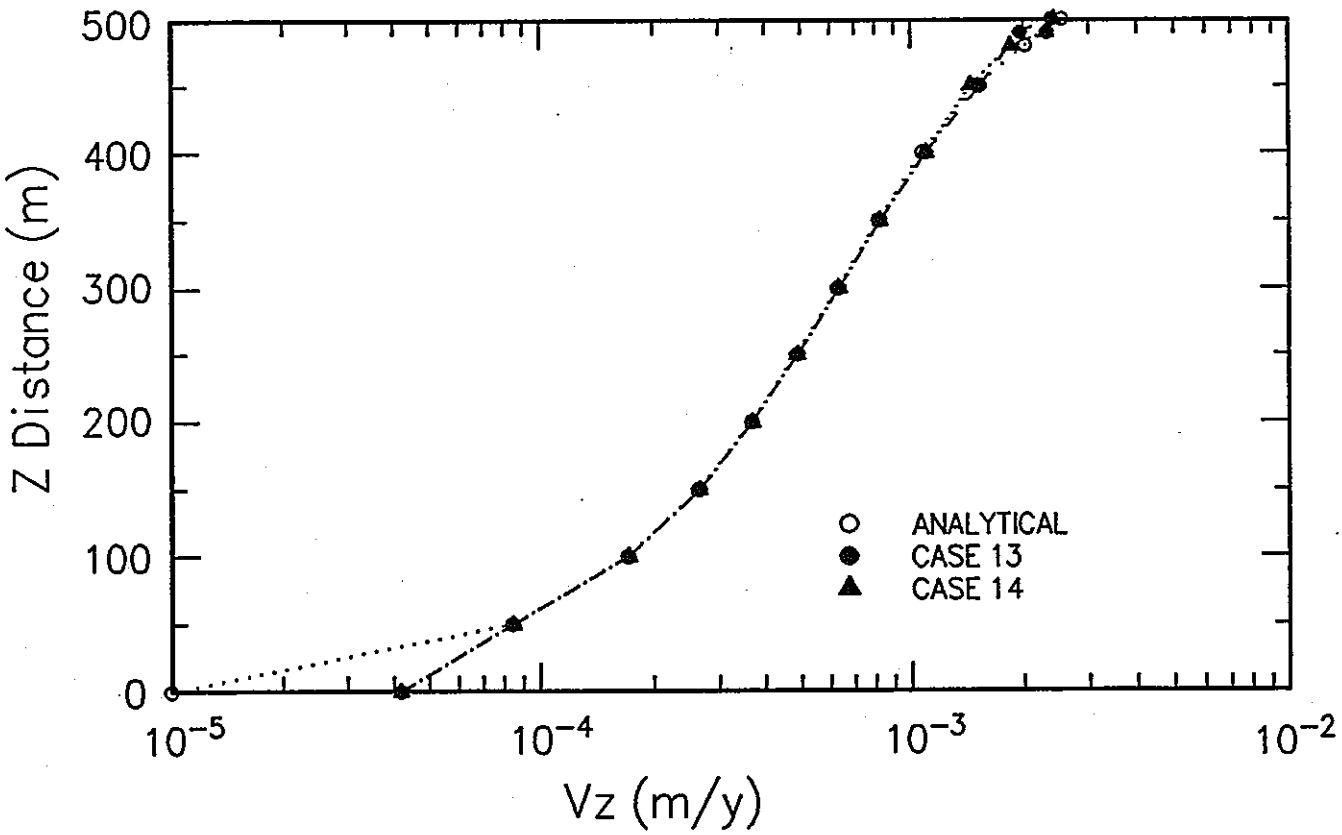


(b) V z

図－69　x＝0 mにおける垂直分布

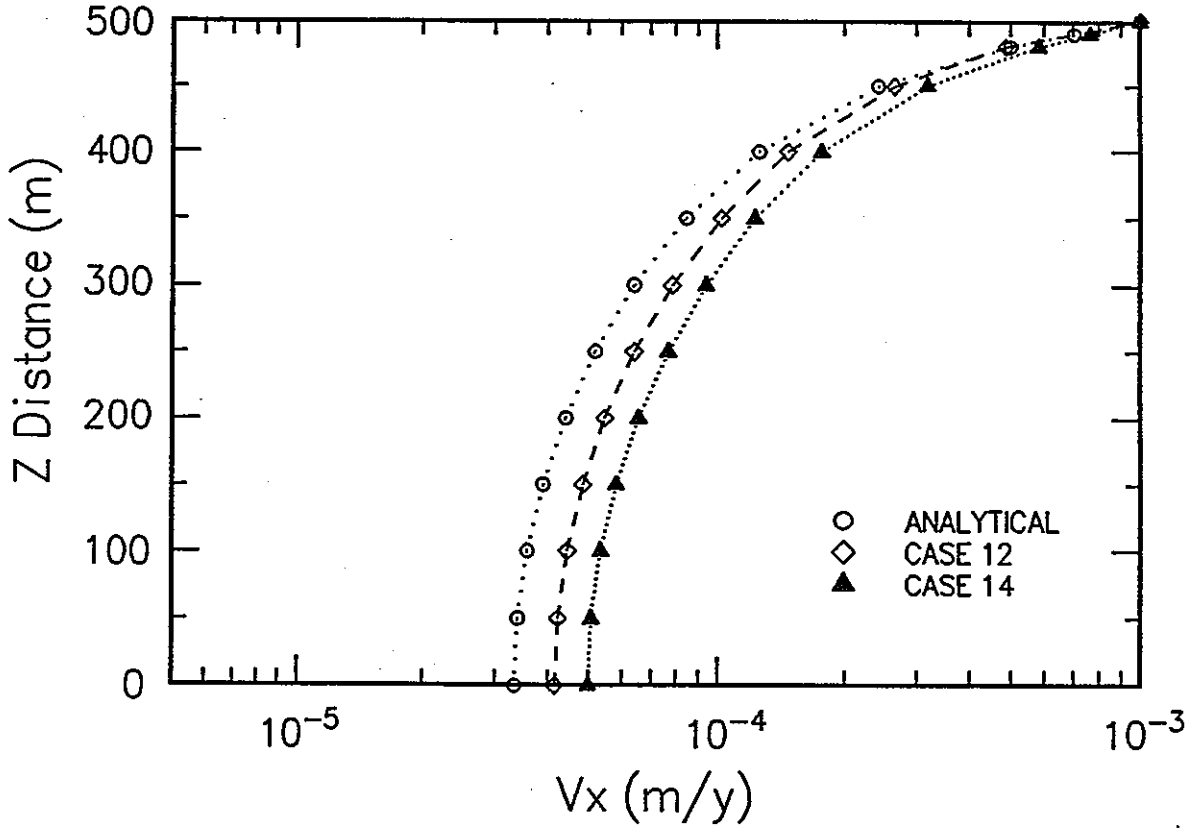


(a) V x

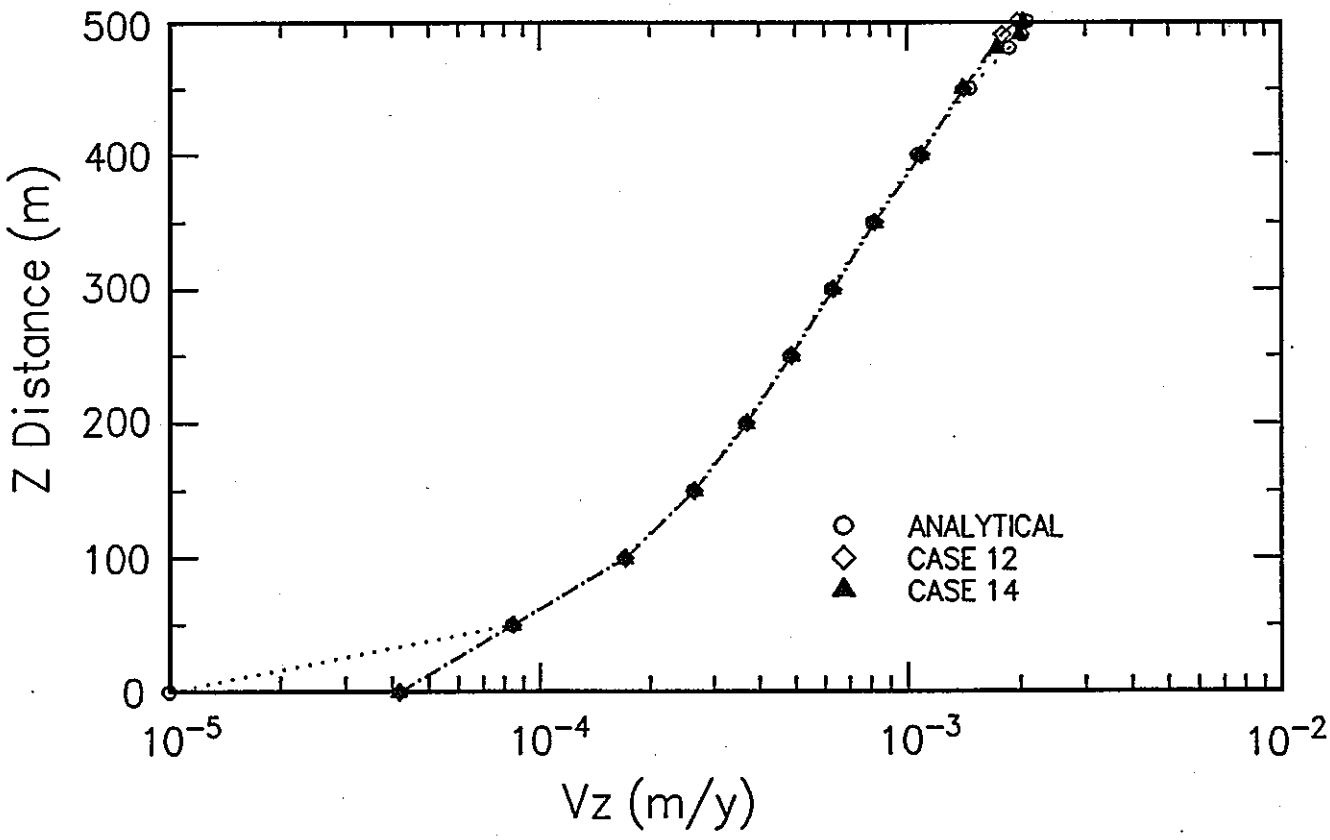


(b) V z

図－70　x＝10mにおける垂直分布

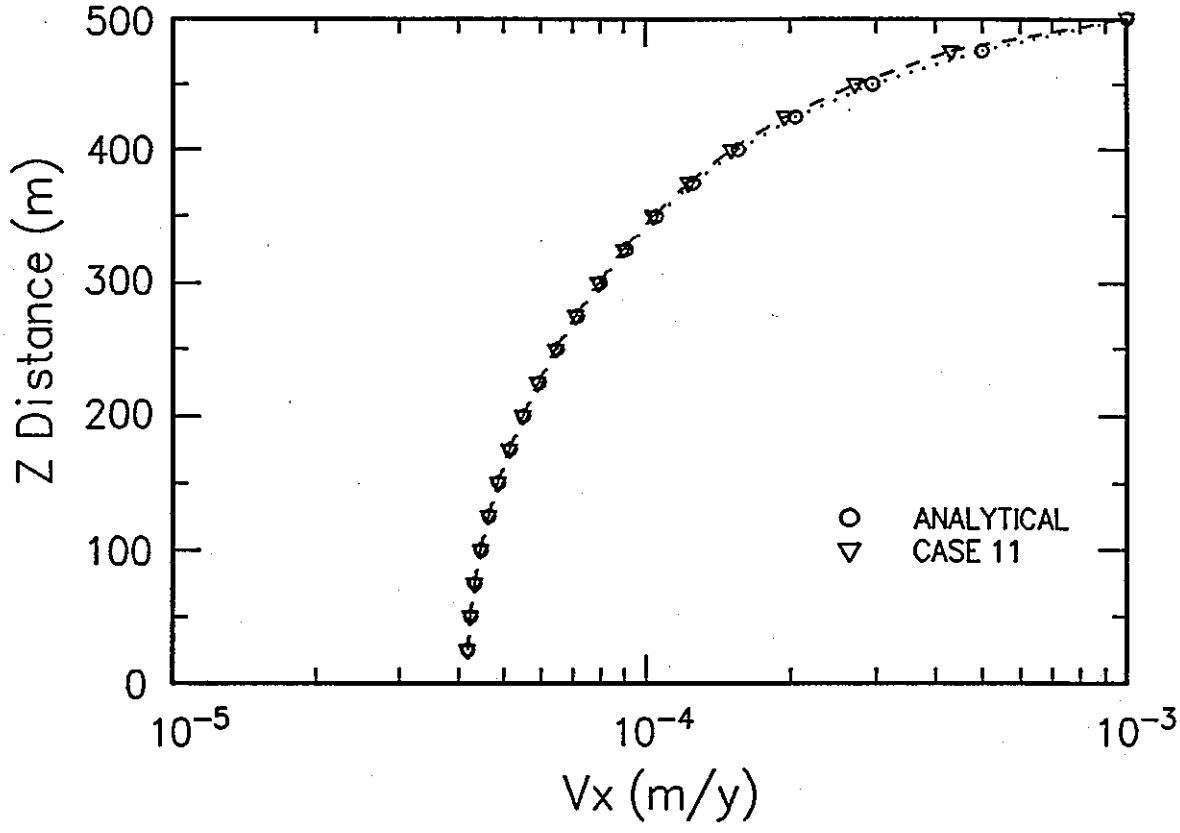


(a) Vx

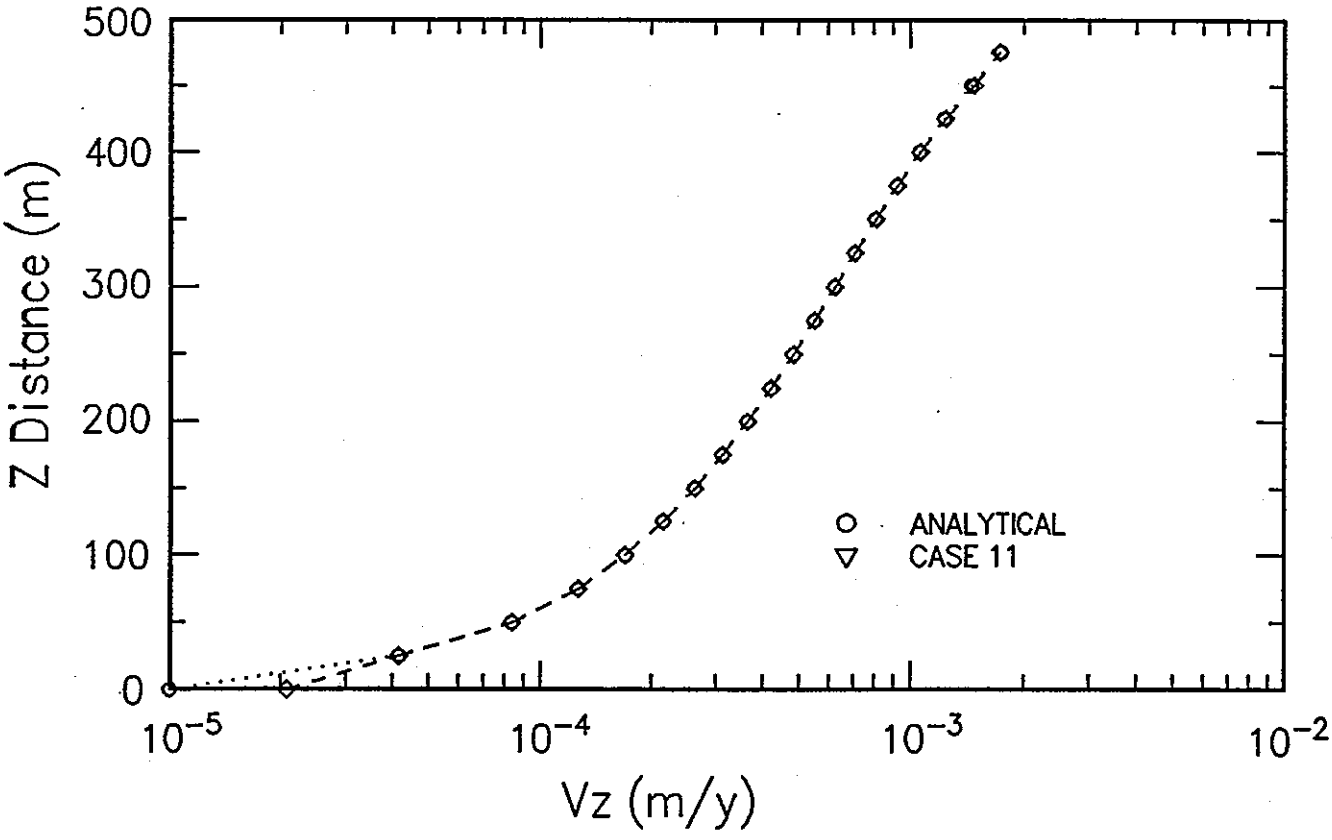


(b) Vz

図－71　x＝20mにおける垂直分布

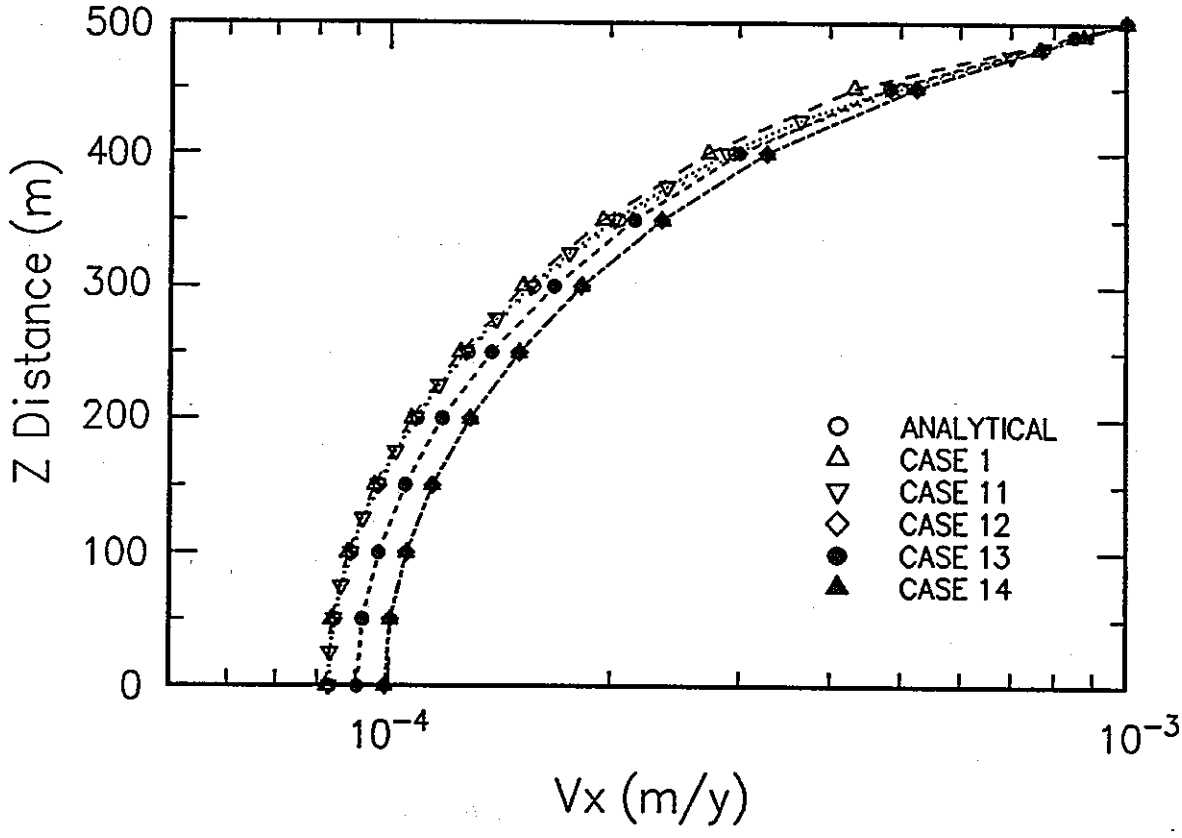


(a) Vx

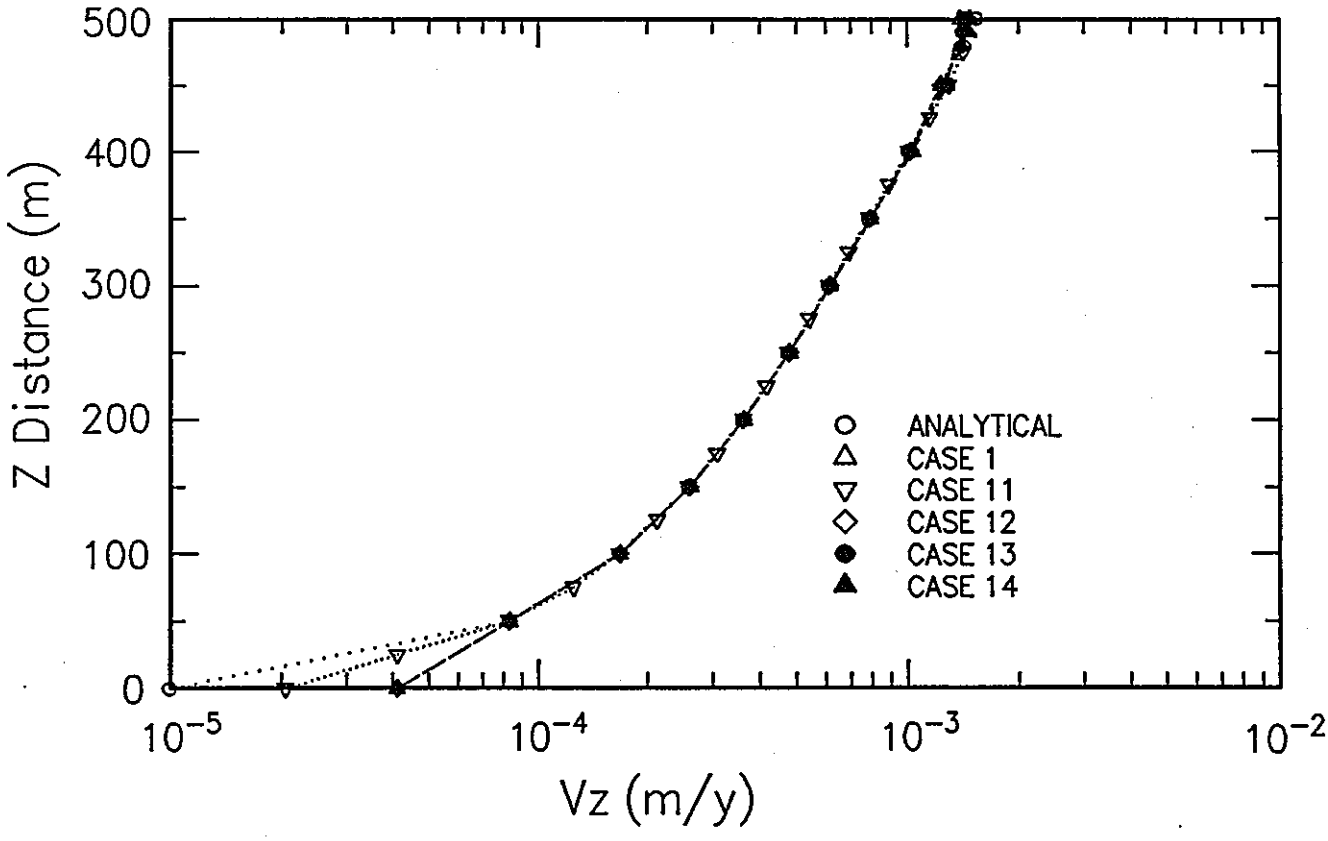


(b) Vz

図－72　x＝25mにおける垂直分布



(a) V x

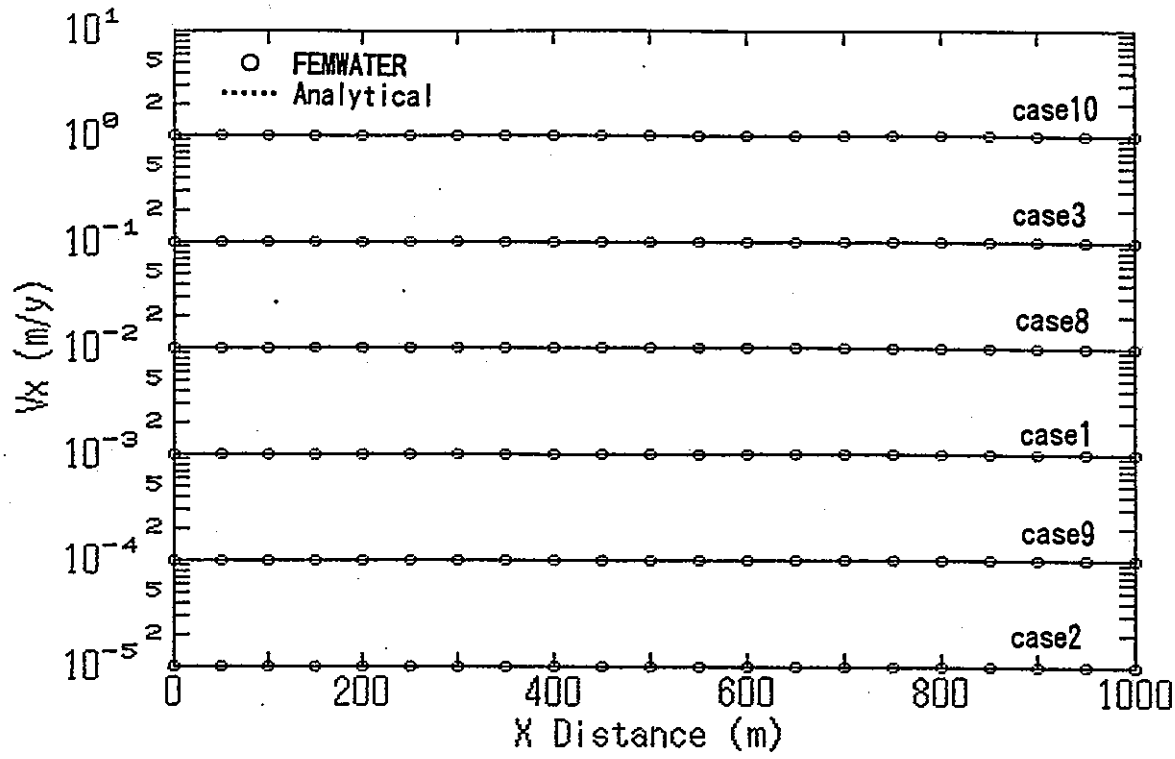


(b) V z

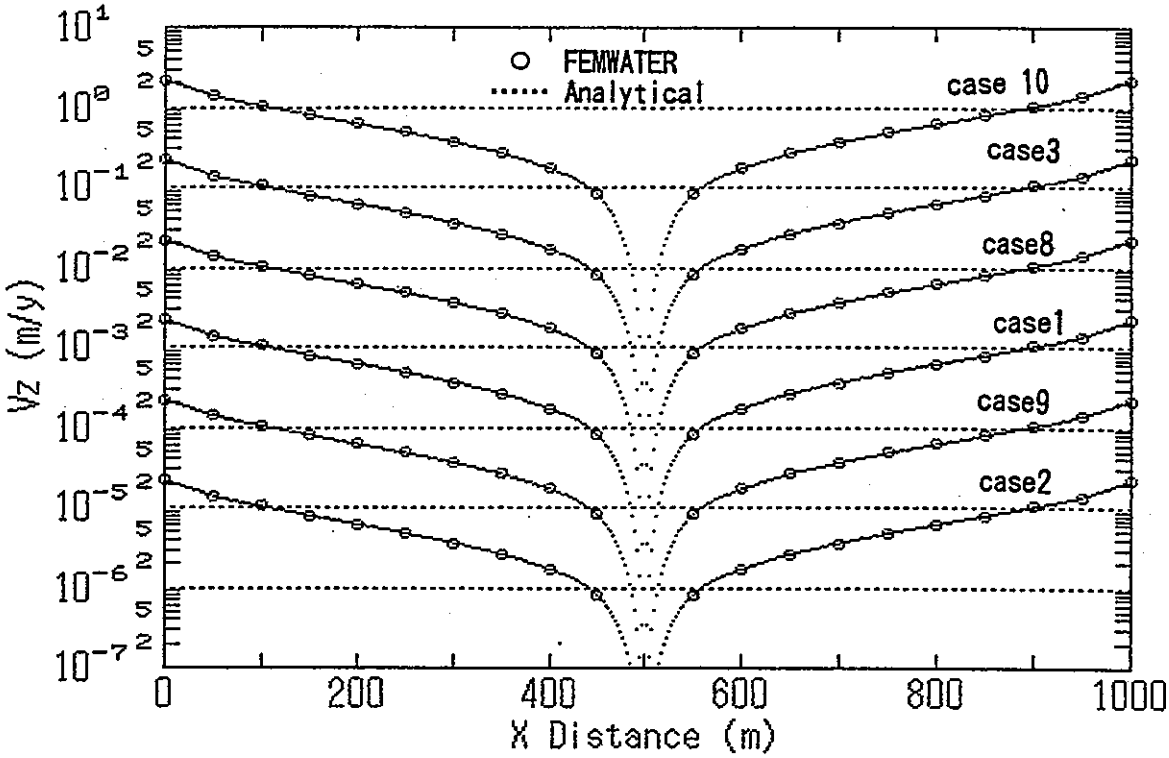
図－73　x＝50mにおける垂直分布

表-29　流出境界節点でのVzの比較

ケース	Vz (m/y)	備　　考
解析解	7.7073×10^{-3}	
case 1	2.168×10^{-3}	メッシュ幅　50
case 4	1.728×10^{-3}	メッシュ幅　100
case 11	2.609×10^{-3}	メッシュ幅　25
case 12	2.573×10^{-3}	境界近傍　Δx=20
case 13	3.197×10^{-3}	境界近傍　Δx=10
case 14	3.194×10^{-3}	境界近傍　Δx=10×2

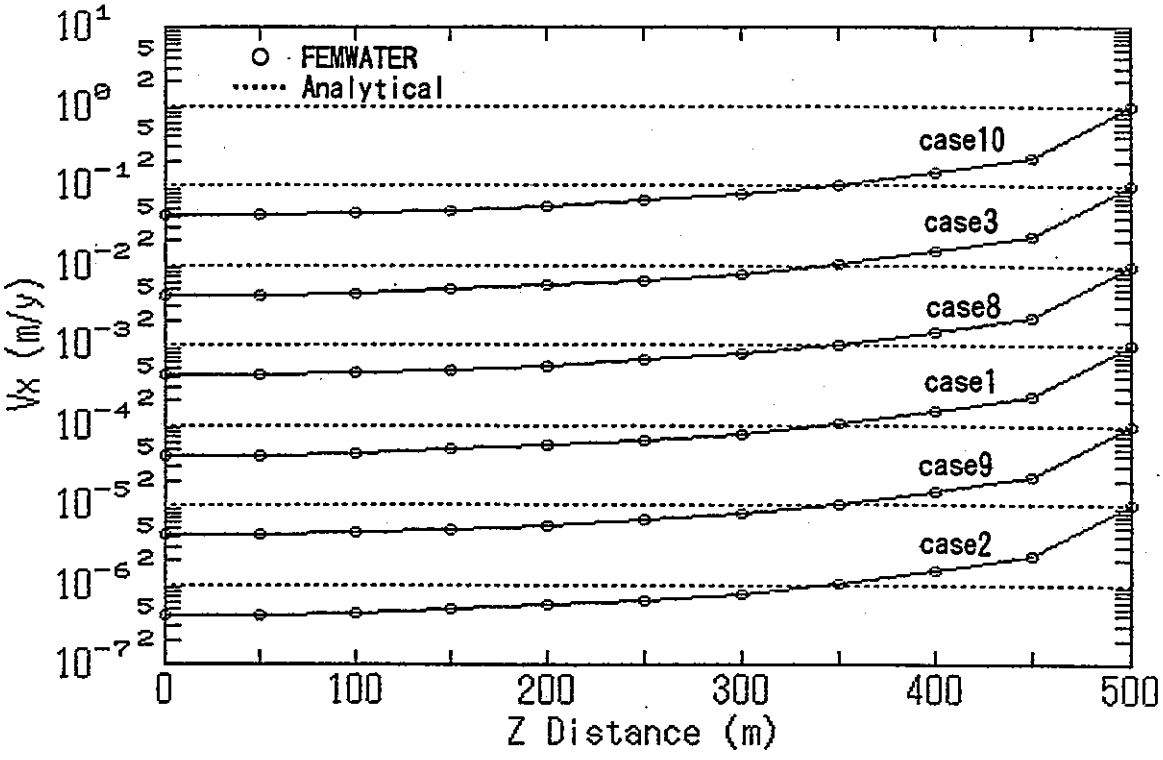


(a) Ｖｘ

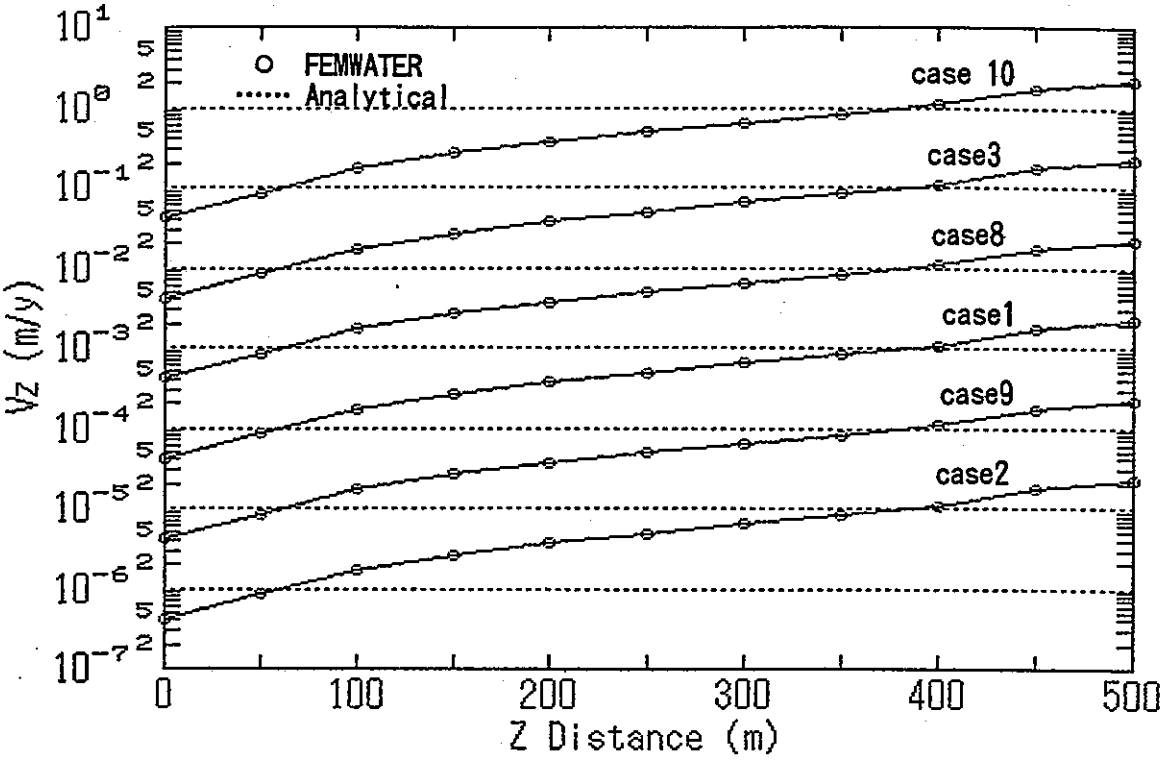


(b) Ｖｚ

図－74　流速の水平分布（ｚ＝500m）



(a) Vx



(b) Vz

図－75　流速の垂直分布（x＝0 m）

7.2.5 検証計算のまとめ

本年度のコード検証は、ファーフィールドでの性能評価を想定した多孔質媒体中の飽和流を対象とし、FEMWATERコードの基本計算能力の確認を目的に行った。元年度委託研究の中で設定した検証ケースの中から、2次元の飽和定常流問題を選び、空間分割の影響、パラメータ（透水係数及び地下水面勾配）の影響について調べた。その結果、以下の事が分かった。

水頭（全水頭）分布では、

- 得られた計算結果は解析解と非常に良く一致し、最大誤差は 0.07 % であった。
- 誤差は要素分割が細かい方が小さく、境界近傍を細かくすると更に小さくなる。
- 本問題は透水係数及び空隙率には依存せず、コード計算結果も同一分布となり、妥当な解が得られた。

ダルシー流束分布では、

- 境界近傍を除いて解析解と良く一致している。しかし、境界上での誤差が大きく、特に数学的な特異点（フラックスが不連続になる点）では正確に近似できない。
- 要素分割は細かい方が精度は良くなり、境界近傍を細かくすると更に良くなるが、長方形要素を用いることになるので分割方法に注意が必要である。
- 透水係数×地下水面の勾配の値に比例したダルシー流速が得られた。

以上から、FEMWATERコードの2次元飽和定常問題の水頭に関しては、全領域において正確に計算できる事が検証された。フラックス（ダルシー流速）に関しては、ほとんどの領域で正確な解が得られたが、周辺領域（境界近傍）では十分な解が得られなかった。これは問題の設定にも関連するが、FEMWATERコードは連続なフラックス場を与えるように作成されており、本問題のような不連続なフラックス場となる問題に対しては正確には近似できないためと考えられる。

7.3 検証のためのユーザ・インターフェイス

コード検証においては、プログラムの能力検査の観点から動的分析手法が適切であり、コードの実行が前提となる。そして、設定した検証対象（解析する現象と場の条件）に対し、様々なコード利用条件（座標系、空間メッシュ分割、時間刻み巾、境界条件等）のもとで多くの計算を行う必要がある。さらにコードテストの結果得られる数値解の収束性、精度、特性等を判断しなければならない。それ故、検証計算は煩雑なものにならざるを得ず、検証作業の効率化のためにはユーザ・インターフェイスの開発は不可欠なものである。ユーザ・インターフェイスを使用することにより、より多くの計算を行うことができ、また多数のユーザ（解析者）による実行が可能となる。

検証作業を進める上でユーザ・インターフェイスに必要な項目・機能について以下に示す。コードにより入力パラメータが異なるので、FEMWATERを例に考えるが、実行に必要な全てのデータが入力でき、それらのデータ管理が可能であることが必要である。

- タイトルの入力

  問題番号、タイトルはFEMWATERの入力項目であるが、データ管理の観点からも入力する必要がある。
- 物理パラメータの入力

  透水係数、空隙率、圧縮率、密度、動粘性係数等の入力が対話形式で行える。
- 計算パラメータの入力

  定常・非定常、飽和・不飽和、地層数、時間差分法等の実行に必要なパラメータの入力が対話形式で行える。
- メッシュ作成機能
- 初期及び境界条件の入力

これらの入力はメニュー選択形式で簡単に行えることが望ましい。また、これらのデータの管理機能が必要で、後日または他のユーザが同一のシミュレーションが再現できなければならない。さらに、FEMWATERのアウトプット（流速等）はFEMWASTE-PNCのインプットとして使われるため、結果に対する管理機能も必要である。

以上のように、ある特定の１つのコード検証作業においてもユーザ・インターフェイス、特に入力用のプリ・プロセッサは必要であるが、連成計算を行うために複数のコードを使用する場合にはユーザ・インターフェイスの開発は不可欠なものである。連成計算では、一人の解析者が複数のコードを使用して一連の計算を行う場合や、複数の解析者がコードを分担して計算を行う場合が考えられるが、各コードのデータ管理やコード間のデータ変換、さらに計算の履歴を記録することができるインターフェイスが必要となる。ユーザ・インターフェイスを使用することにより、検証作業の効率が飛躍的に向上すると考えられる。

7.4 まとめ

本年度のコード検証は、ファーフィールドでの性能評価を想定した多孔質媒体中の飽和流を対象とし、FEMWATERコードの基本計算能力の確認を目的に行った。元年度委託研究の中で設定した検証ケースの中から、2次元の飽和定常流問題－検証ケース名 F1 －を選び、検証計算を実施した。その結果、以下の事が分かった。

水頭（全水頭）分布では、

- 得られた計算結果は解析解と非常に良く一致し、誤差は要素分割が細かい方が小さい。
- 本問題は透水係数及び空隙率には依存せず、コード計算結果も同一分布となり、妥当な解が得られた。

ダルシー流束分布では、

- 境界近傍を除いて解析解と良く一致している。しかし、境界上での誤差が大きく、特に数学的な特異点（フラックスが不連続になる点）では正確に近似できない。
- 要素分割は細かい方が精度は良くなり、境界近傍を細かくすると更に良くなる。
- 透水係数×地下水面の勾配の値に比例したダルシー流速が得られた。

以上から、2次元飽和定常問題に対し、FEMWATERコードは全領域においてモデルを正確に計算できる事が検証された。しかし、フラックス（ダルシー流速）に関しては、ほとんどの領域で正確な解が得られたが、境界周辺の領域では十分な解が得られなかった。特に不連続なフラックスとなる領域に対しては正確な近似ができないと考えられる。

8. あとがき

性能評価予測は、社会的受容の確立と公衆の安全保証上、地層処分システムが長期的な安全性を示すために重要である。このためには、評価上考慮すべき現象を網羅したモデル群を自由に扱うことができる統合解析システムが不可欠である。

本研究では、より包括的、効率的、信頼性の高い解析システムの実現を目差して、

① 出発点となる統合モデル概念の構築と包括的な解析を行なうための技術アプローチの開発

② 個別モデルの解析信頼度を示すための手法の開発

を行ない、長期的な開発展望を拓いた。

今後、この研究を更に進展させるためには、長期的展望に立ち、

① 開発した統合モデル概念を具体化していく開発

② ①の開発を効率的かつ品質保証する技術システムの開発

③ ①で用いる各種モデルの解析信頼度を保証し、高める手法の開発

に努めることが必要である。